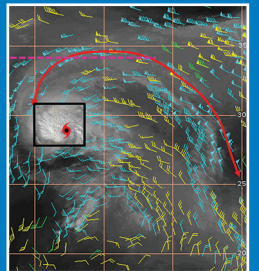
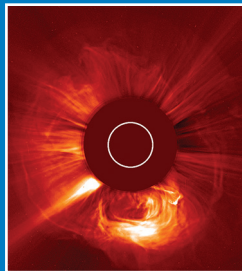
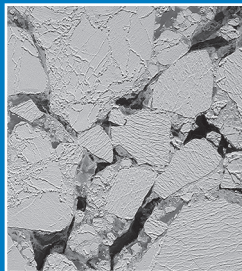
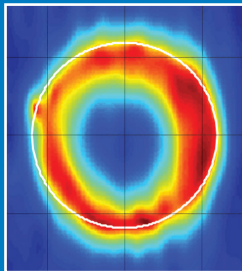
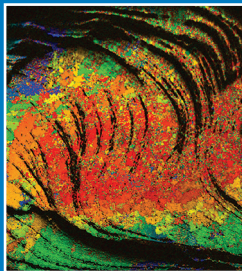
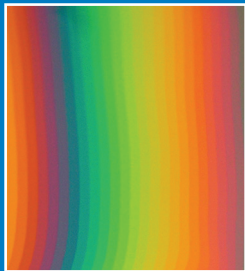


NAVAL RESEARCH LABORATORY
the navy's corporate laboratory

2014 NRL REVIEW

Focusing on cutting-edge
science for the
Navy and the Nation



Washington, DC • Stennis Space Center, MS • Monterey, CA

NRL's MISSION

To conduct a broadly based multidisciplinary program of scientific research and advanced technological development directed toward maritime applications of new and improved materials, techniques, equipment, systems, and ocean, atmospheric, and space sciences and related technologies.

The Naval Research Laboratory provides primary in-house research for the physical, engineering, space, and environmental sciences; broadly based applied research and advanced technology development programs in response to identified and anticipated Navy and Marine Corps needs; broad multidisciplinary support to the Naval Warfare Centers; and space systems technology, development, and support.



NRL REVIEW STAFF

SENIOR SCIENCE EDITOR
John D. Bultman

COORDINATOR
Jonna Atkinson

CONSULTANT
Kathy Parrish

DESIGN, LAYOUT, AND GRAPHIC SUPPORT
Jonna Atkinson

EDITORIAL ASSISTANCE
Saul Oresky
Kathy Parrish
Claire Peachey

PHOTOGRAPHIC PRODUCTION
Gayle Fullerton
Jamie Hartman
James Marshall



COMMANDING OFFICER
CAPT Mark C. Bruington, USN



DIRECTOR OF RESEARCH
Dr. John A. Montgomery

REVIEWED AND APPROVED
NRL/PU/3430--15-600
RN: 15-1231-2091
August 2015

Mark C. Bruington, Captain, USN
Commanding Officer

VIEW FROM THE TOP

from CAPT MARK C. BRUINGTON and DR. JOHN A. MONTGOMERY



The U.S. Naval Research Laboratory (NRL) is a place unlike any other. It's where we advance basic science and nurture unconstrained ideas so that, in the future, the two may merge as an innovative capability. When the Navy and Marine Corps have a tough problem, they come here; but we're not just pushing the envelope for today's warfighters, we're also enhancing the United States' global posture and influence in ways that won't come to light for another 50 years.

When we're asked what makes NRL so special, we always say that it's our people first and foremost. We bring together the best scientists and engineers, and provide them the freedom and the tools to pursue their passions and answer the most urgent applications. We don't know of another place that encourages—requires, even — the kinds of interdisciplinary avenues of research like NRL. As this *NRL Review* shows, it's really at these intersections — where materials science and computational physics, chemistry, and sensing merge — that the most innovative research flourishes.

These kinds of advances are possible because NRL has world-class facilities across the United States,

with one-of-a-kind laboratories like the Laboratory for Autonomous Systems Research, the Institute for Nanoscience, and the Nike Laser Facility. These are the places where we find the space to build our knowledge, expand our creativity, and interface with colleagues to do our work.

The products that emerge are meaningful and cost-effective to transition to our warfighters as we partner with industry. This *Review* provides an in-depth look at some of the most important products from the past year, including global weather prediction systems, alternative energy technologies, and remote sensors and imagers. NRL's advances often come to be used by citizens in their everyday life; this year's *Review* highlights some of those achievements as well.

As we continue to foster research in these and many other areas, we remain confident that NRL will — as it has done since 1923 — keep our nation and our allies ahead of our adversaries, with science and technology benefits for us all.

CONTENTS

2014 NRL REVIEW

NRL'S INVOLVED!

- Our People Make a Big Difference 2
- NRL Demonstrates Capabilities of Coupled Oceanic and Atmospheric Prediction Tools at 2013 Navy Fleet Exercise 7
- GPS Satellite NTS-2 Joins Other NRL Technologies on Display 8
- NRL Hosts Its Third Annual Karles Invitational Conference 12



THE NAVAL RESEARCH LABORATORY

- NRL – Our Heritage 16
- Highlights of NRL Research in 2013 17
- NRL Today 29



FEATURED RESEARCH

- OTHR Gets a Makeover**
2D Oversampled Receive Arrays for Over-the-Horizon Radar 76

- A New Twist on Barnacle Shells!**
Structure and Crystallography of the Barnacle *Balanus amphitrite* 83

- It's RTIME to Shine Light on Arctic Sea Ice Motion**
Measuring Arctic Sea Ice Motion in Real Time 89

- Somewhere, Over the Hurricane, Global Hawks Fly...**
Using Unmanned Aircraft to Probe Hurricanes 97

- TMI about TSI?**
Predicting Total Solar Irradiance 109

- The Quest for Compact Hyperspectral Imaging...Starting with (Very) Small Staircase Steps**
Multiple Order Staircase Etalon Spectroscopy 116

RESEARCH ARTICLES

acoustics

- Atmospheric Acoustic Propagation and Detection of Rotorcraft Noise 126

- Novel Thermophone Acoustic Projectors 127

- Elastic Point Contact and Mechanical Resonators 128

atmospheric science and technology

- Geochemical Data Application to Enhance Seismic Interpretation of Deep Sediment Methane Hydrate Deposits 134

- Monitoring Maritime Conditions with Unmanned Systems During Trident Warrior 2013 136

- Probing the World's Greatest Source of Variability — Madden Julian Oscillation 139

chemical/biochemical research

- Identification of Trace Explosives on Relevant Surfaces at Standoff Distances 144

- Biomolecular Analyses of Ship Hull Biofouling Communities 146

- Hierarchically Organized Microvessels for Vascularized Tissue Models 149

- X-Ray Crystal Structures of Engineered Ricin Vaccine Immunogens 152



electronics and electromagnetics

- Multilayer Polymer Composites for High Energy Density Capacitors 156

- Wideband Dynamic Range Extender (DRE) 157

- An Attractive Hybrid Indirect and Direct Drive Approach to Laser Fusion 159

- Multi-Kilowatt Millimeter-Wave Sheet Beam Amplifiers 161

information technology and communications

- TRIDENT SPECTRE 2013: FIREFLY: Multimodal Signatures for Increased Confidence in Remote Object Detection and Classification 166

- TALON — Robust DoD Laser Communications through the Air 168

materials science and technology

- Novel Spintronic Device for Reconfigurable Logic 172

- Simulation of Cold-X-Ray Effects Using Intense Ion Beams 173

- Prediction of New High Thermal Conductivity Materials for Cooling Electronics 175

CONTENTS

2014 NRL REVIEW

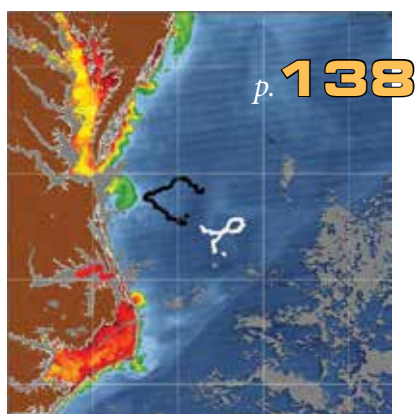
Long-Term Hydrogen-Assisted Cracking
Evaluation of Monel K-500 **176**

nanoscience technology

Photochemistry in 3D Using Visible-Light
Plasmonic-Sensitization **182**

Strained $\text{In}_x\text{Ga}_{1-x}\text{As}$ HEMTs for
Complementary Logic **183**

Energy Distribution through Quantum Dot
Anchored Nanoscale Photonic Wires **185**



ocean science and technology

Ballast Water Compliance Testing **190**

Direct Measurements of Tensile Strength
of Artificial Marine Flocs under Microscopic
Micromanipulation **192**

Laser Profiling System for Laboratory
Sediment Beds **194**

Biogeochemical Control of the Particle Flux in
River-Dominated Coastal Regions **197**

optical sciences

Infrared Gradient Index Optics for Multiband
Imagers **202**

Broadband Nonlinear Metamaterial **203**

remote sensing

Broadband Dielectric Spectroscopy of Several
Energetic and Nonenergetic Materials **208**

Camouflage Paint Scheme for the USS *Fort
Worth* (LCS 3) **210**

Hyperspectral Imager for the Coastal Ocean
(HICO) Goes Public under NASA
Sponsorship **212**

simulation, computing, and modeling

Considering Blast Response in Helmet
Design **216**

The X-Ray Flash of a Z Pinch **217**

From the Stream to the Shore: Forecasting
Complex-Ocean Environments in Trident
Warrior '13 **219**

Integrating the Marine Biosphere into Coupled
Ocean-Atmosphere Models **222**

space research and satellite technology

High-Precision Remote Sensing of Ionospheric
Disturbances **226**

SWORD: Improving the Simulation
Experience **229**

Project CHRONOS **231**



SPECIAL AWARDS AND RECOGNITION

Special Awards and Recognition **236**

Alan Berman Research Publication and
NRL Edison (Patent) Awards **249**

NRC/ASEE Postdoctoral Research
Publication Awards **252**



PROGRAMS FOR PROFESSIONAL DEVELOPMENT

Programs for NRL Employees — Graduate
Programs, Continuing Education, Professional
Development, Equal Employment Opportunity
(EEO) Programs, and Other Activities **256**

Programs for Non-NRL Employees —
Postdoctoral Research Associateships,
Faculty Member Programs, Professional
Appointments, and Student Programs **258**

NRL Employment Opportunities **260**

GENERAL INFORMATION

Technical Output **262**

Key Personnel **263**

Contributions by Divisions, Laboratories,
and Departments **264**

Subject Index **267**

Author Index **269**

Map/Quick Reference Telephone
Numbers **270**

NRL's Involved!

2 Our People Make a Big Difference

7 NRL Demonstrates Capabilities of Coupled Oceanic and Atmospheric Prediction Tools at 2013 Navy Fleet Exercise

8 GPS Satellite NTS-2 Joins Other NRL Technologies on Display

12 NRL Hosts Its Third Annual Karles Invitational Conference

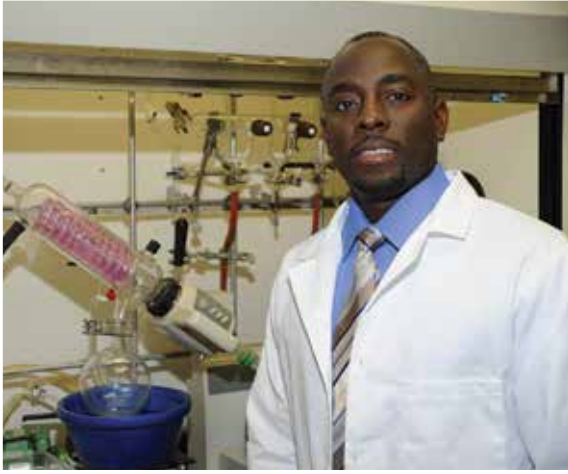


our people make a **BIG** difference



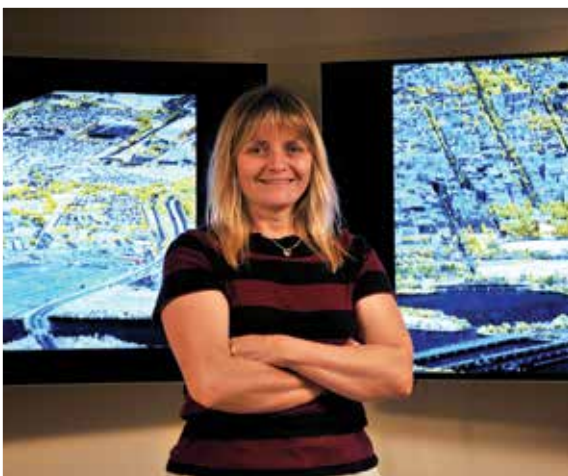
The *NRL Review* dramatically illustrates the range of **research capabilities and innovative technologies** that make the Naval Research Laboratory a leader in so many fields. Driving all of NRL's innovations and successes are the **highly motivated people** who work here. It is these people who provide the talent, creativity, and sustained effort to **turn ideas into realities** in support of the Navy mission. In this section, we proudly highlight some of these special people.





MR. PAUL CHARLES has been a research chemist in the Center for Bio/Molecular Science and Engineering since his arrival at NRL in 1991. His research has focused on the design of novel fluorescence-based biomolecular sensors for the detection of explosives, PCBs, and drugs of abuse. This research has been adapted for field monitoring applications of environmental contaminants in seawater, groundwater, and soil. Mr. Charles's current research has involved sensor integration into underwater autonomous vehicles for use in the marine environment. He has experience in the design and synthesis of 3D polymeric materials for the immobilization of proteins and oligonucleotides in microarrayed formats; synthesis and characterization of molecular products by HPLC, FTIR, and GC-MS; and methods and protocol development for solvent vapor headspace and particulate analysis. Mr. Charles has a B.A. in biological sciences

from the University of Maryland, Baltimore County (UMBC) and a master's degree from the University of Maryland, University College (UMUC) (health care/business administration). He has more than 40 publications (1000+ citations), 5 patents, and numerous presentations at national and international conferences. In addition to his research, Mr. Charles serves as the director of the ONR-sponsored summer internship program at NRL for underrepresented minority undergraduates who attend historically black colleges and universities/minority institutions (HBCU/MI). This program encourages talented students to pursue graduate degrees in the STEM disciplines by providing a 10-week "hands-on" research and mentoring experience with NRL scientists. Students are also provided opportunities such as career development and scientific workshops, teambuilding events, and educational visits to graduate schools to enhance their NRL research experience. To date, more than 260 interns have participated, and more than 25 have co-authored refereed articles published in prestigious scientific journals. "I have been extremely blessed to have worked more than 20 years as an NRL scientist with some of the brightest minds in the world performing state-of-the-art research. I strongly promote diversity in the scientific community and believe it is essential that we encourage our youth and provide opportunities through mentoring programs (especially to talented underrepresented minorities interested in STEM disciplines). I believe the Navy and the DoD can maintain its high level of scientific superiority; however, it must continue to broaden its scope and embrace ideas from all communities. Brilliant ideas know no race, color, or gender. They are just brilliant ideas."



MS. TRIJNTJE DOWNES is a member of the Intelligence, Surveillance, and Reconnaissance (ISR) Systems Section in the Applied Optics Branch within the Optical Sciences Division. She received a master's degree in physics from U.C. Irvine in 1988, and worked at Rockwell International and the RAND Corporation before joining NRL in 1998. She spent five years in the Remote Sensing Division helping to develop and test models for ocean-atmospheric light fields before transferring to Optical Sciences where she has been instrumental in the analysis, development, and field testing of numerous hyperspectral sensors. She leads the data analysis efforts for sensor collections and is one of the key image specialists that evaluate advanced target detection algorithms developed by the branch. In addition, she manages the branch's multilevel security data storage and exploitation facility where all of the classified and

unclassified multisensor data are archived and exploited. "Working at NRL provides both an academic and commercial-industrial experience. We see ourselves as the 'trusted, honest agent' for our customers who rely on our research to provide answers to difficult questions."



MS. LAURIE FIALKOWSKI is a mathematician in the NRL Acoustics Division. Her areas of research include acoustic signal processing and acoustic propagation modeling, with application areas in detection and classification of underwater sound sources, as well as geo-acoustic inversions. As part of the Acoustic Signal Processing and Systems Branch, Ms. Fialkowski has focused much of her research in developing techniques that will provide the Navy with robust target detection and classification capabilities, both for platform-based receivers and for autonomous surveillance. She is currently the principal investigator of an effort to develop and field-test waveguide-invariant-based methods that exploit acoustic guide sources at the ocean surface for use in passive signal processing in littoral regions. In support of this effort, Ms. Fialkowski participated in the planning and execution of at-sea experiments on the

New Jersey Shelf in 2012 and 2014. During these experiments, Ms. Fialkowski worked alongside several NRL scientists to deploy ocean acoustic recording equipment from aboard the University of Delaware's research vessel R/V *Hugh R. Sharp*. During her years at NRL, Ms. Fialkowski has participated in several ocean acoustic experiments, many of which involved multinational collaboration. Ms. Fialkowski first came to NRL as a cooperative education student in 1988 while pursuing a bachelor's degree in applied math at Texas A & M University; she joined NRL full-time after completing her undergraduate degree in 1990. Ms. Fialkowski also completed a master's degree in applied math at the University of Maryland in 1998 while participating in NRL's Edison Memorial Graduate Training Program, a program which enables employees to pursue graduate studies in their fields at local universities. "Working at NRL has offered me interesting and diverse opportunities, many that I never imagined would be available to a mathematician.... From the day I came aboard, experienced scientists enthusiastically offered guidance, and I was encouraged to participate in workshops and field experiments. My time at NRL continues to be an exciting balance between independent research, team development, and field experience."



MR. BRETT HUHMAN has been in the Electromagnetic Launchers and Advanced Systems Section of the Plasma Physics Division since his arrival at NRL as a contractor in 2005; he became an NRL employee in 2007. He graduated from the University of Missouri with a B.S. and M.S. in electrical engineering in 2003 and 2006, respectively. In 2013, he was selected as a recipient of the NRL Edison Memorial Graduate Training Program, and is currently a Ph.D. candidate at Virginia Tech. Since joining NRL, Mr. Huhman has pushed the state of the art in both high-resolution flash x-ray sources and electromagnetic railguns. In 2005, he successfully delivered a modified Febetron unit that combined the casing and Marx capacitor bank of a Febetron with an NRL-designed front end, allowing the use of a much smaller anode on the vacuum diode. The resulting radiographs have demonstrated a 10× increase in radiographic figure of

merit for explosively strained material tests. From 2007 to 2012, he was the operations manager of the NRL Railgun, coordinating the efforts of a multidisciplinary team investigating the pulsed power, materials, and physics of high powered railguns. In 2011, he was a recipient of an Award of Merit for Group Achievement for NRL's 1000th railgun shot. In 2012, Mr. Huhman became the PI for NRL's new effort in battery-based rep-rated pulsed power systems, designing from the ground up an operational system capable of driving a small caliber railgun 10 times per minute for five minutes. "NRL has the greatest working environment for me: I can go to work in jeans and t-shirt, shoot off an indoor artillery gun, and have access to world-class scientists working on nearly any topic."



DR. SANGEET "SUNNY" KHEMLANI is a cognitive scientist at the Navy Center for Applied Research in Artificial Intelligence (NCARAI). He joined NRL in 2011 as a postdoctoral fellow after earning a B.S. in cognitive science from Rensselaer Polytechnic Institute and a Ph.D. in cognitive science from Princeton University. In 2014 he was hired as a Karles Fellow under the auspices of the Intelligent Systems Section at NCARAI. His research goal is to build computational models of higher-level cognitive behaviors. He designed mReasoner, a system that mimics how people reason about abstract concepts like quantity, time, and probability. One of the things he enjoys most about working at NRL is the opportunity to collaborate with talented experts in human-robot interaction, artificial intelligence, and cognitive science at the Laboratory for Autonomous Systems Research (LASR). "The LASR community is unique

in its focus on the difficult problem of how to build autonomous systems that are sensitive to human cognitive abilities and constraints. My goal is to get people and robots reasoning together by designing artificial systems to understand the strengths and weaknesses of human information processing."



MR. ANDREW QUAD is the senior engineering technician responsible for the planning and execution of oceanographic experiments for the Physical Oceanographic Processes Section of the Oceanography Division. In 2002 he earned a B.S. in chemical oceanography from the Florida Institute of Technology. He worked for the U.S. Geological Survey and assisted with ecological mapping of the deep water coral reefs in and around the now active oil drilling operations in the northeastern Gulf of Mexico. In 2004 he joined NRL, working around the globe on many different projects, with many diverse oceanographic devices. Since Oceanography Division field experiments are always unique, he often has to quickly devise effective solutions to complex problems associated with data collection and logistics. Some of his more recent innovative accomplishments include development and implementation of a new type of

pitch/roll/depth sensor important to deployment of Barney-mounted ADCPs; a Set and Drift at Depth (SDD) mission sequencing for gliders; a mechanism for increasing the sampling rates for glider-mounted optical instrumentation, a capability currently unique to NRL; and a power control system for efficiency of an autonomous inverted echo sounder that resulted in high cost savings. He is the Oceanography Division's expert in the deployment and piloting of autonomous underwater vehicles (AUVs) and sensor platforms. His combined experience with instrumentation, theory of operation, and ability to process and quality control various types of data are vital to accomplishing objectives for the numerous field experiments in the Division. Through NRL's Edison program, he earned an M.S. in marine science from the University of Southern Mississippi in 2012. His thesis work is related to NRL's development of a sediment microbial fuel cell, often referred to as the "Bug Battery," in which he was integral to the fabrication and field testing. "I knew I made the correct career choice in 2002, after graduating from the Florida Institute of Technology. I knew I would be seeking employment in the oceanographic field for the rest of my career, and have found a happy home working for NRL. NRL has enabled me to continue my education, which meshes perfectly with the hands-on knowledge of studying dynamic ocean processes, and the technology that is used for sensing the environment. My goals for the Division are to redesign sensor platforms and to incorporate new technology, allowing for more efficient and cost-effective field exercises, while improving observational techniques, data quality and quantity."



MS. TERI THOMAS is head of the NRL Purchasing Branch in the NRL Supply and Information Services Division. Ms. Thomas oversees the full spectrum of the acquisition process and manages the purchasing of required supplies, material, and services up to \$150,000 on the open market; up to the maximum order limit through the Federal Supply Schedule (FSS) program and other indefinite-delivery type contracts; and through the wholesale supply system. In addition, as part of a temporary Federal initiative, Ms. Thomas' branch has procurement authority for purchasing commercial items and services greater than \$150,000 but not exceeding \$6.5 million. These functions are critical to the success of the NRL research missions. In FY14, her branch processed more than 11,000 procurement requests valued at \$96 million, often under extreme deadlines as priority orders. Ms. Thomas has been in the position

since March 2009 and has 34 years of acquisition experience. Throughout her career, she has served as procurement technician, purchasing agent, and procurement specialist. As the branch head, she routinely works with the NRL scientists, researchers, and other technical and support personnel by providing expert advice and guidance on the best way to satisfy the customers' needs. "I am always searching for new ways to simplify and streamline the process, yet maintain the spirit and intent of the myriad complex Federal and other DoD procurement regulations and policies. My goal is to lead and inspire my staff to provide critical and successful customer support to the NRL research community."



DR. SHARON VTIPIL is an aerospace engineer with NRL's Mission Analysis Section of the Naval Center for Space Technology. She applies her astrodynamics expertise to solving space challenges in the areas of orbit determination, coverage analysis, and orbit design. Sharon maintains two NRL astronomical software programs: Orbit/Covariance Estimation and ANalysis (OCEAN) and Ephemeris Propagator Library (EPL). OCEAN is used for orbit determination and data simulation while EPL determines satellite look angles for ground sites. Sharon earned her bachelor of science degree in aerospace engineering from the United States Naval Academy in 1997. Upon graduation, she commissioned into the United States Air Force. As a Space Command officer, she worked for eight years in the areas of space operations and program management. During her time in the Air Force, she earned her master of engineering degree

in aerospace engineering from the University of Florida in 2000. In 2010, she earned a doctorate degree in aerospace engineering from Old Dominion University researching orbit design for Earth observing satellites. "Here at NRL I have the opportunity to pursue my goal of supporting U.S. military warfighting capabilities through enhanced space programs."

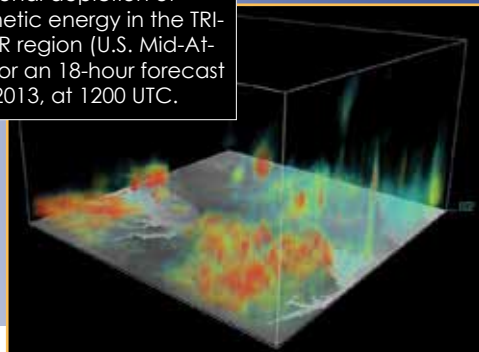
highly motivated people turn ideas into realities...

NRL established the Karles Fellowship in honor of Drs. Jerome and Isabella Karle, two scientists who have dedicated their entire professional lives to innovative advancements in science and technology. The Karles embody the intensity and fervor that NRL wishes to foster and harbor in the workforce of the future. Karles Fellowships are awarded to new NRL hires who are recent graduates and show exceptional scientific abilities and research potential. The Karles Fellowship is one element of NRL's Jerome and Isabella Karle Distinguished Scholar Fellowship Program, which also includes the Karles Senior Research Fellowship, open to established researchers whose credentials are comparable to those of the Karles, and the annual Karles Invitational Conference.

NRL Demonstrates Capabilities of Coupled Oceanic and Atmospheric Prediction Tools at

2013 Navy Fleet Exercise

Three-dimensional depiction of turbulence kinetic energy in the TRIDENT WARRIOR region (U.S. Mid-Atlantic coast) for an 18-hour forecast valid July 16, 2013, at 1200 UTC.



ScanEagle unmanned aerial vehicle is launched during TRIDENT WARRIOR exercises off the Virginia coast.

U.S. Naval Research Laboratory (NRL) scientists in the Marine Meteorology Division and the Oceanography Division, with funding provided by the Office of Naval Research, took part in the Navy fleet experiment TRIDENT WARRIOR 2013 (TW13), July 13–18, demonstrating in situ atmospheric and oceanic sensing systems and real-time operational mesoscale numerical weather prediction models.

“These numerical experiments demonstrate, in real time, the impact of the observations on tactically relevant environmental features of the ocean battlespace environment,” said Dr. James Doyle, head of the Mesoscale Modeling Section, Marine Meteorology Division. “This is the first time feedback between environmental forecasts and targeted observations has been conducted in both the ocean and atmosphere during a Navy exercise.”

Feedback between environmental forecasts and targeted observations has resulted from long-term research at NRL into understanding and developing high-resolution coupled prediction capabilities to diagnose and predict the sensitivity of tactically relevant environmental predictions to observations and develop controlled observation systems.

“This unique opportunity provides a better understanding between environmental forecast systems and controlled observing systems in the coastal marine atmospheric boundary layer,” adds Dr. Gregg Jacobs, head of the Ocean Dynamics and Prediction Branch, Oceanography Division. “These feedbacks will offer a positive impact on future mesoscale model forecasts and tactical decision aid programs for the Navy.”

In collaboration with the Fleet Numerical Meteorology and Oceanography Center and the Naval Oceanographic Office, NRL researchers ran the high-resolution coupled prediction systems — Coupled Ocean/Atmosphere Mesoscale Prediction System (COAMPS) and Navy Operational Global Ocean Model (NCOM) — which made use of the NRL Atmospheric Variational Data Assimilation (NAVDAS) and Navy Coupled Ocean Data Assimilation (NCODA) systems. The model suite was used to assimilate routine satellite, surface, and subsurface atmospheric and oceanic observations

and special TW13 unmanned aerial, surface, and undersea vehicle observations taken during the mid-Atlantic exercise.

NRL further provided an extensive ocean environmental battlespace survey through Naval Air Warfare Center's Air Test and Evaluation Squadron Twenty (VX-20) to test the predictability of frontogenesis in the ocean that can block surface acoustic ducting. Also deployed as network tools were ocean gliders provided by NRL, Oregon State University, and the Naval Oceanographic Office, and wave buoys from UC-San Diego Scripps Institution of Oceanography. NRL researchers assimilated data from these devices to demonstrate nearshore wave prediction systems.

A Scripps ScanEagle unmanned aerial vehicle provided high-fidelity measurements of the atmospheric boundary layer, sea-breeze fronts, inversions, and other structures that impact the electromagnetic (EM) propagation characteristics. The ScanEagle observations along with radiosonde ascents, Naval Postgraduate School kite and buoy observations, and four SHARC (Sensor Hosting Autonomous Remote Craft) Wave Glider unmanned surface vehicles and surface meteorology data provided additional real-time sensing of EM and coupled boundary layer conditions.

Notable firsts also established during the experiment included the first consistent ocean nesting forecasts from global resolutions, down to nearshore forecasts at Virginia Beach, Virginia; high-resolution coupled COAMPS forecasts in real time loosely coupled with wave forecasts; real-time COAMPS adjoint model forecasts at high resolution in a nested mode used to identify regions where EM predictions may benefit the most from observations; and the first automated control of unmanned underwater ocean gliders targeting unmanned undersea vehicles to provide optimal forecasts.

TRIDENT WARRIOR 2013 is part of an advanced field experimentation series designed to place new or improved capabilities into the hands of the Fleet for evaluation in an operational environment. The annual venue allows the Navy and its partners to incorporate real-world warfighter feedback early in the acquisition process.

GPS Satellite NTS-2 Joins Other NRL Technologies On Display



The restored NTS-2 engineering model during installation at the Smithsonian.

In nine decades of operation, the Naval Research Laboratory has developed many technologies that have made a mark on history. One of NRL's most significant technology contributions was recently placed on display at the Smithsonian National Air and Space Museum (NASM) in Washington, DC, where several others are already on view.

NRL's NTS-2 prototype Global Positioning System (GPS) satellite is featured in "Time and Navigation: The Untold Story of Getting from Here to There," a new permanent exhibition that opened at NASM in 2013. The exhibition explores "the surprising connection between time and place" and looks at the technological history of the tools of timekeeping and navigation, from sextants and chronometers to atomic clocks and satellites. The restored engineering model of NTS-2 is in a section of the exhibition that traces the evolution of satellite navigation.

NTS-2 was the fourth satellite designed and built by NRL in the TIMATION (time/navigation) program, initiated in 1964 to explore the concept of navigation based on accurate time signals sent from satellites. The concept grew out of NRL's experiments with ranging (and the attendant need for precise time synchronization) during development of the Naval Space Surveillance System, a radar "fence" that tracked satellites passing over the United States. The TIMATION program proved that accurate, reliable, and real-time navigation could be achieved with a

combination of passive ranging and a constellation of space-borne, high-precision clocks. TIMATION I, launched in 1967, and TIMATION II, launched in 1969, carried quartz clocks and demonstrated accurate positioning and time transfer. In 1973, as NRL was developing TIMATION III, the program was combined with other military programs to form the NAVSTAR Global Positioning System Joint Program Office. TIMATION III was renamed Navigation Technology Satellite (NTS)-1 and launched in 1974 carrying two rubidium atomic clocks, the first atomic clocks in space. NTS-2, launched in 1977, carried cesium atomic clocks and was the first satellite in the initial demonstration constellation of NAVSTAR GPS satellites. GPS revolutionized the science of navigation.

Several other NRL achievements are highlighted at the National Air and Space Museum and at other museums in the Washington, DC area (see the pages ahead). These displays place NRL's work in the context of the science, technology, and exploration history of our nation. They also allow a wider audience to see NRL innovations up close and draw inspiration from them.



XAF Radar (1938)

The “bedspring” antenna from the U.S. Navy's first shipboard radar system, developed and demonstrated at sea by NRL, is on outdoor display at the National Electronics Museum in Linthicum, Maryland. A panel display inside the museum provides technical and historical details. NRL's 200 MHz XAF radar was the prototype that showed the Navy what this new *radio detection and ranging* system – not yet called radar – could do. At-sea exercises aboard USS *New York* (BB 34) in early 1939 demonstrated the detection power of the system, leading Admiral A.W. Johnson, Commander Atlantic Fleet, to call it “one of the most important military developments since the advent of radio itself.” The NRL system went rapidly to production by RCA, and by the time the United States entered World War II, radar systems were installed on 20 Navy vessels.

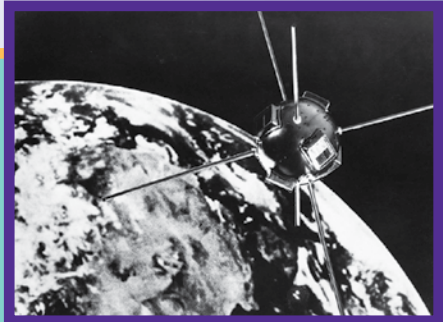
(Photo courtesy of the National Electronics Museum)

Vanguard I Satellite (1958)

A flight backup of NRL's Vanguard I satellite is on display in the “Space Science” exhibit at NASM's Udvar-Hazy Center in Chantilly, Virginia.

Vanguard I was the second U.S. satellite in space, launched on March 17, 1958, and still orbiting Earth today. As part of U.S. participation in the International Geophysical Year, the Vanguard program developed (1) a satellite carrying a scientific experiment, (2) a new rocket type to place satellites in orbit, and (3) the first satellite tracking system, Mini-track. Vanguard I confirmed the Earth's pear shape, used solar cells as a power source, and provided data on atmospheric temperature and density. On display in the “Space Race” gallery of the museum's Washington, DC building is a damaged Vanguard unit recovered after a disappointing rocket failure of December 6, 1957.

The exhibit includes a photo of Vanguard engineers Roger Easton and Martin Votaw inspecting this unit in 2008, the 50th anniversary of the successful launch. NASM recently returned three Vanguard models to NRL that are now taken to conferences and STEM festivals as display and teaching tools.



Vanguard Rocket (1958)

As part of the Vanguard satellite program, NRL led the development of a new, three-stage launch vehicle designed to launch satellites into a high, long-lived orbit. Vanguard's technical ancestor was the Viking sounding rocket, another NRL-directed program, which had reached the highest altitude of any research rocket at that time. A Vanguard rocket transferred by NRL to the Smithsonian in 1958 is on display in NASM's “Space Race” gallery. A 1960s photo shows it on outdoor display in “Rocket Row” together with a Jupiter C, a Polaris, and an Atlas.

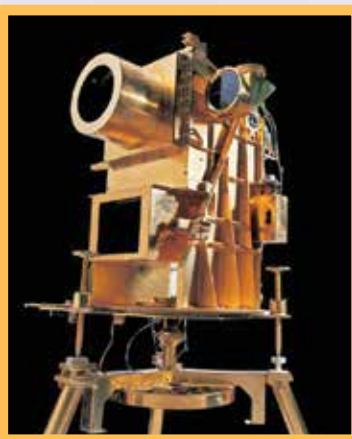


GRAB (1960)

Engineering models of NRL's GRAB (Galactic Radiation and Background) satellites are on display at both the National Air and Space Museum ("Space Race" gallery) and the National Cryptologic Museum. GRAB I was America's first electronic intelligence (ELINT) satellite, launched in 1960 to gather signals from Soviet air defense radars and transpond them to a worldwide network of ground stations for recording and interpretation. The GRAB program provided proof of concept for satellite-based signals intelligence and provided important information on Soviet capabilities during the Cold War. In 1962, GRAB and its successor ELINT satellite program, Poppy, were transferred to the newly established National Reconnaissance Office. The National Cryptologic Museum, located next to National Security Agency headquarters at Fort Meade, Maryland, displays GRAB II and Poppy satellites.

LOFTI (1961)

A model of NRL's first Low Frequency Trans-Ionospheric (LOFTI) radio satellite is hanging with several other early satellites in NASM's Udvar-Hazy Center. Launched February 22, 1961, LOFTI I was designed to explore low-frequency radio wave propagation in the ionosphere. The LOFTI studies were proposed in 1958 at NRL as part of a comprehensive satellite communication research program. LOFTI attempted to determine whether very low frequency (VLF) energy could penetrate through the ionosphere and be received by submerged submarines. The satellites demonstrated that under many ionospheric conditions VLF signals were extremely attenuated and could not be detected, making them unreliable for submarine communication.



Far-Ultraviolet Camera/Spectrograph (1972)

NRL's Far-Ultraviolet Camera/Spectrograph went to the Moon on the Apollo 16 mission in April 1972, becoming the first lunar observatory. An engineering model is on display in the "Apollo to the Moon" gallery at NASM. Developed by Dr. George Carruthers, the instrument was set up on the lunar surface by the mission astronauts to gather images and spectra of Earth, nebulae, star clusters, and other astronomical features at extreme- and far-ultraviolet (FUV) wavelengths. Results included the first photographs of the FUV equatorial bands of atomic oxygen that girdle the Earth, and of the geocoronal hydrogen glow extending many Earth radii into space. Dr. Carruthers received the 2011 National Medal of Technology and Innovation for this invention and his other contributions to space science.



Clementine (1994)

An engineering model of NRL's Clementine satellite, also called the Deep Space Program Science Experiment, hangs on display in the NASM "Lunar Exploration Vehicles" exhibit. Jointly sponsored by NASA and the Ballistic Missile Defense Organization, Clementine completed a high-quality multispectral mapping mission of the entire lunar surface, at the same time testing and space-qualifying new lightweight imaging sensors and other defense technologies. NRL developed Clementine as a next-generation, "smarter" spacecraft

with streamlined costs and space operations. President Clinton called it a "major revolution in spacecraft management and design." Fun Fact: After ordering a Chinese dinner, mission scientists attached their fortune cookie message to the spacecraft. It read, "You will soon take a very pleasant and successful trip."



Dragon Eye (2002)

NASM's "Military Unmanned Aerial Vehicles" display includes Dragon Eye, a small, battery-powered UAV developed by NRL in collaboration with the Marine Corps Warfighting Laboratory to provide reconnaissance and threat detection capabilities to field commanders. Dragon Eye grew out of NRL's concept of developing affordable, expendable airborne sensor platforms for practical warfighter operation. Robust, stealthy, and compact enough to be carried in a Marine's backpack, Dragon Eye weighs only 5.5 pounds and is hand- or bungee-launched. A small ground control station receives the aircraft's video and GPS position. Pre-production units were deployed in 2003 with the 1st Marine Expeditionary Force during

Operation Iraqi Freedom, providing critical on-site intelligence. The well-used combat unit on display, sporting epoxy and duct tape repairs, was flown by the 3rd Marine Division in Afghanistan in 2005.

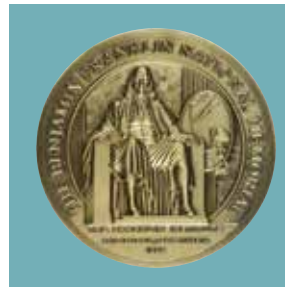
***In nine decades of operation,
the **Naval Research Laboratory** has developed many
technologies that have made a mark on history.***

See more of NRL's technological history, including a prototype excimer laser and other instruments and records, in the Smithsonian's online catalogues at <http://www.si.edu/Collections>.

NRL Hosts Its Third Annual

KARLES INVITATIONAL CONFERENCE

JANUARY 13-14, 2014



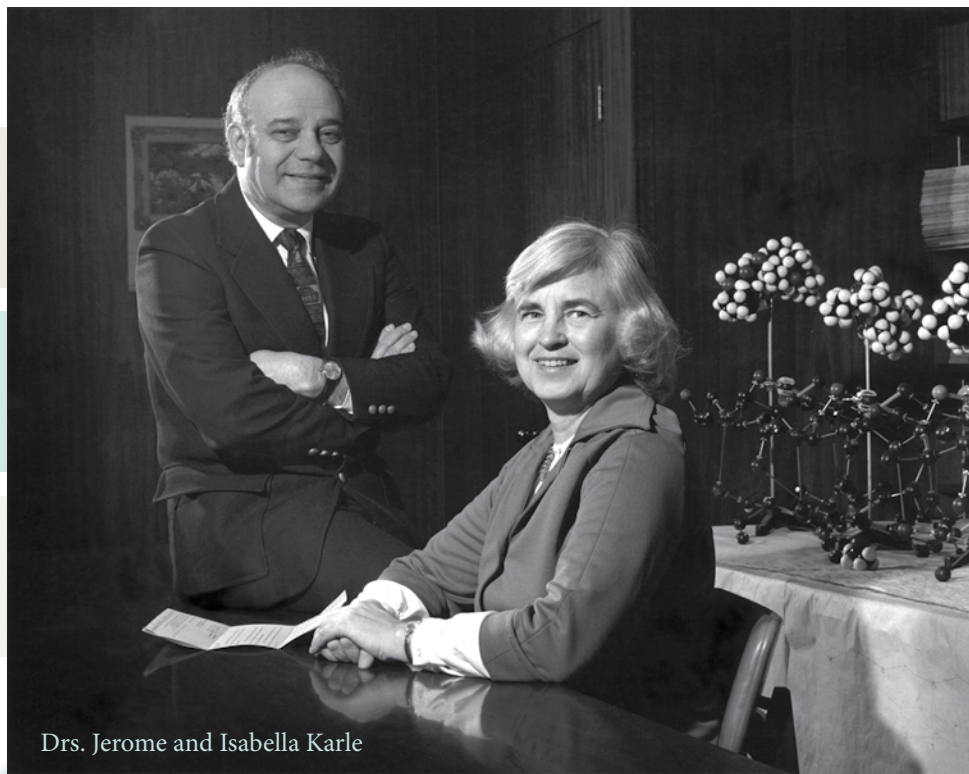
INTELLIGENT AUTONOMOUS SYSTEMS SCIENCE AND TECHNOLOGY

Intelligent Autonomous Systems is an exciting field of exceptional potential that has become one of the most active areas of scientific research around the world. This emerging field is highly multidisciplinary with contributions from cognitive science, neuroscience, computer science, robotics, linguistics, machine learning, and artificial intelligence, among others. Intelligent autonomy takes advantage of the full power of these fields to create new scientific concepts and makes possible entirely new technologies that have the potential to change both society and military capabilities. Important advances have been made in recent years by using concepts from human cognition to enable more intelligent systems, including the areas of computational neuroscience and computational cognitive science. These advances range from focusing on the brain (e.g., building computation models of neural structures to study the emergence of known cognitive processes based on fMRI and EEG data) to focusing on the mind (e.g., building computational cognitive process models based on data collected from human participants solving certain tasks). Both of these approaches have had a large impact on the development of intelligent autonomy, yielding greatly improved computational perception and human-robot interaction, and providing novel methods for control of autonomous systems. The Karles Invitational Conference on Intelligent Autonomous Systems Science and Technology provided a timely program and forum designed to further explore and help assess the future direction of these groundbreaking developments. Presentations were organized into four sessions: Architectures, Methodologies, and Tools; Perceptual Reasoning; Human/Autonomous System Interaction; and Trust, Acceptance, and Ethics.





The professional contributions of 1985 Nobel Laureate in Chemistry Dr. Jerome Karle (June 18, 1918 – June 6, 2013) and of 1993 Bower Award Laureate and 1995 National Medal of Science recipient Dr. Isabella Karle (born December 2, 1921) were critical in enabling the resolution of the molecular structure and function of complex macromolecules. While fundamental in nature, the Karles' contributions continue to have a significant impact on the basic and applied physical, chemical, metallurgical, geological, and biological sciences. In commemoration of their achievements and broad scientific impact, the U.S. Naval Research Laboratory in Washington, DC, has initiated an annual invitational forum that convenes the leading authorities and innovators of a selected scientific research area who are on the verge of producing contributions with similar reach and impact. This year's selected topic was Intelligent Autonomous Systems Science and Technology.



Drs. Jerome and Isabella Karle

The Naval Research Laboratory

A photograph of two men standing in a laboratory. The man on the left is wearing a black beanie, glasses, and a black jacket. The man on the right is wearing a light blue dress shirt, a yellow patterned bow tie, and glasses. They are standing behind a large, white, cylindrical piece of equipment. The background shows various pieces of laboratory equipment and a white wall.

- 16** NRL – Our Heritage
- 17** Highlights of NRL Research in 2013
- 29** NRL Today
- 30** NRL Research Divisions
- 68** Research Support Facilities
- 70** Other Research Sites

NRL — OUR HERITAGE

The early 20th century founders of the Naval Research Laboratory (NRL) knew the importance of science and technology in building naval power and protecting national security. They knew that success depended on taking the long view, focusing on the long-term needs of the Navy through fundamental research. NRL began operations on July 2, 1923, as the United States Navy's first modern research institution, and it continues today as one of the Navy's premier research and development centers.

Thomas Edison's Vision: The first step came in May 1915, a time when Americans were deeply worried about the great European war. Thomas Edison, when asked by a *New York Times* correspondent to comment on the conflict, argued that the Nation should look to science. "The Government," he proposed in a published interview, "should maintain a great research laboratory....In this could be developed...all the technique of military and naval progression without any vast expense." Secretary of the Navy Josephus Daniels seized the opportunity created by Edison's public comments to enlist Edison's support. He agreed to serve as the head of a new body of civilian experts — the Naval Consulting Board — to advise the Navy on science and technology. The Board's most ambitious plan was the creation of a modern research facility for the Navy. Congress allocated \$1.5 million for the institution in 1916, but wartime delays and disagreements within the Naval Consulting Board postponed construction until 1920.

The Laboratory's two original divisions — Radio and Sound — pioneered in the fields of high-frequency radio and underwater sound propagation. They produced communications equipment, direction-finding devices, sonar sets, and perhaps most significant of all, the first practical radar equipment built in this country. They also performed basic research, participating, for example, in the discovery and early exploration of the ionosphere. Moreover, the Laboratory was able to work gradually toward its goal of becoming a broadly based research facility. By the beginning of World War II, five new divisions had been added: Physical Optics, Chemistry, Metallurgy, Mechanics and Electricity, and Internal Communications.

World War II Years and Growth: Total employment at the Laboratory jumped from 396 in 1941 to 4400 in 1946, expenditures from \$1.7 million to \$13.7 million, the number of buildings from 23 to 67, and the number of projects from 200 to about 900. During WWII, scientific activities necessarily were

concentrated almost entirely on applied research. New electronics equipment — radio, radar, sonar — was developed. Countermeasures were devised. New lubricants were produced, as were antifouling paints, luminous identification tapes, and a sea marker to help save survivors of disasters at sea. A thermal diffusion process was conceived and used to supply some of the ^{235}U isotope needed for one of the first atomic bombs. Also, many new devices that developed from booming wartime industry were type tested and then certified as reliable for the Fleet.

Post-WWII Reorganization: The United States emerged into the postwar era determined to consolidate its significant wartime gains in science and technology and to preserve the working relationship between its armed forces and the scientific community. While the Navy was establishing its Office of Naval Research (ONR) as a liaison with and supporter of basic and applied scientific research, it was also encouraging NRL to broaden its scope and become, in effect, its corporate research laboratory. There was a transfer of NRL to the administrative oversight of ONR and a parallel shift of the Laboratory's research emphasis to one of long-range basic and applied investigation in a broad range of the physical sciences.

However, rapid expansion during WWII had left NRL improperly structured to address long-term Navy requirements. One major task — neither easily nor rapidly accomplished — was that of reshaping and coordinating research. This was achieved by transforming a group of largely autonomous scientific divisions into a unified institution with a clear mission and a fully coordinated research program. The first attempt at reorganization vested power in an executive committee composed of all the division superintendents. This committee was impracticably large, so in 1949, a civilian director of research was named and given full authority over the program. Positions for associate directors were added in 1954, and the laboratory's 13 divisions were grouped into three directorates: Electronics, Materials, and Nucleonics.

The Breadth of NRL: During the years since World War II, the Laboratory has conducted basic and applied research pertaining to the Navy's environments of earth, sea, sky, space, and cyberspace. Investigations have ranged widely — from monitoring the Sun's behavior, to analyzing marine atmospheric conditions, to measuring parameters of the deep oceans. Detection and communication capabilities have benefited by research that has exploited new portions of the elec-

tromagnetic spectrum, extended ranges to outer space, and provided a means of transferring information reliably and securely, even through massive jamming. Submarine habitability, lubricants, shipbuilding materials, firefighting, and the study of sound in the sea have remained steadfast concerns, to which have been added recent explorations within the fields of virtual reality, superconductivity, biomolecular science and engineering, and nanotechnology.

The Laboratory has pioneered naval research into space — from atmospheric probes with captured V-2 rockets, through direction of the Vanguard project (America’s first satellite program), to inventing and developing the first satellite prototypes of the Global Positioning System (GPS). Today, NRL is the Navy’s lead laboratory in space systems research, as well as in fire research, tactical electronic warfare, microelectronic devices, and artificial intelligence.

The consolidation of NRL and the Naval Oceanographic and Atmospheric Research Laboratory, with centers at Bay St. Louis, Mississippi, and Monterey, California, added critical new strengths to the Laboratory. NRL now is additionally the lead Navy center

for research in ocean and atmospheric sciences, with special strengths in physical oceanography, marine geosciences, ocean acoustics, marine meteorology, and remote oceanic and atmospheric sensing.

The Twenty-First Century: The Laboratory is focusing its research efforts on new Navy strategic interests in the 21st century, a period marked by global terrorism, shifting power balances, and irregular and asymmetric warfare. NRL scientists and engineers are working to give the Navy the special knowledge, capabilities, and flexibility to succeed in this dynamic environment. While continuing its programs of basic research that help the Navy anticipate and meet future needs, NRL also moves technology rapidly from concept to operational use when high-priority, short-term needs arise — for pathogen detection, lightweight body armor, contaminant transport modeling, and communications interoperability, for example. The interdisciplinary and wide-ranging nature of NRL’s work keeps this “great research laboratory” at the forefront of discovery and innovation, solving naval challenges and benefiting the nation as a whole.

HIGHLIGHTS OF NRL RESEARCH IN 2013

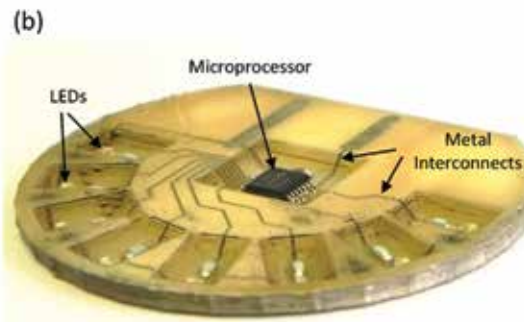
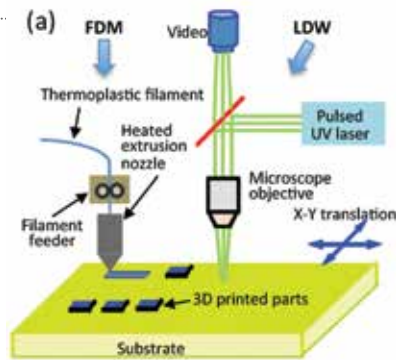
The scientific community at NRL conducts innovative research across a wide spectrum of technical areas, much of it detailed in the *NRL Review* chapters ahead. This section presents a few highlights from the year.



The NRL Reliant autonomous underwater vehicle (AUV), an advanced version of the Bluefin Robotics Bluefin-21 vehicle, is the prototype for the new U.S. Navy Knifefish mine hunter. Reliant completed a record-setting endurance mission of 109 hours, traveling nearly 315 miles from Boston to New York.

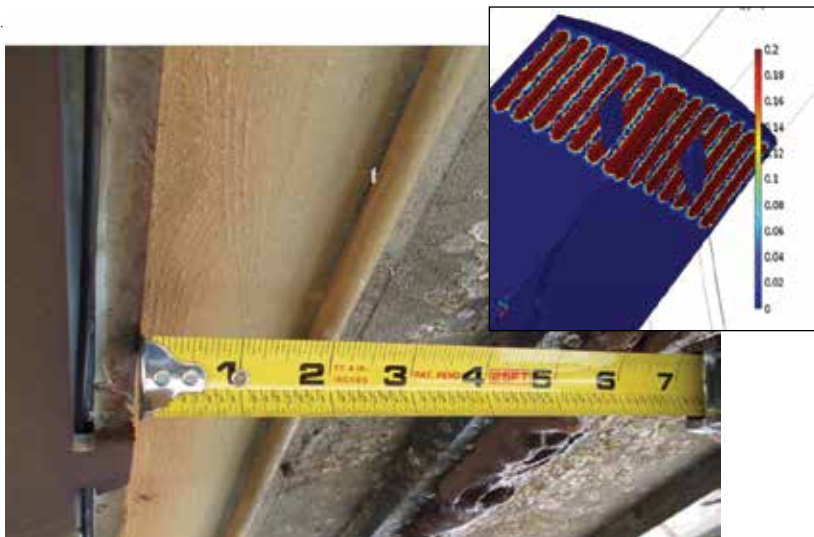
Demonstration of Long Endurance Autonomy with Heavyweight-Class Autonomous Underwater Vehicle (AUV):

The Naval Research Laboratory (NRL) executed a record-setting 500 km “Long Endurance” AUV mission that started in the waters off Boston Harbor and finished at the approaches to New York City. The research mission was designed to exercise state-of-the-art AUV autonomy methods and demonstrate the capability of a new high-capacity energy section on NRL’s Reliant AUV. When equipped with a Low Frequency Broadband (LFBB) sonar system, Reliant is perhaps best known as the prototype for the new U.S. Navy Knifefish mine hunter. The 20 ft long vehicle navigates using a fiber optic gyro based inertial navigation system that is integrated with GPS and a Doppler Velocity Log (DVL), enabling precise navigation underwater for long endurance missions. The vehicle reported its position periodically via Iridium satellite and made it to New York with a 10% energy reserve. This is the first of several planned exercises that will increase autonomy complexity and endurance over the life of NRL’s research program. Conducting long endurance missions such as this is essential to ultimately obtaining the level of performance required in Navy undersea vehicle autonomy and hardware robustness.



(a) Schematic representation of the combined laser direct-write (LDW) and fused deposition modeling (FDM) 3D printing system at NRL. (b) Sample 3D printed electronics comprising interconnects made by LDW over an FDM-generated part.

Direct-Write Processes for Electronic Components: NRL's Materials Science and Technology Division has integrated laser direct-write with additive manufacture processes to develop 3D printed electronics. Additive manufacturing (AM) techniques are capable of fabricating 3D parts layer-by-layer from a computer design; however, integrating electronic circuits within these parts is beyond current AM capabilities. Meanwhile, laser direct-write (LDW) processes can be used to pattern electronic materials into functional circuits and devices; however, these patterns are incorporated only on the surface of the part over which they are printed. The integration of LDW processes with AM techniques will allow the rapid implementation of geometrically precise parts with electronics within their bodies and surfaces. By printing electronic patterns by LDW between the layers generated by the AM processes, highly functional 3D parts with embedded electronics can readily be produced; these are otherwise difficult and expensive to fabricate with current manufacturing techniques. Merging these two processes will enable multifunctional 3D electronic modules required by next-generation autonomous systems. NRL's efforts in this area will be applied to the development of hybrid structures designed for mission-specific tasks such as detecting, processing, and transmitting.



Close-up view of the underside of the PSC-12 hull, where electrodes spaced 8 in. apart generated oxidants from the seawater to keep the hull clear of biofouling. One electrode (black) is visible at the left edge of the image; the lighter color immediately adjacent to it was caused by the oxidants bleaching the grey hull paint. (The protrusion at 2 in. is a guide for cabling to the reference cell.) Inset: Plot of the oxidant concentration above the required 0.2 ppm around each electrode on the hull. The prototype system performed nearly exactly as predicted by the model.

Integrated Underwater Hull Shield: The Integrated Underwater Hull Shield program successfully demonstrated a scaled prototype, on a 64 ft Navy research vessel based out of Panama City, Florida, of an integrated ship hull system that provided cathodic protection to the hull while distributing electrochemically generated oxidant ions that prevented growth of biofouling organisms such as barnacles and oysters. The system used distributed electrodes that operated on a programmed duty cycle to maintain the aluminum hull against corrosion and to generate low concentrations of hypochlorite species that prevented settlement or growth of the biofouling organisms. The integrated system used six distributed silver-chloride reference cells to monitor the hull and electrode potentials, and a single controller that ran off the ship's power that monitored the reference cells and regulated power to the electrodes. The prototype was operational for nine months, during which time the ship (PSC-12) made multi-week deployments from Panama City to Ft. Lauderdale, Florida, and performed all its regular missions.

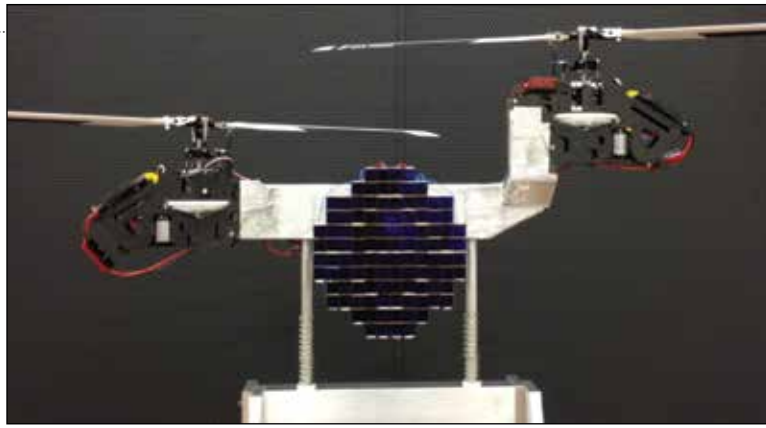
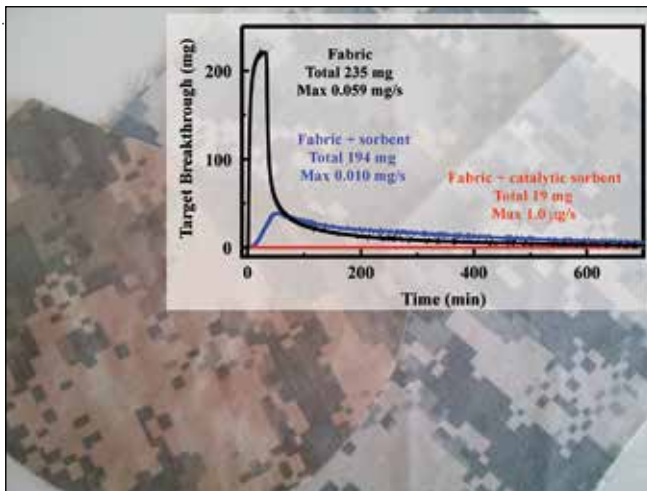


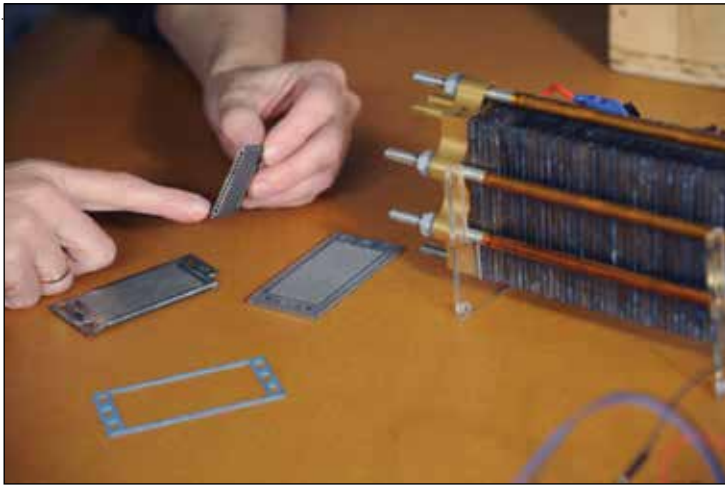
Photo of NRL dual-rotor UAV with photovoltaic array, used in power beaming flight tests with a kW-class cw fiber laser.

Laser Power Beaming to UAVs: NRL researchers from the Plasma Physics and Tactical Electronic Warfare Divisions successfully tested a rotary-wing unmanned aerial vehicle (UAV) powered solely by a high-power fiber laser. A series of flight tests was conducted over a 40 m path in the prototyping high bay in the Laboratory for Autonomous Systems Research at NRL, where a high-power fiber laser was used to beam power to the UAV. A 2 kW, single-mode fiber laser (1.07 μm wavelength) transmits power to a photovoltaic (pv) array fabricated using InGaAs laser power converter chips from Spectrolab (Sylmar, CA). The individual chips are 40% to 50% efficient at the fiber laser wavelength, and the array provides more than 160 W of electricity to power the vehicle. Off-the-shelf components were used to develop the optical tracking system, which automatically positions the laser beam on the center of the pv array during flight. The researchers designed and fabricated a 3.8 lb, dual-rotor UAV that provides air cooling of the pv array using the rotor wash. The NRL approach to long-range laser power beaming uses the same wavelength and technology as Navy designs for 100 kW class solid-state lasers for ship self-defense. Long-range laser power beaming to UAVs can allow for long-duration flights with reduced manpower requirements for many Navy and Department of Defense missions, including offboard decoys, persistent surveillance, and communication relays.



Permeation of target through functionalized fabric is reduced by an order of magnitude. Swatches compare functionalized sample to original uniform fabric.

Mesoporous Materials in Military Uniforms for Personal Protection: Deposition of NRL-developed mesoporous materials onto cotton, military uniform fabrics, and static-dissipative polyester fabrics was demonstrated to provide a protective layer preventing the permeation of both liquid and vapor threat agents. The protective fabrics were further shown to provide catalytic decontamination of organophosphorous targets and sulfur mustard related compounds, effectively regenerating the capacity of the coatings for continued use. Catalysis is facilitated through illumination of the materials by ambient light or through application of an electric current. In contrast to traditional protective layers, water permeation (critical to comfort) was not impeded by these functionalized fabrics. The materials are low density, resulting in minimal weight increase, and are washable. Coatings of this type provide the potential for incorporating protective capabilities into routine use fabrics and surfaces, as well as for improving the function of traditional protective garments.



3D printed titanium bipolar plates are used to make a hydrogen fuel cell stack. The 3D printing allows a hollow internal flow field for coolant flow. The external design is optimized for hydrogen and air flow. The plates are assembled together with gaskets and fuel cell membranes to make the fuel cell stack.

3D Printing in Hydrogen Fuel Cells for Unmanned Air Vehicles: An NRL team from several research divisions has leveraged 3D printing for developing and integrating their next generation of hydrogen fuel cells into unmanned systems. NRL has demonstrated 24- and 48-hour flights of fuel cell systems on the Ion Tiger UAV, and is also using hydrogen fuel cells in its submarine-launched XFC UAV. Fuel cells directly convert the energy in hydrogen to electricity by electrochemically combining with the oxygen in air. The only byproducts are water and low-grade heat, and no combustion occurs. Combined with the high energy of hydrogen, the result is an electric power source that is lightweight and has high energy per unit weight. Additive manufacturing processes such as 3D printing promise rapid prototyping of new designs which can be tested and verified without the expense of traditional manufacturing. The team used the 3D printing process of direct metal laser sintering to make titanium bipolar plates which are the backbone of the fuel cell system. The plate design was optimized with computational fluid design, 3D printed, and then assembled together with fuel cell membranes and compressed together into a 400 W stack. This was integrated with other components of the fuel cell system and electronics, and flown on the Ion Tiger in March 2014. The process demonstrated how 3D printing can be practically used to speed up development time and build prototypes.



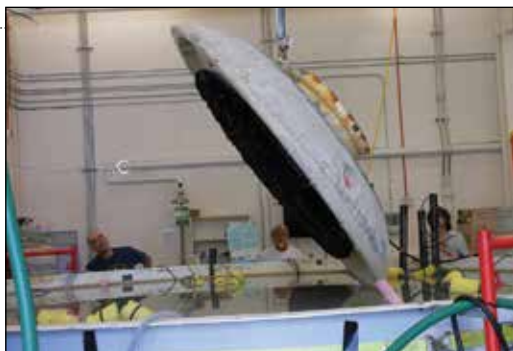
XFC launch from a submerged submarine (time-lapse image). This new capability is expanding undersea influence beyond the current platform-centric sensing capabilities.

Submarine-Launched, Long Endurance UAS: In response to Navy and Department of Defense needs and requirements, NRL demonstrated the launch of an all-electric, fuel-cell-powered, long endurance unmanned aerial system (UAS) from a submerged U.S. Navy submarine. The XFC UAS (eXperimental Fuel Cell UAS) is an expendable, folded-wing (Navy patented), vertically launched, all-electric (stealthy), long endurance small UAS for intelligence, surveillance, and reconnaissance (ISR) and other tactical needs. It was fired from the submarine's torpedo tube using a Sea Robin launch vehicle system. Once deployed, the Sea Robin with integrated XFC rose to the ocean surface where it appeared as a spar buoy. Upon command, the XFC vertically launched from the Sea Robin and flew a successful several-hour mission demonstrating live video streaming back to the submarine and surface support vessels before landing at the Naval Sea Systems Command Atlantic Undersea Test and Evaluation Center (AUTECE). Because the XFC has modular payload capability and is vertically launched, it has a very small footprint and can be easily adapted to other Service and Agency needs. With the fielding of XFC, the submarine's ISR reach will be extended over the horizon. This new capability allows new missions previously not possible, greatly expanding undersea influence beyond the current platform-centric sensing capabilities.



Maritime tracks in the Atlantic Ocean area of responsibility (AOR) from NRL's Mongoose fusion engine.

SENTIENT — Maritime Awareness Technologies: The SENTIENT initiative mission is revolutionizing the intelligence cycle by contextualizing the past and anticipating the future to focus problem-centric, multiple intelligence (multi-INT) collection. Maritime Domain Awareness (MDA) technologies from NRL have been modified and upgraded to support this effort. NRL's Mongoose/Sea-link Advanced Analysis (S2A), a multi-INT correlation software suite, is being used to provide core fusion capabilities and enable Activity Based Intelligence (ABI) for SENTIENT. NRL's MDA solutions are being applied to the problem-centric intelligence hypothesis that the Intelligence Community (IC) can increase its value and performance, become responsive to changing situations, and optimize resources in an anticipatory manner through the adoption of new processes and enabling technologies. NRL processes and technologies are being integrated into the SENTIENT system, enabling the optimal tasking of appropriate sensors with the timeliness required to produce actionable intelligence. These efforts are revolutionizing the tasking, collection, processing, exploitation, and dissemination (TCPED) of information for the Department of Defense and IC. The SENTIENT initiative is being executed within the National Reconnaissance Office Advanced Systems and Technology Directorate, Advanced Systems Office.



Deployment of a BMFC in the mesocosm at LASR. This particular experiment is composed of 70 interconnected carbon fiber bottlebrush anodes attached to the bottom of a SEPTR oceanographic instrument.

The Benthic Microbial Fuel Cell: A benthic microbial fuel cell (BMFC) sits on the sediment/water (benthic) interface of marine environments and generates electrical power, utilizing organic matter naturally residing in marine sediments as its fuel, and oxygen in overlying water as its oxidant. The BMFC can generate power indefinitely — this is due to constant replenishment of organic matter and oxygen by naturally occurring diffusion and advection; durability/regenerative ability of its electrode catalysts consisting of self-forming biofilms comprised of microorganisms naturally inhabiting the benthic interface; and lack of moving/degradable/depletable components. The BMFC is being developed to power persistent in-water intelligence, surveillance, reconnaissance (ISR) capabilities presently limited in operational live time by battery depletion. In field-based research demonstrations, BMFCs have powered a riverine meteorological buoy with a radio transceiver link, a hydrophone with a radio transceiver link, an acoustic modem, and a surveillance camera with a cellular link. It is estimated to be at Technology Readiness Level 6. During the past 10 years, small-scale BMFCs (<0.1 W continuous output) have been deployed in coastal waters ranging in depth from <1 m to >1000 m over durations of <6 months to >2 years before being retrieved without indication of depletion in power output. Development of full-scale BMFCs (>1 W continuous output) commenced at NRL in 2013. In the Laboratory for Autonomous Systems Research (LASR), a 6 m diameter mesocosm was erected to mimic the benthic interface, enabling accelerated iterative design and evaluation of full-scale BMFC-equipped moorings (BEMs). This alleviates the cost, risk, and logistics burden of full-scale field evaluations. Field deployment of optimized BEMs is slated to begin in 2015.

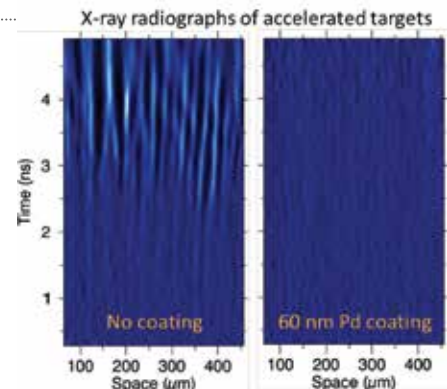
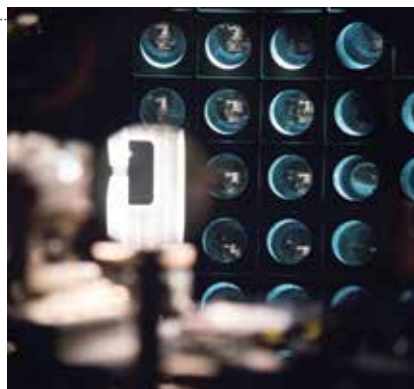


The WANDA UUV.



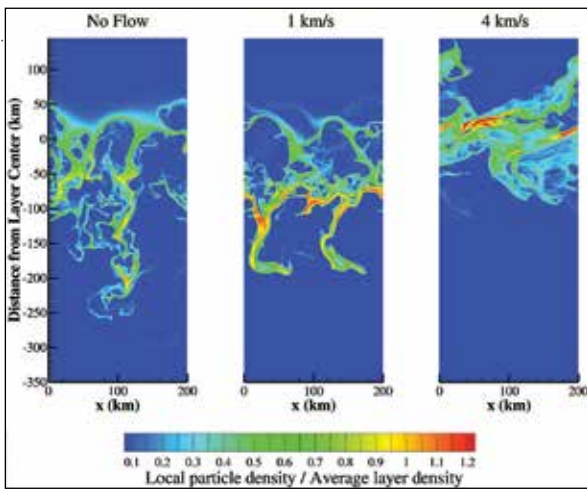
Flimmer vehicle in-flight, using the two aft fins as aerodynamic stability surfaces and the two forward fins as canards. After splashdown, this same vehicle submerges and then swims underwater using the four fins for propulsion and maneuverability.

Unmanned Underwater and Aerial Vehicle — Flimmer: The NRL-developed unmanned underwater vehicle (UUV) WANDA (Wrasse-inspired Agile Near-shore Deformable-fin Automaton) was developed using robotic flapping fins to provide an unmanned platform capable of precise maneuverability and station-keeping for critical Navy missions in dynamic near-shore environments. The original UUV prototype has been modified to increase payload capacity and vehicle speed, through scaling up the size of both the vehicle hull and the fins. Validated computational fluid dynamics (CFD) studies show that this WANDA-II UUV is capable of speeds between 1.7 and 2.3 knots while also expanding the hull volume from 3500 to 3800 cm³. While the design of WANDA-II provides a platform ideal for near-shore mobility, long-range transit to an area of interest requires longer endurance at higher speeds. To address this need, a hybrid vehicle called Flimmer (Flying-Swimmer) was developed. Flimmer employs the same deformable fin technology as WANDA-II, but provides long-range transit capability through the use of a 1.67 m span wing for a flying ingress to a water splashdown. Computational results have characterized Flimmer in its capacity as both an airplane and an underwater swimming vehicle. Further, CFD capability has been extended to simulate the splashdown of this vehicle, transitioning between air and water media. Experimental testing of the aerodynamic, hydrodynamic, and landing characteristics of this vehicle is currently under way.



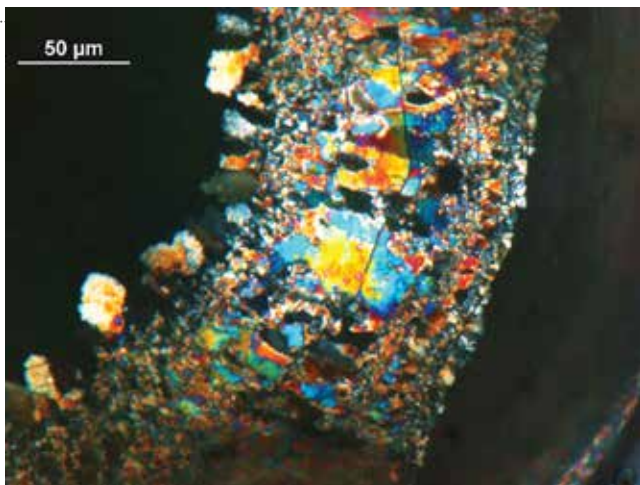
The Nike laser facility overlaps up to 44 focused beams onto planar targets to study aspects of laser-driven fusion. Scientists have found that a thin gold or palladium coating on plastic targets reduces hydrodynamic instability in the laser-accelerated targets, as shown in the comparison figures at right.

An Attractive Hybrid Indirect and Direct Drive Approach to Laser Fusion: High-power lasers are an attractive driver for inertial confinement fusion (ICF) and related high energy density physics experiments. However, the spatial modulations of multiple high intensity laser beams can be the seed for instabilities that grow and destroy the target material. Minimizing these modulations is usually accomplished either by smoothing the beams (direct drive) or by converting the beams into x-rays that are smoother (indirect drive). NRL scientists have developed a hybrid approach that uses a thin coating of gold or palladium over plastic targets to locally generate x-rays that initially drive the target acceleration. Little or no laser imprint is observed in experiments on the NRL Nike KrF laser facility. The laser eventually burns through this layer, and the high efficiency of directly driven targets is retained. This hybrid technique thereby combines advantages of indirect drive and direct drive. This approach will be tested as part of the National Ignition Facility hydrodynamic and ablator physics program and could provide a unique platform for equation of state experiments, as well as an attractive path to fusion energy.



Images show the local density of dust particles normalized by the average dust density in the initial layer after 700 seconds in orbit for several different methods of initializing the layer. The three plots represent dust layers with, from left to right, no imposed flow, an inhomogeneous flow profile with maximum velocity of 1 km/s, and an inhomogeneous flow profile with maximum velocity of 4 km/s. In the figure, the gravitational direction is oriented from top to bottom, the Earth's magnetic field points into the page, and the imposed flow is oriented across the page. The layer in the rightmost figure (4 km/s) is able to maintain a coherent structure throughout the simulation while the others (No Flow and 1 km/s) are severely distorted.

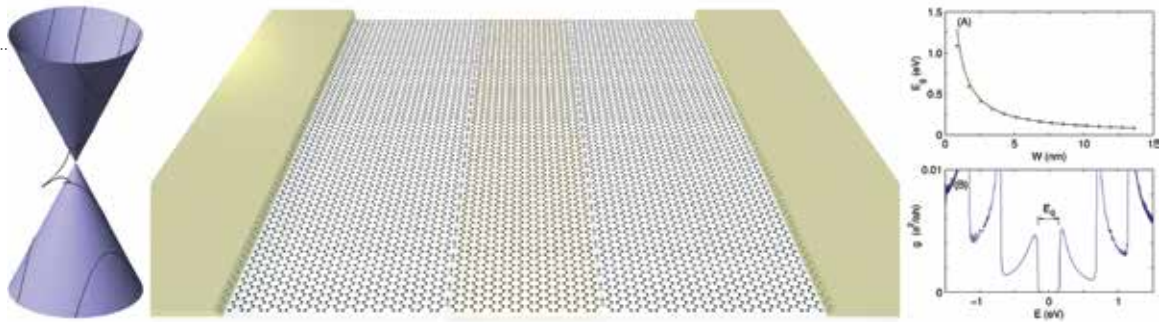
De-Orbiting Space Debris: Scientists in NRL's Plasma Physics Division and Laboratories for Computational Physics and Fluid Dynamics recently proposed a means of passively removing small-scale orbital space debris by releasing in orbit a layer of tungsten dust. The dust layer decelerates the debris by artificially enhancing drag and slowly lowering its orbit until atmospheric friction is sufficient to force its re-entry and, ultimately, incineration. It is crucial that the dust layer remain intact for as long as possible to maximize its effectiveness. Both large (several micron) and small (nanometer) diameter dust grains have been considered. The effect of dust charge on the larger dust grains is negligible and they form a stable ring that can be used for an Active Debris Removal (ADR) system. Detailed numerical simulations have analyzed the behavior of a nanometer diameter tungsten dust layer, for which charging effects are not negligible, in gravitational and magnetic fields using linear stability theory and computational fluid dynamics simulations. We found that a uniformly orbiting dust layer is unstable and rapidly disperses. Several methods of stabilizing the layer were considered. A promising approach is to apply inhomogeneous motions to the layer relative to its orbital speed. Intrinsic gravitational and shear instabilities rapidly destroy the layer at low flow speeds, but at higher speeds the layer remains intact for longer periods of time. These findings suggest it may be possible to tailor the relative motions to maximize this effect. Research on this topic and complementary stabilization techniques is ongoing.



View from below of a calcareous base plate developing under a live juvenile barnacle *Balanus amphitrite* under cross-polarized light. Calcite crystals with differing orientations appear as different colors. The newly formed base plate consists of a wide band displaying a distinct ring of coarse crystals surrounded by bands of fine crystals. (Photo: Dr. Christopher So)

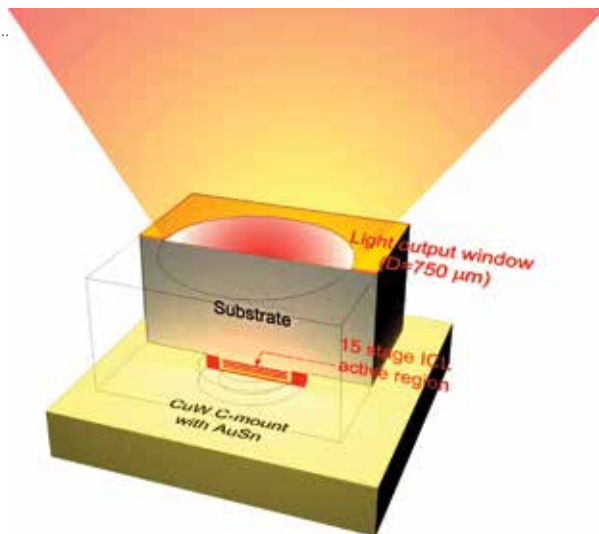
Developing a Fundamental Understanding of Barnacle Adhesion: NRL scientists are using high-resolution microscopy to reveal how a barnacle's "bricks and mortar" adhesion process unfolds in real time. The details of how barnacles cure their adhesive and mineralize the bonded region have remained elusive due to the challenge of the "buried" bonding interface underneath the barnacle. Furthermore,

monitoring barnacle growth, like watching paint dry (or literally glue curing), is a slow process. A team of NRL Materials Directorate scientists, combining expertise in chemistry, biology, and materials science, has revealed this process in three-dimensional detail using high-resolution optical and chemical microscopies. To speed things up, the team uses time-lapse videography through transparent surfaces, from underneath the barnacles. The barnacle builds its interface by expanding the surrounding shell that then pulls along and unfolds a membrane identified as cuticle along the underlying surface. This process is slow and is accompanied by some adhesion. Ductwork is then created that delivers additional protein adhesive to the interface, doubling adhesion. Finally, a calcification front passes on top of the membrane within the barnacle, like bricks and mortar. The process repeats cyclically as the barnacle, a relative of insects, spiders, crabs, and lobsters, goes through the molting process to grow. These new details of how protein secretion, cuticle unfolding and curing, and mineralization combine to create barnacles' robust adhesion is forcing a reevaluation of the overall picture of barnacle adhesion.



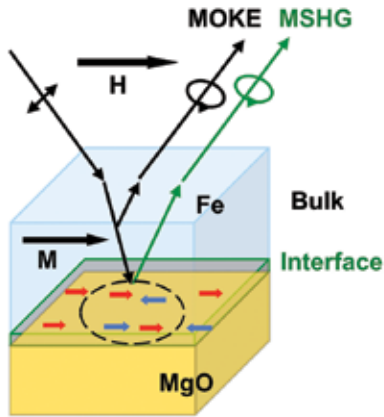
Low-energy electron and hole carriers in 2D graphene occupy states on the surface of a Dirac cone (left). Upon the introduction of two parallel line defects in graphene (center), the states within the railroad structure are further restricted to the set of black curves. These curves highlight a dimensional crossover, at which the 2D states escape the Dirac cone and become 1D boundary-localized states. As only states on the Dirac cone are able to bring carriers across the structure between the two contact electrodes, the structure exhibits a transport gap near the Dirac point, at which the two inverted cones meet. This transport gap depends on the separation, W , between the line defects, and with a gate electrode, can be used to switch on and off the conductance per unit length, g , across the structure (right).

Graphene Resonant Tunneling Transistor: Graphene is a promising material for future nanoelectronic applications, with its atomically thin planar structure ideal for high-density applications and exceptional conduction properties minimizing costly power dissipation. Even at room temperature, electron and hole carriers in graphene could travel past 10,000 atoms, on average, without being scattered, a property matched by few if any other materials. The roadblock for graphene nanoelectronics has been the inability to controllably switch off this exceptional conduction. One solution is to introduce nanoscale interfaces within graphene that create boundary conditions that block conduction of low-energy carriers through quantum interference. A switchable device can then be achieved by electrostatically gating this structure. The interfaces in this graphene resonant tunneling transistor could be realized by structural defects, including the extended 5-5-8 line defect observed in graphene.



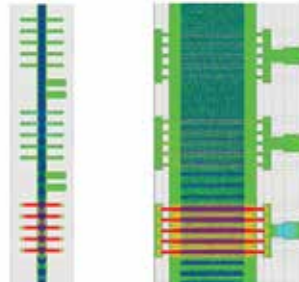
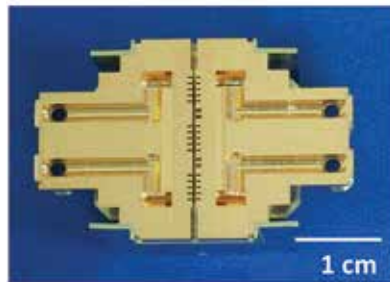
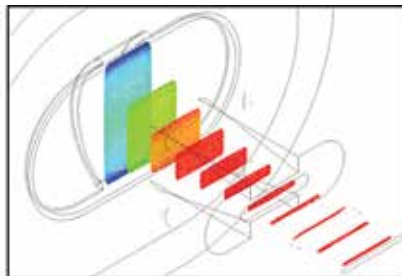
Schematic of interband cascade light-emitting device (ICLED) producing incoherent light in the mid-wave infrared. The mesa device is mounted epitaxial-side-down on a CuW submount for heat dissipation, and the light emerges from the back side after passing through the GaSb substrate.

Interband Cascade Lasers (ICLs) and Light Emitting Diodes (LEDs): NRL interband cascade lasers (ICLs) and light emitting diodes (LEDs) have recently extended the state of the art for coherent and incoherent sources emitting in the 3.0 to 3.6 μm wavelength range. The lasers employ a new innovative design that redistributes the optical mode within the waveguide, lowers the internal loss, and increases the electrical-to-optical power conversion efficiency. Most of the mode is shifted from the cladding and active regions to a low-loss separate confinement layer while sufficient gain is maintained by adding more stages. The resulting ICLs emitting at a wavelength of 3.5 μm generate nearly 600 mW of continuous wave (cw) output power in a high-quality beam at room temperature (25 $^{\circ}\text{C}$). Wallplug efficiencies of 10% are now routine, and values up to 14% are observed even for relatively long cavities. The interband cascade light-emitting devices (ICLEDs) have 15 stages and incorporate NRL's patented "carrier rebalancing" design. They perform well in cw mode because NRL's proprietary epitaxial-side-down mounting architecture is ideal for these devices that emit from the bottom through the GaSb substrate. The ICLEDs produce up to 1.6 mW of cw output at room temperature, in a broad spectral band that is more favorable for chemical sensing. This power is more than a factor of 2 beyond any previous report for the mid-IR, and nearly an order of magnitude higher than the best commercial devices.



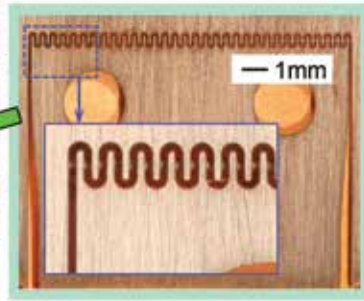
A laser beam is used to measure the magnetic properties in two complementary ways. The linear polarization of the incident laser light is rotated by the sample magnetization and measured in a reflection geometry. The magneto-optic Kerr effect (MOKE) measures the net magnetization (“bulk”) of the Fe film, while magnetic second harmonic generation (MSHG) selectively probes the interface magnetization only.

New Nanoscale Exchange Electron Spin Bias Mechanism: Exchange bias occurs at the interface between an antiferromagnet (AFM) and a ferromagnet (FM) — the hard magnetization of the AFM biases the softer magnetization of the FM to point in a selected direction to optimize some function or performance. Exchange bias is of great technological importance in tailoring the operating characteristics of most magnetic devices, including hard disk read heads, magnetic memory, and magnetic sensors. However, it remains poorly understood and continues to be extensively studied. NRL scientists, in collaboration with researchers at the College of William and Mary, have discovered a new form of exchange bias manifested only in the interface electron spin system, in marked contrast with typical systems where exchange bias is observed in the net magnetization. Atomic magnetic moments at the interface between a ferromagnetic metal (iron) and an oxide (magnesium oxide) were demonstrated to be exchange biased independently of the bulk magnetization, and therefore could be controlled and switched independently of the bulk. These results are very important for ultrathin magnetic films and nanoscale structures, and have broad implications for advanced magnetic memory, sensors, and reprogrammable logic.



NRL's 7.7 kW peak power, 94 GHz sheet-beam extended interaction klystron amplifier: assembled and sectioned circuit photographs (left) and simulations of electron gun and amplifier performance (right).

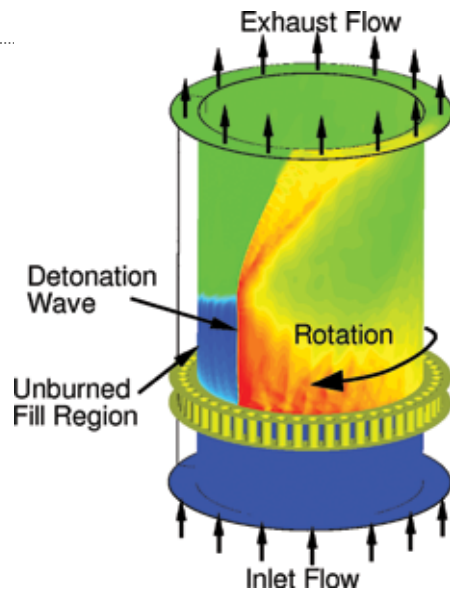
Sheet Electron Beam Gun Powers RF Amplifiers, Delivering Record Power in Ka- and W-Bands in Compact Packages: A novel, 20 kV, 3.5 ampere sheet electron beam gun, designed using NRL's MICHELLE 3D electron beam optics code, has been successfully demonstrated in two new high-power millimeter-wave amplifiers: a Ka-band amplifier centered around 35 GHz generating a record 12.7 kW of peak radio-frequency (RF) power with a half-power bandwidth of ~5 GHz (more than an order of magnitude improvement compared to state-of-the-art conventional round-beam amplifiers of comparable frequency and operating voltage) and a 94 GHz amplifier generating a record 7.7 kW of peak RF power (a more than sevenfold increase in power compared with conventional round-beam amplifiers of comparable frequency and operating voltage). The unprecedented 70 kW of beam power with >98% beam transport in a highly compact package is a key enabling technology for compact, high-power millimeter-wave amplifiers for Navy/Department of Defense electronic warfare systems, directed energy applications, high-resolution radar, and high-data-rate communications with low probability of intercept.



Microfabricated high-power millimeter-wave amplifiers: NRL recently demonstrated over 60 W of power at 214.5 GHz from a compact traveling wave amplifier (left image). The key component, the copper serpentine interaction circuit shown in the right image, was microfabricated using UV-LIGA techniques developed at NRL.

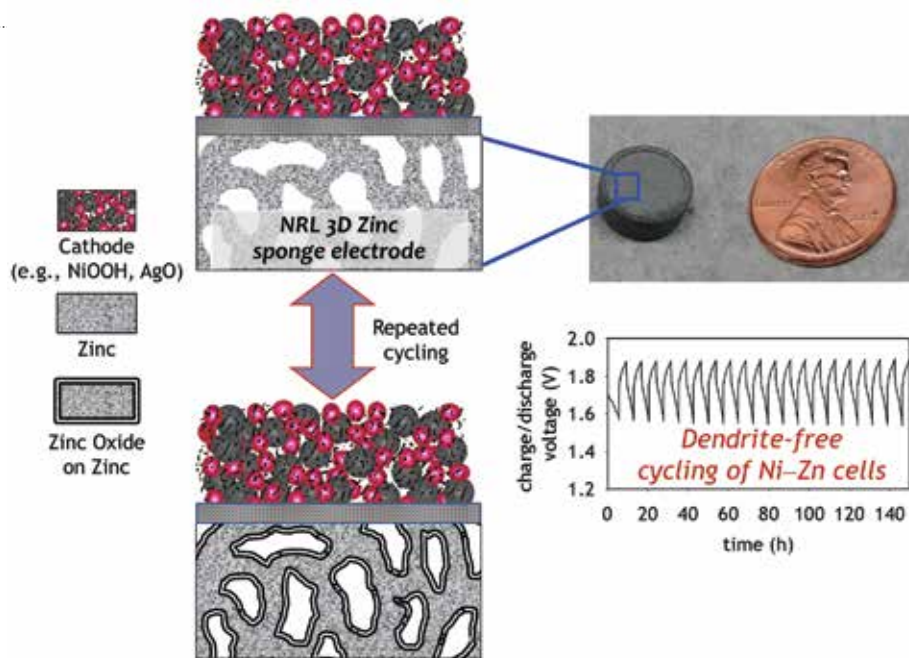
New Ultraviolet Photolithographic Process Demonstrated in a High-Power RF Amplifier Generating a Record 60 W and 15 GHz Bandwidth in G-Band:

A major impediment to the development of practical high average power devices operating above 100 GHz frequency, in the “terahertz gap,” has been the difficulty in creating suitable precision structures that meet the need for tight mechanical tolerances to fabricate finely structured sub-wavelength electromagnetic interaction circuits and that meet the need for solid metal construction to minimize losses and for good thermal management. To surmount these obstacles, NRL scientists have (1) developed a solid metal microfabrication process based on ultraviolet photolithography to create robust, precision, high-power circuit structures for millimeter-wave and submillimeter-wave amplifiers; and (2) demonstrated an amplifier that proves the ability of the microfabricated circuits to produce high power at high frequency. A traveling-wave tube amplifier using a serpentine waveguide circuit structure fabricated with a patent-pending NRL ultraviolet photolithographic process has demonstrated a record peak radio-frequency (RF) output power of over 60 W at a frequency of 214 GHz with a small-signal bandwidth of 15 GHz, offering 12 times the power and 50 times the bandwidth of state-of-the-art commercial devices. This demonstration is the first-ever vacuum electronic amplifier fabricated using the UV lithography process. It is a key enabling technology for a diverse range of Navy capabilities including high-resolution radar imaging, high-data-rate secure communications, all-weather imaging, and stand-off spectroscopic detection of chemical/biological/radiological/nuclear (CBRN) hazards.



A schematic of the rotating detonation engine concept including the computed flow field within the engine.

Rotating Detonation Engines for Reducing Fuel Consumption: NRL has been in the forefront of exploiting the detonative mode of combustion for increasing energy conversion efficiency and thus reducing fuel consumption. Previous research on pulsed or intermittent detonation engines is nearing full-scale engine demonstration. Meanwhile, detailed numerical simulations have shown that going to rotating (a form of continuous) detonation engines can reduce fuel consumption even more than pulsed or intermittent detonation engines. With the science basis established by the NRL simulations, ONR, DARPA, ARPA-E, and AFRL/AFOSR have all initiated programs to increase the Technology Readiness Level of this technology.



Redesigning zinc electrodes as 3D architectures enables dendrite-free cycling and a 30% capacity increase relative to commercial Zn/air batteries.

3D Zinc Sponge Electrodes for Batteries with Dendrite-Free Recharging: To make a breakthrough in a century-old quest in battery technology — to physically suppress formation of dendritic spikes upon charge/discharge cycling of metallic zinc (Zn) electrodes — researchers in the NRL Chemistry Division completely rethought the battery structure. They replaced the thin foils or powder composites comprising typical zinc electrodes with an aperiodic “sponge” form factor to create high-surface-area, 3D-wired porous zinc architectures. The Zn sponge electrode has already been tested in single-use Zn/air batteries and shown to discharge 90% of the zinc (versus <60% utilization of Zn in powder-composite electrodes) while maintaining a monolithic form-factor. Typical Zn batteries can be cycled only 8 to 10 times before dendrites grow long enough to contact the opposing electrode and short out operation. With Zn sponges, dendrite formation is shut off, even after 80 cycles at current loads that otherwise ensure formation of dendrites. Rechargeable, dendrite-free, zinc-based batteries offer viable alternatives to fire-prone Li-based batteries. The NRL team is now evaluating their zinc sponges in rechargeable, aqueous-based batteries capable of hundreds of cycles at high depth-of-discharge of the electron-rich zinc with a focus on Ni/Zn cells (of relevance for electric vehicles and funded by ARPA-E) and Ag/Zn cells (a favorite NASA and military single-use system).

NRL TODAY

ORGANIZATION AND ADMINISTRATION

The Naval Research Laboratory is a field command under the Chief of Naval Research, who reports to the Secretary of the Navy via the Assistant Secretary of the Navy for Research, Development and Acquisition.

Heading the Laboratory with joint responsibilities are CAPT Mark C. Bruington, USN, Commanding Officer, and Dr. John A. Montgomery, Director of Research. Line authority passes from the Commanding Officer and the Director of Research to three Associate Directors of Research, the Director of the Naval Center for Space Technology, and the Associate Director for Business Operations. Research divisions are organized under the following functional directorates:

- Systems
- Materials Science and Component Technology
- Ocean and Atmospheric Science and Technology
- Naval Center for Space Technology

The *NRL Fact Book*, published every two years, contains information on the structure and functions of the directorates and divisions.

NRL operates as a Navy Working Capital Fund (NWCF) Activity. All costs, including overhead, are charged to various research projects. Funding in FY13 came from the Chief of Naval Research, the Naval Systems Commands, and other Navy sources; government agencies such as the U.S. Air Force, the Defense Advanced Research Projects Agency, the Department of Energy, and the National Aeronautics and Space Administration; and several nongovernment activities.

PERSONNEL DEVELOPMENT

At the end of FY13, NRL employed 2613 persons — 33 officers, 47 enlisted, and 2533 civilians. In the research staff, there are 868 employees with doctorate degrees, 344 with master's degrees, and 414 with bachelor's degrees. The support staff assists the research staff by providing administrative support, computer-aided design, machining, fabrication, electronic construction, publication and imaging, personnel development, information retrieval, large mainframe computer support, and contracting and supply management services.

Opportunities for higher education and other professional training for NRL employees are available through several programs offered by the Employee Relations Branch. These programs provide for graduate work leading to advanced degrees, advanced training, college course work, short courses, continuing education, and

career counseling. Graduate students, in certain cases, may use their NRL research for thesis material.

For non-NRL employees, several postdoctoral research programs exist. There are also agreements with several universities for student opportunities, as well as summer and part-time employment programs. Summer and interchange programs for college faculty members, professional consultants, and employees of other government agencies are also available. These programs are described in the *NRL Review* chapter "Programs for Professional Development."

NRL has active chapters of Women in Science and Engineering (WISE), Sigma Xi, Toastmasters International, and the Federal Executive and Professional Association. An amateur radio club, a drama group, and several sports clubs are also active. NRL has a Recreation Club that provides gymnasium and weight-room facilities. NRL also has an award-winning Community Outreach Program. See "Programs for Professional Development" for details on all these programs and activities.

NRL has its very own credit union. Established in 1946, NRL Federal Credit Union (NRLFCU) is a sound financial institution that serves about 20,000 members including NRL employees, contractors, select employee groups and their families as well as consumers via the American Consumer Council. Focusing on its mission of Trusted Partners for Life, NRLFCU provides many free and low-cost products and services, including free checking with free bill pay, Visa CheckCard®, and mobile banking with remote deposit and great rates on auto and personal loans, credit cards, mortgages and more. Plus, NRLFCU offers the convenience of direct deposit, online access, and local branches (including one located in Bldg. 222, one in Waldorf, MD, and one in Alexandria, VA), nationwide access via the National Shared Branching Network with over 30,000 surcharge-free ATMs, and personalized full-service investment and brokerage services. For more information, call 301-839-8400 or visit nrlfcu.org.

Public transportation to NRL is provided by Metrobus. Metrorail service is three miles away.

SITES AND FACILITIES

NRL's main campus in Washington, D.C., consists of 89 main buildings on about 131 acres. NRL also maintains 15 other research sites, including a vessel for fire research and a Flight Support Detachment. The many diverse scientific and technological research and support facilities are described here. More details can be found in the *NRL Major Facilities* publication at www.nrl.navy.mil.

Institute for Nanoscience



NRL researchers working in the Institute for Nanoscience clean room.

The revolutionary opportunities available in nanoscience and nanotechnology led to a National Nanotechnology Initiative in 2001. In that same year, the NRL Institute for Nanoscience was established. The prospect for nanoscience to provide a dramatic change in the performance of materials and devices was the rationale for identifying this emerging field as one of the DoD strategic research areas for basic research funding on a long-term basis.

The mission of the NRL Institute for Nanoscience is to conduct highly innovative, interdisciplinary research at the intersections of the fields of materials, electronics, chemistry, and biology in the nanometer size domain. The Institute exploits the broad multidisciplinary character of the Naval Research Laboratory to bring together scientists with disparate training and backgrounds to pursue common goals at the intersection of their respective fields in systems at this length scale. The Institute provides the Navy and DoD with scientific leadership in this complex, emerging area and identifies opportunities for advances in future defense

technology. NRL's nanoscience research programs and accomplishments directly impact nearly all Naval S&T focus areas.

The Institute's current research program emphasizes multidisciplinary, cross-division efforts in a wide range of science and technology applications:

- Ultra-low-power electronics
- Quantum information processing
- Chemical signaling
- Energy conversion/storage
- Photonics/plasmonics
- Multifunctional materials
- Biomimetics
- Bio/inorganic hybrid materials

The Institute for Nanoscience building, opened in October 2003, provides NRL scientists access to state-of-the-art laboratory space and fabrication facilities. The building has 5000 ft² of Class 100 clean room space for device fabrication, 4000 ft² of "quiet" lab space with temperature controlled to ± 0.5 °C, acoustic isolation at the NC35 standard (35 dB at 1 kHz), floor vibration isolation to <150 $\mu\text{m/s}$ rms at 10 to 100 Hz and <0.3 mOe magnetic noise at 60 Hz, and 1000 ft² of "ultra-

quiet” laboratory space with temperature controlled to ± 0.1 °C and acoustic isolation at the NC25 standard (25 dB at 1 kHz). Equipment includes a complete suite of fabrication tools including deposition and etch systems, optical mask aligners, two electron beam writers, a focused ion beam writer, an optical pattern generator for mask making, a plasma-enhanced atomic layer deposition system, a laser machining tool, and a wide variety of characterization tools including an aberration-corrected transmission electron microscope.



Metrology.



Transmission electron microscopy.



The Institute for Nanoscience research building.

Radar



The AMRFC testbed, located at NRL's CBD, was developed as a proof-of-principle demonstration system that is capable of simultaneously transmitting and receiving multiple beams from common transmit and receive array antennas for radar, electronic warfare, and communications.

NRL has gained worldwide renown as the “birthplace of U.S. radar,” and for more than half a century has maintained its reputation as a leading center for radar-related research and development. A number of facilities managed by NRL’s Radar Division continue to contribute to this reputation.

A major Division facility is the Compact Antenna Range used for antenna design, development, and characterization and also to measure the radar cross section of objects. The range is capable of simulating far-field conditions from 1 to 110 GHz, with a quiet zone approximately 7 ft in diameter and 8 ft in length. Instrumentation currently covers from 1 to 95 GHz. The range was recently upgraded to add a 20 ft × 12 ft near-field scanner supporting near-field array antenna measurements up to 110 GHz. Another strong Division capability is the Computational Electromagnetics (CEM) Facility, which supports complex, high-fidelity electromagnetic modeling of naval platforms, targets, and antennas. The facility produces detailed predictions of the radar cross section of various targets, primarily ships. The CEM Facility includes multiple-CPU supercomputers that are also used during the design

of phased array antennas. The tremendous synergism between the CEM group and the Compact Antenna Range facility provides the ability to design in the CEM environment, test in the compact range, and have immediate feedback between the theoretical and experimental aspects to shorten the development cycle for antennas of novel design and using new materials.

In support of airborne radar applications, the Division operates a supercomputer-based Radar Imaging Facility and an inverse synthetic aperture radar (ISAR) capable of being deployed in the air, on the ground, or shipboard for collecting radar imaging data. The NRL P-3B aircraft equipped with the AN/APS-145 radar and Cooperative Engagement Capability is also available to support experiments.

In support of ship-based radar applications, the Division operates the Radar Test Facility at the

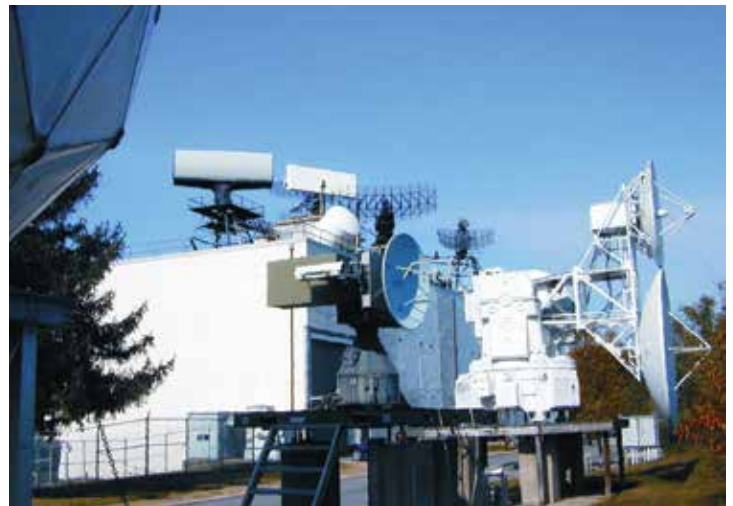
Chesapeake Bay Detachment (CBD) near Chesapeake Beach, Maryland. The site has long-range air search and surface search radars and features the W-band Advanced Radar for Low Observable Control (WARLOC), a fully operational high-power coherent millimeter-wave radar operating at 94 GHz. The WARLOC transmitter is capable of producing a variety of waveforms suitable for precision imaging of targets at long range. Waveforms with a bandwidth of up to 600 MHz can be transmitted at full power. A 6 ft Cassegrain antenna is mounted on a precision pedestal and achieves 62 dB of gain. An S-band waveform development test bed will soon be operational with a 43 dB gain Cassegrain monopulse antenna supporting bandwidths up to 400 MHz.

The Advanced Multifunction Radio Frequency Concept (AMRFC) test bed is an installation at CBD operated by the Radar Division, with significant contributions by other NRL divisions. The goal of the AMRFC program was to demonstrate the integration of multiple shipboard RF functions, including radar, electronic warfare (EW), and communications, by utilizing a common set of broadband array antennas, signal and data processing, and signal generation and display hardware. The test bed consists of separate active transmit and receive arrays that operate over the 6 to 18 GHz band. Functionality of the test bed includes a multimode navigation/surface surveillance Doppler radar, multiple communication links (line-of-sight and satellite), and passive and active EW capabilities. The arrays are mounted on a 15° tilt-back overlooking the Chesapeake Bay, emulating a shipboard installation. Currently, the test bed site is being enlarged and modified to accommodate additional equipment in support of the Integrated Topside (InTop) program. The InTop program, sponsored by the Office of Naval Research, has a similar set of goals as AMRFC, but is broader in scope, covering RF functions across the spectrum from HF through Ka band.

The Division also has access to the Navy's AN/TPS-71 Relocatable Over-The-Horizon Radar (ROTHR). The Division provides direct technical support for the AN/TPS-71 program and has direct access to data. The Division is currently developing a relocatable high frequency surface wave radar that will be used to explore phased array antenna geometries and associated beamforming concepts.

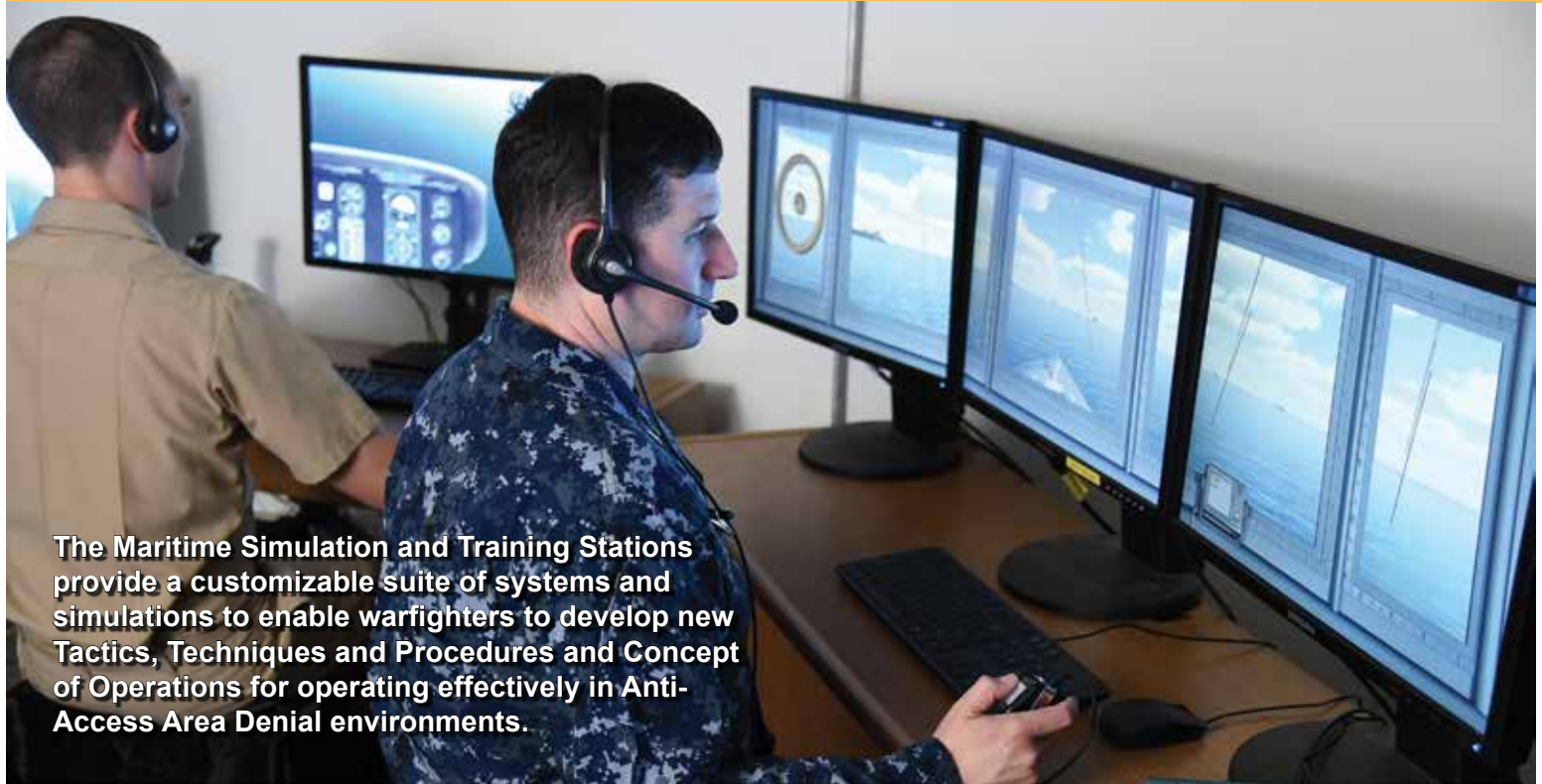


Compact Range Facility.



Radar antennas in front of and on the roof of the Radar Test Facility.

Information Technology



The Maritime Simulation and Training Stations provide a customizable suite of systems and simulations to enable warfighters to develop new Tactics, Techniques and Procedures and Concept of Operations for operating effectively in Anti-Access Area Denial environments.

NRL's Information Technology Division (ITD) conducts basic research, exploratory development, and advanced technology demonstrations in the collection, transmission, processing, dissemination, and presentation of information. ITD's research program spans the areas of artificial intelligence (AI), autonomous systems, high assurance systems, tactical and strategic computer networks, large data systems, modeling and simulation, virtual and augmented reality, visual analytics, human/computer interaction, communication systems, transmission technology, and high performance computing.

NRL's RF Communications Laboratory conducts research in satellite communications systems and modulation techniques, develops advanced systems for line-of-sight communications links, and conducts designs for the next generation of airborne relays. A Voice Communication Laboratory supports the development of tactical voice technology; a Mobile Network Modeling Laboratory supports modeling, emulation, development, and scenario-based performance evaluation of both tactical network and Mobile Ad Hoc Networking (MANET) capabilities; and a Dynamic

Spectrum Allocation/Cognitive Radio Technology Test Lab provides the capability to analyze, test, and develop dynamic, cognitive, networked tactical wireless communications capabilities that efficiently share and exploit the spectrum. A Freespace Laser Communications Laboratory supports the design and development of prototype technical solutions for Naval laser communications requirements.

The Center for Computational Science (CCS) hosts the High Performance Computing (HPC) and Communications efforts at NRL. CCS participates in the DoD HPC Affiliated Research Center (ARC) program providing supercomputer research access to NRL and DoD customers. For high-performance networking, the Center runs the Advanced Technology Demonstration Network (ATDnet) in the Washington, D.C., metro area that provides dark fiber access to research partners. Other research supports high-speed connections (tens to hundreds of Gbps). Current efforts range from mapping traditional large shared memory (SHMEM) problems onto scalar computing systems to emerging cloud architectures to extremely large storage (petabytes and beyond).

CCS network operations provides a full range of IT infrastructure to support Lab-wide needs including equipment that supports a cable TV plant, SIPRNet, backbone fiber based network, services and external

connectivity to the Defense Research and Engineering Network (DREN). DREN is a high-bandwidth wide area network that provides the communications path within the HPC community, to DoD networks and to the Internet. A current research effort includes Open-flow between multiple DREN sites, including NRL.

The Autonomous Systems and Robotics Laboratory provides the ability to develop and evaluate intelligent software, hardware, sensors, and interfaces for human interaction with autonomous systems. The lab includes a number of ground and air platforms, as well as equipment for evaluating interfaces, including eye trackers. A variety of passive and active sensors support research in perception for autonomous systems. The Audio Laboratory combines a state-of-the-art 3D sound environment and multitask test bed for basic and applied human performance studies and Navy information display research. The core of the new Visual Analytics Laboratory is a display wall composed of LCD tiles, which enable teams of analysts to explore massive, diverse streams of data, supporting research into the

science of analytical reasoning facilitated by visual interfaces. The Service Oriented Architecture Laboratory is used to investigate, prototype, and evaluate flexible, loosely coupled Web services that can be rapidly combined to meet dynamically changing warfighter needs. The Behavioral Detection Laboratory features a 50-node Cloud cluster to support the development of algorithms, processes, and sensor suites associated with behavioral indicators of deception.

The Configurable Synthetic Merged Environments (CSME, or Sesame) Laboratory enables the assessment of Naval systems, individuals, and teams using virtual prototyping techniques to simulate future warfighting scenarios within surface, undersea, land (including man-portable wearable gear), and air domains. Individuals and teams are able to interact with each other and synthetic entities in a realistic manner to improve training effectiveness. The CSME Laboratory is a complement to the Department of Navy's warfighter performance portfolio.



Scientist using the Dynamic Spectrum Allocation/Cognitive Radio Technology Test Lab facility to prepare a WNaN radio network for RF spectrum sharing field testing.



Technicians and scientists in the Mobile Network Modeling Laboratory (top) prepare and run a scenario-based, tactical network emulation using the NRL-developed EMANE system (bottom).

Optical Sciences

The Advanced Optical Materials Fabrication Laboratory, a state-of-the-art high vacuum cluster system, consists of a series of interconnected chambers allowing complex, heterogeneous, multilayer films to be deposited and patterned without breaking vacuum during processing.



The Optical Sciences Division has a broad program of basic and applied research in optics and electro-optics. Areas of concentration include fiber optics and fiber-optic sensing, materials and sensors for the visible and infrared (IR) spectral regions, integrated optical devices, signal processing, optical information processing, panchromatic and hyperspectral imaging for surveillance and reconnaissance, and laser development.

The division occupies some of the most modern optical facilities in the country. The newest facility in Optical Sciences is the Advanced Optical Materials Fabrication Laboratory, a state-of-the-art cluster system for vacuum deposition of thin films. The facility consists of a series of interconnected high vacuum chambers, allowing complex, heterogeneous, multi-

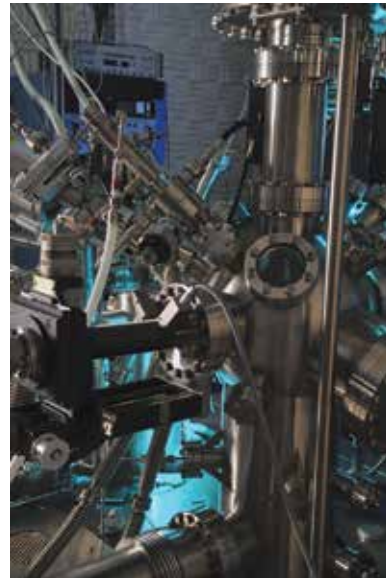
layer films to be deposited without breaking vacuum during processing. The system includes a glove box, sample distribution robot, sputtering chambers for chalcogenide materials and oxides, evaporators for metals and dielectrics, and a mask changing module to enable layers to be patterned in situ while eliminating interface effects that result from exposure to air. Three other recently added facilities include the Optical Fiber Preform Fabrication Facility for making doped and undoped, multimode, single-mode, multicore, and photonic crystal glass preforms at temperatures as high as 2300 °C; the Surface Characterization Facility for ultraviolet and X-ray photoemission spectroscopy, atomic force and scanning tunneling microscopy (STM), and STM-induced light emission measurements; and the molecular beam epitaxial growth system dedicated to infrared lasers and detectors based on GaSb/InAs/AlSb quantum well and superlattice

structures. In addition, an extensive set of laboratories exists to develop and test new laser and nonlinear frequency conversion concepts and to evaluate non-destructive test and evaluation techniques. Fiber-optic sensor testing stations include acoustic test cells and a three-axis magnetic sensor test cell. There is also an Ultralow-loss Infrared Fiber-Optic Waveguide Facility using high-temperature IR glass technology. The facilities for ceramic optical materials include powder preparation, vacuum presses, and a 50-ton hot press

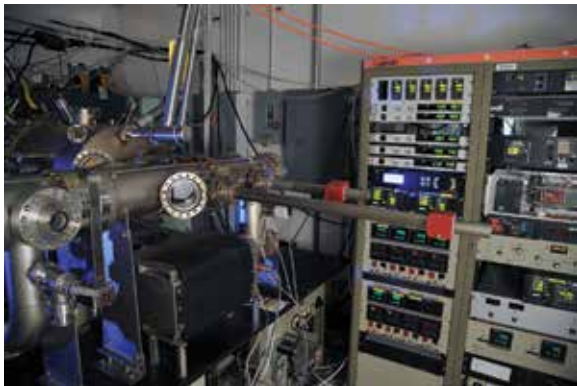
for sintering. The Focal Plane Array Evaluation Facility allows measurement of the optical and electrical characteristics of infrared focal plane arrays being developed for advanced Navy sensors. The IR Missile-Seeker Evaluation Facility performs open-loop measurements of the susceptibilities of IR tracking sensors to optical countermeasures. An ultra-high-vacuum multichamber deposition apparatus is used for fabrication of electro-optical devices and can be interlocked with the Surface Characterization Facility.



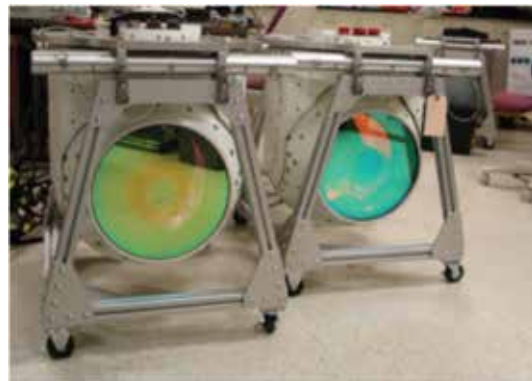
The Optical Fiber Preform Fabrication Facility includes computer control of the glass composition and standard fiber-optic dopants as well as rare earths, aluminum, and other components for specialty fibers.



The Optical Sciences Surface Characterization Facility includes instrumentation for ultraviolet and X-ray photo-emission spectroscopy (UPS and XPS), atomic force and scanning tunneling microscopy (AFM and STM), and STM-induced light emission (STM-LE) measurements.



Molecular beam epitaxy (MBE) system dedicated to quantum confined GaSb/InAs/AlSb structures for midwave infrared laser development.



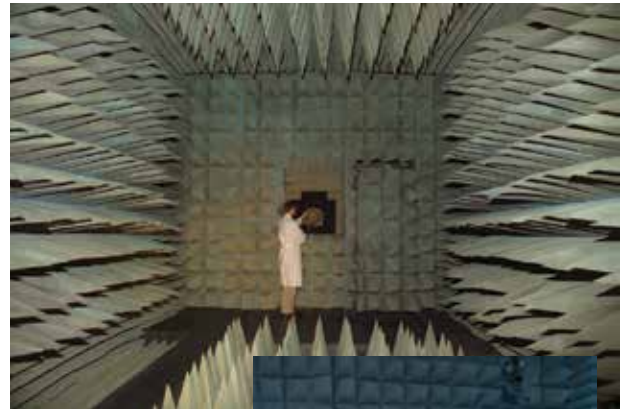
MX-20SW hyperspectral sensors.

Tactical Electronic Warfare

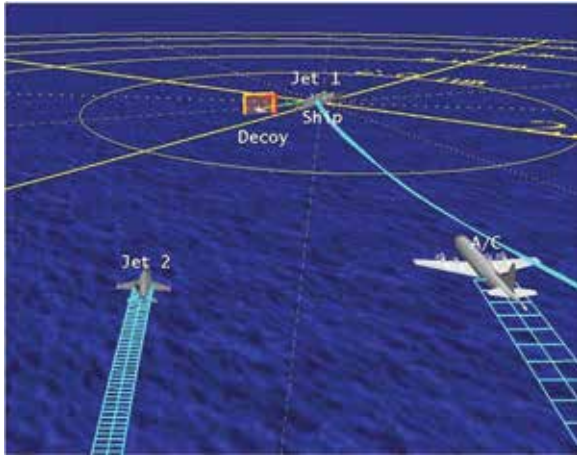


Learjet with simulators during RIMPAC exercises.

The Tactical Electronic Warfare (TEW) Division's program for electronic warfare (EW) research and development covers the entire electromagnetic spectrum. The program includes technology research and advanced developments and their applicability to producing EW products for the Fleet. The range of ongoing activities includes components, techniques, and subsystems development as well as system conceptualization, design, and EW effectiveness evaluation. The focus on the research activities extends across the entire breadth of the battlespace. These activities emphasize providing the methods and means to detect and counter enemy hostile actions via threat neutralization — from the beginning, when enemy forces are being mobilized for an attack, through to the final stages of the engagement. In conducting this program, the TEW Division employs an extensive array of special research and development laboratories, anechoic chambers, and modern computer systems used for modeling and simulation. Dedicated field sites and airborne platforms allow for the conduct of field experiments and operational trials. This combination of scientists, engineers, and specialized facilities also supports the innovative use of all Fleet defensive and offensive EW assets currently available to operational forces.



Radio Frequency Countermeasures anechoic chamber for EW testing.



TEWD develops and implements advanced visualization tools to support EW systems development and analysis.



The Central Target Simulation Facility is a high-performance, hardware-in-the-loop simulator for real-time closed-loop testing and evaluation of electronic warfare systems and techniques to counter the antiship missile threats.



EATES — Electronic Attack Technique Evaluation System, a stand-alone portable EA testing system.



Deployed EW subsystem to improve emitter detection and classification based on conceptualization and development performed in TEWD.

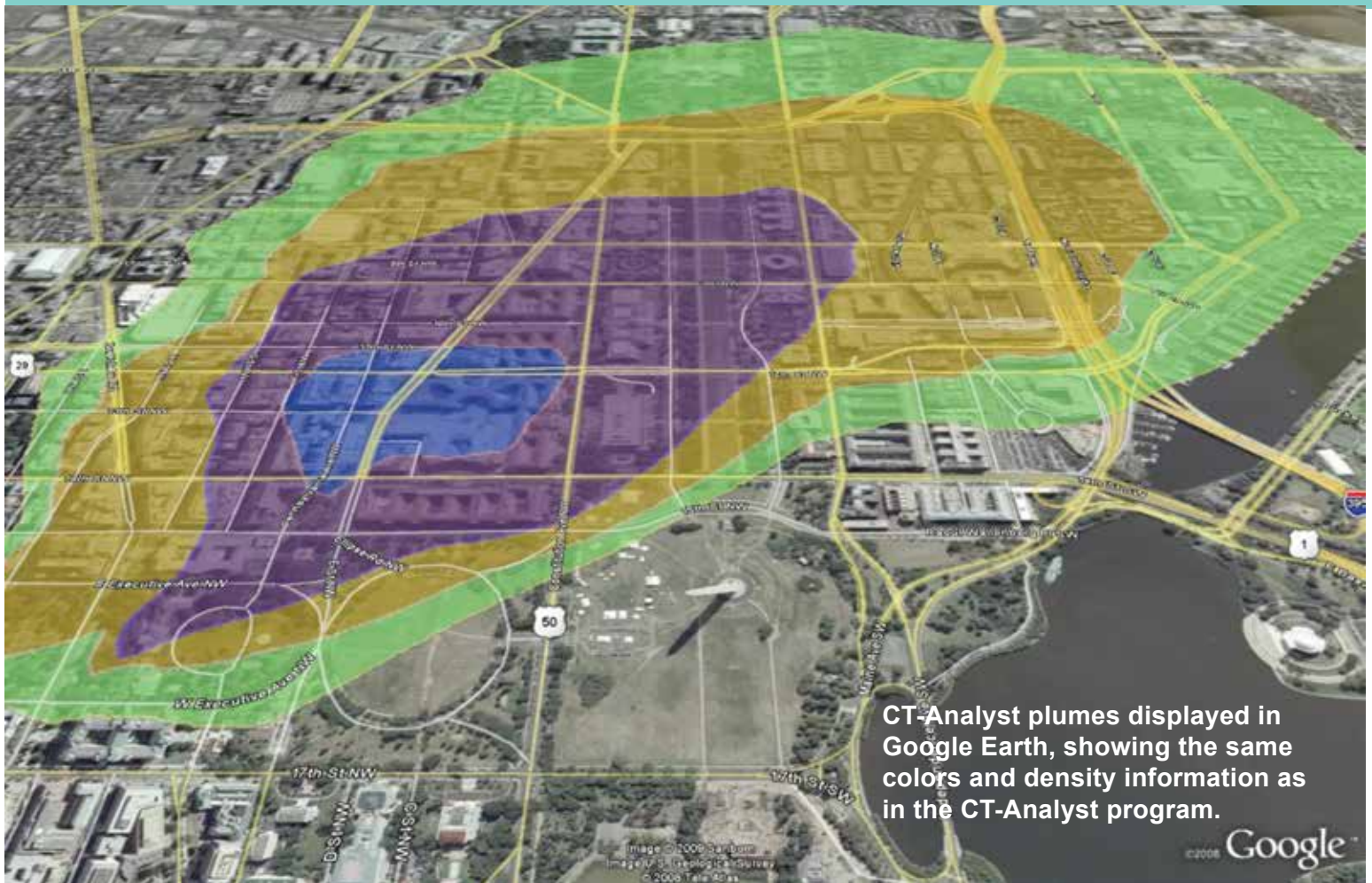


XFC (Experimental Fuel Cell) UAV — tube launch sequence.



XFC prototype in flight under fuel cell power.

Laboratories for Computational Physics and Fluid Dynamics



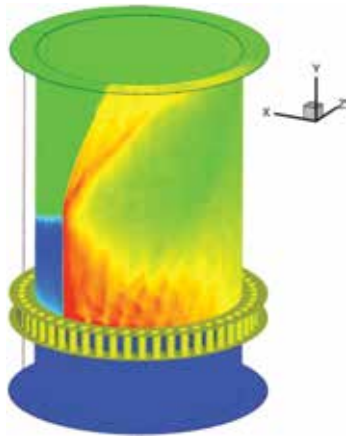
The Laboratories for Computational Physics and Fluid Dynamics (LCP&FD) is staffed by physicists, engineers, and computer scientists who develop software and use high-performance computers to solve priority problems for the Navy, the DoD, and the nation when existing capabilities and available commercial software prove inadequate to the application. For example, the LCP&FD developed the CT-Analyst crisis management software (figure above) so that first responders can have instant predictions of an airborne contaminant spread in an urban environment.

The LCP&FD maintains a very powerful collection of computer systems applied to a broad collection of work. There are currently 3180 clustered x86_64 cores and their associated support systems. In addition, there

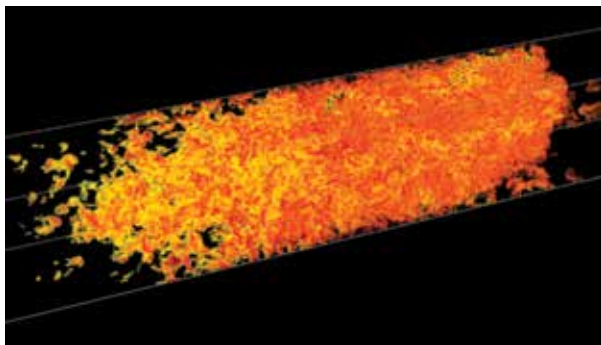
are over 40 Apple workstations in the group, most of which are capable of large calculations both independently and in parallel ad hoc clusters.

There are four 64-bit x86 multicore distributed memory clusters, each well coupled with Infiniband high-speed switched interconnect. Two of the clusters contain many-core coprocessors. The newest of these systems consist of 64 NVIDIA Kepler class GPUs and 8 Intel Xeon Phi coprocessors. The second system is comprised of 88 NVIDIA Fermi class GPUs. All of the many-core processors are tightly coupled to their associated x86_64 multicore processor nodes. A ScaleMP based shared memory machine is available for large memory processing.

All systems share 250 terabytes of storage for use during a simulation and at least one gigabyte of memory per processor core. All unclassified systems share a common disk space for home directories as well as 3 terabytes of AFS space that can be used from any AFS-capable system throughout the allowed Internet.

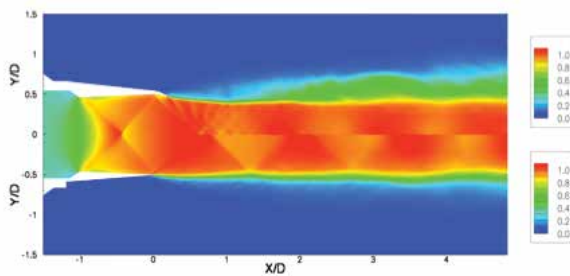


The computed flow field inside a rotating detonation engine with mixture plenum (bottom), injector plate and injectors (center), and combustion chamber (top). This new class of engines has been investigated computationally and been shown to have the potential to reduce fuel consumption by 25% while providing the same performance as current gas-turbine engines.

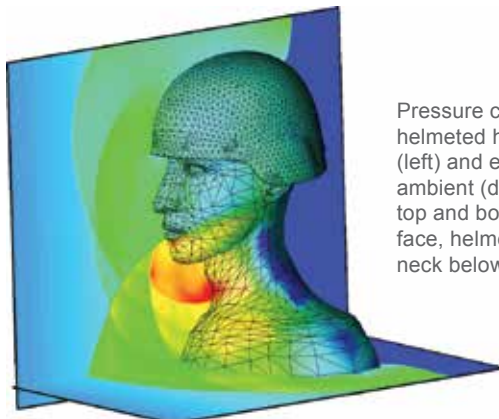


Accelerating unconfined turbulent flame in a methane-air mixture shortly before a spontaneous transition to a detonation. Shown is the volume rendering of the reaction rate in a fully resolved numerical simulation of the flame interaction with the driven, homogeneous, isotropic, and high-speed turbulence.

Chevrons

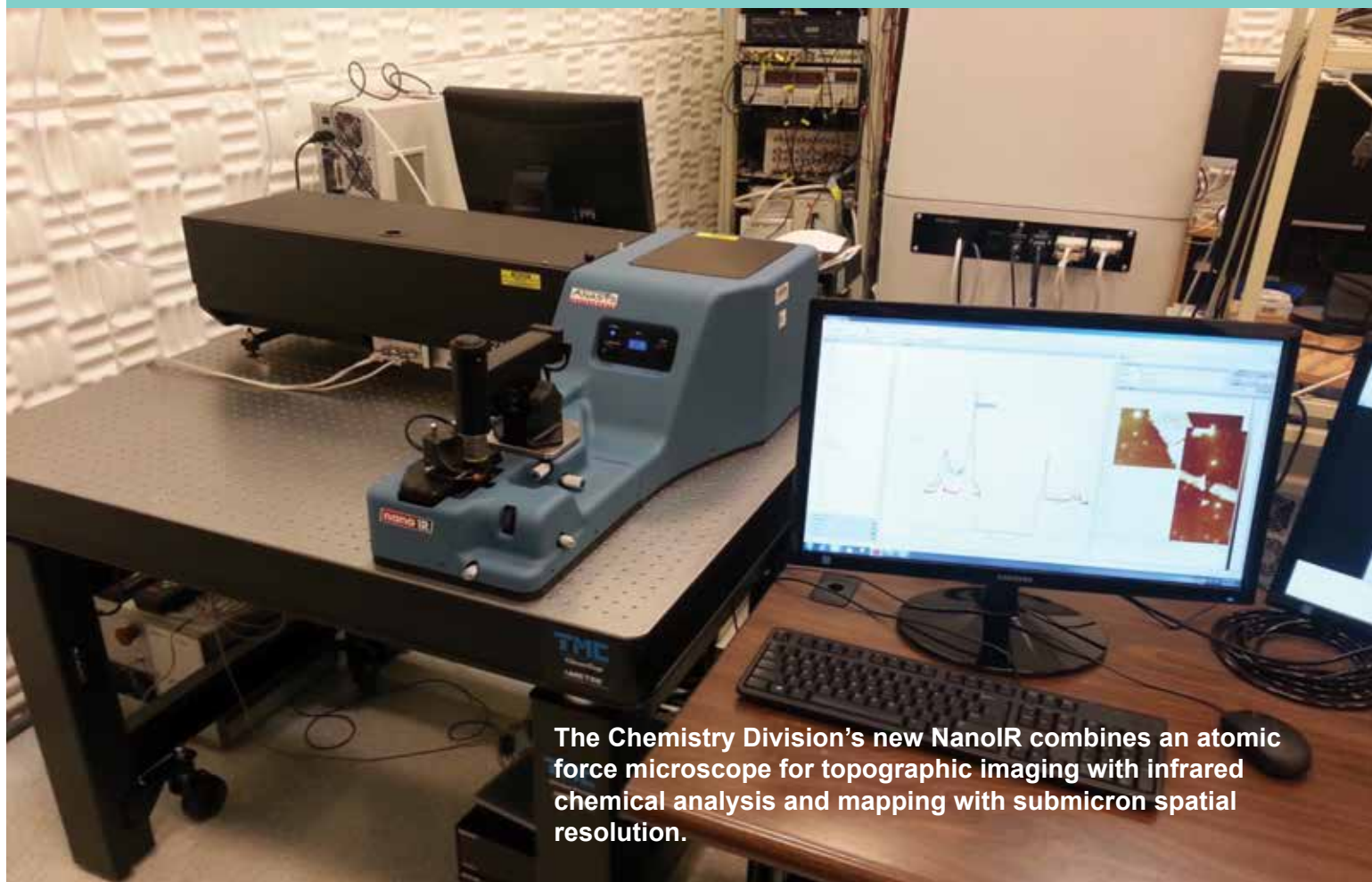


The computed exhaust flow field of a super-sonic military aircraft jet shows the flow modifications (shock disruptions and enhanced jet mixing) created by mechanical chevrons (when compared to the baseline flow field without chevrons). The overall noise intensity is reduced in half with the use of these flow modifiers.



Pressure contours resulting from blast interaction with a helmeted head. The shock wave approaches from the front (left) and envelopes the geometry; the boundary between ambient (dark blue) and post-shock (green) air is seen at the top and bottom right. Interacting shock reflections from the face, helmet, and torso generate high pressures (red) on the neck below the chin.

Chemistry



The Chemistry Division's new NanoIR combines an atomic force microscope for topographic imaging with infrared chemical analysis and mapping with submicron spatial resolution.

NRL has been a major center for chemical research in support of naval operational requirements since the late 1920s. The Chemistry Division continues this tradition. The Chemistry Division conducts basic research, applied research, and development studies in the broad fields of diagnostics, dynamics, synthesis, materials, surface/interfaces, environment, corrosion, combustion, and fuels. Specialized programs currently within these fields include the synthesis and characterization of organic and inorganic materials, coatings, composites, nondestructive evaluation, surface/interface modification and characterization, nanometer structure science/technology, chemical vapor processing, tribology, solution and electrochemistry, mechanisms and kinetics of chemical processes, analytical chemistry, theoretical chemistry, decoy materials, radar-absorbing materials/radar-absorbing structures (RAM/RAS) technology, chemical/biological warfare defense, atmosphere analysis and control,

environmental remediation and protection, corrosion science and engineering, marine coatings, personnel protection, and safety and survivability. The Division has several research facilities.

Chemical analysis facilities include a wide range of modern photonic, phononic, magnetic, electronic, and ionic-based spectroscopic/microscopic techniques for bulk and surface analysis.

The Magnetic Resonance Facility includes advanced high-resolution solid-state nuclear magnetic resonance (NMR) spectroscopy techniques to observe nuclei across much of the periodic table and provides detailed structural and dynamical information.

The Nanometer Characterization/Manipulation Facility includes fabrication and characterization capability based on scanning tunneling microscopy/spectroscopy, atomic force microscopy, and related techniques.

The Materials Synthesis/Property Measurement Facility has special emphasis on polymers, surface-film processing, and directed self-assembly.

The Chemical Vapor and Plasma Deposition Facility is designed to study and fabricate materials such as diamond using in situ diagnostics, laser machining, and plasma deposition reactors.

The Navy Fuel Research Facility performs basic and applied research to understand the underlying chemistry that impacts the use, handling, and storage of current and future Navy mobility fuels.

Fire research facilities include a 11,400 ft³ fire research chamber (Fire I) and the 457 ft ex-USS *Shadwell* (LSD 15) advanced fire research ship. Commensurate support has been devoted to survivability of the new classes of ships, DDX, LPD 17, LCS, CVNX, and LHA(R).

The Marine Corrosion and Coatings Facility located on Fleming Key at Key West, Florida, offers a “blue” ocean environment and unpolluted, flowing seawater for studies of environmental effects on materials. Equipment is available for experiments involving accelerated corrosion and weathering, general corrosion, long-term immersion and alternate immersion, fouling, electrochemical phenomena, coatings applica-

tion and characterization, cathodic protection design, ballast water treatment, marine biology, and corrosion monitoring.

The Chemistry Division has focused on force protection/homeland defense (FP/HD) since September 11, 2001, especially on the development of improved detection techniques for chemical, biological, and explosive threats. As part of a multidivisional program to develop new technology systems, the Chemistry Division is a major contributor to the NRL Institute for Nanoscience. Nanoscience complements FP/HD in that nanoscience is expected to provide dramatic improvements to chemical/biological detection, protection, and neutralization. Chemistry will approach the nanoscale from the bottom up — building smaller atoms and molecules into nanostructures with new properties and developing the directed assembly of nanostructures into hierarchical systems. The NRL Nanoscience building is linked directly into the Chemistry building to provide controlled access and auxiliary space for work not requiring a “low noise” environment.



Thermal gravimetric analysis: The new simultaneous thermal analyzer NETZSCH STA 449 F3 Jupiter allows the measurement of mass changes and thermal effects (TG, TG-DTA, and TG-DSC measurements) between -150 °C and 2400 °C.

The Leica UC7/FC ultramicrotome with cryo attachment can efficiently section materials for further study, and is capable of ultra-thin sections in the 50 nm range.



The Micro-Raman system is a multiwavelength, fully automated spectrometer providing chemical microprobe analysis and mapping of organic, inorganic, and biological specimens.



Materials Science and Technology



Scientist passages cells in preparation for live cell microscopy studies.

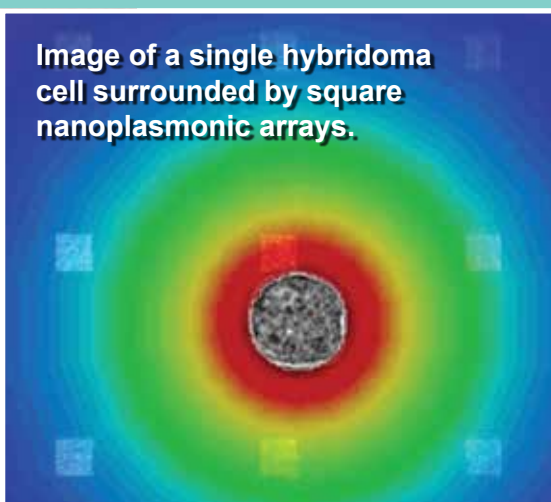
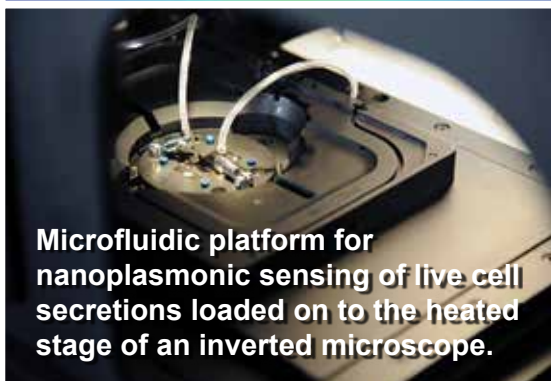


Image of a single hybridoma cell surrounded by square nanoplasmonic arrays.



Microfluidic platform for nanoplasmonic sensing of live cell secretions loaded on to the heated stage of an inverted microscope.

The Materials Science and Technology Division at NRL provides expertise and facilities to foster materials innovation. The Division houses many specialized and unique facilities for carrying out basic and applied materials synthesis and characterization research.

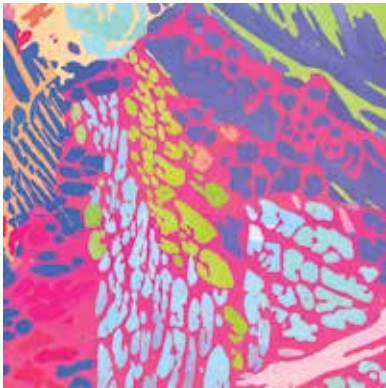
The Magnetolectronics Fabrication Facility consists of a Class 1000 clean room equipped with tools for lithographic construction of magnetolectronic and spintronic devices. It provides pattern definition, metallization, dielectric layer deposition, and both reactive and Ar^+ ion etching of wafers and small pieces.

The Electrical, Magnetic, and Optical Measurement Facility contains several complementary instruments that allow for the magnetic, electrical, optical, and heat capacity characterization of materials and devices. The SQUID (superconducting quantum interference device) uses magnetometry and vibrating sample magnetometry to determine important properties of superconducting, paramagnetic, diamagnetic, and ferromagnetic materials. The transport properties of materials, namely the temperature- and magnetic-field-

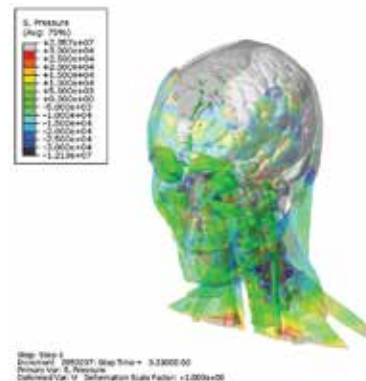
dependent resistivity combined with heat-capacity measurements, allow for a fundamental physical understanding of electronic properties.

The Materials Processing Facility includes apparatuses for powder production by fluid atomization, thermal evaporation, and arc erosion, and a physical vapor deposition system designed to produce and coat submicron powders in situ. Facilities to process powder into bulk specimens by hot and cold isostatic pressing permit a variety of consolidation possibilities. The isothermal heat treatment facility and quenching dilatometer permit alloy synthesis and single crystal growth. Bulk alloys can be prepared by induction melting, while rapidly solidified metals of thin cross section can be made by splat quenching and melt spinning. Ceramic and ceramic-matrix composites processing facilities include a wide variety of conventional, controlled atmospheric furnaces, hot presses, a ball milling apparatus, particle size determination capability, and sol-gel and organometallic coating processing capabilities.

The Mechanical Characterization Facility consists of various testing systems, many with automated computer control and data acquisition, for determining the mechanical response of materials under controlled



Electron backscatter diffraction inverse pole figure map shows the grain orientations of the ferrite and austenite phases in a duplex stainless steel 2205 alloy.



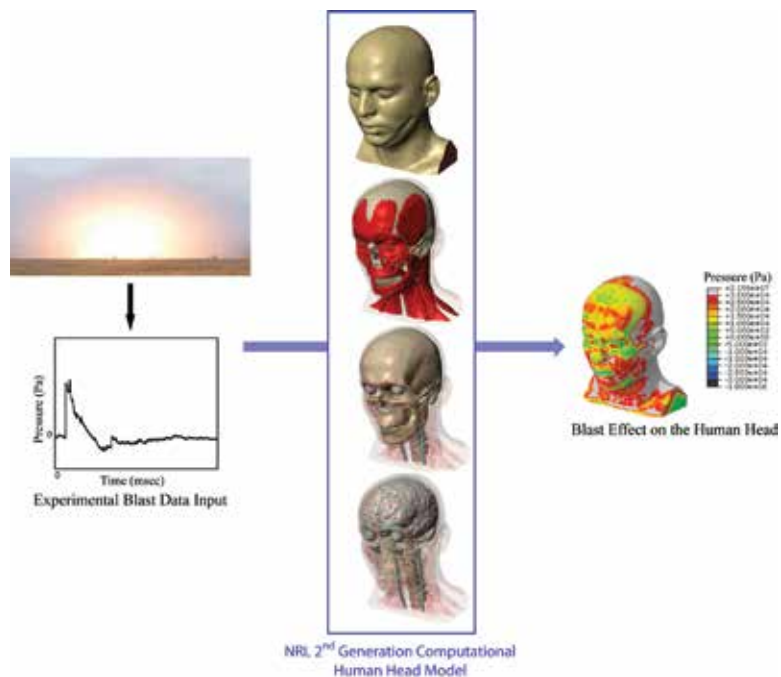
Head dynamic response to front blast pressure wave; translucent image of pressure levels in the head.

loading/deformation and environmental conditions. Basic capabilities include quasistatic tensile and fracture testing, dynamic storage and loss moduli as a function of frequency and temperature, cyclic fatigue crack growth and corrosion fatigue testing, and stress-corrosion cracking testing.

The Thin-Film Materials Synthesis and Processing Facility provides users a wide variety of techniques for growth and processing of thin films (thickness 1 μm or less). Sputter deposition offers a versatile method of depositing metallic and dielectric films and is a primary tool of this facility. Thermal evaporation of metals is implemented in both high-vacuum and ultra-high-vacuum systems. Pulsed laser deposition (PLD) with variable stage temperature and controlled atmosphere allows growth of oxides. Electrolytic deposition offers efficient growth of gold and silver films. Laser direct-write ablation and deposition processes provide unique methods for imposing CAD-defined features via ablation of a substrate film and ablative mass transfer to a substrate.

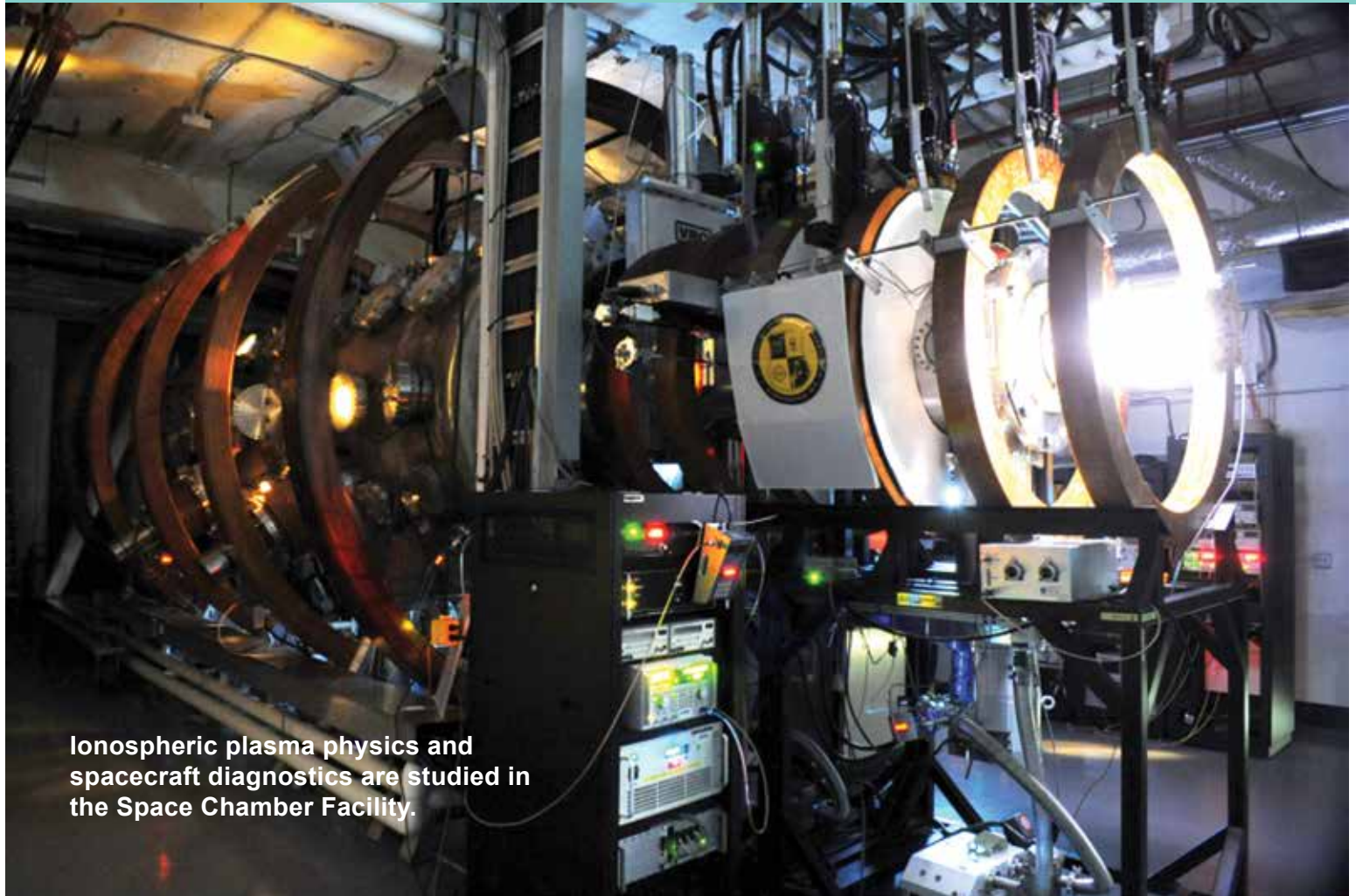
The Micro/Nanostructure Characterization Facility is capable of performing transmission electron microscopy (TEM), scanning transmission electron microscopy (STEM), atomic resolution transmission electron microscopy (ARTEM), electron energy loss spectroscopy (EELS), Z-contrast imaging, and spectral imaging through the use of a JEOL 2010F transmission electron microscope, an FEI Tecnai G² 30 analytical transmission electron

microscope, and a JEOL JSM-7001F Variable Pressure scanning electron microscope with secondary and backscattered electron imaging capabilities, as well as energy dispersive spectrometry (EDS) and electron backscatter diffraction (EBSD). In addition, this field-emission microscope operates in low-vacuum mode, which allows for high-resolution imaging of nonconductive materials without coatings or any additional preparation. Other standard microstructure characterization instruments are also available.



High-fidelity modeling of the human head under blast loading.

Plasma Physics



Ionospheric plasma physics and spacecraft diagnostics are studied in the Space Chamber Facility.

The Plasma Physics Division conducts basic and applied research in space plasmas; inertial confinement fusion (ICF); ultra-short pulse laser interactions; directed energy; railguns; pulsed-power and intense particle beams; materials processing; advanced diagnostics; radiation-atomic physics; and nonlinear dynamics.

The Space Physics Simulation Chamber generates near-Earth plasma environments for studying space plasma phenomena and spacecraft diagnostic development and testing. Nike and Electra are major KrF laser facilities for ICF research, studying ICF target physics and developing repetitively pulsed KrF technologies, respectively. The Ultrashort-Pulse, High-Intensity Laser facility has both a 10 Hz (15 TW) and kilohertz (0.45 TW) Ti:Sapphire laser to investigate laser-driven

acceleration and nonlinear laser-plasma interactions. Directed energy research is performed in the High Energy Laser Lab, which has four multikilowatt fiber lasers to study laser propagation, incoherent beam combining, and power beaming. The Materials Testing Facility houses a 6-meter-long railgun used to study the materials issues of electromagnetic launch for the Navy and DoD's multimission railgun program. A new small caliber railgun will fire repetitively and expand our knowledge of materials, pulsed power, and energy storage. The Division has two large, high-voltage, pulsed-power devices, Gamble II and Mercury, which are used to produce intense electron and ion beams, flash X-ray sources, and high-density plasmas for application to nuclear weapons effects testing, radiography, and active detection of nuclear materials. The Division uses both microwaves and plasmas for materials processing applications. The microwave materials processing laboratory includes a 20 kW, CW, 83 GHz gyrotron.

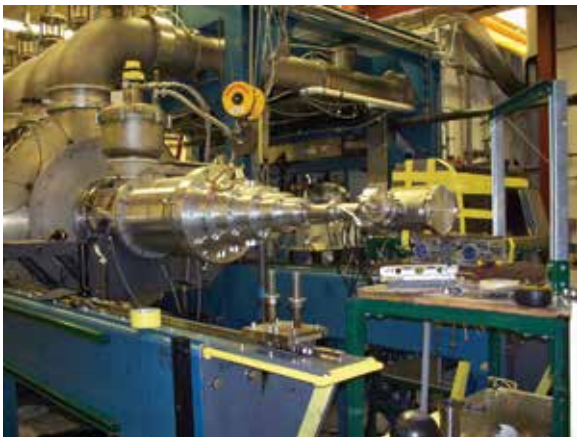
The Large Area Plasma Processing System (LAPPS) generates ultra-low-temperature plasmas for studying the modification of energy sensitive materials such as polymers, graphene, and biologicals. Two atmospheric discharge systems are used to study plasma processing and synthesis, plasma biology, and plasma aerodynamics.



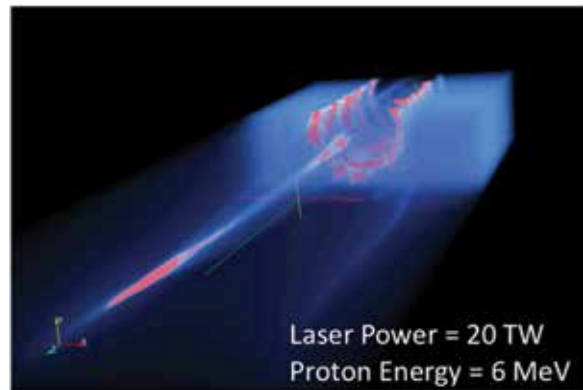
The Materials Testing Facility railgun studies the physics and material science of electromagnetic launch.



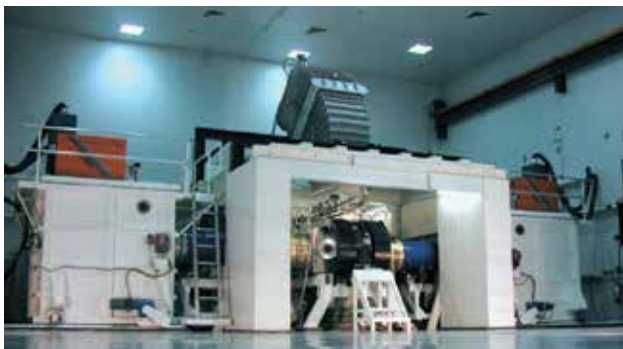
The Large Area Plasma Processing System (LAPPS) is used to develop, characterize, and study plasma-based processing of energy sensitive materials.



Tapered front-end of Mercury accelerator (6 MV, 360 kA, 50 ns) for dual-axis down-hole radiography.



TURBOWAVE simulation proton acceleration from a hydrogen gas target driven by an ultrashort pulse laser.



Electro-repetitive electron beam facility, used to investigate inertial fusion energy, materials modification, waste remediation, and biofuel production.

Electronics Science and Technology



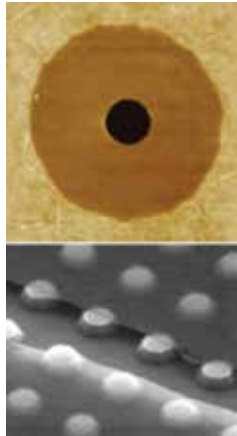
The Electronics Science and Technology Division's Advanced Silicon Carbide Epitaxial Research Laboratory (ASCERL).

The Electronics Science and Technology Division conducts a multidisciplinary basic and applied research program in solid-state electronics; electronic materials including growth, theory, and characterization of semiconductors and heterostructures; surface and interface science; microwave and millimeter-wave components and techniques; microelectronic device research and fabrication; nanoelectronics science and technologies; vacuum electronics; power electronics; photovoltaics and optoelectronics; and modeling and simulation.

The Division operates 13 major facilities: Ultrafast Laser Facility (ULF), Solar Cell Characterization Laboratory (SCCL), Compound Semiconductor Processing Facility (CSPF), Laboratory for Advanced Materials Synthesis (LAMS), Center for Advanced Materials Epitaxial Growth and Characterization (Epicenter), Ultra-Violet Photolithography Laboratory for Submillimeter-Wave Devices (UV-PL), Millimeter-Wave Vacuum Electronics Fabrication Facility (MWVEFF), Advanced Silicon Carbide Epitaxial Research Laboratory (ASCERL), Optoelectronic Scanning Electron

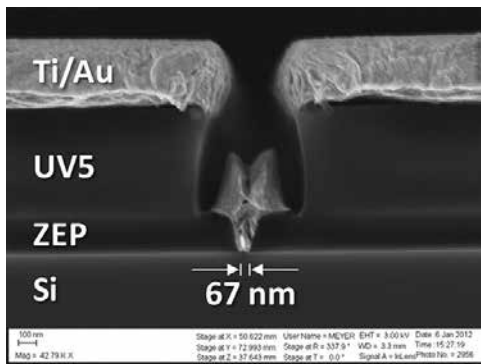
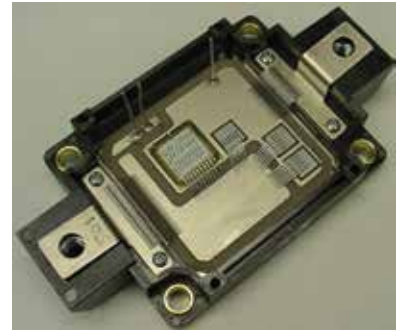
Characterization Facility (OSECF), Infrared Materials and Detectors Characterization Laboratory (IR Characterization Lab), Atomic Layer Deposition System (ALD), Atomic Layer Epitaxy System, and High Pressure Multi-Anvil System (HPMAS).

The CSPF processes compound semiconductor structures on a service basis, especially if advanced fabrication equipment such as electron beam lithography for reactive ion etching is required. But most fabrication can be hands-on by NRL scientists to assure personal process control and history. The LAMS uses metallorganic chemical vapor deposition to synthesize a wide range of thin films, particularly wide bandgap semiconductors such as gallium nitride (GaN) and related alloys. The Epicenter (a joint activity of the Electronics Science and Technology, Materials Science and Technology, Optical Sciences, and Chemistry Divisions) is dedicated to the growth of multilayer nanostructures by molecular beam epitaxy (MBE). Current research involves the growth and etching of conventional III-V semiconductors, ferromagnetic semiconductor materials, 6.1 Å III-V semiconductors, and II-VI semiconductors. The structures grown in this facility are analyzed via in situ scanning tunneling microscopy and angle-resolved electron microscopy. The ASCERL is the focal point of NRL efforts to develop thin-film heterostructure materials needed for high-voltage, high-power silicon carbide

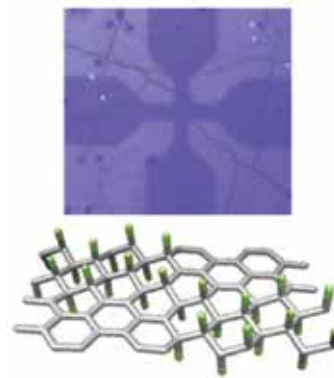


Graphene's high strength (equal to diamond) and low mass are well suited for NEMS sensors and applications. ESTD researchers are developing techniques to broadly engineer mechanical properties of graphene films such as strength, tension, resilience, and quality factors. These materials are being further developed for mass sensors, switches, and filters for RF communications. To date, ESTD researchers have demonstrated state-of-the-art frequency tunability (>500%) and quality factors (Q~30,000) for graphene-based nanomechanical resonators.

ESTD has developed very efficient medium voltage power modules by replacing the traditional Si freewheeling diode with SiC Schottky diodes. The SiC Junction Barrier Schottky (JBS) diodes were rated for 4500 V and replaced the very lossy Si PiN diodes. The combination of SiC diodes and the silicon Insulating Gate Bipolar Transistors (IGBT) demonstrated a factor of 7 reduction in turn-on losses and overall better than a factor of 2 in total power dissipation (switching and conduction losses). The SiC JBS diodes have proven extremely reliable and are expected to be commercialized in the near future.



Scanning electron microscope cross section of a metallized UV5/ZEP resist profile patterned using electron beam lithography. By using a thermal reflow process, T-gates can be fabricated with gate lengths below 30 nm, enabling transistor operation at frequencies greater than 400 GHz.



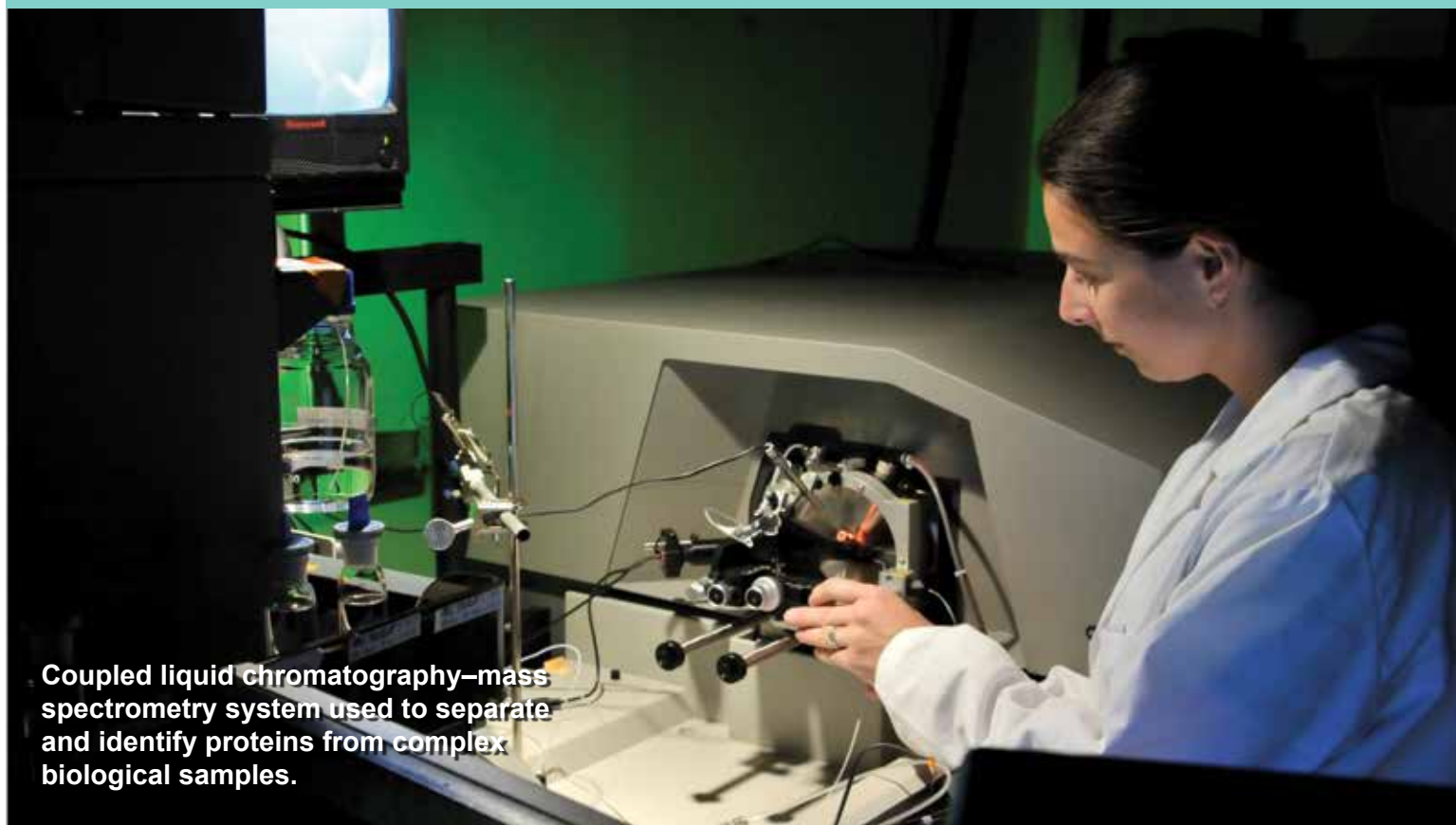
While graphene's intrinsic properties are unsurpassed, specific applications require modifying its nature. ESTD researchers have discovered and studied new fluorinated graphene derivatives with ideal conjugate properties to graphene; it is highly insulating, transparent, and chemically active. Such fluorographene materials are finding their way into nanoelectronic

and sensing applications. ESTD researchers have utilized this idea of fluorine functionalization in the formation of novel graphene nanoribbons, biosensors, and RF transistors.

(SiC) power electronic components in future naval systems. ASCERL uses an EPIGRESS reactor capable of growing thick, low-defect, ultra-high-purity SiC epitaxial layers. The SCCL studies new and emerging solar cell technologies for tactical applications including terrestrial and space environments. The ULF is optimized for the characterization of photophysical and photochemical processes on a timescale of tens of femtoseconds. It includes a synchronously pumped dye laser system for simulating the effects of charge deposited in semiconductors characteristic of space radiation. The UV-PL and MWVEFF are key laboratories for developing precision, all-metal structures for electron optics, electron beam-wave interaction (e.g., amplifiers and oscillators), and passive electromagnetic devices. The UV-PL uses lithographic techniques

and chemical electroforming to create high height-to-width aspect ratio structures (up to 10:1) with feature sizes as small as 5 μm . These dimensions are compatible with devices that can produce coherent electromagnetic radiation at submillimeter wavelengths. The MWVEFF contains a computer numerically controlled (CNC) milling machine and a CNC precision lathe capable of fabricating intricate millimeter-wave vacuum electronic components and a wire electric discharge machining (EDM) tool for fabrication of millimeter-wave and submillimeter-wave components that cannot be fabricated by conventional rotary cutting tools. EDM offers a noncontact process for both hard and soft metals as well as SiC and doped silicon.

Center for Bio/Molecular Science and Engineering



Coupled liquid chromatography–mass spectrometry system used to separate and identify proteins from complex biological samples.

The Center for Bio/Molecular Science and Engineering conducts cross-disciplinary, bio-inspired research and development to address problems relevant to the Navy and the DoD by exploiting biology's well-known ability for developing effective materials and sensing systems. The primary goal is to translate cutting-edge, bio-based discoveries into useful materials, sensors, and prototypes that can be scaled up, are robust, and lead to enhanced capabilities in the field. The challenges include identifying biological approaches with the greatest potential to solve Navy problems and provide new capabilities while focusing on bio-inspired solutions to problems that have not otherwise been solved by conventional means.

Studies involve biomaterial development for chemical/biological warfare defense, structural and functional applications, and environmental quality/cleanup. Program areas include optical biosensors, nanoscale manipulations, genomics and proteomics, bio/molecular and cellular arrays, surface modification,

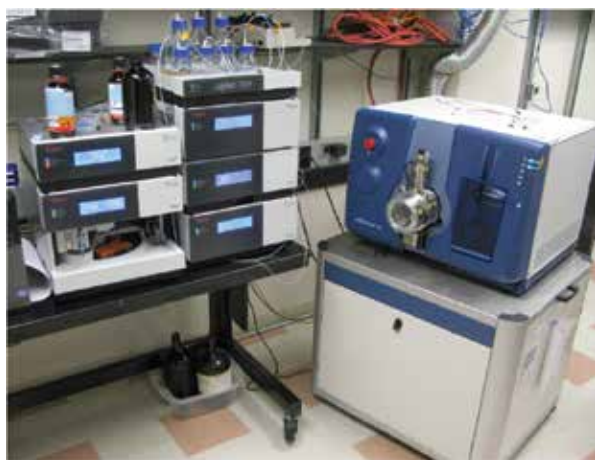
energy harvesting, systems biology, viral particles as scaffolds, and bioorganic materials from self-assembly.

The staff of the Center is an interdisciplinary team with expertise in biochemistry, surface chemistry, biophysics, molecular and cell biology, organic synthesis, materials science, and engineering. The Center also collaborates throughout NRL and with other government laboratories, universities, and industry.

The Center's modern facilities include laboratories for research in chemistry, biochemistry, systems biology, and physics. Specialized areas include controlled-access laboratories for cell culture and molecular biology, an electron microscope facility, a scanning probe microscope laboratory, instrument rooms with access to a variety of spectrophotometers, a multichannel surface plasmon resonance (SPR) sensor, and an optical microscope facility including polarization, fluorescence, and confocal microscopes. Additional laboratories accommodate nuclear magnetic resonance (NMR) spectroscopy, liquid chromatography–mass spectrometry (LCMS), and fabrication of microfluidic and micro-optical systems in polymers. The Center maintains a state-of-the-art X-ray diffraction system including a MicroSTAR-H X-ray generator. In com-

bination with new detectors and components, the system is ideal for data collection on proteins or very small single crystals of organic compounds and is also capable of collecting data on films and powders. Core facilities have been established for fluorescence activated cell sorting (FACS), micro-array analysis, next generation sequencing, circular dichroism (CD) spectroscopy, and 3D printing and rapid prototyping. The Center has recently installed an analytical

ultracentrifuge to facilitate separation and characterization of proteins and protein complexes. The mass spectrometry (MS) facility was also enlarged to enable small molecule and proteomic analyses of biological, environmental, and clinical samples by offering state-of-the-art instrumentation and proteomics expertise in preparing, analyzing and bioinformatic interpretation of experimental data and manual interpretation of MS/MS spectra.



AB SCIEX QTRAP 5500 hybrid triple-quadrupole mass spectrometer coupled with a Dionex UltiMate 3000 liquid chromatography system.



Prototyping facility 3D printer for rapid production of scale models or custom parts.



Applied Biosystems QSTAR Elite mass spectrometer coupled with a Tempo Nano Multi-Dimensional Liquid Chromatography (MDLC) System.

Acoustics

NRL's "Reliant" unmanned undersea vehicle with towed acoustic array being deployed during a long range active acoustics experiment.



The Acoustics Division's research program spans the domains of quantum and classical physics. It addresses spatial scales from nanometers to hundreds of kilometers and temporal scales from less than microseconds to the seasonal and long-term variability of the oceans. The Division's research topics include the following:

(1) The study of the impact of riverine, ocean, and atmospheric fluid dynamics on the phase coherent properties of acoustic signals with the objective of predicting the performance variability of acoustic systems including autonomous unmanned underwater systems and their underwater acoustic communications networks;

(2) The continued development, expansion, and adaptation of full physics underwater acoustic propagation and scattering theories. The use of numerical

simulations to estimate the uncertainty in acoustic field propagation simulations that is caused by limited spatial and temporal sampling of the initialization and updating sound speed fields;

(3) The measurement and theoretical description of the spatial/temporal variability of the deterministic/statistical properties of acoustic signals scattered from marine organisms, the near-surface ocean volume, the air-sea interface and the sea bottom/ subbottom with the objective of reducing the impact of non-target acoustic signal clutter on naval mine countermeasures and antisubmarine warfare system performance;

(4) The prediction and measurement of the angle and frequency dependence of acoustic signals scattered and radiated by complex three-dimensional structures with application to advanced manned and unmanned mine countermeasures and antisubmarine warfare detection concepts;

(5) The design from first principles of microelectromechanical and nanotechnology-based structures (e.g., metamaterials and sensors) that have unique sound

transmission, reflection, and transduction properties.

The experimental and computational components of the Division's research program require the utilization of high-performance computers, the NRL Institute for Nanoscience experimental facilities, the University National Oceanographic Laboratory System's ships and measurement systems, and the design and use of state-of-the-art laboratory, underwater, and atmospheric research instrumentation.

At-Sea Research: The Division uses autonomous unmanned vehicles, fixed autonomous moorings, and measurement systems attached to ships. Undersea acoustic propagation and ambient noise measurements are made with a fully autonomous moored acoustic data acquisition suite composed of two 80 m, 32-channel vertical hydrophone arrays, two 600 m, 96-channel horizontal hydrophone arrays, and two 50% duty cycle programmable acoustic sources operating at center frequencies of 300 and 500 Hz. Data are acquired by two 32-channel and one 96-channel recording systems that continuously acquire 24-bit data for a minimum of 30 days.

Ship-attached instruments are used to investigate the four-dimensional properties of acoustic signals scattered from the ocean's surface, bottom, and volume. They include two flex-tensional XF-4 and one ITC 2077 sound sources; a towable, vertically directional source array operating in the 1.5 to 9.5 kHz frequency band and a 64-channel broadband (500 to 3500 Hz) time reversal source-receiver array.

A 53 cm diameter Bluefin autonomous underwater vehicle (AUV) is used to test autonomous unmanned mine countermeasures, antisubmarine warfare concepts, and autonomous vehicle control algorithms designed to function in environments with unanticipated events. Underwater acoustic communications network research defines future network capacity by deploying programmable modems, two Iver-2 58 in. expandable AUVs, and two 8-channel moored/towed remotely controlled acoustic communications data acquisition modems in a variety of topologies.

Laboratory Facilities: The Acoustics Division has several nationally unique laboratory facilities. The Laboratory for Structural Acoustics supports experimental research where acoustic radiation, scattering, and surface vibration measurements of fluid-loaded and non-fluid-loaded structures are performed. A 3.7-million-liter, in-ground pool facility (17 m dia. \times 15 m deep) has vibration and temperature control, anechoic interior walls, and automated three-dimensional scattering cross section measurement capabilities. Instrumentation includes compact range scatter-

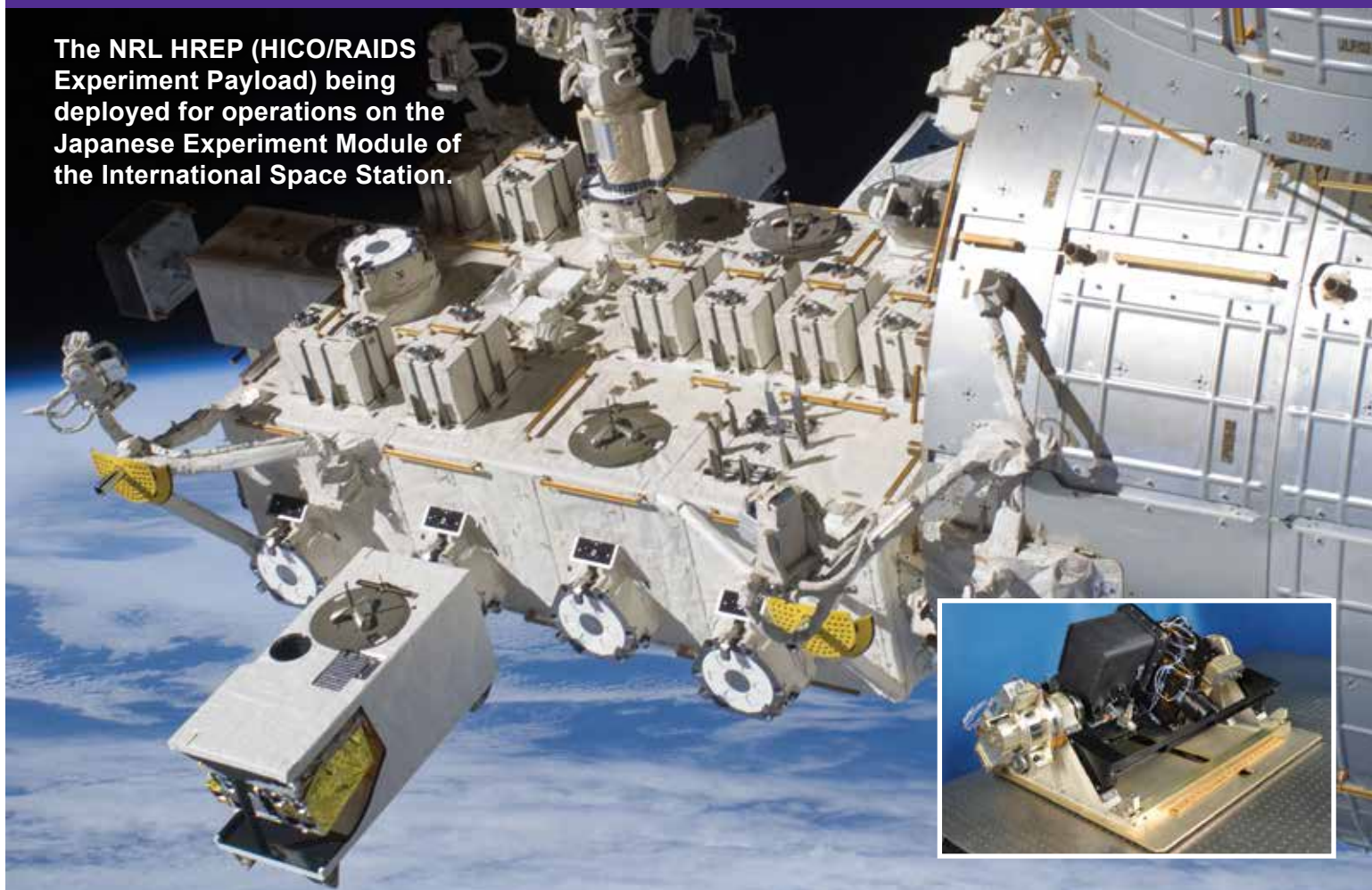
ing, nearfield holography, and scanning laser Doppler vibrometry capabilities. Ultra-high-precision measurements are conducted in this pristine laboratory environment using submarine hull backing impedance simulators, torpedoes, scale-model submarine structures, and deactivated mine targets. A large acoustically treated in-air measurement facility (50 \times 40 ft and 38 ft high) is used for structural acoustic and vibration measurements on satellite payload fairings, active and passive material systems for sound control, and new transducer and sensor systems. It is instrumented with robotic scanners capable of generating nearfield acoustic holography (NAH) radiation, reflection, and transmission databases. Marine sediments are replicated in tanks to study the impact of sediment burial on the structural response of mines or improvised explosive devices. In addition, a salt water tank (6 m \times 6 m \times 3.5 m) facility is designed to study a variety of physical phenomena under both saline and non-saline conditions. These include air-sea interface and subsurface bubble acoustic signal absorption and scatter studies; the characterization of sound generated by laser pulses; and the effectiveness of acoustic metamaterials. A sonomagnetic measurement facility is equipped with a vibration-insulating optical table constructed from nonmagnetic materials and a single three-axis magnetometer capable of measuring fields up to ± 100 μ T with a 1 nT noise floor at 1 kHz. An ultrasonic measurements laboratory is used for small-scale acoustics experiments designed to measure the effectiveness of acoustic metamaterials. Two 1.2 m cubic water tanks are equipped with overhead X-Y-Z positioning systems and LabVIEW-based data acquisition systems. A fabrication workshop equipped with a Haas Mini-Mill and an Objet Connex 500 3D rapid prototyping machine support the laboratory research facilities.



Proteus LDUUV being launched. The Acoustics Division is developing technology for, and recently completed measurements with the Columbia Group vehicle.

Remote Sensing

The NRL HREP (HICO/RAIDS Experiment Payload) being deployed for operations on the Japanese Experiment Module of the International Space Station.



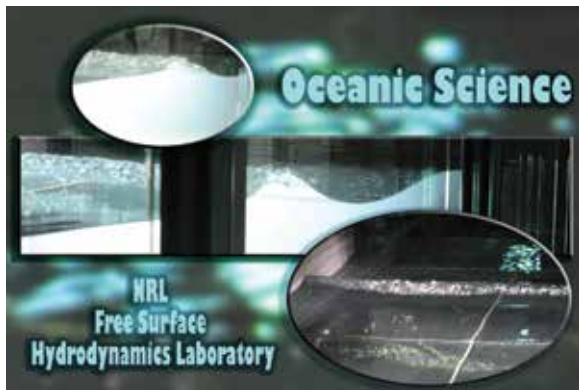
The Remote Sensing Division is the Navy's center of excellence for remote sensing research and development, conducting a broad program of basic and applied research across the full electromagnetic spectrum using active and passive techniques from ground-, air-, and space-based platforms. Current applications include Earth, ocean, atmospheric, astronomy, astrometry, and astrophysical science, and surveillance/reconnaissance activities including maritime domain awareness, antisubmarine warfare, and mine warfare. Special emphasis is given to developing space-based platforms and exploiting existing space systems.

Research in ocean and earth science includes maritime hyperspectral imaging, radar measurements of the ocean surface for the remote sensing of waves and currents, model- and laboratory-based hydrodynamics, and land-based trafficability studies.

Current airborne sensors used for characterization of the littoral environment include visible/near-IR (VNIR) and shortwave IR hyperspectral imagers, a VNIR multichannel polarimetric imager, a non-imaging VNIR polarimetric spectrometer, longwave and midwave IR thermal cameras, and an X-band, 2-channel interferometric synthetic aperture radar. As an outgrowth of our airborne sensing program, the Division developed the Hyperspectral Imager for the Coastal Ocean (HICO), the world's first spaceborne VNIR hyperspectral sensor specifically designed for coastal maritime environmental observations. HICO was launched to the International Space Station in September 2009 and is currently providing scientific imagery of varied coastal types worldwide. After a 3-year Navy mission, HICO is currently supported by NASA. Ground-based instruments for maritime sensing include the NRL Focused Phased Array Imaging Radar (NRL FOPAIR), an X-band, high-frame-rate polarimetric radar system. New research areas include the exploitation of polarized hyperspectral imaging, and active (lidar-based) sensing of the water column.

For radiometric and spectral calibration of the visible and IR imaging sensors, the Division operates a Calibration Facility that includes a NIST-traceable integrating sphere and a set of gas emission standards for wavelength calibration.

The Division's Free Surface Hydrodynamics Laboratory (FSHL) supports ocean remote sensing research. The lab consists of a 10 m wave tank equipped with a computer-controlled wave generator and a comprehensive set of diagnostic tools. Recent work focuses on the physics of breaking waves, their infrared signature,



Snapshots of breakers generated in the Free Surface Hydrodynamics Laboratory. At lower right, a wave traveling toward the viewer is seen breaking across the width (approx. 3 m) of the tank. In the upper images, waves traveling from left to right are breaking and forming surface turbulence.

and their role in producing aerosols. Experiments conducted in the FSHL are also used to test and validate numerical results and analytical theories dealing with the physics of the ocean's free surface.

Current atmospheric science research areas include the measurement of ocean surface winds and middle atmospheric research. NRL (in a collaboration between the Naval Center for Space Technology and the Remote Sensing Division) developed the first spaceborne polarimetric microwave radiometer, WindSat, launched in January 2003 and still operational. Its primary mission was to demonstrate the capability to remotely sense the ocean surface wind vector with a passive system. WindSat provides major risk reduction for development of the microwave imager for the next-generation DoD operational environmental satellite program. WindSat data are processed at the Navy Fleet Numerical Meteorology and Oceanography Center (FNMOC), and operationally assimilated into the Navy's global weather model, as well as that of several civilian weather agencies worldwide. In addition, the Remote Sensing Division is exploiting WindSat's

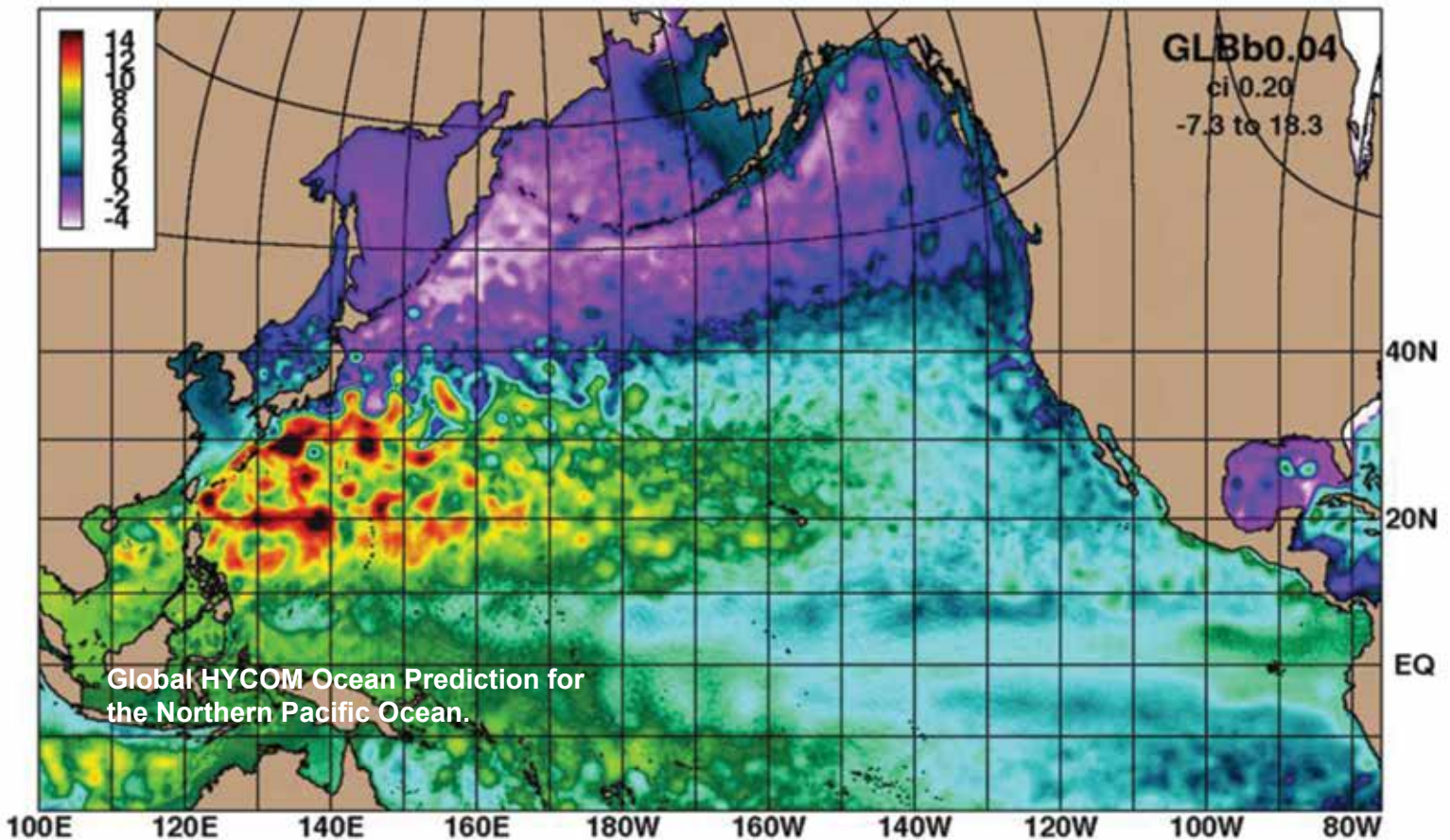
unique data set for other environmental parameters such as sea surface temperature, soil moisture, and sea ice concentration.

The Division also carries out a vigorous research program in the remote sensing of middle atmosphere constituents by ground-based millimeter-wave spectroscopy. The centerpiece of that program is the Water Vapor Millimeter-wave Spectrometer (WVMS). It is part of the international ground-based Network for Detection of Atmospheric Composition Change (NDACC), with sensors based in Lauder, New Zealand, Mauna Loa, Hawaii, and Table Mountain, California. Recently, measurements of chlorine monoxide and ozone have been added as part of a collaboration with the University of Massachusetts and the New Zealand National Institute for Water and Atmospheric Research.

The Division has research programs in astronomy and astrophysics ranging in wavelength from the optical to longwave radio (HF), with an emphasis on interferometric imaging. Facilities include the Navy Precision Optical Interferometer (NPOI), located near Flagstaff, Arizona, a joint project between the U.S. Naval Observatory and the NRL Remote Sensing Division. NPOI is used for optical astrometry, to investigate unfilled aperture imaging technologies, and to conduct astrophysical research. When completed, it will be the highest-resolution ground-based optical telescope in the world. The Division is also at the forefront of research in low-frequency (<100 MHz) radio astronomy and associated instrumentation and interferometric imaging techniques. The Division developed and installed VHF receivers on the National Radio Astronomy Observatory's Very Large Array (VLA), has designed the next-generation HF receiver system for the EVLA (Expanded VLA), and developed imaging techniques necessary to correct for ionospheric phase disturbances, important at HF frequencies. The Division is also collaborating with the University of New Mexico and New Mexico Tech on the Long Wavelength Array, a prototype, next-generation, HF imaging array ultimately with 200 to 300 km baselines.

The Division operates the NRL SEALAB (Sensor Exploitation Lab), which is the primary conduit of Division research to the operational community.

Oceanography



The Oceanography Division is the major center for in-house Navy research and development in oceanography. It is known nationally and internationally for its unique combination of theoretical, numerical, experimental, and remotely sensed approaches to oceanographic problems. The Division's modeling focus is on a truly integrated global-to-coastal modeling strategy, from deep water up to the coast including straits, harbors, bays, inlets, and rivers. This requires emphasis on both ocean circulation and wave/surf prediction, with additional focus on coupling the ocean models to atmospheric, biological, optical, and sediment models. This includes processing and analysis of satellite and in-water observations, development of numerical model systems, and assimilation for predicting the ocean environment. This modeling is conducted on the Navy's and DoD's most powerful vector and parallel processing machines. The Division's in-house Ocean Dynamics and Prediction Computational Network Facility provides computer services to scientists for program development, graphics, data pro-

cessing, storage, and backup. It also provides network connectivity to other Navy sites, to the DoD High Performance Computing centers, and to the Internet. The computational system enables leading-edge oceanographic numerical prediction research applicable to Navy operations affected by environmental variations at scales of meters to hundreds of kilometers and time scales of seconds to weeks. To study the results of this intense modeling effort, the Division operates a number of highly sophisticated graphic systems to visualize ocean and coastal dynamic processes. Problems addressed cover a wide scope of physics including parameterization of oceanic processes, construction and analysis of ocean models and forecast systems, basic and applied research of ocean dynamics, surface waves, thermohaline circulation, nearshore circulation, estuarine and riverine modeling, arctic ice modeling, internal waves, and ocean/atmosphere coupling. Additional emphasis is on optimization of underwater, airborne, and satellite observing systems, representation of ocean processes affecting temperature, salinity, and mixed-layer depth, uncertainty analysis in coupled systems, ensemble and probabilistic ocean forecasting,

targeting ocean observations, representing probability in ocean/acoustic systems, and satellite-observed surface heat fluxes. The end goal is to build cutting-edge technology systems that transition to operational forecast centers.

The Division's Ocean Sciences Branch conducts basic and applied research in ocean physics, air-sea interaction, ocean optics, and marine microbially influenced corrosion. Emphasis of this research is on understanding the oceans' physical processes and their interactions with the atmosphere and biological/chemical systems at scales ranging from basin-scale to microscale. Numerical and analytical models are developed and tested in laboratory and field experiments. The results of this research support the Navy's operational capability for predictions of oceanic atmospheric exchanges, acoustic propagation/detection, light transmission/emission, and influences of microbes on marine corrosion. The seagoing experimental programs of the Division range worldwide. Unique measurement systems include a wave measurement system to acquire in situ spatial properties of water waves; a salinity mapper that acquires images of spatial and temporal sea surface salinity variabilities in littoral regions; an integrated absorption cavity and optical profiler system, and towed optical hyperspectral array for studying

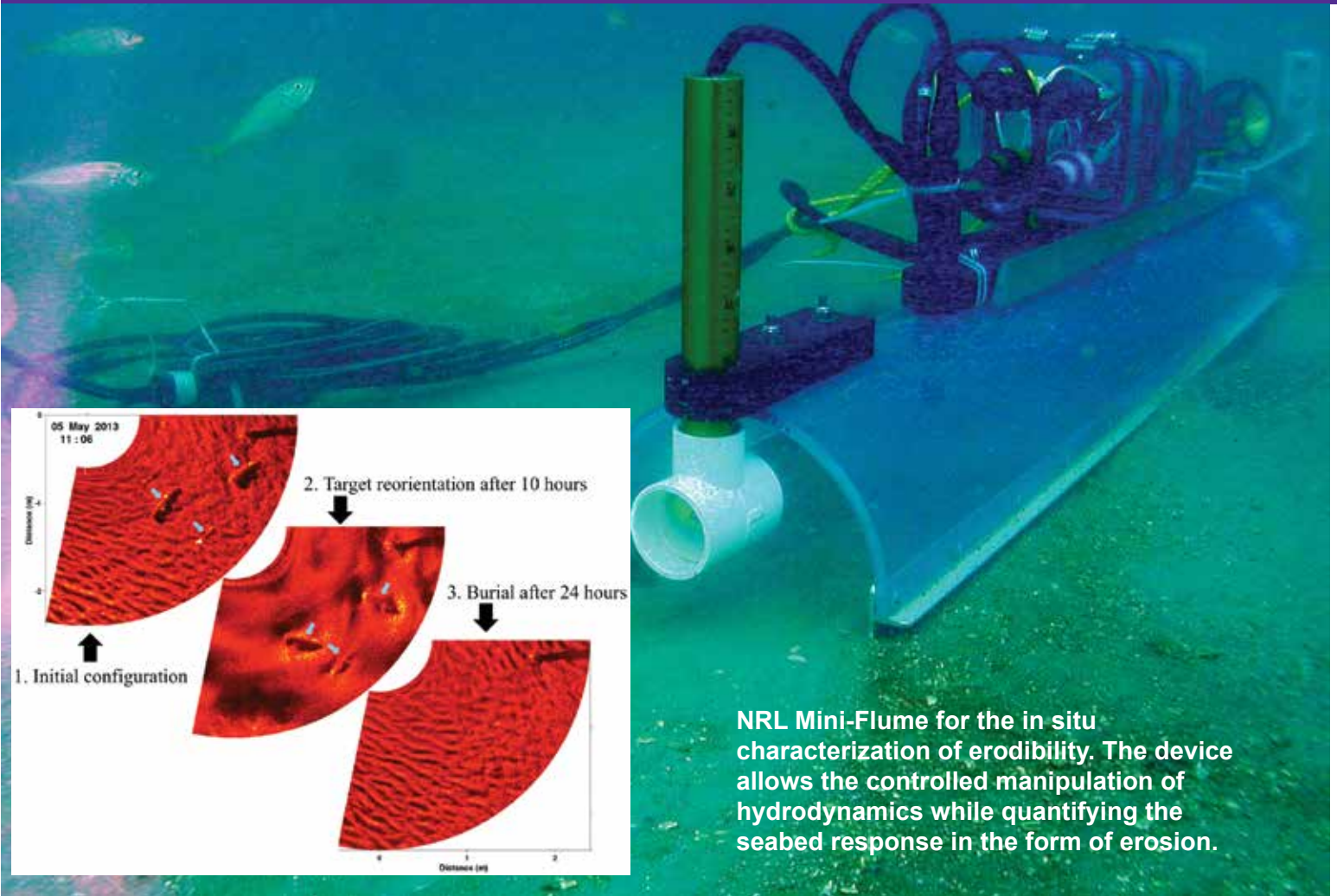
ocean optical characteristics; self-contained, bottom-mounted, upward-looking acoustic Doppler current profilers (ADCPs) for measuring ocean variability; and a Shallow water Environmental Profiler in Trawl-safe, Real-time configuration (SEPTR). A newly acquired Rayleigh Bernard Convective Tank and a Hybrid Underwater Camera support the Division's ocean optics programs providing object detection and identification in extremely turbid underwater environments. Instruments for sensing the littoral environment include a Vertical Microstructure Profiler (VMP), a Scanfish, and four Slocum Gliders.

The Division's remote sensing research focuses on radiative transfer theory, optical ocean instrumentation, lasers and underwater imaging and vision, satellite and aircraft remote sensing, remote sensing of bio-optical signatures, and coupled physical bio-optical modeling. The research includes applying aircraft and satellite ocean color and thermal infrared signatures for understanding the biogeochemical cycles in the surface ocean. Additional emphasis is on algorithm and model development using satellite and aircraft data (SeaWifs, MODIS, MERIS, AVHRR, VIIRS, OCM, GOCI, HICO, and CASI) to address the spatial and temporal variability of coastal optical properties.



Ice lead opening off the coast of Barrow, Alaska, as observed from aircraft in March 2013.

Marine Geosciences



NRL Mini-Flume for the in situ characterization of erodibility. The device allows the controlled manipulation of hydrodynamics while quantifying the seabed response in the form of erosion.

The Marine Geosciences Division is the major Navy in-house center for research and development in marine geology, geophysics, geodesy, geoacoustics, geotechnology, and geo-spatial information and systems, with its research focused in three thrust areas:

Characterization and Prediction in Seafloor and Terrestrial Regions. Research subthrusters: (1) The Division tested the foliage penetration of a prototype ultra-wideband, low-frequency synthetic aperture radar (SAR) in the jungles of Papua New Guinea, successfully finding WWII aircraft wreckage and aircrew remains. (2) In collaboration with Remote Sensing and Oceanography division scientists, research continued to understand the changing Arctic environment, utilizing a prototype airborne SAR, light detection and ranging (lidar), and snow radar instrument suite to calibrate

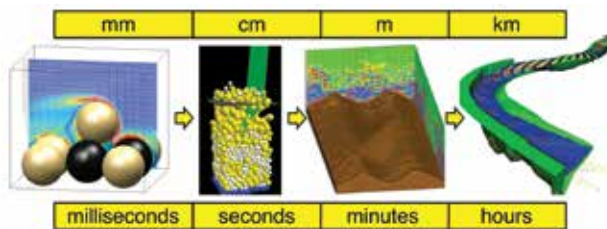
CryoSat2 satellite-derived snow and ice measurements and the Navy's ice-ocean coupled numerical model. (3) As part of the Carbon Flux Project, recently acquired data from the Bering Sea have been analyzed with seismic waveform inversion techniques to quantify gas and gas hydrate in the deep-water Aleutian Basin. Each of the large super chimneys in the area is estimated to hold 0.01 to 0.014 gigatons of carbon (GtC) in the form of methane. There are as many as 1000 super chimneys, holding as much as 14 GtC; by comparison, the atmosphere holds 3.8 GtC as methane.

Dynamic Littoral and Riverine Processes. Research subthrusters: (1) The Division continued its modeling of sediment transport phenomena that spans many orders of magnitude, from the discrete particle scale (in which individual sand grains are simulated) to the continuum scale (in which the flow of rivers is resolved). Modeling the relevant physics of the problem at each scale and identifying links between the adjacent scales is crucial

to developing the operational forecasts needed by Navy warfighters. (2) Development continued on a predictive model for the mechanical strength and erodibility of soft, cohesive sediments by analyzing the physicochemical, micromechanical, and bulk mechanical responses of cohesive sediment constituents under controlled manipulation of variables including hydrodynamics, salinity, and organic matter speciation. (3) Researchers conducted a series of field experiments funded by ONR and CNMOC to assess sensing technologies for the tactical identification of littoral and riverine navigational hazards, flow velocity, water surface level, bathymetry, and other environmental conditions. The various sensing approaches investigated included acoustic Doppler current profilers, single-beam and multibeam sonars, inexpensive GPS-based drifters, UUV-based sampling, and UAV-imagery processing and analysis. (4) Division scientists developed a modified constitutive law for shear strain dependence upon the strength of soft clays and muds applicable to a wide range of strain rates, including extension to the never before modeled high strain-rate region. (5) Marine biogeochemists studied the impact of hypoxic zones in the Gulf of Mexico on benthic communities and on surficial sediment characteristics.

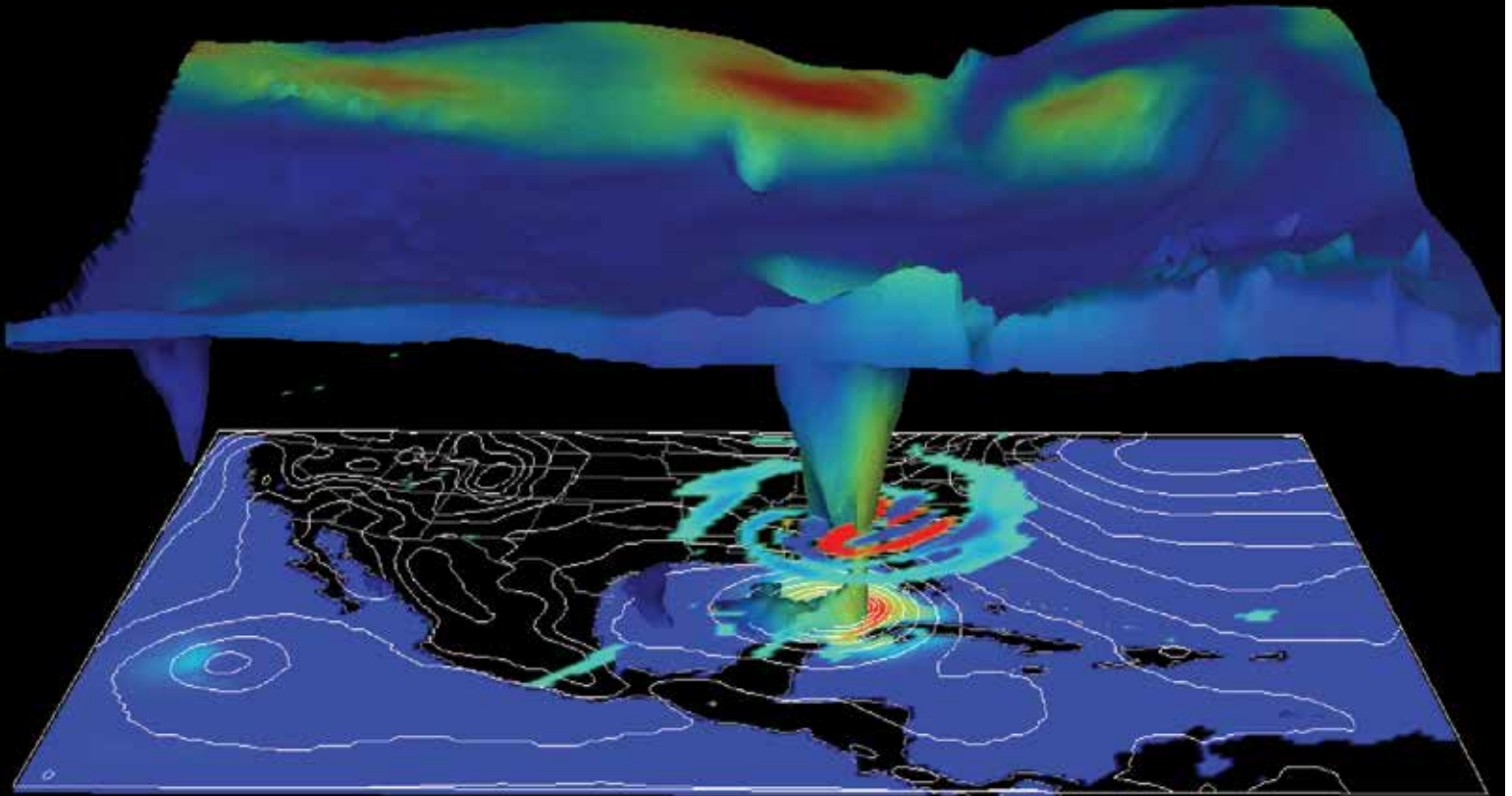
Geospatial Sciences and Technology. Research sub-thrusts: (1) As the Navy's leading science authority on hydrography, the Division continued a multiyear effort to develop a production capability for tactical bathymetry products by combining different sources of data, and incorporate uncertainty to bathymetry soundings and multispectral derived bathymetry to provide the warfighter a better understanding of potentially questionable data sources. Additional work includes a new 6.1 program to develop uncertainty analysis for areas where survey data is scarce, and a Rapid Transition Project for the Oceanographer of the Navy to develop methods for reducing Navy digital database sizes through the use of depth and uncertainty constrained right triangulated integrated networks. (2) The Division continued development of the Geospatial Area Folders concept

which provides the ability to rapidly create geospatially enabled intelligence products from multisource intelligence data, reducing regional headquarters production timelines by 80% to deliver actionable intelligence to the warfighter. Seven Mine Warfare Area Folder (MWAFF) systems were transitioned into operational use, with system delivery and training being provided to CTF 52 in Bahrain, MCMRON 7 in Japan, and operational headquarters in the United States. A new version of the Hydrographic Mission Planner was delivered to NAVOCEANO, providing a geospatial decision making toolset used to analyze survey tasking and schedule survey fleet resources. (3) NRL computer scientists developed and hosted advanced geospatial services for NGA, USMC, USA, and USAF. Geospatial Hub (GHub) is a content management system that provides an automatically synchronized, web-based means of organizing and distributing all types of geospatial information including imagery, maps, weather, and scientific data. NRL mapping systems have features not found in civilian systems, including patented, high-speed, data management technologies and support for an unlimited number of different data layers. (4) The Automated Bottom Feature Navigator was transitioned to the Naval Oceanographic Office, enabling AUV positioning accuracy within 10 m by identifying stationary seafloor objects with onboard sidescan sonar systems, eliminating the need for external positioning systems and infrastructure. (5) Scientists delivered Environmental Post Mission Analysis software for use in the Littoral Combat Ship Mine Countermeasures Mission Module, utilizing on-scene data collections to update environmental databases and reduce timelines for detecting mine-like changes on the seabed. (6) The Division continued its long-term support of Naval Aviation and the Joint Mission Planning System (JMPS), integrating the ability to process and tailor mission-specific, in situ data and ocean bathymetry for cockpit display in MH-60 R/S helicopters supporting antisubmarine warfare missions.



In the Marine Geosciences Division, scientists model sediment transport phenomena that span many orders of magnitude, from the discrete particle scale (far left) where individual grains are simulated, up to the continuum scale (far right) where the flow in rivers is resolved. The goal is to develop reliable forecasting models for operational length and time scales. Consequently, we must simulate the relevant physics of the problem at each scale and identify links between adjacent scales (arrows). Pictures from left to right: a fully resolved simulation of the entrainment of an individual particle into a turbulent boundary layer; simulation of sheet flow transport using a discrete particle model; simulation of sand ripple evolution using mixture theory (SedMix3D); and simulation of flow in a reach of the Kootenai River, Idaho.

Marine Meteorology



3D depiction of Hurricane Katrina 2005 by NRL's high-resolution operational mesoscale model, COAMPS®-TC (Coupled Ocean/Atmosphere Mesoscale Prediction System–Tropical Cyclone).

The Marine Meteorology Division, located in Monterey, California, conducts basic and applied research in atmospheric sciences. The Division develops meteorological analysis and prediction systems and other products to support Navy, DoD, and other customers operating at theater, operational, and tactical levels. The Division is collocated with the Fleet Numerical Meteorology and Oceanography Center (FNMOC), the Navy's operational production center for numerical weather prediction (NWP) and satellite imagery interpretation.

The Division's Earth System Prediction Capability Laboratory is built around multiple LINUX clusters supported by approximately 3000 TB of RAID storage and a tape library capable of expansion to over 10 PB. The Division also maintains nearly 100 LINUX servers,

including a unique Global Ocean Data Assimilation Experiment (GODAE) server hosting data sets suitable for research and development of ocean and atmospheric data assimilation capabilities. In 2012, the DoD HPC Modernization Office (HPCMO) Dedicated HPC Project Investment (DHPI) awarded the Division a Cray XE6m supercomputer consisting of 5376 computer cores, 10.5 terabytes of memory with 54 teraflops of peak performance. These systems, in combination with offsite DoD Supercomputing Resource Centers (DSRC) and FNMOC assets, enable the Division to efficiently develop, improve, and transition numerical weather analysis and prediction systems and coupled air/ocean/ice systems for operational use, producing unique, tailored guidance that is used by Fleet forces around the globe. These systems also support basic research and are used to conduct real-time demonstrations in atmospheric processes such as air-sea-ice interaction, atmospheric dynamics, and cloud/aerosol physics, as well as development of environmental

applications, decision aids, and probabilistic prediction products.

The Division's state-of-the-art Satellite Data Processing Laboratory allows the direct downlink of real-time NOAA geostationary (GEO) digital data (GOES-WEST/EAST) and data relays from four other geostationary satellites that permit global coverage at 30 minute intervals. Data from numerous low Earth orbiting (LEO) satellite sensors are also received in near real time via collaborative interagency agreements, most recently including the NPP Visible Imager Radiometer Suite (VIIRS). NRL-Monterey processes digital satellite data from 32 LEO sensors and six GEO platforms to conduct research and development of multisensor data fusion products to support a variety of scientific endeavors and DoD organizations. A LINUX cluster with approximately 1 teraflop of computing power is incorporated to process 1.5 TB/day and output nearly 100,000 jpeg images and even more kml Google Earth files each day. These enable NRL to actively engage the scientific and operational user community on activities such as monitoring tropical cyclone characteristics, cloud properties, rain, and ocean surface vector winds; and detecting hazardous weather conditions such as airborne dust and volcanic plumes. These products directly support of overseas combat operations.

The Mobile Atmospheric Aerosol and Radiation Characterization Observatories (MAARCOs) are mobile instrumentation suites that can be housed in a pair of climate-controlled mobile laboratories

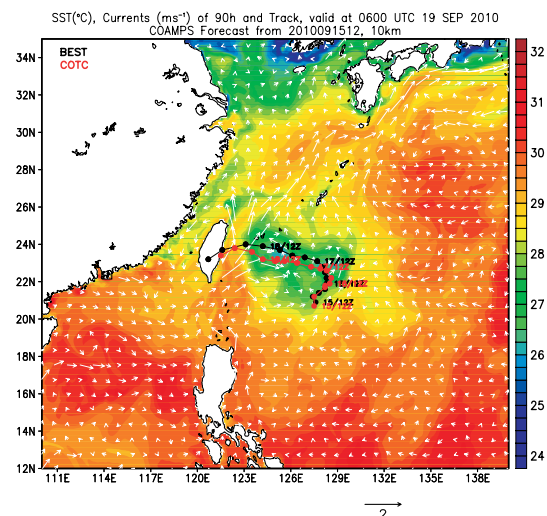


MAARCO is designed as a stand-alone suite for basic atmospheric research and the collection of data to assist in validating aerosol and weather models. Its purpose is to enable research on atmospheric aerosols, gases, and radiation (visible and IR light) in areas of key interest, including remote areas, overseas locales, and aboard ships and aircraft. MAARCO can also be deployed as mobile laboratories in areas with limited facilities, thereby providing maximum flexibility for integration of additional instrumentation.

consisting of modified shipping containers with integrated suites of meteorological, aerosol, gas, and radiation instruments for atmospheric characterization. MAARCOs can be deployed as mobile laboratories, in host laboratory facilities, or on aircraft and ships. They are designed to operate in strategic areas around the globe with the mobile lab providing flexibility to deploy in remote regions. When mounted on aircraft, the instruments are used to investigate boundary layer meteorology, aerosol microphysics, aerosol and cloud radiative properties, and electro-optical propagation.

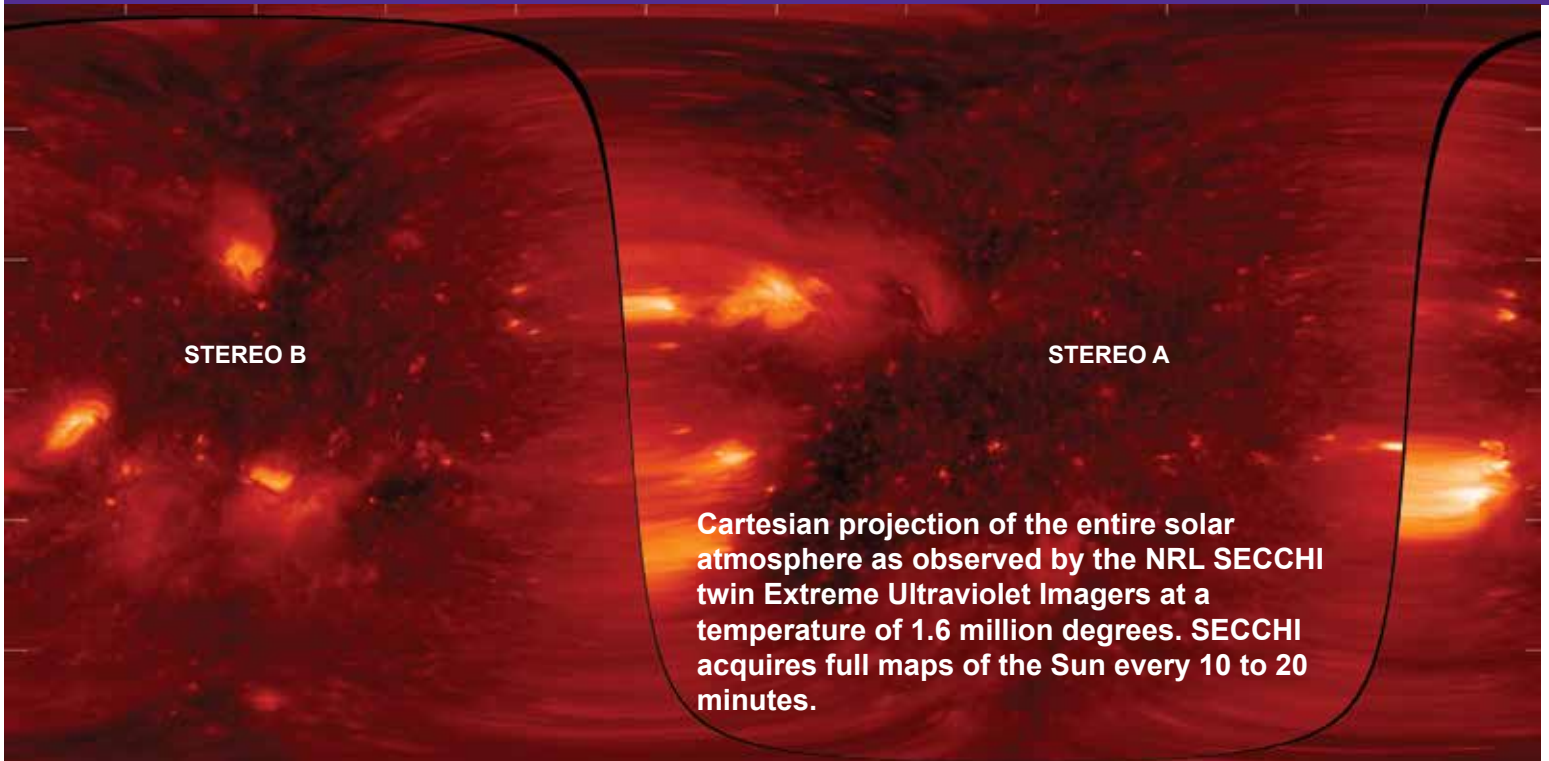


NRL's Marine Meteorology Division processes satellite data from 32 LEO sensors and six geostationary platforms and uses that data to conduct research and development of multisensor data fusion products to support a variety of DoD missions.



The sea surface temperature (shaded, in °C) and surface currents (vectors, ms^{-1}) at 90 hr of the coupled COAMPS®-TC forecast starting at 1200 UTC 15 Sept. 2010, overlaid with the model track (red dots) and the BEST track (black dots).

Space Science



STEREO B

STEREO A

Cartesian projection of the entire solar atmosphere as observed by the NRL SECCHI twin Extreme Ultraviolet Imagers at a temperature of 1.6 million degrees. SECCHI acquires full maps of the Sun every 10 to 20 minutes.

The Space Science Division conducts a broad-spectrum RDT&E program in solar-terrestrial physics, astrophysics, upper/middle atmospheric science, and astronomy. Division researchers conceive, plan, and execute scientific research and development programs and transition the results to operational use. They develop instruments to be flown on satellites, sounding rockets, and balloons; and ground-based facilities and mathematical models. The Division's primary objective is to perform foundational discovery research to ensure Navy and Marine Corps access to critical space capabilities and space force enhancement capabilities on the ground, at sea, and in a contested space environment.

The Division's Vacuum Ultraviolet Solar Instrument Test (SIT) facility is an ultra-clean solar instrument test facility designed to satisfy the rigorous contamination requirements of state-of-the-art solar spaceflight instruments. The facility has a 400 ft² Class 10 clean room and a large Solar Coronagraph Optical Test Chamber (SCOTCH). The SIT clean room is ideally suited for assembly and test of contamination-sensitive spaceflight instrumentation. It contains a large vibration-isolated optical bench and a 1-ton capacity overhead crane. The SCOTCH consists of a

large vacuum tank and a precision instrument-pointing table. The Division also maintains extensive facilities for supporting ultraviolet (UV) spectroscopy sounding rocket programs. These facilities include a dedicated Class 1000 instrument clean room, and a gray room area for assembling and testing the rocket payloads that incorporates all of the fixtures required for safe handling of payloads. Further, the Division rocket facilities include a large UV optical test chamber that is additionally equipped with a large vibration- and thermal-isolated optical bench for telescope testing, which allows the laboratory area to be turned into a schlieren facility. The Division also has a unique facility for developing Doppler Asymmetric Spatial Heterodyne (DASH) thermospheric wind sensors, which are currently being developed in support of future space flight missions.

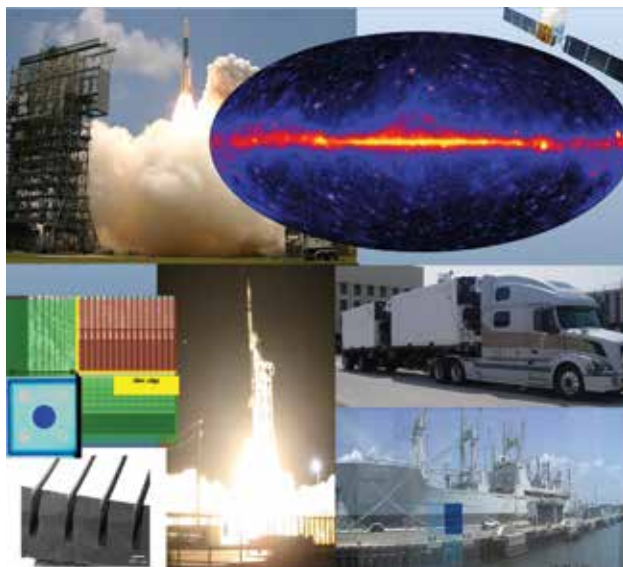
The Division has a wide range of new satellite, rocket, balloon, and ground-based instruments under development. These include the SoloHI heliospheric imager that will image both the quasi-steady flow and transient disturbances in the solar wind when aloft on board the Solar Orbiter mission; the Compact CORonagraph (CCOR), an elegant, externally occulted instrument that uses a single-stage optical design with two lens groups, a polarization analyzer, and a spectral filter to achieve performance comparable to the tra-

ditional three-stage Lyot coronagraph but with significantly lower mass and volume than the traditional design; and the NRL-led SuperMISTI detection system, intended to demonstrate standoff detection, identification and imaging of radiological/nuclear weapons of mass destruction (WMD) in maritime environments. A Division-led thermospheric wind instrument, the Michelson Interferometer for Global High-resolution Thermospheric Imaging (MIGHTI), is being developed for spaceflight onboard the ICON Explorer Mission.

Advanced space-based research is also currently being performed. Division experiments are measuring the Earth's thermosphere and ionosphere to improve space weather forecasting for these near-space atmospheric regions that significantly influence the performance of important operational systems such as GPS navigation, communication, and space debris tracking. The Special Sensor Ultraviolet Limb Imager (SSULI) developed by NRL's Space Science Division and Spacecraft Engineering Department offers a first-of-its-kind technique for remote sensing of the ionosphere and thermosphere from space. Flying on the U.S. Air Force Defense Meteorological Satellite Program (DMSP) satellites, SSULI's characterization of the Earth's upper atmosphere and ionosphere provides necessary scientific data to support military and civil systems. In August 2013, the Fermi Gamma ray Space Telescope, major portions of which were developed and tested by NRL's Space Science Division and Spacecraft Engineering Department, completed five years of successful

operation on orbit. Division scientists have had lead roles in several key scientific discoveries using Fermi, including: confirmation of the long-standing belief that shocks formed from exploding stars are the source of the high-energy cosmic rays seen at Earth; creation of a highly efficient means of discovering new pulsars, the rapidly rotating cores of dead stars that serve as precise astrophysical clocks; and discovery that our Sun accelerates particles to extreme energies even in relatively weak flares, and does so for hours after the impulsive event. Two Space Science Division-led heliophysics space instrument capabilities, the Large Angle Spectrometric and Coronagraphic Telescope (LASCO) on the SOHO Mission and the Sun-Earth Connection Coronal Heliospheric Investigation (SECCHI) on the STEREO Mission, are continuing to advance understanding of the solar corona and the importance of coronal mass ejections in determining space weather at Earth.

Division scientists, using the Division network of computers and workstations and other connected high performance computing assets, develop and maintain physical models in support of their research. These include research to extend the operational Navy Global Environmental Model (NAVGEM) from its current upper boundary to altitudes of ~100 km; and HiFi, a user-friendly, highly parallel, fully implicit adaptive spectral element code framework designed for model development, magnetohydrodynamics, and multifluid numerical modeling in two- and three-dimensional geometries.



NRL's major role in the Fermi Mission (launch 2008, upper left) has enabled broadly based astrophysical investigations including the gamma ray sky map (upper right) identifying over 1800 point sources and new insight into particle acceleration and radiations from pulsars, supernova remnants, active galactic nuclei and many other topics. Space science research in detector design enabled by NRL's Institute for Nanoscience has resulted in three pending patents relating to "slim edge" detectors (middle left) and charge control using atomic layer deposition and three patents on deep reactive ion etching of detectors (lower left). The J-PEX extreme-ultraviolet sounding rocket experiment (lower center) provided unprecedented spectral resolution on White Dwarf stars. Division research in radiological/nuclear weapons of mass destruction (WMD) detection resulted in the dual container SuperMISTI detection system (middle right, in transport to Norfolk maritime testing) providing standoff detection and imaging of WMD. Image (lower right) shows SuperMISTI image of radiation source (blue block) hidden in the hold of USS *Cape Chalmers*.

Space Systems Development Department

Space Systems Development Department Optical Test Facility transmits laser light at both 1064 nm and 1550 nm for both satellite laser ranging and free space optical communication signals.



The Space Systems Development Department (SSDD) is responsible for the end-to-end definition, design, development, integration, test, and operation of space systems that satisfy naval and national defense requirements.

The total system engineering philosophy employed by the SSDD enables seamless sensor-to-shooter capabilities to be deployed that optimize the interfaces between command and control, on-orbit satellite collection, and onboard and ground processing functions; the dissemination of data to tactical and national users; and the design of tools that provide for the automated correlation and fusion of collected information with other sources.

Research and development is conducted in the areas of space system architectures; advanced mission data processing and data analysis techniques; advanced

information systems concepts, including enterprise and cloud computing and networking of space, air, ground, and subsurface sensors; and mission simulation techniques. Intelligence collection, advanced RF, optical, and laser communication, satellite laser ranging, digital signal processing, data management, and space navigation systems are constantly improved upon to satisfy evolving requirements. These systems are engineered for maximum reuse and interoperability.

Having conceived of and developed the payload for the first Global Positioning System (GPS) satellite, the SSDD continues to be a center of excellence in the research and development of advanced GPS technology. Advanced theoretical and experimental investigations are applied to expanding the design and interoperability of systems used for a wide range of military, space, geodetic, and time dissemination applications. These investigations involve critical precise time generation and measurement technology for passive and

active ranging techniques incorporating advanced data transmission and signal design. Precise time and time interval research conducted involves theoretical and experimental development of atomic time/frequency standards, instrumentation, and timekeeping to support highly precise and accurate timescale systems in scientific and military use. Net-centric systems are critically dependent on highly accurate and stable time/frequency standards coordinated to a common timescale through the diverse dissemination comparison techniques developed within the SSDD.

The Precision Clock Evaluation Facility (PCEF) is one of the major facilities within NRL's Naval Center for Space Technology. The PCEF was developed to support development of high-precision clocks for GPS spacecraft and ground applications, primarily atomic standards. Space atomic clocks are evaluated, qualified, and acceptance tested for space flight using the assets of this facility. Testing performed includes long- and short-term performance evaluation, and environmental testing (including shock and vibration). Investigations of on-orbit anomalies are performed within the PCEF to attempt to duplicate similar effects in space-qualified hardware under controlled conditions. The facility was originally developed to evaluate developments in the Global Positioning System concept development program (Block I) and expanded for the

dedicated space clock development conducted during operational system development and deployment. The ability to evaluate and test highly precise atomic clocks, especially in a space environment, requires unique facilities, precise time and frequency references, and precise instrumentation not available anywhere else. The primary time and frequency reference for the PCEF is a specially designed environmental chamber housing a number of hydrogen masers combined with measurement equipment permitting a realization of Universal Coordinated Time (UTC) to be maintained as UTC (NRL) in cooperation with the International Bureau of Weights and Measures (BIPM) for reference and research purposes.

In addition to a wide array of test tools and facilities, the Department operates several field sites including the Midway Research Center satellite calibration facility in Stafford, Virginia; the Blossom Point Satellite Tracking and Command Facility in Welcome, Maryland; and the Chesapeake Bay Detachment Radar Range in Chesapeake Beach, Maryland.



The Naval Center for Space Technology's Precision Clock Evaluation Facility (PCEF).

Spacecraft Engineering Department

Lift-off of TacSat-4 — NRL's 100th satellite.



The Spacecraft Engineering Department (SED) and the Space Systems Development Department, together comprising NRL's Naval Center for Space Technology (NCST), cooperatively develop space systems to respond to Navy, DoD, and national mission requirements with improved performance, capacity, reliability, efficiency, and life cycle cost.

The SED facilities that support this work include integration and test highbays, large and small anechoic radio frequency chambers, varying levels of clean rooms, shock and vibration tables, an acoustic reverberation chamber, large and small thermal/vacuum test chambers, a thermal systems integration and test laboratory, a spin test facility, a static loads test facility, and a spacecraft robotics engineering and control system interaction laboratory.

Integration and Test Facilities: The department maintains a wide range of specialized RF chambers for test of antennas, receivers, transmitters, electronics,

and other flight systems. There are two main anechoic chambers whose main function is the test and verification of antennas and flight systems; the tapered chamber is 31 × 31 × 120 ft, with a 100 ft measurement distance; it is instrumented from 100 MHz to 18 GHz for radiation patterns, and is regularly used for electromagnetic interference (EMI) measurements as well. The rectangular chamber is 10 × 12 × 20 ft, with a 15 ft measurement distance, and is instrumented from 1 to 220 GHz. There is also a 3 × 3 ft millimeter-wave near-field scanner that is instrumented up to 220 GHz, but capable of measurements up to 550 GHz. All the measurement facilities are computer-controlled and fully automated, allowing multiple antennas and polarizations to be measured at the same time. A third RF chamber is dedicated to electromagnetic interference/radio frequency interference (EMI/RFI) testing. This welded steel chamber measures 23 × 23 × 20 ft and provides as much as 120 dB shielding effectiveness up to 18 GHz and 100 dB from 18 to 50 GHz. The chamber uses a hybrid anechoic material consisting of wideband pyramidal absorbers and ferrite tiles for performance from 20 MHz to 50 GHz. The EMI chamber is equipped with instrumentation to perform the full range

of MIL-STD-461 EMI qualification testing. A 10 ft high × 11 ft wide sliding bladder door allows easy access of large test items to the main chamber.

The Laminar Flow Clean Room provides a Class 100 ultraclean environment for the cleaning, assembly, and acceptance testing of contamination-sensitive spacecraft components, and integration of complete spacecraft subsystems. The facility is used primarily to support spacecraft propulsion systems but has been used to support all spacecraft electrical, electronic, and mechanical subsystems.

The Vibration Test Facility, which simulates the various vibration-loading environments present during flight operations and demonstrates compliance to design specifications, consists of the following shakers: Unholtz-Dickie T5000 50K Flb random 2-in. DA stroke, Ling 4022 30K Flb random 2-in. DA stroke, Ling 2022 16K Flb random 2-in. DA stroke, and a Ling 335 16K Flb random 1-in. DA stroke.

The Acoustic Reverberation Simulation Facility is a 10,000 ft³ reverberation chamber that simulates the acoustic environment that spacecraft will experience during launch. The maximum capable sound pressure level is approximately 152 dB.

The Thermal Fabrication and Test Facility supports the design, fabrication, installation, and verification of spacecraft thermal control systems. It also provides for the analytical thermal design and analysis of any spacecraft. This includes conceptual design, analytical thermal model development, definition of requirements, worst-case environments and design conditions, and temperature predictions for all cases. The facility provides the means to go from design and analysis to hardware qualification and acceptance testing and then to orbit.

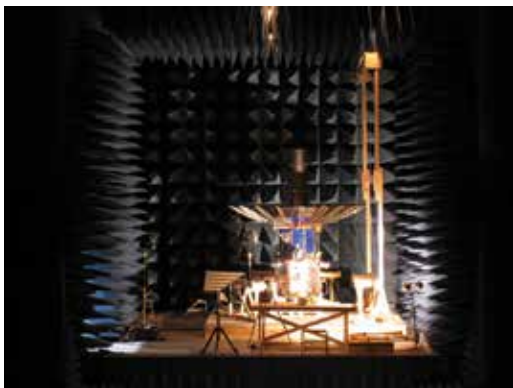
The Thermal Vacuum Test Facility consists of one large, two medium, and several small chambers. The large chamber is a 16 ft diameter by 30 ft long horizontal end loading cylinder, the medium chambers are 7 ft

diameter by 8 ft tall vertical bottom loading cylinders. The large and one medium chamber are cryogenic pumped, providing an oil-free vacuum environment. The other medium chamber has a diffusion pump system capable of evacuation rates similar to the rates that occur during launch ascent. All three chambers are equipped with gaseous nitrogen conditioned thermal shrouds capable of temperatures between -150 °C and +125 °C. The large chamber and both medium chambers are enclosed within a 2100 ft² clean room that is specified at ISO 7 (Class 10,000) and certified to ISO 5 (Class 100).

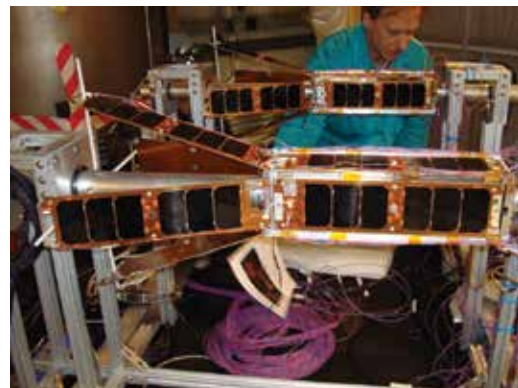
The Spin Test Facility contains two spin balancing machines (one horizontal and one vertical) to handle various types of balancing requirements. Both machines are provided with a plane separation network to obtain correction readings directly in the plane of correction. Moment of inertia (MOI) tables of various capacities are used to verify MOI and center of gravity for units under test.

The Static Loads Test Facility provides the capability to perform modal survey testing on a wide variety of spacecraft and structures. It consists of two 6 ft × 12 ft × 6 in. thick, ~15,500 lb steel plates (attachable) with floating base, six 75 Flb stinger shakers (1/2-in. DA stroke), two 250 Flb stinger shakers (4-in. DA stroke), and a ~300-channel data acquisition system (expandable).

Spacecraft Robotics Engineering and Controls Laboratory: This facility, which is the largest dual-platform motion simulator of its kind, is operated by NCST in collaboration with NRL's Naval Center for Applied Research in Artificial Intelligence. It supports research in the emerging field of space robotics including autonomous rendezvous and capture, remote assembly operations, and machine learning. It allows full-scale, hardware-in-the-loop testing of flight mechanisms, sensors, and logic of space robotic systems.



SED's Tapered Anechoic Chamber.

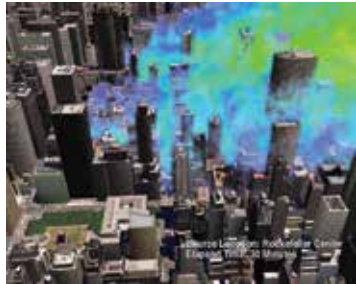


Cubesats being prepared for environmental testing.

RESEARCH SUPPORT FACILITIES

Technology Transfer Office

The NRL Technology Transfer Office (TTO) is responsible for NRL's implementation of the Federal



NRL's CT-Analyst, which provides instantaneous, 3D predictions of airborne particle transport in urban settings, has been developed for use in specific cities.

Technology Transfer Act. It facilitates the transfer of NRL's innovative technologies for public benefit by marketing NRL technologies and by negotiating patent license agreements and Cooperative Research and Development Agreements (CRADAs).

TTO markets NRL technology through its Web site, by exhibiting at trade shows and scientific conferences, posting videos on NRL's social media sites, and through DoD-contracted Partnership Intermediaries such as TechLink. It also works with state and local economic development offices to identify small companies manufacturing and selling related technologies.

A license grants a company the right to make, use, and sell NRL technologies commercially in exchange for equitable licensing fees and royalties. Revenue is distributed among inventors and NRL's general fund. TTO reviews the commercialization plan submitted by the potential licensee in support of its application for a license. The plan must provide information on the licensee's capabilities, proposed development expenditures, a time line to commercialization, and an assessment of the planned market.

A license may be exclusive, partially exclusive (exclusive for a particular field of use or geographic area), or non-exclusive. Once a license is executed, TTO monitors the licensee for timely payments and for its diligence in commercializing the licensed invention.

TTO also negotiates Government Purpose Licenses to transition NRL technologies for manufacture and sale solely for Navy and other U.S. Government purposes.

CRADAs provide a vehicle for NRL scientists and engineers to collaborate with their counterparts in industry, academia, and state and local governments. Under a CRADA, a company may provide funding for collaborative work between it and NRL and is granted an exclusive option to license technologies developed under that CRADA's Statement of Work (SOW). TTO works with the NRL scientist to develop a SOW that has sufficient detail to define the scope of the CRADA partner's rights.

Technical Information Services

The Technical Information Services (TIS) Branch combines publication, printing and duplication, graphics, photographic, multimedia, exhibit, and video services into an integrated organization. Publication services include writing, editing, composition, publications consultation and production, and printing management. The Service Desk provides quick turnaround digital black-and-white and color copying/printing/CD/DVD duplicating, as well as passport and ISOPREP photos. TIS uses digital publishing technology to produce scientific and technical reports that can be used for either print or



Photographer and videographer capture footage for a technical presentation.

Web. Graphics support includes technical and scientific illustrations, computer graphics, design services, display posters, and framing. The HP large format printers offer exceptional color print quality up to 1200 dpi and produce indoor posters and signs up to 56 inches. Lamination and mounting are available. Photographic services include digital still camera coverage for data documentation, both at NRL and in the field. Photographic images are captured with state-of-the-art digital cameras and can be output to a variety of archival media. Photofinishing services provide custom printing and quick service color prints from digital files. Video services include producing video reports and technical videos, and capturing presentations of scientific and technical programs. TIS digital video editing equipment allows in-studio and on-location editing. TIS' photoarchivist is digitizing and ingesting all of NRL's historical and recent photos/negatives into an integrated database. The TIS Exhibits Program works with NRL's scientists and engineers to develop exhibits that best represent a broad spectrum of NRL's technologies and promote these technologies to scientific and nonscientific communities at conferences throughout the United States.

Administrative Services

The Administrative Services Branch is responsible for collecting and preserving the documents that comprise NRL's corporate memory. Archival documents include personal papers and correspondence, laboratory notebooks, and work project files — documents that are appraised for their historical or informational value and considered to be permanently valuable. The Branch



Employees of the Administrative Services Branch working in the mail room.

provides records management services, training, and support for the maintenance of active records, including electronic records, as an important information resource. The Branch is responsible for processing NRL's incoming and outgoing correspondence and provides training and support on correct correspondence formats and practices. The Branch is responsible for NRL's Forms and Reports Management Programs (including designing electronic forms and maintaining a Web site for Lab-wide use of electronic forms), and is responsible for providing NRL postal mail services for first class and accountable mail and for mail pickup and delivery throughout NRL. The Branch also provides NRL Locator Service.

Ruth H. Hooker Research Library

NRL's Ruth H. Hooker Research Library continues to support NRL and ONR scientists in conducting their research by making a comprehensive collection of the most relevant scholarly information available and useable; by providing direct reference and research support; by capturing and organizing the NRL research portfolio; and by creating, customizing, and deploying a state-of-the-art digital library.

Print and digital library resources include extensive technical report, book, and journal collections dating back to the 1800s housed within a centrally located research facility that is staffed by subject specialists and information professionals. The collections include 45,000 books; 54,000 digital books; 80,000 bound historical

journal volumes; more than 3,500 current journal subscriptions; and approximately 2 million technical reports in paper, microfiche, or digital format (classified and unclassified). Research Library staff members provide advanced information consulting; literature searches against all major online databases including classified databases; circulation of materials from the collection including classified literature up to the SECRET level; and retrieval of articles, reports, proceedings, or documents from almost any source around the world. Staff members provide scheduled and on-demand training to help researchers improve productivity through effective use of the library's resources and services.

The Research Library staff has developed and is continuing to expand the NRL Digital Library. The Digital Library currently provides desktop access to thousands of journals, books, and reference sources to NRL-DC, NRL-Stennis, NRL-Monterey, and the Office of Naval Research.

Library systems provide immediate access to scholarly information, including current and archival journals, trade magazines, and conference proceedings that are fully searchable at the researcher's desktop (more than 15,400 titles). Extensive journal archives from all the major scientific publishers and scholarly societies are now available online. The breadth and depth of content available through TORPEDO, NRL's locally loaded digital repository, continues to grow and



Librarians working in the Ruth H. Hooker Research Library.

provides a single point of access to scholarly information by providing full text search against journals, books, conference proceedings, and technical reports from 20 publishers (14.5 million items by May 1, 2014). The NRL Online Bibliography, a Web-based publications information system, is ensuring that the entire research portfolio of written knowledge from all NRL scientists and engineers since the 1920s will be captured, retained, measured, and shared with current and future generations.

OTHER RESEARCH SITES

NRRL has acquired or made arrangements over the years to use a number of major sites and facilities outside of Washington, D.C., for research. The largest facility is located at Stennis Space Center (NRL-SSC) near Bay St. Louis, Mississippi. Others include a facility near the Naval Postgraduate School in Monterey, California (NRL-MRY), and the Chesapeake Bay Detachment (CBD) and Scientific Development Squadron One (VXS-1) in Maryland. Additional sites are located in Virginia, Alabama, and Florida.

Stennis Space Center (NRL-SSC)

The NRL Detachment at Stennis Space Center, Mississippi (NRL-SSC), consists of NRL's Oceanography Division and portions of the Acoustics and Marine Geosciences Divisions. NRL-SSC, a tenant at NASA's John C. Stennis Space Center (SSC), is located in the southwest corner of Mississippi, about 40 miles north-east of New Orleans, Louisiana, and 20 miles from the Mississippi Gulf Coast. NRL-SSC personnel have been located at SSC since the early 1970s, when they were part of the Navy Ocean Research and Development Activity and, later, the Navy Oceanographic and Atmospheric Research Laboratory before becoming an NRL detachment. Other Navy tenants at SSC include the Commander, Naval Meteorology and Oceanography Command (CNMOC), the Naval Oceanographic Office (NAVOCEANO), Naval Oceanography Operations Command, Naval Oceanography Antisubmarine Warfare Center, Naval Oceanography Mine Warfare Center, Fleet Survey Team, Naval Small Craft Instruction and Technical Training School, Special Boat Team Twenty-two, and Navy Office of Civilian Human Resources Southeast.



Vertical microstructure profiler.

Other Federal and State agencies at SSC involved in marine-related science and technology include the National Oceanic and Atmospheric Administration (NOAA) National Coastal Data Development Center and the NOAA National Data Buoy Center, the U.S. Geological Survey, the Environmental Protection Agency (EPA) Gulf of Mexico Program and EPA Environmental Chemistry Laboratory, the Center of Higher Learning, University of Southern Mississippi Department of Marine Science, and Mississippi State University. NRL-SSC benefits from the collocation of CNMOC and NAVOCEANO, which are major opera-

tional users of the oceanographic, acoustic, and geosciences technology developed by NRL-SSC researchers. NAVOCEANO operates the Navy DoD Supercomputing Resource Center, one of the nation's High Performance Computing Centers, which provides operational support to the warfighter and access to NRL for ocean and atmospheric science and technology.

The Acoustics branch (Code 7180) and Marine Geosciences and Oceanography Divisions occupy more than 155,000

ft² of research, computation, laboratory, administrative, and warehouse space. Facilities include the sediment core laboratory, transmission electron micro-



The JEOL JEM-3010 transmission electron microscope.

scope, moving-map composer facility, underwater navigation control laboratory, computed tomography scanning laboratory, real-time ocean observations and forecast facility, ocean color data receipt and processing facility, environmental microscopy facility, maintenance and calibration systems, Ocean Dynamics and Prediction Computational Network Facility, and numerous laboratories for acoustic, geosciences, and oceanographic computation, instrumentation, analysis, and testing. Special areas are available for constructing, staging, refurbishing, and storing seagoing equipment.

Monterey (NRL-MRY)

The NRL Detachment Monterey is located in Monterey, California, on a 5-acre Annex about one mile from the Naval Support Activity, Monterey (NSAM) main base and the Naval Postgraduate School (NPS) campus. The Marine Meteorology Division has



NRL Monterey's 15,000 ft² Marine Meteorology Center. The building was dedicated in October 2012.

occupied this site since the early 1970s, when the U.S. Navy collocated its meteorological research facility with the operational center, Fleet Numerical Meteorology and Oceanography Center (FNMOC). FNMOC started in Monterey around 1960 to be able to share resources and expertise with NPS. This collocation of research, education, and operations continues to be a winning formula. FNMOC remains the primary customer for the numerical weather prediction and satellite product systems developed by NRL-MRY. The Division was awarded a Cray XE6m supercomputer by the DoD HPCMO Dedicated HPC Project Investment (DHPI) program. Procurement of an additional Cray with CPP funds further enhanced this robust research system, located in the FNMOC computer center. Additionally, NRL-MRY scientists have direct access to FNMOC's supercomputers, allowing advanced development using the real-time, on-site, global atmospheric and oceanographic databases, in the same computational environment as operations. Such access offers unique advantages for successfully implementing new systems and system upgrades and allows for rapid integration of new research results into the operational systems. Proximity to NPS also offers unique opportunities for collaborative research, as well as educational and teaching/mentoring opportunities for NRL staff.

NRL-MRY occupies portions of three out of the five primary buildings on the Annex. A new building, the Marine Meteorology Center, was completed and dedicated in October 2012. The state-of-the-art, LEED-certified building includes an atmospheric aerosol laboratory, computer facility, the Meteorology Applications Development Branch (Code 7540), and the Division's front office suite. A configurable, cutting-edge aerosol and radiation measuring and observation platform is situated on the roof of the building for long-term monitoring of the air quality in Monterey, complementing the standard meteorological observation suite of the National Weather Service Forecast Office for San Francisco/Monterey Bay, collocated in the Annex. In 2014, the Division's Atmospheric Dynamics and Prediction Branch (Code 7530) will vacate a portion of one building and fully move into the building adjacent to the new building. When the move is completed, NRL-MRY will wholly occupy two buildings on the Annex, with a total floor space of approximately 40,000 ft².

Chesapeake Bay Detachment (CBD)

NRL's Chesapeake Bay Detachment (CBD) occupies a 168-acre site near Chesapeake Beach, Maryland, and provides facilities and support services for research in radar, electronic warfare, optical devices, materials, communications, and fire research.

Because of its location high above the western shore of the Chesapeake Bay, unique experiments can be performed in conjunction with the Tilghman Island site, 16 km across the bay from CBD. Some of these experiments include low-clutter and generally low-back-

ground radar measurements. Using CBD's support vessels, experiments are performed that involve dispensing chaff over water and characteriz-



CBD's LCM-8 providing test support for electronic warfare research.

ing aircraft and ship radar targets. Basic research is also conducted in radar antenna properties, testing of radar remote sensing concepts, use of radar to sense ocean waves, and laser propagation. A ship motion simulator (SMS) that can handle up to 12,000 lb of electronic systems is used to test and evaluate radar, satellite communications, and line-of-sight RF communications systems under dynamic conditions (various sea states).

CBD also hosts facilities of the Navy Technology Center for Safety and Survivability that are primarily dedicated to conducting experimental studies related to all aspects of shipboard safety, particularly related to flight decks, submarines, interior ship conflagrations, and other field activities that may affect the marine environment. The Center has a variety of specialized facilities including two fully instrumented real-scale fire research chambers for testing small (28 m³) and large (300 m³) volume machinery spaces, a gas turbine engine enclosure and flammable liquid storeroom fire suppression systems; three test chambers (0.3, 5, and 324 m³) for conducting experiments up to 6 atmospheres of pressure; a 50 ft × 50 ft fire test chamber fitted with a large-scale calorimeter hood rated up to 3 MW; a 10,000 ft² mini-deck that affords capabilities for studying characteristics and suppression of flight deck fires and suppression techniques; two mobile instrument vans for remote field tests support; and an LCAC gas turbine engine module. The 5 m³ chamber was upgraded with new instrumentation and equipment to study cell-to-cell failure propagation in lithium-ion batteries. These upgrades include high-speed visible and infrared (IR) cameras, a Fourier transform infrared (FTIR) spectrometer for in situ, real-time chemical species identification, temperature, pressure, and heat flux measurements, and remote, real-time non-dispersive infrared (NDIR) monitoring of selected chemical species.

The Radar Range facility at CBD, together with the Maritime Navigation Radar (MNR) Test Range at Tilghman Island, provide the emitters and analysis tools for developing comprehensive Maritime Domain Awareness capabilities. The MNR consists of dozens of radars that represent a precise cross section of today's actual MNR environment. An integrated suite of advanced sensors has been developed for data collection and processing to identify and classify vessels. A suite of similar sensors and processors has been integrated into a transportable shelter, the Modular Sensor System (MSS), that can be rapidly deployed to ports or other sites for enhanced maritime awareness reporting.

Scientific Development Squadron ONE (VXS-1)

Scientific Development Squadron ONE (VXS-1), located at Naval Air Station (NAS) Patuxent River, Maryland, is manned by 12 Naval Officers, 51 Enlisted Sailors, and nine civilian contractors and government civil servants. VXS-1 provides airborne science and technology (S&T) research platforms to support Naval Research Laboratory and Office of Naval Research (ONR) projects. VXS-1 is the sole airborne S&T squadron in the U.S. Navy and conducts scientific research and advanced technological development for the Department of Defense, the Department of the Navy, Naval Air Systems Command (NAVAIR), the National Science Foundation (NSF), the Missile Defense Agency (MDA), the National Oceanic and Atmospheric Administration (NOAA), and many other governmental and nongovernmental agencies. VXS-1 operates and maintains three NP-3 and one RC-12 research aircraft. In addition, the squadron serves as the Aircraft Report-



RC-12M.

ing Custodian (ARC) for nine ScanEagle unmanned aircraft systems and the U.S. Navy's only manned airship, the MZ-3A.

VXS-1 routinely conducts a wide variety of S&T missions from remote detachment sites around the globe. In 2014, the squadron completed research detachments to Marine Corps Air Station Kaneohe Bay, Hawaii; U.S. Air Force Forward Operating Location,

Curacao; Juneau, Alaska; and numerous local flights from NAS Patuxent River, Maryland. The squadron has provided flight support for diverse research programs: ONR Code 31's ROUGH WIDOW system, focused on



NP-3D Orion.

systems integration, sensor fusion, and performance testing of systems in operational maritime patrol environments; multiple detachments supporting the MDA's testing and experimentation, vital to the success of air- and surface-based missile tracking and interceptor tests; NRL's Tactical Electronic Warfare Division, supporting the Navy's electronic warfare requirements; Johns Hopkins University Applied Physics Laboratory, providing capabilities testing for the U.S. Navy's Multi-Band Terminal; ONR's PMR-51 GAMERA Project sensor development and testing; and multiple RC-12 detachments supporting NOAA's Gravity for the Redefinition of the American Vertical Datum (GRAVD) survey and Multiple-Link Common Data Link System (MLCS) testing for NRL's Information Technology Division. The squadron's ongoing contributions to the Naval Research Enterprise now total over 72,000 flight hours spanning 51 years of Class "A" mishap-free operations.

Midway Research Center

The Midway Research Center (MRC) is a worldwide test range that provides accurate, known signals as standards for performance verification, validation, calibration, and anomaly resolution. In this role, the MRC ensures the availability of responsive and coordinated scheduling, transmission, measurement, and reporting of accurate and repeatable signals. The MRC, under the auspices of NRL's Naval Center for Space Technology, provides NRL with state-of-the-art facilities dedicated to Naval communications, navigation, and basic research. The headquarters and primary site is located on 162 acres in Stafford County, Virginia. The main site consists of three 18.2 m, radome-enclosed precision tracking antennas and a variety of smaller antennas. The MRC has the capability to transmit precision test signals with multiple modulation types. Its normal configuration is transmit but can be configured to receive as required. The MRC also provides cross-mission and cross-platform services from worldwide locations using

a combination of fixed and transportable resources and a quick-reaction, unique signals capability. Assets include Pulsar Systems (several worldwide locations), a 45 m tracking antenna in Palo Alto, California, and a 25 m tracking antenna system on Guam. The MRC instrumentation suite includes nanosecond-level time



Midway Research Center satellite calibration facility in Stafford, Virginia.

reference to the U.S. Naval Observatory, precision frequency standards, accurate RF and microwave power measurement instrumentation, and precision tracking methodologies. The MRC also contains an Optical Test Facility with two specialized suites of equipment: a multipurpose Transportable Research Telescope (TRTEL) used for air-to-ground optical communications and for passive satellite tracking operations, and a satellite laser ranging (SLR) system built around a 1 m telescope as a tool for improving customer ephemeris validation processes.

Pomonkey Facility

The Naval Research Laboratory's Pomonkey Facility is a field laboratory with a variety of ground-based antenna systems designed to support research and development of space-based platforms. Located 25 miles south of Washington, D.C., the facility sits on



The NRL Pomonkey Facility.

approximately 140 acres of NRL-owned land, which protect its systems from encroaching ground-based interferers. Among its various precision tracking antennas, the facility hosts the largest high-speed tracking antenna in the United States. Boasting a diameter of 30 m, its range of trackable platforms includes those in low Earth orbit

through those designed for deep space missions. The facility's antenna systems are capable of supporting missions at radio frequencies from 50 MHz through 20 GHz and can be easily configured to meet a variety of mission requirements. The ease of system configuration is due to the facility's stock of multiple antenna feeds, amplifiers, and downconverters. Other facility assets include an in-house ability to design, fabricate, test, and implement a variety of radio frequency components and systems. The facility also hosts a suite of spectrum analysis instrumentation that, when coupled to its antenna systems, provides a unique platform for a variety of research and development missions.

Blossom Point Satellite Tracking and Command Facility

The Blossom Point Tracking and Command Facility (BPTF) provides engineering and operational support to several complex space systems for the Navy and other

sponsors. BPTF provides direct line-of-sight, two-way communications services with spacecraft in multiple bands and multiple orbits including LEO, HEO, GEO, and lunar. Additionally, with



Blossom Point Satellite Tracking and Command Facility.

BPTF as an external node on the Air Force Satellite Control Network (AFSCN), it has the capability to provide coverage worldwide. BPTF consists of a satellite mission operations center, multiple antennas, and an infrastructure capable of providing space system command, control, and management to most on orbit assets worldwide.

Specific BPTF resources include the following:

Neptune/Common Ground Architecture Software. This government-owned software provides infrastructure and reusable components facilitating construction of command, control, and monitoring systems for space vehicle development, integration, test, and operations. Neptune/Common Ground Architecture with Automated Ground Operations software allows for 5 × 8 (lights out) operations on 24 × 7 operations. Current missions include 13 satellites with 186 worldwide contacts per day. The GAO-10-55 report dated October 2009, titled *Challenges in Aligning Space Systems Components*, lauds BPTF with Neptune/Common Ground

Architecture as one facility that can control a variety of satellites.

Hardware Architecture: Based on RF, video, and matrix switching with net-centric control and processing, virtually any hardware asset can be “switched” into a path to create the correct capability required for any mission. This architecture supports both classified and unclassified operations and missions, and internal LANs support multiple simultaneous mission operations. Salient resources include antennas; receivers; telemetry, tracking, and command (TT&C); command encoder; front-end processors; operations automatic data processing (ADP) resources; and satellite health and monitoring/engineering.

Marine Corrosion Facility

The Chemistry Division’s Marine Corrosion Facility (MCF) located in Key West, Florida, is a tenant command to the Naval Air Station, Key West on its Trumbo Point Annex. The site offers a “blue” ocean environment with natural seawater characterized by historically small compositional variation and a stable biomass. This continuous source of stable, natural seawater provides a site ideally suited for studies of marine environmental effects on materials, including accelerated and long-term exposure testing and materials evaluation.

The MCF began as a small field exposure site for NRL in the late 1960s, encompassing only a small office and outdoor laboratory on shared facilities. The MCF was staffed full time by NRL researchers starting



NRL's Marine Corrosion Facility in Key West, FL.

in 1986 and has experienced significant growth since; today, the MCF includes several buildings on a 4-acre site. The major facilities include a Marine Coatings Application and Test Facility, a Full-Scale Shaft Bearing Test Facility, a Ballast Water Treatment System Evaluation Facility and associated marine biology laboratory, a 20,000 ft² atmospheric test site, once-through natural seawater exposure troughs and the Navy’s only

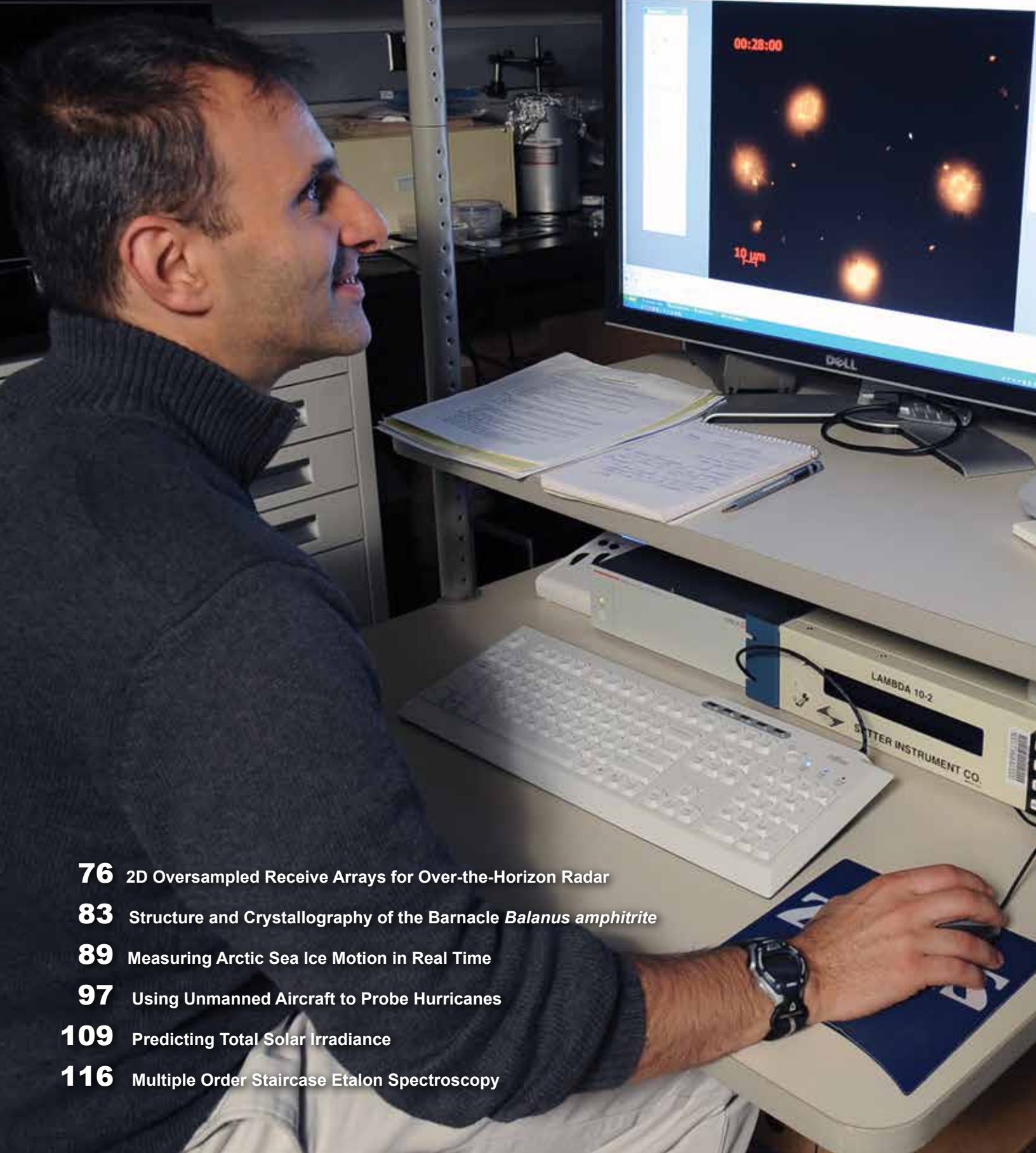
Cathodic Protection Physical Scale Modeling (CP-PSM) Design Facility. The CP-PSM provides a highly accurate capability to physically model the electrochemical behavior of ship hulls and outboard structures to understand both the characteristics and adequacy of corrosion control systems and their relation to underwater electromagnetic fields. The CP-PSM has been the cornerstone to Navy impressed current cathodic protection systems, providing new construction design requirements for NAVSEA Program Executive Offices and Allied navies.

The MCF maintains extensive capabilities for RDT&E of marine engineering and coatings technologies and supports a wide array of Navy and industrial sponsors. Equipment is available for experiments involving accelerated corrosion and weathering, general corrosion, long-term immersion and alternate immersion, fouling, electrochemical phenomena, coatings application and characterization, ballast water treatment, marine biology, and corrosion monitoring. In 2009, the facility received a comprehensive refurbishment due to hurricane damage.

Ex-USS *Shadwell* Research Platform

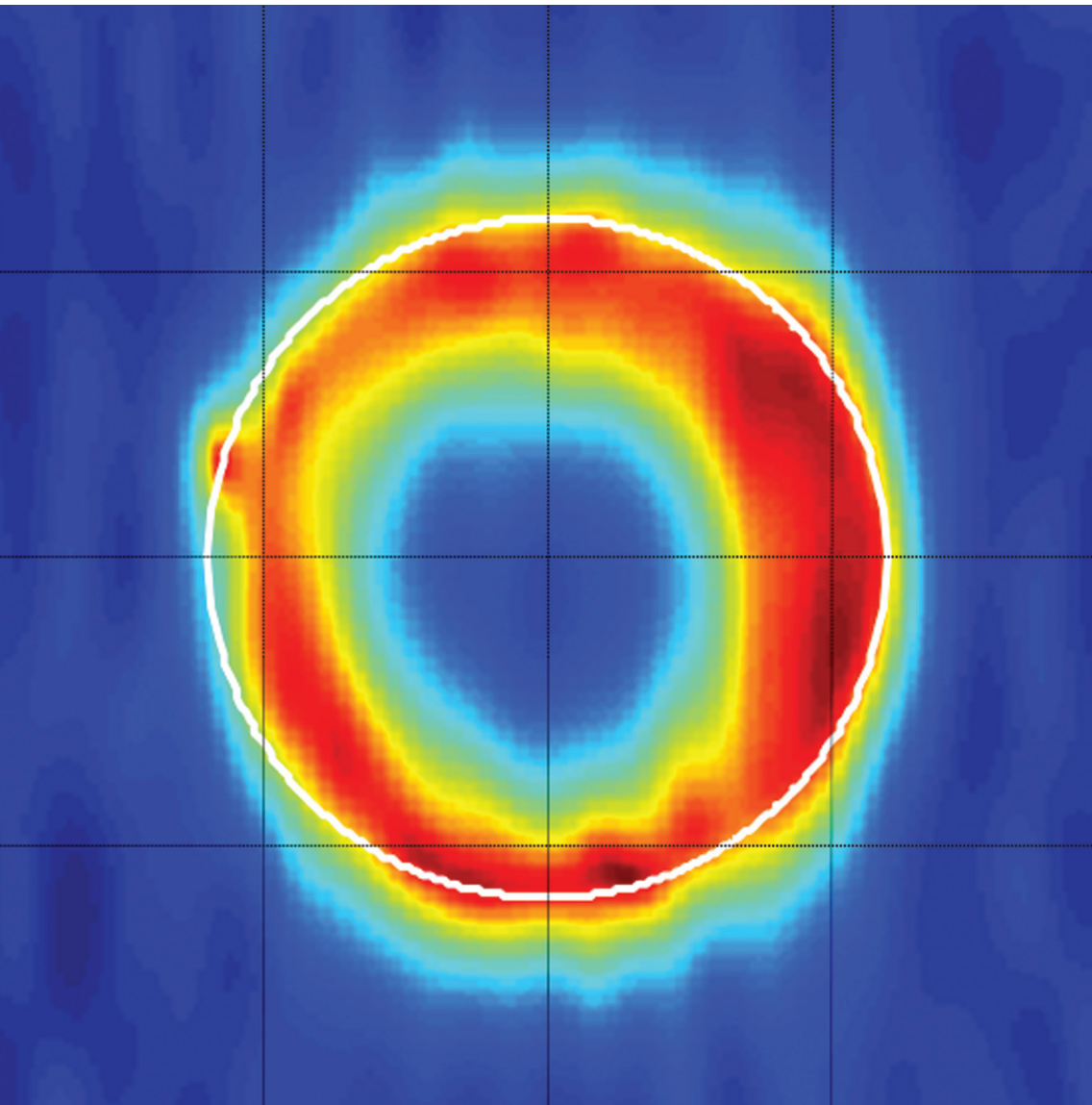
The Navy Technology Center for Safety and Survivability has a full-scale test ship, the ex-USS *Shadwell* located at the Joint Maritime Test Detachment (JMTD), Little Sand Island, Mobile, Alabama. *Shadwell* is a 457 ft, 9000 ton dock landing ship (LSD). All ship systems germane to damage control are maintained, including heating and air conditioning (HVAC), smoke ejection system (SES), one complete Collective Protection System (CPS) (replicating zone two of the DDG 51 class ships), and electrical, lighting, and internal communication systems (including wire-free and WLAN communications). Specialized test areas include a hangar bay, flight deck with helicopter mockup, submarine test area, machinery space, shipboard magazine including a PVLS magazine, and well deck/vehicle stowage areas. Three damage control lockers are also maintained. The data are collected and displayed via a blown fiber gigabit network that is distributed throughout the ship. In addition, Little Sand Island has a wave tank that is used for in situ burn tests and studies for oil spill containment.

Featured Research



- 76** 2D Oversampled Receive Arrays for Over-the-Horizon Radar
- 83** Structure and Crystallography of the Barnacle *Balanus amphitrite*
- 89** Measuring Arctic Sea Ice Motion in Real Time
- 97** Using Unmanned Aircraft to Probe Hurricanes
- 109** Predicting Total Solar Irradiance
- 116** Multiple Order Staircase Etalon Spectroscopy

OTHR Gets a Makeover



You're not likely to see over-the-horizon radar (OTHR) at retirement seminars. That's because after more than 60 years in use, OTHR isn't cashing in – far from it. Over-the-horizon radar's usefulness in wide area surveillance, in fact, is better than ever since its makeover by NRL's rejuvenating researchers. Using revolutionary advancements in receive array technology and architecture, especially two-dimensional spatially oversampled arrays and adaptive signal processing, NRL is making OTHR more sensitive and more able to operate at night at low frequencies. An enhanced understanding of the high frequency noise environment made 2D arrays the logical choice for OTHR nighttime surveillance due to their ability to achieve signal-to-external-noise ratio enhancement. By matching appropriate receiver architectures with proper beamforming techniques, future OTHRs will be more mission-capable.



2D Oversampled Receive Arrays for Over-the-Horizon Radar

G. San Antonio¹ and Y.I. Abramovich²

¹*Radar Division*

²*WR Systems Ltd., Fairfax, VA*

Over-the-horizon radar (OTHR) is a well-established tool for wide area surveillance that has been used extensively over the past 60 years. Recently, revolutionary advancements have been made with regard to receive array technology that will increase the overall radar sensitivity and help extend mission capability. The technology advancements that have made this sensitivity improvement possible are two-dimensional (2D) spatially oversampled arrays and adaptive signal processing.¹ Recent studies focused on understanding the high-frequency noise environment have revealed that particular array geometries can provide optimal signal-to-external-noise ratio enhancements.² Ongoing work includes efforts to demonstrate advanced signal processing techniques that will optimally use the newly developed array architecture.³⁻⁶

BACKGROUND

Over-the-horizon radar (OTHR) is a well-established technology that provides persistent (near 24 hours/365 days/year), wide area (thousands of square miles) surveillance. Target detection is achieved through the propagation of RF energy “over” the visual horizon either by a surface attached high-frequency (HF) electromagnetic wave or by a refracted electromagnetic wave via the Earth’s ionosphere. These two forms of RF propagation broadly delineate two classes of OTHRs known as surface wave OTHR and skywave OTHR. Both classes of OTHR are generally required to have a large frequency span of operation (3 to 30 MHz) so that radar operation can be optimized for the continually varying environmental conditions.

A particularly vexing problem for OTHR is the ability to achieve noise-limited target detection at night using frequencies from the lower half of the HF spectrum (3 to 15 MHz). The increased level of difficulty of this particular detection problem vice that of noise-limited target detection during the day using upper-half HF frequencies (15 to 30 MHz) or even lower-half HF frequencies for surface wave systems is due in large part to two factors. The first factor limiting target detection at lower HF frequencies is simply an overall reduction in the target radar cross section (RCS). Typical fast moving targets appear as resonant structures in the 20 to 30 MHz frequency range (15 to 10 m wavelengths, respectively). A decrease in the radar RF frequency below these resonant frequencies is accompanied by roll-offs in the RCS at a rate of -40 dB/decade. Thus, the raw signal component of the target backscatter can be extremely small at lower HF frequencies. The

second and probably more interesting factor that limits target detection at the lower HF frequencies at night is an increase in the overall background “environmental” noise power. The main mechanism for determining the background noise level in the HF section of the RF spectrum is the ionosphere. The ionosphere is a section of the Earth’s upper atmosphere from 80 km to 600 km above the Earth’s surface. This region contains electrically charged ions with spatial densities driven to a large degree by the Sun. During the daytime, areas of the Earth in view of the Sun experience an increase in the ionosphere electron density as well as the development of a lower ionospheric layer called the D-layer. Electrons contained within this layer are not dense enough to refract HF electromagnetic waves; however, they do cause large amounts of attenuation. Absorption/attenuation is inversely proportional to the RF frequency; lower HF frequencies, therefore, suffer more absorptive losses. The net effect is to limit the amount of noise or signal that can be propagated long distances at these frequencies during the day. In contrast, as night arrives and the Sun moves from overhead, the ionosphere electron density is lowered and the absorptive D-layer disappears. Thus, noise can be propagated over longer distances at lower frequencies at night. The net effect is that a receiver operating at night in the lower HF band will have to cope with the combination of noise sources covering nearly the entire Earth. Figure 1 provides a visual example of the time–frequency behavior of the HF spectrum covering 3 to 30 MHz over a 30 h period.

The challenge, therefore, with improving the detection performance of OTHR systems (both surface wave and skywave) operating in the lower HF band at night

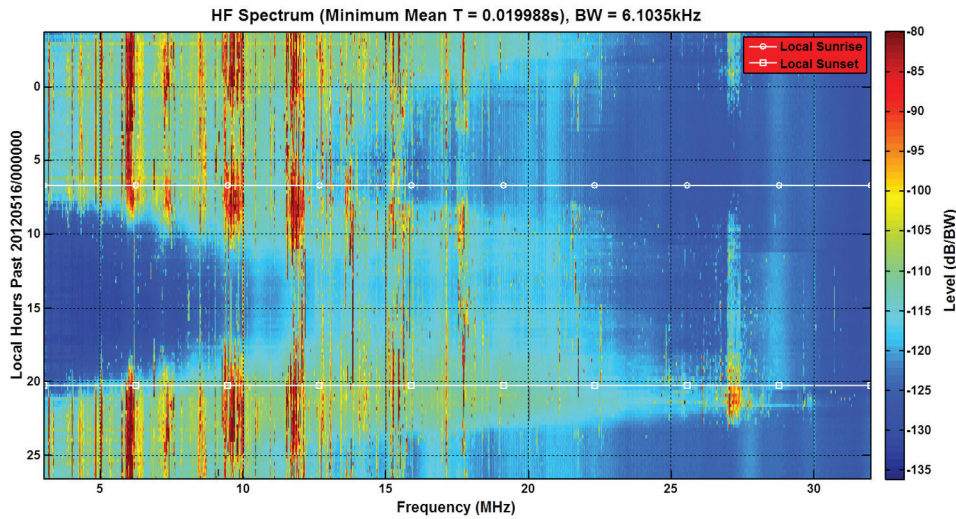


FIGURE 1 Variation of the HF spectrum over a period of 30 hours. Horizontal white lines indicate the local sunrise and sunset periods. Note the dramatic power level difference in frequencies below 10 MHz as a function of time of day.

is both to understand the space–time characteristics of the background noise field and to design receive array architectures that might achieve the highest levels of signal-to-external-noise ratio (SEN) gains.

SPACE-TIME NOISE MODELING

The design of an optimal receive array architecture cannot be completed without an accurate enough noise and signal space–time model. Prior to the initiation of the work described in this article, very little was definitively known concerning the spatial noise distribution of lower HF nighttime noise. Here the spatial noise distribution refers to the spatial distribution of noise power in azimuth and elevation for a particular spot on the Earth. Large studies, most notably the International Geophysical Year of 1957–1958, have been conducted to characterize the temporal and seasonal variation of HF noise at various locations on the Earth’s surface.

Among all the users of the HF spectrum, OTHR systems are unique in their use of highly directional multichannel phased array receive antennas. It is possible to achieve directional beams with beamwidths of less than 1 degree, sidelobes of less than –30 dB, and directional gains approaching 25 dB. Therefore, the noise characteristics as measured on a single antenna in no way represent the noise field as sampled and measured by a modern OTHR system. A challenge that exists, however, is that OTHR systems currently exist in only a handful of locations and are most often one-dimensional in design, thus limiting the applicability of their measurements. Therefore, it was necessary to build one or more two-dimensional receive arrays to measure and construct spatial noise models. Part of a study² conducted over a two-year period did this task. Several 2D

receive arrays were constructed ranging in size from 30 to 300 elements with various geometric configurations. This resulted in empirical measurements of the lower HF nighttime 2D directional spectrum and empirically derived parametric noise models that could be used for future array design and performance prediction. Figure 2 shows an example of an empirical noise spatial spectrum measurement. Correspondingly, Fig. 3 is an example of a parametric noise model spatial spectrum. The results of the empirical noise study can be summarized by a few important points. First, to a large extent, there is minimal variation of the lower HF noise power as a function of azimuth. Absent geographic areas of enhanced noise, the noise is equally likely to be propagated from long distances at all azimuths. Second, there

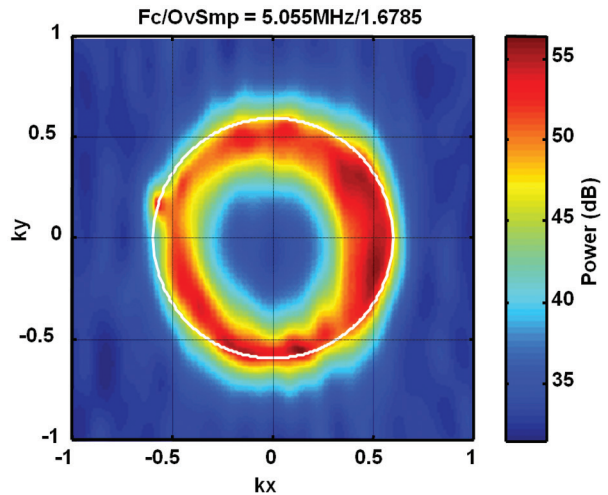


FIGURE 2 Empirically measured noise spatial spectrum using 2D planar antenna array. Visible and invisible space (due to array spatial oversampling) are shown.

Noise/Elmt Mod = $\sin^{10}(\sin^2 \cos^{0.7})$, Fc/OvSmp = 5MHz/1.697

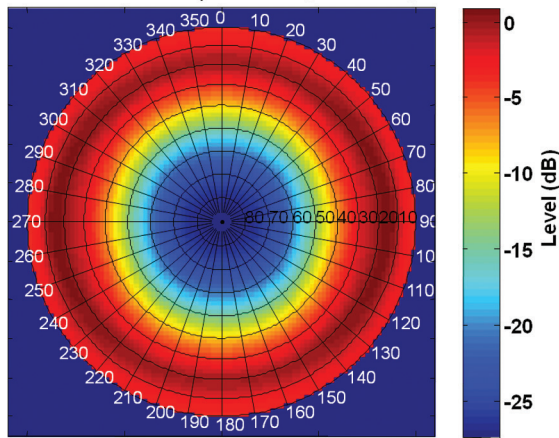


FIGURE 3
Parametric modeled noise spatial spectrum.

is significant variation of the noise power as a function of elevation angle. The variation in elevation can be physically linked to the propagation mechanism, which in this case is the ionosphere. At any particular RF frequency, there is an elevation angle called the critical angle at which all ray paths at higher elevation angles completely penetrate the ionosphere and continue into space. Therefore, noise energy propagated via the ionosphere may only arrive at a receive array at elevation angles below the critical angle. The critical angle is dependent on the radar RF frequency and the ionospheric electron density. For a given electron density profile, higher RF frequencies will have lower (closer to the horizon) critical angles. Thus, a parametric noise model was developed that is parameterized by the elevation critical angle.

RECEIVE ARRAY DESIGN

The current generation of skywave and surface wave OTHR systems have evolved to use long (greater than 2 km in total length) one-dimensional receive apertures. The genesis of this concept can be traced to pioneering work performed by Stanford University's SRI laboratory with an experimental OTHR called WARF in the 1970s and 1980s. Experimental evidence showed that long receive apertures on the order of ~2 km were about the limit to which signal wavefront coherence could be maintained across the aperture. An array made any longer will fail to produce coherent gains on target signals. This therefore presents a problem when trying to design new receive apertures that could potentially require 10 dB more array gain. The corresponding linear aperture producing 10 dB gain over an existing 2 km aperture would have to be more than 20 km long, which is at the very least impractical. As a result, one need consider the design of 2D receive apertures.

Traditional array design theory would suggest that 2D planar arrays operated near endfire (a 2D planar HF antenna array for long-range surveillance must form beams near the horizon) will not produce effective array gain, especially not when spatial oversampling occurs in the endfire dimension. However, traditional array theory does not usually consider spatially inhomogeneous noise fields, as the HF background noise has been shown to be, as well as the use of adaptive spatial beamforming. These two factors can be exploited in practice if a 2D dimensional oversampled array architecture is adopted. To be clear, the term spatial oversampling refers to spatial sampling schemes in which array elements are spaced less than half the specified radar wavelength. For example, at a frequency of 5 MHz, the half-wavelength spacing is 30 m. Array elements placed 15 m apart would be spatially oversampled by a factor of 2. Spatial oversampling is heavily used in today's modern OTHR systems. The existing 1D receive apertures are close to five times oversampled at 5 MHz. In fact, it can be shown that this oversampling in 1D is actually an inefficient use of radar hardware resources. However, in the extension to 2D apertures, spatial oversampling can be exploited to produce increased array gains through the use of optimal beamforming (i.e., beamforming that optimally accounts for the noise spatial distribution). The array property that 2D spatially oversampled arrays exploit is an old concept called "superdirectivity."

Superdirectivity refers to beamforming techniques that achieve higher directive gain than would normally be achieved with conventional beamforming. In the context of low-frequency nighttime HF noise and 2D oversampled arrays, superdirectivity allows one to trade gain on low-level system noise for decreased gain on more powerful external background noise. To be precise, though, we use optimal beamforming techniques that happen to exhibit the properties of traditional superdirectivity. This is in contrast to prior work on superdirectivity that intentionally sought to generate superdirective beams. The key point here is that beamforming is tailored and dictated by the actual noise environment. In practice, one would employ an adaptive beamformer that would adapt to the actual sensed noise. A visual difference between conventionally formed beams and optimally formed beams is seen in Figs. 4 and 5, respectively. The circular region near the center of both figures denotes the boundary between real physical azimuth and elevation angles (here shown in k-space) and nonphysical/invisible angles. The optimal beamformer places more energy into the nonphysical angle space, thereby achieving 7 dB of signal-to-external-noise ratio gain. Extensive analysis of both simulated data based on parametric noise models and empirically measured data demonstrate that

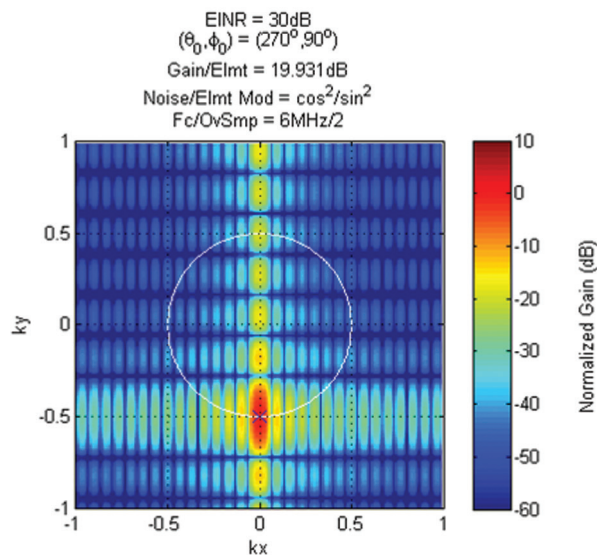


FIGURE 4
Beampattern of a conventionally steered beam.

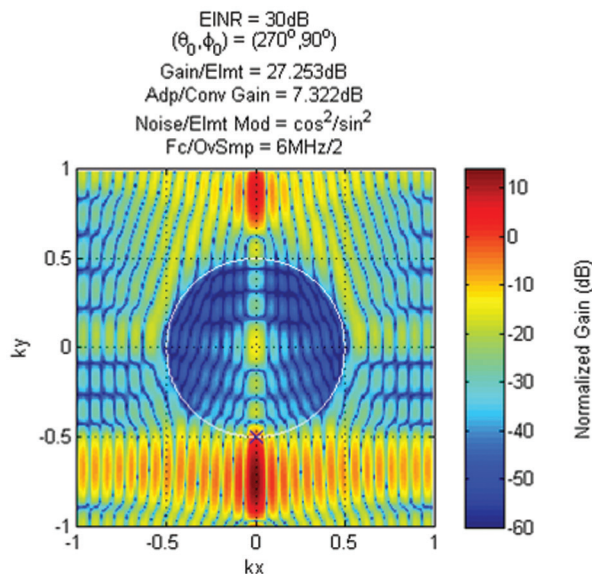


FIGURE 5
Beampattern of an optimally steered beam.

similar gains can be achieved across a broad range of frequencies and angles.^{1,2} Figure 6 shows an example of the variation in SENR for an example array geometry.

ADVANCED SIGNAL PROCESSING TECHNIQUES

Theoretical studies show the performance potential of 2D array geometries assuming the use of fully optimal beamforming techniques. In practice, one must resort to scenario-dependent techniques such as adaptive beamforming. Implementation of adaptive beamforming in practice can often become problematic as real-world issues of finite training sample support

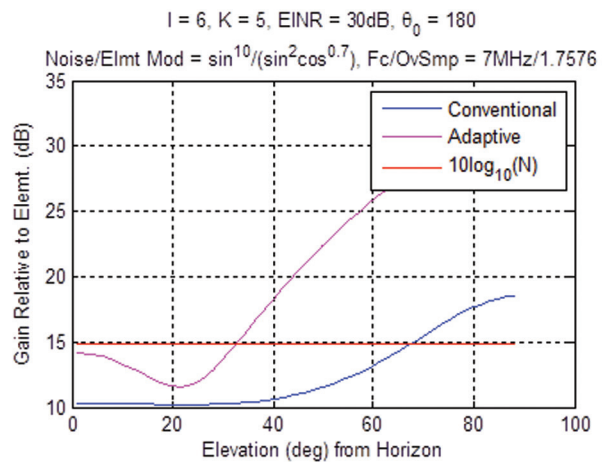


FIGURE 6
Variation in array signal-to-external-noise ratio gain as a function of elevation angle for conventional and optimal beamformers.

are encountered. For example, future OTHR systems may have thousands of receive elements. Implementing a fully adaptive beamforming scheme with correspondingly low stochastic adaptive signal processing losses is a near-impossible task as there might never be a way to collect the required number of training samples. Alternative partially adaptive beamforming techniques can be developed that leverage some existing a priori known information about the data. Two partially adaptive beamformers have been developed for the specific application of 2D oversampled receive arrays.

The first technique³ exploits a 2D aperture varying autoregressive model to reduce the required sample support from a multiple of the total number of sensors N , to a multiple of the model order parameters P and M , where $P, M \ll N$. The additional advantage of this beamforming technique is that the parameters P and M can be fixed as the receiver aperture grows in total sensor count N . The second beamforming technique⁴ combines the prior technique with a method for mitigating spatially localized point sources. The discussion of HF noise thus far has been limited to include only spatially distributed noise fields. In practice, with a high gain/high directivity receive array, one will always encounter a limited number of spatially localized sources. It is well known that adaptive beamformers can be constructed to efficiently handle a small number of sources K with the required sample support proportional to K , not the total number of sensors N . The challenge then is to combine point source adaptive beamforming with spread source adaptive beamforming in an efficient manner.

Another aspect of oversampled receive arrays that has been addressed is array calibration.⁵ Typically, array calibration is performed by measuring the response to a single far-field source. This method is practically infeasible for OTHR applications as the required far-

field distances are on the order of +100 km. Alternative techniques have been developed specifically for oversampled receive geometries that exploit the presence of physical and nonphysical beamspace. In fact, the algorithms that have been developed are essentially self calibration on clutter.

Finally, it has also been shown that the direction-of-arrival (DOA) estimation accuracy can be significantly enhanced using an oversampled receive array geometry.⁶ Through the use of optimal beamforming, superdirective receive beams can be formed that exhibit “sharper” beams capable of providing enhanced DOA accuracy in comparison to conventionally formed beams with the same aperture.

CONCLUSION

This article has discussed the application of 2D oversampled receive arrays to the problem of realizing enhanced nighttime low frequency OTHR performance. It was shown how the very nature of nighttime low frequency HF noise leads one to consider 2D oversampled arrays for practical use. In the design of any future OTHR system, the discussed receiver architecture may be used as a solution to provide required SENR gains when coupled to the proper adaptive beamforming technique, such as those discussed. The practicality of the proposed architecture becomes evident as one considers 2D receive arrays potentially covering tens of square kilometers.

ACKNOWLEDGMENTS

This work was performed cooperatively by the NRL Radar Division and WR Systems Ltd.

[Sponsored by the NRL Base Program (CNR funded)]

References

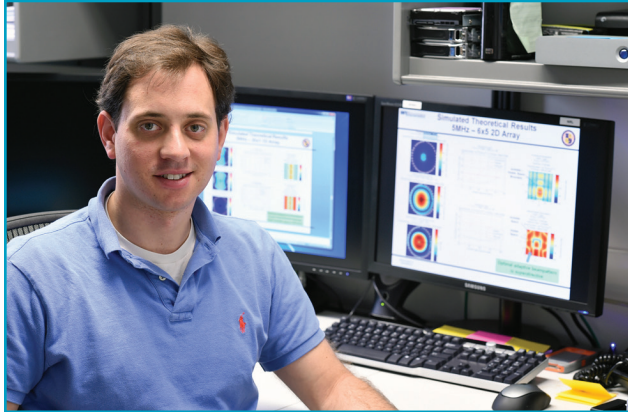
- ¹ Y.I. Abramovich, G.S. San Antonio, and G.J. Frazer, “Over-the-Horizon Radar Signal-to-External Noise Ratio Improvement in Oversampled Uniform 2D Antenna Arrays: Theoretical Analysis of Superdirective SNR Gains,” IEEE Radar Conference, Ottawa, Canada, May 2013.
- ² Y.I. Abramovich, G.S. San Antonio, R. Barnes, and S. Mondschlein, “Coalition Warfare Program: Over-the-Horizon Radar Signal-to-External Noise Ratio Improvement in Oversampled Uniform 2D Antenna Arrays: Summary Report Part II – Analysis of Experimental Results,” RPO, Chesapeake, VA, RPO-TR-CWP-0513-003.
- ³ Y.I. Abramovich and G.S. San Antonio, “Aperture Varying Autoregressive Covariance Modeling for 2D Oversampled Receive Arrays,” IEEE CAMSAP Workshop, St. Martin, Dec. 15–18, 2013.
- ⁴ Y.I. Abramovich and G.S. San Antonio, “Regularized Finite-Order Rank Covariance Matrix Approximation for Adaptive Beamforming in Oversampled 2D HF Antenna Arrays,” IEEE Radar Conference, Cincinnati, OH, May 19–23, 2014.

⁵ G.S. San Antonio and Y.I. Abramovich, “Oversampled OTHR Receive Array Calibration,” Tri-Service Radar Conference, Boulder, CO, June 2012.

⁶ Y.I. Abramovich and G.S. San Antonio, “Over-the-Horizon Radar Potential Signal Parameter Estimation Accuracy in Harsh Sensing Environments,” IEEE ICASSP Conference, Florence, Italy, May 4–9, 2014.



THE AUTHORS

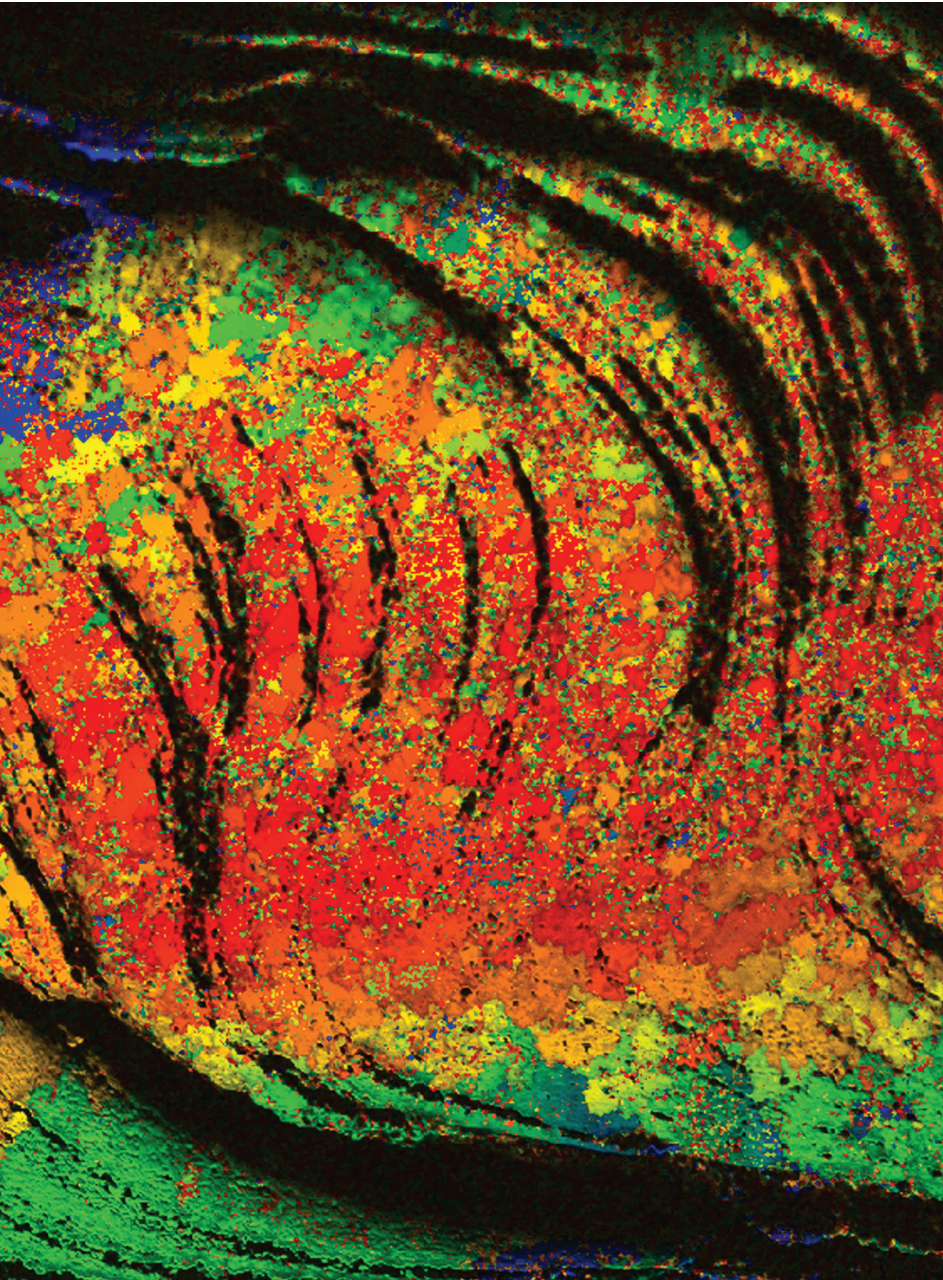


GEOFFREY SAN ANTONIO has been member of the Radar Systems Branch since 2008. He received a B.S. in electrical engineering from Worcester Polytechnic Institute in 2003, an M.S. in electrical engineering from Washington University in St. Louis in 2005, and a Ph.D. in electrical engineering from Washington University in St. Louis in 2007. His research interests include over-the-horizon radar and multichannel adaptive signal processing.



YURI I. ABRAMOVICH received the Dipl. Eng. (Hons.) degree in radio electronics and the Cand. Sci. degree (Ph.D. equivalent) in theoretical radio techniques, both from the Odessa Polytechnic University, Odessa, Ukraine, Russia, in 1967 and 1971, respectively, and the D.Sc. degree in radar and navigation from the Leningrad Institute for Avionics, Leningrad, Russia, in 1981. From 1968 to 1994, he was with the Odessa State Polytechnic University, Odessa, Ukraine, as a research fellow, professor, and ultimately as Vice-Chancellor of Science and Research. From 1994 to 2006, he was at the Cooperative Research Centre for Sensor Signal and Information Processing (CSSIP), Adelaide, Australia. Since 2000, he has been with the Australian Defence Science and Technology Organisation (DSTO), Adelaide, as principal research scientist, seconded to CSSIP until its closure. Currently he is on leave from DSTO with WR Systems, USA. His research interests are in signal processing (particularly spatio-temporal adaptive processing, beamforming, signal detection, and estimation), its application to radar (particularly over-the-horizon radar), electronic warfare, and communication. Dr. Abramovich is currently an associate editor of *IEEE Transactions on Aerospace and Electronic Systems* and previously served as associate editor of *IEEE Transactions on Signal Processing* from 2002 to 2005.

A New Twist on Barnacle Shells!



In an ongoing effort to really understand what makes barnacles stick, NRL researchers are interrogating the nasty little biofoulants both inside and out. How do their shell microstructure and overall shape affect their ability to adhere so strongly to ships? Using advanced electron imaging and crystallographic tools, these NRL researchers are determined to turn the tables on these tenacious critters. Their recent investigation has yielded some answers – the calcium carbonate that composes the barnacle *Balanus amphitrite*'s base plate forms with a convoluted structure while the parietal “sidewalls” seem to have no coherent crystallographic pattern. With this new information, improved, image-based 3D simulations of the barnacle’s mechanical response to removal stresses can be performed. There is still a lot to learn about these persistent miscreants. The real payoff will come when barnacle adhesion can be captured in real time – you see, what grows around, comes around . . .and off.

Structure and Crystallography of the Barnacle *Balanus amphitrite*

A.C. Lewis,¹ R.K. Everett,¹ K.J. Wahl,² and D.K. Burden³

¹Materials Science and Technology Division

²Chemistry Division

³National Research Council Postdoctoral Associate

We present novel mappings of the structure and crystallography of the shell of the barnacle *Balanus amphitrite*. Calcium carbonate in the form of hexagonal calcite (CaCO_3) was observed, with fine crystallites forming clusters with similar orientations. While no apparent preferred orientation was measured in the parietal (side) shell cross section, the base plate shell cross section revealed a preference for the alignment of the $\langle 0001 \rangle$ direction at the exterior of the shell, rotating by 90° toward the center of the base plate cross section. These maps will be used to construct image-based models of the barnacle shell for further study of mechanical response.

INTRODUCTION AND MOTIVATION

Barnacles are a common biofoulant that add significant drag to Naval vessels, causing increased energy use and maintenance costs. Improving approaches to defeat barnacles without ablative toxins requires evaluation of adhesion mechanisms. Prior work has shown that the nature of the barnacle base plate and adhesive may impact release characteristics.^{1,2} How the overall shape³ and shell microstructure contribute to adhesion and release processes is part of ongoing research at NRL.

Acorn barnacles like *Balanus amphitrite* develop protective shells around their soft tissues, consisting of a base plate, multiple interlocked side (parietal) plates, and movable plates covering the top opening (operculum), as shown in the X-ray tomography reconstruction in Fig. 1(a).² Shells of many marine organisms including mollusks and crustaceans are composed primarily of calcium carbonate and organic material. The calcium carbonate in shells is typically found to have crystalline structures comprised of aragonite or calcite, which are also well-known geologic mineral structures. While mollusk shells are typically found to be composed of aragonite, the majority of studies of barnacle shell crystalline structure show that the calcium carbonate is primarily in the form of calcite, which has a trigonal-rhombohedral structure (Fig. 2). Crystallography of barnacle shells, primarily the side shell plates, has been measured previously in detail for the giant barnacle *Austromegabalanus psittacus*⁴ and recently for the opercular plates of *Balanus amphitrite*.⁵

NRL researchers are developing image-based three-dimensional simulations of the barnacle mechanical response to removal stresses, including quantified structure and crystallography. Simultaneous mapping of the crystallography and microstructure will enable

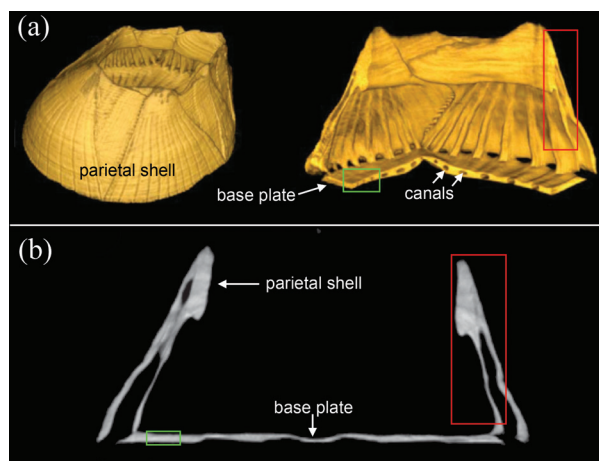


FIGURE 1
(a) X-ray computed tomography images of *B. amphitrite* shell. The base plate, parietal shell, and canals are labeled. (b) Cross section of the barnacle shell. In (a) and (b), the areas examined in this study are indicated by large red and small green boxes.^{2,6}

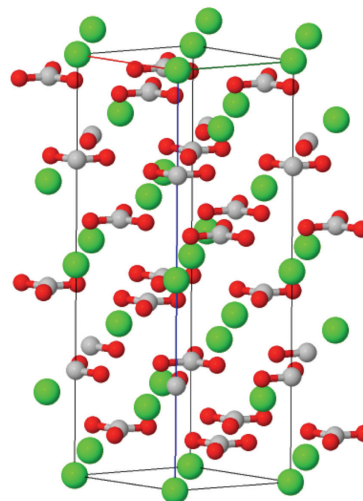


FIGURE 2
The crystal structure of calcite: calcium (green), carbon (grey), and oxygen (red).

development of a functional model of the barnacle shell combining shell ultrastructure, morphology, microstructure, and crystallographic texture to simulate mechanical response of the shell structure to removal stresses.

The microstructures and orientations of individual grains in polycrystalline materials can be imaged and quantified by electron backscatter diffraction (EBSD). Recently this approach has been used to examine biomineralization of marine organisms. In this work, we imaged cross sections of barnacle shells using scanning electron microscopy (SEM) and EBSD to determine the composition and phase of the shell calcium carbonate, quantify the hierarchical structure of the base plate and parietal shells, determine the degree of crystallinity and mineralization, and measure crystallographic texture.⁶

MATERIALS AND METHODS

Balanus amphitrite shells (between 4 and 18 mm in diameter) grown on silicone panels were gently released from the substrate and the barnacle body and soft tissue removed. Shell specimens were mounted in epoxy or acrylic, and sectioned through the center of the

crystallographic measurements, collected patterns were indexed against calcite (CaCO_3). EBSD data were collected from two barnacles in regions represented in Fig. 1(b): on the base plate (green boxes) and on the parietal shell (red boxes).

STRUCTURE AND CRYSTALLOGRAPHY

Two separate parts of the barnacle shell structure were examined in cross section: the base plate and the parietal shell. Cross-sectional scanning microscopy (Fig. 3) reveals bands of discrete grains or crystallites with a diamond-like cross section (inset) ranging from hundreds of nanometers to several microns in width on the long axis. The parietal shells also showed layered morphology with similar grain cross-section geometries and laminar morphologies to the base plate.

The crystallographic orientations of the barnacle shell mineral phases were measured and mapped by EBSD, a microscopy technique by which the crystallographic structure is quantified by scanning the electron beam across the surface, and collecting and indexing diffraction patterns at each point. The crystallographic orientation, i.e., the alignment of atoms at each measured point, is depicted in an inverse pole figure (IPF),

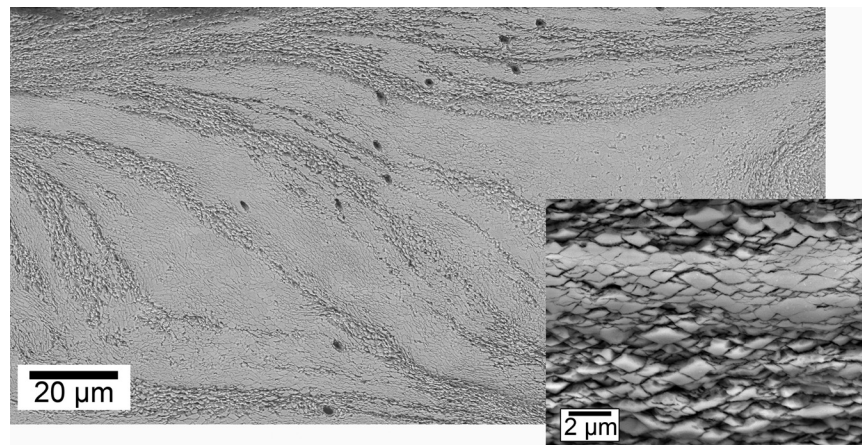


FIGURE 3 Scanning electron micrograph of barnacle base plate cross section from a region similar to that highlighted by the small green boxes in Fig. 1. Rotation of calcite crystals is visible in the higher-magnification inset.

barnacle in the plane perpendicular to the base plate before polishing. Standard mechanical polishing was followed by vibratory polishing for approximately 4 h. While the mechanical polishing resulted in flat surfaces that were generally sufficient to collect EBSD patterns, in some regions, crystallite pull-out occurred, leaving crystallites that were below the plane of polish. Since the resulting surfaces of the remaining crystallites were not highly polished, they did not produce patterns that could be indexed to crystallographic orientations. For

which maps the measured structure by coloring each point based on the corresponding crystallographic alignment. Figure 4 shows an IPF of a barnacle base-plate cross section, showing calcite crystallites grouped in clusters of similar orientations. This clustering was observed in all barnacle base plate cross-sectional specimens. The low-magnification IPF map shows the measured crystallography across the thickness of the entire base plate (where the outer surface of the shell is towards the bottom of the image, and the interior

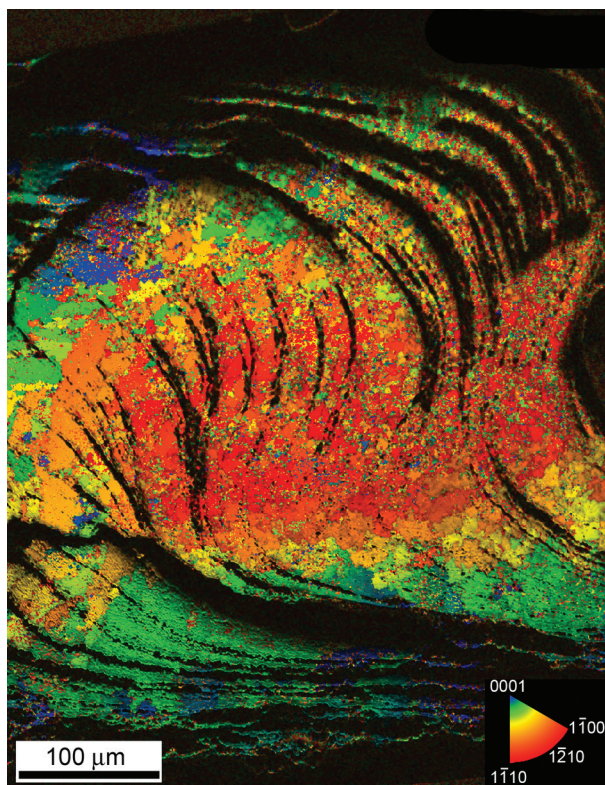


FIGURE 4 Crystal rotation map of the barnacle base-plate cross section. Calcite crystals are oriented with $\langle 0001 \rangle$ direction normal to the base plate at the outer surface of the shell (bottom of the image), rotating to 90° away from $\langle 0001 \rangle$ in the middle of the base plate.

of the shell is towards the top). The crystal direction is plotted and colored according to degrees away from the $\langle 0001 \rangle$ direction (vertical direction in Fig. 2). Those crystals closest to the outer surface of the base plate (i.e., the surface that adheres to the substrate) have near- $\langle 0001 \rangle$ orientation, and rotate to 90° away from $\langle 0001 \rangle$ at the center of the base plate. This suggests that the first calcite crystals to form adopt a low-energy orientation and rotate away from that low-energy orientation as growth proceeds, or alternately that growth proceeds from multiple surfaces. Clusters of similarly oriented crystallites maintain their orientation through a global rotation (black areas in the IPFs), suggesting that the global and crystallographic orientations of calcite crystals in these barnacle shells develop simultaneously.

The crystallographic structure of the barnacle parietal (side) shell is seen in the IPFs in Fig. 5. In the low-magnification image, it is evident that the calcite crystallite clusters do not maintain a uniform size or shape in the parietal shell, compared to the somewhat uniform clusters observed in the base plate. The shell growth in the parietal shell and in the base plate do not follow the same growth pattern. However, the side

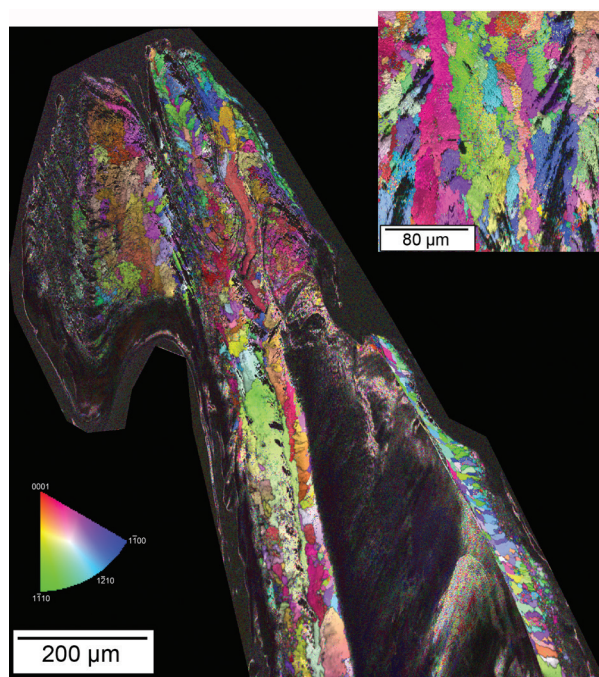


FIGURE 5 Inverse pole figure map of barnacle parietal shell cross section. Color corresponds to the crystallographic orientation perpendicular to the page.

plates do exhibit much larger domains of crystallites with similar orientation (inset).

DISCUSSION AND SUMMARY

The SEM and EBSD images of the barnacle shell revealed micron-scale calcite crystallites with well-defined texturing relative to the shell structures. At the micron length scale, calcite was the only observed form of calcium carbonate. The calcite crystallites had shapes similar to the calculated rhombohedral equilibrium shape, and were rotated about the axis normal to the base plate in some regions of the base plate. The crystallographic orientations, however, do not follow the same rotation. These features are not observed in the parietal shell, where crystallographic orientation appears to be random, even though the global calcite crystallite inclination does conform to the shell features and thus the growth pattern of the shell. The NRL researchers are working to evaluate the crystallization processes in real time, inside growing barnacles, as well as outside barnacles using protein and calcium carbonate solutions.

Other measurements of the global crystallographic orientation of calcite in the parietal shell have shown preferred orientations; however, for image-based simulation of the mechanical response of the barnacle shell, local orientations in barnacle base plate and parietal shells are needed. Measurement of the crystalline phas-

es present, the inclination of calcite crystallites, and the distribution of calcite clusters and orientations are all critical input to enable refinements to finite element simulations of the mechanical response of the barnacle shell to applied load. Future studies will incorporate the aforementioned features into 3D microstructure-based models to determine liftoff forces and to predict crack propagation in the shell.

In summary, this work presents novel mapping of the structure and crystallography of the shell of the barnacle *Balanus amphitrite*. Calcium carbonate in the form of hexagonal calcite was observed, with fine crystallites on the order of 1 micron in diameter forming clusters of similar orientation. While no apparent preferred orientation was measured in the parietal shell cross section, the base plate shell cross section revealed a preference for the alignment of the <0001> direction at the exterior of the shell, rotating by 90° towards the center of the base plate cross section. These maps will be used to construct image-based models of the barnacle shell for further study of mechanical response.

ACKNOWLEDGMENTS

The authors thank G. Wetzel and J. Hudson at Clemson University for preparing the barnacle shell cross sections for EBSD, and B. Orihuela and D. Rittschof of the Duke Marine Laboratory for providing barnacles.

[Sponsored by the NRL Base Program (CNR funded)]

References

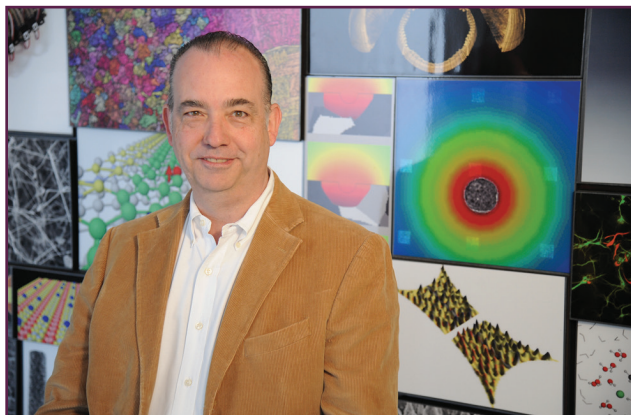
- ¹ M.P. Schultz, J.A. Bendick, E.R. Holm, and W.M. Hertel, "Economic Impact of Biofouling on a Naval Surface Ship," *Biofouling* **27**(1), 87–98, doi: 10.1080/08927014.2010.542809 (2011).
- ² D.K. Burden, D.E. Barlow, C.M. Spillman, B. Orihuela, D. Rittschof, R.K. Everett, and K.J. Wahl, "Barnacle *Balanus Amphitrite* Adheres by a Stepwise Cementing Process," *Langmuir* **28**, 13364–13372 (2012).
- ³ C.Y. Hui, R. Long, K.J. Wahl, and R.K. Everett, "Barnacles Resist Removal by Crack Trapping," *J. Roy. Soc. Interface* **8**, 868–879 (2011).
- ⁴ A.B. Rodriguez-Navarro, C. CabraldeMelo, M. Batista, N. Morimoto, P. Alvarez-Lloret, M. Ortega-Huertas, V.M. Fuenzalida, J.I. Arias, J.P. Wiff, and J.A. Arias, "Microstructure and Crystallographic-texture of Giant Barnacle (*Austromegabalanus psittacus*) Shell," *J. Structural Biol.* **156**, 355–362 (2006).
- ⁵ G.M. Khalifa, S. Weiner, and L. Addadi, "Mineral and Matrix Components of the Operculum and Shell of the Barnacle *Balanus amphitrite*: Calcite Crystal Growth in a Hydrogel," *Crystal Growth & Design* **2011**(11), 5122–5130 (2011).
- ⁶ A.C. Lewis, D.K. Burden, K.J. Wahl, and R.K. Everett, "Electron Backscatter Diffraction (EBSD) Study of the Structure and Crystallography of the Barnacle *Balanus Amphitrite*," *JOM* **66**(1), 143–148 (2014).



THE AUTHORS



ALEXIS C. LEWIS received her S.B. in 1997 from the Massachusetts Institute of Technology and Ph.D. in 2003 from the Johns Hopkins University, both in materials science and engineering. In 2003, she joined the Naval Research Laboratory as an NRC postdoctoral associate, and became a staff scientist in the Multifunctional Materials Branch in 2005. Her research interests center around advanced materials characterization, including 3D analysis of the crystallography and mechanical response of materials. Dr. Lewis is a member of the Materials Research Society, TMS, and ASM.



RICHARD K. EVERETT is the Associate Superintendent of the Materials Science and Technology Division and has been with NRL for over 35 years. He is also the Acting Branch Head of the Materials and Sensors Branch, Code 6360. He received his B.S. in materials science from Cornell University and his Ph.D. in engineering materials from the University of Maryland. From 2002 to 2005, he did a tour of duty as the Associate Director for Materials Science at Office of Naval Research – Global in London. His research interests include damage accumulation in Naval steels, synthesis and processing of advanced materials, micromechanics in multiphase materials, and X-ray tomography. He has over 100 publications and seven patents.

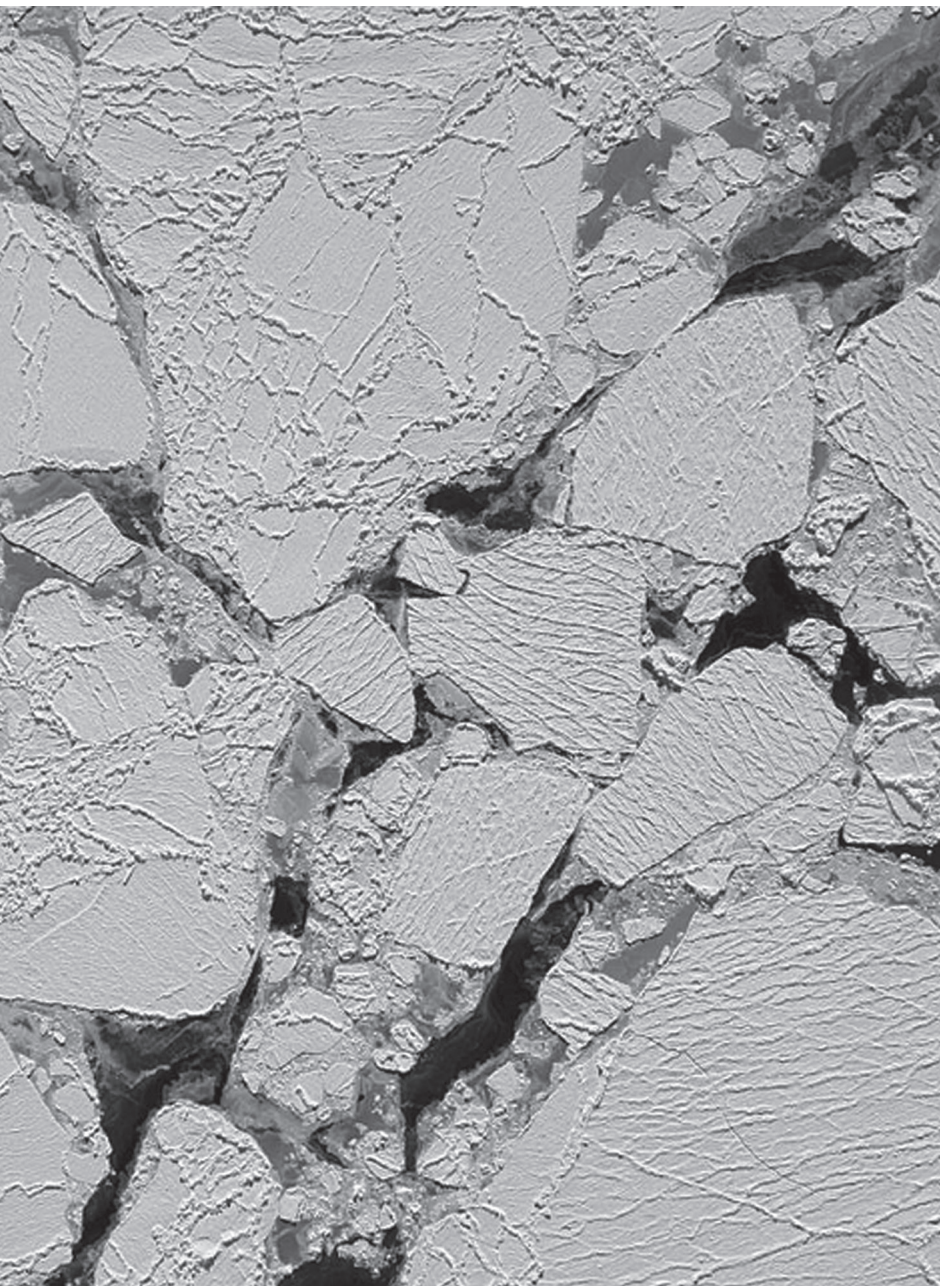


KATHRYN J. WAHL heads the Molecular Interfaces and Tribology Section at the Naval Research Laboratory. She received a B.A. in physics and mathematics from St. Olaf College (Northfield, MN, 1987) and a Ph.D. in materials science and engineering from Northwestern University (Evanston, IL) in 1992. She came to the NRL Chemistry Division as a National Research Council postdoctoral researcher and became a research staff member in the Chemistry Division in 1995. Her research focuses on the fundamental physics and chemistry of sliding and adhesive interfaces, from macroscopic to nanometer scales. She and her coworkers and postdocs have developed a broad array of in situ spectroscopic and mechanical methods to examine buried sliding and adhesive interfaces. Currently she leads a cross-disciplinary team of NRL Materials Directorate researchers tackling barnacle adhesion from the inside out by applying advanced analytical approaches: protein biochemistry and bioinformatics, surface chemistry and interfacial spectroscopies, and electron microprobe analyses and X-ray tomography. She also applies her interfacial wear and materials expertise to submarine and surface ship propulsion journal bearings tribology problems. She serves on the editorial boards of the journals *Wear* and *Tribology Letters*, is a recipient of the Department of the Navy Meritorious Civilian Service Award, and is a Fellow of the American Vacuum Society (AVS) and Society of Tribologists and Lubrication Engineers (STLE).



DANIEL K. BURDEN is an instructional assistant at Thomas Jefferson High School for Science and Technology. He earned his Ph.D. in physical chemistry at the University of Wisconsin, Madison, in 2010, where he studied chemical kinetics and reactions at the gas/liquid interface. Dr. Burden spent three years as a postdoctoral researcher at the Naval Research Laboratory, Washington, DC, where he employed multiple optical techniques to observe and interpret barnacle adhesion in situ. Currently, he is pursuing a career in secondary education teaching high school chemistry.

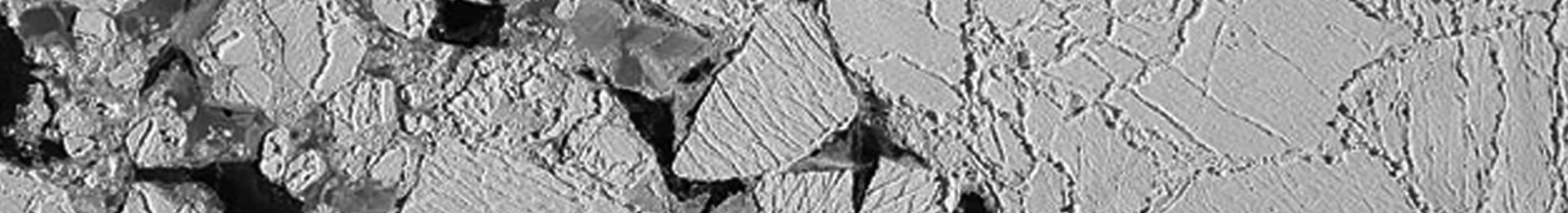
It's RTIME to Shine Light on Arctic Sea Ice Motion



Sea ice (frozen ocean water) plays a crucial role in planetary health. It helps to cool Earth's temperature by reflecting light and heat back into the atmosphere that the ocean water would otherwise absorb. Since sea ice can tell us a lot about global weather megatrends and more immediate meteorological concerns, measuring it accurately via satellite and aircraft is important. In an effort to more precisely characterize ice drift, a phenomenon that makes collecting contiguous data difficult, NRL has developed Real Time Ice Motion Estimation (RTIME), an airborne system that applies two computers and a real-time, orthographic photogrammetric camera to this task. In studies conducted in the Arctic off the northern coast of Alaska, RTIME has provided rapid (near real-time) point-to-point tracking of specific ice patches, which is used to achieve full-coverage radar and lidar surveys

to compare to satellite data, thus helping to calibrate CryoSat-2 satellite flyovers.

Going with the flow of drifting sea ice means collecting such data as ice thickness and velocity in real time and using orthorectification software to modify airborne survey coverage on the fly to avoid data gaps. The system's success was proven by the lack of data gaps between the flight lines of the 2013 surveys and the creation of complete lidar- and photo-mosaics of seven survey areas.



Measuring Arctic Sea Ice Motion in Real Time

R.A. Hagen,¹ M.F. Peters,¹ R.T. Liang,¹ J.M. Brozena,¹ and D.E. Ball²

¹*Marine Geosciences Division*

²*Exelis Information Systems, Herndon, VA*

The U.S. Naval Research Laboratory (NRL) has been collecting sea ice data in the Arctic off the northern coast of Alaska with an airborne system employing a radar altimeter, lidar, and a photogrammetric camera in an effort to obtain wide swaths of measurements coincident with CryoSat-2 track footprints. Because the satellite tracks traverse regions of moving pack ice, and the aircraft speed and measurement footprint are smaller than that of the satellite, it is necessary to know the local sea ice motion in order to plan and fly a full-coverage survey. With the advent of functional, real-time orthographic photogrammetric systems, we have developed a Real Time Ice Motion Estimation (RTIME) system that permits the rapid determination of sea ice motion. RTIME enables tracking of specific patches of ice, allowing direct comparison of airborne data to satellite data on a point-by-point basis. This system should be useful to other Arctic airborne science programs that often need to compensate for the effect of ice drift.

INTRODUCTION

Concern over changes in the characteristics of Arctic ice has driven demand for better monitoring of changes in the sea ice cover. In 2011, NRL, in coordination with the NASA IceBridge mission and the U.S. Army Corps of Engineers Cold Regions Research and Engineering Laboratory (USACE CRREL), began a five-year study focused on sea ice thickness and distribution variability with the intent of optimizing state-of-the-art sea ice forecasting models.¹ Field efforts continued in collaboration with the Alfred Wegener Institute for Polar and Marine Research, University of Alaska Fairbanks Geophysical Institute, and University of Alaska at Fairbanks Seasonal Ice Zone Observing Network (SIZONet) project in 2012 and 2013, and with the U.S. Naval Academy Polar Science Program in 2013.

NRL's airborne suite of sensors in 2011 and 2012 included a 10 GHz (incoherent) short-pulse radar altimeter built at NRL, a Riegl Q560 lidar, and an Applanix DSS439 photogrammetric camera system. In 2013, the lidar was upgraded to a Riegl Q680i (on loan from NOAA), and the radar was redesigned to allow coherent timing of the pulses.

In 2011, data for calibration and validation of airborne data were collected near a camp established in support of the U.S. Navy's Ice Expedition 2011 (ICEX 2011). We used this opportunity to develop techniques for collecting large swaths of data over moving ice in order to collect future survey grids centered beneath CryoSat-2. The flight tracks were planned in advance, using data from three GPS buoys that had been de-

ployed along an in situ line. However, local velocities from these buoys were only available up until aircraft takeoff, and the actual ice velocity at the time of survey was poorly known. Thus, the spacing between tracks was too large and the planned overlap between lidar swaths was inadequate in some cases, producing data gaps. Determining the sea ice motion, and incorporating that knowledge in near real time to modify flight-line layout and mitigate data gaps was a key objective for future airborne surveys.

To date, most of the existing data on sea ice motion have come from buoys drifting on the ice or from satellite images. While buoys can provide data with relatively high temporal resolution, their spatial sampling is poor. Also, the buoys quickly drift out of the survey area and must be frequently replaced at large expense. Satellite images can provide velocities over large areas with high spatial density, but poor temporal resolution.^{2,3} Neither method provides both the high temporal and high spatial resolution necessary for airborne survey planning. Aerial photography has been used for decades to determine glacial ice motion, and the collection of sea ice motion data with both high temporal and spatial resolution using airborne camera systems has been possible for several years. However, processing the aircraft trajectory and orthorectification of the imagery could only be done post-flight, rendering the method unsuitable for survey planning. The recent development of in-flight orthorectification software makes a near-real-time ice velocity measurement system possible, and led us to develop this capability.

HARDWARE, SOFTWARE, AND OPERATIONAL PROCEDURE

For the spring 2013 field season, we developed a Real Time Ice Motion Estimation (RTIME) system to determine sea ice motion using images from an Applanix DSS439 camera system and a beta version of Applanix's In-FlightOrtho software.⁴ Two computer systems were used: the camera operation and logging system and the separate orthorectification/RTIME computer. The camera system's POSAV 410 unit used the best GPS positioning available from either its internal dual-frequency GPS receiver or an external NAVCOM SF3050 GPS receiver, with a satellite real-time correction subscription service that has approximately 1 m accuracy with highly correlated errors over time. The camera had a 40 mm lens with 60-degree field of view to match the lidar coverage. The computer running the In-FlightOrtho and RTIME software had a direct Gigabit Ethernet connection to the camera system's computer. In-FlightOrtho software ran under Windows 7 and wrote the orthophotos to a solid-state disk, while RTIME software ran in a virtual CentOS 6 environment using the Geospatial Data Abstraction Library (GDAL).⁵ RTIME consisted of an image-correlation/velocity-estimation suite and front-end programs to let a user select orthophotos from a map for velocity determination.

The camera system captured images that were 7212 by 5408 pixels across- and along-track. At our survey altitude (nominally 840 m), this resulted in images of the ice surface covering approximately 1080 m across-track and 810 m along-track at a 0.15 m resolution. The In-FlightOrtho software used the aircraft trajectory and orientation information, along with a digital elevation model of the sea surface (EGM 2008 geoid) to orthorectify the images.

For the CryoSat-2 underflights, data were collected along six long transits beginning approximately 30 km offshore of Barrow, Alaska, and extending to the NNE 60 to 170 km beneath descending satellite tracks. Additionally, a survey block consisting of multiple flight lines was flown at selected locations along each of these transits (Fig. 1). This survey layout gave us the opportunity to compare our data against numerous CryoSat-2 radar waveforms in various areas.

Initially we had hoped to determine ice motion continuously and automatically using consecutive photos. However, the time difference of 6 s between consecutive photos was too short, and the ice motion too slow (on the order of 15 cm or 1 pixel in the images in 6 s), to generate enough offset between photos to get reliable ice velocities. Instead, the operational procedure for each flight started with a prospecting flightline along the satellite track. When a suitable ice region was iden-

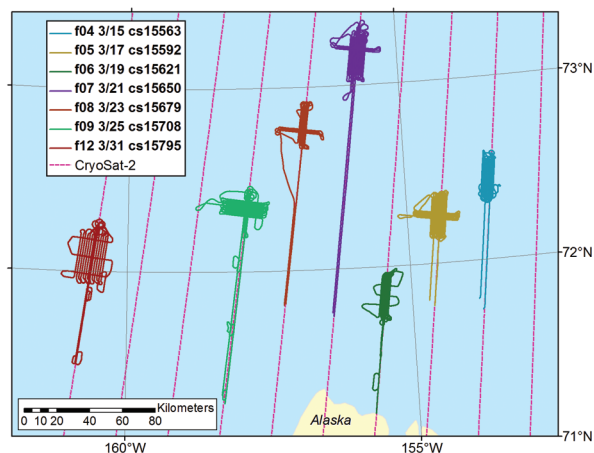


FIGURE 1
Locations of NRL 2013 CryoSat-2 underflights. Figure key shows flight number, date, and satellite orbit number. CryoSat-2 tracks are shown in magenta. Survey tracks shown are as flown (not ice drift corrected).

tified, the camera was turned on and In-FlightOrtho was used to make five or six orthophotos. The plane would turn around, taking about 2 min, and re-fly the same portion of the track, collecting a similar number of orthophotos. The operator used RTIME and a web browser interface to select likely pairs of overlapping photos for the correlation/velocity estimation suite to use.

RTIME finds photo footprints, plots the locations, and generates an HTML page that links those locations to JPEG versions of the orthophotos. The photo footprint plot is then displayed in a web browser interface, where the operator can examine the images and select a pair for processing. Selected photos are then passed to the correlation software, which selects a series of "chips" in the first photo and performs 2D correlations to find the best matches in the second photo. Processing time is dependent on the chip size, the number of chips, and how much area must be searched for matches. If the chip size is $N \times N$ and the search image size is $M \times M$, the total number of multiplications that must be performed for each chip is N^2M^2 . In practice, 10 to 20 chips that were 15.15 m square (101 0.15-m-pixels in each dimension) were used, and the search area was constrained with an initial estimate of ice velocity so that only a limited portion of the second image had to be searched. Additionally, we found that the chips could be decimated by up to a factor of 5 to further speed up the correlation with no detrimental effect on the results.

During the field surveys, it took less than 3 min to generate the orthophotos, select the overlapping pair(s), and determine the ice velocity. The velocity estimates were used to plan track layout for the rest of the flight. The survey operators also generated orthophotos near

the end of survey lines and at the beginning of subsequent lines to check for ice velocity changes (temporal and spatial) during the day's survey flight in case the flight tracks needed to be adjusted. This was the case on the last flight, where the flight team determined during the survey that the ice motion differed greatly between the northern (0.08 m/s) and southern (0.03 m/s) regions of the survey area.

ALGORITHM

Correlation techniques to measure shifts between digital images have been used since at least 1975.⁶ Our technique tries to find the maximum correlation coefficient between two or more images by examining pixel intensity subsets.

Cross-correlation was performed on each chip in the first image against all possible chips within the search area in the second image. The chip with the highest correlation coefficient in the second image was chosen as representing that chip-pair displacement. The resulting set of correlations from all of the chips was then passed to a routine that uses a density-based clustering algorithm⁷ on the chip displacements to determine the overall displacement of the photo-pair. Finally, the software used the photo times and displacement to compute the ice motion vector for the orthophoto pair. Although even minor rotation between the image pairs will cause reduced correlation values using this simple method, in practice this is not a significant source of

error given the short time period (2 to 20 min) between the acquisitions of the two images. Another source of error is ice deformation occurring within the images. We have observed significant localized deformation in image pairs during the course of our surveys, but again, this is not generally a problem in the short time frame of the images collected to generate ice velocities.

RESULTS

During the 2013 field season, NRL deployed a GPS buoy on the pack ice near the survey areas. Figure 2 shows comparisons of the ice velocity results from the buoy and from the RTIME system during several of the surveys. The RTIME generated velocities generally follow the same overall velocity trends as the buoy. However, in some instances, the velocities are quite different (not unexpectedly, given the large distances between the buoy and survey locations; the buoy was about 32 km NW of the flight 05 survey, 86 km SSE of the flight 07 survey, and 32 km S of the flight 09 survey). Because of the improved flight planning resulting from using the RTIME system, the 2013 surveys do not have the data gaps between flight lines seen in prior years. Post-flight application of the RTIME software to photos collected during the survey allows for calculation of x- and y-shifts necessary to correct the photo positions to a single instant in time (Fig. 3). The image-to-image corrections computed by RTIME can be added together to get total corrections for each image relative to a single

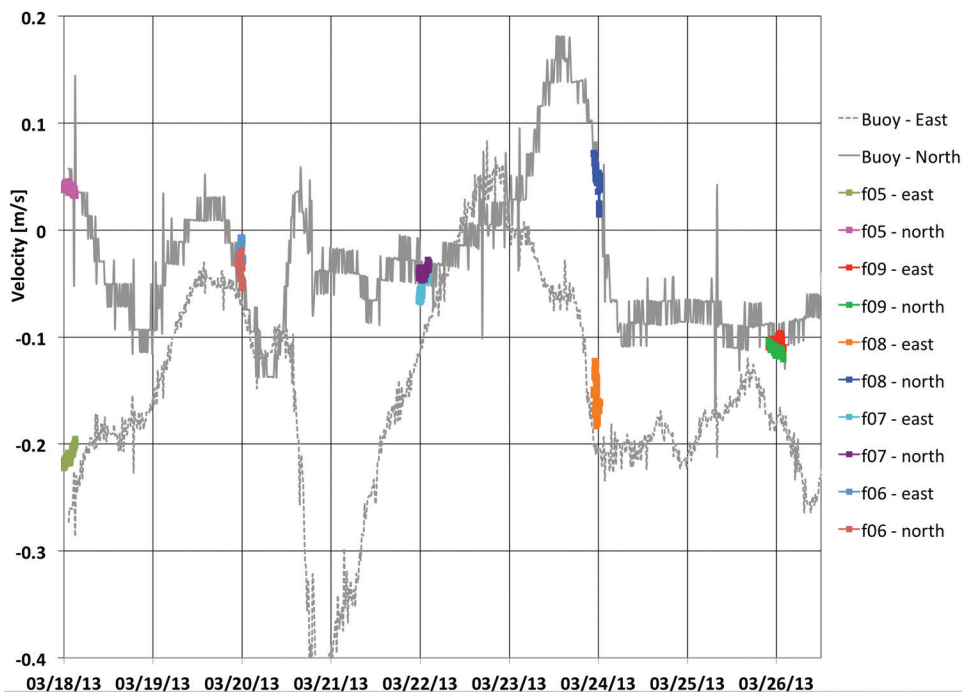


FIGURE 2
Comparison of RTIME-derived sea ice velocities for 2013 surveys with results from a nearby GPS buoy. Easterly and northerly components of the drift are shown separately.

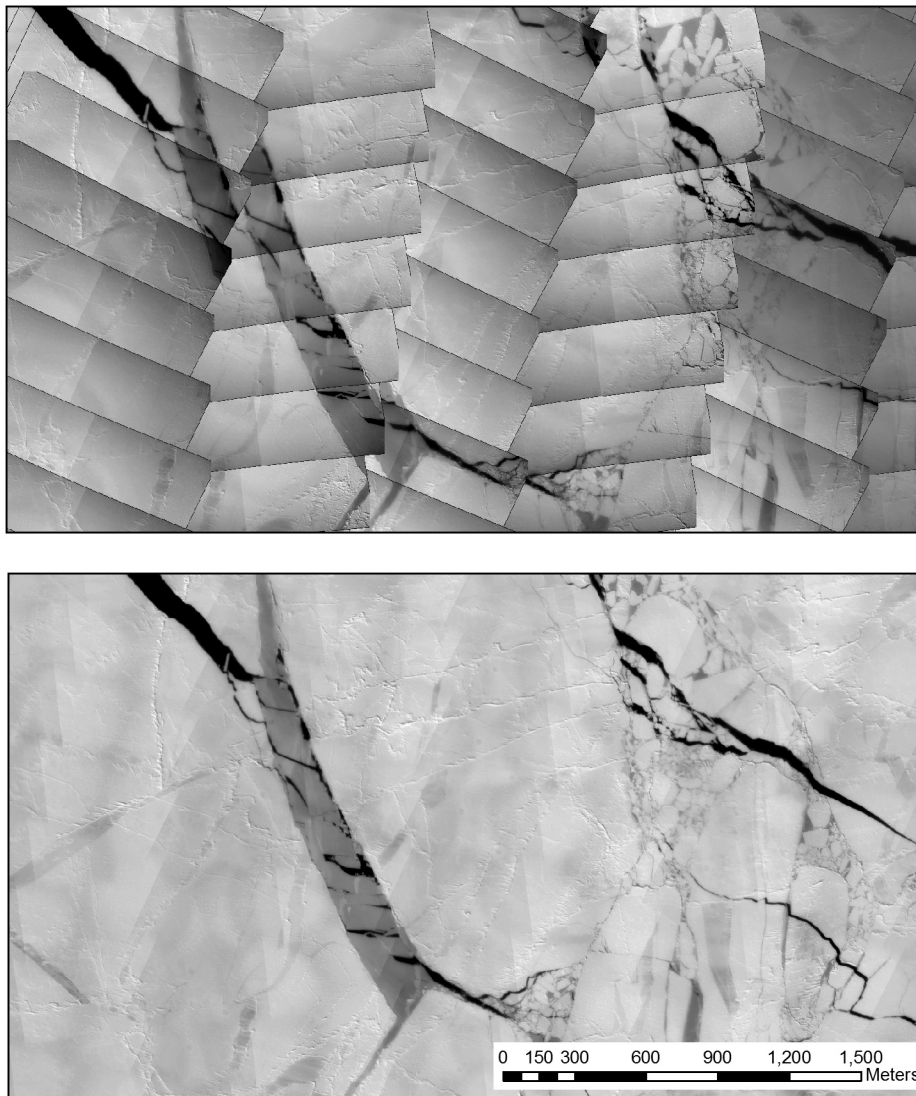


FIGURE 3

Example of images collected during flight 04 uncorrected for sea ice motion (top), and corrected for motion and mosaicked into a single image (bottom). The sequential images (along NNE-SSW flightlines) are ~ 6 s apart, and the columns of images are separated by ~ 5 to 12 min and 100 to 200 m of ice drift each in this area.

reference image. For the purposes of our project, the photos were all shifted to their positions at the instant that the CryoSat-2 satellite passed directly overhead.

A further key use of the RTIME system is to provide corrections for local ice drift in other, coincident data sets. Because lidar (and radar) data are collected continuously and not at discrete intervals like photos, the linear translation estimates from RTIME must be used post-collection to generate a continuous model of ice velocities in both geographic space and time. This model is then used to create a drift-corrected “pseudo aircraft trajectory” that is applied to the lidar data to generate a corrected lidar point cloud (Fig. 4).

CONCLUSIONS

Knowledge of surface motion is required for the efficient collection of complete grids of airborne lidar data over moving sea ice. Temporal and spatial deficiencies in existing methods commonly used to measure these velocities, when applied to a real-time situation, led to the investigation of new techniques. Advances in the software used to produce orthophotos, coupled with precise real-time navigation and aircraft orientation, makes possible a near-real-time velocity measurement system that does not have extensive new equipment or power requirements when used with an existing camera

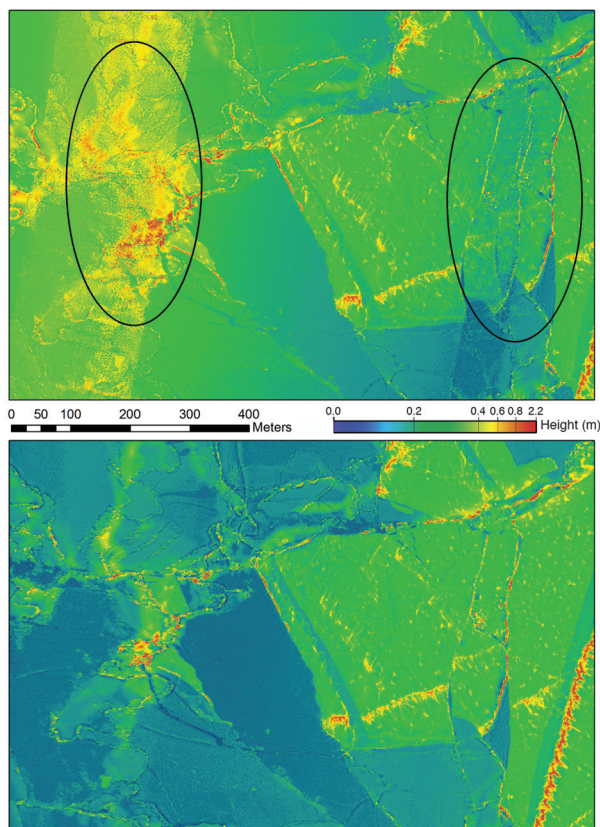


FIGURE 4
Example of lidar data collected during flight 07. The upper image shows the non-drift-corrected data from three lidar lines. The lower image has been corrected for sea ice drift. Note the duplicated features in the overlap areas indicated by the black ovals that have been corrected in the lower image.

system. Such a system was developed and successfully deployed in a March 2013 Arctic sea ice survey. Not only were sea ice velocities determined sufficiently rapidly to plan survey flight tracks in the air, but local geographic and temporal changes requiring track adjustment were detectable. The same software system has been readily modified to provide adjustments for the creation of post-flight photo-mosaics and large lidar grids.

Inadequate knowledge of the velocity and direction of movement of the sea ice beneath a satellite pass makes it difficult to collect airborne data over the exact strip of ice imaged by the satellite. Therefore, typical airborne underflights can only be compared to satellite data on a statistical basis. RTIME provides accurate sea ice motion velocities when conducting our surveys, enabling us to image the same patch of ice as the satellite and allowing us to directly compare our airborne data to the satellite on a point-by-point basis.

This system should be useful to other arctic airborne science programs such as the NASA IceBridge mission, the European Space Agency's CryoVex program, and

the Alfred Wegener Institute's PAMARCMIP program, that often also wish to compensate for the effect of ice drift (e.g., as they overfly in situ field surveys, or underfly satellites).

ACKNOWLEDGMENTS

We would like to thank Mike Vermillion of NRL, Chase Stoudt of Qinetiq, and the U.S. Naval Academy cadets who set up targets on the fast-ice, as well as the pilots of Twin Otter International who did an excellent job flying the exacting survey tracks.

[Sponsored by the NRL Base Program (CNR funded) and ONR]

References

- ¹ J. Gardner, J. Richter-Menge, S. Farrell, and J. Brozena, "Coincident Multiscale Estimates of Arctic Sea Ice Thickness," *Eos Trans. Amer. Geophys. Union* **93**(6), 57–58 (2012).
- ² B. Holt, D.A. Rothrock, and R. Kwok, "Determination of Sea Ice Motion from Satellite Images," in *Microwave Remote Sensing of Sea Ice* (ed. F.D. Carsey), Geophysical Monograph 68 (American Geophysical Union, Washington, DC), pp. 343–354 (1992).
- ³ R. Kwok, "Satellite Remote Sensing of Sea Ice Thickness and Kinematics: A Review," *J. Glaciology* **56**, 200 (2011).
- ⁴ R. Smith, "DSS - Mobile Mapping and Positioning Solutions Accurately and Reliably Capture and Measure the World Around Us," <http://www.applanix.com/solutions/airborne/dss.html>, Applanix Corp., Richmond Hill, Ontario, Canada (accessed October 1, 2013).
- ⁵ Open Source Geospatial Foundation, "GDAL - Geospatial Data Abstraction Library," <http://www.gdal.org/index.html> (accessed October 1, 2013).
- ⁶ T.J. Keating, P.R. Wolf, and F.L. Scarpace, "An Improved Method of Digital Image Correlation," *Photogrammetric Engineering and Remote Sensing* **41**(8), 993–1002 (1975).
- ⁷ J. Sander, M. Ester, H. Kriegel, and X. Xu, "Density-based Clustering in Spatial Databases: The Algorithm GDBSCAN and its Applications," *Data Mining Knowledge Discovery 2* (Kluwer Academic Publishers, the Netherlands, 1998), pp. 169–194.

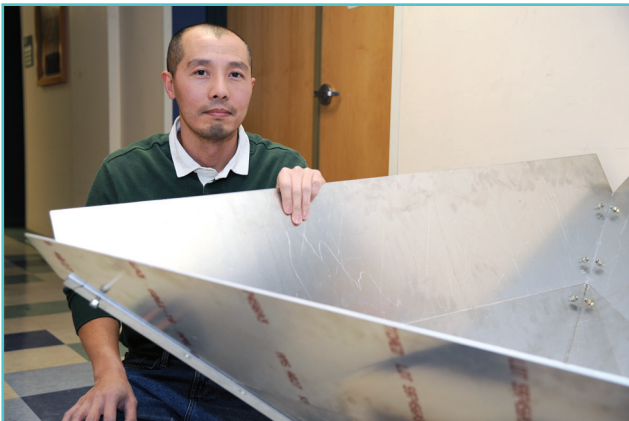
THE AUTHORS



RICK A. HAGEN received his Ph.D. in geology and geophysics from the University of Hawaii in 1992. He was a postdoc at the Alfred Wegener Institute for Polar and Marine Research from 1993 to 1996, and an NRC postdoc at NRL from 1996 to 1998. After working for Fugro Seafloor Surveys International from 1998 to 2002, he returned to NRL in 2003 as a research scientist in the Marine Geosciences Division. His current research projects include airborne characterization of Arctic sea ice using photogrammetry and lidar data, and MBSAR radar processing for change detection.



MARY PETERS received a B.S. with honors in mathematics from the University of Maryland in 1982. After being a student employee while an undergraduate and later graduate student, she joined the Naval Research Laboratory in 1985 and is currently a mathematician in the Marine Physics Branch of the Marine Geosciences Division. Over the past 30 years she has worked on software for airborne remote sensing and data acquisition systems including aircraft positioning; software and algorithms for the analysis and modeling of geo-potential data including gravity meter off-level and error modeling; gravity and gradient modeling software; and analysis of the occasional shipboard data set.



ROBERT T. LIANG received his B.S. degree in electrical engineering in 1993 and his M.S. in telecommunications and computers in 1999 from George Washington University. He started at NRL as a co-op student in 1990 and is now the senior engineer for the Marine Physics Branch. He has worked on an airborne acquisition system for gravity and magnetic surveys of the Arctic Ocean aboard NRL P-3 aircraft, and also on a system to collect oceanographic and hydrographic data from existing receivers installed on P-3s. He has logged numerous flight hours in the Arctic and Gulf of Mexico. He was the lead engineer for multisensor airborne survey and counter-IED work in Afghanistan and Iraq. He has also worked on smaller fixed-wing aircraft, most recently integrating the Multi-Band Synthetic Aperture Radar on a Pilatus PC-12.



JOHN BROZENA is head of the Marine Physics Branch at the Naval Research Laboratory. He received his B.A. in physics from the University of Virginia in 1976, an M.A. in applied mathematics from the University of Maryland in 1986, and a Ph.D. in geophysics from Cambridge University in 1996. He has worked on the development of airborne remote sensing techniques for the past 35 years at NRL and in the process has acquired more than 6000 flight hours experience on various research projects in geophysics, geodesy, acoustics, and oceanography including pioneering the first successful airborne gravimetry system for fixed-wing aircraft, and the development of long-baseline kinematic GPS for aircraft positioning at the centimeter level. Most recently he was project manager and chief scientist for Projects Rampant Lion and Perseus, multisensor airborne geophysical surveys of the major portion of Afghanistan that included synthetic

aperture radar, digital photogrammetry, hyperspectral imaging, gravity and magnetic sensors, and then counter-IED work in Iraq. Besides the Afghanistan experiment, he has led major multisensor airborne field experiments over Antarctica, Greenland, and the Atlantic, Pacific, and Arctic ocean basins.

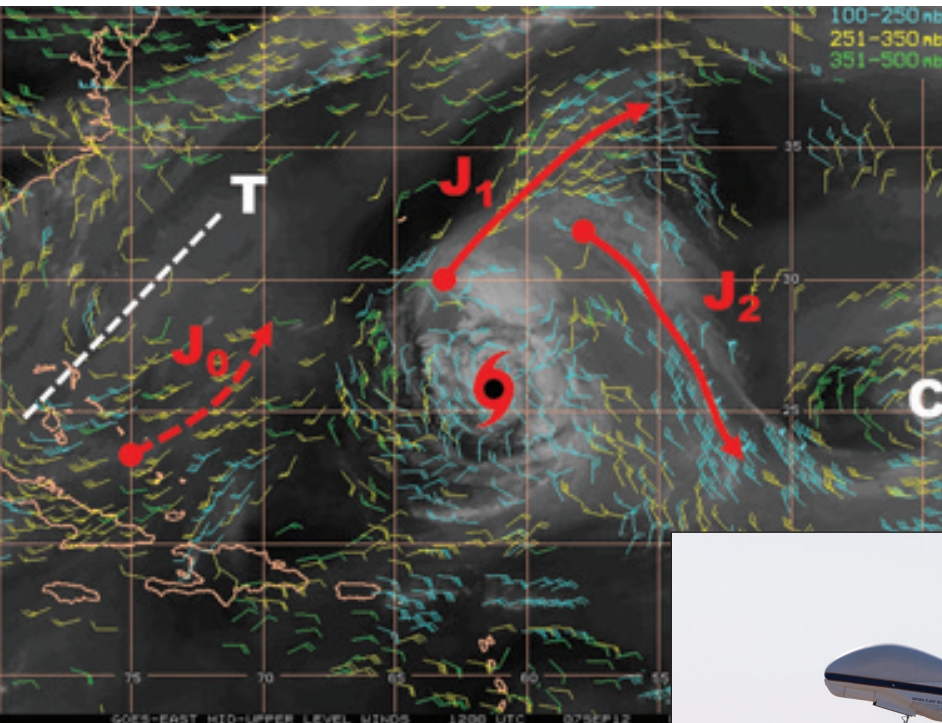


DAVID BALL received his B.S. in electrical engineering in 1990 from Virginia Polytechnic Institute and State University. He was employed by Locus, Inc. in Alexandria, Virginia, and started working on a one-person contract with the Marine Physics Branch of NRL in 1991. Since then, his company has been sold, merged, bought out, split, and renamed around seven times. He still works under contract to Marine Physics with his employer's current incarnation, Exelis Information Systems, working on airborne and marine data collection, reduction, exploitation, and presentation. During his years at NRL he has worked on gravimetry, geomagnetics, ocean topography, photogrammetry, lidar, radar, and SAR.

Somewhere, Over the Hurricane, Global Hawks Fly...

...and when these high-altitude, long-endurance unmanned air vehicles (UAVs) do, they learn crucial information about storm intensity and structure. Using a suite of in situ and remote instruments and their ability to fly over storms for more than 20 hours, Global Hawk UAVs can reach more distant storms than other hurricane reconnaissance aircraft and provide far more

in-depth data on the storms and their environments. NASA's three-year Hurricane and Severe Storm Sentinel (HS3) campaign, which is conducted in collaboration with NRL science team members, has been observing hurricanes from the surface to 60,000 ft above the Atlantic and Gulf of Mexico and uses the pair of Global Hawks to probe both the upper-

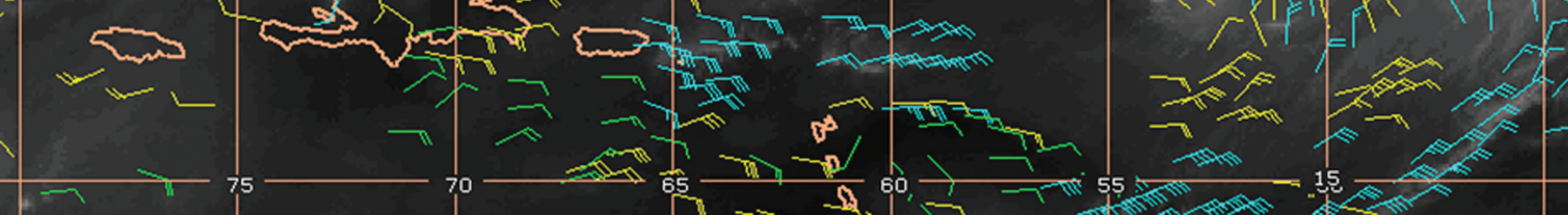


tropospheric outflow layer and the near-surface inflow layer of tropical cyclones (TCs). Their observations, tied with the Navy's Coupled Ocean/ Atmosphere Mesoscale Prediction System for Tropical Cyclones (COAMPS-TC) model, have shed new light on the

complex relationship between those two key regions and fluctuations in storm intensity, and have highlighted the influence of the outflow layer on TC intensity and structural changes.



Photo of Global Hawk, AV-6, used for observing tropical cyclones and the surrounding environments (Courtesy of NASA).



Using Unmanned Aircraft to Probe Hurricanes

J.D. Doyle,¹ J. Moskaitis,¹ P. Black,² E. Hendricks,¹ P.A. Reinecke,¹ Y. Jin,¹ and S. Braun³

¹Marine Meteorology Division

²SAIC, Inc.

³NASA Goddard Space Flight Center

New insight into tropical cyclone intensity change is attained through participation in a multiyear NASA field campaign aimed at observing hurricanes from the surface to 60,000 ft above the Atlantic and Gulf of Mexico using unmanned aircraft and instruments, both with unprecedented capabilities. The Hurricane and Severe Storm Sentinel (HS3) mission, conducted in collaboration with science team members from the Naval Research Laboratory, uses a pair of NASA Global Hawk unmanned aircraft equipped with remote and in situ meteorological instrumentation. These High-Altitude, Long-Endurance (HALE) unmanned aircraft have the capability to fly over storms for long periods of time (20+ hours), which provides a more complete sampling of the storm and environment, and can reach storms much farther away from base. Simultaneously probing both the upper-tropospheric outflow layer and near-surface inflow layer provides an unprecedented opportunity to unravel the complex relationship between these key regions leading to tropical cyclone intensity change. Global Hawk observations and the Navy's Coupled Ocean/Atmosphere Mesoscale Prediction System for Tropical Cyclones (COAMPS-TC™) model results suggest that the outflow layer plays a more important role in tropical cyclone intensification and structural changes than previously thought.

TROPICAL CYCLONE INTENSITY CHANGE

Understanding and predicting changes in tropical cyclone (TC) intensity remains one of the greatest challenges in atmospheric science today. Previous TC research programs and field campaigns predominantly have focused on processes associated with the atmospheric boundary layer, deep convection, large-scale environmental conditions, and the ocean mixed layer, all of which have been found to impact TC development and intensification to varying degrees. However, TC outflow jets that spiral away from the storm center in the upper troposphere remain largely unexplored due to a lack of high-altitude research aircraft capable of making sustained measurements in this portion of the TC. This region is a critical one, as changes in the TC outflow jets can directly cause changes in the TC secondary (in-up-out) circulation. The secondary circulation consists of radial inflow near the surface, ascent in deep convection concentrated near the storm center (i.e., the hurricane eyewall), and radial outflow in the upper troposphere. TCs intensify through enhanced radial inflow, which subsequently allows for increasing heat, moisture, and high angular momentum air to be transported into the inner core, which in turn reinforces vigorous deep convection. Continuity must be maintained between the inflow, upward, and outflow branches of the secondary circulation, and therefore changes in one branch will directly impact the other branches.

HURRICANE AND SEVERE STORM SENTINEL

The Hurricane and Severe Storm Sentinel (HS3) program is a three-year NASA field campaign aimed at observing hurricanes from a unique vantage in the lower stratosphere, above the storm. The Global Hawk platform used in HS3 is ideal for probing the storm from the outflow layer to the surface. One Global Hawk is focused on measuring the environmental conditions, especially the hurricane outflow layer, with a new mini-drosonde: small tube-shaped devices, equipped with parachutes, that gather and transmit data as they fall to the ocean surface while profiling atmospheric pressure, temperature, humidity, and wind. The environmental Global Hawk is also equipped with onboard remote sensors such as the Cloud Physics Lidar (CPL) from the NASA Goddard Space Flight Center (GSFC) and the Scanning High-resolution Interferometer Sounder (S-HIS) from the University of Wisconsin. The former detects aerosol and cloud tops, especially upper-level thin cirrus clouds associated with hurricane outflow channels, while the latter remotely profiles atmospheric temperature and humidity in the clear-air environment below. A second Global Hawk is used to probe the inner core of the storm using other instruments developed by NASA. The Hurricane Imaging Radiometer (HIRAD) from Marshall Space Flight Center is a multifrequency radiometer system used to map ocean surface winds and rainfall rate, especially in the hurricane eyewall, where the strongest winds and heaviest rainfall

occur. The High-altitude Wind and Rain Atmospheric Profiler (HIWRAP) from GSFC is a conically scanning Doppler radar that maps the hurricane's inner-core 3D wind and rainfall structure, and the High-Altitude MIMIC Sounding Radiometer (HAMSR) from the Jet Propulsion Laboratory maps precipitation features and measures the large thermal anomaly in the hurricane eye.

OBSERVATIONS OF TROPICAL CYCLONE OUTFLOW DURING HS3

During the HS3 program in 2012 and 2013, mini-dropsondes deployed from the NASA Global Hawk environmental aircraft revealed the vertical and horizontal structure of TC outflow jets. An overflight of Hurricane Leslie's outflow occurred during the very first HS3 flight, on September 6 and 7, 2012. The flight made a long loop around Leslie, deploying a series of mini-dropsondes along the axis of an equatorward-directed outflow jet (J_2 in Fig. 1) located between the center of the tropical cyclone and an upper-tropospheric trough. Figure 2 shows a height-latitude cross section

of potential temperature and wind created from the dropsonde data. The highest wind speeds of 35 m s^{-1} in the jet are located at 14 km, which is just below the tropopause. This wind maximum at 14 km is coincident with the top of the cirrus cloud deck, as indicated in the CPL observations (courtesy of Dennis Hlavka, GSFC). Above 14 km, at the top of the outflow jet, there is a very sharp shear zone in which the wind speed drops by approximately 20 m s^{-1} in 1 km of altitude. Figure 3 shows the corresponding Richardson number ($Ri = \frac{g}{\theta} \frac{\partial \theta}{\partial z} / \left[\left(\frac{\partial u}{\partial z} \right)^2 + \left(\frac{\partial v}{\partial z} \right)^2 \right]$, where θ is the potential temperature, g is the acceleration due to gravity, z is the altitude, and u, v are the zonal and meridional wind components). The shear zone is associated with an Ri between 0.25 and 1 (blue shading), with embedded layers of Richardson number less than 0.25 (red shading). Turbulence occurs when $Ri < 0.25$ (although reported critical values have ranged from roughly 0.2 to 1.0), which is a necessary condition for velocity shear to overcome the tendency of a stratified fluid to remain stratified. When Ri is large, turbulent mixing is generally suppressed. The strong shear above the wind

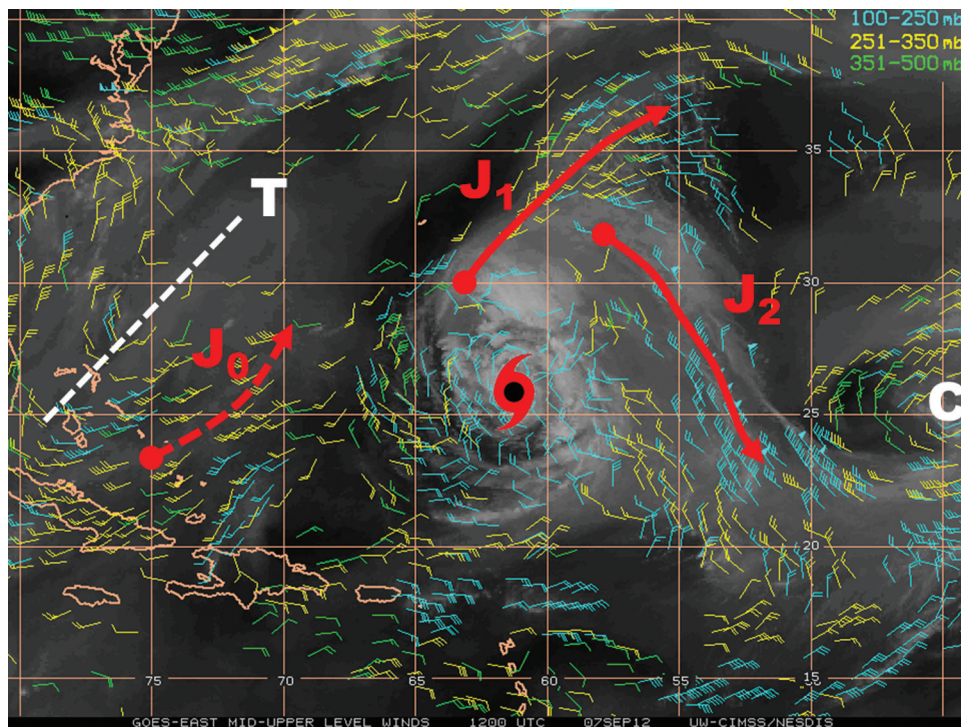


FIGURE 1 Middle and upper tropospheric atmospheric motion vectors, superimposed on water vapor imagery, for 12 UTC September 7, 2012 (from the U. of Wisconsin Cooperative Institute for Meteorological Satellite Studies, UW-CIMSS). The approximate center of Hurricane Leslie is marked by the red hurricane symbol. An upper level trough to the west of the center is marked by a "T" and a white dashed line, while an upper cold-low to the east of the center is marked by a "C." An upper subtropical jet associated with the trough is indicated by a dashed line and marked by "J₀," while poleward- and equatorward-directed outflow jets are indicated by solid red lines and marked by "J₁" and "J₂," respectively, as well as by the blue wind barbs indicating average winds for the 100 to 250 mb pressure layer. The Global Hawk dropped sondes along the axis of the equatorward-directed outflow jet, J₂.

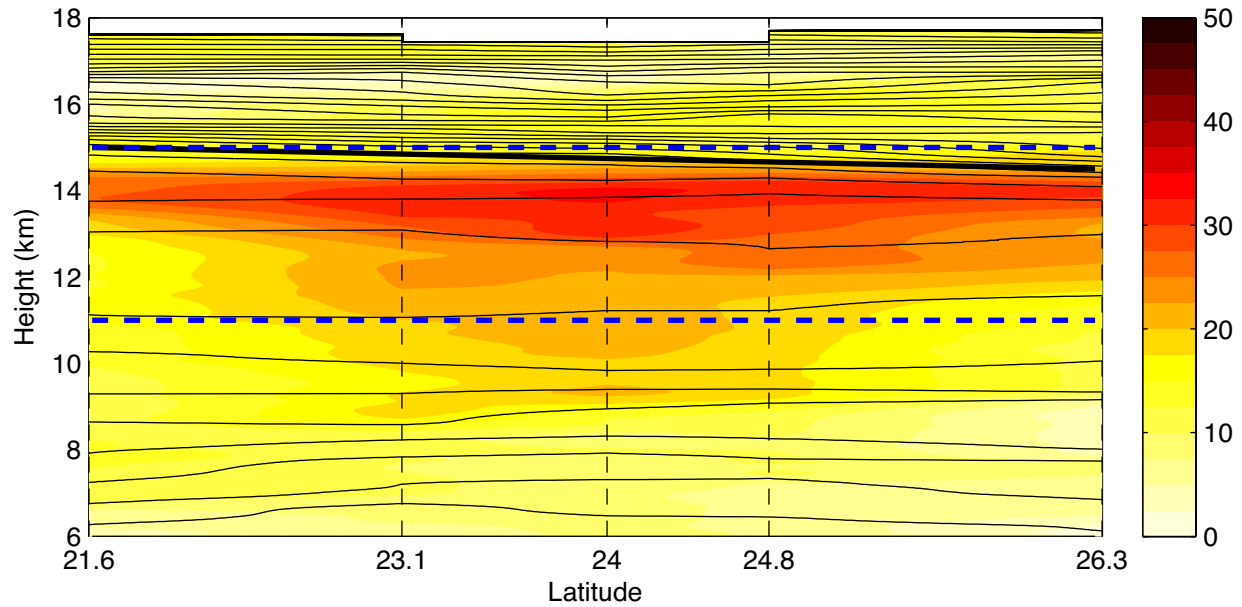


FIGURE 2
 The upper plot shows a height–latitude cross section created from five Global Hawk dropsondes released during the HS3 flight around Hurricane Leslie. The color shading indicates wind speed (contoured at 2.5 m s^{-1} intervals) and the black contours are isentropes (every 2.5 K). The thick black line indicates the approximate location of the tropopause. The dashed black lines indicate the latitudes of the drops. The blue dashed lines broadly defines the outflow layer region.

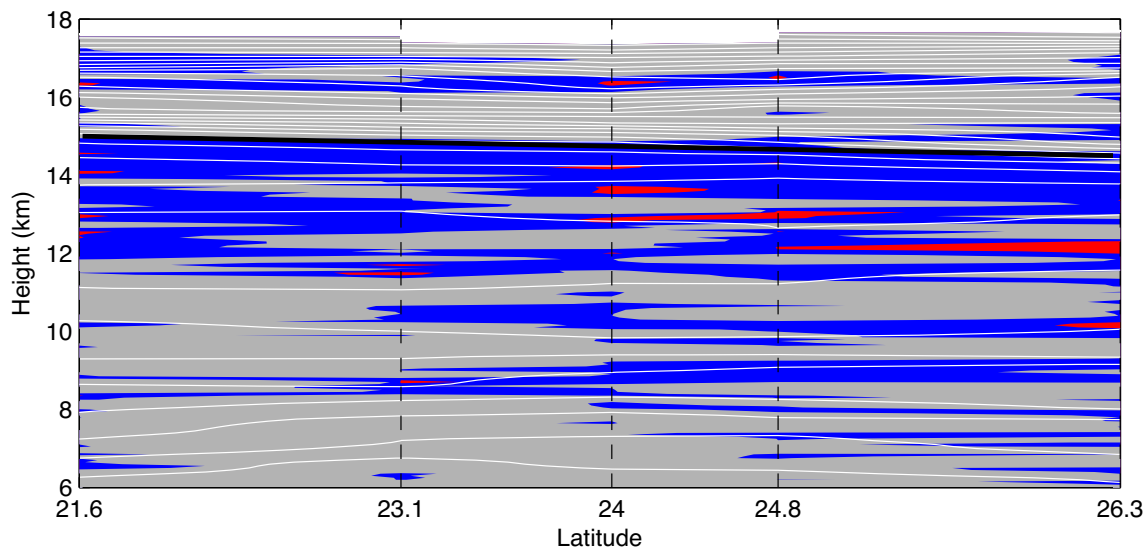


FIGURE 3
 As in Fig. 2, a height–latitude cross section is created from five Global Hawk dropsondes released during the HS3 flight around Hurricane Leslie. The color shading indicates Richardson number (Ri): gray for $Ri > 1$, blue for $0.25 \leq Ri \leq 1$, and red for $Ri < 0.25$. The white contours are isentropes, drawn at 2.5 K intervals. The thick black line indicates the approximate location of the tropopause. The dashed lines indicate the latitudes of the drops.

maximum combined with moderate stability results in Richardson numbers at or below the critical value of $\frac{1}{4}$. This observation is repeated over all the sondes deployed along the axis of Leslie’s equatorward-directed outflow jet. From this result, we conclude that vertical shear or Kelvin–Helmholtz instability exists in this

region, acting as a powerful mixing mechanism in the exchange of upper tropospheric and stratospheric air parcels.

During the 2012 field campaign, the environmental Global Hawk made five lawnmower pattern flights around Hurricane Nadine. The first leg of the second

Nadine flight (September 14–15, 2012) was by far the best overflight of an outflow jet emanating from Nadine. This east-west oriented flight leg intersected the anticyclonically curving outflow jet (indicated by the red curved outflow axis in Fig. 4) that emerged from the convectively active northwest side of Nadine.

IMPACT OF HS3 DROPSONDES ON COAMPS-TC PREDICTIONS

COAMPS-TC is a regional model developed specifically for the prediction of tropical cyclones at forecast times up to 5 days. The COAMPS-TC system includes

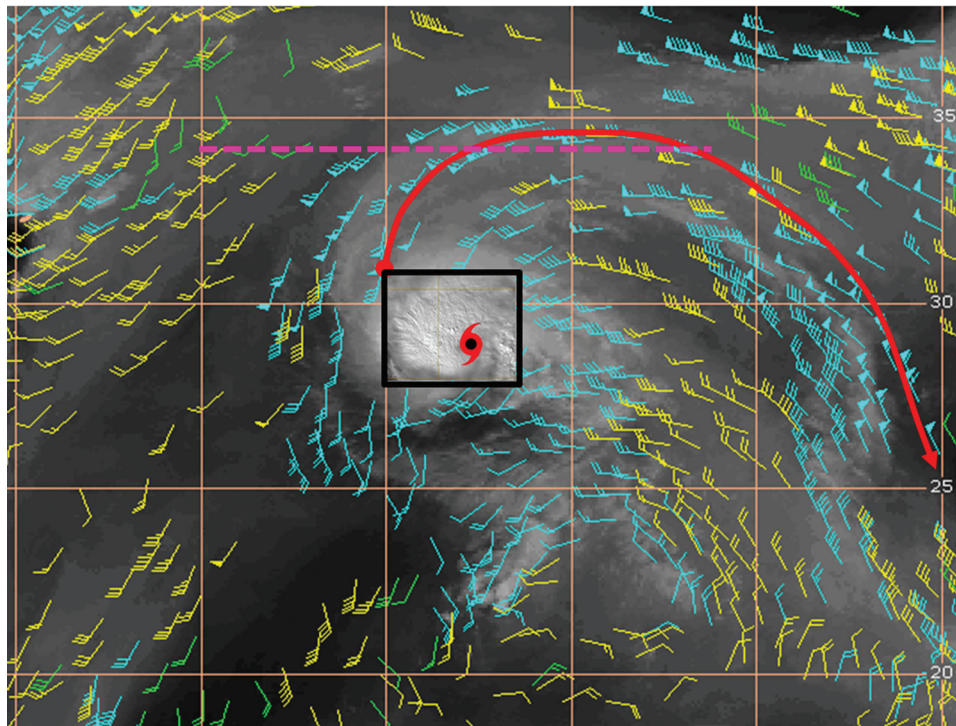


FIGURE 4 UW-CIMSS middle and upper tropospheric atmospheric motion vectors, superimposed on water vapor imagery, for 18 UTC September 14, 2012. The approximate center of Hurricane Nadine is marked by the red hurricane symbol. Strong convection to the NW of the center shown by the overshooting tops (shaded cauliflower appearance) in the MODIS visible image inset outlined in black gives rise to an outflow jet, shown by the solid red curve, that spirals anticyclonically away from the storm center directed equatorward (see blue wind vectors, which are for the 100 to 250 mb pressure layer). The dashed magenta line indicates the approximate flight path of the Global Hawk.

A height–longitude cross section of potential temperature and wind speed created based on the dropsonde data from the aforementioned flight leg is shown in Fig. 5. In Nadine, the outflow jet is deeper than for Leslie, but like Leslie, the jet maximum is located just below the tropopause (where the isentropes begin bunching together just above 14 km). Above the jet maximum is a shear zone located in the lower stratosphere, for which the Richardson number is below 1 (see Fig. 6). Similar to the Leslie case, the Richardson number is driven to such low values by the strong shear, overcoming the moderate static stability of the lower stratospheric vertical temperature gradient.

data quality control, analysis, initialization, and forecast model subcomponents. The Navy Atmospheric Variational Data Assimilation System (NAVDAS) has been modified for tropical cyclone applications to blend the available atmospheric observations from a variety of sources, along with synthetic observations that define the TC structure and intensity. The COAMPS-TC atmospheric model uses the nonhydrostatic and fully compressible form of the dynamical equations, and includes representations of cloud microphysical processes, convection, radiation, boundary layer processes, and surface layer fluxes, and allows for moving nested grid families that independently follow individual tropi-

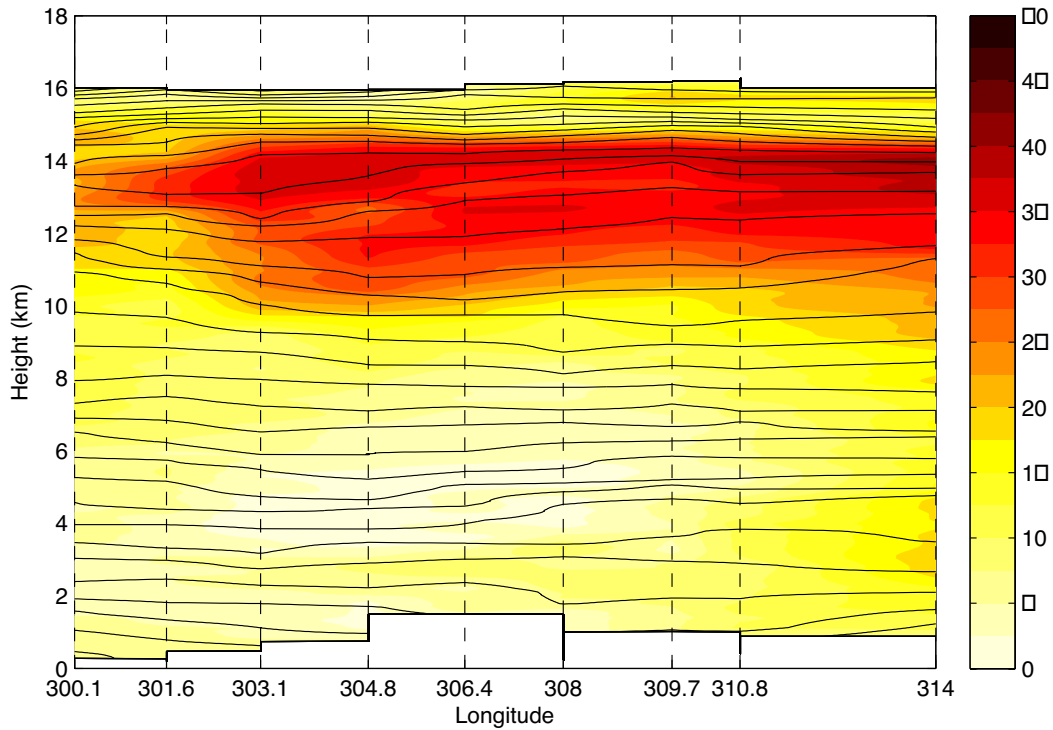


FIGURE 5
 A height–longitude cross section created from nine Global Hawk dropsondes released during the first leg of the mission to Hurricane Nadine on September 14–15, 2012. The color shading indicates wind speed (contoured at 2.5 m s^{-1} intervals) and the black contours are isentropes (every 2.5 K). The dashed lines indicate the longitudes of the drops.

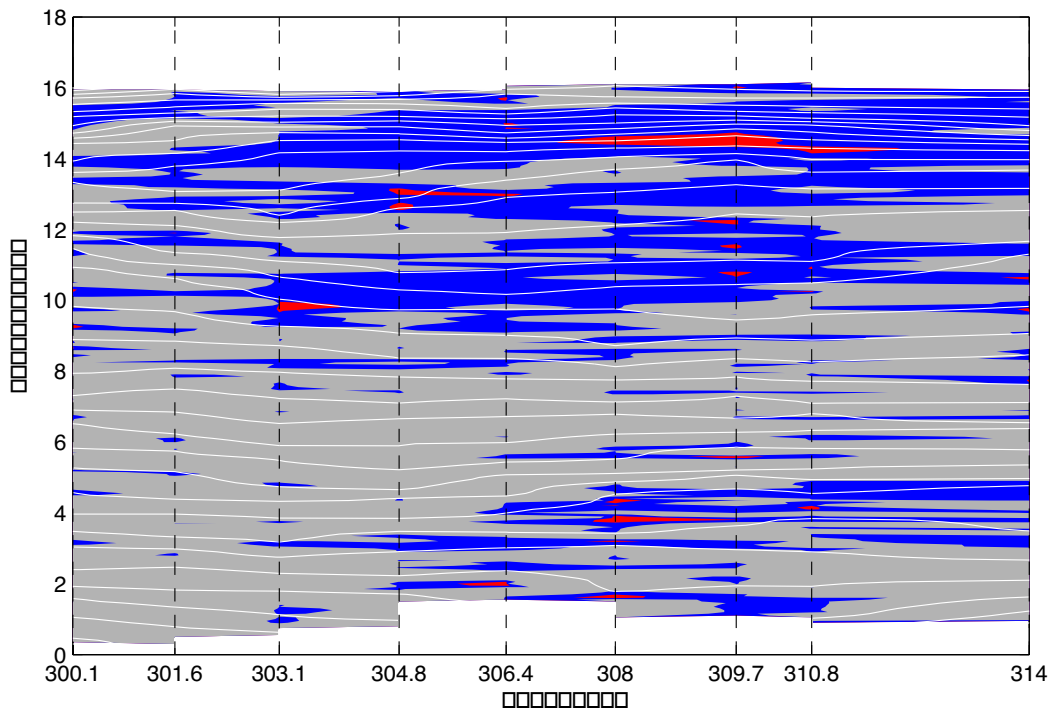


FIGURE 6
 As in Fig. 5, a height–longitude cross section created from nine Global Hawk dropsondes released during the first leg of the mission to Hurricane Nadine on September 14–15, 2012. The color shading indicates Richardson number (Ri): gray for $Ri > 1$, blue for $0.25 \leq Ri \leq 1$, and red for $Ri < 0.25$. The white contours are isentropes, drawn at 2.5 K intervals. The dashed lines indicate the longitudes of the drops.

cal cyclone centers.^{1,2} The system has the capability to operate in atmosphere-only mode or in a fully coupled air-sea interaction mode using the Navy Coastal Ocean Model (NCOM) and the Simulating WAVes Nearshore (SWAN) model.³ The COAMPS-TC is a robust and skillful prediction system for tropical cyclones, and was transitioned into operations at Fleet Numerical Meteorology and Oceanography Center (FNMOC) in June 2013.²

Here we apply the COAMPS-TC to better understand the impact of the HS3 dropsondes on predictions of tropical cyclone track and intensity using a triple-nested grid setup of the model with a 5 km resolution on the finest mesh and 40 vertical levels. Two experiments were executed for Hurricane Nadine. The first experiment did not assimilate any observations from the HS3 dropsondes, while the second experiment assimilated the HS3 dropsonde observations. In this second experiment, the density of the dropsondes was sufficient to initialize the tropical cyclone vortex, and thus synthetic observations were not used to initialize the storm, which is the typical method used for COAMPS-TC (and is used in the first experiment). Conventional satellite, surface, and radiosonde observations were assimilated in both experiments. The experiments were run over a 9 day period from September 19 to 28, which featured three HS3 flights into Hurricane Nadine, resulting in approximately 30 forecasts. The average forecast performance for the two experiments is summarized in Fig. 7. The assimilation of the HS3 dropsondes improves the track prediction by over 50 nm at the 120 h lead time. However, the HS3 dropsondes have an even larger positive impact on the maximum wind error and minimum sea-level pressure error relative to the track error. For example, assimilation of the HS3 dropsondes reduces the maximum wind mean absolute error from 15 knots to less than 10 knots at 48 h, with similar reductions at later lead times. The minimum sea-level pressure mean absolute error is reduced considerably from 16 hPa to 10 hPa at 48 h. We are currently analyzing these results further to better understand this strong positive impact that the HS3 dropsondes have on the forecast performance.

An ensemble prediction system (EPS) for COAMPS-TC has also been developed to better quantify the forecast uncertainty for TC track, intensity, and storm structure. The COAMPS-TC EPS consists of an 80-member ensemble Kalman filter (EnKF) data assimilation component and a 20-member forecasting component. The EnKF is based on the Data Assimilation Research Testbed (DART) and is used for the assimilation of radiosonde data, aircraft data, cloud-track winds, surface station data, and the tropical cyclone intensity and position. The COAMPS-TC model setup consists of three two-way interactive grids with

horizontal resolutions of 27, 9, and 3 km. The 9 km and 3 km meshes are designed to track the location of the storm independently for each ensemble member. Initial condition perturbations, drawn from a static background-error covariance matrix, are then added to the initial fields. The 80-member EnKF system is cycled by assimilating observations every 6 hours into the three nested grids for the duration of the storm. A 20-member forecast ensemble is drawn from the 80-member data-assimilation ensemble and integrated for 120 h.

The 20-member forecast ensemble was initialized at 00 UTC September 16, 2012 for Hurricane Nadine during HS3. Figure 8 depicts the 120 h ensemble track forecasts, with symbols showing the position of the storm every 24 h. Two experiments are run: the first assimilates the Global Hawk dropsonde observations, while the second does not. For the first 48 h, the track forecast is tightly clustered around the ensemble mean with little error relative to the observed track. However, beyond the 48 h time, the 20-member ensemble track forecasts show considerable spread among the members, with the greatest spread exhibited in the experiment that did not assimilate dropsondes. The additional dropsondes from the Global Hawk decrease the spread of predicted ensemble member tracks, and increase the forecast confidence for the storm path. The COAMPS-TC EPS also provides a probabilistic intensity and storm size forecast capability (not shown).

SUMMARY

The NASA Hurricane and Severe Storm Sentinel (HS3) mission, focused on observing hurricanes from the surface to 60,000 ft above the Atlantic and Gulf of Mexico, has yielded an unprecedented set of observations that provide new insight into tropical cyclones and the associated upper-level outflow jets. The Global Hawk UAVs deployed during HS3 allow for HALE missions that are able to fly over storms for long periods of time (20+ hours), enabling a more complete sampling of the storm and its environment. The Leslie and Nadine cases have already led to some new insights about the nature of these jets, in particular the strong shear at the top of these jets and associated Richardson numbers that suggest the presence of turbulent vertical mixing. Analysis of additional cases is under way. These cases will be needed to gain a more complete understanding of the morphology of tropical cyclone outflow jets. The nature of the turbulent layer at the top of the outflow jet could have important implications for regulation of the wind speed in the jet core and the vertical mixing of atmospheric constituents from the troposphere into the lower stratosphere. Outflow layer turbulence may also play an important role in governing the structure of the outflow layer near the storm

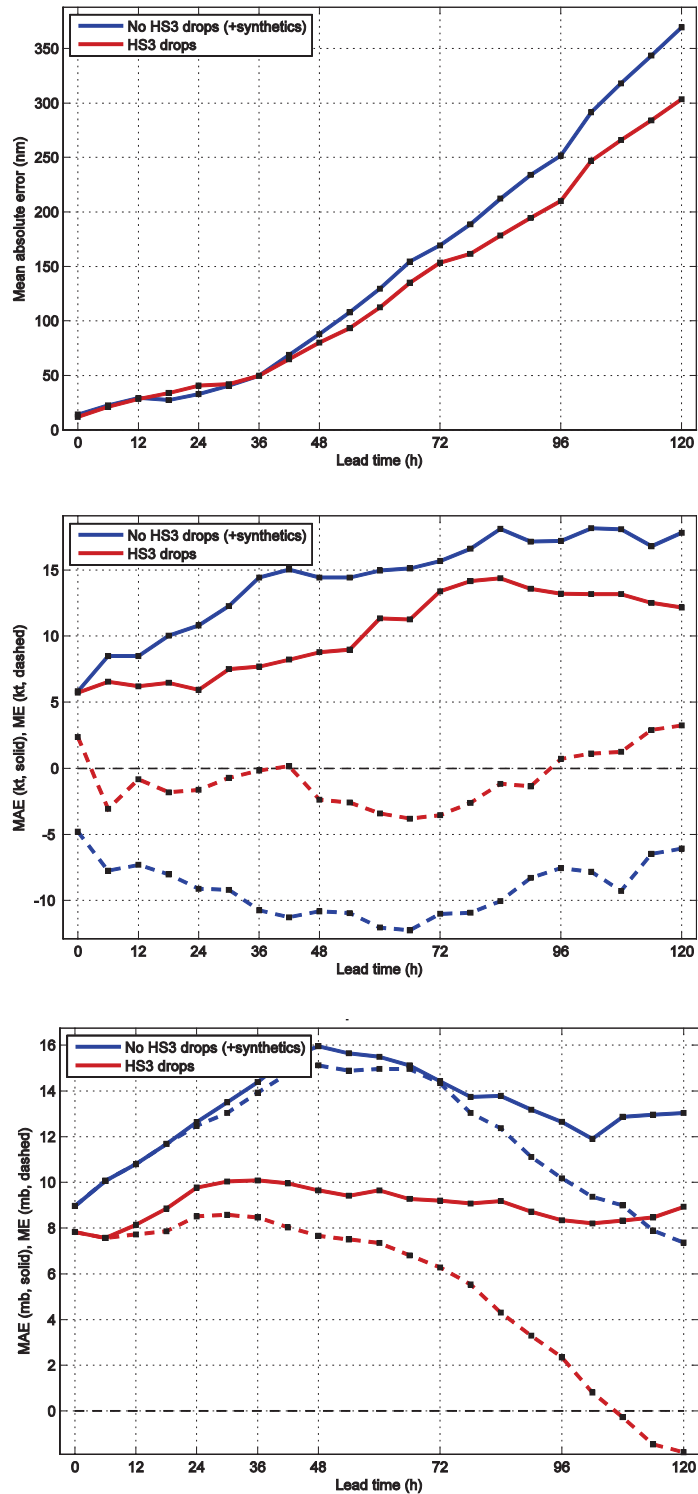


FIGURE 7
Track mean absolute error (nm) (top panel) for Hurricane Nadine (September 19–28, 2012) as a function of forecast time for the experiment that used HS3 dropsondes in the assimilation system (red line) and the experiment that did not assimilate HS3 dropsondes (blue line). Maximum wind speed mean absolute error (MAE, solid lines) and mean error (ME, dashed lines) (knots; 1 knot = 0.514 m s^{-1}) (middle panel) and minimum sea level pressure MAE and ME (lower panel) as a function of forecast time for the two experiments. The number of cases is approximately 30.

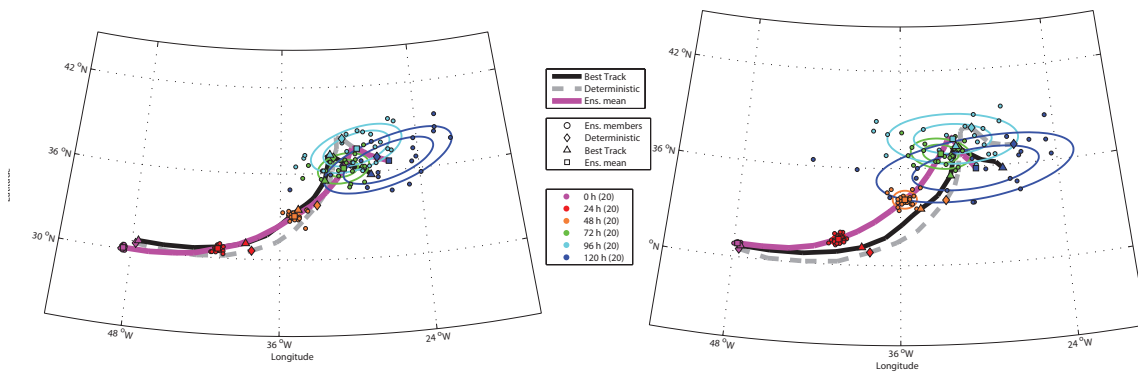


FIGURE 8

Probabilistic track forecasts from the COAMPS-TC ensemble for Hurricane Nadine for the experiment with dropsonde assimilation (left) and the experiment without dropsonde assimilation (right). This forecast was initialized at 00 UTC September 16, 2012. The plots show the TC position from the individual ensemble members every 24 h and ellipses that encompass one third and two thirds of the ensemble members. The purple line indicates the track for the ensemble mean, the gray dashed line for the deterministic forecast, and the black line shows the observed track.

core and in regulating changes in TC intensity. Finally, we have seen that assimilation of HS3 dropsonde observations contribute positively to the performance of COAMPS-TC and COAMPS-TC EPS forecasts of Hurricane Nadine, but more cases and further analysis are needed to better quantify of impact of HS3 dropsondes on overall TC forecast performance.

ACKNOWLEDGMENTS

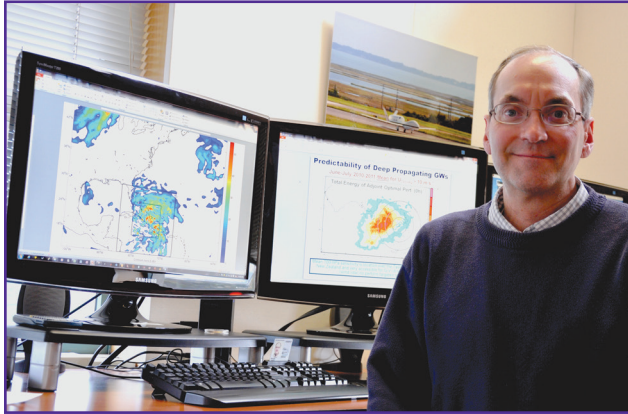
We acknowledge the support of the Office of Naval Research (ONR) and the NASA HS3 program. We acknowledge the collaboration with NRL Oceanography Division in Stennis, MS, related to the air-sea coupled capability for COAMPS. We also appreciate support for computational resources through a grant of Department of Defense High Performance Computing time from the DoD Supercomputing Resource Center at Stennis, MS, and Vicksburg, MS. COAMPS® is a registered trademark of the Naval Research Laboratory.

[Sponsored by the NRL Base Program (CNR funded), ONR, and NASA]

References

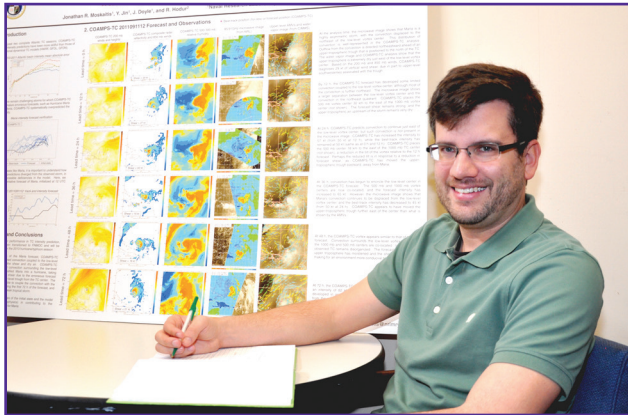
- ¹ J.D. Doyle, Y. Jin, R. Hodur, S. Chen, H. Jin, J. Moskaitis, A. Reinecke, P. Black, J. Cummings, E. Hendricks, T. Holt, C. Liou, M. Peng, C. Reynolds, K. Sashegyi, J. Schmidt, and S. Wang, "Real time Tropical Cyclone Prediction Using COAMPS-TC," *Advances in Geosciences* **28**, C.-C. Wu and J. Gan, eds. (World Scientific Publishing Company, Singapore, 2012), pp. 15–28.
- ² J.D. Doyle, Y. Jin, R. Hodur, S. Chen, Y. Jin, J. Moskaitis, S. Wang, E.A. Hendricks, H. Jin, and T.A. Smith, "Tropical Cyclone Prediction Using COAMPS-TC," *Oceanography* (submitted) (2014).
- ³ S. Chen, T.J. Campbell, H. Jin, S. Gaberšek, R.M. Hodur, and P. Martin, "Effect of Two-Way Air-Sea Coupling in High and Low Wind Speed Regimes," *Mon. Wea. Rev.* **138**, 3579–3602 (2010).

THE AUTHORS



JAMES D. DOYLE earned his B.S. degree in atmospheric science and mathematics from University of Wisconsin at Milwaukee in 1983 and his Ph.D. in meteorology from the Pennsylvania State University in 1991. He joined the Marine Meteorology Division in Monterey, CA, in 1992, and has served as the head of the Mesoscale Modeling Section in the Atmospheric Dynamics and Prediction Branch since 1997. He is one of the primary developers of the Navy's Coupled Ocean/Atmosphere Mesoscale Prediction System (COAMPS) and COAMPS-Tropical Cyclone (COAMPS-TC), which are used to support operational Navy and DoD interests globally, as well as basic research at NRL and numerous other universities and laboratories. Currently, he is leading efforts for improving the physical understanding and prediction of mesoscale phenomena such as topographically forced flows and gravity waves, tropical cyclones, and

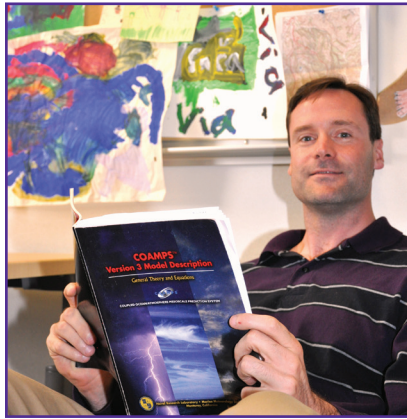
marine boundary layer circulations using both deterministic and probabilistic approaches. He is a recipient of the Top Navy Scientists and Engineers of the Year Award and is a Fellow of the American Meteorological Society. He has published over 120 peer-reviewed publications and has received seven NRL Alan Berman Research Publication Awards.



JONATHAN R. MOSKAITIS received a B.S. in meteorology from the Pennsylvania State University in 2002, and a Ph.D. in atmospheric science from the Massachusetts Institute of Technology in 2009. He then came to NRL as a National Research Council Postdoctoral Research Associate before joining the staff as a meteorologist in 2010. Dr. Moskaitis specializes in the validation of numerical weather prediction models, such as COAMPS-TC and NAVGEM (Navy Global Environmental Model), both of which began operational production at the Fleet Numerical Meteorology and Oceanography Center in 2013. He also has research interests in tropical cyclone dynamics, probabilistic prediction of extreme weather events, and atmospheric predictability.



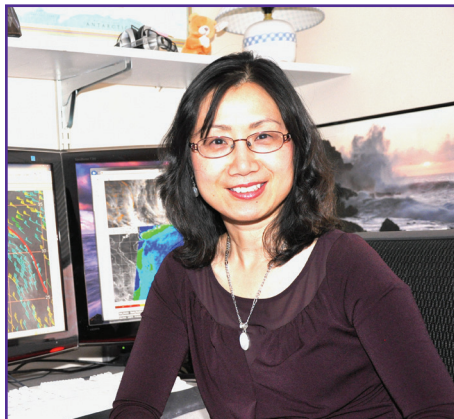
PETER G. BLACK works at NRL as a senior scientist contractor with SAIC, Inc. He received his M.S. from the University of Chicago in 1969 and Ph.D. in meteorology from Penn State University in 1983. Dr. Black worked at the NOAA Hurricane Research Division for 40 years, designing and participating in hurricane research flights, with over 400 penetrations into hurricane eyes. He led a team that developed the first operational airborne instrument for measuring hurricane surface wind speeds, the Stepped Frequency Microwave Radiometer, for which he received the U.S. Department of Commerce Bronze Medal awards in 2008 and 2009 and, together with his team, the AMS Special Award in 2010. He also received the Banner Miller Best Paper Award in 2009 and was elected Fellow of the AMS in 2010. Dr. Black received the Interdepartmental Hurricane Conference Hagemeyer Award for career achievements in 2011. Under ONR sponsorship, he has served as Chief Scientist for the Hurricane Coupled Boundary Layer Air-Sea Transfer project (2002–2004) as well as lead aircraft scientist for the TPARC/Tropical Cyclone Structure and Interaction of Typhoons Over the Pacific experiments in 2008 and 2010, respectively. He is presently (2012–2014) serving as a mission scientist for Global Hawk UAV flights during NASA's Hurricane and Severe Storm Sentinel (HS3) project, with which NRL is working collaboratively.



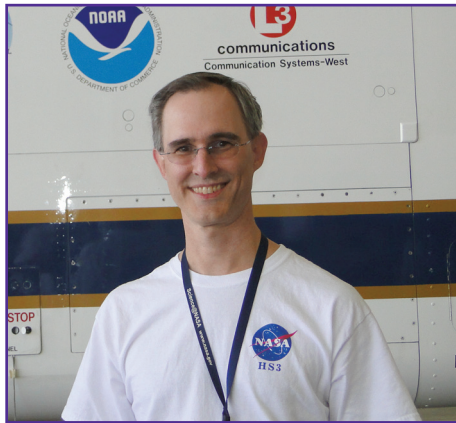
ERIC A. HENDRICKS received his doctorate degree in atmospheric science from Colorado State University in 2008. He was a National Research Council postdoctoral fellow at NRL until 2010, and then joined NRL as a meteorologist under the Karle Distinguished Scholar fellowship. At NRL, he performs basic research on hurricane dynamics and applied research on improving the numerical weather prediction of tropical cyclones. In 2004, he discovered the fundamental role of rapidly rotating deep convection in tropical cyclogenesis, and he has also published numerous papers on the role of hurricane eyewall instability in intensity and structural variability. He is lead or coauthor of 25 peer-reviewed publications, and he received an NRL Alan Berman Research Publication Award in 2012 as a lead author.



P. ALEXANDER REINECKE received his doctorate degree in atmospheric science from the University of Washington in 2008. He was a National Research Council postdoctoral fellow at NRL until 2009, when he joined the Marine Meteorology Division in Monterey, CA, as a meteorologist. He currently is a member of the Mesoscale Modeling Section in the Atmospheric Dynamics and Prediction Branch. Dr. Reinecke has extensive experience in mesoscale numerical weather prediction and is interested in mesoscale dynamics, model development, and ensemble data assimilation. He is the principal investigator of an NRL base project investigating the impact of observations assimilated from unmanned aerial systems on the prediction of tropical cyclone track and intensity.



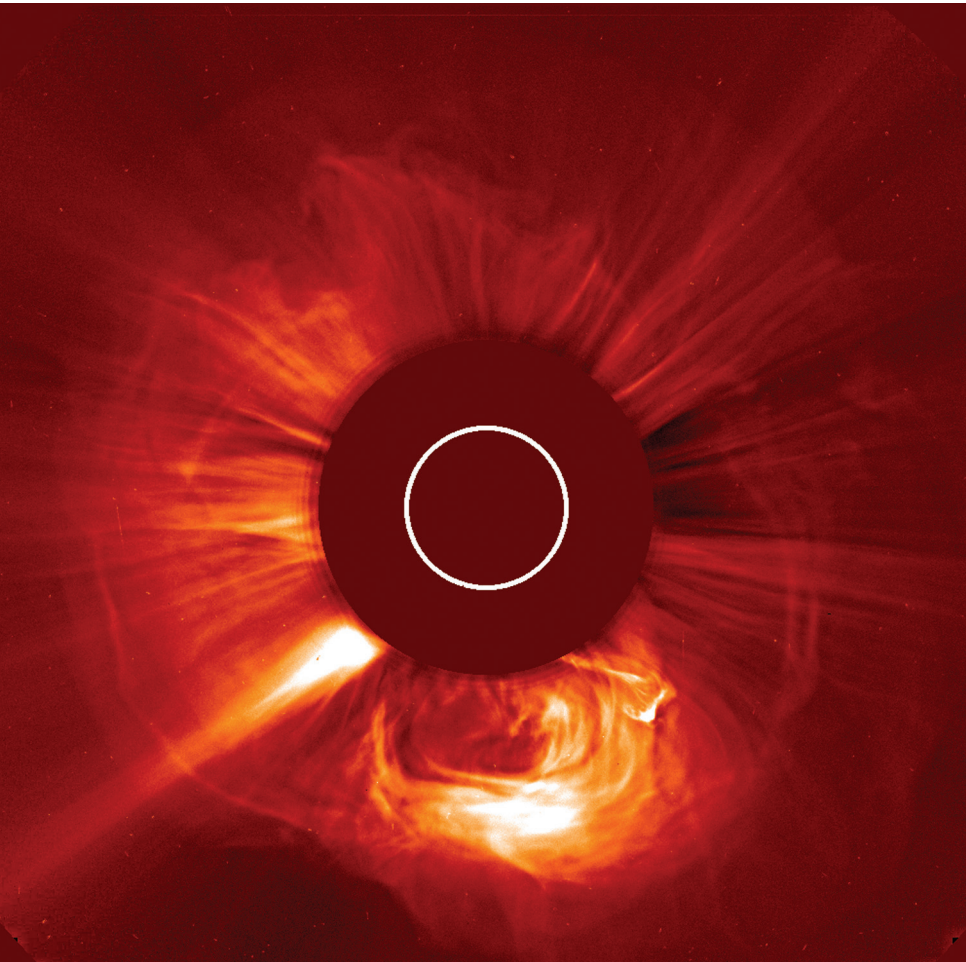
YI JIN earned her Ph.D. degree in atmospheric sciences from the North Carolina State University in 1997 with an emphasis on mesoscale dynamics and numerical modeling. She also holds B.S. and M.S. degrees in atmospheric sciences from Nanjing University, China. After receiving her Ph.D., she worked at Science Applications International Corporation for 5 years. In 2002, she joined the Mesoscale Modeling Section of the Naval Research Laboratory's Marine Meteorology Division, first as a contractor and was then hired into the section. Over the years, she has been actively involved in developing and improving physical parameterizations in numerical weather prediction models. Her research interests include mesoscale dynamics and physical processes in tropical cyclones, cloud and boundary layer interactions, coastal processes, and air-sea interactions. Currently she serves on the American Meteorological Society Committee on Coastal Environment. She is a recipient of the NRL Alan Berman Research Publication Award.



SCOTT A. BRAUN is a research meteorologist at NASA's Goddard Space Flight Center. He has a doctorate in atmospheric sciences from the University of Washington in Seattle. He was a postdoctoral fellow at the National Center for Atmospheric Research (NCAR) in Boulder, Colorado, and has worked at Goddard since 1997. Dr. Braun is the principal investigator for NASA's Hurricane and Severe Storm Sentinel (HS3) investigation, a multiyear mission specifically designed to investigate hurricanes in the Atlantic Ocean basin. As PI, he leads a team of hurricane and instrument scientists to design and conduct experiments using unmanned aircraft to understand better the meteorological conditions that favor storm formation and intensity change. Dr. Braun is also the project scientist for the Tropical Rainfall Measuring Mission (TRMM) satellite, now in its 17th year of operations. Dr. Braun has received the Goddard Earth Science Achievement Award, the NASA Exceptional Scientific Achievement Medal, and group achievement awards for participating in NASA's CAMEX-4, TCSP, and GRIP missions. He has 47 peer-reviewed papers as first author or coauthor.

TMI about TSI?

No, we don't think you can ever know enough about total solar irradiance (TSI), considering how important it is in understanding long-term climate change on Earth. Quantifying the fluctuations in TSI, the total amount of energy from the Sun (in all wavelengths) that is received on Earth, has



interested scientists for more than a century, but getting this data remains difficult and is best done from space. Eight satellites have borne instruments to measure TSI, but small differences between their measurements have cast doubt on whether there has been fundamental change in the solar output. (That is, is the “solar constant” really constant?)

However, for almost 18 years, NRL's Large Angle and Spectrometric Coronagraph (LASCO), from its SOHO spacecraft platform, has been imaging the dynamic solar corona to produce a wealth of information about the Sun and its processes, such as coronal mass ejections (CMEs). Now we know that it has also been able to detect the small changes in

TSI behavior. By analyzing LASCO's daily visible light observations of the solar corona (visible light being the largest component of TSI) and comparing that data to other TSI measurements and different TSI models, NRL researchers have been able to spot trends in solar activity, calibrate TSI measurements, and compute expected TSI. While it is yet unknown how the TSI fluctuations will affect us, what is sure is that NRL, NASA, and many others are glad to have this information.



Predicting Total Solar Irradiance

R.A. Howard, K. Battams, and H.A. Dennison
Space Science Division

The Earth is being continually bathed in radiant energy from the Sun, our nearest star. The total amount of energy incident on the Earth is termed the total solar irradiance (TSI). TSI drives the long-term climate change here on Earth, so fluctuations in this quantity are of paramount importance. The fluctuations in TSI are on the order of 0.2%, which is about 4 W/m^2 . The measurement of TSI is best done from space, but even then it is still difficult, requiring special and very involved techniques to maintain the calibration. A Naval Research Laboratory instrument, the Large Angle and Spectrometric Coronagraph (LASCO), has been regularly imaging the solar corona since 1996. Designed to observe the dynamic solar corona, LASCO is also able to detect the changes in the TSI that bathes the Earth in an almost constant flux of energy. LASCO's high sensitivity and stability over nearly 18 years gives us the TSI behavior as a serendipitous byproduct of the primary instrument function. The Sun is currently at the peak of its activity cycle, but we find that it is undergoing some unpredicted changes — both the rate of coronal mass ejections (CMEs) and the level of the TSI are much lower than at the previous activity maxima. These reductions appear to be returning the Sun to the lower levels that were present before the beginning of the space age. The long baseline of LASCO observations allow us to provide a relative calibration from one TSI instrument to another. The advantage of this indirect method is that the calibration is relatively straightforward. In this article, we review the LASCO and TSI measurements and the method we use to predict the TSI.

WHAT IS TSI?

The photosphere of the Sun — the disk that we see in the sky — is radiating away energy produced in its core from burning helium. This radiance lowers the temperature from about 15 MK to a cool 5700 K. The solar energy that reaches the Earth is about 1461 W/m^2 , and for many years this output of the Sun was thought to be constant, thus being called the solar constant. Most of the energy is in the visible part of the wavelength spectrum. Figure 1 shows the disk of the Sun in the visible with the dark sunspots and the faculae (the brighter areas around groups of sunspots, indicating concentrated magnetic fields). As the sunspots and faculae traverse the disk, the solar output can increase or decrease the total solar irradiance (TSI). These three regions (solar disk, sunspots, and faculae) are the basis of an empirical model developed by Judith Lean of the Naval Research Laboratory (NRL) that reproduces the observed TSI.¹

Samuel Pierpont Langley and Charles Greeley Abbot² of the Smithsonian Institution were the first to measure the solar constant in the early 1900s. They developed many different styles of instruments and procedures to remove the effect of the absorbing atmosphere from their observations, making their measurements initially from the ground, and then on balloons to get higher in the atmosphere. Abbot carried on the work of Langley, lowering the value that Langley had estab-

lished, but in spite of extremely careful measurements, his accuracy was still on the order of 50%.

TSI is defined as the total amount of energy that is falling on a square meter at the top of the Earth's atmosphere, when the Earth is at its mean distance from the Sun (1 astronomical unit or $1.5 \times 10^8 \text{ km}$). Figure 2 shows the measurements of TSI that have been made from space. As can be seen, the consistency of the absolute level has been difficult to achieve, but there is general agreement that there are cycles. At the peaks of the solar activity cycle (1980, 1991, and 2002), the TSI is greater than at the solar activity minima. The colors indicate the observations from a similar type of instrument. For example, the green points are from the Active Cavity Radiometer Irradiance Monitor (ACRIM) experiment on three different satellites — the Solar Maximum Mission (SMM), the Upper Atmospheric Research Satellite (UARS), and finally the ACRIM Satellite (ACRIM-SAT). Even though the three instruments were a similar design and provided by the same institution, there is a very small (0.15%) but obvious difference between the three missions. The controversy has been whether this difference was real and were there fundamental changes in the solar output. Kopp and Lean³ have suggested that the latest measurements of the TSI at solar minimum from the SORCE/TIM instrument are providing the correct absolute levels of 1361 W/m^2 instead of the previously accepted value of 1364 W/m^2 .

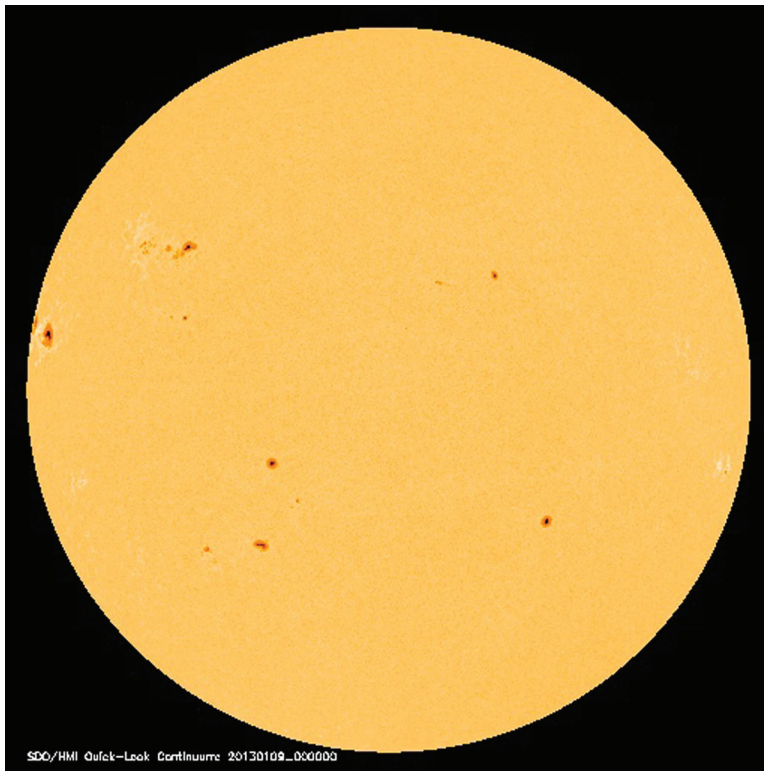


FIGURE 1
An image of the solar disk taken on January 9, 2013, by the Heliomagnetic Imager on the Solar Dynamics Observatory mission. This image of the solar photosphere illustrates the uniformity of the solar disk except for the dark sunspots and the bright faculae.

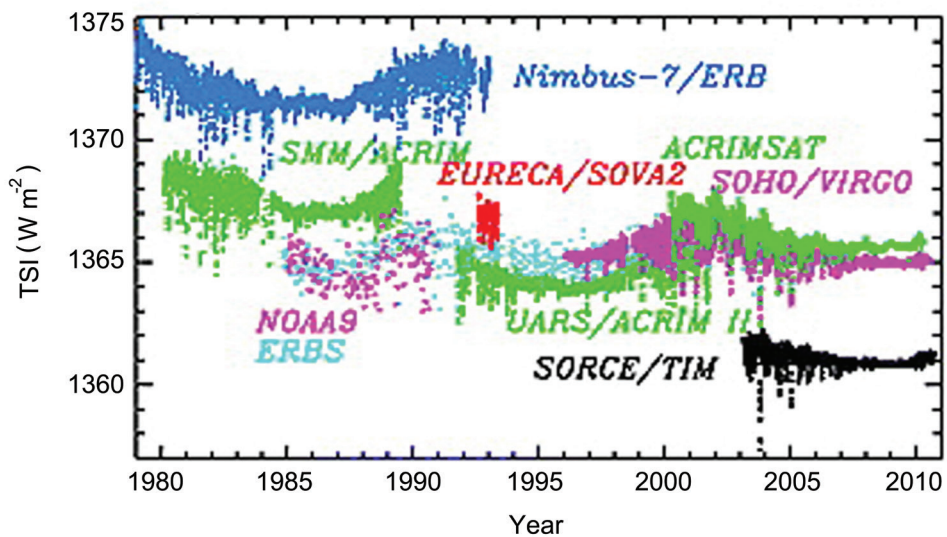


FIGURE 2
Daily averaged values of the Sun's total irradiance (TSI) from radiometers on different space platforms. The data from each platform/instrument combination are indicated by a different color. The offsets from one instrument to another are due to calibration errors.

THE SOHO/LASCO INSTRUMENT

The Large Angle and Spectrometric Coronagraph (LASCO) experiment is one of 12 instruments included on the European Space Agency's Solar and Heliospheric Observatory (SOHO) spacecraft, which was launched by NASA on December 2, 1995. LASCO was designed to answer questions on the quiescent and dynamic structure of the corona and its relation to the solar magnetic field. One of the dramatic dynamic events is the expulsion of plasma from the Sun, called a coronal mass ejection (CME), illustrated in Fig. 3. Here, a large CME is seen in the LASCO/C2 telescope coming toward the observer with a large, bright structure going toward the bottom of the image. The size and position of the Sun is indicated by the white circle in the center. The Sun is behind an occulting disk, which blocks the sunlight and enables us to see the very faint emission surrounding the Sun. The CME has already expanded to be many times larger than the Sun, although certainly much less dense. The linear structures, coming

apparently radially away from the Sun, are streamers, regions of high electron density tracing the magnetic field lines.

LASCO records such structures as the streamers and CMEs as scattering photospheric light from the electrons in the corona. The intensity of the scattered light depends on the number of electrons, but it is also dependent on the intensity of the incident photospheric light. The TSI is a good indicator of the photospheric intensity. LASCO is only sensitive to visible wavelengths, whereas TSI encompasses all wavelengths, but the visible wavelengths are the dominant component. Thus, LASCO could provide a good measure of TSI.

Figure 4 illustrates the analysis technique used in this study. The LASCO/C2 coronagraph observes the solar corona from about 2 to 6 solar radii. About 75 images each day are collected from which we obtain a daily background image, which removes dust streaks, stars, CMEs, and other transient effects, but keeps streamers and other semistationary structures. The intensities in the daily C2 background image at a

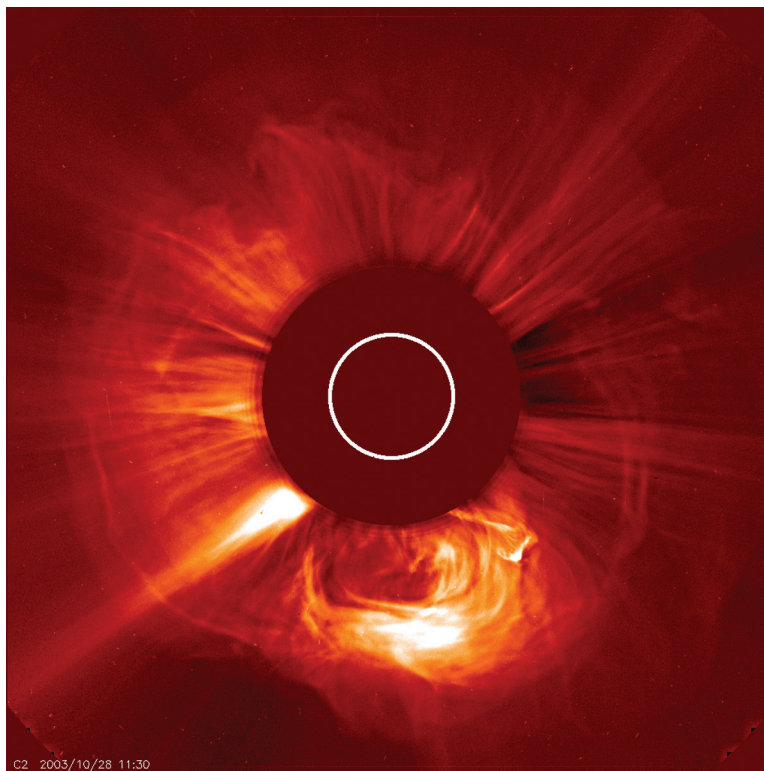


FIGURE 3

An image of the solar corona taken by the LASCO/C2 white light coronagraph on the SOHO satellite. The direct sunlight from the solar disk is blocked by an occulting disk in front of the telescope lens, to enable the very faint emission in the corona to be seen. The position and size of the Sun is shown by the white circle in the center. The visible light in this image arises from scattering of the photospheric light from free electrons in the coronal plasma at about 2 MK. Pixels that are brighter have more electrons along the line of sight than those that are dimmer. In this image, several coronal mass ejections can be seen in addition to the streamers that are tracing the coronal magnetic field.

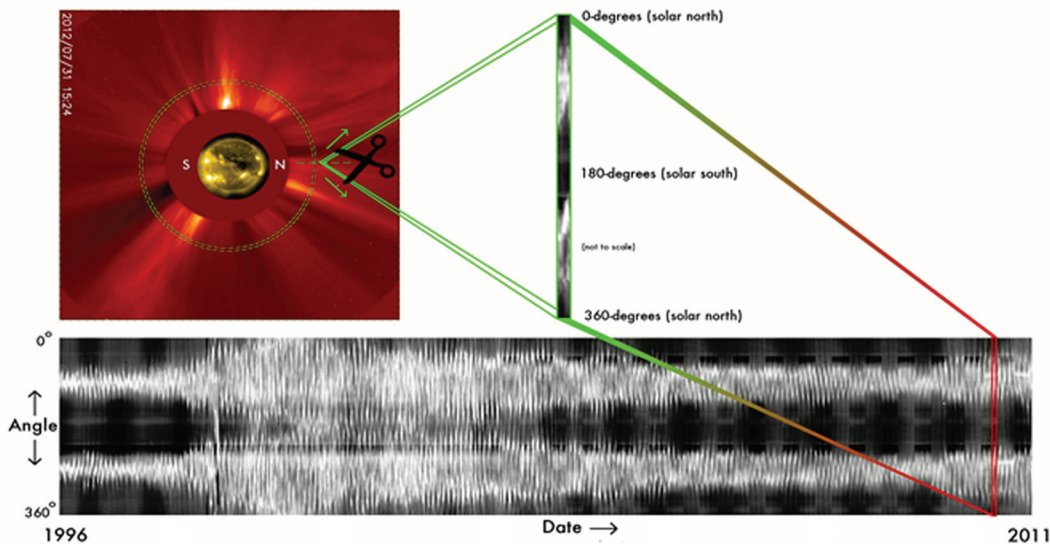


FIGURE 4 A composite image illustrates the procedure to obtain a single number for each day of the total coronal brightness. Starting with a daily LASCO image, a scan is made at a constant distance from the center of the Sun. An individual scan (at 2.8 solar radii) is shown to the right of the daily image. The scan around the Sun starts at the north pole and goes counterclockwise to the eastern equator, the south pole, the western equator, and back to the north pole. All of these daily scans are put into a new image, each column of the image being one scan. This image gives a Mercator-like projection of the corona and shows the evolution of coronal patterns throughout a solar cycle.

constant distance from the Sun center (2.8 solar radii) are computed, correcting for the variable distance of the instrument from the Sun. These scans start at the solar north pole and proceed counterclockwise around the Sun, passing first the eastern equatorial region, the south polar region, the west equatorial region, and finally back to the north pole. The grayscale image shows all the scans together from the beginning of the mission. The solar activity cycle of about 11 years is clearly shown in this record. At minimum activity, the coronal brightness is confined to the east and west equatorial regions, whereas at maximum activity, the entire corona is bright. By totaling the intensities in each scan, we obtain a single number for each day, which is plotted in Fig. 5. This format enables us to compare to TSI directly.

You can see that the total brightness varies by about 30% between solar minimum and solar maximum. This is due to the increased number of electrons in the corona. At minimum, the poles have large regions, called coronal holes, which are lower in density than at maximum. At minimum, the solar magnetic field is primarily dipolar, so that the regions of enhanced electron density are confined to the equatorial regions, in what is called the streamer belt. As the solar activity cycle proceeds toward maximum, the strength of the polar coronal holes declines and the streamers rise to higher latitudes until, finally at maximum, they disappear and enhanced electron density is all over the disk.

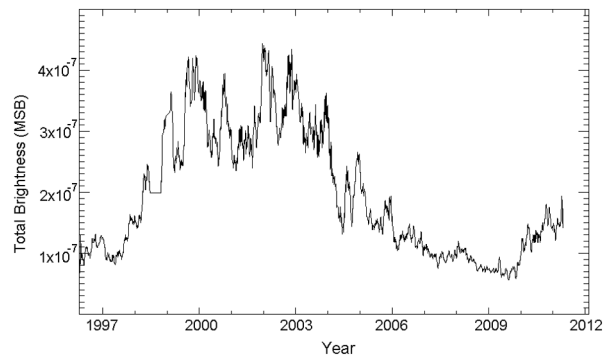


FIGURE 5 The daily total coronal brightness at 2.8 solar radii. The daily scans shown in the image at the bottom of Fig. 4 are summed into a single number and plotted here.

COMPARING TSI TO LASCO BRIGHTNESS

By performing a correlation analysis between the daily brightness values in Fig. 5 with the different TSI measurements shown in Fig. 2, we can establish a linear relation between them. We find that the correlation coefficient varies between 0.72 and 0.83 depending upon which TSI data set we use for the TSI. For this study we used two TSI data sources^{4,5} and one TSI model.¹ The best correlation (0.92) was to the faculae component of the TSI model. Faculae are the brightenings (see Fig. 1) associated with concentrated magnetic fields. The plasma is hotter in these regions and so the faculae are a

little brighter. Figure 6 (bottom) compares the predicted value of TSI to the values of the TSI observed from the Solar Radiation and Climate Experiment (SORCE) spacecraft, launched in 2003, while Fig. 6 (top) compares the same to a composite index generated from various sources by Fröhlich⁴ and called PMOD after his institute in Switzerland, Physikalisch-Meteorologisches Observatorium Davos. The prime data source in the PMOD is the Variability of Solar Irradiance and Gravity Oscillations experiment (VIRGO) on SOHO.

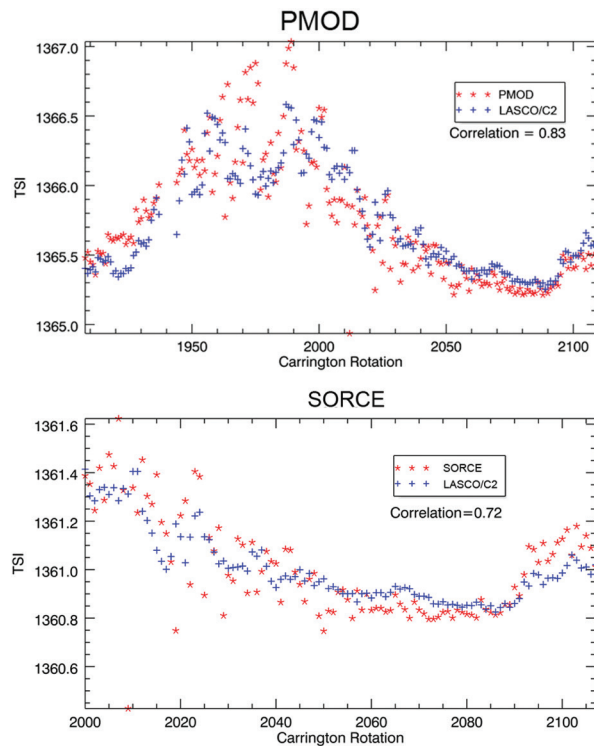


FIGURE 6
The observed and predicted TSI plotted in time as measured by Carrington Rotations, units of the solar rotation of about 27.3 days. The correlation of the LASCO observations from Fig. 5 with the TSI observations from Fig. 2 allows us to compute the expected TSI from the LASCO observation. The upper plot compares the PMOD TSI data with LASCO and the bottom plot compares the SORCE TSI data.

CONCLUSIONS

White light observations of the corona from LASCO are well correlated to TSI and thus can be used to intercompare observations from different TSI instruments. The on-orbit absolute calibration of LASCO is tied to stellar brightness measurements, whereas the TSI observations do not have such a capability. The TSI shows different behavior compared to the NRL predictions for the rise to the current maximum. Here, the PMOD is rising more slowly than the NRL prediction and SORCE is rising more rapidly. This confirms

the need to have well-calibrated instruments and that the coronagraph observations of the corona give a good proxy for the long-term behavior of the total amount of solar energy impacting our Earth.

The excellent calibration allows us to compare the most recent solar minimum with the previous one. Figure 5 shows that the 2008/2009 minimum was about 28% lower than the 1996 minimum. Scientists⁶ have found that the current minimum has the weakest solar wind since the beginning of the space age in terms of speed, mass flux, temperature, momentum flux, energy flux, and many other parameters. What effect this is going to have on us is not known, but it will certainly be interesting.

ACKNOWLEDGMENTS

We are grateful for useful discussions and encouragement from Judith Lean who supplied the TSI data. This work was funded by NRL and by NASA grants to SOHO/LASCO.

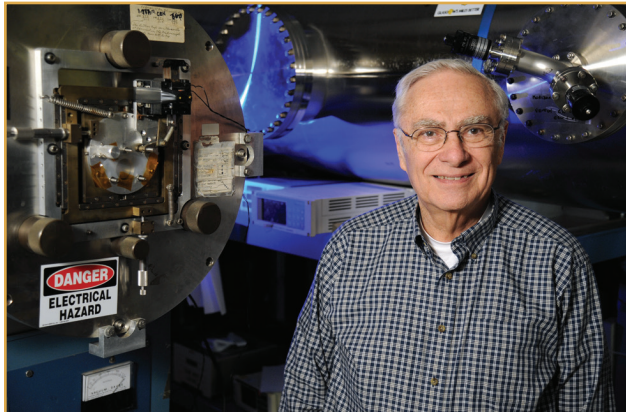
[Sponsored by NRL and NASA]

References

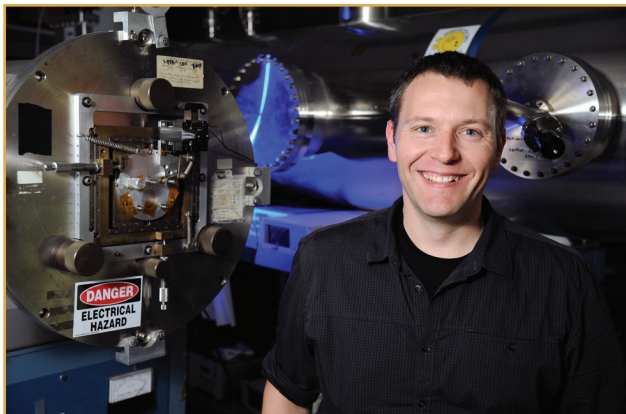
- ¹ J.L. Lean, "Short Term, Direct Indices of Solar Variability," *Sp. Sci. Rev.* **94**, 39–51 (2000).
- ² D.H. DeVorkin, "Defending a Dream: Charles Greeley Abbot's Years at the Smithsonian," *J. History Astronomy* **21**, 121–136 (1990).
- ³ G. Kopp and J.L. Lean, "A New, Lower Value of Total Solar Irradiance: Evidence and Climate Significance," *Geophys. Res. Lett.* **38**, L01706 (2011).
- ⁴ C. Fröhlich, "Solar Irradiance Variability Since 1978. Revision of the PMOD Composite During Solar Cycle 21," *Space Sci. Rev.* **125**, 53–65 (2006).
- ⁵ G. Rottman, "The SORCE Mission," *Sol. Phys.* **230**, 7–25 (2005).
- ⁶ D.J. McComas, N. Angold, H.A. Elliott, G. Livadiotis, N.A. Schwadron, R.M. Skoug, and C.W. Smith, "Weakest Solar Wind of the Space Age and the Current 'Mini' Solar Maximum," *Astrophys. J.* **779**, 1–10 (2013).



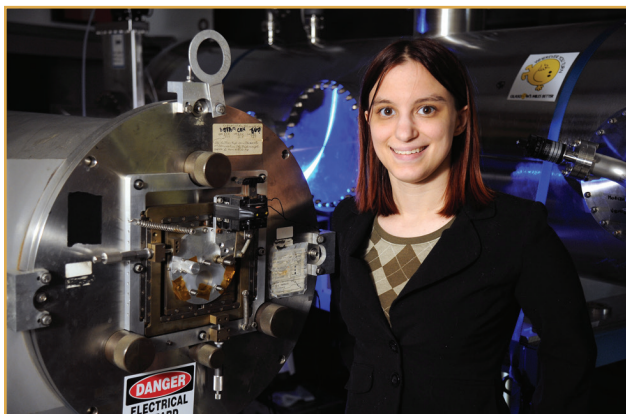
THE AUTHORS



RUSSELL A. HOWARD joined NRL in 1969 as an NRC Resident Research Associate in ultraviolet spectroscopy, having just received his Ph.D. in chemical physics from the University of Maryland. After a two year postdoctoral period, he was hired by the Rocket Spectroscopy Branch in the Space Science Division to analyze data from a white light coronagraph instrument that had just been launched by NASA on the Orbiting Solar Observatory #7 satellite. This was the first orbiting coronagraph to observe an eruption of plasma — what we now call a coronal mass ejection. He continues to study CMEs and solar structures and their effect on Earth and geospace. He has worked on a number of ultraviolet and white light coronagraphs, culminating in him being the principal investigator of two instruments currently flying in space on the SOHO and STEREO missions, and of two instruments in development for launch in 2017 and 2018 on the Solar Orbiter and Solar Probe Plus missions, respectively.

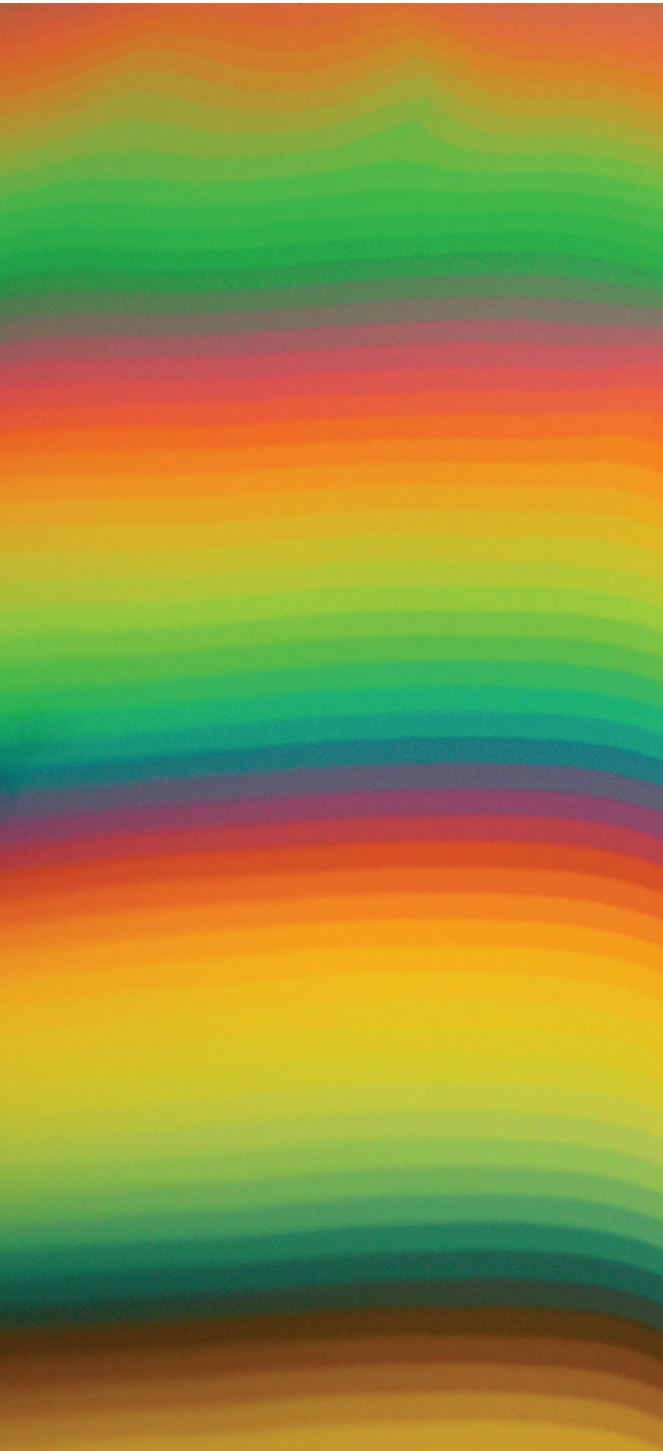


KARL BATTAMS received a B.S. in astrophysics from University College London, UK, in 2002, and an M.S. in computational science from George Mason University (GMU) in 2008. He is currently pursuing his Ph.D. in computational sciences at GMU. In 2003, he was hired to support the NRL Solar and Heliospheric Physics Branch LASCO and SECCHI projects, and he became an NRL employee in 2008. He is primarily involved in the analysis, processing, exploration, and visualization of solar data, with an interest in the application of high-performance computing to this work. Since 2003, he has been the PI of the NASA-funded “Sungrazer” project, enabling the discovery of previously unknown comets in the LASCO and SECCHI data. He has subsequently studied these near-Sun objects as means of characterizing and probing the solar wind in the inner heliosphere.



HILLARY A. DENNISON began working at NRL in 2010 as an intern as part of the STEP program. As an intern, she assisted with the cataloging of “Sungrazer” comets seen in the LASCO and SECCHI data. In 2011, upon completing her B.S. in physics from George Mason University, she was hired by the NRL Solar and Heliospheric Physics Branch to assist with data analysis, processing, and visualization of the solar data. She is primarily involved with improving analysis/processing software and in analyzing the test data for an instrument in development for launch in 2017 on the Solar Orbiter mission. In 2012, she entered into the SCEP (Pathways) program and began pursuing her M.S. in computational science, focusing on astrophysics and high-performance computing. She will receive her M.S. from George Mason University in May 2014.

The Quest for Compact Hyperspectral Imaging...Starting with (Very) Small Staircase Steps



The benefits offered by spectral sensing to military, medicine, industry, and agricultural applications are nearly limitless. Until recently, hyperspectral spectrometers' size, weight, power requirements, and cost have made them unavailable to handheld applications. NRL researchers first did the math to enable hyperspectral sensors to be made from a specially designed optical filter placed in contact with a sensing array. Then, with the help of NRL nanotechnology expertise, they used Fabry-Pérot spectroscopy combined with a multiplexing technique to design and build a staircase arrangement of Fabry-Pérot etalons spanning multiple optical orders. This novel, compact filter will enable the design of hyperspectral sensors no larger or more power-consuming than a digital B&W camera. By working on the nanoscale to yield enormous results, NRL researchers have reached the upper echelons of etalon spectroscopy, and in doing so, are putting spectrometry literally into the hands of the warfighter.

Multiple Order Staircase Etalon Spectroscopy

M. Yetzbacher,¹ C. Miller,¹ A. Boudreau,¹ and M. Christophersen²

¹*Optical Sciences Division*

²*Space Science Division*

Spectral sensing is becoming more pervasive for Department of Defense, medical, industrial, and agricultural applications. While good progress has been made towards engineering imaging spectrometers to reduce size, weight, power, and cost, hyperspectral sensing cannot at present be reliably performed by handheld instruments. We describe the mathematics that will enable hyperspectral imaging using only a specially designed optical filter placed in contact with the sensing array. Our approach combines Fabry-Pérot spectroscopy with the same kind of multiplexing technique used in Fourier transform spectroscopy, using a staircase arrangement of Fabry-Pérot etalons spanning multiple optical orders. We demonstrate the construction of a staircase etalon filter, enabled by recent advances in nanofabrication techniques developed at NRL's Institute for Nanoscience. This development of complementary mathematics and fabrication techniques allows for a novel approach to spectroscopy. This approach enables hyperspectral imaging using devices negligibly different in size, weight, power consumption, and cost than a simple panchromatic camera system.

INTRODUCTION

Hyperspectral imaging (HSI) is an important tool in present Navy operations, being used in counter-camouflage, friend/foe or material identification, and detection and tracking applications. Most hyperspectral sensors use mechanically scanned filters or dispersive optics to achieve color discrimination. The size, weight, and power (SWAP) required by these conventional methods of color separation has restricted the use of HSI to large platforms, prohibiting the widespread tactical collection of HSI data. Within the Navy and Department of Defense (DoD), there is a significant desire to extend the availability of HSI intelligence, surveillance, and reconnaissance capabilities from their current use on large regional assets (manned aircraft, Reaper, or Global Hawk) to smaller systems such as the U.S. Marine Corps Blackjack unmanned airborne system. Extending hyperspectral capabilities to larger numbers of soldiers requires sensor systems that are smaller, lighter, cheaper, and use less power. In tomorrow's Navy, spectral measurement is desired to be expanded from the limited domain of large, configurable equipment to a broader world accessible by smaller, more mobile, specialized measurement tools. A compact hyperspectral sensor could be deployed at the squad level for real-time utilization by large numbers of warfighters. To this end, NRL engaged in research to provide the warfighter with a high performance, compact imaging spectrometer.

An ideal compact imaging spectrometer would have negligibly different SWAP from a panchromatic (black and white) camera system. Color video imagery has

been routinely used for decades using devices no larger than panchromatic cameras. Color video is most commonly collected through the use of mosaic array filters. Mosaic array filters are arrays of pixel-sized filters that allow the transmission of particular wavelengths of light onto particular pixels. These filters can have thicknesses on the order of a few microns and do not appreciably increase the size, weight, or power consumption of a camera. However, mosaic array filters do not display the spectral resolution necessary for HSI. The principal research problem is then to combine the low SWAP of the mosaic array filter concept with the spectral resolution of the HSI sensor.

There are a large number of techniques used for collecting HSI data. While the collection technique for different instruments varies, the spectral sensitivity of the detector must vary in at least one measurement dimension (time or space). For simplicity, we will describe a sensing array of one dimension, capable only of the measurement of a single spectrum, with the understanding that the principles used can be extended to a two-dimensional sensing array capable of collecting a three-dimensional data cube in accordance with a reasonable scanning technique.

CONTACT OPTICAL SPECTRAL FILTERS

A mosaic array filter is an example of a contact optical spectral filter (COSF). A COSF is an optical element that is placed in contact with a photosensitive array detector and that provides spectral sensitivity for different parts of the array detector (see Fig. 1).

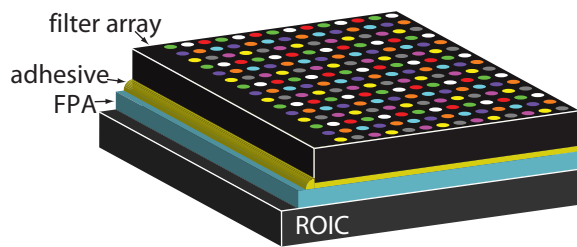


FIGURE 1
Schematic of a contact optical spectral filter (COSF). The pixelated focal plane array (FPA) has elements that distinguish colors via a filter array placed in optical contact with the FPA. In the example here, an adhesive is used to make optical contact. This example shows a two-dimensional, 9-color filter array with circular apertures. COSFs may have square apertures, larger or smaller numbers of distinct colors, or may be arranged to vary only in one dimension.

Dielectric filters and interference filters are the most promising technologies for the creation of HSI-capable COSFs. Current manufacturing technology, however, does not allow for the creation of the requisite large-scale mosaic patterns containing the needed several hundred spectrally independent single-pixel-sized filters. Thus, most previous work involving COSFs for HSI has relied on a systematic variation of fabrication parameters across a detector array in order to create a simple architecture in which (for example) an optical cavity thickness varies in a wedge-like fashion. These wedged COSFs can have a continuous or digital wedge profile (see Fig. 2) and have been demonstrated by several groups.¹⁻³

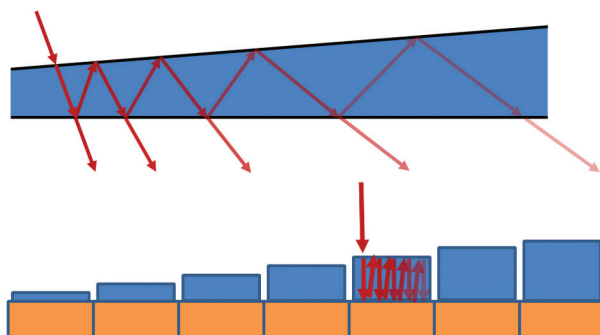


FIGURE 2
Examples of optical wedges used as COSFs. The spectral discrimination is brought about by the constructive and destructive interference of multiple reflections from the top and bottom surfaces of the wedge. Transmission occurs when a given wavelength is resonant with the location-specific optical cavity thickness. (Top) A continuous wedge, where the wavelength of maximum transmission varies smoothly with the wedge thickness. (Bottom) A digital wedge, where the wavelength of maximum transmission varies discretely with each wedge segment's thickness.

The most common form of color discrimination, simplex spectroscopy, senses a single wavelength range with a single pixel (e.g., Refs. 2 and 3). The advantage of

a simplex spectrometer is that there is an unambiguous design, i.e., a different resonant cavity thickness, correlated to each desired wavelength. The disadvantages of a simplex spectrometer are challenging trade-offs between bandwidth, resolution, and throughput. Typical spectral resolutions required for Navy/DoD applications are on the order of a few nanometers in the visible. Optical cavities for simplex spectrometers with spectral widths equal to or smaller than a few nanometers require high cavity finesse and, therefore, will reject a large portion of the incident light. Simplex spectrometers must also be constructed for bandwidths less than one octave (the maximum wavelength must be less than twice the minimum wavelength) due to multi-order interference. In theory, this bandwidth limit can be overcome by using additional filter layers, but this significantly increases the complexity and cost of the device and has not previously been demonstrated for a COSF. There is, therefore, not a clear path to a compact, broadband, simplex spectrometer. Next-generation compact spectrometers must use some future technology, or use a multiplexing technique.

MULTIPLEXED SPECTROSCOPY

Multiplexed spectroscopy involves measuring more than one wavelength range on each pixel. This has the advantage that it is not limited to a single octave and therefore enables spectral sensitivity across all wavelengths to which the detector is sensitive. Determination of the input spectrum is then achieved through processing the measured signals arising from a group of pixels. The main disadvantage for a multiplex spectrometer is the computational complexity required to reconstruct a spectrum from the multiplexed detected signal.

A few multiplexing techniques have been widely utilized, such as Fourier transform and Hadamard spectroscopies. Fourier transform methods were successfully applied to a COSF spectrometer in Ref. 1. However, because of the nature of the Fourier transform, the device necessarily operates in the low finesse limit, and this limits the device's achievable signal-to-noise ratio (SNR). Therefore, Fourier transform spectroscopy is not anticipated to produce a compact device that could be deployed into the field and used for rapid measurements. A new multiplexing technique is required, one that uses moderate-to-high finesse and is capable of simultaneously achieving broadband sensing, adequate spectral resolution, and good SNR. Given a desired wavelength axis, how will we know what series of optical cavities to build? How can we assure ourselves that the conversion matrix will be stable? We will need to derive a mathematical conversion matrix to transform the multiplexed measured signal into a spectrum.

FINDING THE NATURAL AXIS

Fixed optical cavities of moderate-to-high finesse are known as etalons. The transmission, T , of an etalon of thickness d , as a function of wavenumber σ , can be described by the Airy function derived for Fabry-Pérot spectroscopy:

$$T_d(\sigma) = \frac{\left(\frac{\pi}{2}\right)^2}{\left(\frac{\pi}{2}\right)^2 + F^2 \sin^2[\phi_d(\sigma)]},$$

where $\phi_d(\sigma)$ is the optical phase acquired by light of wavenumber σ on a single pass through the etalon and F is the etalon finesse. For an ideal etalon, the finesse is related to the reflectance R of each surface of the etalon by the relation $F = \pi\sqrt{R}/(1-R)$. Figure 3 shows plots of the Airy function in the wavelength space for different values of the finesse and different etalon thicknesses.

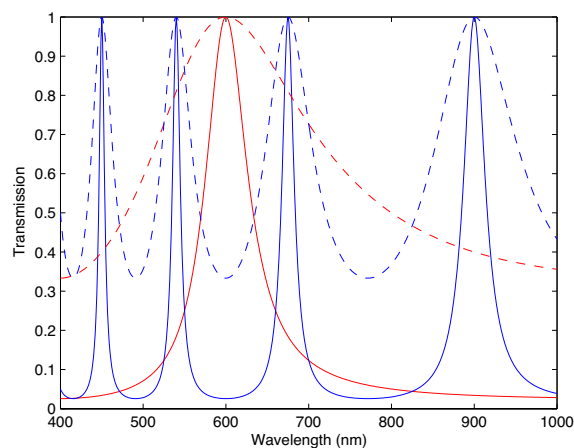


FIGURE 3 Transmission spectra of ideal optical cavities with a constant refractive index of 1.5. Transmission of simple optical cavities is determined by the Airy function (see text for equation). The reflectance R of top and bottom surfaces of the optical cavities determines the sharpness of the features. The cavity thickness and index of refraction determine the wavelength separation between transmission peaks. Cavity reflectance $R = 0.5$ (dashed lines); $R = 0.85$ (solid lines). Cavity thicknesses of 200 nm (red) and 900 nm (blue) are shown. Over the displayed wavelength range, the 200 nm cavity transmits a single order, while the 900 nm cavity transmits information content from four orders.

For any interference spectrometer, there must be found a relationship between the range and resolution of the varied parameter (in this case the cavity thickness d) and the range and resolution of the extracted variable (in this case the wavenumber σ), these dimensions are known as the natural axes of the system. Research at NRL has shown that a combination of the resolution and Nyquist sampling rules derived for the standard Fabry-Pérot and Fourier transform spectroscopies can be used to derive a natural axis for sampling

a multiplexed Airy-function spectrometer. Given a wavelength axis defined by maximum wavenumber σ_{\max} , wavenumber resolution $\Delta\sigma$, and some number of extracted spectral values N , the natural Airy function axis can be described by a staircase of cavities defined by three parameters: the thinnest etalon, d_{\min} , the etalon thickness step size, δ , and the range of etalon thicknesses, $d_r = d_{\max} - d_{\min}$. The required range and resolution parameters for the conjugate axis can be calculated using $d_r = \frac{1}{2 F \Delta\sigma}$ and $\delta = \frac{1}{4 F \sigma_{\max}}$

respectively. The value of d_{\min} is essentially a free parameter. Under typical solar illumination conditions, SNR considerations lead to a desire to keep d_{\min} as small as possible, preferably $d_{\min} = \frac{1}{2 \sigma_{\max}}$. Using the

above relations to guide system design thus ensures that spectral values can be calculated from the multiplexed measured signal. Figure 4 shows a numerical estimation of the stability of the transform as the values of δ and d_r deviate from the values recommended in the above equations.

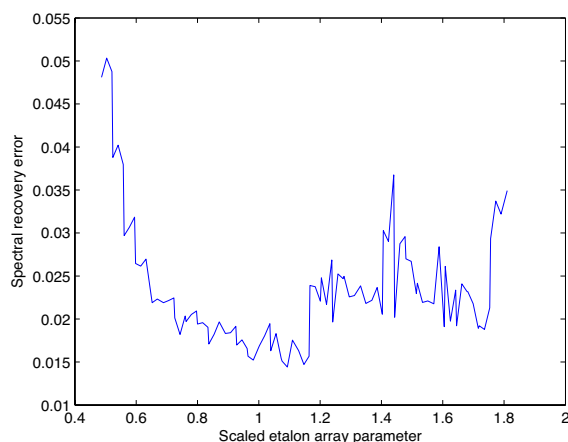


FIGURE 4 Spectral recovery error as a function of a scaled etalon array parameter. The spectral recovery was estimated by encoding and recovering a spectrum containing both sharp and broad features. The spectral recovery contained 100 distinct spectral bins over the entire silicon sensitivity bandwidth (air wavelength range from 450 to 1000 nm). The scaled etalon array parameter is the step size for 360 etalons, scaled by the recommended value in the text. The minimum recovery error (and best numerical stability) is very near the recommended value (scaled etalon array parameter = 1).

For typical HSI applications in the visible band, $\sigma_{\max} \approx 33,300 \text{ cm}^{-1}$ (450 nm wavelength in air) and $\Delta\sigma \approx 92 \text{ cm}^{-1}$ (wavelength resolutions between 1 and 6 nm in the collection band 450 to 1000 nm). This results in 200 spectral bins over a typical silicon detector bandwidth. Cavities with a reflectance of 65% on each surface ($F = 7.24$) will ensure that broadband signals

contain adequate contrast for analysis. Using the above expressions leads to device parameters of $d_{\min} = 150$ nm, $\delta = 10$ nm, and $d_r = 7.5$ μm . This is an extremely challenging optical device to manufacture. Such a system requires deposition of over 700 different etalon thicknesses, each having a flatness much less than the 10 nm step size. Low-cost fabrication methods for this type of structure were not found to be available. Thus, a robust method for fabricating the stair-stepped etalon structures was developed in NRL's Institute for Nano-science.

NANO-STAIRCASE FABRICATION

The standard way to microfabricate a series of material thicknesses is to sequentially etch levels into a dielectric material. Each level is fabricated in an independent lithographic and subsequent etching step, requiring K steps for K levels. The combinatorial etching used in Ref. 3 is able to reduce the number of etch steps to $\log_2(K)$; however, even this approach leaves ~ 20 microfabrication steps for a structure having between 512 and 1024 levels. Since each microfabrication step is time consuming and adds costs and complexities, minimizing the number of fabrication steps is desired. For comparison, a typical commercial camera chip requires 8 to 32 lithography steps. Thus, the additional fabrication of a 700 level structure by traditional means

would significantly add to the device cost and complexity, making this path highly undesirable. Other approaches use gray-tone lithography⁴ to fabricate levels using a single lithograph step, but the variability of etch processes and material homogeneity usually limit the number of truly distinct levels to around 100 levels.

Our process is based on gray-tone lithography of a repeated bilayer stack.⁵ Figure 5 presents a schematic of the process sequence. This process is based on four basic steps: (i) stack deposition, (ii) gray-tone lithography, (iii) structure transfer, and (iv) selective chemical etch. Standard lithography generates a “black-white” image with a distinct two-level profile. Gray-tone lithography, on the other hand, can generate a full three-dimensional (3D) structure such as a wedge. In gray-tone lithography, a 3D photoresist structure can be transferred by reactive ion etching (RIE) into almost any type of material. We transfer a gray-tone photoresist wedge into a stack of 10 nm thick bilayers repeatedly deposited up to a total thickness of a few micrometers. After the RIE step, a rough wedge-shaped layer remains due to variability in material and photoresist homogeneity, and the inherent variability of the etch process. This variability has historically limited the number of resolvable gray-tone levels.

In our process, following the RIE step, a chemical etch is used to digitize the levels. Each bilayer is comprised of two dielectric materials wherein one material

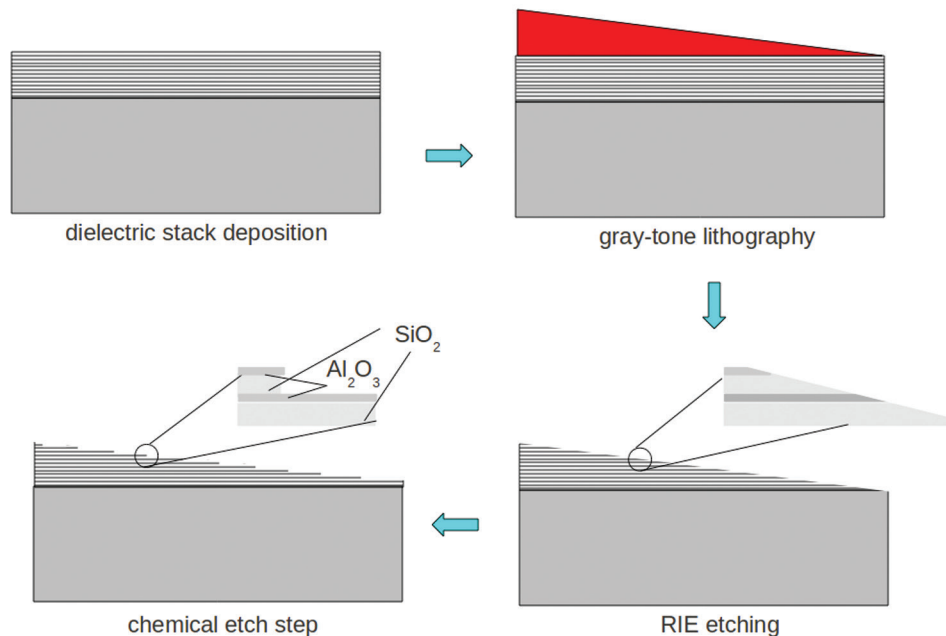


FIGURE 5

Basic process sequence for fabrication of a nano-staircase (clockwise from upper left). (i) A dielectric stack consisting of a large number of bilayers of SiO_2 and Al_2O_3 is deposited on a substrate by atomic layer deposition. Each layer has atomic-level smoothness. (ii) Gray-tone lithography is used to fabricate a continuous wedged structure in photoresist on top of the bilayers. (iii) Reactive ion etching is used to transfer the wedge pattern into the bilayer stack, leaving a roughened surface due to material and etching inhomogeneity. (iv) A chemical etch removes one material of the bilayer, leaving a series of atomically flat surfaces having finely resolved steps.

acts as a chemical etch stop (i.e., one etches quickly and the other one very slowly when exposed to the same etch process). The physical separations of the etch stop layers then define the resolvable thicknesses of the final structure.

The repeating bilayer stack is comprised of two materials, silicon dioxide (SiO_2) and alumina (Al_2O_3), that are alternately deposited to form the spacer and etch stop layers. The bilayer stack can be deposited using any one of several thin-film deposition techniques. For this system, atomic layer deposition (ALD) was chosen for the deposition process. Figure 6 shows an SEM cross section of a bilayer stack deposited using ALD and clearly shows the thick SiO_2 and thin Al_2O_3 layers.

Forming a wedge from the dielectric stack is enabled by fabricating the desired shape in photoresist on the dielectric stack material. The gray-tone photoresist structures may be transferred, for example by plasma etching, to reproduce, in the target material, a scaled version of the three-dimensional photoresist structure. As the etch proceeds, the photoresist mask slowly erodes, exposing the underlying material, in our case the dielectric stack, to the high etch rate plasma. Gray-tone technology relies on specifically developed RIE chemistries and plasma conditions to control the relative etch rate of the dielectric stack to photoresist called “etch selectivity.” This aspect defines the final vertical dimensions of a 3D structure. In our case, the SiO_2 and Al_2O_3 etch rates are similar to that of the photoresist, thus allowing a transfer in approximately a

1:1 scale. However, due to variability in the RIE process, the resulting structure is somewhat distorted from that originally established in the photoresist.

After transferring the gray-tone photoresist into the stack, a chemical etch step is performed to create distinct thicknesses in the structure, each level being optically flat. The chemical selectively only etches one material of the bilayer. Vapor hydrofluoric acid (HF) was used to etch SiO_2 selectively over Al_2O_3 . This leads to digitally distinct levels at a flatness controlled by the deposition technique of the bilayer stack, which in this case is of atomic layer precision due to the single-atom nature of the ALD deposition process. Figure 7 shows a reflection micrograph of the stair-step structure on a test substrate. The colors are due to the different transmission characteristics of the different etalon heights. Having demonstrated nano-staircase fabrication, the next step was construction of a prototype device by fabricating a nano-staircase on top of a pixelated detector.

PROTOTYPE DEVICE

Our device used a commercially available imaging sensor provided by Aptina (model MT9V111). Mirrors and a nano-staircase were deposited directly onto the imaging array. Figure 8 shows a photograph of one of the first devices. Schedule and budget constraints limited the prototype device to 140 steps. As of this writing, the device is still undergoing calibration and characterization. Preliminary calibration data indicate

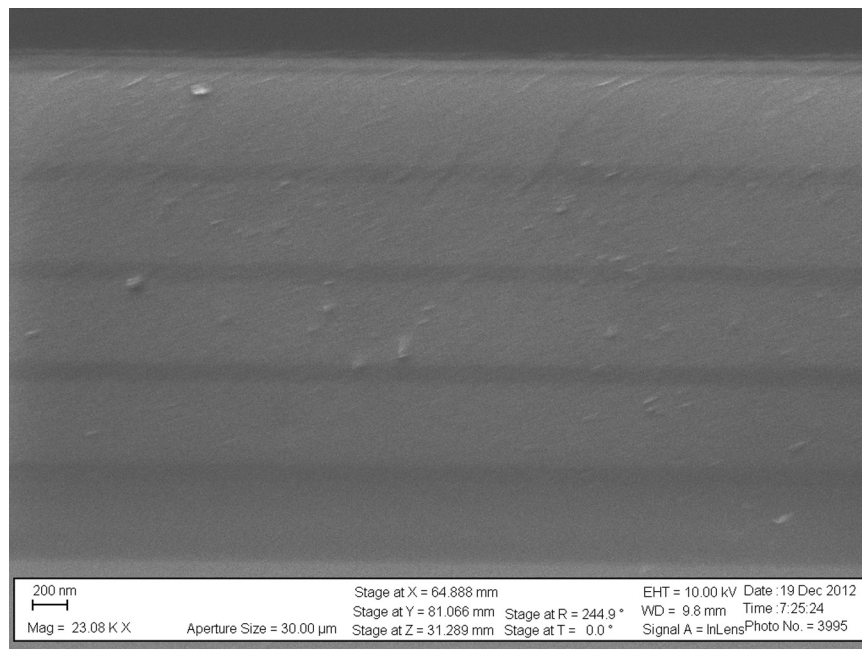


FIGURE 6 Scanning electron microscope (SEM) micrograph, cross section of a bilayer stack. This example shows a repeating pattern of 200 nm of SiO_2 interspersed with 20 nm of Al_2O_3 .

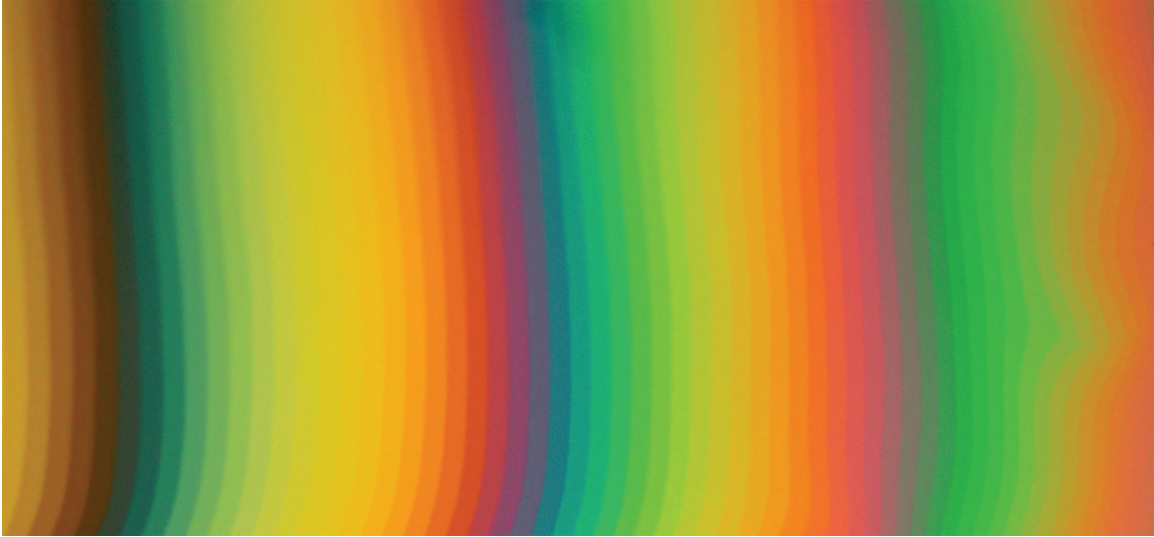


FIGURE 7

Optical micrograph, top view, white light fringe pattern (step width $\sim 10 \mu\text{m}$, bilayer step height 10 nm: 7 nm SiO_2 + 3 nm Al_2O_3). Approximately 70 distinct levels are visible. The sharp transitions between steps are due to the finely digitized staircase. This micrograph shows only a section of the wedge. Overall, the Fabry-Pérot etalon array is comprised of 140

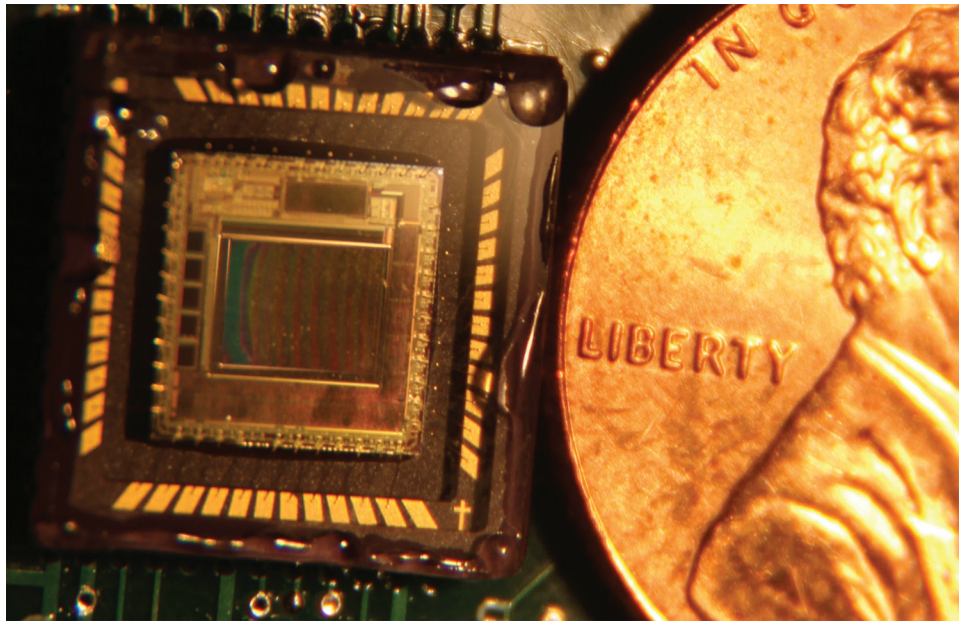


FIGURE 8

Photograph of the prototype device with a penny for scale. The wedged etalon array on the sensing chip is composed of 140 distinct levels. The striping of the first two layers is clearly visible on this scale. Since the color resolution of our device is much finer than that of the camera used to take this image, groups of etalon levels may appear to be the same color. A moiré pattern of interfering colors is visible over the larger steps. The shortest steps have etalon thicknesses of approximately 150 nm, while the tallest steps have etalon thicknesses of approximately $1.5 \mu\text{m}$.

that the device displays the expected spectral sensitivity. This prototype is negligibly different in SWAP from the panchromatic array and offers the capability of compact hyperspectral imaging to the warfighter.

[Sponsored by ONR]

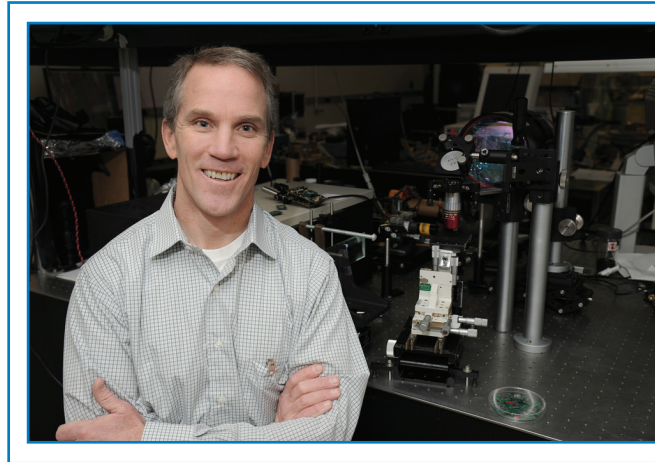
References

- ¹ S. Rommeluere, N. Guerineau, R. Haidar, J. Deschamps, E. De Berniol, A. Million, J.P. Chamonal, and G. Destefanis, "Infrared Focal Plane Array with a Built-in Stationary Fourier-Transform Spectrometer: Basic Concepts," *Opt. Lett.* **33**(10), 1062–1064 (2008).
- ² A. Emadi, H. Wu, S. Grabarnik, G. De Graaf, K. Hedsten, P. Enoksson, J.H. Correia, and R.F. Wolffenbuttel, "Fabrication and Characterization of IC-Compatible Linear Variable Optical Filters with Application in a Micro-spectrometer," *Sensors and Actuators A* **162**(2), 400–405 (2010).

- ³ S.-W. Wang, C. Xia, X. Chen, W. Lu, M. Li, H. Wang, W. Zheng, and T. Zhang, "Concept of a High-Resolution Miniature Spectrometer Using an Integrated Filter Array," *Opt. Lett.* **32**(6), 632–634 (2007).
- ⁴ J. Xiao, F. Song, K. Han, and S.-W. Seo, "Fabrication of CMOS-compatible Optical Filter Arrays Using Gray-Scale Lithography," *J. Micromech. Microeng.* **22**(2), 025006 (2012).
- ⁵ A. Boudreau et al., "Fabrication Method for Digital Etching of Nanometer-Scale Level Structures," U.S. Patent pending (2013).



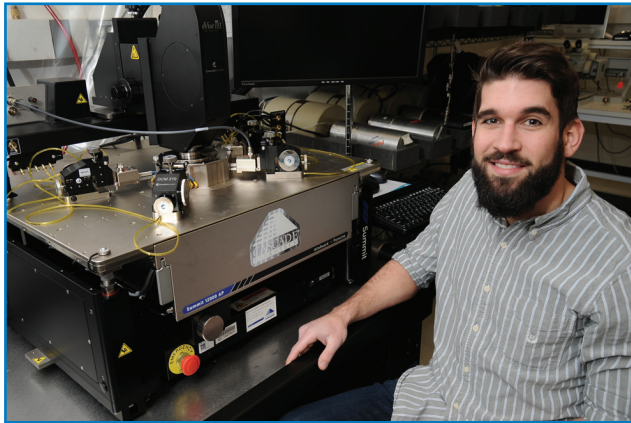
THE AUTHORS



MICHAEL YETZBACHER has been with NRL since 2010 where his research is focused on the development of sensor technology and its application to airborne sensing. His duties include laboratory and field testing of novel systems that broaden the limits of spectroscopic and radiometric sensing. His research interests include the development and characterization of micro-optical components for polarimetric, hyperspectral, and multispectral sensing. He received a Ph.D. in physical chemistry and a certificate in optical sciences from the University of Colorado in 2008.



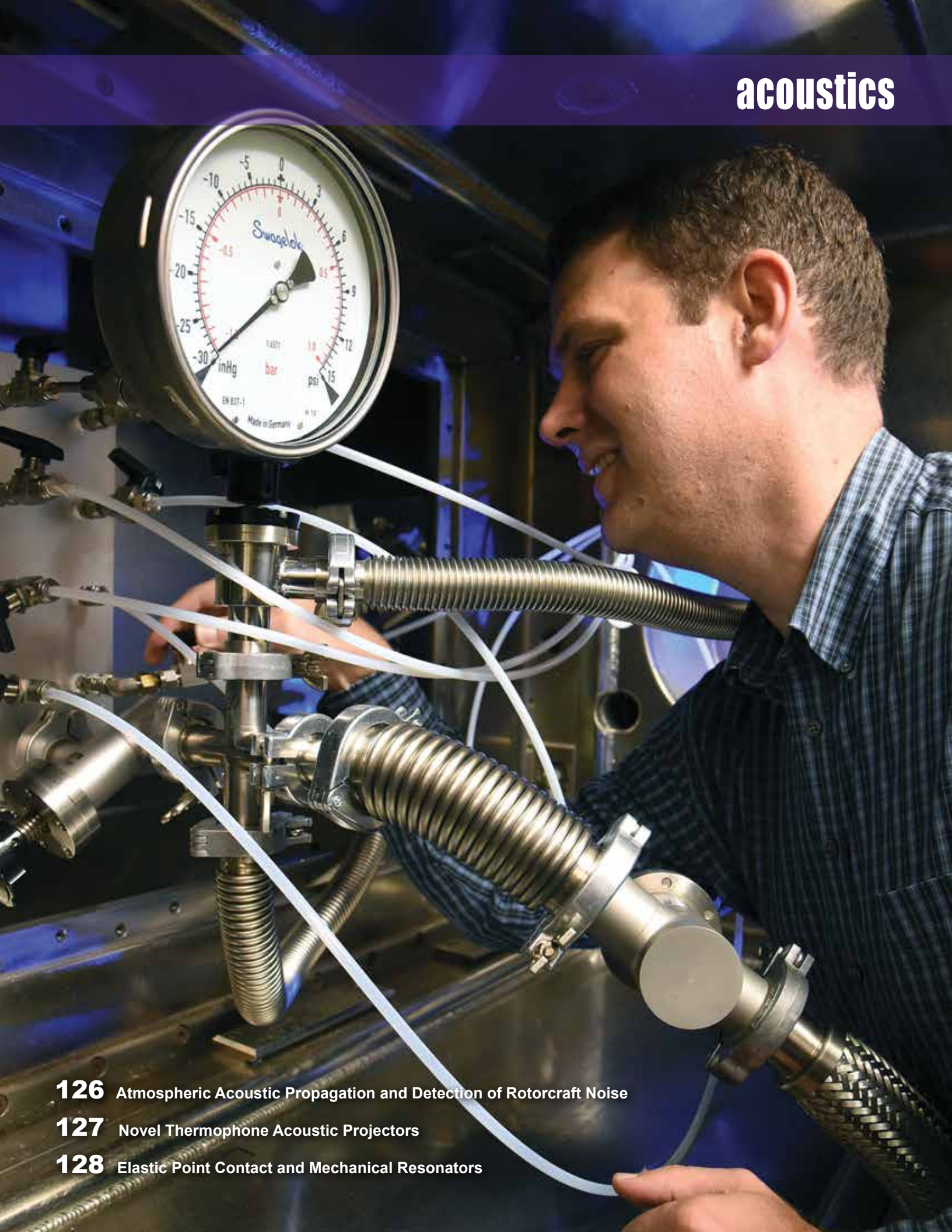
CHRISTOPHER W. MILLER joined NRL as a Karles Fellow in 2012 working on atmospheric correction for hyperspectral imagery. Since then his work has focused on solving ill-posed inverse problems within the domains of computer vision and signal processing. Dr. Miller graduated in 2012 with his doctoral degree in applied mathematics and scientific computation from the University of Maryland at College Park, specializing in numerical solvers for stochastic partial differential equations. His research interests include applied harmonic analysis, statistical learning theory, and the development of real-time algorithms in target detection.



ANDREW BOUDREAU received his B.S. and M.S. in electrical engineering from The George Washington University in 2008 and in 2010, respectively. His M.S. work focused on electronics, photonics, and micro-electromechanical systems. In 2010, he joined NRL's Applied Optics Branch and has designed hardware systems for synthetic aperture radar and hyperspectral imaging systems. His work has also focused on microfabrication techniques for complex optical structures. His research interests include mixed signal integrated circuit design, simulation, and fabrication.



MARC CHRISTOPHERSEN joined NRL as an NRC post-doctoral fellow in 2007. Since 2009, he has been a Federal employee in the Radiation Detection Section of the High Energy Space Environment Branch in the Space Science Division. Marc Christophersen worked on different MEMS (micro-electromechanical systems) applications ranging from electrochemistry to biomedical applications. His current research interests are focused on the development of silicon radiation detectors and low-level light sensors for high-energy physics experiments and DoD/Homeland Security applications. He received his Ph.D. and M.S. in materials science from the University in Kiel in Germany. He received the 2011 U.S. Navy Dr. Delores Etter Top Scientists and Engineers of the Year and 2012 NRL Sigma Xi Edison Chapter Young Investigator awards.



126 Atmospheric Acoustic Propagation and Detection of Rotorcraft Noise

127 Novel Thermophone Acoustic Projectors

128 Elastic Point Contact and Mechanical Resonators

Atmospheric Acoustic Propagation and Detection of Rotorcraft Noise

J.F. Lingeitch,¹ J. Cook,² C. Hutchins,² and D. Martinez³

¹Acoustics Division

²Marine Meteorology Division

³Computer Sciences Corporation

Introduction: Rotorcraft often fly at low altitudes where they are vulnerable to acoustic detection by human listeners. The propagation of the highly directional vehicle noise through an inhomogeneous atmosphere and interaction with terrain features introduce complexity and variability into the acoustic signal received by a distant listener or microphone. The NRL Acoustics and Marine Meteorology Divisions are developing and testing a new application to predict the acoustic detection footprint of a rotorcraft noise source by a human listener. This application leverages advanced acoustic propagation and high-resolution numerical weather prediction models developed in the NRL base program to forecast an estimate of the acoustic spectral attenuation between the source and a grid of listeners in an area of interest. A developmental version of the application is currently being validated with existing acoustic data and was exercised during a recent U.S. Marine Corps (USMC) exercise. The acoustic predictions provide probability-of-detection (PoD) estimates and the forecasts offer a tactical advantage to mission planners.

Multidisciplinary Approach: Long-range acoustic noise propagation is a multifaceted problem requiring a

forecast of atmospheric conditions (e.g., temperature, wind, and humidity profiles), knowledge of terrain elevation and type, and an acoustic model for propagating the noise through an inhomogeneous waveguide. Our approach, the NRL Atmospheric Acoustic Propagation (AAP) model, integrates an advanced propagation model developed in the Acoustics Division as a reach-back application utilizing the Coupled Ocean/Atmosphere Mesoscale Prediction System (COAMPS®) On-demand System (COAMPS-OS®) software running on the Fleet Numerical Meteorology and Oceanography Center (FNMOC) A2 and DoD Supercomputer Resource Center (DSRC) clusters. This capability is currently being developed and tested for transition to operations via upgrades to the COAMPS-OS software suite which provides products with the necessary detail and accuracy to support the Navy and USMC missions following the reach-back concept of operations and applying net-centric principles.

We have developed and implemented a wide-angle, energy conserving parabolic wave equation with a linear-shift-map to compute acoustic transmission loss through a variable atmosphere over uneven terrain.¹ Atmospheric refraction due to temperature and wind gradients, diffraction by terrain features, frequency-dependent atmospheric attenuation, and variable ground impedance are included in the transmission loss calculation between the source and a grid of ground listener locations. Figure 1 shows a vertical slice (i.e., range/altitude) of a transmission loss calculation over realistic terrain (the color scale from red to blue indicates low to high transmission loss). The source

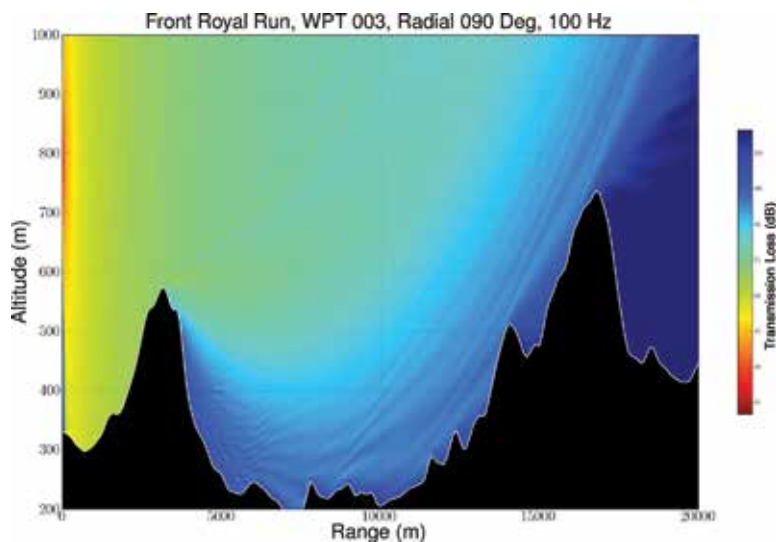


FIGURE 1

Transmission loss for a sample calculation for an air acoustic propagation problem with a refracting atmosphere and significant terrain features. The color scale from red to blue indicates low to high transmission loss. The source is located at 0 m range at an altitude of 800 m.

is located at 0 m range at an altitude of 800 m. In this case, the atmosphere is upward refracting, and sharp terrain features block the direct propagation of sound into the valley between the two ridges, but diffracted sound energy reaches the valley floor.

Testing and Evaluation: The AAP application integrates the transmission loss calculations discussed above with existing helicopter noise characterizations and a human listener probability-of-detection model (AUDIB) developed for the NASA Rotorcraft Noise Model.² The AAP application was evaluated by end users in USMC training exercises conducted during October 2013 by the Marine Aviation Weapons and Tactics Squadron One, Yuma, Arizona, as a component of their Weapons and Tactics Instructor Course.

[Sponsored by SPAWAR PMW-120]

References

¹ D.J. Donohue and J.R. Kuttler, "Propagation Modeling over Terrain Using the Parabolic Equation," *IEEE Trans. Antennas and Propagat.* **48**, 260–277 (2000).

² J.A. Page, C. Wilmer, and K.J. Plotkin, "Rotorcraft Noise Model Technical References and User Manual (Version 7)," Wyle Laboratories Research Report WR 07-04, April 2007.



Novel Thermophone Acoustic Projectors

B. Dzikowicz, J. Baldwin, and J. Tressler
Acoustics Division

Introduction: The ability to produce sound in the audio frequency band due to periodic heating of a very thin metal foil by an alternating electrical current has been known and generally understood since the early part of the 20th century. The rapidly oscillating surface temperature change gives rise to expansions and contractions in the surrounding gas layer, which generates outgoing acoustic waves. The sound field produced by these early thermophone devices was limited by the amount of energy required to raise the temperature of the metal foil. This ability is quantified by the heat capacity per unit area which is predicted to be inversely proportional to the efficiency.¹ Because metal foils available at that time did not possess a sufficiently low heat capacity per unit area, their efficiencies were quite low. Thermophones were therefore eventually abandoned as practical sources of sound as they were unable to compete with more efficient conventional acoustic sources such as piezoelectric ceramics and moving coil loudspeakers.

Carbon Nanotube Thermophones: Recent advances in the manipulation and large-area synthesis of suspended carbon nanotube films and similar nanoscale materials have renewed interest in examining thermophones as a viable acoustic source technology, particularly for very low frequency applications.² Carbon nanotube films are arrays of nanoscale filaments that are effectively one dimensional. These nanoscale suspended films have very low mass, high surface area, and a heat capacity per unit area that is several orders of magnitude lower than legacy metal foils (see Table 1). Because a thermophone is ultimately a heat engine, it becomes more efficient as the temperature difference between the sink and source becomes greater. As such, the very high melting points of these carbon nanotube materials are also advantageous.

We are also investigating a number of other modern nanoscale films that also meet the low heat capacity per unit area criteria. These include graphene, metallic nanowire arrays, and composite structures.

Enclosing the nanofilm within a thin layer of gas causes its efficiency at low frequencies to increase enormously. This effect is particularly important when the external medium, such as water, is nearly incompressible. Choice of enclosure gas is also important. In order to get as much thermal energy into the gas layer as possible, the gas should have a high thermal conductivity and a low heat capacity. The best candidate gases that meet these criteria are helium and neon.

Properties and Applications: Thermophones have a number of advantages over conventional sound projectors. Since they are essentially resistive heaters, they are electrically simple and do not require complex circuitry or specialized amplification to drive them. Because the enclosure structure can be made nearly massless, the harmonic structure is greatly simplified. This unique feature explains their broad frequency band response. Sources with flat response, especially at low frequencies, are of particular interest for naval sonar applications.

The most straightforward naval application of nano-thermophone projectors is for low frequency sources for sonar systems on small-diameter autonomous underwater vehicles (AUVs). These sources could be mounted to the exterior of an AUV or submarine without appreciably altering the vehicle profile. State-of-the-art low-frequency broadband projectors take up a large fraction of an AUV's volume and mass. Replacing these with nano-thermophone projectors would lower both volume and mass considerably. Other potential underwater applications include acoustic communication transducers and navigation beacons, as well as active surfaces for stealth applications. All

TABLE 1 — Comparison of candidate thermophone films. Legacy models show an inverse relationship between the heat capacity per unit area and the efficiency. The bottom three materials have only been available relatively recently.

Film	Thick-ness (nm)	Density (kg/m ³)	Bulk Heat Capacity (J/kg* ^o K)	Heat Capacity per Area (J/m ² * ^o K)	Conduc-tivity (1/ Ω *m)	Melting Point (^o C)
Platinum ¹	700	21,450	134	2.0	9.4 x 10 ⁶	1,770
Gold	700	19,320	128	1.7	45.0 x 10 ⁶	1,060
Graphite	700	2,250	710	1.1	1.54 x 10 ⁶	3,650
Single-Walled Carbon Nanotube Film	0.6 - 2	1,300 – 1,400	710	0.92 x 10 ⁻³	19 x 10 ⁶	2,800
Multi-Walled Carbon Nanotube Film ²	2 - 10	1,300 – 1,400	710	7.7 x 10 ⁻³	19. x 10 ⁶	2,800
Graphene	.34		710	0.31 x 10 ⁻³	2.6 x 10 ⁶	2,800

these applications would take advantage of the nano-thermophone’s ability to be thin and conform directly to the hull of a vehicle.

Work at NRL: Existing models of the efficiency of thermophones^{1,3} do not take into account all of the heat transfer mechanisms, such as losses due to radiation, or the heat-sinking effect of the barrier material. These deficiencies led to an overly optimistic result. We developed a more complete numerical model of the system, taking into account these more subtle mechanisms. Although our results (Fig. 2) revealed sound levels and efficiencies lower than that of earlier models, there remains a significant advantage to moving to nanoscale films.

Initial experiments demonstrated the efficacy of the device over a broad range of frequencies. We are

in the process of producing an experimental apparatus giving us the ability to test a large array of nanoscale films, enclosure gases, barrier materials, and geometries. It is expected that these experiments will lead to a theoretical verification of the model and guide us to new naval applications.

[Sponsored by the NRL Base Program (CNR funded)]

References

- ¹ H.D. Arnold and I.B. Crandall, “The Thermophone as a Precision Source of Sound,” *Phys. Rev.* **10**, 22 (1917).
- ² A.E. Aliev, M.D. Lima, S. Fang, and R.H. Baughman, “Underwater Sound Generation Using Carbon Nanotube Projectors,” *Nano Letters* **10**, 2374–2380 (2010).
- ³ L. Xiao, Z. Chen, C. Feng, L. Liu, Z.-Q. Bai, Y. Wang, L. Qian, Y. Zhang, Q. Li, K. Jiang, and S. Fan, “Flexible, Stretchable, Transparent Carbon Nanotube Thin Film Loudspeakers,” *Nano Letters* **8**, 4539–4545 (2008).

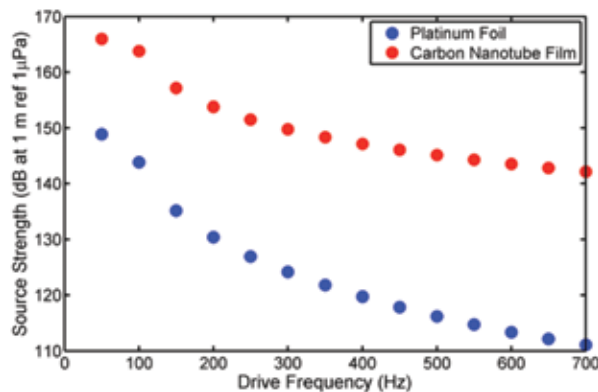


FIGURE 2 Theoretical source strength from the model developed at NRL, assuming an 8 mm thick projector with a surface area 0.24 m by 0.24 m. The heat capacity of the carbon nanotube film is 260 times lower than that of the platinum foil.

Elastic Point Contact and Mechanical Resonators

D.J. Goldstein, D.M. Photiadis, and M.K. Zalalutdinov
Acoustics Division

Introduction: Mechanical resonators, generally described as coupled networks of springs and masses, are present throughout nature and technological applications. We demonstrate here that the compliance associated with the deformation of the contact area between these elements becomes significant for sufficiently small attachment area, the case of an elastic point contact. Although local compliance at an

interface region has long been understood for the static case, particularly by geophysicists, perhaps surprisingly, dynamic effects related to elastic point compliance such as resonance frequency shifts and inelastic absorption have not yet been reported and are typically not taken into account by researchers unless exact elasticity theory simulations are employed. Instead, the point attachment of a spring element to a mass/base has generally been regarded either as rigid or as a source of radiative phonon loss into an effectively infinite medium or phonon cavity, a mechanism distinct from the nearfield phenomenon we consider here. Our model is adequate to describe the behavior of basic nanoscale objects such as nanowires and nanorods. Such objects are envisioned as components of complex electromechanical systems, but reconciling theoretical predictions of their mechanical properties with experiment has been inconclusive due to the difficulty in carrying out measurements.

A Contact Impedance Model: We offer a simple analytical model that accounts for the compliance of the elastic point contact through the introduction of a contact impedance, an approach that is similar to the introduction of contact resistance in electrical circuits. We demonstrate the validity of this model (described in Fig. 3) using a series of appropriately designed mechanical resonators. In the experimental results we present (shown in Fig. 4), an attachment area radius varying from 1 to 2 mm in a resonator with nominal resonance frequencies of order 5 kHz leads to frequency shifts of 15% to 25%. The model is an approximation based on classical elasticity theory and is scale invariant. Thus, we expect it will predict effects that may be significant in systems ranging from engineering structures to biological and nanoelectromechanical systems.

Elastic point contacts are commonly used in nanoelectromechanical systems to achieve weak mechanical and thermal coupling. Our results show that in addition to introducing an elastic compliance, a point contact creates a channel that allows for the transport of energy from an attached oscillator or phonon cavity to the nearfield of the point contact in the substrate. For sufficiently weak coupling, we predict that this channel dominates the radiative phonon transport thought to set a fundamental limit in such geometries.

This simple model is sufficient to predict the observed frequency shifts to within an accuracy of a few percent in the experiments we have carried out, but the model can be generalized in many ways. Perhaps of most interest, the normal stress need not be constant, allowing for applied moments and enabling the analysis of cantilever-type oscillators. We have carried out this analysis; the details are different, but the main phenomenon is unchanged.

Results: In outline, our main theoretical results are as follows. Suppose that the nanowire exerts an oscillatory normal force $F e^{-i\omega t}$ upon the mass m and assume for simplicity that the mass is free. For a circular contact area of radius $a \rightarrow 0$, the average displacement of the attachment point is given to leading order in a by $\langle x \rangle = F \langle G \rangle_r(\omega) + F/K_s$, where K_s is the stiffness associated with the short-time compliance of the mass and $\langle G \rangle_r(\omega)$ is a complex reverberant field. The stiffness K_s is given by the simple expression $K_s = \kappa G a$, where G is the shear modulus of the mass and κ is a dimensionless constant of order unity.

A straightforward argument based on our results indicates that there is an alternative coupling path between a suspended device and a substrate resulting from direct excitation of the nearfield. This coupling channel arises from the fact that any substrate will possess inelastic mechanisms that convert strain energy to electronic excitations or thermal phonons. This mechanism can be taken into account by allowing the elastic contact stiffness to acquire an imaginary part, giving a contribution to the inverse Q of an attached oscillator, $\delta Q^{-1} = \alpha' \omega_0^2 / (\omega_0^2 + (\Omega')^2)$. Here, the frequency $\Omega' = \sqrt{K_s/M}$ is determined by the nearfield stiffness and α' is proportional to the internal friction of the substrate. The ratio of this quantity to the radiative phonon contribution is given by $\alpha' C / (k_L a)$, where C is an order unity constant. Because of the singular behavior of the nearfield, this ratio can become larger than 1 as $k_L a \rightarrow 0$. For $\alpha' \sim 0.01$ and $f = 1$ GHz, this limit is reached for $a \sim 17$ nm. Based on the Landauer formula, we predict that the same phenomena will become important in thermal transport for temperatures less than or of order 20 mK.

One potentially interesting application of our result is to use the simple nature of the relationship given by $K_s = \kappa G a$ to measure the modulus of elastic systems on the nanoscale, an area of great recent interest in both biological and material systems. Currently, the method of choice for this measurement is to use an atomic force microscope (AFM) in either a static or dynamic mode. To obtain predictions from such measurements, a detailed knowledge of the tip geometry is typically combined with a nonlinear Hertzian contact theory of the tip/sample interaction. Our results suggest that configuring the AFM with a nanowire or a carbon nanotube, rather than a conventional conical tip, would enable absolute measurements because of the constant cross section of the cylindrical geometry, and may be preferable.

Our model may also be used in the analysis of larger, more complex systems, in analogy to the analysis of electrical circuits. In such scenarios, full, three-dimensional, elasticity theory-based numerical calculations, which automatically include the effects we describe here, are quite large and costly and are limited

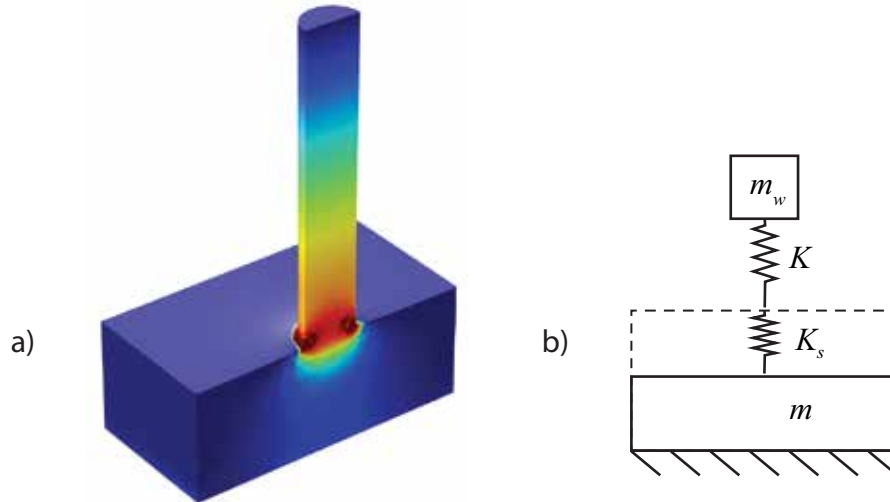


FIGURE 3
 An elastic (nano)wire coupled to a mass m . (a) A three-dimensional, elasticity finite element model (COMSOL) prediction for the stress field in a cross section of the geometry for the fundamental extensional mode. In the simulation, the mass is rigidly supported from below and composed of Si. The stress field extends into the mass and results in compliance of the attachment point. (b) Equivalent lumped parameter representation in which the compliance at the attachment point is replaced by a spring K_s , and the nanowire is itself replaced by a spring and effective mass. Regarding the bottom of the mass to be "fixed" as shown in the figure is done for numerical convenience and is not important; the boundary condition can be regarded as introducing an additional force on the mass.

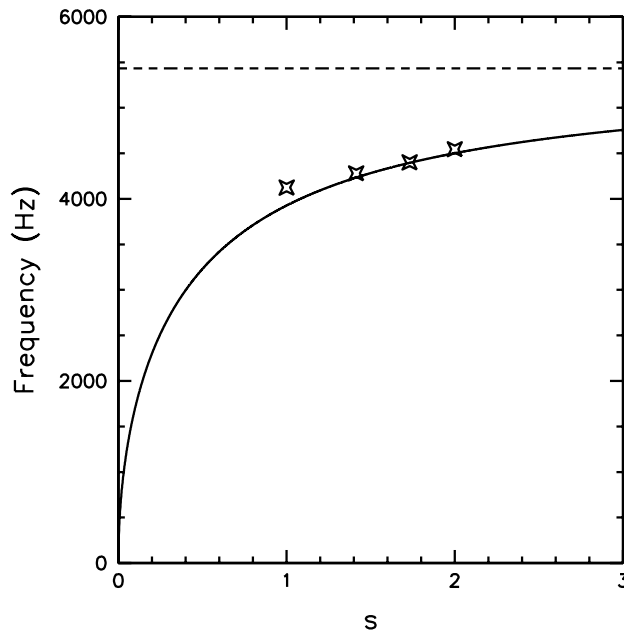


FIGURE 4
 Measured oscillator resonance frequencies vs theory as a function of scale factor s . The stars are the measured resonance frequencies. The solid line is the theoretical prediction of our model, while the dashed line shows the resonance frequency of the spring-mass system without taking the elastic contact stiffness into account.

to relatively low frequencies. Approximate techniques that use lumped parameter models involving spring, mass, plate, and shell elements are widely used in these circumstances. Such models omit the effects of elastic point compliance, while the actual geometry often contains point attached elements. Our results show that the effects of elastic point contact can be included in such simplified models, for example in finite element models, with relatively little effort and cost.

Acknowledgments: The authors acknowledge J.M. Willey for providing support in carrying out the measurements; J.A. Bucaro, N. Lagakos, P. Herdic, and K. Reynolds for providing help in carrying out initial measurements; C. Carter for fabricating the samples; and K. Wahl for measuring the Young's modulus of Cotronics EE-4461 epoxy.

[Sponsored by ONR]



atmospheric science and technology

A person wearing camouflage clothing and a bucket hat is seen from behind, holding a blue and white handheld electronic device. They are standing in a dense, tropical forest with many trees and large green leaves. The scene is brightly lit, suggesting daylight.

134 Geochemical Data Application to Enhance Seismic Interpretation of Deep Sediment Methane Hydrate Deposits

136 Monitoring Maritime Conditions with Unmanned Systems During Trident Warrior 2013

139 Probing the World's Greatest Source of Variability — Madden Julian Oscillation

Geochemical Data Application to Enhance Seismic Interpretation of Deep Sediment Methane Hydrate Deposits

R. Coffin,¹ W. Wood,² and I. Pecher³

¹Chemistry Division

²Marine Geosciences Division

³School of Environment, University of Auckland

Introduction: Deep-water gas hydrates, distributed through the world coastal ocean (Fig. 1), are recognized as a potential energy source, a key component in ocean floor slope stability, and a contributor to ocean and shallow sediment carbon cycling. There is a strong interest in determining the Arctic shallow sediment

profiles from piston cores retrieved across different seismic expressions have shown hydrate instability due to salt diapirs, a total absence of hydrates, and elevated hydrate loadings that did not correspond with seismic images. Future exploration integrating seismic and geochemical data will provide a more thorough understanding of the coastal gas hydrate distribution.

Seismic Surveys: Reflection seismology was developed to analyze the shapes and reflectivities of structures in the sub-seafloor (Fig. 2). Most applications consist of an airgun sound source and an array of hydrophones towed at the sea surface to image the sub-seafloor echoes of the source. Because sound propagation is so strongly affected by gas, flat lying accumulations of gas create strong, easily identifiable reflections in seismic images. NRL has also used its deep towed

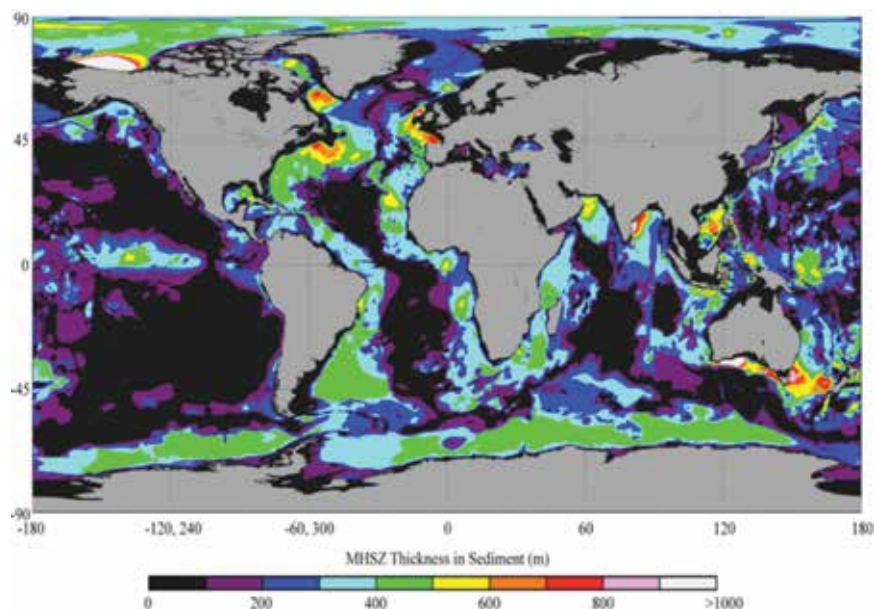


FIGURE 1

Global summary of coastal methane hydrate deposits estimated with a review of the thickness of the methane hydrate stability zone (MHSZ) in seafloor sediments. This estimate is based on water depth, sediment thickness, and geothermal gradients. (Ref. 5)

methane contribution to the atmosphere and climate change. Coastal exploration of hydrates over the past 30 years has focused on seismic data acquisition and interpretation. Where gas hydrates are present, seismic data frequently exhibit a bottom-simulating reflection caused by free gas; above this expression, stable gas hydrate deposits are present. We also observe regions with strong seismic blanking, which suggests either free gas or significant lateral variability and potentially significant vertical fluid and gas migration. Geochemical patterns above deep sediment hydrates have been used at many locations around the world for a more thorough interpretation of seismic data and hydrate locations. Analyses of porewater methane and sulfate

acoustic geophysics system (DTAGS) to image gas hydrates off the U.S. Atlantic Coast, Gulf of Mexico, Chile, Vancouver Island, and Japan.

Geochemical Assessment: Vertical methane (CH_4) fluxes are used to survey potential deep methane hydrate deposits (Fig. 3).^{1,2} The flux is estimated using sulfate (SO_4^{2-}) and CH_4 concentration profiles, where SO_4^{2-} concentrations decrease in the shallow sediment by consumption as the terminal electron acceptor during anaerobic oxidation of methane (AOM).³ In sediments with vertical CH_4 flux, AOM is the dominant pathway for sulfate reduction¹⁻³ and can be described by the following net reaction:

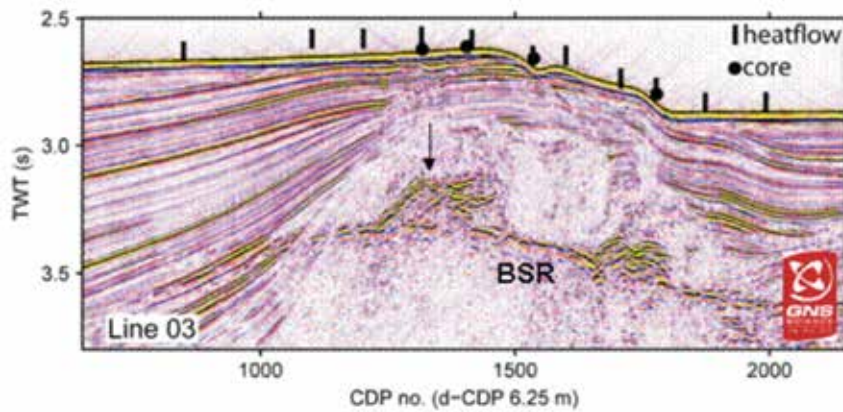


FIGURE 2
Seismic survey to address coring and heat flow focus sites in the assessment of methane hydrate deposits across the Porangahau Ridge, on the Hikurangi Margin, New Zealand. Here a seismic amplitude anomaly is observed (arrow) above bottom-simulating reflection (BSR) marking the base of gas hydrate stability (data courtesy GNS Science). (Ref. 6)

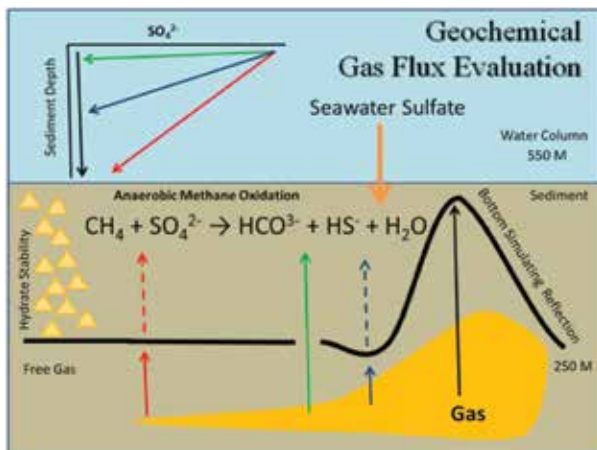
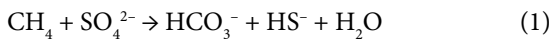


FIGURE 3
Geochemical assessment of deep sediment hydrate deposits based on shallow sediment anaerobic oxidation of methane and reduction of sulfate.



The sedimentary horizon where CH_4 and SO_4^{2-} co-occur and are consumed during AOM is termed the sulfate methane transition (SMT) and the depth of this zone is controlled by the rate of vertical CH_4 diffusion.⁴

Findings: These data collected from distinct locations around the world demonstrate the strength of combining geophysics and geochemistry to survey the presence and distribution of deep sediment methane hydrate deposits. In a recent study off the eastern coast of New Zealand, across the Chatham Rise, seismic data showed shallow and deep blanking patterns that were interpreted to be past and present gas pockets (Fig. 4). Sulfate data are presented as an indication of the vertical methane flux (Eq. (1)); if large, deep methane deposits exist, we expect to measure no sulfate in the sediment deeper than 100 to 400 cm. Vertical sulfate profiles were extremely deep through all of these locations and indicated no current-day vertical methane

flux exists. Data are now being studied to assess methane fluxes 20,000 to 900,000 years ago. Previous studies have provided additional interesting results with the interpretation of seismic and geochemical profiles. Off the mid-Chilean Margin, seismic blanking suggested a strong vertical gas flux down the continental slope while piston cores suggested a moderate gas flux. Further assessment of geochemical data taken along the slope showed a much more intense vertical methane flux up the slope where the seismic blanking was less intense. At Atwater Valley in the Gulf of Mexico, the seismic data showed an elevated bottom-simulating reflection, suggesting a high vertical flux at a mound. In this case, the geochemical data concurred with this interpretation of seismic data; however, including pore-water chloride analyses showed the high methane flux that corresponded to a hydrate instability caused by salt diapirs below the hydrate layers.

Conclusions: Geochemical analyses at methane seeps allow us to constrain not only the amount of gas

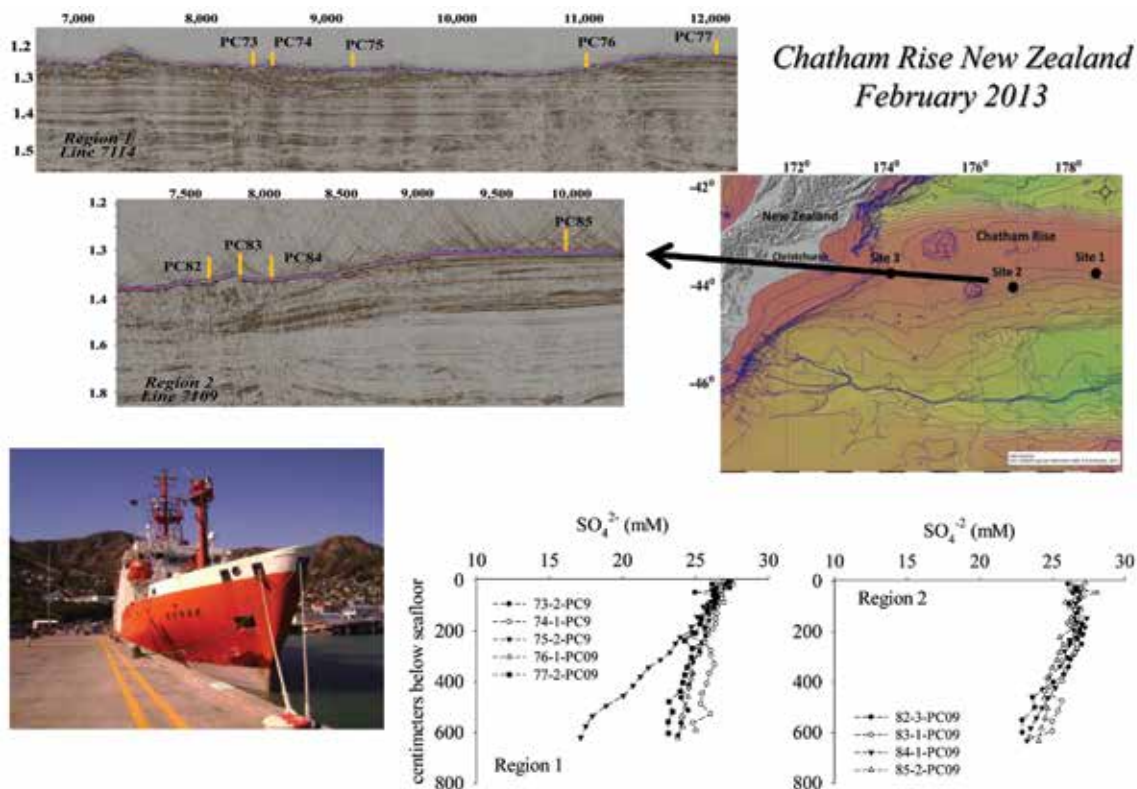


FIGURE 4
A comparison of geophysical and geochemical data from a 2013 expedition aboard the RV *Sonne*, off the coast of New Zealand across the Chatham Rise. Two seismic lines were studied at this location to evaluate the vertical methane flux. Here we present sulfate data related to the spatial variation in sediment methane concentrations. These sulfate profiles show there was no vertical methane flux at any location.

(almost all methane) entering the ocean–atmosphere system, but also in many cases to determine the origin and history of the carbon in that gas. The seismic data allow us to constrain the possible fluid pathways on scales of meters (high-resolution systems like DTAGS) to hundreds of kilometers for larger surface-towed airgun systems. The successful marriage of these two disciplines continues to be an effective means of quantifying the dynamics of gas hydrate in ocean sediments.
[Sponsored by ONR]

References

- ¹R.B. Coffin, L. Hamdan, R. Plummer, J. Smith, J. Gardner, and W.T. Wood, “Analysis of Methane and Sulfate Flux in Methane Charged Sediments from the Mississippi Canyon, Gulf of Mexico,” *Marine Petroleum and Geology* **25**, 977–987 (2008).
- ²R.B. Coffin, L. Hamdan, J.P. Smith, R. Plummer, L. Millholland, and R. Larson, “Spatial Variation in Shallow Sediment Methane Source and Cycling along the Alaskan Beaufort Sea,” *Marine Petroleum and Geology* **45**, 186–197 (2013).
- ³W.S. Borowski, C.K. Paull, and W. Ussler III, “Marine Porewater Sulfate Profiles Indicate In Situ Methane Flux from Underlying Gas Hydrate,” *Geol.* **24**, 655–658 (1996).
- ⁴W.S. Borowski, C.K. Paull, and W. Ussler III, “Global and Local Variations of Interstitial Sulfate Gradients in the Deep-Water, Continental Margin Sediments: Sensitivity to Underlying Methane and Gas Hydrates,” *Mar. Geol.* **159**, 131–154 (1999).

- ⁵W.T. Wood and W.Y. Jung, “Modeling the Extent of the Earth’s Methane Hydrate Cryosphere,” Proceedings of the 6th International Conference on Gas Hydrates (ICGH 2008), Vancouver, British Columbia, Canada, July 6–10, 2008.
- ⁶I.A. Pecher, R. Coffin, S.A. Henrys, and GNS Science (NZ), and CHARMNZ Working Group, *Tangaroa TAN0607 Cruise Report: Gas Hydrate Exploration on the East Coast, North Island, New Zealand*, GNS Science Report 2007/29 (Lower Hutt, NZ, 2007).

Monitoring Maritime Conditions with Unmanned Systems During Trident Warrior 2013

C.N. Barron,¹ S.D. Ladner,¹ A.J. Quaid,¹ L.F. Smedstad,¹ K.P. Grembowicz,² A. Mask,² E.M. Coehlo,³ E.A. Holmberg,³ and G. Peggion³
¹Oceanography Division
²Naval Oceanographic Office
³University of New Orleans

Introduction: Before predicting future conditions in the maritime environment, we must sense what the

ocean is doing now. Humans perceive the environment through our senses; comparable perception is also becoming available in autonomous observing platforms. These can feel the warmth of the ocean, taste its saltiness, and see and hear changes in light and sound. Ocean forecasts are improved through the assimilation of these data; our challenge is efficiently obtaining observations and using them in ways that have the greatest impact. NRL researchers teamed with other Navy and academic institutions to address this challenge under the aegis of July's Trident Warrior 2013 (TW13) exercise off the Virginia shore. TW13 hosted deployments of two types of unmanned ocean observing platforms: undersea ocean gliders (Slocum and Spray models) to see, feel, and taste visibility, temperature, and salinity; and surface wave gliders (Sensor Hosting Autonomous Remote Craft or SHARC model) that emit sounds and listen for reflected changes in response to ocean currents. Experiments tested how to guide, adapt, and use observations from these unmanned underwater (UUV) and surface (USV) vehicles. The observations were supplemented with traditional in situ and satellite measurements for assimilation into real-time forecasts of the maritime environment relevant for antisubmarine and mine warfare (ASW/MIW).

Exercise: Trident Warrior is an annual exercise coordinated by the U.S. Fleet Forces Command that provides an operational Fleet environment to assess the impact of new tactics and technology on warfighter needs. The experiments in TW13 were conducted with the cooperation of several ships and aircraft from various participating Navy and Air Force commands, in

and around the waters east of Virginia and Maryland during July 13 through 18. Researchers from NRL's Oceanography Division joined with contributors from other NRL, Navy, and university groups in an effort coordinated by the Office of Naval Research (ONR) to demonstrate the effectiveness of unmanned observing systems for characterizing the ocean environment within the framework and constraints of a Fleet exercise.

Gliders: Figure 5(a) shows NRL personnel deploying one of the 10 profiling gliders released and recovered from the R/V *Knorr* during the exercise. Data from the two NRL and two Naval Oceanographic Office (NAVOCEANO) gliders were transmitted to Stennis Space Center, processed using the Local Automated Glider Editing Routine (LAGER), and displayed in the NRLSSC real-time display laboratory. Oregon State University controlled and provided data from the six remaining ocean gliders. Four SHARC gliders from UC-San Diego Scripps Institution of Oceanography were also deployed; these provided Acoustic Doppler Current Profiler (ADCP) 3D measurements of the ocean currents as well as measurements of the surface meteorology. Figure 5(b) shows a schematic representation of one wave glider and two ocean gliders superimposed on the real-time forecast of ocean temperature. Glider location tracks (Fig. 6(a)) were updated in real time for the duration of the exercise. In addition to the standard measurements of temperature and salinity, the NRL gliders included bio-optical observation packages with measurements of chlorophyll-a, colored dissolved organic matter (CDOM), beam attenuation coefficient at 660 nm, and backscatter coefficient at 532 nm. Cross

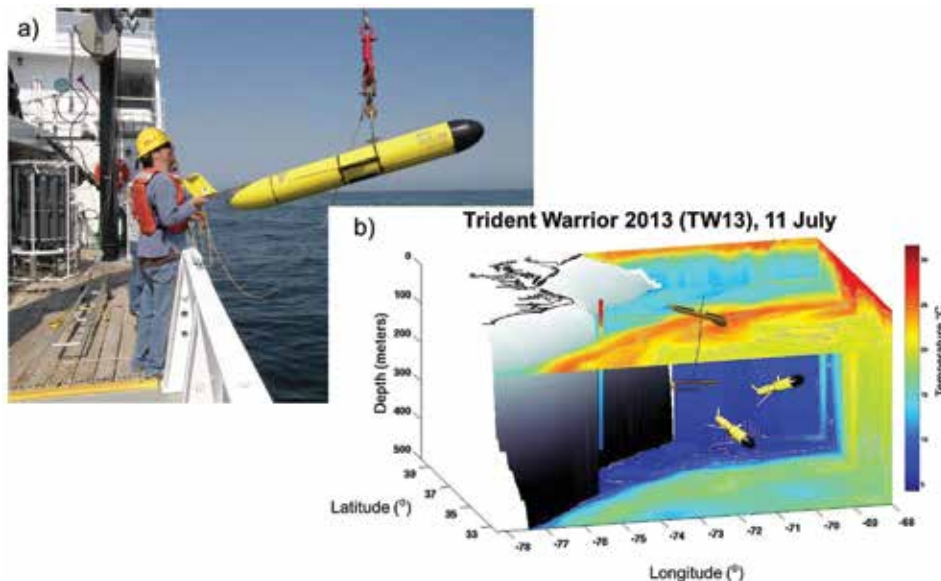


FIGURE 5
 (a) NRL personnel deploy a profiling Slocum ocean glider. (b) Two ocean gliders and one SHARC are superimposed on a 3D TW13 ocean temperature forecast valid at 00:00 UTC 11 July 2013.

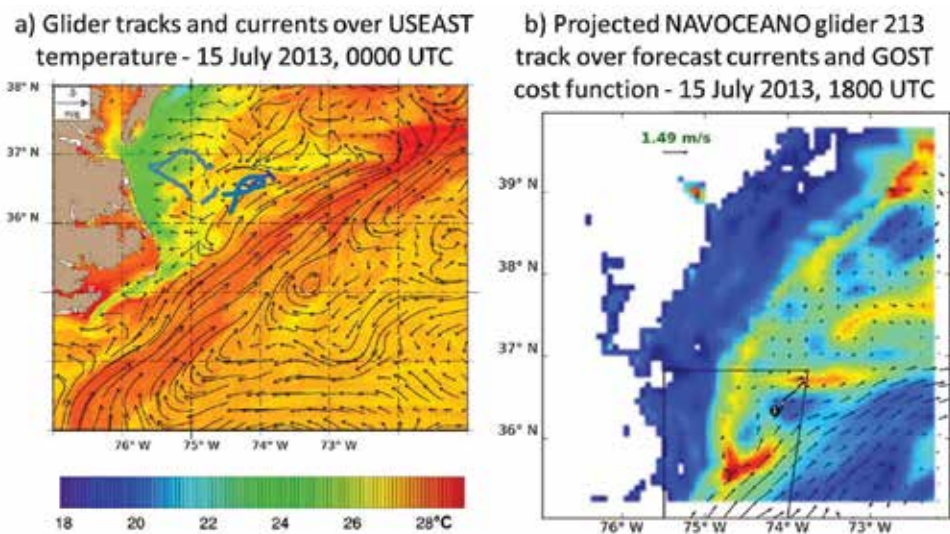


FIGURE 6
 (a) NRL and NAVOCEANO gliders focus on optical properties in the inshore region and temperature and salinity for acoustics in the offshore. (b) GOST projects a path for NAVOCEANO glider that is optimized according to the mission-dependent cost function, identifying high-value samples in red. The polygon informs GOST of the waterspace management mandated for the exercise, restricting the gliders to remain south of the main shipping lanes into Chesapeake Bay.

sections of the data received and processed by NRLSSC were on display in real time along with corresponding satellite data and ocean model outputs and products from the region.

GOST: The Glider Observation Strategies (GOST) system developed by NRL identifies glider paths that are likely to cover times and locations with the most impact on assimilative ocean forecasts in the operational area while avoiding areas restricted by waterspace management or challenging operating conditions.¹ GOST uses the forecasts to identify efficient paths through the shifting currents and targets areas where predictions of sound speed or other conditions are uncertain or changing in ways that influence warfighter decisions. During TW13, GOST ran on NAVOCEANO's operational systems and implemented communication links between the ocean modeling and glider operations groups, using model forecasts to project glider paths anticipated to be best suited for the mission and providing this as guidance for the glider pilots (Fig. 6(b)). A new GOST rendezvous option was demonstrated, identifying glider trajectories that maintain high observation value while enabling timely recovery by the R/V *Knorr*.

Optical Forecasts: Additionally, some of the optical and physical ocean data from the gliders are combined with satellite-derived surface optical properties (Fig. 7) and physical models to tune coefficients in a 3D optical model.² The Tactical Ocean Data System

(TODS) 3D Optical Generator (3DOG) provides optical parameters in a 3D volume at 1 km grid spacing. These data are combined with ocean current forecasts to feed BioCast, a system to solve for the three-dimensional advection-diffusion-reaction of dissolved or

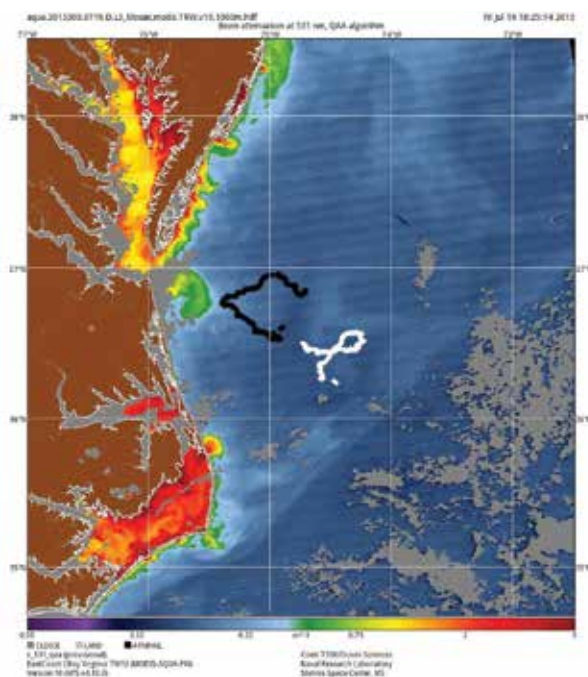


FIGURE 7
 Trajectories of NRL's gliders superimposed on a satellite image processed to estimate beam attenuation at 531 nm. The satellite and glider data are combined in TODS to predict 3D optical parameters and are forecast using RELO-NCOM.

particulate tracers in aquatic environments and forecast changing optical properties out to 24 hours.

Acknowledgments: Our work in Trident Warrior 2013 was made possible through the support of the Office of Naval Research (ONR) and its efforts to leverage this exercise to test a wide range of technologies being developed to support Navy and Air Force operations. The authors acknowledge Kipp Shearman of Oregon State University and the many other scientists and crew aboard the R/V *Knorr* and at participating activities around the country for their valuable contributions to the success of this exercise. Particular thanks at NRL are extended to Jan Dastugue, Courtney Kearney, Pete Spence, and David Sitton for work on data processing and visualization.

[Sponsored by ONR]

References

- ¹L.F. Smedstad, K.D. Heaney, G. Peggion, C.N. Barron, and E. Coelho, "Validation Test Report for a Genetic Algorithm in the Glider Observation Strategies (GOST 1.0) Project: Sensitivity Studies," NRL/MR/7320--12-9361, Naval Research Laboratory, Stennis Space Center, MS (2012).
- ²S.D. Ladner, R. Arnone, J. Jolliff, B. Casey, and K. Matulewski, "Forecasting the Ocean Optical Environment in Support of Navy Mine Warfare Operations," *Proceedings of SPIE* **8372**, 83720Z-1, doi: 10.1117/12.920784 (2012).
- ³C.N. Barron, A.B. Kara, P.J. Martin, R.C. Rhodes, and L.F. Smedstad, "Formulation, Implementation and Examination of Vertical Coordinate Choices in the Global Navy Coastal Ocean Model (NCOM)," *Ocean Modelling* **11**(3-4), 347-375, doi:10.1016/j.ocemod.2005.01.004 (2006).

Probing the World's Greatest Source of Variability — Madden Julian Oscillation

M. Flatau,¹ S. Chen,¹ T. Jensen,² T. Shinoda,² J. Cummings,² and P. May³

¹*Marine Meteorology Division*

²*Oceanography Division*

³*Computer Sciences Corporation, Monterey, CA*

Introduction: The Madden-Julian Oscillation (MJO), named after Roland Madden and Paul Julian, who first described this phenomenon, is a primary mode of atmosphere/ocean variability. The MJO consists of a large, planetary-scale convective anomaly propagating eastward along the Equator over the Indo Pacific warm pool with a phase speed of about 5 to 8 m/s. It influences the atmosphere and ocean on various temporal and spatial scales — from tropical cyclones through monsoons and El Niño in the tropics, to mid-

latitude, and even polar, atmosphere, and ocean circulation patterns. The effects of this tropical phenomenon can be observed as far away as ocean current anomalies in the Drake Passage.

MJO behavior depends on multiscale interactions between the global circulation and local convective patterns, as well as feedback between the atmosphere and the ocean. The MJO "cycle" consists of the dry (suppressed) phase, in which clear skies and large insolation allow for heating of the upper ocean and energy is accumulated in the atmosphere/ocean system, and the active phase, in which the energy is released in the form of atmospheric convection (precipitation). A synthesis of the MJO based on model simulations, field measurements, and a conceptual model is shown in Fig. 8(a-d).

MJO Forecast: From the forecasting point of view, the MJO represents a link between the weather and climate. Its relatively long time scale forms a base for extended weather prediction and, therefore, understanding of the MJO became a Holy Grail for the forecasting community. However, in spite of its importance, the MJO presents a formidable forecasting challenge, mostly because of its multiscale nature. The MJO system includes eastward and westward moving tropical disturbances with various spatial and temporal scales that interact with the large-scale "MJO envelope"; the air-sea interaction creates another level of complexity.

An interdisciplinary NRL team participated in an international effort, called Cooperative Indian Ocean Experiment on Intraseasonal Variability (CINDY) / Dynamics of Madden-Julian Oscillation (DYNAMO), directed toward understanding MJO dynamics, with the focus on MJO initiation in the Indian Ocean that appears to be especially difficult to predict. During the CINDY/DYNAMO field campaign (October to December 2011), three MJO episodes were observed, providing a wealth of data for MJO investigation. In this campaign, the NRL air-sea-ocean-wave Coupled Ocean-Atmosphere Mesoscale Prediction System (COAMPS) model was used, the first fully coupled high-resolution model run in real time. The model consists of the atmospheric regional model, ocean model Navy Coastal Ocean Model (NCOM), and wave model Simulating WAVes Nearshore (SWAN) with the boundary forcing provided by Navy global models and data assimilation in the atmosphere and in the ocean. The model nested grid setup used for the DYNAMO forecasts, with the cloud resolving nest centered on the DYNAMO observational array, reflected the multiscale nature of the MJO. With this model, combined with the atmospheric and ocean observations collected during the field program, we analyzed the transitions from the suppressed stage to the active stage of the

MJO. Our research was focused on the air–sea interaction between the atmospheric convectively coupled waves and the development of the temperature, surface current, and salinity anomalies in the upper ocean.

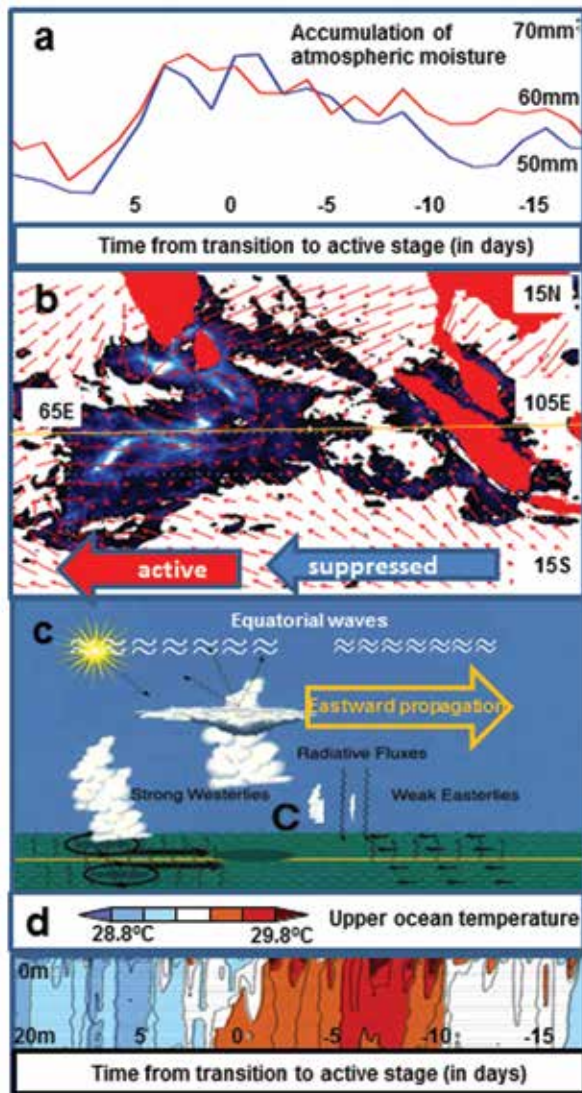


FIGURE 8
The synthesis of MJO transition from convectively suppressed to active phase based on DYNAMO observations, COAMPS simulations, and conceptual model. Spatial patterns from the model and point observations from DYNAMO instruments are combined. (a) The buildup of atmospheric moisture in the suppressed phase and the release during the active phase at 80E 0N, as observed in DYNAMO atmospheric soundings (courtesy of R. Johnson and P. Ciesielski) and COAMPS simulation adapted from Ref. 3. (b) The surface winds and precipitation from the COAMPS 11/23/2011 forecast of MJO. The area with strong winds and precipitation corresponds to the active phase, while the area to the east of the moving convection represents the suppressed phase. (c) The conceptual model of air-sea interaction in MJO adapted from Ref. 4. (d) The time series of the ocean temperature in the upper 20 m of the ocean, measured by the Sea-Glider near 80E 2N (courtesy of A. Matthews and D. Baranowski). The high temperatures and large diurnal cycle develop during the suppressed MJO phase.

Multiscale Air–Sea Interaction: Our research addressed the multiscale nature of the MJO, from equatorial waves in the atmosphere and the ocean to local air–sea interaction. Using satellite observation, we have shown the remote effects of the wind anomalies associated with MJOs observed during DYNAMO.¹ Satellite-derived precipitation patterns indicated also that atmospheric equatorial waves play a role in MJO initiation (Fig. 9). The role of atmospheric disturbances and their interaction with the ocean surface was further studied using COAMPS simulations that focused on the transition between the suppressed and active MJO phases.^{2,3} Our model experiments indicate that during the MJO suppressed phase, equatorial waves and air–sea interaction are essential for the moisture buildup in the atmosphere shown in Fig. 8(a), preconditioning the atmosphere for the deep convection ahead of the active phase of MJO (Fig. 8(b)). The warm diurnal layer that develops in the upper ocean on clear days (Fig. 8(d)) appears to be particularly important for air-sea interaction, especially on short time scales.

The equatorial disturbances play an important role in the MJO active phase as well. We have shown that the interaction between the eastward and westward propagating waves (Fig. 8(c)) leads to rapid development of the deep convection observed during the MJO active phase. The enhanced equatorial winds in the active phase shown in Fig. 8(b) are the result of such interactions. COAMPS simulations indicate that air/sea interactions play a role at this stage of the MJO by strengthening the equatorial waves.

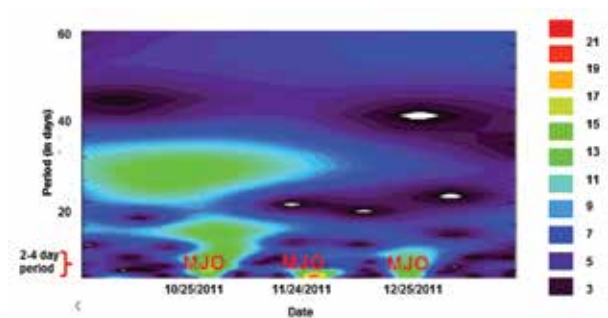


FIGURE 9
Multiscale character of MJO as shown by wavelet analysis of eastward propagating precipitation disturbances with small zonal scales (zonal wave numbers 9–40, corresponding to zonal wavelengths below 4000 km). The dominant period of large-scale (zonal numbers 1–8) perturbations was 30 days, corresponding to frequency of MJO episodes. However, each MJO initiation was accompanied by a burst of short, high-frequency perturbations with 2–4 day period. The precipitation data are obtained from NASA TRMM analysis.

Summary: Our research indicates that even though the MJO is mainly an atmospheric phenomenon, the interaction with the ocean surface plays an

important role in its evolution and it is critical for skillful forecasts. On the shorter time scales (1 to 2 weeks), local interactions with the upper ocean appear critical, demanding high vertical resolution near the ocean surface in the ocean model. On the longer time scales, the remote response of the ocean to atmospheric anomalies requires that the ocean dynamics are properly resolved. In the atmosphere, MJO forecasts depend on the simulation of the equatorially coupled convective waves and their interactions.

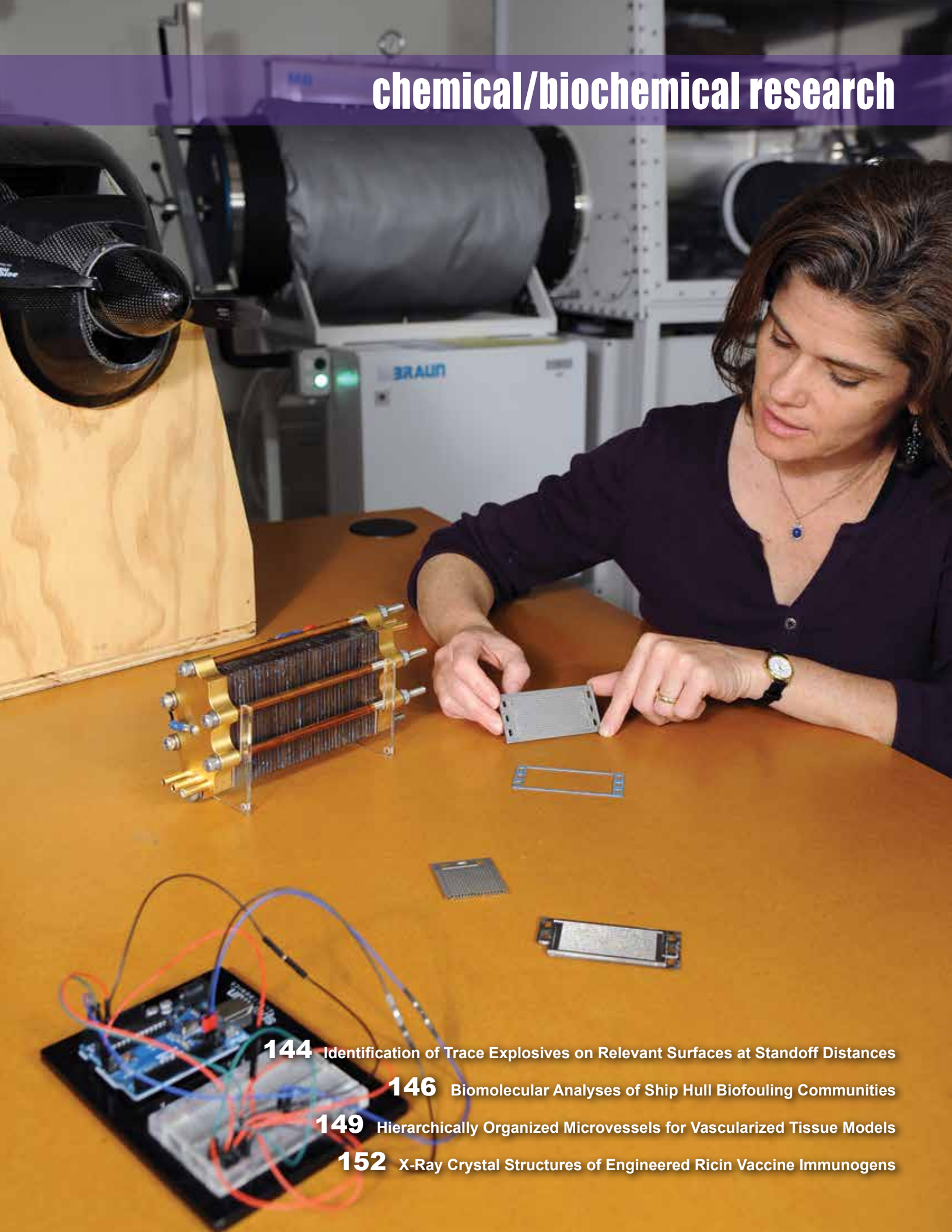
[Sponsored by ONR]

References

- ¹ T. Shinoda, T. Jensen, M. Flatau, S. Chen, W. Han, and C. Wan, "Large-Scale Oceanic Variability Associated with the Madden-Julian Oscillation during the CINDY/DYNAMO Field Campaign from Satellite Observations," *Remote Sensing* **6**, 2072–2092 (2013).
- ² T. Shinoda, T.G. Jensen, M. Flatau, and S. Chen, "Surface Wind and Upper-Ocean Variability Associated with the Madden-Julian Oscillation Simulated by the Coupled Ocean-Atmosphere Mesoscale Prediction System (COAMPS)," *Mon. Wea. Rev.* **141**, 2290–2307 (2013).
- ³ S. Chen, M. Flatau, T.G. Jensen, T. Shinoda, J. Cummings, J. Schmidt, P. May, M. Liu, P.E. Ciesielski, C.W. Fairall, R.-C. Lien, D.B. Baranowski, N.-H. Chi, S. de Szoeke, and J. Edson, "A Study of CINDY/DYNAMO MJO Suppressed Phase," *J. Atmos. Sci.*, in review (2014).
- ⁴ M. Flatau, P.J. Flatau, P. Phoebus, and P.P. Niiler, "The Feedback between Equatorial Convection and Local Radiative and Evaporative Processes: The Implications for Intraseasonal Oscillations," *J. Atmos. Sci.* **54**, 2373–2386 (1997).



chemical/biochemical research



144 Identification of Trace Explosives on Relevant Surfaces at Standoff Distances

146 Biomolecular Analyses of Ship Hull Biofouling Communities

149 Hierarchically Organized Microvessels for Vascularized Tissue Models

152 X-Ray Crystal Structures of Engineered Ricin Vaccine Immunogens

Identification of Trace Explosives on Relevant Surfaces at Standoff Distances

C. Kendziora, R. Furstenberg, V. Nguyen, M. Papantonakis, J. Byers, and R.A. McGill
Materials Science and Technology Division

Toward the critically important DoD goal of detection of trace explosives at standoff, selectivity is almost as important as sensitivity. The need for high sensitivity is evident due to the very small amount (micrograms) of explosives that can be left behind on surfaces, for instance in a fingerprint. However, selectivity (the ability to distinguish the explosives analyte of interest from the substrate or from other surface bound chemicals) is just as important because the vast majority of relevant surfaces will not contain threats. False positive alarms (indicating the presence of a threat when one does not exist) can be highly disruptive. To demonstrate both sensitivity and selectivity for our standoff photothermal infrared method, we use carefully prepared and characterized trace level residues of explosives or related materials (TNT, RDX, ammonium nitrate, and sugar) on relevant substrates (painted car panels, glass, steel, and polyethylene).

Photothermal infrared imaging spectroscopy (PT-IRIS) measurements were performed by illuminating the samples (or analytes) with a range of wavelengths (both on and off absorption resonances characteristic of different materials) while imaging the samples with an infrared camera. Figure 1 is a schematic illustration of the PT-IRIS configuration. By comparing the

pixel-by-pixel results from “known” samples and bare substrates, we were able to identify the different analytes on relevant surfaces at standoff distances featuring trace level surface loadings.

As part of an ongoing effort toward eye-safe standoff detection of trace explosives, we have developed the PT-IRIS approach with increasingly portable instrumentation. To date, four U.S. patents relating to this technology development have been issued.¹ Testing the methods and instrumentation on relevant samples is a crucial step toward demonstrating the utility of the technique. Precisely for this purpose, we use carefully prepared sample coupons with each of four types of analytes (TNT, RDX, ammonium nitrate, and sugar) deposited on each of four types of substrates (painted car panel, glass, steel and polyethylene). Two trace mass loadings (nearly invisible) of $\sim 10 \mu\text{g}/\text{cm}^2$ and $\sim 100 \mu\text{g}/\text{cm}^2$ were used. Figure 2 shows the four substrate types, each with $\sim 100 \mu\text{g}/\text{cm}^2$ of RDX deposited in a circular area near the coupon center. For the purpose of building a representative analytical “library,” we also examined the “blank” substrates and the “pure” analytes separately. Combining all of these test elements, the measured sample matrix consisted of 40 fully characterized sample coupons.²

The signature infrared absorption spectra derived from intrinsic molecular properties provides the spectroscopic basis for chemical identification by PT-IRIS. Some infrared wavelengths are highly absorbed by the analytes of interest, while others (even with very similar wavelengths) are not. However, rather than presume which experimental parameters (such as infrared laser wavelength) would provide the best sensitivity or selec-

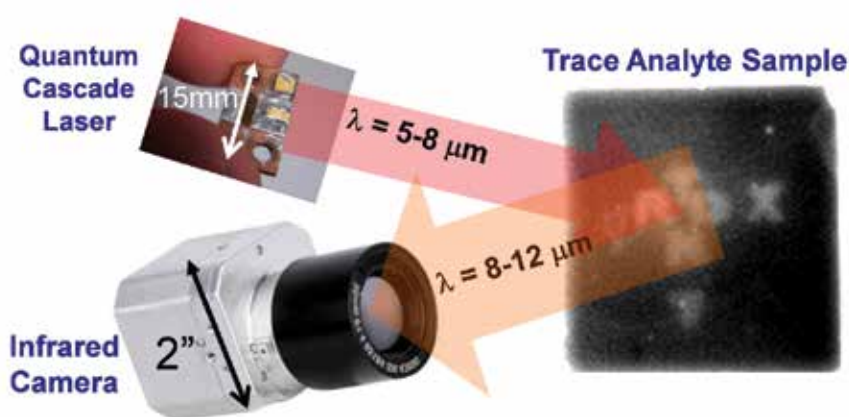


FIGURE 1

Schematic of PT-IRIS. In the photothermal infrared imaging spectroscopy (PT-IRIS) technique, an infrared quantum cascade laser (QCL) is tuned through a series of wavelengths in the 5 to 8 μm range. This beam is directed toward a sample surface that is potentially contaminated with trace explosives or other analyte. Certain wavelengths are selectively absorbed in the analyte, causing the analyte particles to heat slightly. This heating is observed using an infrared camera sensitive to the wavelength range from 8 to 12 μm . The figure elements are not shown to scale. During testing, the sample can be up to 10 m or more from the QCL and camera.

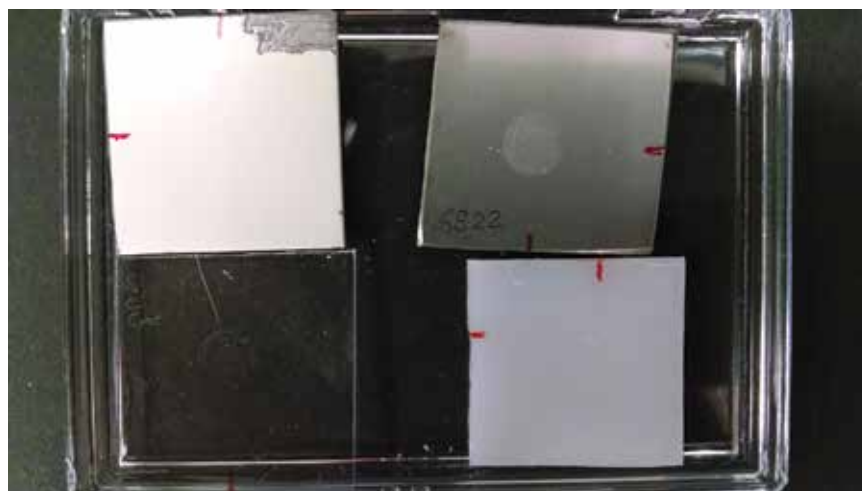


FIGURE 2
 Photograph of sample coupons (each 1 in. [2.54 cm] square) of the four substrate types: white car panel (upper left), steel (upper right), glass (lower left), and polyethylene (lower right). The samples are in a clear case on a black background. Each panel has RDX deposited at a mass loading of $\sim 100 \mu\text{g}/\text{cm}^2$ in a circular area near the coupon center.

tivity, we decided to measure an extensive number of these “features” and implement an analytical algorithm on the complete data set. This allowed us to empirically measure the most important discrimination factors with the goal of optimizing future systems and methods to reduce the overall redundancy and complexity. Spectroscopically, we selected 75 laser wavelengths between 5.8 and 7.75 μm that could propagate over several meters to the targets without attenuation due to water vapor bands in the air. Also, each laser sequence was repeated while the target was imaged using each of four long-wave IR camera filters to provide additional chemical selectivity. This permutation resulted in a total of 300 spectral “features” for subsequent analysis.²

Once the PT-IRIS signal from each of the 40 samples was measured for each of the 300 spectral features, the resulting “feature vector matrix” was analyzed for patterns that could identify specific analytes independent of the substrate they were on.² This is important from a practical point of view since, in the field, stand-off analyte detection must be made on an arbitrary substrate. One challenge was that the number of features (rows) exceeded the number of samples (columns), leaving the matrix mathematically “underdetermined.” Alternatively, we exploited the imaging nature of our method to extract the signal from 197 individual pixels (within a 17×17 pixel circle) corresponding to the laser illuminated sample area. By considering each pixel as a unique “sample,” we could expand the width (number of columns) of the feature vector matrix and avoid underdetermination. For classification, we selected the “Boost” algorithm, which assigns numerical scores to the degree of match between a set of (known) “train-

ing” samples and a (unknown) “testing” sample. We randomly selected roughly half of the pixels for “training” and reserved the other half for “testing.” Positive (> 0) scores indicate an increasingly good match, while negative scores indicate an increasingly poor match.

Figure 3 illustrates an example result of the Boost classification for the $100 \mu\text{g}/\text{cm}^2$ mass-loaded samples of each analyte on a white painted car panel substrate. In the figure, the pixel-by-pixel classification scores from the same five sample coupons are shown in each row. Light-shaded pixels represent positive Boost scores, indicating likely detection. Dark-shaded pixels represent negative Boost scores, indicating the likely absence of that specific analyte on that specific pixel of that sample coupon. Pixels shaded with the neutral gray (defined as zero score) were set aside for use as the “training data” and therefore excluded from the “testing.” Across the top row, the different samples are scored using the “TNT” classifier. As desired, the TNT sample (second column) has mostly light-colored pixels, indicating that TNT is detected. Some variation in the intensity is expected given the inherent inhomogeneity of analyte coverage. Conversely, the other samples are mostly colored dark, indicating that no TNT is found. It is interesting that the sample with RDX (middle column) has some lighter colored pixels, indicating that there is some “overlap” in the classifier for RDX and TNT. This is not surprising given that the two materials have somewhat similar IR spectra in the range of wavelengths used. Across the second, third, and fourth rows, the PT-IRIS data from the same samples are scored using the RDX, ammonium nitrate and sucrose classifiers, respectively. As expected, these

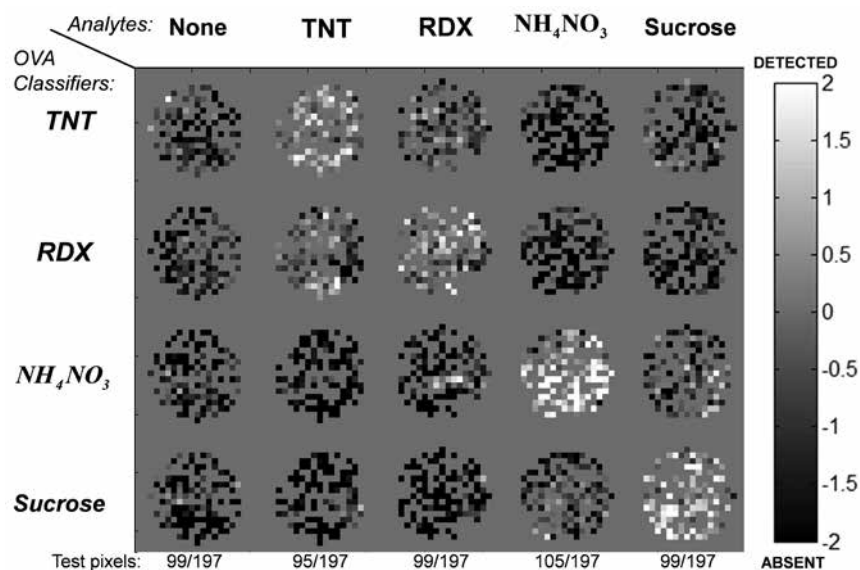


FIGURE 3
Results of the analyte classification tests on white painted car panels. Trace levels of TNT, RDX, ammonium nitrate (NH_4NO_3), and sugar (sucrose) on white painted steel panels were examined using PT-IRIS in a circular area comprised of 197 pixels. Half of the pixels (same gray as background) were used for “training” and the other half for testing. Light-shaded pixels indicate detection, while dark pixels indicate the absence of that particular analyte. As expected, the TNT classifier (top row) detected TNT (indicated by white pixels) predominantly on the sample where TNT was present (second column). Similar results were found for the RDX, NH_4NO_3 , and sucrose classifiers (rows 2, 3, and 4). Not surprisingly, there was some cross identification between TNT and RDX due to their similar IR spectra.

classifiers generally yield high scores for the sample with that specific analyte and low scores for the other sample coupons.

Overall, the results of the Boost classification algorithm provide high confidence in the selectivity of our PT-IRIS technology at trace levels, with high detection rates and low false alarm rates. While not shown here, the results on the glass, steel, and polyethylene substrates are very similar. It is worth reinforcing that these results were generated on a pixel-by-pixel basis using eye-safe IR lasers under a standoff configuration on trace level sample coupons with relevant substrates. This is a critical step toward the development of standoff detection of trace explosives. This work is ongoing at NRL with the long-term goal of providing a new paradigm in standoff detection and protection for the warfighter and Homeland Security communities.

[Sponsored by Army CERDEC]

References

- R.A. McGill, C. Kendziora, R. Furstenberg, M. Papantonakis, J.S. Horwitz, and G.K. Hubler, “Detection of Chemicals with Infrared Light,” Patent Nos. US8101915, US8222604 (2012), and US8421018, US8421017 (2013).
- C.A. Kendziora, R. Furstenberg, M. Papantonakis, V. Nguyen, J. Borchert, J. Byers, and R.A. McGill, “Infrared Photothermal Imaging of Trace Explosives on Relevant Substrates,” *Proc. SPIE* **8709**, 87090O-1 (2013). ◆

Biomolecular Analyses of Ship Hull Biofouling Communities

D.H. Leary,¹ W.J. Hervey IV,¹ L.J. Hamdan,²
N. Lebedev,¹ Z. Wang,¹ J.R. Deschamps,¹ R.W. Li,³
A.W. Kusterbeck,¹ and G.J. Vora¹

¹Center for Bio/Molecular Science and Engineering

²Chemistry Division

³U.S. Department of Agriculture

Introduction: The overall cost associated with biofouling on the hulls of *Arleigh Burke*-class destroyers is estimated to be \$56M per year.¹ Despite this fact and the decades of research that have focused on understanding the formation of marine biofouling communities, relatively little is known about the soft fouling consortia that are responsible for their formation and function. This gap in our understanding is due in large part to the current inability to cultivate the vast majority of marine microbes in the laboratory. However, a new suite of innovative and culture-independent molecular techniques that includes high-throughput DNA sequencing to determine all environmental genetic material (metagenomics) and mass spectrometry-based analysis of the protein components (metaproteomics)

now allows us to circumvent this obstacle and offers a unique opportunity to deconvolute the inherent complexity of these physically associated multispecies communities. Using these high-throughput analysis tools, a multidisciplinary team of NRL scientists has completed the first comparative characterization of environmental ship hull biofouling communities at the biomolecular level.

Sample Collection: Multiple biofouling samples with a Fouling Rating 20 (i.e., “advanced slime,” Naval Ships’ Technical Manual Chapter 081, 2006) were scraped from the starboard, midship hull air-water interface of two *Arleigh Burke*-class destroyers [USS *Laboon* (DDG 58) and USS *Bainbridge* (DDG 96)] at Norfolk Naval Station, Norfolk, Virginia (Fig. 4(a) and (b)). Both hulls were sampled after a seven-month deployment (January through July 2010). While both deployments started and concluded in Norfolk, USS *Laboon* traveled to ports in the North and Baltic Seas, whereas USS *Bainbridge* traveled to Rota, Spain. Each

biofouling sample was collected at a distance of ~1 m from the previous sample and immediately snap frozen. Surface water samples (1 L from 0.1 m depth) were also collected at a distance of ~5 m from the hulls and all planktonic material was captured on 0.22 μm filters and snap frozen.

Analyses: We used PhyloChip 16S rDNA microbial profiling, metagenomic DNA sequencing, qualitative and quantitative nano-flow liquid chromatography–tandem mass spectrometry (LC-MS/MS) metaproteomic analyses, elemental analyses, and fluorescence spectroscopy to begin to determine the composition and function of ship hull air-water interface marine biofouling communities formed in different environments (Fig. 4(c)). High-throughput metagenomic DNA sequencing from both communities generated a total of 49,426,099 and 33,516,399 raw sequence reads that were assembled into contiguous sequences. Analyses of the relative read abundance demonstrated that both biofouling communities were dominated by bacte-

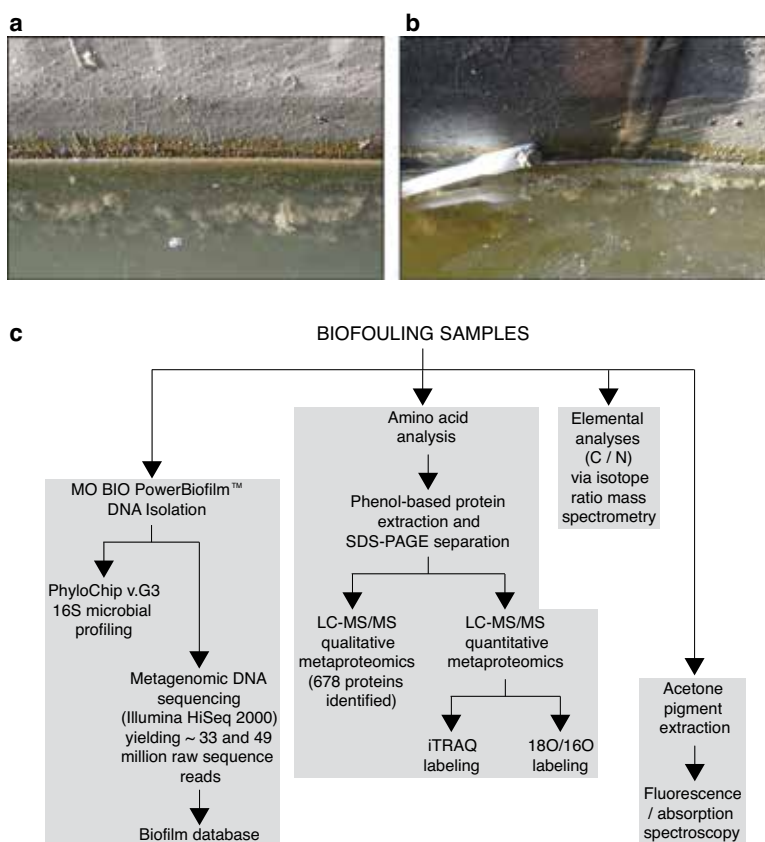


FIGURE 4 Several grams of marine biofouling samples were harvested from the hulls of USS *Laboon* and (a) USS *Bainbridge* at Norfolk Naval Station in Norfolk, Virginia. (b) Samples with a Fouling Rating 20 (i.e., “advanced slime,” Naval Ships’ Technical Manual Chapter 081, 2006) were scraped from the air-water interface (starboard, midship) and immediately snap frozen. (c) Individual biofouling samples were utilized for PhyloChip Array 16S microbial profiling, and pooled samples (all samples collected from the same hull, midship) were utilized for every other aspect of the study.

ria (Table 1), with the majority of reads belonging to members of the Proteobacteria (specifically Alphaproteobacteria and Gammaproteobacteria). Significant compositional differences were observed between the two communities on the phylum (e.g., Cyanobacteria), class (e.g., Flavobacteria), and genus (e.g., *Erythro-bacter*) levels. Although the eukaryota were relatively minor constituents of the metagenomes (Table 1), marked compositional differences were also observed between the two ships. At the phylum level, 65.94% of the eukaryotic sequences from the USS *Bainbridge* were associated with the microscopic Bacillariophyta (i.e., diatoms, 4 times the number found on the USS *Laboon*). In contrast, the USS *Laboon* had a far greater number of sequences from macroscopic eukaryotic phyla (e.g., Cnidaria, Chordata, and Arthropoda).

community was enriched for proteins involved in all aspects of photosynthesis, carbon fixation, membrane transport, photorespiration, and electron transport. Proteins generally associated with housekeeping functions (e.g., ATP-binding, GTP-binding, ribosomes, and translation) and the plasma membrane were detected at comparable levels in both biofouling communities.

Conclusions: Unlike biofouling communities from relatively stable marine environments, communities that are formed on ship hulls are more likely to be highly complex and dynamic as they are not only subject to strong physical selection pressures (e.g., insolation, oxidative stress, predation, and shearing) but also accumulate and potentially interchange members from the surrounding environment during transit and over

TABLE 1 — Biofouling Community DNA Sequencing Read Classification Summary

Domain	USS <i>Laboon</i> reads		USS <i>Bainbridge</i> reads	
	Abundance	%	Abundance	%
Bacteria	12,414,111	93.48	9,739,391	91.87
Eukaryota	826,897	6.23	835,647	7.88
Archaea	23,334	0.18	17,916	0.17
viruses	8,529	0.06	2,413	0.02
unclassified	7,209	0.05	5,380	0.05
other sequences	548	0.00	450	0.00
total	13,280,628	100	10,601,197	100

MG-RAST classifications determined using the "lowest common ancestor" method.

Based on the dominance of bacterial DNA sequences in both metagenomes, we expected the majority of identified proteins in the matched metaproteomes to also be of bacterial origin. Instead, the LC-MS/MS metaproteomic findings (generated using methods specifically designed for the interrogation of marine biofilms²) contrasted with the metagenomic findings in that the majority of identified and annotated proteins were of eukaryotic origin (Fig. 5(a) and (b)). At the organismal level, the greatest number of unique proteins from the USS *Laboon* belonged to macroscopic eukaryotes such as *Hydra* and *Nematostella*. On the USS *Bainbridge*, most of the unique proteins belonged to photosynthetic marine diatoms (fouling microalgae) such as *Phaeodactylum tricorutum*, *Thalassiosira pseudonana*, and *Odontella sinensis*. Further partitioning into biological processes revealed that the metaproteome from the USS *Laboon* demonstrated an enrichment of proteins involved in cell adhesion, DNA binding, calcium binding, and eukaryotic cytoplasmic components and structures, while the USS *Bainbridge*

time. Despite being harvested from identical substrates, the communities sampled from the USS *Laboon* and USS *Bainbridge* demonstrated significant qualitative and quantitative differences in their organismal and biomolecular properties, thus highlighting the role different geographic environments play in determining the composition and function of biofouling communities. By using such a large-scale and relatively unbiased approach,³ we have established a baseline understanding of the microfouling and macrofouling species that constitute marine biofouling communities and, in turn, have generated first-in-kind data that may inform environment-specific antifouling coatings development. Similar analyses are now under way on biofouling communities sampled from the hulls of USS *Arleigh Burke* (DDG 51), USS *Elrod* (FFG 55), and USS *Nicholas* (FFG 47).

Acknowledgments: The LC-MS/MS equipment for high-throughput peptide and protein analyses was purchased through the Capital Procurement Program

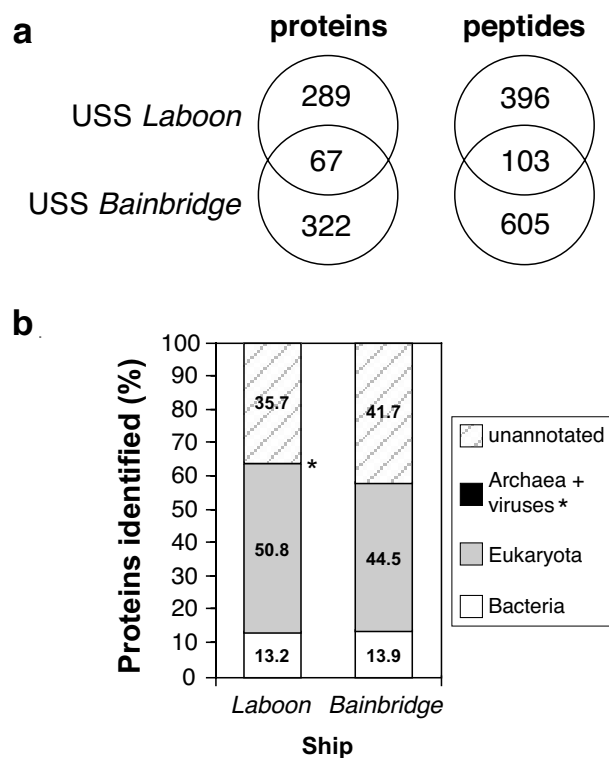


FIGURE 5
 (a) Venn diagrams depicting the total number of proteins and peptides identified from both biofouling metaproteomes. (b) Superkingdom-level classification of all identified proteins from both biofouling metaproteomes. Percent of Archaea/virus proteins identified (asterisk).

of the Naval Research Laboratory. We also acknowledge DDG CLASS Advocate Brian D. McClain for coordinating the sampling efforts and the Executive Officers of USS *Laboon* and USS *Bainbridge* for their cooperation and assistance.

[Sponsored by the NRL Base Program (CNR funded)]

References

- ¹ M.P. Schultz, J.A. Bendick, E.R. Holm, and W.M. Hertel, "Economic Impact of Biofouling on a Naval Surface Ship," *Biofouling* 27(1), 87–98 (2011).
- ² D.H. Leary, W.J. Hervey 4th, R.W. Li, J.R. Deschamps, A.W. Kusterbeck, and G.J. Vora, "Method Development for Metaproteomic Analyses of Marine Biofilms," *Anal. Chem.* 84(9), 4006–4013 (2012).
- ³ D.H. Leary, W.J. Hervey 4th, J.R. Deschamps, A.W. Kusterbeck, and G.J. Vora, "Which Metaproteome? The Impact of Protein Extraction Bias on Metaproteomic Analyses," *Mol. Cell. Probes* 27(5-6), 193–199 (2013).

Hierarchically Organized Microvessels for Vascularized Tissue Models

M.A. Daniele,¹ S.H. North,² and A.A. Adams²

¹National Research Council Postdoctoral Fellow

²Center for Bio/Molecular Science and Engineering

Introduction: Comprehensive models of bioagent infection and pathogenesis will rely upon engineered tissue constructs that mimic cardiopulmonary behavior. To date, in vitro tissue and organ system models rely upon planar co-culture of various cell types without the requisite ability to accurately simulate blood flow with vascular constructs. The ability to generate microvessels from biocompatible polymers and biochemical hybrids provides a key resource for the improvement of these in vitro tissue models as well as the understanding of vascular cell–cell and cell–material interactions. To these ends, we synthesized and characterized a tissue scaffold that could be rapidly polymerized while harboring the desired cell type, and we then employed a microfluidic method for the production of microscale fibers and tubes from the macromer/cell solutions.

Fabrication of Multiaxial Microvessels: By inducing spatial control of material with cellular components by hydrodynamic focusing, the macromer precursor fluids can be arranged into complex patterns at the microscale.^{1,2} Hydrogel microvessels were generated by the photopolymerization of macromer solutions introduced into a microfluidic device and shaped by 3D hydrodynamic focusing. Figure 6(a) illustrates the design and operating mechanism of the hydrodynamic shaping microchannel for producing microvessels. The basic unit of the microfabrication device consists of three inlet channels, converging on a central channel and one shaping region. The inlet channels are used to flow reagents that will form the concentric layers of the microflow. The central microchannel then leads to the modular focusing region. The focusing region of the microchannel is patterned with chevron-shaped grooves in the top and bottom channel walls. Additional inlets and shaping regions can be directly appended onto the outlet of the microchannel to produce nested layers of fluid flow, e.g., a hollow or two-layer coaxial microfiber would require two shaping regions and a tetra-axial microfiber would require four shaping regions. In Fig. 6(b), an exemplary micrograph of a sectioned hollow microvessel is shown to illustrate the uniformity of structure. This microfluidic design uses hydrodynamic shaping to generate laminar flow in which a macromer solution and template fluid are directed into concentric flow regimes. To design the

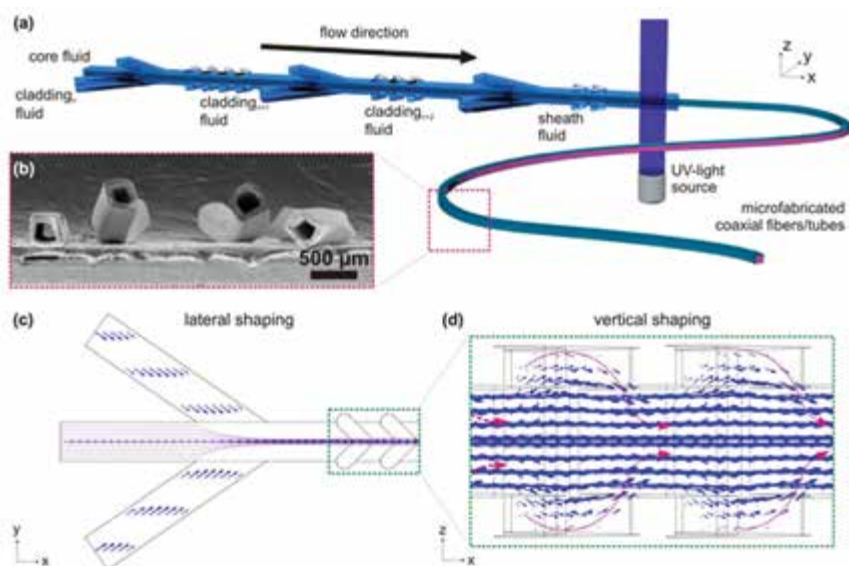


FIGURE 6 Hydrodynamic focusing. (a) The design and operating mechanism of a coaxial hydrodynamic shaping device. (b) Electron micrographs of a sectioned microvessel. (c-d) Computational model of lateral and vertical hydrodynamic focusing within the microchannels.

microfabrication device and visualize the hydrodynamic shaping, computational fluid dynamics was used to simulate fluid flow. Hydrodynamic focusing at the inlet channels sets the lateral dimension of the focused fluid (Fig. 6(c)), while the chevron grooves induce advection, which sets the vertical dimension of the focused fluid (Fig. 6(d)).

Generation of Endothelial Cell Containing Microvessels: The heterogeneous network architecture of native extracellular matrix (ECM) impacts mechanical strength, mass transport capacity, degradation rate, and subsequent cellular behavior. To emulate the microstructural composition and activity of native ECM, we fabricated interpenetrating networks that physically and covalently incorporated a protein phase within a synthetic polymer network (Fig. 7).³ Gelatin methacrylamide (GelMA) and poly(ethylene glycol)

(PEG) macromers were integrated by concurrent photoinitiated thiol-click reactions. First, a PEG network was generated by thiol-yne coupling, and the second interlocking network was formed by thiol-ene coupling between GelMA and PEG. GelMA, PEG-tetrathiol, and PEG-tetra alkyne provided photoreactive methacrylate, thiol, and alkyne functional groups, respectively. Gelatin and PEG were selected to emulate the combination of asymmetric physiochemical properties of ECM — a rigid macromolecular network interpenetrated with a soft, bioactive protein network — which is hypothesized as the key to enhanced mechanical and biological performance.

To demonstrate the advantage of the bio/synthetic network, the mechanically robust GelMA-PEG network was evaluated as a viable material for the construction of microfiber cell scaffolds via our microfluidic fabrication method. For the encapsulation of endothe-

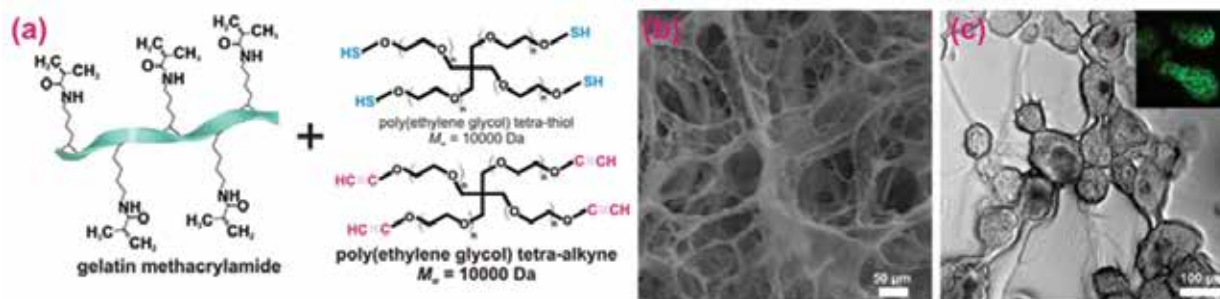


FIGURE 7 Polymer + protein hydrogel matrices. (a) The biological (gelatin methacrylamide) and synthetic (PEG) components of the bio-hybrid hydrogel developed to support encapsulated cells. (b) Electron micrograph of the porous biosynthetic hydrogel. (c) Proliferation of ea.Hy 926 endothelial cells encapsulated within the biosynthetic hydrogel network. (c, inset) Phalloidin stained encapsulated cells.

lial cells in microvessels, the hydrodynamic focusing apparatus was used to direct and photopolymerize the bio/synthetic macromer solution around the endothelial cells. As illustrated in Fig. 8, the endothelial cells were encapsulated within the bio/synthetic microfibers and collected in culture media. The encapsulated cells were stained to examine viability (calceinAM/ethidium homodimer). Micrographs of endothelial cells encapsulated within the microvessels showed a predominately viable population (green) and uniform distribution throughout the center of the fibers. The fully swollen

microchannel walls focused the multilayered, laminar fluid flow to generate concentric fluid regimes. By combining this hydrodynamic shaping with in situ photopolymerization, we continuously generated biomimetic microvessels, while avoiding the limitations of “concentric-needle” microfluidic devices and the bio-“incompatibility” of previously reported microfluidic methods. Microfluidic production of individual blood vessels will provide the necessary level of architectural and cellular control at the microscale for building large-scale 3D tissue models with complex vascular networks

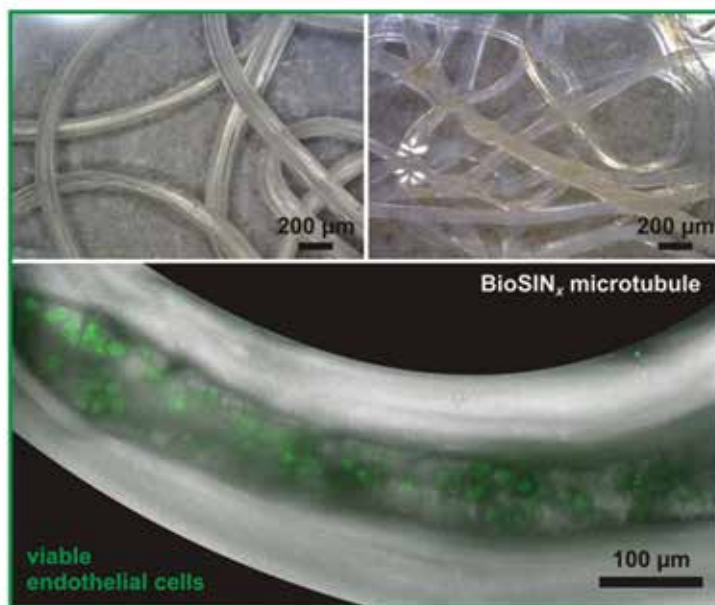


FIGURE 8
From microtubule to blood vessel. Photopolymerization solidified the biosynthetic hydrogels into microvessels containing a viable population of endothelial cells.

fibers were ca. 250 µm in diameter, but it is important to note that the versatility of the hydrodynamic shaping microchannel allows for control of fiber size solely by the adjustment of fluid flow rates. With these advantages and the robust mechanical integrity, smaller microfibers and finer focusing of cell placement will be explored with cell-laden microvessels fabricated on the scale of arterioles and venules; “capillary-sized” fibers can also be achieved with this method.

Conclusions: We reported a cytocompatible strategy to fabricate multiaxial microfibers and microvessels using the combination of hydrodynamic shaping and in situ photopolymerization of a bio/synthetic hydrogel. We found that hydrodynamic shaping and photoinitiated polymerization produced minimal cellular stressors, and with the appropriate cytocompatible macromer system, we were able to generate microfibers containing endothelial cells. These coaxial microfibers and microvessels mimic biological microvessels. In this design, surface features directly milled into the

that recapitulate the given human physiology. This technology may afford new insights into studying the efficacy of potential medical counter measures (MCM) and may be used to identify biomarkers.

Acknowledgments: Work performed by Michael A. Daniele was supported by a National Research Council Postdoctoral Fellowship. This work was supported by the Naval Research Laboratory (NRL) and the Office of Naval Research (ONR).

[Sponsored by NRL and ONR]

References

- ¹ M.A. Daniele, S.H. North, J. Naciri, P.B. Howell, S.H. Foulger, F.S. Ligler, and A. Adams, “Rapid and Continuous Hydrodynamically Controlled Fabrication of Biohybrid Microfibers,” *Advanced Functional Materials* **23**(6), 698–704 (2013).
- ² D.A. Boyd, M.A. Daniele, A.A. Adams, and F.S. Ligler, “Microfluidic Fabrication of Polymeric and Biohybrid Fibers with Predefined Size and Shape,” *J. Visualized Experiments* **83**, e50958–e50958 (2014).
- ³ M.A. Daniele, A.A. Adams, J. Naciri, S.H. North, and F.S. Ligler, “Interpenetrating Networks Based on Gelatin Methacrylamide

and PEG Formed Using Concurrent Thiol Click Chemistries for Hydrogel Tissue Engineering Scaffolds,” *Biomaterials* 35, 1845–1856 (2013).

X-Ray Crystal Structures of Engineered Ricin Vaccine Immunogens

P.M. Legler,¹ J.R. Compton,¹ and COL C.B. Millard (ret.)²

¹Center for Bio/Molecular Science and Engineering

²U.S. Army Medical Research and Materiel Command, Ft. Detrick, Maryland

Ricin is a well-known plant toxin that can be extracted easily from castor beans and has a history of use as a deadly human poison. The protein consists of a catalytic A-chain (RTA) coupled with a lectin B-chain (RTB) that binds the galactosyl moieties found on many cell surface oligosaccharides (Fig. 9(a)). Although ricin is noninfectious, it is closely related in structure and function to the bacterial Shiga toxins and Shiga-like toxins (also known as Verotoxin) of *Shigella dysenteriae* and *E. coli*. Antibiotic-resistant *E. coli* producing Shiga toxin was responsible for 54 deaths in Germany in 2011.¹ RTA and Shiga toxins belong to a family of enzyme toxins known as “ribosome inactivating proteins (RIPs)” that work by blocking essential protein synthesis.

The RTA N-glycosidase catalyzes the hydrolysis of an adenine from ribosomal RNA (Fig. 10). It targets a specific loop in the ribosome known as the ricin-sarcin

loop. Once the adenine is removed, the ribosome is inactive and protein synthesis is halted. One internalized ricin molecule can potentially inactivate the ribosomes of an entire cell, ultimately killing the cell. Human intoxication by a lethal dose of these proteins is essentially irreversible since there is currently no FDA-approved small molecule ricin therapeutic or anti-toxin. From sub-lethal doses, however, immunity can be acquired, as ricin is also immunogenic. Vaccination is a useful prophylaxis for personnel who may be at risk of exposure.

Because the RTA subunit is primarily responsible for the toxicity of ricin, it has formed the basis of several subunit vaccines.² In the 1990s, the U.S. Army tested deglycosylated RTA purified from castor beans as a vaccine. Purified RTA in the absence of the RTB subunit is a promising candidate because it is at least 1000-fold less toxic compared to ricin holotoxin and, therefore, may be safely injected in the microgram quantities needed for human vaccination. As recombinant technologies and protein engineering became more common, the A-chain was produced in *E. coli* apart from the B-chain. In 2002, Vitetta et al. developed a ricin vaccine for humans called RiVax (Fig. 9(b)) that is based upon recombinant RTA containing two mutations, V76M and Y80A.³

RTA has one important limitation, however, to its practical development as an immunogen. Ricin evolved as a dimeric protein and artificial removal of the RTB subunit from RTA exposes a relatively hydrophobic interfacial surface formed by the C-terminus of RTA. The

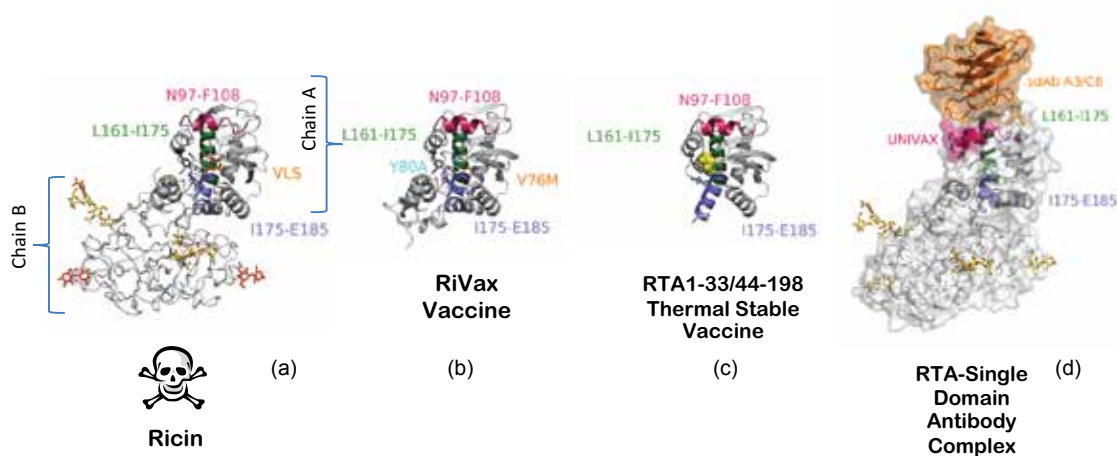


FIGURE 9

Ricin vaccines derived from the A-chain of the toxin. (a) Ricin consists of an A-chain and a B-chain. The A-chain is shown in ribbon. (b) The ricin A-chain can be produced recombinantly in *E. coli* apart from the B-chain. The structure of RiVax (PDB 3SRP) is similar to the structure of the A-chain of the toxin. (c) Truncation of the hydrophobic C-terminal residues of the A-chain and the loop increased the thermal stability of the protein and reduced its propensity to aggregate. The incorporation of disulfide bonds (yellow spheres) further enhanced the thermal stability of the immunogens (PDB 3MK9, 3LC9, and 4IMV). (d) Structure of an anti-ricin single domain antibody, A3/C8, identified by Dr. Goldman’s lab at NRL in complex with RTA. The structure shows the epitope recognized by this antibody. The protective epitopes are colored on each protein. The UNIVAX R70 epitope is shown in magenta (Ref. 9); the B-cell epitope recognized by human neutralizing antibodies between Leu161-Ile175 was identified by Castelletti et al. (Refs. 10,11) and is shown in green. The T-cell epitope between Ile175-Tyr183 is shown in blue. The complex has been overlaid onto ricin.

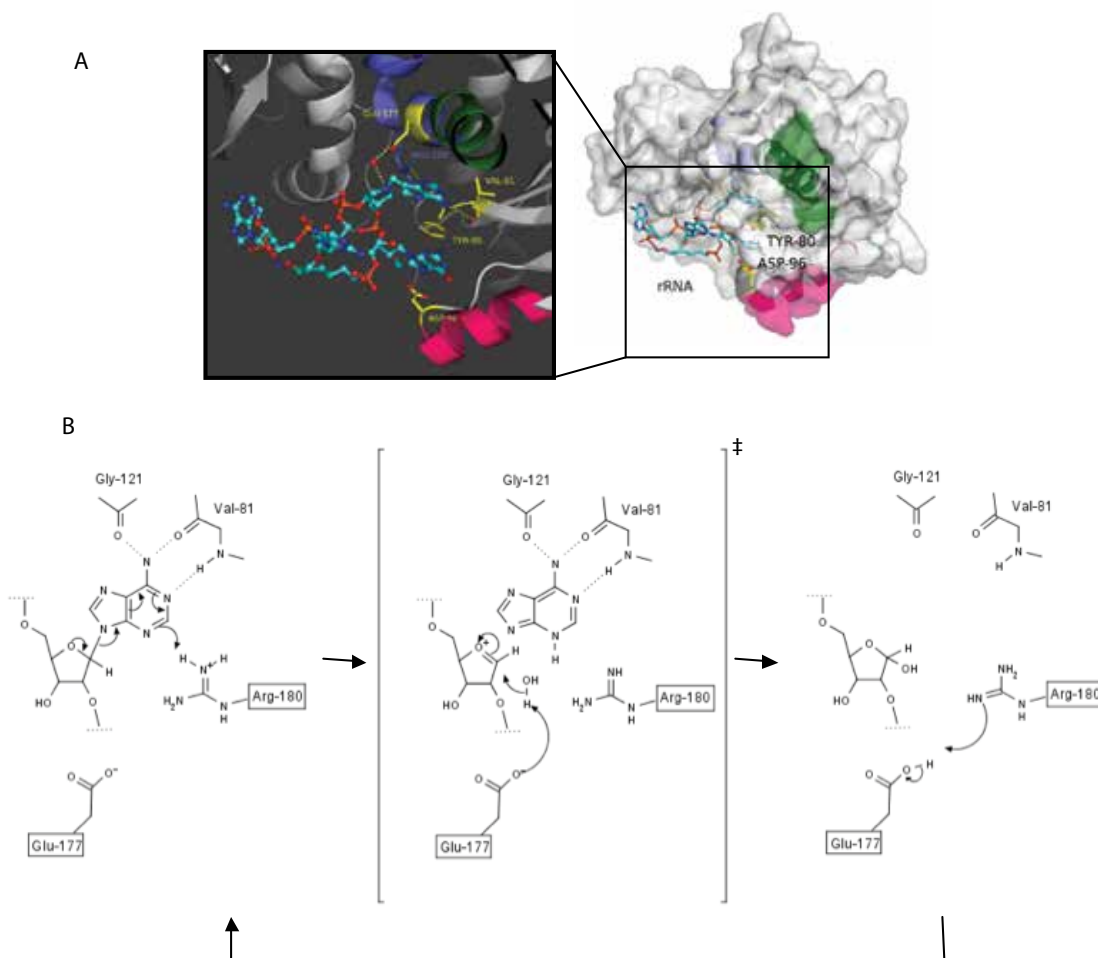


FIGURE 10

RTA catalyzed depurination reaction. (a) Structure of a cyclic G(9-DA)GA 2'-OMe transition state mimic determined by Roday et al. (PDB 3HIO) (Ref. 12). A methylene carbon between the nitrogen of the aza-sugar and the adenine mimics the increased ribosyl-adenine distance in the dissociative transition state (Ref. 13). (b) Proposed mechanism of the RTA catalyzed depurination reaction. The hydrolysis reaction is thought to proceed via a dissociative mechanism with an oxocarbenium transition state. Arg-180 protonates the leaving group (adenine) and the N-glycosidic bond is broken. Glu-177 deprotonates the hydrolytic water that attacks at carbon to complete the depurination reaction.

exposed surfaces promote undesirable self-aggregation and precipitation of RTA during vaccine production and storage. Large protein aggregates also are undesirable because they are difficult to quantify from batch to batch, and also may impede optimal immune system processing by human macrophages.

To address the low solubility and instability of the protein, next-generation thermostable recombinant RTA immunogens were later developed by scientists at the U.S. Army Medical Research Institute of Infectious Diseases (USAMRIID), the Walter Reed Army Institute of Research (WRAIR), and the Naval Research Laboratory (NRL).⁴⁻⁶ These immunogens are truncations of RTA and lack the C-terminal residues 199-276 as well as the loop residues 34-43 (Fig. 9(c)). The hydrophobic loop residues pack against the C-terminal domain and their removal further enhanced the stability of the pro-

tein. The RTA1-33/44-198 vaccine immunogen (also known as RVEc) retains all of the protective epitopes of RTA, but is more stable and less prone to aggregation. RTA1-33/44-198 is currently in Phase I Clinical trials sponsored by the Department of Defense Joint Vaccine Acquisition Program.⁷

The RTA1-33/44-198 immunogen was improved further by the addition of an engineered disulfide bond (R48C/T77C or V49C/E99C).⁴ The engineered RTA variants have melting temperatures 13 °C higher than the wild type RTA. More stable vaccines can reduce the costs of storage and frequency of replenishment of strategic stockpiles, as well as improve the reliability of protein products if the cold-chain of storage is broken during military operations.

After making such major changes to the natural RTA structure to optimize it for use as a vaccine, it

was important to verify the structural integrity of the engineered proteins, especially the known protective epitopes. X-ray crystallography^{4,5} was used to determine the 3D structure of these proteins. The structure determination was an integral part of the functional characterization of these recombinant engineered vaccines. The structure of the antibody-RTA complex (Fig. 9(d)) identified the specific epitope recognized by an anti-ricin single domain antibody produced by Dr. Goldman's lab at NRL. The structures of the truncated RTA1-33/44-198 variants,⁴ RiVax,⁸ and an antibody RTA complex were determined by NOVA contractor Jaimee R. Compton and NRL scientist Patricia M. Legler. These structures were highlighted in the Protein Data Bank as the Molecule of the Month in May 2013 (www.rcsb.org, doi: 10.2210/rcsb_pdb/mom_2013_5) after ricin was found in letters sent to the U.S. Capitol's off-site mail facility in April 2013.

Acknowledgments: The protein sequences of the RTA immunogens were originally proposed by COL Charles B. Millard and Dr. Mark Olson at USAMRIID (Ft. Detrick, MD). Ms. Compton and SPC V.B. Clingan carried out the biochemical characterization and construction of the mutants under the technical guidance of Dr. Legler. The single domain antibody was provided by Dr. Ellen Goldman's lab at NRL. X-ray crystal structures of RiVax, RTA1-33/44-198 V49C/E99C and R48C/T77C, and RTA-antibody complex were determined by Ms. Compton and Dr. Legler at WRAIR and NRL. This work was funded by the Defense Threat Reduction Agency.

[Sponsored by the Defense Threat Reduction Agency]

References

- ¹ C. Frank, D. Werber, J.P. Cramer, M. Askar, M. Faber, H.M. an der Heiden, H. Bernard, A. Fruth, R. Prager, A. Spode, M. Wadl, A. Zoufaly, S. Jordan, M.J. Kemper, P. Follin, L. Muller, L.A. King, B. Rosner, U. Buchholz, K. Stark, and G. Krause, "Epidemic Profile of Shiga-Toxin-Producing *Escherichia coli* O104:H4 Outbreak in Germany," *N. Engl. J. Med.* **365**, 1771–1780 (2011).
- ² C.B. Millard and R.D. LeClaire, "Ricin and Related Toxins: Review and Perspective," in *Chemical Warfare Agents: Chemistry, Pharmacology, Toxicology, and Therapeutics* (J.A. Romano, B.J. Lukey, and H. Salem, eds.), second edition (CRC Press/Taylor & Francis Group, LLC, Boca Raton, 2008), pp. 423–467.
- ³ J.E. Smallshaw, A. Firan, J.R. Fulmer, S.L. Ruback, V. Ghetie, and E.S. Vitetta, "A Novel Recombinant Vaccine which Protects Mice against Ricin Intoxication," *Vaccine* **20**, 3422–3427 (2002).
- ⁴ J.R. Compton, P.M. Legler, B.V. Clingan, M.A. Olson, and C.B. Millard, "Introduction of a Disulfide Bond Leads to Stabilization and Crystallization of a Ricin Immunogen," *Proteins* **79**, 1048–1060 (2011).
- ⁵ L. Janosi, J.R. Compton, P.M. Legler, K.E. Steele, J.M. Davis, G.R. Matyas, and C.B. Millard, "Disruption of the Putative Vascular Leak Peptide Sequence in the Stabilized Ricin Vaccine Candidate RTA1-33/44-198," *Toxins (Basel)* **5**, 224–248 (2013).
- ⁶ M.A. Olson, J.H. Carra, V. Roxas-Duncan, R.W. Wannemacher, L.A. Smith, and C.B. Millard, "Finding a New Vaccine in the Ricin Protein Fold," *Protein Eng. Des. Sel.* **17**, 391–397 (2004).
- ⁷ U.S. Army Medical Research and Materiel Command, *Safety and Immunogenicity Study of Recombinant Ricin Toxin A-Chain Vaccine (RVEc™)*, NCT01317667 (2011).
- ⁸ P.M. Legler, R.N. Brey, J.E. Smallshaw, E.S. Vitetta, and C.B. Millard, "Structure of RiVax: a Recombinant Ricin Vaccine," *Acta Crystallogr. D. Biol. Crystallogr.* **67**, 826–830 (2011).
- ⁹ P.V. Lemley, P. Amanatides, and D.C. Wright, "Identification and Characterization of a Monoclonal Antibody that Neutralizes Ricin Toxicity In Vitro and In Vivo," *Hybridoma* **13**, 417–421 (1994).
- ¹⁰ D. Castelletti, G. Fracasso, S. Righetti, G. Tridente, R. Schnell, A. Engert, and M. Colombatti, "A Dominant Linear B-Cell Epitope of Ricin A-Chain is the Target of a Neutralizing Antibody Response in Hodgkin's Lymphoma Patients Treated with an Anti-CD25 Immunotoxin," *Clin. Exp. Immunol.* **136**, 365–372 (2004).
- ¹¹ D. Castelletti and M. Colombatti, "Peptide Analogues of a T-Cell Epitope of Ricin Toxin A-Chain Prevent Agonist-Mediated Human T-Cell Response," *Int. Immunol.* **17**, 365–372 (2005).
- ¹² S. Roday, T. Amukele, G.B. Evans, P.C. Tyler, R.H. Furneaux, and V.L. Schramm, "Inhibition of Ricin A-chain with Pyrolydine Mimics of the Oxocarbenium Ion Transition State," *Biochemistry* **43**, 4923–4933 (2004).
- ¹³ M.C. Ho, M.B. Sturm, S.C. Almo, and V.L. Schramm, "Transition State Analogues in Structures of Ricin and Saporin Ribosome-Inactivating Proteins," *Proc. Natl. Acad. Sci. U.S.A.* **106**, 20276–20281 (2009).



A photograph of two men in a laboratory setting. They are both wearing safety glasses and are focused on a small electronic component held by one of them. The background is dark with various pieces of equipment and glowing green and red lights, suggesting a high-tech or research environment. The overall tone is professional and technical.

electronics and electromagnetics

156 Multilayer Polymer Composites for High Energy Density Capacitors

157 Wideband Dynamic Range Extender (DRE)

159 An Attractive Hybrid Indirect and Direct Drive Approach to Laser Fusion

161 Multi-Kilowatt Millimeter-Wave Sheet Beam Amplifiers

Multilayer Polymer Composites for High Energy Density Capacitors

M.A. Wolak
Optical Sciences Division

Synopsis: Emerging Naval technologies such as rail guns and electromagnetic aircraft launch systems require pulsed power systems capable of rapid delivery (<10 ms) of massive amounts of energy (>10 MJ). These pulsed power systems rely on high energy density capacitors (HEDCs) to play the central role of storing and discharging energy. HEDCs are also needed for various civilian applications such as electric vehicles and defibrillators. We, in collaboration with Case Western Reserve University (CWRU), recently developed a new multilayer polymer capacitor material that can attain maximum energy densities up to 17 J/cm³, more than double that of biaxially oriented polypropylene (BOPP), the current state-of-the-art pulsed power capacitor material. Increasing the energy density of the polymer dielectric will result in a substantial decrease in both the size and weight of capacitors used in on-ship Naval pulsed power systems. Our research, highlighted below, focuses on identifying how the multilayer structure affects the breakdown mechanism. This information is then used to optimize the structure for improved dielectric performance.

Multilayer Polymer Composites: For a linear dielectric material, the maximum energy storage density (U_d) is proportional to its permittivity (ϵ_r) times the square of the dielectric strength (E_b), which is defined as the maximum field the material can withstand prior to electrical breakdown. We postulated that a multilayer structure could be used to alter the breakdown mechanism and enhance both E_b and U_d . The multilayer films contain alternating layers of a high ϵ_r polymer (such as polyvinylidene fluoride, PVDF) interleaved with a high E_b polymer (such as polycarbonate, PC). The films are prepared via melt coextrusion by CWRU. Most films have a nominal thickness of 12 μm and contain 32 to 256 layers. Figure 1 shows a cross section of a 32-layer 50 vol% PC/50 vol% PVDF film.

Dielectric Properties: The bulk permittivity of the multilayer composites is well understood and follows an effective medium model as detailed in Ref 1. First-generation PC/PVDF composites show enhanced E_b relative to pure PC or PVDF films, with a maximum E_b nearing 800 V/ μm for 90/10 PC/PVDF films (Fig. 2). The discharged energy density of the PC/PVDF composites reaches a maximum of 13.5 J/cm³ at a 50/50 volume fraction, representing a 60% increase relative to pure PVDF films, and a 100% increase relative to pure

PC films.¹ The enhancement in dielectric strength and energy density is due to the so-called Barrier Effect, whereby the layer interfaces impede the propagation of an electrical breakdown tree, allowing the film to withstand higher electric field than single component films of its source polymers. The Barrier Effect was confirmed by scanning electron microscopy (SEM) imaging of treeing patterns on the surface of films driven to electrical breakdown under divergent field conditions.²

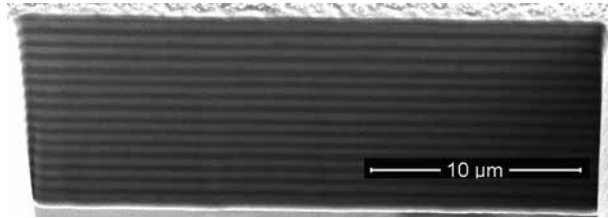


FIGURE 1
FIB/SEM micrograph of a 12 μm thick, 32-layer 50 vol% PC / 50 vol% PVDF film. The dark layers are PC and the light layers are PVDF. Each layer is ~ 375 nm thick here. The relative layer thickness (PVDF/PC) varies with relative concentration, and an increase in the number of layers provides overall thinner layers.

To further examine breakdown in multilayer films, we pioneered a novel failure analysis technique using dual-beam focused ion beam (FIB)/SEM.³ FIB is used to mill a site-specific hole in the film, and SEM is used to image the resulting cross section. Sequential FIB milling followed by SEM imaging can give a 3D image of the internal structure of a film near a breakdown site, as seen in Fig 3. Figure 3 also depicts an internal cross section of a film after breakdown, in which the layer structure is grossly distorted and voids are formed at the interfaces between adjacent PC and PVDF layers. These images, and many others like them collected on different samples, show that layer delamination may be a precursor to “through-film” breakdown. We therefore conclude that the layer interfaces play an important role in the breakdown mechanism. Based on the FIB/SEM studies, we recently studied new interface-modified films that are designed to prevent layer delamination and also control electric field distributions within the film. These films contain a thin interfacial layer of polymethylmethacrylate (PMMA) between discrete PC and PVDF layers. The improved layer adhesion in new PC:PMMA:PVDF films results in enhanced dielectric properties: $E_b > 900$ V/ μm and $U_d = 17$ J/cm³. We have also investigated additional approaches to further enhance E_b , such as biaxial stretching or introducing a third polymer as a thin interfacial adhesion layer.

Conclusion: Multilayer polymer composites show enhanced E_b and U_d relative to monolithic single

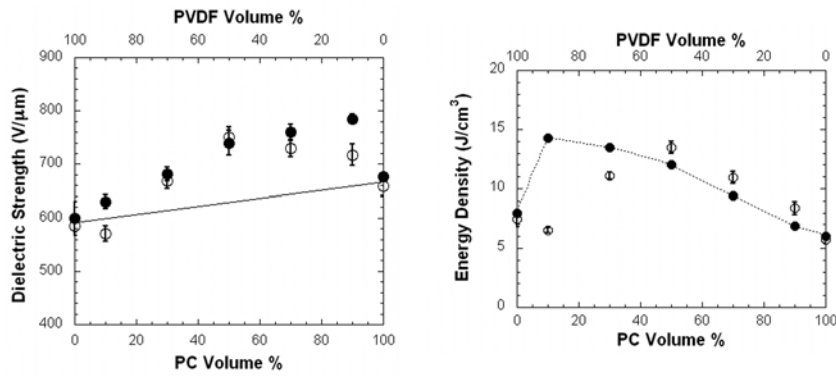


FIGURE 2 (Left) Dielectric strength as a function of composition for 32-layer PC/PVDF films (filled circles) and 256-layer films (unfilled circles). The thinnest layers in the 256-layer films are apparently less effective as barriers. (Right) Measured stored energy density of 32-layer PC/PVDF films (unfilled circles) vs the theoretical energy density (filled circles). Polarization hysteresis in the PVDF reduces the recoverable energy density. It is inhibited in thinner PVDF layers.

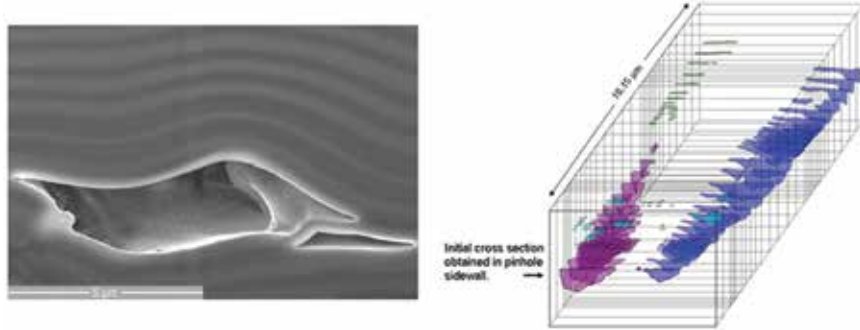


FIGURE 3 (Left) FIB/SEM image of an internal cross section of a 32-layer 50/50 PC/PVDF film subjected to electrical breakdown. The layer structure is grossly distorted and voids have formed at the interfaces between adjacent layers. (Right) A quasi-3D reconstruction of voids and layer delaminations as a function of distance from a breakdown pinhole with the closest cross section milled directly in the pinhole sidewall. The reconstruction features 30 successive FIB milling cross sections covering a distance of 16.15 μm in length. Note that some voids are not connected to the site of the “through-film” breakdown, suggesting that smaller breakdown events are delocalized throughout the film.

polymer films because the layer interfaces provide barriers to the propagation of through-film electrical breakdown. By optimizing the structure and composition, we have achieved a maximum U_d of 17 J/cm³ for interface-modified PC:PMMA:PVDF films, more than double that of BOPP. The enhanced energy density will allow for the fabrication of smaller, lighter capacitors to be deployed in on-ship Naval pulsed power systems, or in civilian applications such as electric vehicles.

[Sponsored by ONR]

References

- ¹ M.A. Wolak, M.-J. Pan, A. Wan, J.S. Shirk, M. Mackey, A. Hiltner, E. Baer, and L. Flandin, “Dielectric Response of Structured Multilayered Polymer Films Fabricated by Forced Assembly,” *Appl. Phys. Lett.* **92**(11), 113301 (2008).
- ² M. Mackey, A. Hiltner, E. Baer, L. Flandin, M. Wolak, and J. Shirk, “Enhanced Breakdown Strength of Multilayered Films Fabricated by Forced Assembly Microlayer Coextrusion,” *J. Phys. D: Appl. Phys.* **42**, 175304 (2009).

- ³ M.A. Wolak, A. Wan, J.S. Shirk, M. Mackey, A. Hiltner, and E. Baer, “Imaging the Effect of Dielectric Breakdown in a Multilayered Polymer Film,” *J. Appl. Polym. Sci.* **123**(4), 2548 (2012).

Wideband Dynamic Range Extender (DRE)

B. Nousain,¹ J. Goodman,¹ K. Lorenz,¹ M. McKeon,¹ and G. Stantchev²

¹Tactical Electronic Warfare Division

²Electronics Science and Technology Division

Introduction: Receivers currently designed to operate across wide bandwidths are limited in dynamic range by frequency spurs resulting from nonlinearities in analog and mixed-signal components. These spurs

are unaffected by traditional noise floor reduction techniques. As a result, receivers are severely desensitized and, thus, weak signals will go undetected. We have developed and demonstrated a digital nonlinear equalization (NLEQ) algorithm^{1,2} that has suppressed these spurs and subsequently extended the dynamic range of these receivers by up to two orders of magnitude (20 dB) over 500 MHz of instantaneous bandwidth.

Motivation: Receiver spurs are problematic when detecting and characterizing weak signals. Traditional detection algorithms cannot discriminate the spurs from a legitimate signal. Conventional techniques to reduce the noise floor, such as averaging, are ineffective at suppressing the spurs. This is because the spurs are not random and are actually coherent with the averaging process.

Figure 4 illustrates the detection problem by highlighting a narrowband signal at approximately the same power level as the spurs before equalization. After spur suppression, the narrowband signal is detected as legitimate. Spur suppression is often addressed through the use of lookup tables. However, lookup tables are not effective against spurs with memory. Our technique has the ability to suppress spurs with and without memory, including those created by interleaving multiple digitizers.

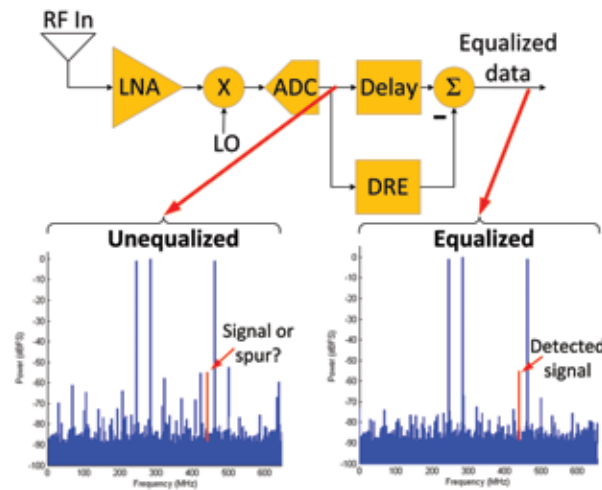


FIGURE 4 Typical receivers cannot discriminate between receiver spurs and legitimate signals.

Nonlinear Model: We predict spur location by mathematically modeling the nonlinear receiver response as linear combinations of a nonlinear basis that is weighted over a sliding window. This equates to the input signal being multiplied by delayed versions of itself followed by a finite impulse response (FIR) filter. The FIR filter is vital to account for the memory of the nonlinearities. The result is a modular architecture (Fig. 5) that can be scaled to fit available processing re-

sources. When fewer processing resources are available, fewer nonlinear bases, or processing elements, are used at the expense of reduced spur suppression. After the spur locations are predicted, they are subtracted from the original signal (Fig. 4). This technique is powerful, because it works for arbitrary inputs to the receiver.

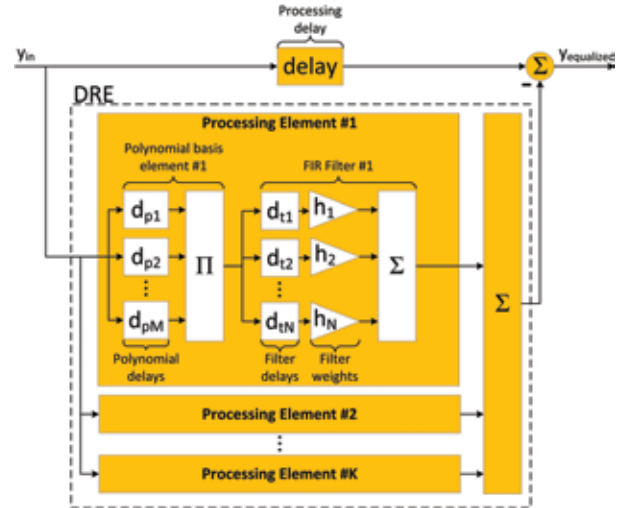


FIGURE 5 Dynamic range extender (DRE) block diagram.

Architecture Identification: The key to developing the nonlinear system model is to select an appropriate basis to represent the nonlinear system response. The number of possible bases is extremely large, so identifying an optimal one is computationally infeasible. Instead, forward sequential estimation is used to choose a basis with a fixed computational complexity. The basis selection algorithm remains computationally demanding, but the architecture only needs to be identified once for each receiver. Over time, the receiver may need to be recalibrated to update coefficient values, but this is computationally inexpensive.

Receiver Characterization Test Bed: The nonlinearities of a receiver are excited by injecting many sets of tones and the receiver output is precisely measured. Our algorithm does not require synchronization between the tone sets and the receiver. This prevents amplitude estimation errors of the excitation source from adversely affecting the identification of distortions. After the data are collected, the forward sequential estimation algorithm is used to project the receiver nonlinearities onto basis functions.

Architecture Verification: The equalization architecture is tested on independent tone sets to verify the equalization model is effective against tone sets not used to build the model.

To demonstrate spur suppression performance, a benchtop receiver was constructed using commercial

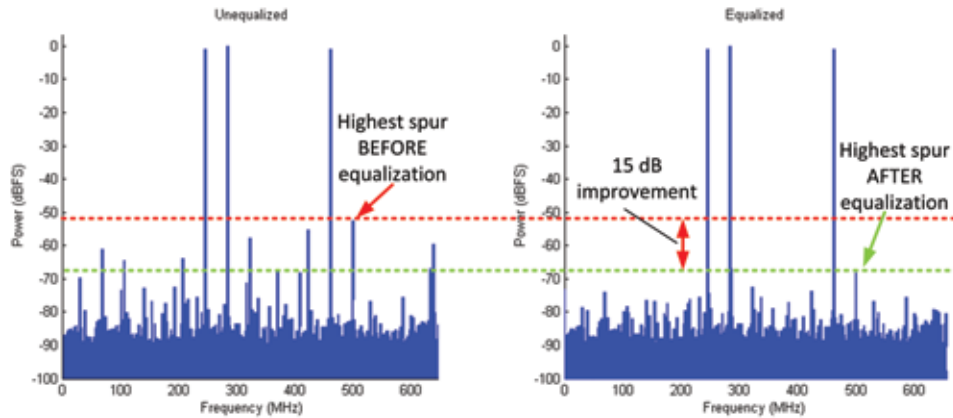


FIGURE 6
Demonstrated spur suppression showing a 15 dB improvement in spurious free dynamic range.

components and injected with 100 tone sets across over 500 MHz of bandwidth – 75 sets for training and 25 sets for testing. To suppress nonlinear spurs in this receiver, eight processing elements were used with an eight-tap FIR filter. This processing architecture yielded a 15 dB improvement in spurious free dynamic range (Fig. 6).

Summary: Our algorithm has been demonstrated to suppress nonlinear spurs by up to 20 dB. The process to identify a suppression architecture is computationally intensive, but only needs to be performed once for each receiver. Once identified, the architecture is scalable and can trade spur suppression performance for processing resources.

[Sponsored by the National Security Agency]

References

- ¹J. Goodman, B. Miller, M. Herman, M. Vai, and P. Monticciolo, “Extending the Dynamic Range of RF Receivers Using Nonlinear Equalization,” 2009 International Waveform Diversity and Design Conference, pp. 224–228, February 8–13, 2009.
- ²J. Goodman, B. Miller, M. Herman, G. Raz, and J. Jackson, “Polyphase Nonlinear Equalization of Time-Interleaved Analog-to-Digital Converters,” *IEEE J. Selected Topics Sig. Proc.* 3(3), 362–373 (2009).



An Attractive Hybrid Indirect and Direct Drive Approach to Laser Fusion

M. Karasik,¹ J.L. Weaver,¹ A.J. Schmitt,¹ J.W. Bates,¹ V. Serlin,¹ S.P. Obenschain,¹ Y. Aglitskiy,² and J. Oh³

¹Plasma Physics Division

²SAIC, Inc.

³RSI

Generating High Pressures Uniformly with High Power Lasers: When a high-power laser is focused on

the surface of a material, the surface is rapidly heated, resulting in ablation of the material at a very high rate. The ablation generates pressure on the surface, just like exhaust generating thrust in a rocket engine. With sufficiently high laser intensity, pressures of 10 to 100 million atmospheres can be achieved with UV lasers. These high pressures can be used to rapidly accelerate targets to the extreme velocities (>300 km/s) required for inertial fusion implosions. This type of research is supported by National Nuclear Security Administration (NNSA) as part of their stockpile stewardship program. In the longer term, inertial fusion may be a source for clean, plentiful energy.¹

Nonuniformities in laser illumination, present in all high energy laser systems, can produce pressure variations across the driven surface, imprinting perturbations that can be amplified by hydrodynamic instabilities — the process known as laser imprint. Laser imprint can limit the quality of the data obtained or spoil the uniformity of an imploding fuel capsule in inertial confinement fusion. Two major approaches have been developed to minimize laser imprint in fusion implosions (see Fig. 7). The first uses “indirect” drive, where laser beams are first used to heat the walls of a cavity made of a high atomic number material (such as gold) to emit X rays, which then ablate the target more uniformly. This approach is being pursued at the National Ignition Facility (NIF) at Lawrence Livermore National Laboratory. The second approach is to shine the laser beams on the target directly (“direct” drive), but smooth the laser beams by breaking up and rapidly varying the laser perturbations, leaving a more uniform drive on the time scale of the ablation. This is accomplished most successfully on the Nike laser at the Naval Research Laboratory. Nike is a krypton fluoride (KrF) gas laser that operates at 0.25 μm (deep-ultraviolet) wavelength. The laser smoothing technique invented at NRL and the KrF laser architecture allow Nike to have the world’s most uniform high-energy laser drive.

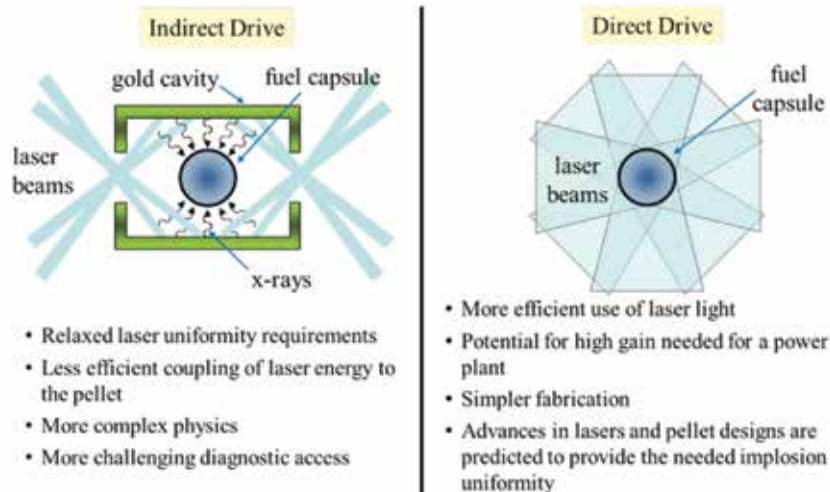


FIGURE 7

The two methods of fusion capsule illumination. Advances in laser technology and capsule designs allow the use of the advantageous direct drive for capsule implosions.

The indirect drive approach currently used at the NIF comes at a cost of increased complexity and reduced coupling of the available laser energy to the fuel capsule. While the NIF is thought to have sufficient energy to ignite a fuel capsule using direct drive, it cannot provide as uniform target illumination as the Nike laser, and that limits its capability to implode fusion targets by direct drive. Researchers on Nike have found a way of mitigating imprint that retains the uniformity benefit of the indirect drive without sacrificing the efficiency of direct drive, yet is relatively easy to implement and produces a highly uniform drive.

Suppression of Laser Imprint with Thin Metal Coatings: In this method of imprint suppression, a thin overcoat of high atomic number (high-Z) metal, such as gold or palladium, is applied to the surface of the target. The initial rise of the laser pulse on target is almost entirely absorbed in the thin metal coating, rapidly heating it to the point of X-ray emission. Half of the emitted X rays are absorbed in the underlying target, generating the initial ablation by indirect drive. The large standoff that forms between the laser absorption region and the target ablation region allows smoothing of short-scale laser perturbations to take place. Figure 8 shows this schematically in planar geometry.

Originally developed on Nike at NRL over a decade ago,² the use of high-Z coating for imprint suppression has now been demonstrated to work with the intensities and laser pulse shapes relevant to the fusion ignition-scale lasers such as the NIF. An example of the effect of the coating on the smoothness of the laser drive with such a pulse shape can be seen in Fig. 9, which shows measurements of laser imprint with and without the

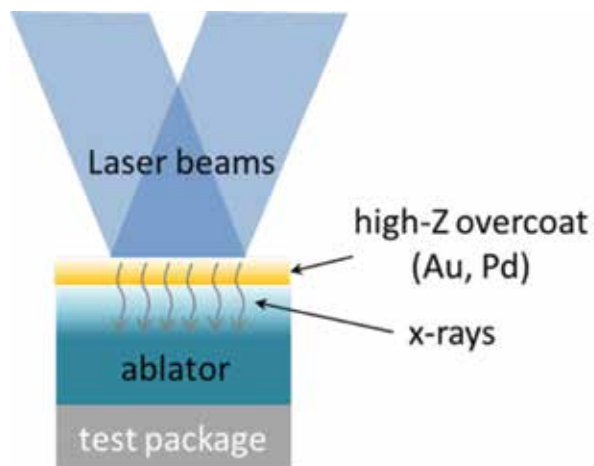


FIGURE 8

Schematic of the use of a thin overcoat of a high atomic number metal coating to suppress laser imprint. The laser is first absorbed in the coating, resulting in initial ablation of the target by X rays.

coating. The coating suppresses laser imprint to below the instrument measurement noise.

The thickness of the coating is an important part of the design. Once long separation between laser absorption and target ablation is established and smoothing of laser perturbations can take place, the drive should transition to direct laser ablation of the target to minimize X-ray preheat of the payload and maximize drive efficiency as the laser power ramps up. This transition requires the initially absorbing high-Z layer to become transparent to the laser at the appropriate time. On the Nike laser, we find coating thickness of 400 to 800 Å of gold or palladium to be optimal. Figure 10 shows an example of the transition of emission from the gold layer

in front of the target to the underlying plastic target, indicating that the gold density has dropped sufficiently for the laser light to ablate the target directly.

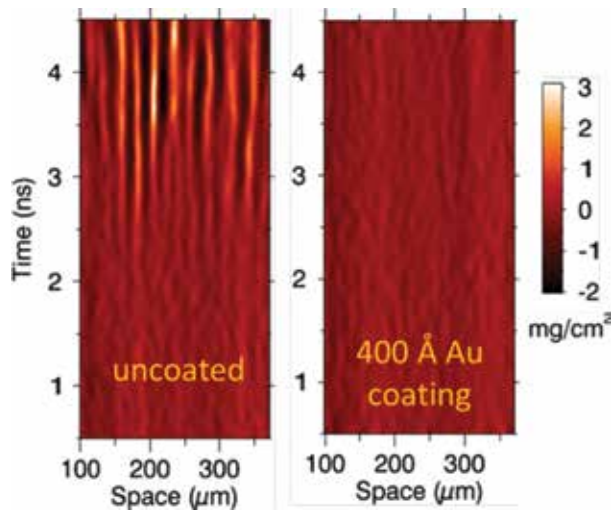


FIGURE 9 Example of the effect of a thin gold coating on laser imprint. The left image shows the growth in time of areal mass perturbations caused by laser imprint amplified by the Rayleigh-Taylor instability for an uncoated plastic target. Large amplitude perturbations are evident starting at about 3 ns. The right image shows the same conditions but with a 400 Å gold coating on the target. No perturbations above the measurement noise are present in this case. Measurement was performed using curved crystal monochromatic X-ray radiography pioneered on Nike at NRL.

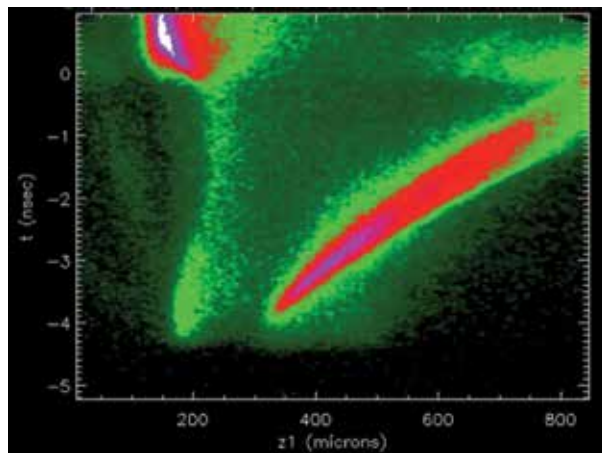


FIGURE 10 Streaked image of X-ray emission from a gold-coated plastic target. Strong emission is seen from the gold layer early in the pulse ($t = -4$ to 0 ns) as it is pushed away from the target by the ablating underlying plastic. Around $t = 0$, the emission switches from the gold to the underlying plastic (located at $z =$

Enabling Future Advances: The success of the high-Z coatings in suppressing imprint is expected to enable a range of new experiments on the NIF, where

laser beam smoothing is insufficient for most direct drive experiments. If successfully “ported” to the laser conditions there, it would not only improve planar experiments, but may also enable higher performance direct drive fusion capsule implosions there. Looking toward the inertial fusion energy application,³ the coating would not only improve fusion capsule implosion performance, but may also improve the cryogenic fuel capsule’s ability to survive injection into the hot reactor chamber due to the high reflectivity of the metal coating for infrared wavelengths.

[Sponsored by DOE/NNSA]

References

- S.P. Obenshain, J.D. Sethian, and A.J. Schmitt, “A Laser Based Fusion Test Facility,” *Fusion Science and Technology* **56**, 594–603 (2009). Also available at <http://www.dtic.mil/cgi-bin/GetTRDoc?AD=ADA521296>.
- S.P. Obenshain, D.G. Colombant, M. Karasik, C.J. Pawley, V. Serlin, A.J. Schmitt, J.L. Weaver, J.H. Gardner, L. Phillips, Y. Aglitskiy, Y. Chan, J.P. Dahlburg, and M. Klapisch, “Effects of Thin High-Z Layers on the Hydrodynamics of Laser-Accelerated Plastic Targets,” *Physics of Plasmas* **9**, 2234 (2002).
- J.D. Sethian et al., “The Science and Technologies for Fusion Energy with Lasers and Direct-Drive Targets,” *IEEE Trans. Plasma Science* **38**, 690–703 (2010).

Multi-Kilowatt Millimeter-Wave Sheet Beam Amplifiers

J. Pasour,¹ D. Abe,¹ S. Cooke,¹ B. Levush,¹ K. Nguyen,² E. Wright,² D. Pershing,² and A. Balkcum³

¹Electronics Science and Technology Division

²Beam Wave Research, Inc.

³Communications and Power Industries, Inc.

Introduction: Multi-kilowatt, broad-bandwidth, compact amplifiers in the millimeter-wave (MMW) regime (~ 30 GHz and above) are urgently needed for a variety of military applications, including electronic warfare and high-resolution radar. To achieve such challenging performance goals, researchers at NRL have replaced the round electron beam used in conventional vacuum electronic devices with a thin, ribbon-shaped sheet beam with thickness equal to the round beam diameter. A wide sheet beam can carry much higher electron current through an interaction circuit whose thinnest dimension must be less than a tenth of a wavelength for strong beam-wave interaction. At higher frequencies this condition severely limits the power that can be extracted from a round beam of modest voltage. While sheet beams are significantly more difficult to generate and transport than round beams, an even larger challenge is the development of stable and efficient sheet beam interaction circuits,

which are inherently subject to parasitic oscillations that have foiled all previous attempts at practical implementations of sheet-beam devices.

Approach: A team led by scientists and engineers from the NRL Electronics Science and Technology Division (ESTD) has devised a novel sheet beam electron gun that generates a powerful ~ 70 kW electron beam at ~ 20 kV. The beam's transverse dimensions are 0.3×4 mm, thin enough for devices at frequencies up to about 100 GHz. A specially designed permanent magnet transports the beam with 99% efficiency through a 0.4×5.5 mm beam tunnel.¹

To develop the interaction circuits needed to extract MMW power from this beam, extensive analyses and computer simulations have been performed using physics-based modeling tools developed over the past decade by ESTD scientists. Ultimately, two circuits have been conceived, developed, and demonstrated, as shown in Fig. 11. First is a 94 GHz extended interaction klystron (EIK). This narrowband structure has a high gain per unit length and can deliver very high power. Keys to achieving stable operation of this amplifier are (a) a new circuit topology that produces extremely uniform electromagnetic fields in the circuit midplane while providing good separation of adjacent competing modes, (b) incorporation of radio frequency “chokes” in the beam tunnel to prevent feedback between cavities, and (c) the implementation of small mechanical tuners in each cavity to compensate for small (~ 10 – 20 μm) fabrication errors.

tivity to stabilize the circuit against oscillations. Both amplifiers incorporate a collector depressed to -11 kV, significantly enhancing the device efficiency. The overall size of both amplifiers is determined by the magnet, which for the CC-TWA is $22 \text{ cm} \times 17 \text{ cm} \times 29 \text{ cm}$, quite compact for an amplifier of this power.

Results: The EIK is driven by either a 1 W solid state amplifier or by a pulsed 1 kW extended interaction oscillator. Adjustments are made by tuning one or more of the individual cavities and by varying the beam voltage. Figure 12 illustrates the performance as the center, or buncher, cavity is tuned by 50 MHz. The maximum output power shown in Fig. 12(b) is 7.7 kW, which is about five times that achieved by any other 94 GHz amplifier operating at such a modest voltage. The EIK is stable and its efficiency with the depressed collector is over 17%, also high for amplifiers at this frequency. Small signal gain varies from 30 to 40 dB, depending on operating parameters. Performance agrees very well with simulations by NRL's Neptune code.² The CC-TWA is driven by a round beam traveling wave tube (TWT). Measured output power at a constant drive power of 150 W is shown in Fig. 13(a), along with Neptune predictions. Figure 13(b) shows the predicted saturated output power across the operating band along with the corresponding drive power. Although a new 750 W, 32 to 37 GHz round beam CC-TWT driver will ultimately be used to validate these simulations more fully, initial measurements using a more limited driver are shown here and confirm a 10.5 kW output power at about 34

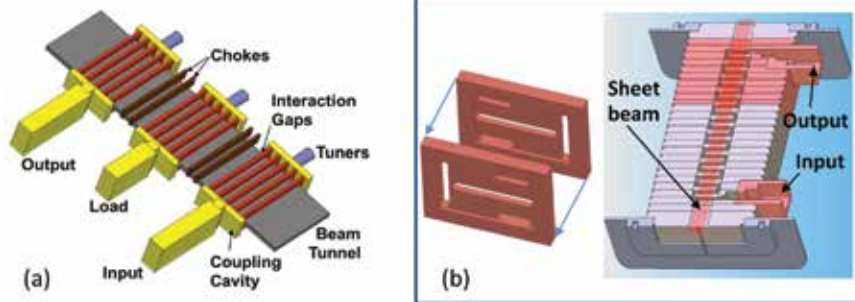


FIGURE 11 (a) EIK circuit with three identical 5-gap copper cavities. Total length is 2.2 cm. (b) Coupled-cavity TWA circuit model, showing plate fabrication technique and cutaway view of 4-cm-long assembled circuit.

The second circuit, centered at 34 GHz, is a coupled-cavity traveling wave amplifier (CC-TWA), selected for its potential for both high power and broad bandwidth. This circuit consists of 22 individual plates, each containing three coupling slots and a beam tunnel, brazed together in alternating fashion. The first 14 plates are made from cupro-nickel, with higher resis-

GHZ. Again, the measurements of Fig. 13 agree exceedingly well with Neptune simulations. The measured power represents more than a 10-fold increase relative to comparable state-of-the-art round beam CC-TWTs. The efficiency is $\sim 33\%$ with the collector depressed to -11 kV. The small signal gain is about 21 dB, decreasing by 6 dB at saturation (as is typical of TWA's).

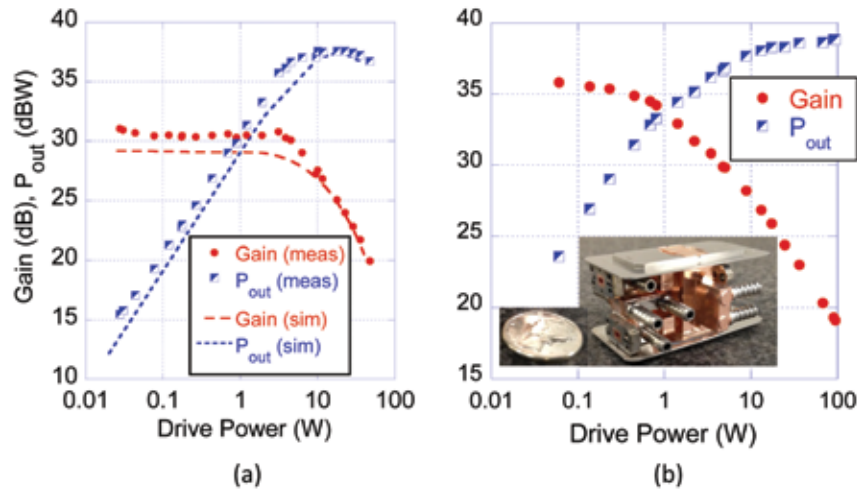


FIGURE 12 EIK gain and output power at 94 GHz vs input power at two different buncher frequencies and beam voltages. (a) Comparison of measured and simulated performance at 20.4 kV. (b) Measured performance at 21.3 kV when tuned for maximum power. Circuit photo is inset.

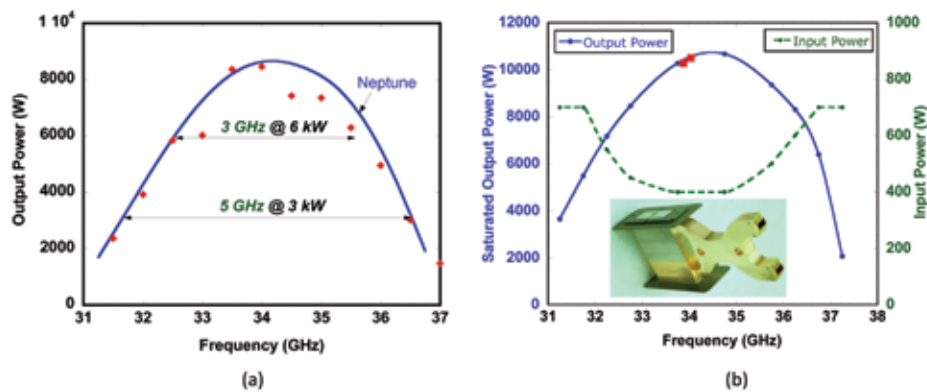


FIGURE 13 (a) Comparison of measured and simulated output power of CC-TWA at a constant 150 W drive power. (b) Neptune-predicted saturated output power and corresponding drive power across the full operating band. Red squares are initial measurements and photo of circuit is inset.

Summary: NRL researchers have demonstrated unprecedented millimeter-wave power from novel slow-wave amplifiers by employing a sheet electron beam. NRL's unique sheet beam electron gun has powered both a 10.5 kW CC-TWA at 34 GHz, with a 3 dB bandwidth of 5 GHz, and a 7.7 kW EIK at 94 GHz. The successful demonstration of these amplifiers proves that the fundamental challenges of beam transport and electromagnetic stability faced by sheet beam devices can be overcome to achieve up to an order-of-magnitude increase in output power in a compact slow-wave device with modest operating voltage (~20 kV).

[Sponsored by the NRL Base Program (CNR funded)]

References

¹ J. Pasour, K. Nguyen, E. Wright, A. Balkcum, J. Atkinson, M. Cusick, and B. Levush, "Demonstration of a 100-kW Solenoi-

dally Focused Sheet Electron Beam for Millimeter Wave Amplifiers," *IEEE Trans. Electron Devices* **58**, 1792–1797 (2011).

² S. Cooke, "GPU-Accelerated 3D Large-Signal Device Simulation Using the Particle-in-Cell Code 'Neptune,'" *2012 IEEE Thirteenth Int. Vacuum Electronics Conf. Proc.*, Monterey, CA, pp. 21–22, April 2012.

information technology and communications



166 TRIDENT SPECTRE 2013: FIREFLY: Multimodal Signatures for Increased Confidence in Remote Object Detection and Classification

168 TALON — Robust DoD Laser Communications through the Air

TRIDENT SPECTRE 2013: FIREFLY: Multimodal Signatures for Increased Confidence in Remote Object Detection and Classification

G.C. Gilbreath,¹ D.J. Bonanno,¹ C.O. Font,¹
B. Bajramaj,¹ T.J. Walls,¹ F. Pipitone,¹ and M. Sartor²
¹Information Technology Division
²RDIS, LLC, Princeton Junction, NJ

In May 2013, the U.S. Naval Research Laboratory (NRL) led a multimodal (multiple sensor) airborne data collection campaign at the 2013 Trident Spectre Exercise (TS13) in Little Creek, Virginia, cosponsored by Naval Special Warfare and the Department of Defense (DoD). This effort, entitled FIREFLY, was an adjunct experiment that flew six sensors on three aircraft that collected data using different airborne patterns and altitudes. The effort was designed to collect data on objects and vehicles of interest using multiple data types. FIREFLY was planned and executed by the NRL Information Technology Division and was underwritten by the DoD and DARPA, with leveraged support from the Army Night Vision Laboratory (NVL). The effort drew on talent from NRL's Information Technology Division and Optical Sciences Division, as well as from ten contributing contractors. Figure 1 provides sensor specifications.

The sensor modes included hyperspectral imaging (HSI) in the visible and near-infrared (VIS/NIR), mid-wave infrared (MWIR), and long-wave infrared (LWIR) portions of the spectrum. Modalities also included LWIR and visible wide area motion imagery (WAMI), synthetic aperture radar (SAR) at 1.2 GHz, lidar at 1.06 μm , and high-resolution framing cameras that were used to generate 3D data using stereoscopy through structure-from-motion. The goal of FIREFLY was to evaluate the utility of multimodal data to support problems relevant to the DoD. The NRL team has been leading the effort to combine the data types for the signatures products. To date, we have combined lidar with 3D stereo, with SAR, and with HSI. These composites have enabled automated classification of objects and tracking of vehicles with probability of detection greater than 95% with nominal false alarm rates. Other products are in development. For this effort, we have developed techniques to automatically detect and classify vehicles of interest using a variation on "tripod operators." These unique algorithm-based operators were invented at NRL¹ and adapted to the TS13 problem of quickly discriminating vehicles from other objects in a scene.

Georectified composite images were enabled by the collections. For example, a standard 2D visible image was taken of a scene and then combined with the commensurate image taken with SAR. The SAR modality identifies the metals and other manmade objects that

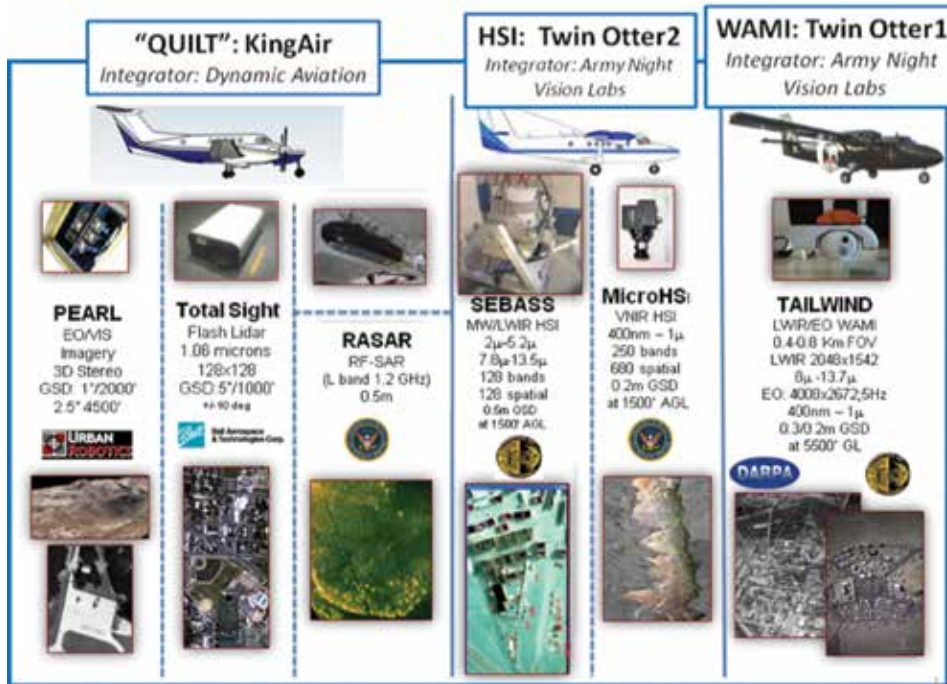


FIGURE 1
Sensors and aircraft used in the 2013 Trident Spectre adjunct demonstration FIREFLY.

are not necessarily detectable at shorter wavelengths. The 3D imaged products are also combined with the composite. The 3D image might be generated from structure-from-motion stereoscopy or from lidar. Metadata included with the image enables the analyst to not only identify objects, foliage, and other details in the scene, but also to estimate the object's geospatial position and dimensions to centimeters of accuracy. The value of such an "image" with its commensurate geospatial and dimensional accuracies is that power lines and fences, for example, can be identified to assist in mission planning, or vents can be detected for detections of chemical effluents.

Timeliness from data-collect-to-product-availability was also noteworthy. The FIREFLY team produced 3D, hyperspectral, and video-based products within 24 hours of collection that were used by the TS13 intelligence cell and quick reaction teams to plan their missions. FIREFLY products allowed 3D terrain evaluation, identification of obstacles and structures, and situational awareness through thermal imaging of the site. In particular, the TS13 mission planners indicated that some of the structures discovered by FIREFLY were not known to them through their own surveillance systems. The FIREFLY team made products available to TS13 participants through RAPTOR-X, an operational mission planning tool used outside of the continental United States (OCONUS).

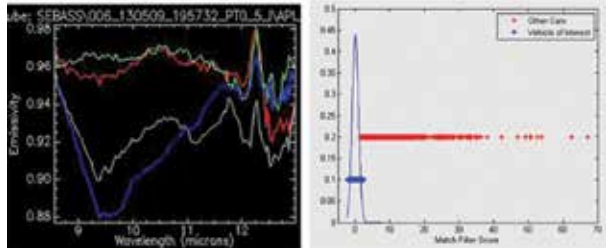
Within FIREFLY at TS13, spectral sensing was used for tagging, tracking, and locating (TTL) to find, track, and reacquire vehicles across time and geospatial locations. The goal was to capture the signature of a targeted vehicle using hyperspectral sensing and use it to reacquire the vehicle later in different locations, times, and contexts. Under TS13, scenarios were set up to capture designated vehicle targets (high value targets, or HVTs) across several days and different locations. In the exercise, only nadir data was used. Off-nadir algorithms for HSI sensing is an open area of research and was not within the scope of this effort.

The FIREFLY team was able to demonstrate vehicle detection and reacquisition of an HVT (a white Hyundai) across a time span of 6 days in populations of hundreds of vehicles (some of which were the same color and type) with only two false alarms. These false alarms were mitigated by eliminating non-vehicle targets (vehicles were detected by using 3D data and HSI detection of other cues). By using 3D classification data (stereoscopy and lidar), the false alarm rate was reduced by almost an order of magnitude (8x). The FIREFLY team was able to demonstrate that the signature of the HVT could be uniquely separated from a population of 723 detected vehicles that were present in the field of regard during a specific day collection. Figure 2 illustrates some of these results.

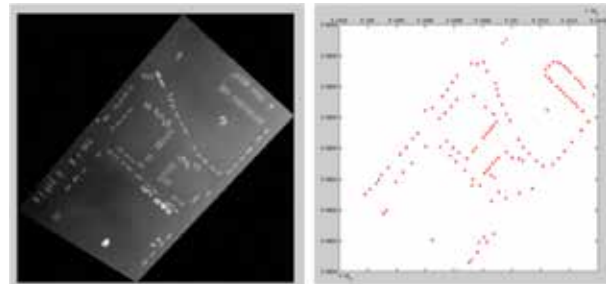
Hyperspectral wide area imagery enables vehicle detection.



High Value Target is identified with its unique HSI signature.



Shape methods are used to create a detection map to align the other modalities.



3D signatures are extracted and automated algorithms using tripod operators are used to classify vehicle types.

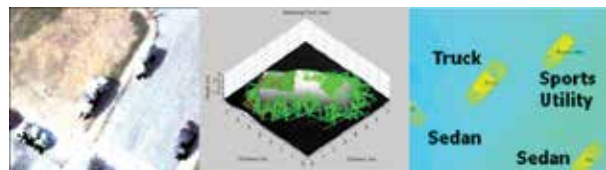


FIGURE 2

Multimodal sensing enabled the NRL team to acquire and tag a high value target and reacquire it 5 and 6 days later in different locales using the HSI + 3D composite signatures.

Techniques to generate other composite products are under way by the NRL team with their collaborators.

[Sponsored by DoD]

Reference

- 1 F. Pipitone and W. Adams, "Tripod Operators for Recognizing Objects in Range Images; Rapid Rejection of Library Objects," Proceedings of the 1992 IEEE International Conference on Robotics and Automation, Nice, France, May 1992, pp. 1596–1601 (1992).



TALON — Robust DoD Laser Communications through the Air

C.I. Moore,¹ L. Thomas,¹ W. Rabinovich,² T.N. Smith,³
D. Baker,¹ H.R. Burris,¹ R. Mahon,² D. Rabinovich,^{1,4}
W.R. Smith IV,¹ M. Vilcheck,¹ N. Walker,¹ and
L. Willstatter^{1,4}

¹Space Systems Development Department

²Optical Sciences Division

³Information Technology Division

⁴Summer student

Introduction: The Office of Naval Research and the Naval Research Laboratory, in collaboration with Exelis Inc., Novasol Inc., IJK Inc., and LGS Inc., are developing robust, low-cost, automated free space optical (FSO) terminals for the Tactical Line-of-sight Optical Network Communications Future Naval Capability (TALON FNC) program. TALON FSO terminals are eye-safe out of the aperture and capable of providing higher speed, more secure, line-of-sight communications than RF communications while also alleviating RF spectrum congestion. However, atmospheric turbulence and inclement weather can significantly affect an FSO system's performance. Numerous past FSO research and development programs have attempted to use complex technology to reduce turbulence and weather effects and improve performance. However, the successes from these systems came at a significant price in cost, size, weight, power, and complexity.

TALON is unique in its approach. It attempts to optimize performance at useful ranges (up to 70 km) and data rates (100 Mbps) for the warfighter while maintaining lower cost and simplicity. This approach results in a system that provides the attributes of FSO most important to the warfighter today, while leaving options for improvements in capabilities later. This has resulted in highly capable compact terminals that are an order of magnitude lower in cost than previous DoD attempts to develop laser communications (lasercomm) systems. As a result of these efforts, both the United States Marine Corps (USMC) and the United States Navy (USN) have expressed an interest in transitioning TALON lasercomm terminals.

TALON Testing Description: TALON is a three-phase program to incrementally develop terminals capable of transition to environmental testing and validation followed by deployment. Phase 2 culminated in June 2013 with rigorous system performance evaluations. System evaluation was conducted between 100-foot-tall masts at Camp Pendleton (Fig. 3) and over a 50 km range in a harsh environment at Naval Air Weapons Station (NAWS) China Lake in midsummer (Fig. 4).

Primary testing used NRL's MGEN testing software to quantitatively measure packet error rate and latency at data rates of 95 Mbps. Goals for this testing were to demonstrate packet error rates less than 0.1% and latencies less than 50 ms.

Secondary testing evaluated the TALON system's ability to autonomously acquire and maintain a link using each terminal's coordinates as inputs, and assessments of link quality for typical user data: VoIP, SD, and HD video cameras, chat, and file transfers.

Results: Phase 2 testing at Camp Pendleton was performed over a 4 km link with terminals mounted on 100-foot-tall masts. This testing evaluated the TALON system's ability to establish and maintain a low packet error rate and latency 100 Mbps communications link while mounted on relatively unstable masts.

The tests performed at Camp Pendleton successfully demonstrated the primary goal of establishing and maintaining a low packet error rate and latency link. Average raw packet error rates were much less than 1% and latencies were less than 50 ms.

Autonomous link establishment based on coordinates was also successfully performed but not with 100% reliability. The causes of the unsuccessful tests are known and are being remedied in phase 3.

Autonomous link maintenance after acquisition was completely successful, with tracking maintained 100% of the time with no drops in tracking despite the very high winds (>30 knots) present during the testing. Qualitative assessments were completely successful with VoIP, video teleconferencing, and chat being used as the primary communication methods between the two test sites after link establishment. These applications were also useful for demonstrations to base personnel and visitors.

Phase 2 testing at NAWS China Lake was performed over a 50 km range between Cinder Peak and Laurel Mountain. Similar tests were used at China Lake as at Camp Pendleton with the exception of autonomous link establishment, which was not tested. Systems were primarily evaluated for link quality over a long-range, highly turbulent link.

As was the case at Camp Pendleton, average packet error rate and latency were well below the goals of less than 0.1% and less than 50 ms, respectively. Tracking was excellent as well, although a few short drops occurred. In these cases, the link was automatically reestablished in less than 1 second. As at Camp Pendleton, VoIP, video teleconferencing, and chat were used as the primary forms of communication between the two sites.

Conclusions: Overall, TALON phase 2 testing results were excellent. Fundamental questions of whether



FIGURE 3
TALON terminal being raised on USMC mast (a) and mounted on mast at 100 ft elevation (b).



FIGURE 4
TALON terminal mounted on Cinder Peak at NAWS China Lake pointed at Laurel Mountain 50 km away.

the systems could operate in harsh conditions at long range and whether the systems could acquire and track from relatively unstable masts at a maximum extension of approximately 100 ft were clearly answered in the affirmative. These fundamental questions were the most important to answer in phase 2. Phase 3 is currently focusing on improvements to harden the system and to advance the automated operation of the system to allow users to reliably use these systems with minimal training and effort.

[Sponsored by ONR]



materials science and technology

A photograph of two men in a laboratory or industrial setting. The man on the left is wearing a red polo shirt and has a beard. The man on the right is wearing a green polo shirt and is sitting on a metal structure. The background shows various pieces of equipment, including what looks like a control panel with several monitors or displays.

- 172** Novel Spintronic Device for Reconfigurable Logic
- 173** Simulation of Cold-X-Ray Effects Using Intense Ion Beams
- 175** Prediction of New High Thermal Conductivity Materials for Cooling Electronics
- 176** Long-Term Hydrogen-Assisted Cracking Evaluation of Monel K-500

Novel Spintronic Device for Reconfigurable Logic

M.B. Johnson

Materials Science and Technology Division

Introduction: Spintronic devices, found in integrated electronics applications, incorporate magnetic material components, and their operation uses carrier spin to represent the binary values 0 and 1. By contrast, conventional semiconductor electronics is based on charge. Spintronic devices have excellent performance with characteristics uniquely suited to Naval applications. They have found success in low-power, high-performance, radiation-hard nonvolatile magnetic random access memories (MRAM) that serve several commercial niche markets. Products for avionics and space platforms and for extended temperature range applications are especially relevant to Navy needs.

However, spintronic devices lack power gain and other characteristics that are required for broader information processing applications where complementary metal oxide semiconductor (CMOS) circuits are dominant but draw high power. A focus of spintronics research is to combine the low-power attribute of spintronics with the broader capabilities of semiconductor logic.

Device Experiments: We describe the development of a magnetic-field-controlled avalanche diode as a novel semiconductor magnetoelectronic device.¹ In this structure (Fig. 1(a)), the electric field along the channel accelerates electrons until they have enough energy to scatter and create new carriers by impact ionization. The number of carriers increases with increasing voltage, resulting in a nonlinear current-voltage (I - V) characteristic. An external magnetic field B can be applied along an axis perpendicular to the channel (the z -axis in Fig. 1(a)). By using both p -type and n -type doped layers in the diode channel, field orientation along $-z$ deflects the electrons towards the bilayer interface where they are lost because of recombination (Fig. 1(b)). Orientation along $+z$ deflects electrons away from the interface and recombination is minimal. Thus, the magnetic field is a control parameter that changes the carrier concentration and diode conductance. For a given voltage bias, the diode has two distinct device states that are determined by the orientation of magnetic field and the device can be used as a current switch. At $V_{\text{bias}} = 11.0$ V (Fig. 1(c)), the two stable states have different output current values, $I_{\text{LOW}} = 20$ mA and $I_{\text{HIGH}} = 100$ mA.

Applications: Spintronic logic has unique attributes that enable new kinds of applications. Boolean logic gates are the base level of logic circuits. More complex

and sophisticated mathematical and logic functions are built up from subcircuit arrangements of Boolean gates. In digital semiconductor technology, these subcircuits are “hard-wired,” meaning that a single function is determined by the gate configuration when they are fabricated. Logic cells that use magnetic-field-controlled devices are reconfigurable. The configuration of a basic Boolean logic gate can be controlled by an input pulse to perform as an AND, NAND, OR, NOR, XOR, or XNOR gate. This ability gives new flexibility to the design of information processing chips. The number of basic Boolean cells on a chip can be reduced and the remaining subcircuits can perform multiple tasks

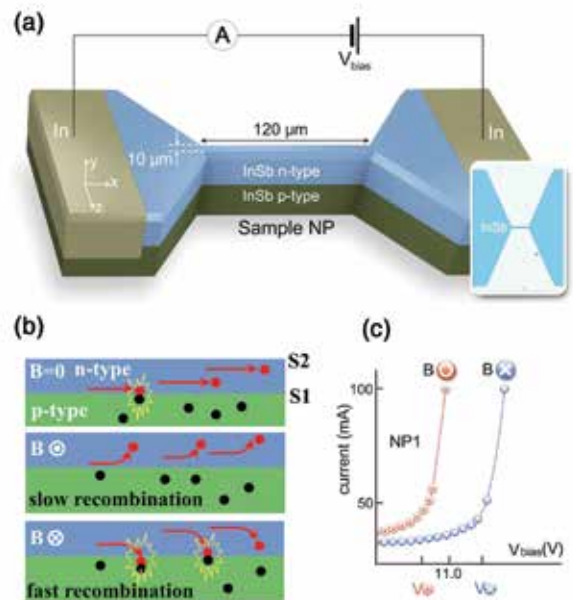


FIGURE 1

(a) A perspective sketch of an avalanche diode with a p - n bilayer channel. (b) Schematic description of electron transport. New carriers are generated when the electrons scatter in the n -layer, and are lost because of recombination when they scatter near the p - n interface. A magnetic field along $-z$ increases recombination, whereas the opposite sign field decreases recombination. (c) Current-voltage data for the device are different for the two magnetic field conditions and form the basis of digital operation.

Circuit Experiments: Prototype circuits comprising a few diodes were made for a demonstration of dynamically reconfigurable Boolean logic. Figure 2(a) is a schematic depiction of a configurable cell. Three diodes are in series with a constant voltage bias and the binary output value is either LOW (~ 35 mA) or HIGH (~ 100 mA) current. The orientation of magnetic field applied to the function selector (diode PN2) determines whether the circuit functions as an AND or OR gate. The magnetic fields at the two other diodes (NP5 and NP6) are the binary inputs. Operation of the cell can be described in qualitative terms. When the conductance of the function selector is high, that diode has a low

resistance and there is a large voltage drop V_{12} across the two input diodes. Only when both NP5 and NP6 are in a high conductance state (red trace in Fig. 1(c)) will the circuit have HIGH current output and the circuit truth table matches that of an AND gate (Fig. 2(b)). When the conductance of the function selector is low, that diode has a high resistance and voltage drop V_{12} across the two input diodes is small. Only when both NP5 and NP6 are in a low conductance state (blue trace in Fig. 1(c)) will the circuit have LOW current output and the circuit truth table matches that of an OR gate. Other simple circuits have demonstrated NOR, NAND, XOR, and XNOR operations. These circuits operate with individual pulses and require neither a clock circuit nor constant power. The result of the operation is stored in a nonvolatile way (storage requires zero power) and the result can be read out and used at any later time.

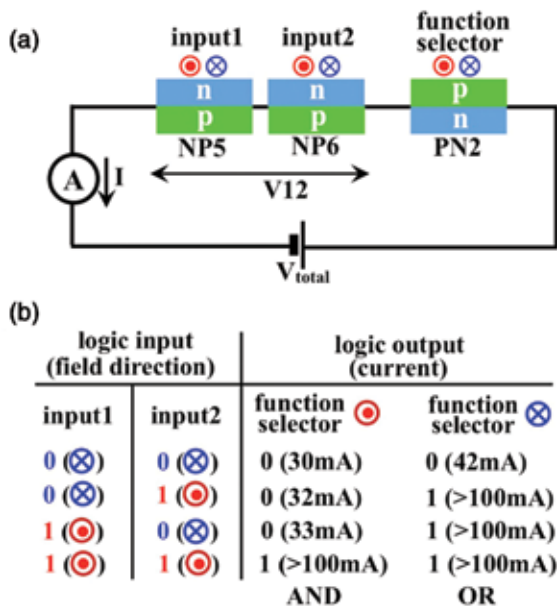


FIGURE 2
 (a) A magnetic field controlled circuit that demonstrates nonvolatile reconfigurable Boolean logic as confirmed by (b) experimentally measured truth tables.

Summary: This article describes the characteristics of a novel semiconductor spintronic device. A magnetic field controls the channel conductance of an avalanche diode and provides two characteristic states. The demonstration of a simple circuit that operates as a reconfigurable Boolean logic gate has been presented. Dynamically reconfigurable gates offer new ways to implement logic operations with low power. Other spintronic device families use electric current as input and provide output as a voltage. This new device is uniquely different: it uses current as input and also provides output as a current. Ongoing research is focused on logic cells with integrated sources of magnetic field inputs.

Acknowledgments: This work was performed in collaboration with Sungjung Joo, Taeyueb Kim, Sang-Hoon Shin, Ju Young Lim, Jin Dong Song, Joonyeon Chang, Suk Hee Han, and Kyung-Ho Shin of the Korean Institute of Technology (KIST); Kungwon Rhie of Korea University; and Hyun-Woo Lee of Pohang University. Device fabrication was performed at KIST and Pohang University. Device and circuit testing was performed at KIST. The author (NRL) contributed to designing the experiments and interpreting the results.

[Sponsored by the NRL Base Program (CNR funded)]

Reference

¹ S. Joo, T. Kim, S.H. Shin, J.Y. Lim, J. Hong, J.D. Song, J. Chang, H.-W. Lee, K. Rhie, S.H. Han, K.-H. Shin, and M. Johnson, "Magnetic-field-controlled Reconfigurable Semiconductor Logic," *Nature* **494**, 72–76 (2013).

Simulation of Cold-X-Ray Effects Using Intense Ion Beams

D.D. Hinshelwood,¹ D. Phipps,¹ G. Williams,² M. Lynch,² and G. Paderewski²

¹Plasma Physics Division

²Exelis, Inc.

Introduction: United States and United Kingdom military systems must be able to withstand intense cold X-ray irradiation. Suitable laboratory sources of cold X-rays are limited to very large facilities (for example, the ZR machine at Sandia National Laboratories). In addition to being costly, relevant X-ray fluence is only available very close to the source where debris complicates data collection. Intense MV-level proton beams are an attractive complement to cold X-rays, as they deposit energy in materials to a similar depth. Because they feature a directed flux, the material being studied can be located much further away, significantly reducing debris issues. Furthermore, relevant fluences can be produced using much smaller facilities at higher shot rate and lower cost. A series of material-response experiments on NRL's Gamble II pulsed power machine validated the use of intense pulsed proton beams to simulate cold X-ray fluence on materials of interest. Tests were carried out by the U.K. Atomic Weapons Establishment (AWE) and the U.S. Naval Surface Warfare Center. This work was performed in collaboration with Exelis, Inc. (Colorado Springs, CO), who oversaw the target diagnostics.

Gamble II: The Gamble II generator produces a 50 ns, 30 kJ ion beam. The ion beam, mostly protonic with a small carbon component, is produced by a pinch-reflex diode,¹ and then injected into 1 Torr air through

a thin foil, which removes the carbon fraction. Ionization of the gas background provides charge and current neutralization for the beam so that it propagates ballistically to the target. Varying the distance between the diode and the target varies the target fluence from 3 to 80 cal/cm². We use two operating modes, with endpoint energies/ion currents of 1.3 MV/500 kA, and 1.9 MV/400 kA. Varying the proton energy spectrum allows us to control the energy deposition profile. This is also accomplished by selectively filtering the beam using a mosaic comprising variable filter thicknesses.

Beam Characterization: It is a challenge to characterize an ion beam that is intense enough to ablate any material it encounters. We locate most diagnostics behind small apertures at the target plane with enough separation for beam expansion to provide a reduced fluence on the diagnostic. Graphite calorimeters provide the primary measure of ion-beam fluence. However, these respond on a tens of milliseconds timescale and so can be affected by late-time debris. Carbon activation by the ¹²C(p, γ)¹³N reaction, unaffected by debris, provides a useful corroboration.² Results from the two diagnostics agree within their 10% uncertainties. Activation can also provide an image of the beam: after the shot, a radiographic image plate records decay radiation from the activated carbon. Rutherford scattering of the ions off a distant foil produces a time-resolved signal from which the peak ion energy may be determined by time-of-flight. A depth-dose stack of thin (~10 μm) doped nylon films helps to diagnose the ion-beam energy spectrum. Results of both diagnostics are in agreement with calculations using the measured beam voltage and current, and published values for proton stopping.³ This verifies that there is no anomalous energy loss during transport.

Photonic displacement interferometry (PDI)⁴ is the primary target-response diagnostic fielded by our collaborators. We have constructed a separate, 4-channel PDI system to diagnose the response of known materials as an additional beam-fluence diagnostic. The beam from a fiber laser is reflected off the rear of the target in a Michelson configuration and then mixed with a reference beam from a second laser at a fixed frequency offset. Analysis of this beat signal measures the target displacement with a sensitivity below 10 nm (~0.005 waves).

In practice, a target assembly, comprising the sample under test, surrounded by an array of calorimeters and other diagnostics, is located at various distances from the diode. Figure 3 shows such an assembly mounted on Gamble II.

Materials Tests: Material response is diagnosed using multichannel PDI, along with impulse and strain measurement. The relatively long (ms) delay before

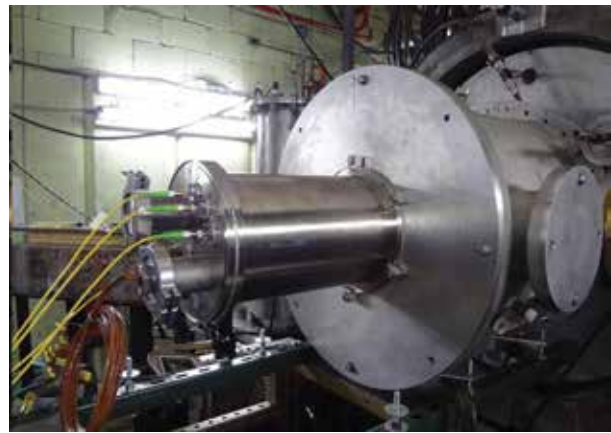


FIGURE 3
A target assembly mounted on Gamble II.

debris arrival makes total impulse measurement possible. Representative displacements obtained from PDI are shown in Fig. 4. Both relevant systems materials, and generic benchmark materials, have been tested. The material-response results are being used by our U.S. and U.K. sponsors to validate codes and to evaluate new materials of interest. Both sponsors have planned

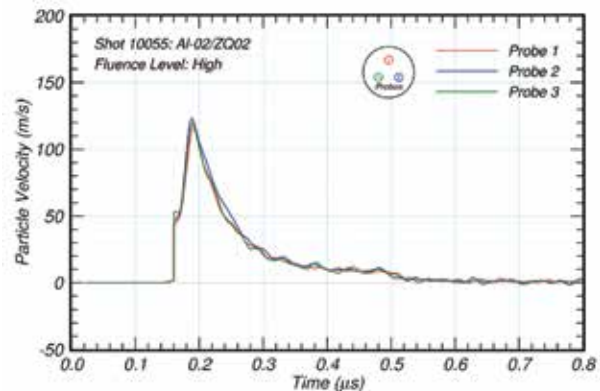


FIGURE 4
Typical rear surface particle velocity measurement in Al6061 using a multiprobe photonic displacement interferometer (PDI) at high fluence, indicating excellent beam uniformity across the face of the 32 mm diameter exposure.

successor experiments in FY2014. A separate round of experiments sponsored by the U.K. AWE is also planned in FY2014. These will involve the Navy Strategic Systems Programs organization. Having established contacts with two distinct Navy groups, we should be well positioned to respond to future Navy needs for component hardness and vulnerability assessment.

[Sponsored by the Naval Surface Warfare Center and the U.K. Atomic Weapons Establishment through the Defense Threat Reduction Agency]

References

- S.J. Stephanakis, D. Mosher, G. Cooperstein, J.R. Boller, J. Golden, and S.A. Goldstein, "Production of Intense Proton

Beams in Pinched-Electron-Beam Diodes,” *Phys. Rev. Lett.* **37**, 1543 (1976).

² F.C. Young, J. Golden, and C.A. Kapetanakis, “Diagnostics for Intense Pulsed Ion Beams,” *Rev. Sci. Instrum.* **48**, 432–443 (1977).

³ J.F. Ziegler, “SRIM-2003,” *Nuclear Instruments and Methods in Physics Research B: Beam Interactions with Materials and Atoms* **219–220**, Proceedings of the Sixteenth International Conference on Ion Beam Analysis, Albuquerque, NM, USA, June 29 – July 4, 2003, G. Vizkelethy, F.D. McDaniel, S. Thevuthasan, and J.R. Tesmer, eds. (Elsevier B.V., Amsterdam, June 2004), pp. 1027–1036, doi:10.1016/j.nimb.2004.01.208.

⁴ O.T. Strand, D.R. Goosman, C. Martinez, T.L. Whitworth, and W.W. Kuhlow, “Compact System for High-Speed Velocimetry Using Heterodyne Techniques,” *Rev. Sci. Instrum.* **77**, 083108 (2006).



Prediction of New High Thermal Conductivity Materials for Cooling Electronics

L. Lindsay,¹ T.L. Reinecke,¹ and D.A. Broido²

¹*Electronics Science and Technology Division*

²*Physics Division, Boston College*

Need for Cooling: Thermal management is becoming increasingly important for electronic devices as they continue to become faster and smaller. This is especially so for high-power, high-frequency devices used by the Navy and elsewhere in the Department of Defense. Thus, identifying new and innovative ways for managing waste heat is essential. Thermal management typically uses use high thermal conductivity, k , materials to spread heat from the active regions in devices. Diamond is an attractive candidate because it has by far the highest known bulk thermal conductivity ($k > 2000 \text{ Wm}^{-1}\text{K}^{-1}$ at room temperature, $T = 300 \text{ K}$). However, it is expensive, and quality material is difficult to produce. Thus, the identification of alternative ultra-high k materials is of great current interest. However, this requires reliable quantitative theoretical approaches for predicting k of a material, which are not currently available.

New Theoretical Tools: In nonmetallic systems, heat is transported primarily by low-frequency, high-velocity lattice vibrations, i.e., by acoustic phonons. In most systems at room temperature and higher, thermal resistance is dominated by intrinsic phonon-phonon scattering for which high-frequency optic phonons play an important role by scattering the acoustic phonons. The complex nature of this intrinsic scattering mechanism has made the development of rigorous, microscopic theoretical treatments of k challenging. As a result, theoretical approaches for calculating k have relied

on ad hoc approximations with adjustable parameters determined from experiment, and such techniques lack predictive capabilities.

In this work, a pioneering first-principles thermal transport approach has been developed that employs a full solution to the Peierls-Boltzmann transport equation for phonons with interatomic forces determined from density functional theory. This microscopic first-principles approach accurately determines the intrinsic phonon-phonon scattering and the thermal conductivity k in bulk and in novel low-dimensional materials without use of adjustable parameters. This approach can treat a wide range of systems and has demonstrated excellent agreement with measured k data for a number of materials (including diamond, silicon carbide (SiC), gallium nitride (GaN), and aluminum nitride (AlN)), thus validating its predictive power.

Cubic Boron Arsenide (BAs): This powerful theoretical approach has been used to predict that an unlikely material, cubic boron arsenide (see Fig. 5), will have a room temperature k larger than all other bulk

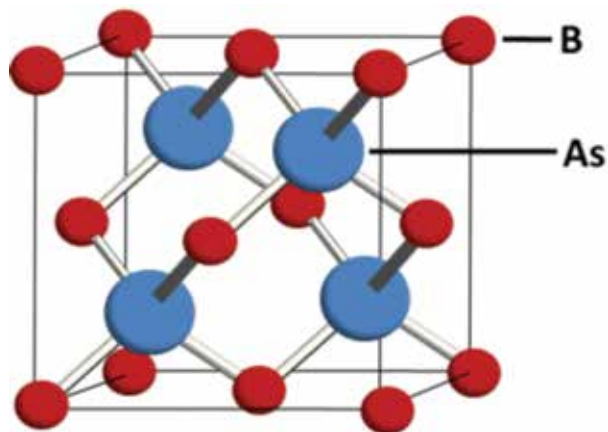


FIGURE 5
Crystal structure of cubic boron arsenide (BAs).

materials except diamond and have a k higher than that of diamond above room temperature (see Fig. 6).¹ The ultra-high k of BAs is especially surprising when comparing its vibrational properties to those of diamond. Figure 7 gives the calculated phonon frequencies vs wave vector (i.e., phonon dispersions) for BAs, silicon (Si), and diamond. The slopes of the curves give the phonon velocities. Diamond’s ultra-high k is largely understood in terms of extremely fast acoustic phonons, which carry much of the heat. From Fig. 7 it is apparent that BAs has significantly lower acoustic phonon velocities than diamond, velocities comparable to those of Si. However, the k of BAs is comparable to that of diamond, while Si has significantly lower thermal conductivity, $k = 150 \text{ Wm}^{-1}\text{K}^{-1}$ at room temperature.

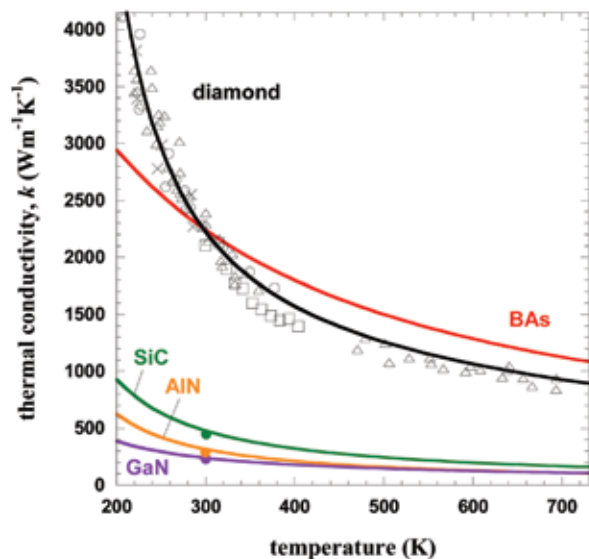


FIGURE 6
Thermal conductivity, k , vs temperature for BAs and some other high k materials. Symbols give measured k data.

The ultra-high k of BAs can be understood in terms of an unusual combination of basic vibrational properties, which include (i) a large frequency gap between the optic phonon branches and the lower frequency acoustic phonons, called the a - o gap, (ii) a bunching of the acoustic phonon branches, and (iii) isotopically pure heavy arsenic atoms. Features (i) and (ii) are illustrated in Fig. 7. Since each phonon-phonon scattering process must obey conservation of energy and momentum conditions, the large a - o gap in BAs eliminates much of the important acoustic-optic phonon scattering resistance, while the bunching of the acoustic branches severely

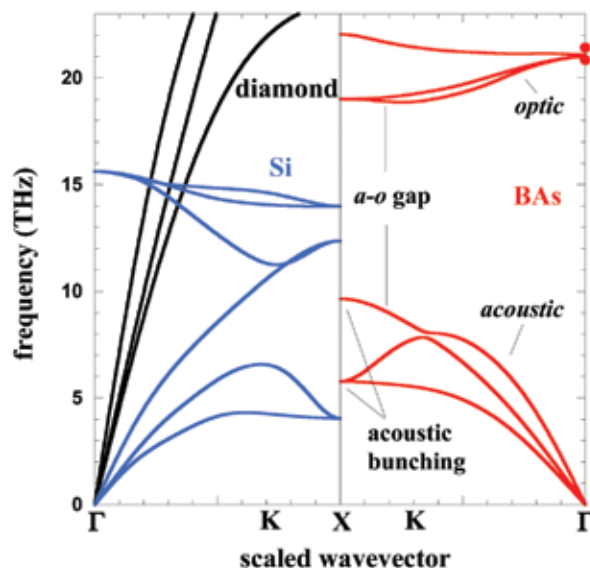


FIGURE 7
Phonon frequency vs scaled wave vector (i.e., phonon dispersion) in the $\Gamma \rightarrow K \rightarrow M$ high symmetry direction. Solid red circles give measured Raman data for cubic BAs.

restricts the all-acoustic phonon scattering. These features give much longer phonon lifetimes and higher k . Silicon, on the other hand, does not have an a - o gap or bunching of the acoustic branches, and thus it has much lower k . Further, acoustic vibrations are governed by the heavy atoms in a crystal, especially for materials with a large mass difference between the constituent atoms such as in BAs. Since the heavy As atoms in BAs are isotopically pure, the scattering of phonons from isotopic mass differences is significantly weaker than in comparable materials, like boron nitride. Thus, BAs has large thermal conductivities for both isotopically purified material, $k > 3000 \text{ Wm}^{-1}\text{K}^{-1}$, and material with naturally occurring isotope concentrations, $k > 2000 \text{ Wm}^{-1}\text{K}^{-1}$, both of which are comparable to those of diamond at room temperature.

Matching thermal expansion coefficients (CTEs) of thermal interface materials with the sensitive electronics that they are cooling is also required to avoid thermal stresses and warping. Cubic BAs has an advantageous CTE that is closely matched with that of Si,² which is ubiquitous in the electronics industry. Diamond's CTE is less than half that of Si, and the CTE of copper (another popular heat spreader) is many times larger than that of Si.

This work provides new insight into the microscopic nature of thermal transport at a quantitative level, and it illustrates the predictive power of computational techniques for thermal transport. The growth and use of high quality cubic BAs material may open new opportunities for passive cooling of state-of-the-art electronic devices. This exciting discovery has already attracted considerable interest in the materials growth and electronics engineering communities.

[Sponsored by ONR and DARPA]

References

- Lindsay, D.A. Broido, and T.L. Reinecke, "First-Principles Determination of Ultrahigh Thermal Conductivity of Boron Arsenide: A Competitor for Diamond?" *Phys. Rev. Lett.* **111**, 025901 (2013).
- D.A. Broido, L. Lindsay, and T.L. Reinecke, "Ab Initio Study of the Unusual Thermal Transport Properties of Boron Arsenide and Related Materials," *Phys. Rev. B* **88**, 214303 (2013).

Long-Term Hydrogen-Assisted Cracking Evaluation of Monel K-500

R. Bayles,¹ T. Lemieux,¹ F. Martin,¹ D. Lysogorski,¹ B. Weathers,¹ K. Williams,¹ L. Drake,¹ P. Pao,² E. Hogan,² A. Geltmacher,² T. Newbauer,³ W. Hyland,³ W. Kinee,³ M.R. First,³ A. Rubinoff,³ P. Stencel,⁴ MIDN E. Arnold,⁵ E. Knudsen,⁶ and D. Horton⁶

¹Chemistry Division

²Materials Science and Technology Division

³Excet, Inc., Springfield, VA

⁴Honeywell

⁵United States Naval Academy '11

⁶VisionPoint

Introduction: The nickel alloy Monel K-500 is a workhorse alloy for Navy immersion service. Its applications include fasteners and actuator components. However, this alloy is susceptible to hydrogen-assisted cracking (HAC), particularly in the presence of cathodic protection, the application of an electrochemical potential to suppress corrosion, which causes hydrogen to be produced on the surfaces of the protected components. HAC can lead to catastrophic failure and, due to the extremely slow diffusion of hydrogen in nickel alloy, these failures may not occur until the component has been in service for many years.

For critical components, knowledge of the response of the alloy to HAC is necessary for component life prediction and setting of inspection and replacement intervals. Fracture mechanics is a methodology that allows the application of laboratory data to structures with a variety of different geometries in which prudence demands the assumption that a crack exists at a vulnerable location in the structure.

Procedure: Two kinds of experiments were performed. One kind involved measuring the rate of hydrogen uptake in Monel K-500 over a period of more

than 1-1/2 years. The other, longer-term experiment involved exposing 108 fracture mechanics test specimens to seawater at NRL's Key West Marine Corrosion Facility for four years. The primary variables in the long-term experiments were electrochemical potential (the cathodic protection voltage) and the stress-intensity factor (SIF). The potentials ranged from minimal cathodic protection to over-protection. Within that range are the potentials of the conventional zinc anodes (-1000 mV vs Ag/AgCl) and the new low-voltage anodes (LVA, -850 mV vs Ag/AgCl). Ag/AgCl is the standard seawater reference cell that provides a basis for the measured potential. SIF is the driving force for growth of an existing crack, based on applied load and specimen geometry. In this experiment, a wide range of SIF was chosen to ensure that crack growth would not occur in some cases.

The long-term specimens used were 19 mm slices from round bar stock machined into disc compact tension (DCT) specimens (PacMan shape) having a notch, fatigue precrack and loading pin holes per ASTM E 399 and spring-loaded as shown in Fig. 8. Two bars of Monel K-500 were used, representing the upper and lower bounds of the QQ-N-286 specification. The high strength bar was "direct aged" by the producer and had a hardness of 34 Rc and the low strength bar was annealed bar, heat treated to a hardness of 26 Rc.

The hydrogen uptake experiments involved exposing 5 mm diameter "pencil" specimens to the same



FIGURE 8

Closeup of DCT specimen (left) and overview of half the tests (right); 54 more tests are out of view behind these.

electrochemical potentials as the long-term specimens. One specimen at each potential was removed for hydrogen analysis every 1000 hours during the first 15,000 hours of the overall program (the initial intended duration).

Results: The hydrogen uptake experiment showed that less negative cathodic protection potentials dramatically reduce the rate of hydrogen absorption as shown in Fig. 9 and, therefore, indicate a benefit of LVAs vs zinc anodes. The long-term fracture mechanics specimens that broke during the course of the experiment and the rest that were broken open after four years' exposure were evaluated for the presence and extent of cracking to identify a stress-intensity/potential regime that is safe. Figure 10 shows the intergranular cracking that indicates HAC. The data presented in Table 1 show a concentration of the cracking in the high-SIF, low-potential corner of the grid. There is ob-

vious scatter in the results. This program determined a potential vs SIF region beyond which cracking was not observed. This can be used to guide a fracture mechanics evaluation of component designs.

Future Work: The analysis of the broken specimens continues with an emphasis on fractographic analysis in the scanning electron microscope and further analysis to understand the cause of the scatter in the results. The program also inspired a related effort to directly measure crack growth rates in Monel K-500 that can be integrated to produce a fracture mechanics life prediction value using relatively short term experiments. A robust life prediction capability will permit extension of the present data to much longer, often relevant, times. It has also informed ongoing experiments to evaluate proposed alternative alloys to ultimately replace Monel K-500.

[Sponsored by NAVSEA]

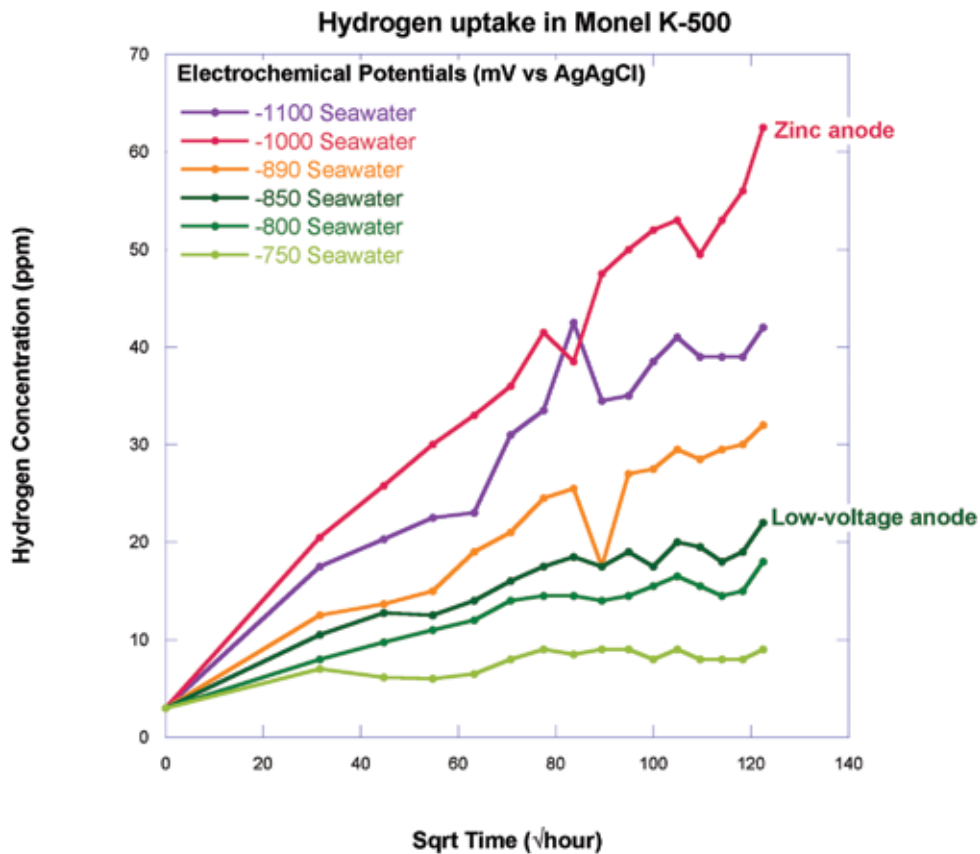


FIGURE 9 Plot of hydrogen uptake data showing that the zinc anode potential introduces the most hydrogen.

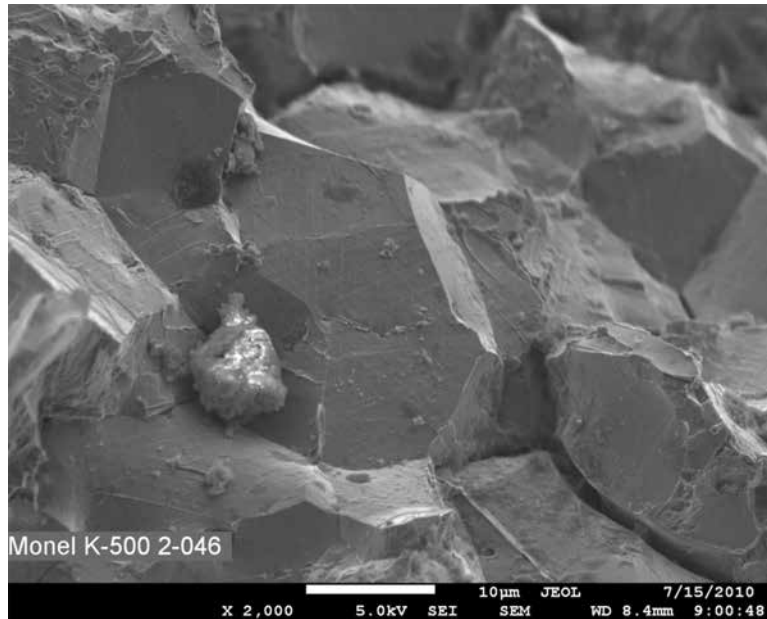


FIGURE 10
Intergranular fracture surface typical of hydrogen-assisted cracking of Monel K-500.

TABLE 1 — Failed Specimens Indicated by Date of Failure and Specimens Having Visible Crack Extension But No Failure in Four Years

		Potential (mV)						
		-1100	-1000	-890	-850	-800	-750	
High Strength	K (MPa√m)	99	200909	4 Years	☺	4 Years	☺	☺
		88	4 Years	4 Years	☺	4 Years	☺	☺
		77	4 Years	4 Years	☺	☺	4 Years	☺
		66	4 Years	☺	☺	☺	☺	☺
		55	4 Years	☺	☺	☺	☺	☺
		44	☺	☺	☺	☺	☺	☺
		33	☺	☺	☺	☺	☺	☺
		22	☺	☺	☺	☺	☺	☺
		11	☺	☺	☺	☺	☺	☺
Low Strength	K (MPa√m)	99	200909	201110	☺	☺	☺	☺
		88	☺	201005	201007	201105	☺	☺
		77	201101	☺	☺	201204	☺	☺
		66	4 Years	4 Years	☺	201304	☺	☺
		55	201008	4 Years	☺	☺	☺	☺
		44	☺	☺	☺	☺	☺	☺
		33	201109	☺	☺	☺	☺	☺
		22	☺	☺	☺	☺	☺	☺
		11	☺	☺	☺	☺	☺	☺
Test Start:	Sep-2009	Failure Date	Visual cracking on fracture face.					
Test End:	Sep-2013	☺	No visually observed cracking.					



182 Photochemistry in 3D Using Visible-Light Plasmonic-Sensitization

183 Strained $\text{In}_x\text{Ga}_{1-x}\text{As}$ HEMTs for Complementary Logic

185 Energy Distribution through Quantum Dot Anchored Nanoscale Photonic Wires

Photochemistry in 3D Using Visible-Light Plasmonic-Sensitization

P.A. DeSario,¹ J.J. Pietron,² D.R. Rolison,²

T.H. Brintlinger,³ and R.M. Stroud³

¹National Research Council Postdoctoral Fellow,
Chemistry Division

²Chemistry Division

³Materials Science and Technology Division

Introduction: Without heterogeneous photochemistry, solar fuels cannot be made because the sunlight-driven conversion of water and carbon dioxide into fuels requires catalyzed processes. The long-standing roadblock to implementation of solar fuels chemistry has been the paucity of aqueous-stable catalysts that efficiently use visible light to drive photochemical water splitting. Local surface plasmon resonances on metal nanoparticles offer a promising workaround mechanism because they can improve energetic overlap with the solar spectrum and sensitize visible-light-driven photocatalytic activity of wide-bandgap semiconductors, such as titania (TiO₂).^{1,2}

Plasmonic Sensitization: Plasmonic nanostructures efficiently absorb light due to the resonance of incident photons with the collective oscillations of valence electrons (surface plasmon resonance, SPR). When surface plasmons decay, they transfer either hot electrons or energy that can initiate photocatalytic processes. Noble metal plasmonic sensitizers, in particular Au, are broadly appealing because their SPR substantially overlaps the peak intensity of the solar spectrum and they are chemically robust. Plasmonic sensitization efficiency for gold is primarily a function of particle size and shape. In order to fully exploit the benefits of coupling oxide photocatalysts with plasmonic Au, the nanoparticulates must be size-controlled, stabilized

against aggregation, and highly dispersed among the supporting oxide particles — all without sacrificing the surface area and porosity of the host.

Composite Au–TiO₂ Aerogels: Using a guest–host sol–gel method in which thiolate-capped Au nanoparticles are added to sol–gel precursors before gelation,³ we demonstrated control over the size, shape, and dispersion of Au nanoparticles to high weight loadings when the Au is sited within the titania nanoparticulate networks that comprise ultraporous aerogel architectures.^{1–3} Characterization of the materials by transmission electron microscopy confirms that upon gelation, the Au particle becomes a component of the oxide network with size uniformity and high dispersion preserved (Fig. 1(a) and 1(b)). Each Au nanoparticle contacts multiple TiO₂ nanoparticles (Fig. 1(c)), which locks the Au nanoparticle in place and prevents agglomeration. The Au–TiO₂ composite aerogel retains the pore size distribution, cumulative pore volume, and surface area of gold-free TiO₂ aerogels. In comparison, when Au of the same size and shape is deposited on preformed TiO₂ aerogels, there is a roughly 20% to 30% loss in surface area and a loss of two-thirds of the free volume relative to the Au-free aerogel.¹

Optical Properties and Photoelectrochemical Activity: The Au–TiO₂ aerogels exhibit a broad surface plasmon resonance centered at ~550 nm that covers a wide range of the solar spectrum (Fig. 2(a)). The intensity of the SPR feature increases with increasing Au weight loading. We calculated incident photon-to-electron conversion efficiency (IPCE) values to determine the photoefficiency of plasmonically initiated water oxidation at TiO₂ and Au-modified TiO₂ aerogels as a function of wavelength. The IPCE reaches peak values between 520 and 580 nm for the Au-modified materials (Fig. 2(b)), which matches the maxima of the Au SPR and also corresponds to the peak intensity of the solar

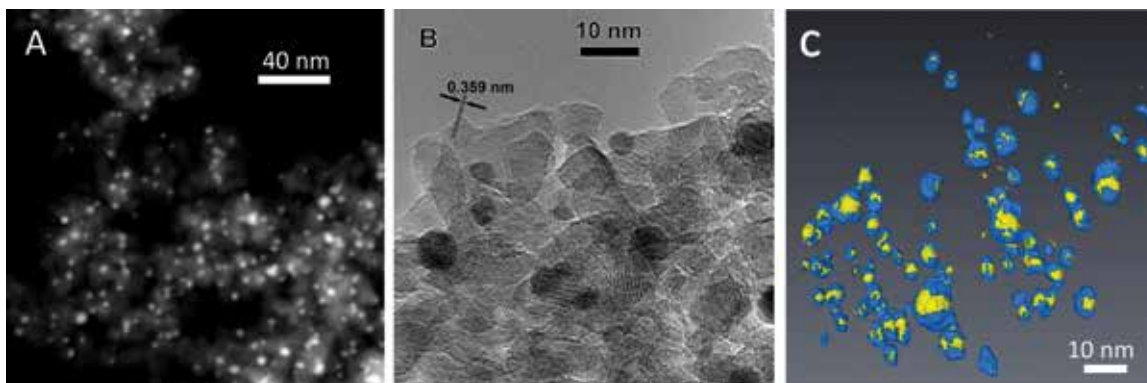


FIGURE 1

(A) Dark-field and (B) bright-field transmission electron micrographs of Au–TiO₂, 8.5 wt.% Au. (C) Tomogram of Au–TiO₂ aerogels (8.5 wt.% Au) compiled from bright-field tilt series showing TiO₂ regions (blue) within 1 nm of Au nanoparticles (yellow).

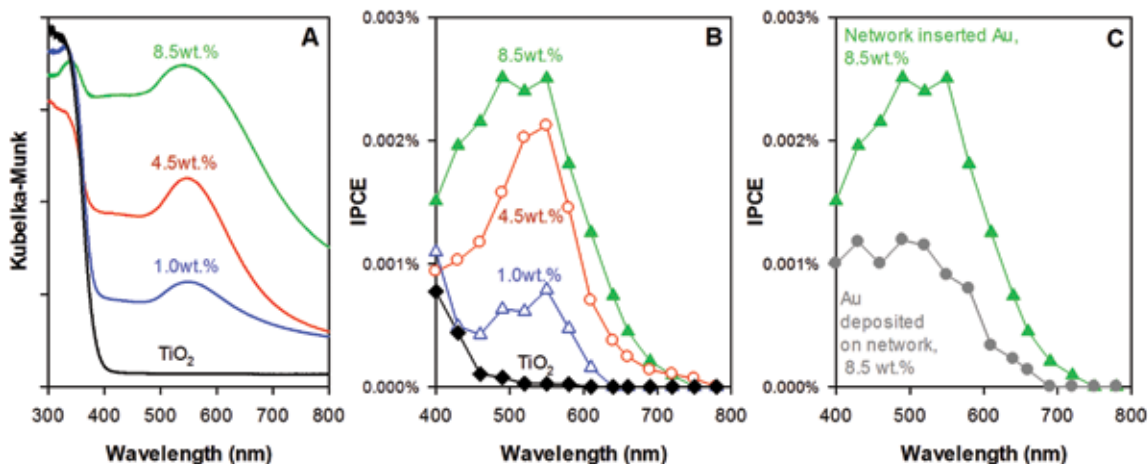


FIGURE 2
 (A) UV-visible absorption spectra for Au-TiO₂ aerogels; (B) IPCE action spectra for aerogel forms of TiO₂ and Au-TiO₂; (C) IPCE action spectra for aerogels containing 8.5 wt.% Au with network-inserted Au (green) and Au deposited on pre-formed TiO₂ aerogels (gray).

spectrum. In comparison, Au-free TiO₂ has no photo-oxidative activity at visible wavelengths. When Au of the same size, shape, and weight loading is deposited on preformed TiO₂ aerogels, the IPCE is lower at all wavelengths (Fig. 2(c)). This lower activity is due in part, but not entirely, to the decrease in surface area and free volume when Au is deposited on TiO₂ aerogels.

The photoactivity of composite Au-TiO₂ aerogels increases over the entire visible-light range with increased Au weight loading (in this study to 8.5 wt.%). In contrast, the photoactivity of Au/TiO₂ composites typically peaks at weight fractions around 1 wt.% with photoactivity decreasing at higher weight fractions. In typical Au/TiO₂ composites, deposition of plasmonic nanoparticles comes at the expense of surface area and porosity of the host oxide, and the critical factors that control sensitization efficiency — size and shape of the plasmonic nanoparticle — cannot be controlled independently of weight loading. Larger, agglomerated particles tend to be less efficient sensitizers, but because of the unique Au||TiO₂ interfacial arrangement in NRL's composite aerogels, we can maintain the small diameter and high dispersion of Au nanoparticles even at high weight loadings, thus maintaining the sensitization efficiency of individual Au particles.

Conclusion: Capturing a higher percentage of solar photons and converting them into charge carriers that participate in fuel-relevant chemistry is critical to improving the utility of photoactive semiconductors such as TiO₂ for solar fuels generation. We have shown that local surface plasmon resonances on Au nanoparticles substantially improve overlap with the solar spectrum and sensitize visible-light-driven photocatalytic activity in high surface area, mesoporous titania aero-

gels. Our composite aerogel synthetic route offers great flexibility in nanoscale photocatalyst design, enabling the incorporation of Au of controlled size and dispersion at high weight fractions without sacrificing surface area or porosity of the semiconducting architecture.

[Sponsored by the NRL Base Program (CNR funded) and ONR]

References

- 1 P.A. DeSario, J.J. Pietron, D.E. DeVantier, T.H. Brintlinger, and D.R. Rolison, "Plasmonic Enhancement of Visible Light Water Splitting with Au-TiO₂ Composite Aerogels," *Nanoscale* **5**, 8073–8083 (2013).
- 2 D.A. Panayotov, J.R. Morris, P.A. DeSario, J.J. Pietron, T.H. Brintlinger, L.C. Szymczak, and D.R. Rolison, "Ultraviolet and Visible Photochemistry of Methanol at 3D Mesoporous Networks: TiO₂ and Au-TiO₂," *J. Phys. Chem. C* **117**, 15035–15049 (2013).
- 3 J.J. Pietron, R.M. Stroud, and D.R. Rolison, "Using Three Dimensions in Catalytic Mesoporous Nanoarchitectures," *Nano Lett.* **2**, 545–549 (2002).

Strained In_xGa_{1-x}As HEMTs for Complementary Logic

J.G. Champlain,¹ B.R. Bennett,¹ J.B. Boos,¹ D. Park,¹ H.S. Newman,¹ N.A. Papanicolaou,¹ and R. Bass²

¹Electronics Science and Technology Division

²Sotera Defense Solutions, Inc.

Introduction: The Navy has a growing need for high-speed, low-power digital, analog, and mixed-signal electronics for burgeoning areas of electronic warfare (EW), high-performance radar, communications, application specific integrated circuits (ASICs),

and signal processing, particularly for miniature air vehicles (MAVs) and autonomous sensing applications that have strict weight and power requirements. Currently, silicon-based complementary metal-oxide-semiconductor (SiCMOS) devices have been the preeminent technology for digital electronics. However, the device scaling that has been required to obtain high-frequency performance has also resulted in higher dissipated power and thermal loads, limiting the overall performance of Si-based components and making them less suitable for these advanced Naval applications.

III-V-based electronics offer lower power and lower thermal operation while providing the superior electrical performance required for Naval applications; however, the desirable InP-based (n-channel) high electron mobility transistors (HEMTs) and antimony (Sb)-based p-channel heterostructure field-effect transistors (HFETs) exist in material systems at two greatly differing lattice constants, conventionally restricting their integration. In order to achieve the very large scale integration necessary to produce high-performance CMOS electronics, the constituent n- and p-channel transistors should preferably coexist on the same substrate, at a single lattice constant.

NRL researchers have now shown that it is feasible to produce both high-performance n-channel HEMTs and p-channel HFETs upon the same buffer/substrate stack, which is critical to producing high-performance, integrated electronics, paving the way for III-V CMOS. The demonstrated technology — high-performance, strained InGaAs HEMTs on an Sb-based buffer — coupled with previously developed Sb-based p-channel HFETs¹ offers an opportunity for III-V CMOS that meets the power and thermal demands of Navy applications while providing the required performance in speed.

Design and Performance: Researchers have developed a technology consisting of an AlGaAsSb buffer upon a semi-insulating substrate (InP or GaAs) with an intermediate lattice constant upon which both the InP-based HEMT and Sb-based p-channel HFET can be grown (Fig. 3), enabling the level of integration necessary for the production of III-V CMOS.

The strained InGaAs HEMTs were designed to be compatible with Sb-based p-channel HFETs and were therefore grown on an Sb-based buffer.² To study the effect of buffer and channel composition, which is directly related to lattice constant and therefore strain, on the electronic transport properties of the transistors, researchers prepared transport study samples from HEMT material grown on varying $\text{Al}_x\text{Ga}_{1-x}\text{As}_y\text{Sb}_{1-y}$ composition buffers having lattice constants ranging from 5.92 to 6.04 Å. High indium content $\text{In}_x\text{Ga}_{1-x}\text{As}$ channels ($x = 0.64, 0.8, 1$) were selected due to the

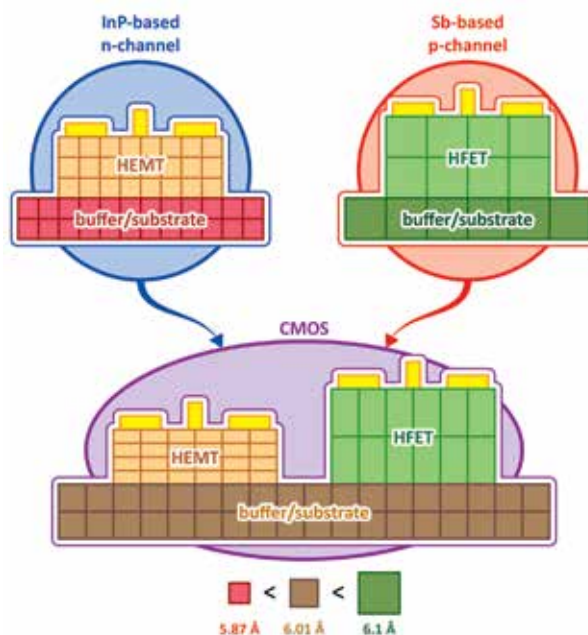


FIGURE 3 Conceptual illustration of integration of an InP-based n-channel HEMT and Sb-based p-channel HFET onto the intermediate AlGaAsSb buffer/substrate.

improved electron transport seen in such materials and because high indium content materials have slightly larger lattice constants, which may mitigate some of the strain in the HEMT due to lattice mismatch with the buffer layer. Figure 4 shows the measured electron mobility (i.e., the “speed” of the electron under a given field) within the HEMT channel as a function of buffer lattice constant for the different channel compositions, with peak mobilities observed in all cases for lattice constants in the range of 5.96 to 6.01 Å. This corresponds to the range of lattice constants where peak

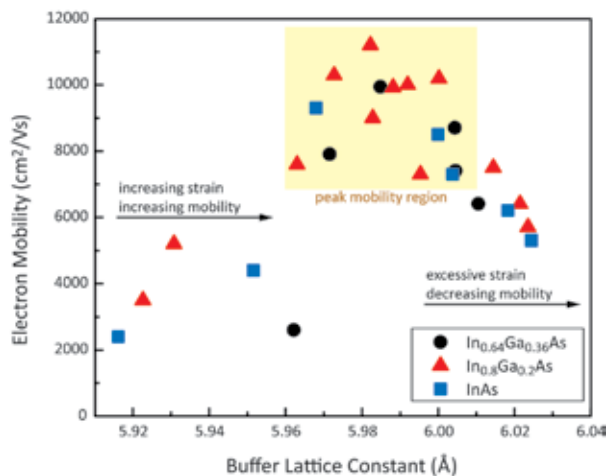


FIGURE 4 Electron mobility in the channel vs lattice constant for the three high indium content $\text{In}_x\text{Ga}_{1-x}\text{As}$ channels. The region of peak mobility between 5.96 and 6.01 Å is highlighted on the plot.

hole mobilities were observed in p-channel HFETs.¹ This confirms that buffers in this lattice constant range provide an excellent substrate for both HEMTs and p-channel HFETs.

NRL researchers then fabricated strained $\text{In}_x\text{Ga}_{1-x}\text{As}$ HEMTs with a channel composition of $x = 0.64$ and a buffer lattice constant of 6.01 \AA (corresponding to the lattice constant at which peak hole mobilities were observed for the p-channel HFETs).^{1,3} At this lattice constant, the barrier layers were strained in tension (2.4%) with the $x = 0.64$ channel strained in tension (1.6%). Transport measurements on the epitaxy used to fabricate the HEMTs showed an excellent electron (sheet) concentration and mobility of $n = 3.5 \times 10^{12} \text{ cm}^{-2}$ and $\mu = 7900 \text{ cm}^2/\text{Vs}$. Fabrication of T-gate HEMTs consisted of standard photolithography and e-beam lithography, metal evaporation, and etching techniques. Low source/drain ohmic contact resistances of $0.42 \text{ } \Omega\text{-mm}$ have been measured. Examples of standard output and transfer characteristics for the strained InGaAs HEMTs (gate length, $L_g = 100 \text{ nm}$) are shown in Fig. 5. These devices show excellent characteristics with good drain current densities up to 250 mA/mm and high transconductances up to 300 mS/mm . Scattering parameter measurements show devices capable of reaching short circuit, current gain cutoff frequencies (f_c) of 134 GHz , and maximum frequency of oscillation

(f_{max}) of 150 GHz . Further research is needed to bring these devices to state-of-the-art performance; however, these excellent results show the feasibility of this technology for achieving high-speed, low-power III-V CMOS that outperforms SiCMOS.

Summary: NRL researchers have demonstrated an alternative low-power, high-speed technology to SiCMOS, necessary for the Navy's growing need for high-speed, low-power digital, analog, and mixed-signal electronics. The technology consists of an Sb-based buffer/substrate stack, with an intermediate lattice constant in the range of 5.92 to 6.04 \AA , upon which both InP-based n-channel HEMTs (5.87 \AA) and Sb-based p-channel HFETs (6.1 \AA) can be grown. The strained InGaAs HEMTs demonstrated here ($I_D = 250 \text{ mA/mm}$, $g_m = 300 \text{ mS/mm}$, $f_r = 134 \text{ GHz}$, $f_{max} = 150 \text{ GHz}$) can be combined with previously developed Sb-based p-channel HFETs to enable the production of high-performance III-V CMOS.

[Sponsored by ONR]

References

- B.R. Bennett, M.G. Ancona, and J.B. Boos, "Compound Semiconductor for Low-Power p-Channel Field-Effect Transistors," *MRS Bulletin* **34**, 530–536 (2009).
- B.R. Bennett, T.F. Chick, J.B. Boos, J.G. Champlain, and A.A. Podpirka, "Strained InGaAs/AlInAs Quantum Wells for Complementary III-V Transistors," *J. Crystal Growth* **388**, 92–97 (2014).
- B.R. Bennett, T.F. Chick, M.G. Ancona, and J. B. Boos, "Enhanced Hole Mobility and Density in GaSb Quantum Wells," *Solid-State Electronics* **79**, 274–280 (2013).

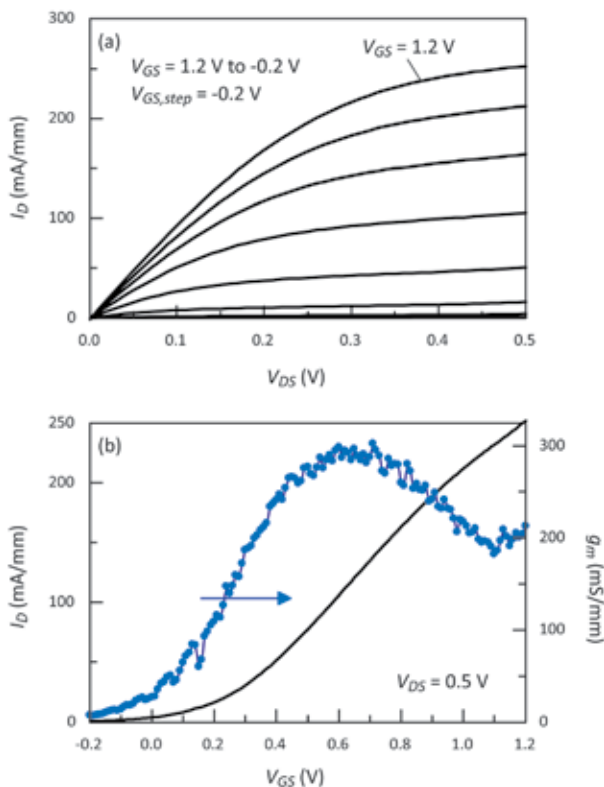


FIGURE 5 Example of standard (a) output and (b) transfer characteristics for the strained InGaAs HEMTs.

Energy Distribution through Quantum Dot Anchored Nanoscale Photonic Wires

C.M. Spillmann,¹ S. Buckhout-White,² E.R. Goldman,¹ I.L. Medintz,¹ M.G. Ancona,³ M.H. Stewart,⁴ K. Susumu,⁵ A.L. Huston,⁴ and W.R. Algar⁶
¹Center for Bio/Molecular Science and Engineering
²George Mason University
³Electronics Science and Technology Division
⁴Optical Sciences Division
⁵Sotera Defense Solutions, Inc.
⁶University of British Columbia

Introduction: A primary goal in nanotechnology is the development of systems that harness energy from an external source and direct it through a nanoscale network. Such systems are widespread in the light-harvesting complexes of photosynthetic bacteria and

green plants, but analogous artificial systems are poorly developed because of the difficulties of organizing the requisite photoactive materials at the nanoscale. One promising approach to this challenge that we have explored is to use deoxyribonucleic acid (DNA)-based architectures, where the specificity of Watson-Crick base-pairing, the stiffness of double-stranded DNA, and the availability of custom sequences make this a powerful approach for the self-assembly of complex structures. By chemically modifying specific sites along the DNA helix with dye molecules that can relay energy, one can convert these DNA assemblies into designer wires for directing photonic energy. In this article, we summarize the efforts of our multidivisional team to produce simple structures of this type in which a double-stranded segment of DNA is transformed into an active nanoscale photonic wire and sensitized by a quantum dot (QD) antenna (see Fig. 6).

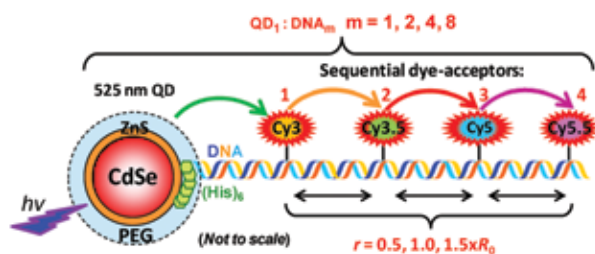


FIGURE 6

Schematic of a central QD donor assembled with a DNA photonic wire; only one wire is shown for clarity. Pertinent characteristics examined in these structures include fluorophore pairings, the interfluorophore distances, and the number of arms displayed around the QD, which are doubled incrementally from 1 to 8. These variables are highlighted in red.

Harvesting and Distribution Strategy: At the center of the photonic wire designs described herein are cadmium selenium–zinc sulfide (CdSe–ZnS) core-shell QDs synthesized at NRL. These unique nanomaterials offer several advantages for use as the primary light-harvesting antenna, including broad absorption coupled to strong photoluminescence (PL), biocompatibility over a wide range of pH and ionic concentrations, and sufficient surface area for coupling of multiple photonic wires.

The fully assembled constructs consist of these QDs decorated with one or more photonic wires. The latter are composed of DNA duplexes that display up to four dyes at specific sites (Fig. 6), with each photoactive element chosen to have large spectral overlap with its neighbors, meaning that the emission spectrum of a given donor fluorophore has significant overlap with the absorption spectrum of the next downstream acceptor fluorophore (Fig. 7). This creates a relay chain such that the QD, as the primary donor, is able to transfer energy to the first acceptor, Cy3, which, in turn, is

able to donate energy to the next downstream acceptor, Cy3.5, and so forth. The energy relay mechanism uses Förster resonance energy transfer (FRET), where an exciton from a donor is transferred to a proximal acceptor fluorophore through a dipole-dipole coupling interaction. In this way, a full construct with five fluorophores (the QD plus the organic dyes) will involve four FRET relay steps and is termed a FRET cascade.

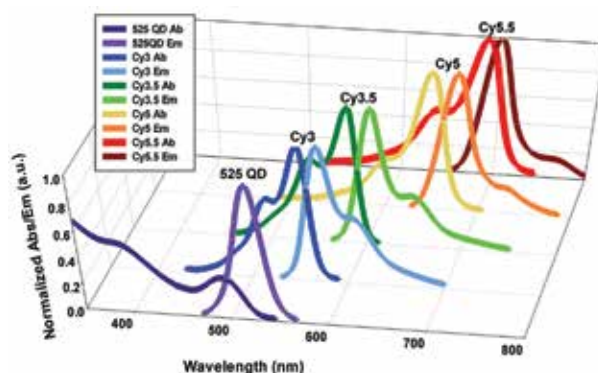


FIGURE 7

Three-dimensional plot showing the absorption and emission of the initial light-harvesting QD donor along with the sequential donor/acceptor of Cy3, Cy3.5, Cy5, and Cy5.5 cyanine dyes.

Energy Transfer Efficiency: The inherently modular DNA-based design of this photonic wire system allows us to control key variables and thereby follow and understand the various energy transfer processes. These variables include (i) the number of wires per QD ($m=1,2,4,8$ in Fig. 6), (ii) the spacing between each fluorophore (r in Fig. 6), and (iii) the composition of each photonic wire, i.e., fully decorated with four fluorophores vs having one, two, or three fluorophores present at a designated position.¹

Mechanistically, following QD excitation, absorbed photon energy is emitted and relayed through downstream acceptor fluorophores and various PL emission spectra are recorded. Figure 8(a) shows representative PL spectra as the construct is built up from only the initial QD donor (red and green curves) to the full QD-4 dye construct (pink curve). Each composite curve is then decomposed into contributions from the individual fluorophores (Fig. 8(b)). These data are in turn used to assess the donor loss and acceptor sensitization, as well as the overall end-to-end efficiency of the system. Figure 8(c) summarizes the latter as a function of both the particular construct and the number of photonic wires per QD. In the full construct (pink), we demonstrate a remarkable end-to-end efficiency approaching 10%. We note that this is almost a two orders of magnitude improvement over a first-generation system developed a few years prior.² Analyzing the results within the context of Förster theory suggests near-ideal

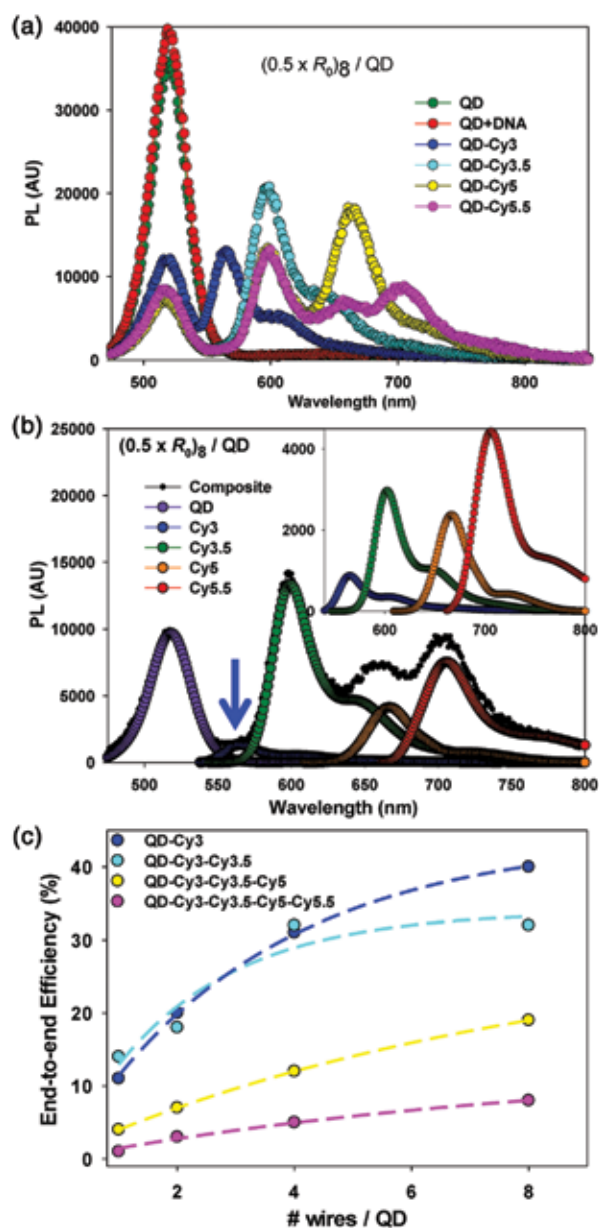


FIGURE 8
 (a) Representative FRET progression with an average of eight DNA-wires coupled to the QD. Excitation for all samples was at 400 nm. Note the decrease in QD PL and increase in Cy-dye sensitization. (b) Composite spectrum of full QD-Cy3-Cy3.5-Cy5-Cy5.5 eight DNA-wire construct in (a) with overlay of the deconstructed contributions from each fluorophore. The contribution from Cy3 is indicated by the blue arrow. Inset: corresponding FRET-sensitized contributions for the Cy3 through Cy5.5 dyes. (c) End-to-end efficiency of the QD-photonic wire constructs as a function of number of fluorophores per wire and number of wires per QD.

behavior when the photonic wires have two sequential acceptor fluorophores (Cy3 and Cy3.5). As additional dyes are added to each wire, the poor photophysical performance of the last two acceptor dyes (Cy5 and Cy5.5) leads to significant transfer losses.

These results demonstrate improvement in exciton transfer efficiency along photonic wires as we better understand nanoscale energy distribution. Thus, we have developed a nanoscale system capable of distributing energy and, perhaps more importantly, defining the design rules necessary to improve these systems so they are relevant to energy harvesting applications. Overall, development of these types of energy harvesting systems has important ramifications for next-generation warfighter capabilities and battle system components. Clearly, warfighter demands for energy in all forms will only grow, and energy harvesting and power sources must become more efficient while shrinking down dramatically in size/weight. Such constructs as discussed here can form the basis for artificial photosynthetic systems that can harvest energy to power nanoscale sensors and electronics.

Acknowledgments: The authors acknowledge ONR and the NRL Institute for Nanoscience for financial support.

[Sponsored by ONR and NRL NSI]

References

- ¹ C.M. Spillmann, M.G. Ancona, S. Buckhout-White, W.R. Algar, M.H. Stewart, K. Susumu, A.L. Huston, E.R. Goldman, and I.L. Medintz, "Achieving Effective Terminal Exciton Delivery in Quantum Dot Antenna-Sensitized Multistep DNA Photonic Wires," *ACS Nano* 7, 7101–7118 (2013).
- ² K. Boeneman, D. Prasuhn, J. Blanco-Canosa, P. Dawson, J.S. Melinger, M. Ancona, M. Stewart, K. Susumu, A. Huston, and I.L. Medintz, "Self-assembled Quantum Dot-Sensitized Multivalent Photonic Wires," *J. Amer. Chem. Soc.* 132, 18177–18190 (2010).

ocean science and technology



190 Ballast Water Compliance Testing

192 Direct Measurements of Tensile Strength of Artificial Marine Flocs under Microscopic Micromanipulation

194 Laser Profiling System for Laboratory Sediment Beds

197 Biogeochemical Control of the Particle Flux in River-Dominated Coastal Regions

Ballast Water Compliance Testing

L.A. Drake,¹ T.P. Wier,² J.F. Grant,³ M.R. First,² S.H. Robbins-Wamsley,² S.C. Riley,² M.N. Tamburri,⁴ and C.S. Moser²

¹Chemistry Division

²Excet, Inc., Springfield, VA

³Battenkill Technologies, Inc., Manchester Center, VT

⁴Chesapeake Biological Laboratory, University of Maryland Center for Environmental Science, Solomons, MD

Introduction: Water — and living organisms within it — is taken aboard ships into ballast tanks and cargo holds to manage the draft, stability, trim, and stress on the vessel. As awareness grew that organisms transported in ballast water may become nuisance species in the waters into which they are discharged, national and international attention became focused on the issue of ship-mediated biological invasions, and standards limiting the discharge of living organisms in commercial vessels' ballast water were promulgated (Table 1). In order to meet the discharge standard, most vessels will likely install a “ballast water management system” (BWMS) to treat the water by, for example, combining physical separation (e.g., filtration) and disinfection (e.g., ultraviolet radiation or electrochlorination).

appropriately. If an additional examination of the ballast water is warranted, a sample could be collected and analyzed.

Water Sample Collection: To determine, with statistical confidence, the number of living organisms in water with a sparse population of organisms (here, ballast water meeting the discharge standard), relatively large volumes of water (e.g., cubic meters) must be concentrated, and samples must be collected to ensure they are representative of the volume of interest. To that end, a flow-through sampling device was designed, constructed, and validated at the land-based ballast water treatment test facility at NRL-Key West.¹ To accommodate shipboard design requirements, an updated prototype was constructed. It consisted of two filter housings (each containing a 35 µm mesh filter bag to capture organisms ≥50 µm), a “whole water” (unfiltered) sampler (to capture organisms ≥10 µm and <50 µm), and its own pump and computer controller (Fig. 1). In validation trials at NRL-Key West, the skid operated as designed, and there was no significant difference in mortality or in the number of living organisms captured in the filter skid vs a plankton net, the device typically used to collect plankton.² Next, the filter skid was installed aboard a bulk carrier in the Great Lakes. Validation trials again showed the skid operated as designed. For example, the coefficient of variation of the

TABLE 1 — Ballast water discharge standards.

Organization and standard	Living organisms ≥50 µm in minimum dimension ^A	Living organisms ≥10 µm and <50 µm in minimum dimension ^B	Toxigenic <i>Vibrio cholerae</i> ^C	<i>Escherichia coli</i>	Intestinal enterococci
USCG Discharge Standard	<10 m ⁻³	<10 mL ⁻¹	<1 cfu 100 mL ⁻¹	<250 cfu 100 mL ⁻¹	<100 cfu 100 mL ⁻¹
IMO Regulation D-2 Ballast Water Performance Standard	<10 m ⁻³	<10 mL ⁻¹	<1 cfu 100 mL ⁻¹ or <1 cfu g ⁻¹ (wet weight zoopl.)	<250 cfu 100 mL ⁻¹	<100 cfu 100 mL ⁻¹

^ANominally zooplankton. ^BNominally protists. ^CSerotypes O1 and O139. cfu = colony forming unit, IMO = International Maritime Organization, USCG = U.S. Coast Guard, and zoopl. = zooplankton.

When vessels arrive in port, a means to determine compliance with the discharge standard will need to proceed quickly, so as not to impede operations. As such, the initial determinations of compliance will likely be made without directly enumerating the exact number of all living organisms in the ballast water discharge. For example, as a first step, the BWMS logs might be examined to show the system had been used

water flow rate through the filter skid was less than 20% (Fig. 2). It was not feasible to compare the filter skid to a plankton net aboard the vessel, but the filter skid captured living, soft-bodied organisms, and the community structure of samples collected in the filter housings was similar to that in the whole water samples.



FIGURE 1
 Photograph of the shipboard filter skid (the filter housings, each containing a 35 μm filter bag, are the silver, oblong canisters).

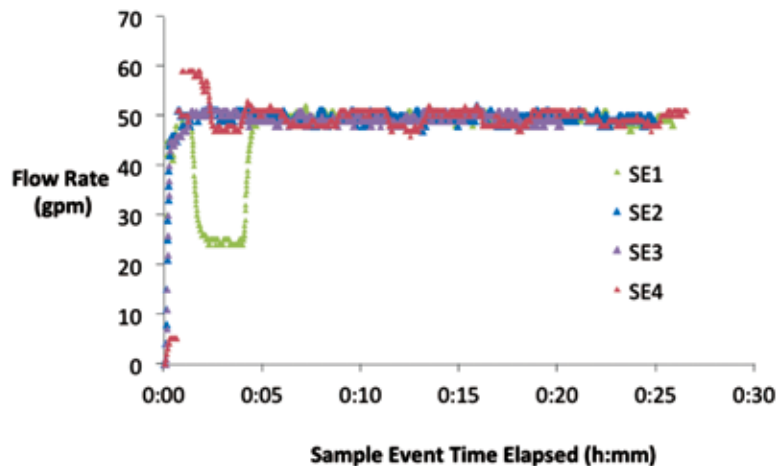


FIGURE 2
 Water flow rate through the filter skid during shipboard trials. The colored triangles represent data from each sample event (SE). The large excursions from the target flow rate were due to variations in flow in the main ballast pipe.

Compliance Tools: When a ballast water sample is analyzed, the first step will likely use “indicative analysis,” that is, measurement to determine gross non-compliance with the discharge standard (e.g., exceedance of the standard by 10- or 100-fold). For example, the operational characteristics of the BWMS may be evaluated (e.g., by measuring the concentration of residual chemicals), or living organisms may be evaluated (e.g., by measuring a bulk metric, such as chlorophyll a). Once a representative water sample is collected (as above), analysis will proceed, ideally with a hand-held tool that will quickly yield reliable data.

Of course, any tool used to determine compliance must be rigorously vetted. To assess, validate, and select compliance tools, NRL, with colleagues at the University of Maryland, the University of Michigan, and Moss Landing Marine Laboratories, has developed a framework consisting of three parts: a proof-of-concept stage, a validation and verification stage, and a final selection stage.³ Such a series of steps will provide confidence that compliance tools generate repeatable, accurate results. The framework is accompanied by a case study using variable fluorescence, which is an approach used to approximate the concentration of living photoauto-

trophs (in the context of ballast water, photoautotrophic protists in the $\geq 10 \mu\text{m}$ and $< 50 \mu\text{m}$ size class). The case study describes laboratory and field studies that indicate variable fluorescence is a promising metric to gauge compliance. Indeed, the focus of compliance tool development by commercial vendors is, at present, on variable fluorescence, as it can be used to determine the physiological status of photoautotrophs rapidly (within minutes).

Summary: As ballast water regulations enter into force, sampling and analysis methods will be required for compliance testing. A flow-through filter skid was designed, constructed, and validated, and these trials showed it to be an appropriate device for sample collection. Regarding sample analysis, tools will be required to rapidly assess ballast water, and prior to their implementation, they will need to be validated. To that end, a validation framework was constructed to ensure any ballast water compliance tools yield robust and reliable data.

Acknowledgments: The U.S. Coast Guard (USCG) Office of Environmental Standards (CG-OES-3) and the USCG Research and Development Center (RDC) sponsored this work, which does not represent official USCG policy. Throughout this research, Richard Everett and Regina Bergner (CG-OES-3), as well as Penny Herring, Chris Turner, and Lew Lewandowski (RDC) provided advice and guidance. William “B.J.” Kinee, Barron Stringham, and Samuel Howarth assisted with the construction of the filter skid, and Diane Lysogorski (Section Head, Naval Research Laboratory Code 6136 and Director, Center for Corrosion Science and Engineering, Key West, FL) supported this work. The American Steamship Company generously provided access to the vessel. We are grateful to all.

[Sponsored by the U.S. Coast Guard]

References

- ¹ M.R. First, E.J. Lemieux, W.B. Hyland, J.F. Grant, C.S. Moser, S.C. Riley, S.H. Robbins-Wamsley, M.K. Steinberg, T.P. Wier, and L.A. Drake, “Validation of a Closed-Housing Filter Skid for In-Line Sampling of Aquatic Organisms,” *J. Plankton Res.* **34**(4), 321–331 (2012).
- ² L.A. Drake, C.S. Moser, S.C. Riley, S.H. Robbins-Wamsley, T.P. Wier, J.F. Grant, P.R. Herring, and M.R. First, “Validation Trials of a Shipboard Filter Skid (p3SFS) Demonstrate its Utility for Collecting Zooplankton,” *Mar. Pollut. Bull.* (in press).
- ³ L.A. Drake, M.N. Tamburri, M.R. First, G.J. Smith, and T.H. Johengen, “How Many Organisms are in Ballast Water Discharge? A Framework for Validating and Selecting Compliance Monitoring Tools,” (in review).



Direct Measurements of Tensile Strength of Artificial Marine Floccs under Microscopic Micromanipulation

A. Abelev¹ and P. Amarasinghe²

¹*Marine Geosciences Division*

²*National Research Council Postdoctoral Fellow*

Introduction: Most sediments in near-shore and coastal areas are represented by mixtures of granular sediments, such as gravels, sands, and silts, and of cohesive materials such as clays. This second group of materials exhibits properties and behaviors that are often markedly different from the former group and are governed by some unique physico-chemical interactions¹ not present or not consequential in the granular material group. These cohesive materials, in the presence of water, plentiful organic matter (e.g., polysaccharides and humic acids), and dissolved salts, are engaged in a slew of short- and long-range force interactions that include forces such as van der Waals and double-layer.² As a result of these characteristics, clayey materials are not (or are rarely) present in the aqueous environment as individual particles, as would be the case with gravel and sand grains, but are part of complex and variable aggregates, often called floccs, which contain clay minerals, organic components, and occasionally small granular (silt) particles.

Modeling the interaction, transport, erosion, and deformation of these sediments can take many forms; discrete element approaches (e.g., Ref. 3) are common and gaining strength with the continuous increase in computing power and the ability to handle larger domains and more complex element-to-element physical laws. While this has direct and immediate effect on modeling granular materials, modeling cohesive aggregates, or floccs, presents challenges, as often the common mechanical interaction laws are not applicable or not very accurate in representing these relatively loosely bound and amorphous clumps of matter, which can range from tens to hundreds of microns or more,^{4,5} in some cases. In these cases, a fundamental understanding of mechanical behavior and strength of individual floccs as a function of their ingredients in an aqueous medium is needed. This is best provided by direct mechanical measurements, whereby an individual flocc is loaded, deformed, and fractured to yield information on strength and deformability characteristics of the floccs. Such a system has been designed and constructed at the NRL Marine Physics Branch of the Marine Geosciences Division.

Experimental Methods: The micromanipulation system developed is shown in Fig. 3, including an

overall view (top right) and a schematic representation (bottom right). The system includes an ability to test individual flocs by using a combination of rigid and flexible micropipettes; a single floc can be located in suspension, attached to a rigid micropipette under suction, and positioned where a second flexible pipette is pierced through it. The rigid holding pipette is then moved away from the flexible one until the floc is fractured in tension (Fig. 3, bottom left). A close-up of a sample slide with the two pipettes is shown in Fig. 3 (top left). The optically recorded deformation of the flexible pipette, as observed under the microscope, can be related to the force imposed on the floc via a pipette calibration. This pipette calibration consists of hanging

to the moment of fracture, where the flexible pipette is bent from its initial position. The top right part of Fig. 4 shows the final fractured floc, split approximately down the middle. The fracture area is estimated from the measurements of the recorded digital video of the entire loading sequence, assuming symmetry of the floc and of the rupture surface. Additional imaging of multiple flocs demonstrates that this assumption of symmetry holds quite well, even though no two flocs appear exactly alike.

The series of measurements conducted so far included flocs composed of Na-montmorillonite clay mineral (Clay Mineral Society, Chantilly, VA), guar gum (a polysaccharide that closely resembles natural

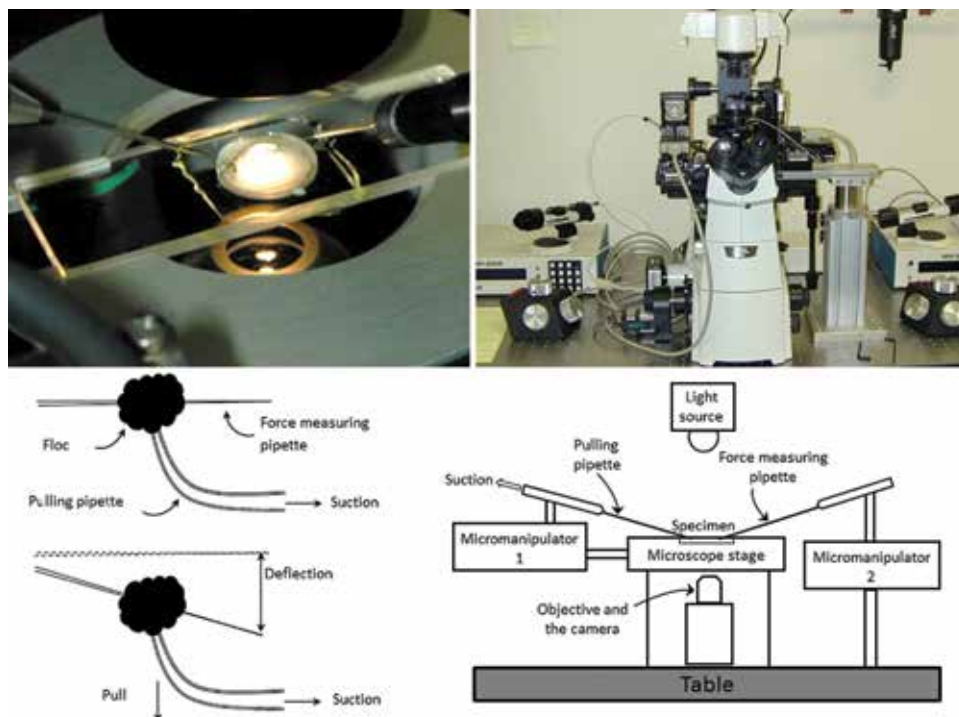


FIGURE 3 NRL micromanipulation system: overall view (top right), schematic representation (bottom right), floc fracturing in tension schematics (bottom left), and a close-up of the sample slide with the two pipettes (top left).

small segments of a copper wire (of precisely known density and dimensions) near the tip in a cantilever fixed configuration. This procedure produces a reliable and repeatable pipette calibration curve, relating displacement to force. Microscope measurements also allow for estimation of the size of the floc and of the floc rupture area, thus allowing us to compute the failure tensile stress at the time of floc rupture.

Results and Discussion: A typical test showing the two micropipettes with the tested floc are shown in Fig. 4. The top left part of the figure displays an initial position and the bottom left shows applied load, close

marine organic matter), and artificial sea salt. The suspension prepared included clay concentration of 5 g/L, 5% of guar gum relative to clay, and salinity of 35 PSU (typical ocean water), and was prepared imitating natural estuarine and littoral formation processes.

All floc tests performed indicated brittle or near-brittle (with elements of plastic behavior) fracture modes with little observable floc deformation prior to failure and only at a larger tensile stress levels. Recorded maximum tensile force is plotted vs the floc fracture area in Fig. 4 (bottom right). The overall average of 15 trials resulted in tensile strength of the flocs of 667 ± 189 Pa. A rather wide standard deviation is expected,

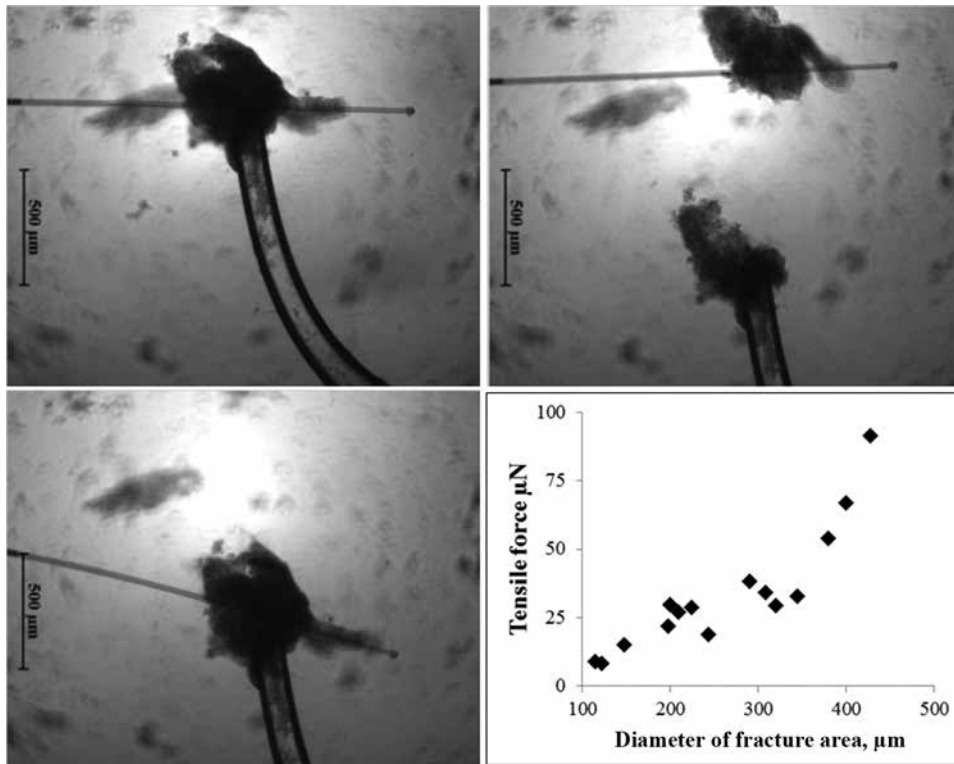


FIGURE 4

A test, showing the two micropipettes with the floc attached, showing initial position (top left), near maximum force applied (bottom left), floc after fracture (top right), and a result of a series of tests, showing tensile force plot vs diameter of the fracture area.

considering the complexity and the delicate nature of the manual measurements and the natural variability of the flocs and their internal structure.

Overall, the system of an inverted microscope, micromanipulators, and custom drawn micropipettes demonstrated the ability to conduct direct measurements of load-deformation and fracture response of simulated marine clayey flocculated material, laying the groundwork for direct and more physically based incorporation of this type of material into discrete element models.

[Sponsored by ONR]

References

- ¹ A. Anandarajah and P.M. Amarasinghe, "Discrete Element Study of the Swelling Behavior of Na-Montmorillonite," *Geotechnique* **63**(8), 674–681 (2013).
- ² Y. Furukawa, J.L. Watkins, J. Kim, K.J. Curry, and R.H. Bennett, "Aggregation of Montmorillonite and Organic Matter in Aqueous Media Containing Artificial Seawater," *Geochemical Transactions* **10**(2), doi:10.1186/1467-4866-10-2 (2009).
- ³ J. Calantoni and C.S. Thaxton, "Simple Power Law for Transport Ratio with Bimodal Distributions of Coarse Sediments under Waves," *J. Geophys. Res.* **113**, C03003 (2008).
- ⁴ A. Abelev, "Examination and Manipulation of Clay Aggregates – Initial Inquiry," NRL Report NRL/FR/7420--11-10,206, Naval Research Laboratory, Washington, DC (2011).
- ⁵ D. Bouyer, A. Liné, and Z. Do-Quang, "Experimental Analysis of Floc Size Distribution under Different Hydrodynamics in a Mixing Tank," *AIChE J.* **50**, 2064–2081 (2004). ♦

Laser Profiling System for Laboratory Sediment Beds

A.M. Penko,¹ A. Bordelon,² and B. Landry³

¹Marine Geosciences Division

²Naval Research Enterprise Internship Program

³University of Illinois

Introduction: Understanding the formation of three-dimensional (3D) bedforms on the seafloor resulting from fluctuating and interacting waves and currents is vital to numerous coastal processes such as sediment transport, wave attenuation, boundary layer development, and seafloor acoustic properties. Despite extensive laboratory investigations conducted to study sediment transport, most work has either reduced the problem to two dimensions (vertical and with the dominant flow) or has focused on constant and equilibrium flow conditions. For example, the equilibrium state of bedforms (their size and shape after many hours of constant forcing) is fairly well known. Historical laboratory and field data have been combined to formulate empirical equations calculating equilibrium bedform height and length based on the wave conditions. How-

ever, limited work exists on the transitional nature of bedforms from one equilibrium state to another and the effects of the transitional states on bottom boundary layer dynamics. Additionally, recent findings have demonstrated the importance of 3D analysis (vertical, along-, and cross-flow)¹ and the role of the transitional state of bedforms under changing flow conditions in sediment transport and bedform migration.² By using a state-of-the-art laser bed profiling system, we can study the 3D and transitional nature of bedforms. The laser bed profiling system measures the changing 3D bed surface due to varying flow conditions in a laboratory flow tunnel. The system includes a fan beam laser projecting a laser line on the bed in the along-flow direction while a high-precision motor shifts the laser in across the width of the tunnel. Simultaneously, a camera captures images of the laser projection on the bed. Images are post-processed with custom algorithms to quantify the spatial and temporal changes of the bed surface with submillimeter accuracy. The resulting time-dependent elevation data are analyzed to extract bedform heights, lengths, migration rates, and three-dimensionality.

Bed Profiling System and Experiment: The laser bed profiling system is mounted above the Small-Oscillatory Flow Tunnel (S-OFT) in the Sediment Dynamics Laboratory at NRL, Stennis Space Center. The flow tunnel has a 2 m long test section and a flow cross section of 25 cm × 25 cm (Fig. 5). Oscillatory flow is generated

with a piston flywheel to drive sediment transport and ripple formation. The profiling system includes a 520 nm, 75° fan beam, continuous wave laser that projects a 3 mm wide and 1 m long laser line on the bed in the along-flow direction. A high-precision stepping motor shifts the laser and camera 20 cm across the width of the tank in 1 cm steps at ~0.6 Hz, while a DSLR camera with a 10 mm fisheye lens captures images of the laser line at every step, resulting in 21 images per scan. One complete scan of the bed takes approximately 35 s. The image size is 5184 × 3456 pixels, resulting in an average of 5 to 6 pixels/mm resolution.

In order to examine the 3D bed transition occurring during changing flows, we performed an experiment that was initialized with bedforms generated by a higher energy flow and measured the resulting bed change caused by a decrease to a lower energy flow. The higher energy flow ran continuously for 17 min (291 wave periods) to generate the rippled bed that would initialize the measurements. Then, the laser bed profiling system began taking measurements as the flow was decreased to a lower energy. The system ran continuously for 5.5 h (8344 wave periods), taking a 35 s scan across the width of the tank and a 60 s pause before scanning back in the opposite direction, resulting in the bed surface elevation of an area approximately 80 cm by 20 cm every 95 s.

Results: The raw images captured by the DSLR camera are post-processed in MATLAB to rectify the

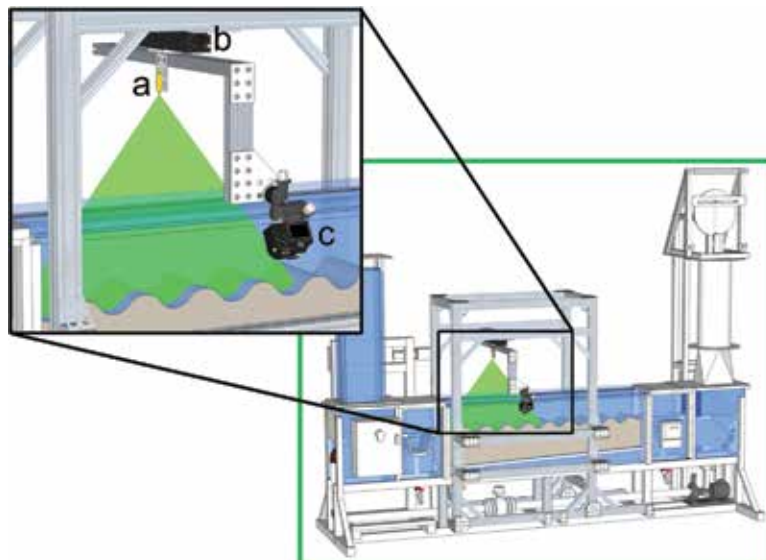


FIGURE 5 Schematic drawing of NRL's Small-Oscillatory Flow Tunnel (S-OFT) and zoomed inset of the laser bed profiling system. The system includes a fan beam continuous wave laser (a) that projects a 3 mm wide and 1 m long laser line on the bed in the along-flow direction. A high-precision motor (b) shifts the laser and camera 20 cm across the width of the tank in 1 cm steps at ~0.6 Hz. A DSLR camera with a 10 mm fisheye lens (c) captures images of the laser line at every step, resulting in 21 images per scan.

fish-eye lens distortion, extract the laser line, correct for camera view refraction, and assign dimensioned coordinates to the laser line to quantify the spatial and temporal changes of the bed surface. Rectification of the fish-eye images requires intrinsic properties of the lens. Figure 6 shows the raw and rectified images of the calibration checkerboard and one laser line. Custom MATLAB algorithms then extract the location of the laser line from each image and apply a corrective 2D-spatial transformation³ using the checkerboard calibration image to assign a dimensioned coordinate system

(x, z) to the pixels in the laser line. The cross-flow horizontal (y) coordinate is determined from the location of the step motor. Lastly, the laser line coordinates are corrected for the refraction of the camera view through the tunnel wall (3 cm thick acrylic) and water (distance depends on location of camera). The 21 along-flow horizontal bed elevations from each scan are stacked to obtain the 3D surface elevation of the bed at every time step (~95 s). Figure 7 plots the bed surface elevation after 17 min of the higher energy forcing and after 5.3 h of the lower energy forcing.

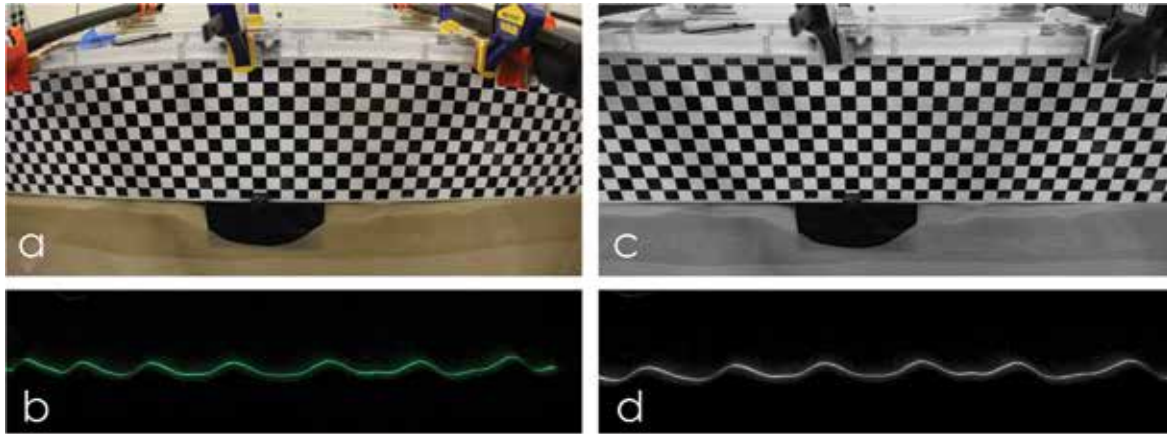


FIGURE 6 Shown are the distorted raw images taken with the 10 mm fish-eye lens of (a) the calibration checkerboard and (b) the laser line on the bed. The images are rectified using intrinsic properties of the lens to obtain the undistorted images for the (c) calibration to a dimensioned coordinate system from the checkerboard and (d) extraction of the laser line coordinates.

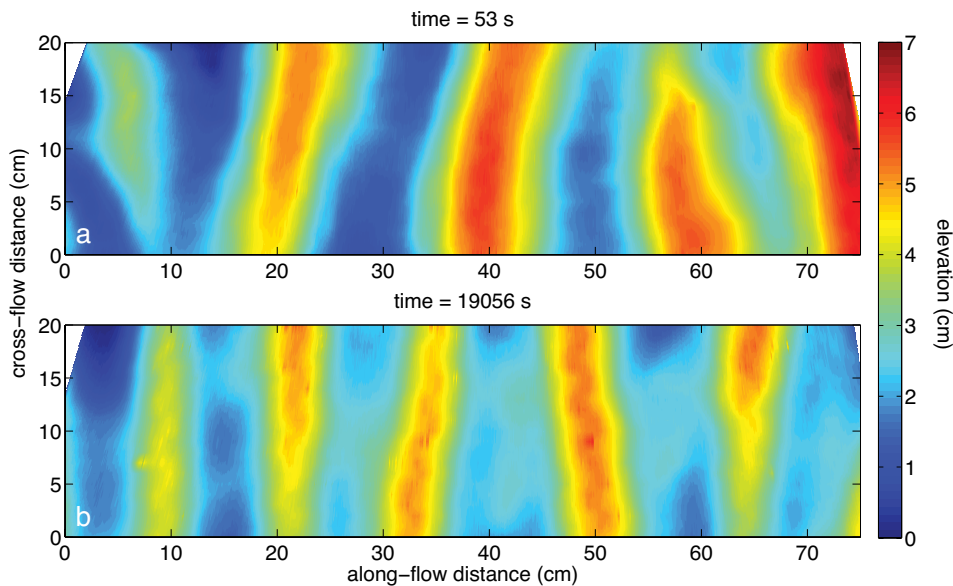


FIGURE 7 Contours of the bed surface elevation (a) after 17 min of higher energy forcing and (b) after 5.3 h of lower energy forcing. The bedforms decreased in wavelength and height, the crests became more peaked, and the troughs became flatter. Both times illustrate the 3D nature of the bedforms.

Summary: The size and shape of bedforms on the seafloor have a significant effect on bottom roughness and sediment transport in the nearshore coastal zone. We can quantify the impact of the evolving seabed surface on boundary layer dynamics by measuring the time-dependent bed evolution and examining the effect of varying flows on bedform migration and sediment transport in the laboratory. The laser bed profiling system is state-of-the-art in that it allows for continuous measurements at low power, in conjunction with other instruments, and without interfering with the environment. A better understanding of seabed evolution will benefit Naval operations including oceanographic forecasting, navigation and trafficability, and the search for mines on the seafloor.

Acknowledgments: The authors thank Tim Kooney and In Mei Sou (Code 7434) for their help with the laboratory setup and the running of the experiment. Special thanks also to Meg Palmsten (National Research Council Postdoctoral Fellow) for her enlightening discussions about image processing.

[Sponsored by ONR]

References

- ¹ A.M. Penko, J. Calantoni, S. Rodriguez-Abudo, D.L. Foster, and D.N. Slinn, "Three-Dimensional Mixture Simulations of Flow over Dynamic Rippled Beds," *J. Geophys. Res.- Oceans* **118**, 1543–1555, doi:10.1002/jgrc.20120 (2013).
- ² J. Calantoni, B.J. Landry, and A.M. Penko, "Laboratory Observations of Sand Ripple Evolution Using Bimodal Grain Size Distributions under Asymmetric Oscillatory Flows," in *Proceedings 12th International Coastal Symposium* (Plymouth, England), D.C. Conley, G. Masselink, P.E. Russell, and T.J. O'Hare (eds.), *J. Coastal Res.*, Special Issue No. 65, pp. 1497–1502 (2013).
- ³ B.J. Landry, "Sand Bed Morphodynamics under Water Waves and Vegetated Conditions," University of Illinois at Urbana-Champaign, Ph.D. dissertation, <http://hdl.handle.net/2142/24055> (2011).

Biogeochemical Control of the Particle Flux in River-Dominated Coastal Regions

Y. Furukawa,¹ A.H. Reed,¹ and G. Zhang²

¹*Marine Geosciences Division*

²*University of Massachusetts, Amherst*

Introduction: Riverine particles undergo a rapid transformation when they reach the land-ocean interface. The rapid succession of hydrodynamic and biogeochemical regimes forces the particles to flocculate, settle, and enter the sediment pool. However, the net effect (i.e., net rates of floc growth and settling) depends on the nature of the particles, especially on

the types and quantities of organic matter, which varies widely between different rivers as well as within a single river due to seasonal climate and land use variability. We found that the flocculation dynamics of riverine particles is a complex function of organic matter types, quantity, aqueous phase biogeochemistry, and hydrodynamics. We quantified the complex dynamics by employing the laboratory flocculation experiments and population balance equation model (PBE) using model mixtures of pure montmorillonite and organic molecules (i.e., guar gum, xanthan gum, humic acid). Both conceptual and quantitative models for the fate of riverine particles (i.e., a rapid flocculation and settling vs slow flocculation and transport offshore) were established.

Background: When riverine suspended particles are transported downstream and enter land-ocean interfaces and estuaries, they undergo a rapid transformation including flocculation and settling. This is caused by the rapid succession of hydrodynamic and biogeochemical regimes.¹ The rate and magnitude of this transformation are important. If the transformation is rapid, then the riverine particles will flocculate, settle, and enter the bottom sediment pool within the immediate vicinity of the river mouth. If the transformation is slow, the riverine particles will remain suspended to yield optically and acoustically turbid water.

However, a generalized, robust, and comprehensive understanding of this transformation has not fully been achieved. This is because the net effect depends on the nature of the particles, especially on the types and quantities of organic matter, which varies widely between different rivers as well as within a single river due to seasonal climate and land use variability. Consequently, the purpose of this study was to evaluate the effect of different types of organic matter species on the estuarine and coastal flocculation of suspended particles.

Methods: For each experimental run, 100 mg of soil montmorillonite powder was combined with an appropriate mixture of milli-Q water and organic matter (guar gum, xanthan gum, or humic acid) stock solution, as well as artificial seawater (ASW), to yield a 400 mL aqueous mixture. The total suspended solid in each experimental run was 250 mg L⁻¹. The mixing ratio was determined such that the organic carbon to mineral weight ratio varied between 0% and 9%, and salinity varied between 0 and 17.5 psu. Montmorillonite, milli-Q water, and the organic matter (OM) stock solution were combined and stirred for at least 5 min before ASW was added. Once ASW was added, the floc size distribution of the suspended materials was measured every 5 to 10 min using the laser diffraction technique (see below) until the size distribution reached the

temporal steady state. The solution pH was monitored using a combination electrode calibrated with NBS buffers, and was adjusted to be between 6.9 and 7.1 using 0.1 N NaOH or 0.1 N HCl. The steady-state median diameter (d_{50}) is reported from each experimental run in this study.

The floc size distribution of the montmorillonite-OM suspensions was characterized using the CILAS 1190 laser diffraction particle size analyzer. Whereas the laser beams were activated only intermittently (i.e., every ~5 min) for the time-series size measurements, the stir paddle and peristaltic pump stayed on for the entire duration of each run. For all experiments, the stir paddle was operated at 210 rpm, and the peristaltic pump was operated at 60 rpm.

Results and Discussion: Among the organic matters tested, guar gum is the most effective in enhancing the flocculation (Fig. 8). However, the effect is nonlinear. The steady-state median floc size exhibits the maximum value at around 2% loading. When the guar gum loading exceeds 2%, the floc size is smaller. The effect of salinity is negligible, meaning that the overall shapes of the organic matter vs d_{50} plots are similar for the guar gum + montmorillonite systems at all different salinity values. Whereas the magnitude is much smaller, xanthan gum also enhances flocculation (Fig. 9). Besides the magnitude of the flocculation, xanthan gum differs from guar gum in that its flocculation is affected by salinity. The effect of xanthan gum is insignificant at salinity = 0 psu, while the effect is more pronounced

in higher salinity solutions. The nonlinear nature of the effect is also apparent. At salinities of 7 and 17.5 psu, the greatest flocculation occurs when the xanthan gum loading is approximately 2% TOC. At higher TOC loading levels, the steady state floc sizes are smaller. Meanwhile, humic acid does not affect flocculation, as the humic acid plots in Fig. 10 exhibit slopes that are nearly zero regardless of the salinity.

Conceptual Models for Estuarine Flocculation:

The schematic diagram shown in Fig. 10 summarizes that the effect of organic matter on montmorillonite flocculation is diverse and nonlinear. These observations may be illustrated by the following conceptual models:²

1. Humic acid exerts steric repulsion at a wide range of salinity values. As a result, humic acid does not affect flocculation at either low or high salinity.
2. The positive flocculation behavior of biopolymers is likely due to the polymer bridging.
3. The nonlinear nature of the biopolymers as the flocculant is likely due to the difference between the clay-biopolymer bond and biopolymer-biopolymer bond.³ Single strands of polymers can act as bridges by adsorbing onto the montmorillonite surface at both ends of the polymer strands. The attachment between clay surfaces and polymer ends may be due to hydration pressure or noncharge transfer Lewis acid-base interactions. Meanwhile, as homoflocculation between biopolymer molecules alone is unlikely because of the hydrophilicity,

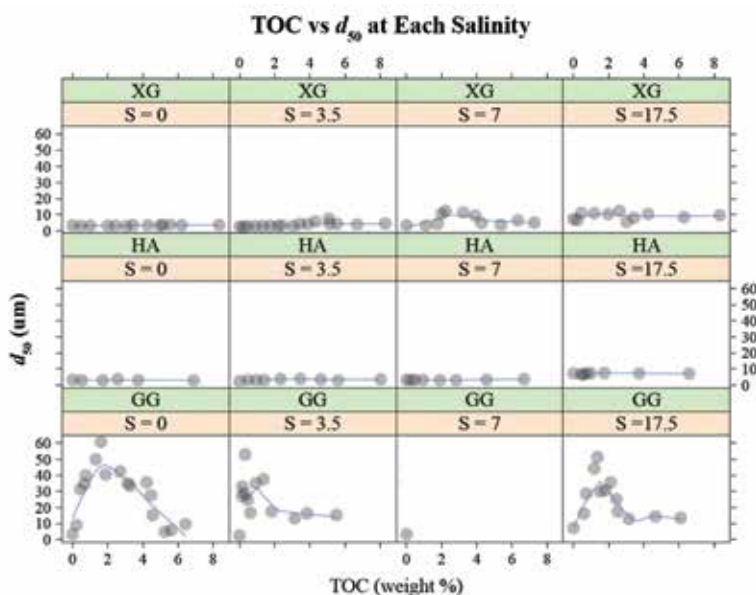


FIGURE 8

The mean steady-state floc diameter of the montmorillonite suspensions (d_{50} , μm) with a range of organic matter loadings (xanthan gum (XG), humic acid (HA), and guar gum (GG)). The organic matter loadings are expressed in terms of the total organic carbon (weight % carbon over total solids, TOC).

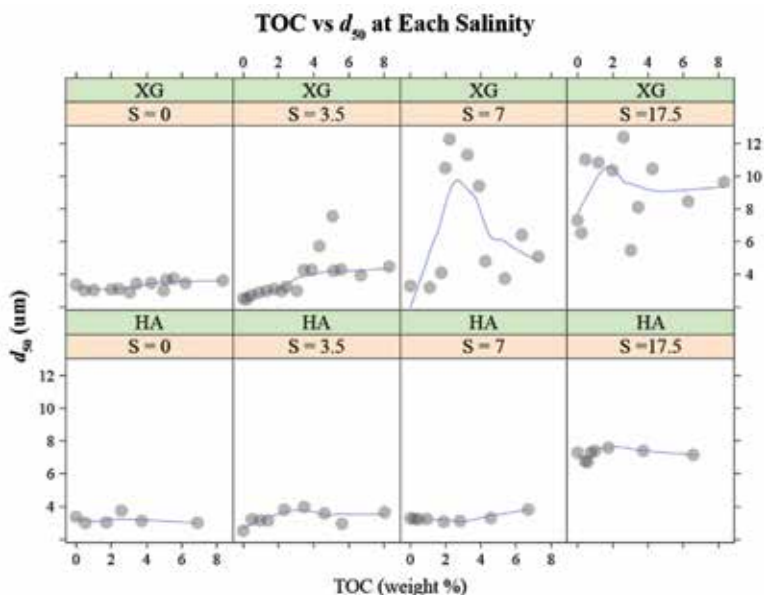


FIGURE 9
 These plots show the same data as in Fig. 8 for XG and HA but on a different y-axis scale to illustrate the difference between XG and HA.

multiple layers of biopolymers on the clay surface due to excess biopolymers may lead to fewer bridges and less flocculation.

- Salinity influences the xanthan gum flocculation but not the guar gum flocculation. Ionic xanthan gum becomes less polar at higher salinities due to specific adsorption of cations. The reduction in polarity can lead to the reduction in repulsive hydration as well as the reduction in electrostatic repulsion. Consequently, more polymer bridging would form. For nonionic guar gum, a change in salinity affects neither the polarity and the resulting repulsive hydration, nor the electrostatic repulsion.

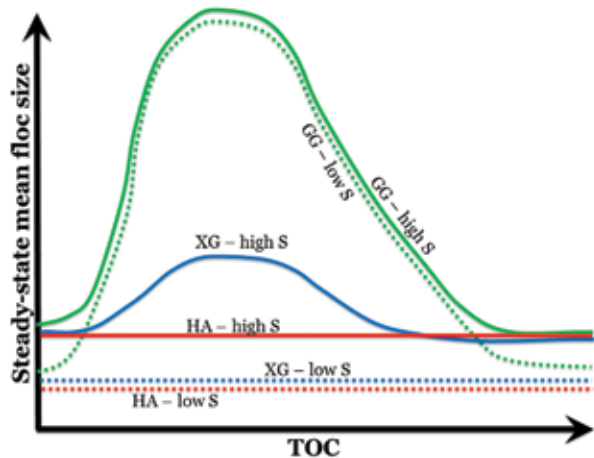


FIGURE 10
 Schematic diagram showing the effect of various organic matter (GG: guar gum; XG: xanthan gum; HA: humic acid) on the flocculation of aqueous montmorillonite suspension at low (~0 psu) and high (~7–17.5 psu) salinity.

Acknowledgments: YF designed the experiments and conducted the size analysis. AR selected the field stations and carried out the sample collection. GZ advised YF in the experimental design and participated in the manuscript draft. All authors read and approved the final manuscript. This study was supported by NRL/ONR.

[Sponsored by the NRL Base Program (CNR funded)]

References

- R. Dalrymple and K. Choi, "Morphologic and Facies Trends through the Fluvial-Marine Transition in Tide-Dominated Depositional Systems: A Schematic Framework for Environmental and Sequence-Stratigraphic Interpretation," *Earth Sci. Rev.* **81**(3-4), 135–174 (2007).
- Y. Furukawa, A. Reed, and G. Zhang, "Effect of Organic Matter on Estuarine Flocculation: A Laboratory Study Using Montmorillonite, Humic Acid, Xanthan Gum, Guar Gum, and Natural Estuarine Floccs," *Geochem. Transact.* **15**(1), doi:10.1186/1467-4866-15-1 (2014).
- T. van de Ven and B. Alinec, "Heteroflocculation by Asymmetric Polymer Bridging," *J. Colloid Interface Sci.* **181**(1), 73–78 (1996).

202 Infrared Gradient Index Optics for Multiband Imagers

203 Broadband Nonlinear Metamaterial

Infrared Gradient Index Optics for Multiband Imagers

D. Gibson, S. Bayya, and J. Sanghera
Optical Sciences Division

Introduction: Infrared (IR) imaging is becoming ubiquitous in DoD missions as it affords the warfighter situational awareness in day or night and in adverse atmospheric conditions. IR imaging is used in each of the four infrared atmospheric transmission bands: near- (NIR, 0.9 to 1.7 μm), short-wave (SWIR, 1.7 to 3 μm), mid-wave (MWIR, 3 to 5 μm), and long-wave (LWIR, 8 to 14 μm) on a variety of platforms including ship-board, airborne, ground combat, and soldier-carried devices. Mission objectives, the environment in theater, and cost determine the IR band to be used. In many applications, coverage of multiple bands with a large field-of-view (FOV) is needed (e.g., LWIR for threat detection and imaging through smoke, MWIR for threat identification, and SWIR for obscurant penetration, such as fog and camouflage). Since the different bands require different refractive optics and detectors, multiband imaging has been typically accomplished by deploying multiple complete imaging systems (e.g., optics and detectors) or using large, narrow-FOV reflective optics. Multiband imagers have therefore been bulky and costly, not well suited to payload-sensitive platforms such as unmanned aerial vehicles or soldier handheld or helmet-mounted systems.

address aberrations or optical noise (e.g., chromatic, spherical, coma, astigmatism, and spherochromatism). For multiband applications, where the refractive optics must perform over a very wide range of wavelengths, chromatic aberration (or color blur) poses a significant challenge due to the small library of multiband compatible materials available and the tendencies of these materials to be more dispersive at some wavelengths and less dispersive at others. As a result, multiband imagers often use a large number of elements and are heavy and complex. Minimizing the number of lens elements in a multiband optical assembly and reducing the complexity is critically needed for imagers on payload-sensitive platforms.

GRIN IR Optics: Gradient index (GRIN) optics are optical elements in which the refractive index within the optic is carefully tailored to manipulate light. GRIN optics are commercially available for visible and near-infrared light, but not for IR wavelengths beyond $\sim 2 \mu\text{m}$. GRIN allows an additional degree of freedom for the optical designer that can be used for optical power or aberration correction.

NRL's diffusion-based IR-GRIN material is comprised of chalcogenide glasses based on arsenic (As), sulfur (S), and selenium (Se) and transmits wavelengths from 0.7 μm to 12 μm , covering all four IR wavebands. A variety of GRIN profiles can be made in axial, radial, or spherical orientation as shown schematically in Fig. 1. The internal refractive index gradient from 2.4

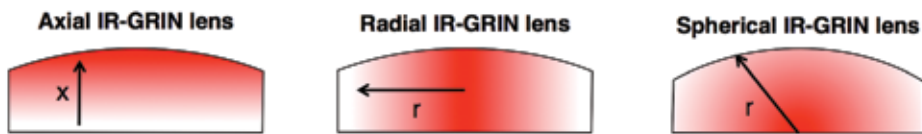


FIGURE 1 Schematic of IR-GRIN lenses in axial (left), radial (center), and spherical (right) configurations.

IR Imaging: Advancements in detector technology have been driving efforts to reduce the size, weight, power, and cost (SWaP-C) of multiband imagers, but conventional refractive optics are limiting miniaturization. Dual-band detectors use a dichroic beamsplitter to separate and direct the optical signal to separate focal plane arrays (FPAs) for each waveband. Newly available dual-band quantum well infrared photodetectors (QWIPs) combine pixels for different wavebands in the same FPA for an extremely compact dual-band detector, but the optics are still heavy and complex.

Imagers based on reflective optics are bulky and offer only a narrow FOV. Imagers based on refractive optics offer very wide FOV, but since the light travels through the refractive elements, these imagers have to

to 2.5 is achieved by controlling the S/Se ratio within the material. Figure 2 shows an example composition profile (top), and corresponding refractive index profile (bottom). The IR-GRIN material can be formed into an IR-GRIN lens by conventional grinding and polishing techniques or by single-point diamond turning (SPDT).

In addition to an internal refractive index gradient, the IR-GRIN material has an internal dispersion gradient that imparts a chromatic effect to the GRIN that contrasts the chromatic dispersion of the glass. The IR-GRIN designer can leverage the two chromatic effects against each other to create lens elements with low-dispersion (and even zero- or negative-dispersion) across a wider wavelength range than possible with conventional materials. These low-dispersion IR-GRIN

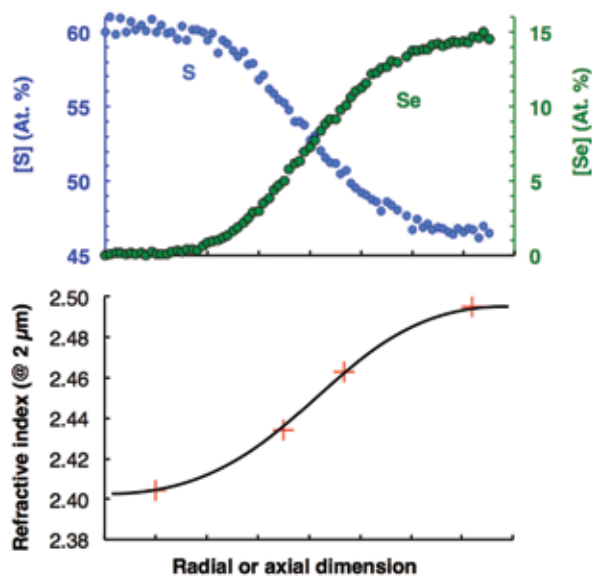


FIGURE 2
Example IR-GRIN composition (top) and refractive index (bottom) profiles.

elements can replace several elements in multiband lens designs, reducing the number of elements by 50% or more compared to conventional lens designs.

Summary: We have developed technologies for infrared gradient index lenses in axial, radial, and spherical configurations. The IR-GRIN material transmits in all IR wavebands and allows an additional degree of freedom for designers of multiband lenses for the efficient correction of chromatic aberrations. IR-GRIN lenses will enable compact, lightweight, multiband imagers for payload-sensitive platforms.

[Sponsored by the NRL Base Program (CNR funded)]

Broadband Nonlinear Metamaterial

W.S. Wall, S.M. Rudolph, S.K. Hong, K.L. Morgan, and V.M. Mendez
Tactical Electronic Warfare Division

Introduction: Nonlinear metamaterials are arrays of subwavelength structures engineered to exhibit power-dependent properties on a macroscopic scale. These materials can be used to create passive microwave devices such as antennas, radomes, and waveguides, which behave differently at high and low powers. While previous demonstrations of nonlinear metamaterials have been able to achieve this nonlinear behavior only over a limited frequency range, many naval and commercial applications require microwave devices with

substantial bandwidths. Therefore, developing a broadband nonlinear metamaterial structure is a critical step in making this technology ready for these applications. Using a novel traveling-wave design loaded with high-speed Schottky diodes, the Naval Research Laboratory (NRL) has experimentally demonstrated a nonlinear metamaterial structure that is capable of switching from a highly reflective state to a reflectionless state over a 30% 3-dB bandwidth.¹

Design: The broadband switching behavior of this metamaterial is achieved by creating two distinct sets of effective material properties that are dependent on the geometry of the metamaterial structure and the characteristics of diodes that load it. This metamaterial structure (Fig. 3) consists of two separate components: an inductive element that provides an exclusively electric response and a magnetic element that exhibits both electric and magnetic effects. When excited with a vertically polarized electromagnetic wave, the response of

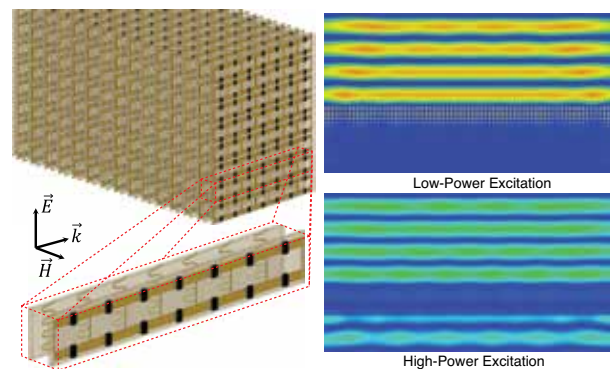


FIGURE 3
A cartoon representation of the metamaterial structure is shown on the left with a single row enlarged to show detail. The metamaterial responds to electromagnetic waves polarized as shown by the vector triad, where E represents the electric field, H represents the magnetic field, and k represents the propagation direction. The resulting field maps on the right depict low- and high-power excitations (top and bottom, respectively) normalized to their incident amplitude.

this structure can be described by one of two limiting cases: broadband reflective (low power) and broadband nonreflective (high power). In the low-power case, magnetic elements resonate and produce an imaginary index of refraction, which blocks the propagation of the wave through the medium.² This behavior is similar to an electromagnetic wave encountering a metal, so the material appears highly reflective. As the incident power is increased, the diodes turn on and destroy the magnetic resonance. In the absence of the resonance, the index of refraction is almost purely real as it would be in glass or other low-loss dielectrics. As a result, the medium becomes transparent to the incident wave.

The bandwidth of this effect is enhanced by electrically connecting the magnetic elements along the direction of propagation. This creates a traveling wave along the magnetic resonators and allows the resonances of the individual elements to couple, resulting in significantly wider bandwidth.³

Experiment: To investigate the performance of this broadband nonlinear metamaterial structure, an experiment was conducted in a rectangular waveguide. A custom waveguide was built to hold nine magnetic and nine electric boards within its cross section (Fig. 4). Both magnetic and electric elements were printed on a low-loss circuit board using standard printed

dBm) state, this structure exhibited broadband reflectivity ($S_{11} > -1$ dB) over a 24% bandwidth centered at 3.7 GHz, and at high power, a difference in reflectivity of 10 dB over an 18% bandwidth and 3 dB over a 31% bandwidth was observed with a maximum difference in reflection of nearly 30 dB. Compared to previous demonstrations designed to operate in a transmission configuration,⁴ this structure exhibited a 72% wider 3 dB bandwidth and a maximum difference between low-power and high-power states that was 24 dB larger.

Summary: NRL has demonstrated a nonlinear metamaterial structure capable of transitioning from a broadband reflective to a broadband reflectionless state.

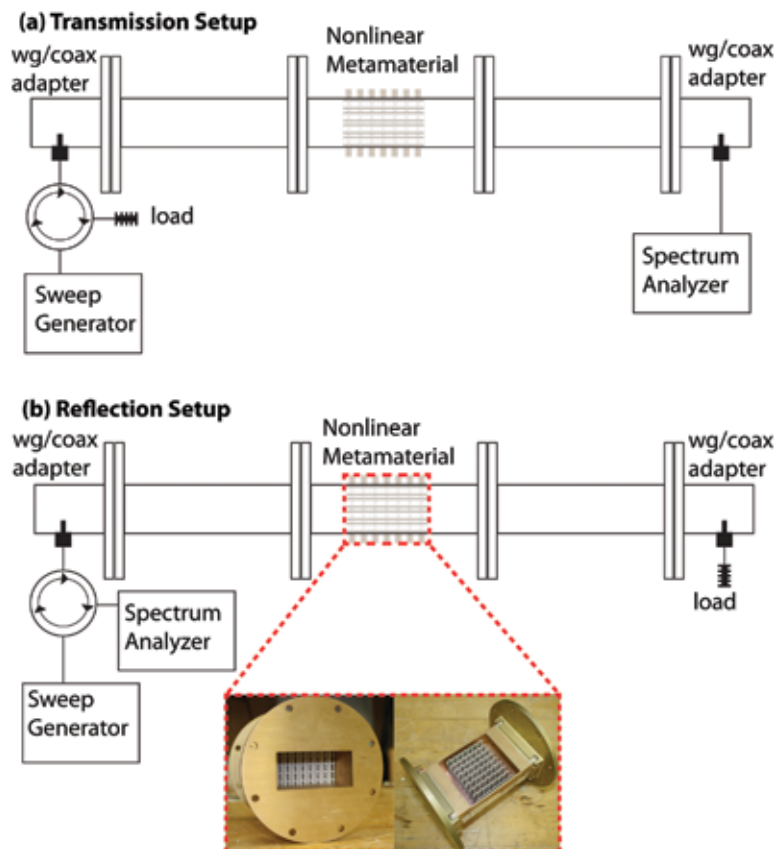


FIGURE 4

Schematic diagram of experimental setup used to measure (a) transmission and (b) reflection characteristics of broadband nonlinear metamaterial structure. Inset shows photographs of metamaterial structure placed inside waveguide.

circuit board (PCB) fabrication techniques. For the nonlinear elements, high-speed Schottky diodes were chosen for their low capacitance and high resistance in the off state, and low resistance in the on state. Reflection and transmission measurements were made at low (<0 dBm) and high (33 dBm) incident powers levels. These measurements are compared to simulated results in Fig. 5, with good agreement. In the low-power (<0

This performance was achieved by carefully engineering the effective material properties of a traveling wave metamaterial structure to achieve broadband “metal-like” properties at low power levels and nonreflective, “dielectric” characteristics at high power levels. The performance of this broadband nonlinear metamaterial was demonstrated through reflection and transmission measurements inside an S-band waveguide at various

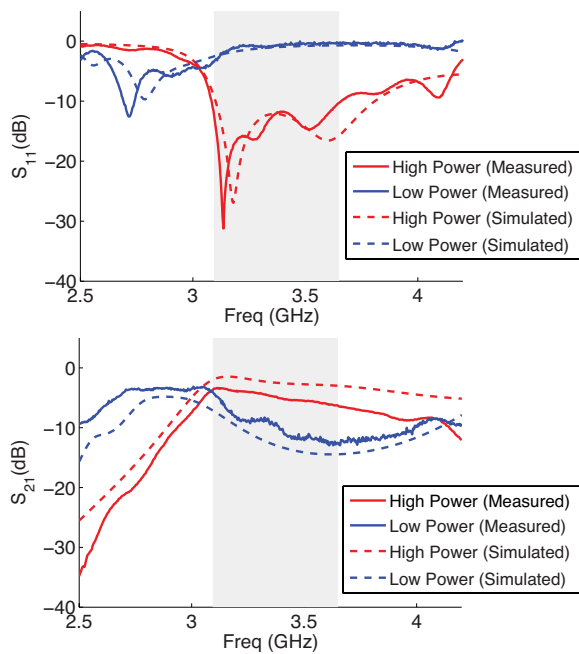


FIGURE 5 Simulated (dashed) and measured (solid) reflection (top) and transmission (bottom) coefficients of the wideband nonlinear metamaterial structure inside waveguide. High and low power states of the diodes were simulated by changing the resistance values. The 10 dB bandwidth of this structure is highlighted in gray.

power levels. These measurements demonstrated a difference in reflectivity of 10 dB over an 18% bandwidth with a maximum difference in reflection of nearly 30 dB. By allowing nonlinear properties to be integrated into bulk materials over usable communication and radar bandwidths, such structures have the potential to enable practical microwave devices like antennas and radomes, which can passively respond to changes in incident power, allowing for reduced radar cross sections and improved immunity to electronic attack.

[Sponsored by ONR]

References

- ¹ W.S. Wall, S.M. Rudolph, S.K. Hong, and K.L. Morgan, "Broadband Switching Nonlinear Metamaterial," *IEEE Ant. Wireless Propagation Lett.*, under review, January 2014.
- ² J.B. Pendry, A.J. Holden, D.J. Robbins, and W.J. Stewart, "Magnetism from Conductors and Enhanced Nonlinear Phenomena," *IEEE Trans. Microwave Theory Tech.* **47**, 2075–2084 (1999).
- ³ S.M. Rudolph and A. Grbic, "Volumetric Negative-Refractive-Index Medium Exhibiting Broadband Negative Permeability," *J. Appl. Phys.* **102**, 013904 (2007).
- ⁴ A.R. Katko, A.M. Hawkes, J.P. Barrett, and S.A. Cummer, "RF Limiter Metamaterial Using PIN Diodes," *Ant. Wireless Propagation Lett.* **10**, 1571–1574 (2011).



208 Broadband Dielectric Spectroscopy of Several Energetic and Nonenergetic Materials

210 Camouflage Paint Scheme for the USS *Fort Worth* (LCS 3)

212 Hyperspectral Imager for the Coastal Ocean (HICO) Goes Public under NASA Sponsorship

Broadband Dielectric Spectroscopy of Several Energetic and Nonenergetic Materials

B. Bajramaj,¹ M.A. Nurge,² and D.J. Bonanno¹

¹Information Technology Division

²NASA Kennedy Space Center

Introduction: Dielectric spectroscopy is used to measure the capacitive response of materials when exposed to a frequency-changing, alternating electromagnetic field. The goal of the NRL Dielectric Spectra Analysis project was to provide high-quality broadband dielectric spectra of several materials that have been known to be the primary substance or constituent of improvised explosive devices (IEDs). The study concentrated on building a library of several key inert and energetic materials' capacitive response under controlled laboratory settings. NRL and NASA Kennedy Space Center teams worked jointly to collect, catalog, and analyze the dielectric response of selected materials of interest. The materials were tested in dry form and with a fixed amount of moisture over a wide temperature range. The data analysis aimed to exploit possible markers that could be used to discriminate the energetic materials from the nonenergetic materials and determine whether low-frequency dielectric spectroscopy can be used as a discriminating method.

Background: NRL had been previously engaged in a similar dielectric spectra collection campaign utilizing a contractor-designed and built dielectric system prototype. The prototype used free space low-frequency dielectric spectroscopy to collect bulk properties of energetic materials. When the prototype was developed, no reference high-quality contact dielectric spectra existed for materials of interest in the hertz to kilohertz range. For the prototype's proof of concept, the contractor designed a capacitive measurement test fixture and collected nonbulk contact spectra for several energetic and inert materials. The data analysis results stated that the material signatures were separable, specifically at the lower end of the frequency range used, and that dielectric spectroscopy could be considered as a method of material discrimination. Further work was done to transition to noncontact measurements and the development of a dielectric system prototype for energetic material detection application.

The separable signatures, however, were directly associated with the testing setup. Discriminating features at the lower frequencies were not purely due to the materials themselves but rather to electrode-material interaction at the contact boundary. This interaction leads to an unwanted parasitic effect known as electrode polarization, which can affect dielectric

measurements at lower frequencies.¹ Positive discrimination between energetic and inert materials from the developed free space prototype was therefore configuration based: it came from bulk material placement, encasing, relative position with respect to sensors, and other test-specific factors, and not necessarily from the materials themselves. Such a system would not be able to provide reliable results as it did not look for unique, material-specific features, but rather for test-specific features. The suggestion from NASA's team to look for material markers by analyzing the materials in pure form and in contact configuration led to a collaborative campaign between the two organizations. Over a period of several months, the dielectric spectra of the energetic materials and other inert materials were measured from 0.1 Hz to 1 GHz, for temperatures between -10°C and 40°C .

Dielectric relaxation is a phenomenon that can be exploited as a discriminating marker. It was first described by Peter J.W. Debye² in 1929 and is directly related to the polarizability of the material. Molecular dipoles and ions in the material will move to align themselves with the changing electric field. As the frequency of the changing electric field is increased, the motion of the dipoles and ions begins to lag behind the changing field, resulting in relaxation. This relaxation typically takes place over a range of frequencies below 10 GHz, with ionic relaxation occurring at lower frequencies than the dipole relaxation. As a result of materials having different ionic and molecular content, the resulting dielectric spectra will also vary from one another. Some materials undergo more than one low-frequency dielectric relaxation, while others only exhibit a small relaxation at much higher frequencies due to the nonpolar nature of their molecules.

Experimental Equipment and Setup: The energetic materials tested were ammonium nitrate fuel oil (ANFO), ammonium nitrate aluminum (ANAL), pentaerythritol tetranitrate (PETN), trinitrotoluene (TNT), cyclotrimethylenetrinitramine (aka RDX), and C-4. The Novocontrol Turnkey Concept 80 System (Fig. 1) used for the data collection provides a wide range of frequency- and temperature-dependent high-quality dielectric measurements. It consists of two separate spectrometers that cover two separate but overlapping frequency ranges: the Alpha-A Modular System (3 μHz to 40 MHz) and the Agilent E4991A Impedance Analyzer (1 MHz to 3 GHz). Both systems use impedance measurements to calculate the complex permittivity for a given sample geometry. The material temperature was controlled by the Quatro Cryosystem, which can vary temperature from -160°C to 400°C with 0.01°C accuracy. For all the tests, the pure material was built into a parallel plate capacitor between the measuring electrodes of 12 mm and 13 mm diameter for the high

and low range of frequencies, respectively. The material was vacuum pressed into a 13 mm pellet with thickness average of 0.8037 mm as shown in Fig. 2. The weight of the pellet ranged from 0.138 to 0.183 g depending on the material. Measures were taken to avoid charge buildup in the energetic materials by keeping them in airtight,

electrostatic discharge safe (ESD) containers. All materials were also kept from absorbing moisture with the use of desiccant packs placed in the storing containers. For the moisture testing, the desired moisture level in the materials was reached by following the American Society for Testing and Materials (ASTM) procedure E104-02.

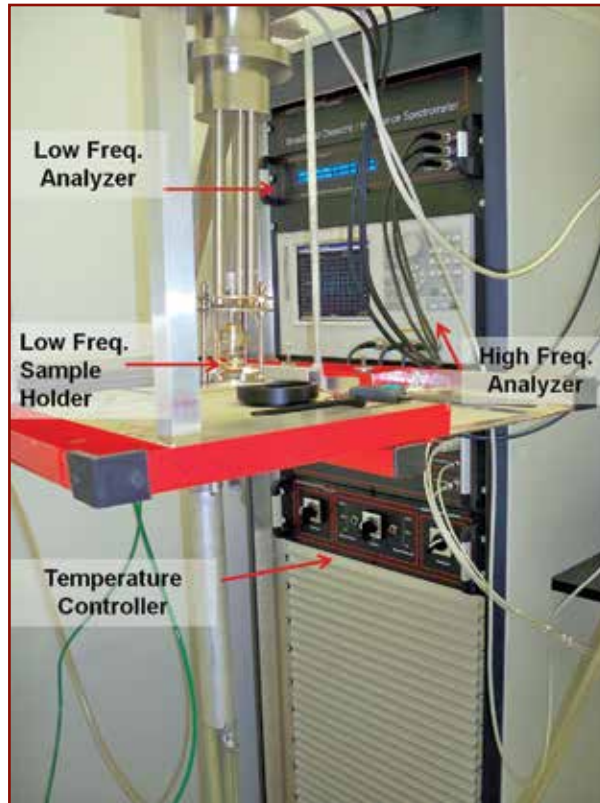


FIGURE 1 Novocontrol Concept 80 system used for dielectric spectra collection.

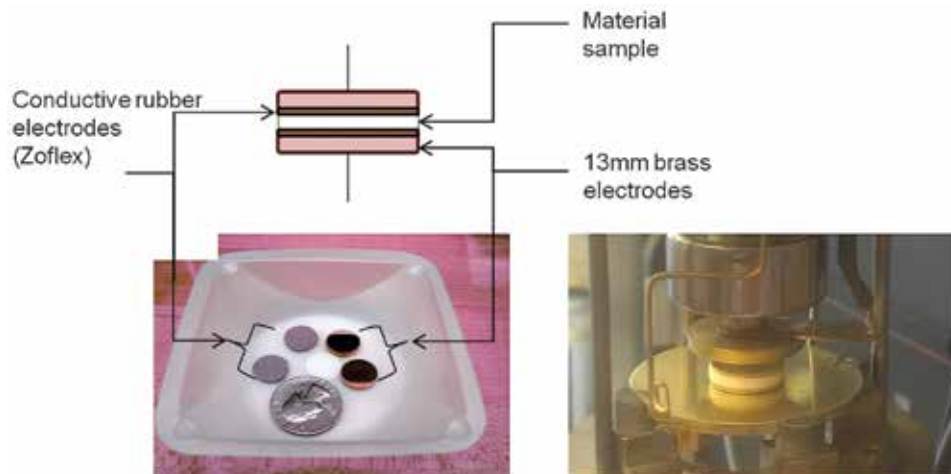


FIGURE 2 Ammonium nitrate pellet along with auxiliary electrodes (left) and in parallel plate capacitor configuration for low-frequency tests (right).

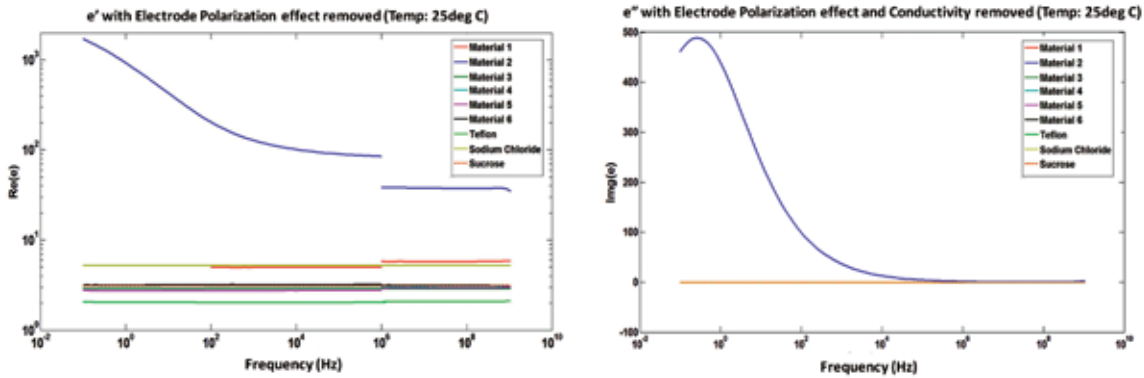


FIGURE 3 Real and imaginary components of the complex permittivity for the energetic materials tested along with three inert materials. The energetics labeled as Material 1 through 6 were ammonium nitrate fuel oil (ANFO), ammonium nitrate aluminum (ANAI), pentaerythritol tetranitrate (PETN), trinitrotoluene (TNT), cyclotrimethylenetrinitramine (aka RDX), and C-4, respectively.

Results: The study showed that the energetic materials did not exhibit a discriminating feature in the frequency range tested and they would not be able to be distinguished from other inert materials in a blind test. Only ammonium nitrate aluminum showed a feature in the spectra that was due to the moisture absorbed by the material (Fig. 3). As such, it is not a unique and reliable marker, and therefore not optimal for identification purposes. The rest of the energetics had no spectral features and their identification would not be possible in a blind test. This work showed that low-frequency dielectric spectroscopy (specifically below 1 GHz) cannot be used as a method to identify these particular energetic materials. These results also confirmed that positive discriminating results reported from the free space prototype were not due to unique material properties, but rather the difference in testing configurations.

Acknowledgments: The authors would like to thank Dr. A. Wolf, Mr. C. Font, Mr. C. Hawley, Dr. C. Gilbreath, Ms. J. McFall, Dr. R. Albo, Dr. R. Richardson, and Mrs. T. Lawhorn for their assistance in data collection and valuable scientific input.

[Sponsored by Patrick AFB]

References

- ¹ F. Kremer and A. Schoenhals, *Broadband Dielectric Spectroscopy* (Springer, Berlin, 2003), pp. 91–92.
- ² P. Debye, *Polar Molecules* (Chemical Catalog Co., Inc., New York, 1929), pp. 83–95.

Camouflage Paint Scheme for the USS Fort Worth (LCS 3)

R. Gignilliat
Tactical Electronic Warfare Division

Introduction: In 2013, the Electro-Optical/Infrared (EO/IR) Measurements and Simulation Section of NRL's Tactical Electronic Warfare Division (Code 5757) was tasked to develop a camouflage paint scheme for the Freedom-variant of the Littoral Combat Ship (LCS) class. Prior to NRL's involvement, the flagship of the class (LCS 1) had been painted with a camouflage pattern that was reminiscent of counter-recognition and counter-targeting paint schemes of the past. For future hulls of the LCS Freedom-variant, Naval Sea Systems Command (NAVSEA) decided that it would be preferable to have a camouflage paint scheme that was designed for counter-detection purposes vs counter-recognition. The objective of a counter-detection scheme is to make the task of finding an object within a scene more difficult, whereas a counter-recognition scheme is intended to make the task more difficult on the observer in discerning the type of object (e.g., cargo ship vs naval combatant) but may not actually reduce detectability. The new paint scheme also needed to possess a number of other attributes in addition to being counter-detection in design. The camouflage design was required to conceal the diesel exhaust ports and surrounding soot areas, use only paints within the Navy's current supply line, reduce labor costs associated with ship painting, and be aesthetically pleasing. To meet the design goals, NRL Code 5757 leveraged research, funded by the Office of Naval Research (ONR), in the field of maritime camouflage design to adapt camouflage concepts to the LCS ship geometry.

How Do You Disguise a Ship?: NRL Code 5757's research led to maritime camouflage design goals that are consistent with the counter-detection camouflage concepts found in other domains, such as ground vehicle camouflage, personnel uniform camouflage, and even camouflage found in nature (e.g., leopards and cuttlefish). Across all domains, an effective camouflage matches the object to the background and mitigates discrimination cues for an observer. Background-matching is achieved by addressing the overall luminance, color, and texture of the object. Discrimination cues are anything identifiable as being dissimilar to the environment. For example, the silhouette shape of a person is easily differentiated from the background if nothing disrupts the continuous boundary. Boundary-disruptive patterning is incorporated into many camouflage designs because of this. However, even though the general approach seems simple, the task of producing a camouflage scheme for a ship that achieves the primary goals of background-matching and denial of discrimination cues becomes complex when the broad range of observation scenarios is considered.

Statistically Speaking: To produce a general-solution maritime counter-detection camouflage solution for the LCS that is equally applicable across operational environments, NRL Code 5757 used statistical analyses as well as modeling and simulation to guide the design process. The effort focused on the most common observation scenario, which is a shore-based (or low altitude) observer scanning the area near the horizon.

This area near the horizon represents the background to which the camouflage paint scheme was designed to match in terms of color, brightness, and texture. The resulting camouflage paint scheme for the LCS Freedom class produced by NRL is shown in Fig. 4 as applied to USS *Fort Worth* (LCS 3). To match color, the paints were selected based on a statistical study of predominant colors in terms of hue, saturation, and lightness. The scheme concentrates darker shaded paints nearer the waterline of the ship to reduce contrast against the sea surface, and lighter shades of gray further up the ship to reduce contrast of those surfaces against the area of sky just above horizon. The luminance on specific areas of the ship, such as the bow-flare and forward deckhouse surfaces, are controlled by applying a concept called countershading. The curvature at the bow-flare creates surfaces that are generally downward facing and away from direct sunlight, creating a shadow on a mono-colored hull. To counteract this, these surfaces were specified to be slightly lighter shades vs the other areas of the hull. Conversely, the sloped-back surfaces on the forward faces of the superstructure were specified to have darker shades of paint to reduce the reflected sunlight coming from this area of the ship. Second-order statistical measures of the background texture/spatial properties established that a horizontally oriented pattern is a much better match of the background texture orientation than any vertically oriented pattern. The scale of the pattern was based on modeling and simulation, which determined the minimum feature size that can be resolved at typical detection range



FIGURE 4
USS *Fort Worth* (LCS 3) exhibits NRL's camouflage paint scheme.

distances. Boundary-disruptive patterning has also been introduced along the edges of the superstructure and hull. Ultimately, NRL Code 5757 met all the design goals for the camouflage paint scheme and simplified the complexity compared to the original LCS 1 scheme, which produced a cost savings of \$300K/ship for the Navy.

[Sponsored by ONR]



Hyperspectral Imager for the Coastal Ocean (HICO) Goes Public under NASA Sponsorship

M. Kappus

Remote Sensing Division

What is HICO?: NRL built the Hyperspectral Imager for the Coastal Ocean (HICO) as the world's first spaceborne imaging spectrometer focused on the coastal ocean. A typical HICO image covers 50 km by 200 km spatially, in which each 100-meter-sized pixel contains values representing the light reflected from the water or land at dozens of contiguous wavelengths throughout the visible and near-infrared range of the spectrum. Displayed as an image (Fig. 5(a)), HICO data illustrate coastal ocean features like eddies, river plumes, or harmful algal blooms; displayed as reflected light spectra from a small spatial region (Fig. 5(b)), HICO data reveal the composition of those features, such as concentrations of different chlorophyll types or entrained sediments.

Initial Navy Operations: Through the Navy's Innovative Naval Prototype program, the Office of Naval Research (ONR) funded HICO's construction and operations from 2010 through 2012 aboard the International Space Station (ISS) as a fast, inexpensive

pathfinder mission to gather data about the coastal regime. NRL scientists developed procedures for the imaging chain, including tasking, processing, exploitation, and dissemination. We developed techniques to determine HICO's position and attitude, accounting for the challenges of the unusual ISS orbit and frequent adjustments for space maneuvers, in order to plan the location and timing of image collections and to properly associate the position of each image with the appropriate location on Earth. We calibrated the sensor in the laboratory using calibration sources traceable to the National Institute of Standards and Technology (NIST), and followed up with adjustments based on cross-correlations in known areas and with other sensors. NRL scientists used HICO data in their research on a range of topics, including determination of surface flow velocity from image sequences over time and investigation into transient mesoscale eddies. We partnered with Oregon State University (OSU) to distribute data to interested users and to engage scientists around the world through the HICO web site hosted at OSU (<http://hico.coas.oregonstate.edu/index.shtml>).

HICO Transitions to NASA: HICO's early achievements grabbed the interest of NASA's ISS Office, which saw HICO both as a successful current science payload and as a risk reducer for planned future hyperspectral sensors. In January 2013, NASA assumed sponsorship of HICO operations, which enabled this robust sensor to continue collecting data. By the end of 2013, HICO had collected 8570 images during its lifetime. NASA sponsorship provided a new outlet for data viewing and distribution: HICO data can be browsed and downloaded from NASA's Ocean Color website (<http://oceancolor.gsfc.nasa.gov/>) alongside traditional ocean color data, encouraging multisensor investigations. HICO data presence on the well-known NASA website has broadened the user base: in the first seven months online, 4370 images have been downloaded by users worldwide (Fig. 6). NASA has enjoyed more



FIGURE 5(a)

Spatial view of a HICO image: A harmful algal (microcystis) bloom appears green, dominating Lake Erie in this September 3, 2011 HICO image.

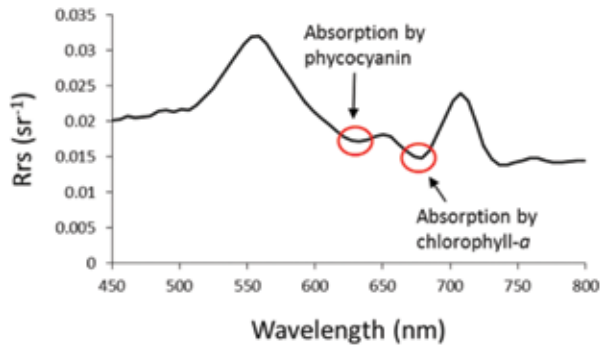


FIGURE 5(b)
Spectral view of the same HICO image: Reflectance spectrum from the portion of the lake with high algae concentration shows the distinguishing absorption features of chlorophyll-a and phycocyanin, the characteristic pigment of the toxic cyanobacteria.

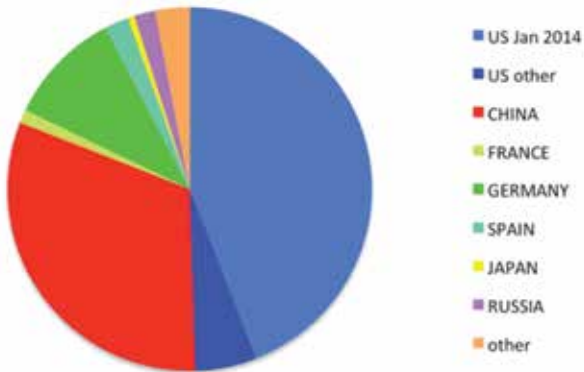


FIGURE 6
Distribution of users downloading 4370 images from the NASA Ocean Color website during the first 7 months of availability (July 2013 – January 2014).



FIGURE 7
HICO image from February 27, 2013 of Taganrog Bay and the Sea of Azov. The milky white color indicates a heavy load of suspended sediments. Colleagues in Russia make in situ measurements of chlorophyll-a concentrations, while NRL researchers extract these values from the processed HICO images. Agreement has been excellent, even during highly variable conditions.

direct access to HICO to support its International Disaster Response Charter mission, capturing images of fires, volcanoes, and floods around the world. Increased international collaboration includes a joint project between NRL and the Russian Academy of Sciences examining the effects of land use and land cover change on the water quality in the Sea of Azov (Fig. 7).

The closer tie to NASA enabled the NRL operations team to make significant improvements to operations by obtaining access to additional accurate time and position information from the ISS platform, which improved the accuracy of the location information for HICO images. The direct relationship secured higher data link rates, which in turn have increased our ability to adjust tasking for weather and to increase the number of images collected each day. Because of the ongoing NRL-NASA affiliation on HICO, NASA had the confidence to explicitly include HICO in its recent call for Earth science research proposals (as part of the PACE science teams).

The successful transition of HICO to NASA illustrates the synergy between the Navy and NASA in remote sensing applied research. NRL looks forward to several more years of partnership with NASA to provide insights about the coastal ocean through the eyes of HICO.

[Sponsored by NASA]

Reference

¹ R.L. Lucke, M. Corson, N.R. McGlothlin, S.D. Butcher, D.L. Wood, D.R. Korwan, R.R. Li, W.A. Snyder, C.O. Davis, and D.T. Chen, "Hyperspectral Imager for the Coastal Ocean: Instrument Description and First Images," *Applied Optics* **50**, 1501–1516 (2011).

simulation, computing, and modeling



216 Considering Blast Response in Helmet Design

217 The X-Ray Flash of a Z Pinch

219 From the Stream to the Shore: Forecasting Complex Ocean Environments in Trident Warrior '13

222 Integrating the Marine Biosphere into Coupled Ocean–Atmosphere Models

Considering Blast Response in Helmet Design

D.R. Mott,¹ T.R. Young, Jr.,² and D.A. Schwer¹

¹Laboratories for Computational Physics and Fluid Dynamics

²Berkeley Research Associates, Beltsville, MD

Overview: The need to understand and ultimately mitigate traumatic brain injury (TBI) has led to significant efforts in characterizing blast loading on helmeted-head geometries. Although the precise mechanisms producing TBI are not well understood, equipment designs that reduce the aerodynamic loading on the head during a blast event are sought. Optional protective equipment, such as removable mandible protection and face shields, are under consideration for the next generation of military helmet. A blast interacts with these components in complex and sometimes counterintuitive ways.

The current work investigated a variety of configurations of the Army's Conformal Integrated Protective Headgear System (CIPHER) prototype geometry to quantify the effect of proposed protective equipment on under-helmet pressures generated by a blast event. In most cases, the additional protective equipment reduced the pressure loading on areas of the head facing the blast source that would otherwise be struck directly by the blast wave. Blast waves also typically penetrated the gap between the helmet brim and the head. These penetrating waves subsequently interacted with other waves or were reflected from helmet components and generated higher localized peak pressures in some areas on the head. Furthermore, in a typical IED scenario targeting an unmounted (i.e., walking) Marine or soldier, these results indicate that the loading on the head can be critically influenced by the reflection of the blast wave from the torso.

Test Cases and Approach: Figure 1 shows the CIPHER prototype geometry including mandible and face shield, as well as a view of the suspension under the helmet shell. This suspension consists of an array of cylindrical supports and pads. The current study considered four equipment configurations:

- (1) helmet
- (2) helmet + mandible
- (3) helmet + face shield
- (4) helmet + mandible + face shield.

The blast is generated by 1.5 kg of C4 placed at chest height and 3 m from the warfighter, and blasts from the front, side, and rear were studied. The mannequin geometry includes the helmet and accessory equipment, head, neck, shoulders, and a simplified torso

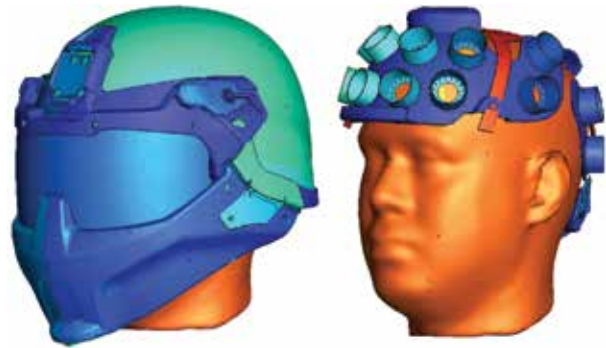


FIGURE 1
CIPHER component and liner geometries.

produced by extending the outline of the shoulders, back, and chest down toward the ground.

The computation of the blast interaction occurs in two steps. First, a compressible reacting-flow simulation of the explosion event generates the blast profile (i.e., pressure emanating from the blast source as a function of time and location), including the ground reflection of the spherically expanding wave, in the absence of the mannequin geometry. The results of this simulation provide boundary conditions that drive a three-dimensional simulation of the blast striking the complex head-helmet-torso geometry. Both calculations are completed using software developed within the Laboratories for Computational Physics and Fluid Dynamics, and the simulation approach has been detailed previously.¹ The results presented below focus on a front blast approaching the CIPHER geometries, but previous work^{2,3} includes results for additional helmet and suspension geometries and blast orientations.

Results: Figure 2 includes pressure histories at selected locations on the head for a blast approaching each equipment configuration from the front. For the helmet worn alone (top left), the pressure plots include three large spikes. The first two are on the eyes and on the forehead and correspond to the blast arriving unabated and reflecting from the face at approximately 0.001 s. The third peak is seen for a location on the back of the head under the edge of the helmet but exposed below the helmet suspension. The initial shock wave splits to envelop the head and helmet as it traverses the geometry, and this third peak results from the wave converging at the back of the head prior to 0.0015 s. The converging wave reinforces and amplifies the pressure at this point on the head away from the blast source.

Adding the face shield mitigates the effect of the blast wave on the eyes and forehead in this scenario and reduces the peak pressures on these areas. Adding the mandible protection to the face shield, however, traps a wave produced when the initial shock reflects from

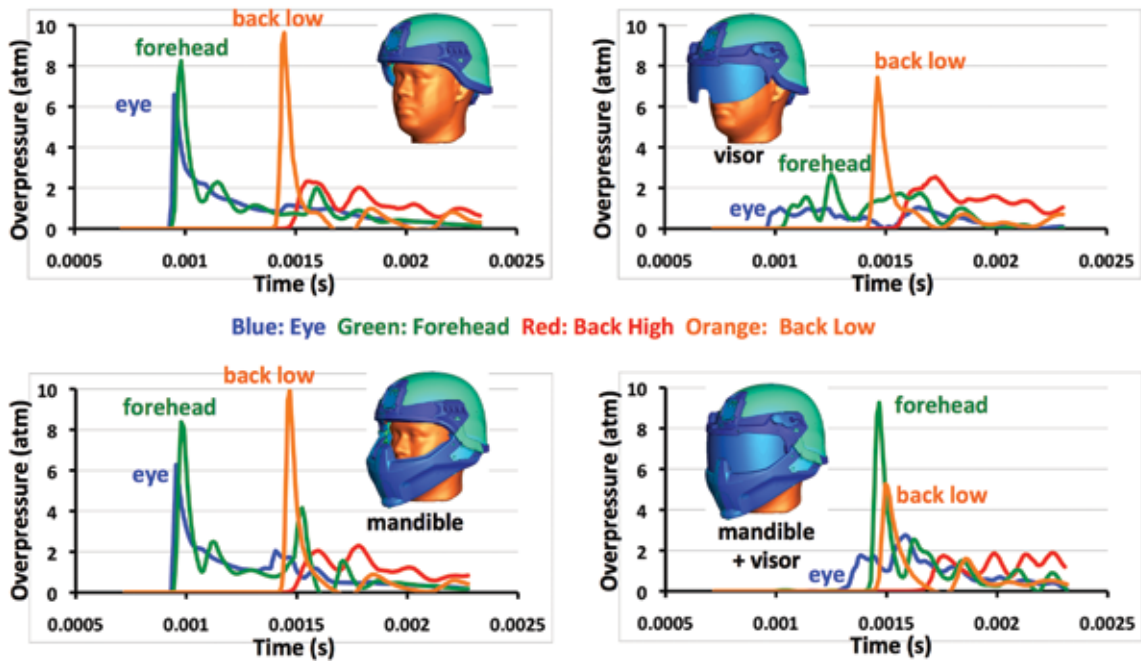


FIGURE 2
Pressure histories for selected points for a blast approaching from the front.

the torso. The trapped wave is channeled up toward the forehead, reflects from the helmet suspension, and amplifies the peak pressure on the forehead. This peak in the forehead pressure comes considerably later than the peaks generated when the initial blast wave strikes the forehead directly in the absence of the face shield. However, the reflected wave trapped by the mandible produces an even higher peak pressure on the forehead than in the unprotected case.

Conclusions: During a blast event, the flow field about a realistic head, helmet, and torso is very complicated. For a given helmet configuration, the peak pressures on the head will likely increase in some locations and decrease in others relative to other configurations. The current results show a potential for significant pressure amplification on various head locations when blast waves enter the region below the helmet. The details of the torso and any additional equipment that the soldier or Marine is wearing (e.g., a collar or vest) can affect the vulnerability to these under-helmet waves. As long as the blast waves can reach that volume adjacent to the head, the potential for this localized pressure amplification remains.

Acknowledgments: The U.S. Army Natick Soldier Research, Development, and Engineering Center (NSRDEC) sponsored this research, under Program Manager Don Lee. The authors also wish to acknowledge Marine Corps Systems Command and NRL's Materials

Science and Technology Division for their support and stewardship of previous efforts in this critical field.

[Sponsored by U.S. Army NSRDEC]

References

- ¹D.R. Mott, D.A. Schwer, T.R. Young, Jr., J. Levine, J.-P. Dionne, A. Makris, and G. Hubler, "Blast-Induced Pressure Fields Beneath a Military Helmet," Proceedings of the 20th International Symposium on Military Aspects of Blast and Shock, Sept. 1–5, Oslo, Norway (2008).
- ²D.R. Mott, D.A. Schwer, and T.R. Young, Jr., "Predicting and Mitigating Blast Loading on the Head Beneath a Military Helmet," Proceedings of the 22nd International Symposium on Military Aspects of Blast and Shock, Nov. 4–9, Bourges, France (2012).
- ³D.R. Mott, T.R. Young, Jr., and D.A. Schwer, "Blast Loading on the Head Under a Military Helmet: Effect of Face Shield and Mandible Protection," AIAA-2014-0948, SciTech 2014, Jan. 13–17, National Harbor, MD (2014).

The X-Ray Flash of a Z Pinch

J.L. Giuliani,¹ J.W. Thornhill,¹ A. Dasgupta,¹ A.L. Velikovich,¹ Y.K. Chong,¹ T.A. Mehlhorn,¹ E. Kroupp,² Y. Maron,² J.P. Apruzese,³ and C. Deeney⁴

¹Plasma Physics Division

²Weizmann Institute of Science, Israel

³Engility Corp.

⁴National Security Technologies

Introduction: An incandescent bulb burns out because the tungsten filament has evaporated to the point that the sudden injection of 0.33 A current breaks the filament and produces a plasma arc and a flash of visible light. Now consider increasing the current by more than a million times and replacing the single wire filament with a cylindrical array of metal wires or a puff of noble gas. Under these conditions, the azimuthal magnetic field generated by such large currents actually compresses, or implodes, the material together into a highly ionized plasma with electron temperatures near 10 million degrees Kelvin. This describes a z pinch, and the flash is not only visible light but also an abundance of X rays. The z pinch is a complex combination of physics: magnetohydrodynamics (MHD) to force the implosion, atomic physics to describe the ionization kinetics, and photon transport to track the radiation. One of the grand challenges in high energy density physics is the self-consistent treatment of these different, but interacting, physical processes into a numerical simulation that can reliably explain the observed behavior. This article describes the application of a radiation-MHD code to model a particular z pinch for code validation and investigate some contentious issues remaining in z-pinch research.

A Gas Puff Z Pinch: The Weizmann Institute of Science in Israel has a 500,000 A pulsed power generator that has been used to produce a z pinch from a neon gas puff. The initial density distribution prior to the current input has been measured with laser interferometry as shown in Fig. 3. The puff is roughly comprised of an outer shell and a central jet, but is quite structured. During the implosion phase and stagnation on axis, visible and X-ray imaging were used to capture the dynamics, while calibrated photo-conducting diodes and high-resolution spectroscopy measured the radiated properties, particularly K-shell emissions from atoms that have retained only one or two of their original electrons.¹ Such an extensive suite of detailed data has never been available before and presents a stringent test, as well as opportunity, for code validation.

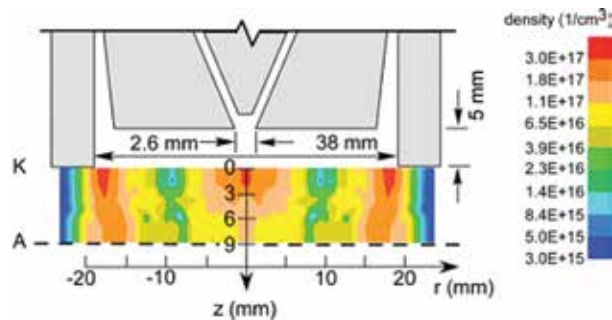


FIGURE 3
The density of the neon gas puff at the Weizmann Institute prior to initiating the current pulse.

Simulation Code: The Mach2-TCRE code was used to simulate this neon z pinch. Mach2 is an Arbitrary Lagrangian-Eulerian, 2D(r,z), MHD code. At NRL, we have added several major components in application to z pinches. First, we have incorporated a circuit model that is non-linearly coupled to the changing inductive and resistive load voltage. The most significant addition to the Mach2 code is the Tabular Collisional-Radiative Equilibrium (TCRE) component, which treats the non-local thermodynamic equilibrium (non-LTE) character of the plasma.² Third, we used a discrete ordinates technique in 3D to properly follow the transport of radiation throughout the plasma.

Results: Figure 4 compares observed visible images of the pinch during implosion against the synthetic images calculated from the numerical simulations. The modeling was also able to match the observed K-shell radiated yield of 25 kJ, the peak K-shell power of 7 GW, the electron density, and the electron temperature (T_e).

One of the most intriguing aspects of z pinches is the ion temperature at stagnation on axis. The only way to measure an ion temperature is through the spectral width of emission lines. But such values, called effective ion temperatures (T_i^{eff}), have consistently been found

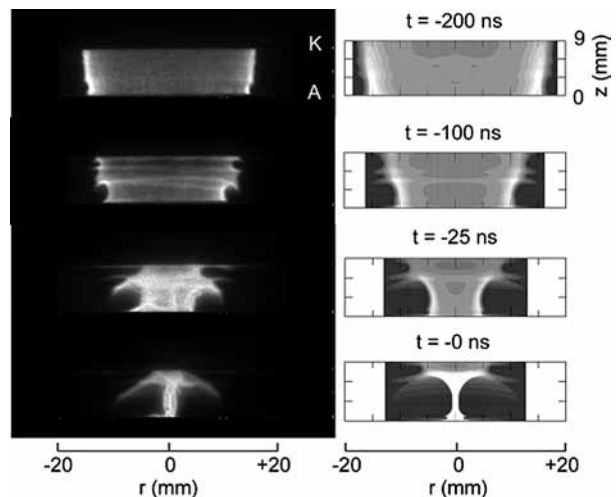


FIGURE 4
Visible images of the implosion of the pinch on the left, compared with synthetic images calculated from the simulations on the right. Times in nanoseconds are shown relative to that of peak X-ray emission.

to be $>10T_e$, although the high densities of a z pinch suggest that the thermal ion temperature (T_i) should be close to T_e . There have been speculations that the large T_i^{eff} represents MHD turbulence or rotation of the pinch. The solid lines in Fig. 5 show the calculated results for these three temperatures from the simulations, and the symbols show the data. We have found that the large values of T_i^{eff} , which match the data, arise from

the Doppler shifts in the radiation transport and reflect large radial velocity gradients near the axis, not rotation or 3D turbulence.³

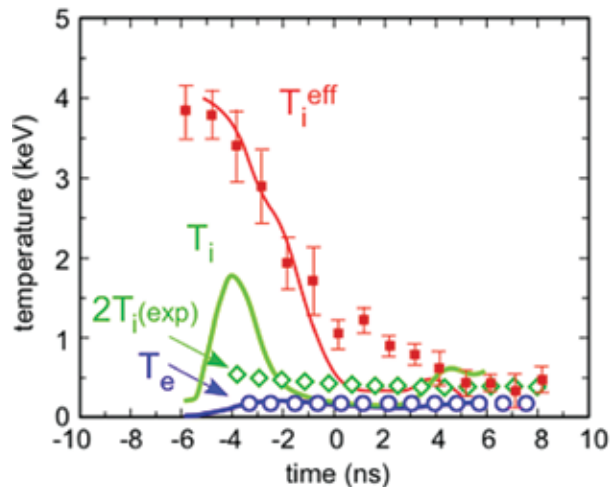


FIGURE 5

The symbols show the measured values for the electron (T_e), ion (T_i), and effective ion (T_i^{eff}) temperatures, and the solid lines are from the simulations. Along the ordinate, 1 keV equals 11 million degrees Kelvin. The modeling shows the large T_i^{eff} arises from Doppler shifts in the observed spectra of the imploding pinch.

Significance: Experiments on a university scale generator as discussed above are important because multiple experiments can be run with specialized diagnostics to build a large database. The largest currents for z pinches are produced on the ZR generator at Sandia National Laboratories and can reach >20 million A and produce hundreds of kilojoules of X rays. The above work describes fundamental research at NRL that contributes to improved understanding and performance of z pinches. These radiation sources are used to test components and enhance the overall stewardship of the U.S. nuclear deterrent.

[Sponsored by DOE National Nuclear Security Administration]

References

- ¹E. Kroupp, D. Osin, A. Starobinets, V. Fisher, V. Bernshtam, L. Weingarten, Y. Maron, I. Uschmann, E. Förster, A. Fisher, M.E. Cuneo, C. Deeney, and J. L. Giuliani, "Ion Temperature and Hydrodynamic-Energy Measurements in a Z-Pinch Plasma at Stagnation," *Phys. Rev. Lett.* **107**, 105001 (2011).
- ²J.W. Thornhill, J.P. Apruzese, J. Davis, R.W. Clark, A.L. Velikovich, J.L. Giuliani, Y.K. Chong, K.G. Whitney, C. Deeney, C.A. Coverdale, and F.L. Cochran, "An Efficient Tabulated Collisional Radiative Equilibrium Radiation Transport Model Suitable for Multidimensional Hydrodynamics Calculations," *Phys. Plasmas* **8**, 3480 (2001).
- ³J.L. Giuliani, J.W. Thornhill, E. Kroupp, D. Osin, Y. Maron, A. Dasgupta, J.P. Apruzese, A.L. Velikovich, Y.K. Chong, A. Starobinets, V. Fisher, Y. Zarnitsky, V. Bernshtam, A. Fisher, T.A. Mehlhorn, and C. Deeney, "Effective vs Ion Thermal Temperatures in the Weizmann Ne Z pinch: Modeling and Stagnation Physics" (to be published in *Physics of Plasmas*, February 2014). ♦

From the Stream to the Shore: Forecasting Complex Ocean Environments in Trident Warrior '13

C.N. Barron,¹ T.J. Campbell,¹ K.L. Edwards,¹ G.A. Jacobs,¹ J.G. Richman,¹ T.A. Smith,¹ T.L. Townsend,¹ J. Veeramony,¹ and P.L. Spence²
¹Oceanography Division
²QinetiQ North America

Introduction: Navy ocean forecasts must support tactical and strategic Fleet decisions within the diverse range of environments Navy operations face. During July's Trident Warrior 2013 (TW13), researchers from the NRL Oceanography Division tested a suite of prediction capabilities spanning conditions from the swift Gulf Stream to waves breaking along the Virginia/Maryland shore. A hierarchy of computer models with increasingly fine resolution followed evolving ocean conditions, spanning from the 7 km global system to a 3 km nest over the Continental Shelf and nearby Gulf Stream to finer nests covering coupled air-sea interactions and culminating in a 50 m mesh detailing ocean waves approaching the Virginia shore. A series of NRL-directed AXBT (Airborne Expendable BathyThermograph) flights supplemented observations from satellite platforms and autonomous vehicles. Validation of the model forecasts relative to the in situ observations showed both the value of new assimilation capabilities and the fidelity of model forecasts supporting Navy decisions.

From the Globe to the Mouth of the Bay: NRL's support for TW13 included the first demonstration during a Navy exercise of a hierarchy of ocean models consistently nested from the global down to a local fine-scale model at 50 m resolution (Fig. 6(a)). In each stage of nesting, an outer model provides initial and boundary conditions to an inner nest covering a subset of the outer domain. For TW13, the Hybrid Ocean Model (HYCOM) from the Global Ocean Forecast System (GOFS 3.0) at the Naval Oceanographic Office (NAVO) provided the boundary/initial conditions for a 3 km nest of the Navy Coastal Ocean Model (NCOM¹) that extends from the Carolinas to New Jersey and offshore to the Sargasso Sea. Both use 3D-variational Navy Coupled Ocean Data Assimilation (NCODA) systems to guide the ocean models toward ocean conditions observed from satellite and in situ platforms. The ocean models use atmospheric forcing from the Navy Global Environmental Model (NAVGEN) and regional implementations of the Coupled Ocean/Atmosphere Mesoscale Prediction System (COAMPS[®]). The NCOM cases also include tidal forcing. More detailed models

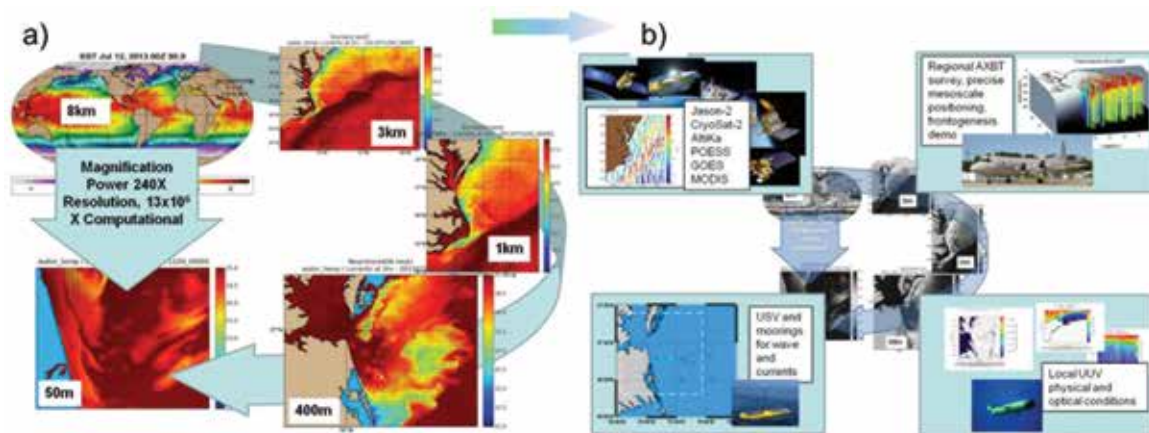


FIGURE 6

(a) TW 13 was the first demonstration during a Navy exercise of a consistently nested ocean modeling system spanning from the globe to a 50 m domain. (b) The corresponding observing system telescoped from global satellite altimeter and sea surface temperature measurements to regional AXBT coverage to local observations from moorings and unmanned underwater (UUV) and surface (USV) vehicles.

successively focus into the Continental Shelf in a 1 km NCOM to COAMPS ocean model covering the mouth of the Chesapeake Bay at 400 m and a portion of the Virginia coast at 50 m. The ocean modeling work demonstrated during TW13 reveals the Navy's operational capability to forecast complex ocean environments from scales from the globe to the Gulf Stream to the shore.

AXBT Survey: Accurate ocean model forecasting requires a complementary ocean observing system to feed the ocean data assimilation systems that guide the realistic forecasts toward the real ocean. Observations supporting TW13 include global and geostationary satellite systems, air-deployed instruments, unmanned autonomous vehicles, and moored observing networks (Fig. 6(b)). A key component consisted of 262 Airborne Expendable BathyThermographs deployed over four flights of a Navy P-3 operated out of the Patuxent River Naval Air Station on a series of legs extending from the slope waters east of Norfolk, Virginia, crossing the Gulf Stream and into the warm Sargasso Sea water between July 11, 2013 (prior to the intensive field program of Trident Warrior 2013) and July 18, 2013 (the end of the intensive field program). The AXBTs were deployed approximately every 16 km along tracks extending from the slope water across the Gulf Stream into the Sargasso Sea. On July 11, one leg followed a track of the AltiKa satellite altimeter (Fig. 7), while for the last flight on July 18, one leg followed a track of the Jason-2 altimeter. The AXBT temperature profiles were processed in near real time and transmitted to NAVO for assimilation into the real time forecast model runs and used as validation data to evaluate forecast skill.

The temperature profiles along the altimeter tracks provided data to evaluate the skill of a new vertical

projection technique, Improved Synthetic Ocean Profiles (ISOP; Fig. 7), examined as a new capability in NCODA to replace the legacy Modular Ocean Data Assimilation System (MODAS) within the 3 km and 1 km NCOM nests. Only the ISOP cases are able to capture several aspects of the circulation important for Navy antisubmarine- and mine-warfare support, including accurate strength of the Gulf Stream front, temperature inversions in the mixing of fresher slope with salty Sargasso waters, and ageostrophic thinning of the layers offshore of the main front (Fig. 7). In addition, mixed layer depths from the temperature profiles are used to test a new hypothesis about conditional predictability of frontogenesis.²

Nearshore Modeling: The innermost TW13 model nests featured demonstrations of COAMPS and the Simulating Waves Nearshore (SWAN) model (Fig. 8). COAMPS uses NCOM to model the ocean and SWAN for the waves. As noted above, a two-way coupled NCOM-SWAN grid was set up with a 400 m grid, with NCOM boundary conditions from a host 1 km grid and SWAN boundary conditions from global WaveWatchIII. Figure 8 depicts the 400 m ocean-wave domain, which extends from the mouth of Chesapeake Bay to approximately 80 km east of the northern Virginia coast. The simulation accurately represented the increased stratification and shallowing of the mixed layer during a weakening of winds from July 10 to 14 (Fig. 8(a)). An additional implementation of SWAN during TW13 examined new wave data assimilation capabilities,³ examining the impact of observations from an array of mini-wave buoys on wave forecasts along the shore south of Chesapeake Bay (Fig. 8(b)). From stream to shore, TW13 demonstrated the capabilities NRL has developed to forecast the broad range of complex ocean environments.

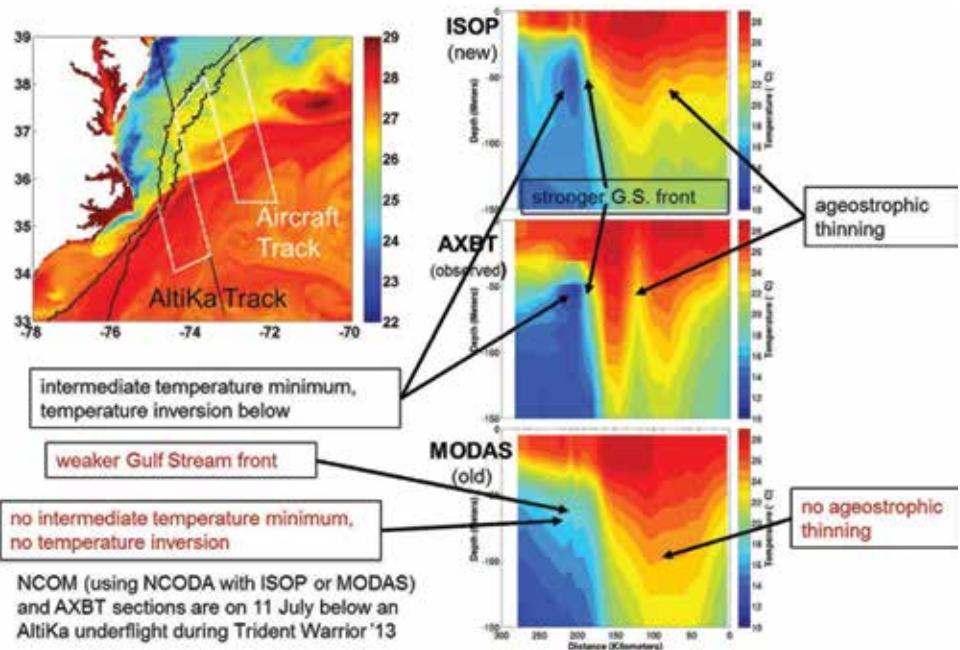


FIGURE 7
 Temperature sections following an AltiKa underflight track on July 11 compare RELO NCOM forecasts to independent AXBT observations. Critical observed phenomena affecting acoustic antisubmarine warfare (intermediate temperature minimum, temperature inversion, Gulf Stream front strength, layer thinning) are forecast only when NCOM uses the new ISOP 1.0 with NCODA.

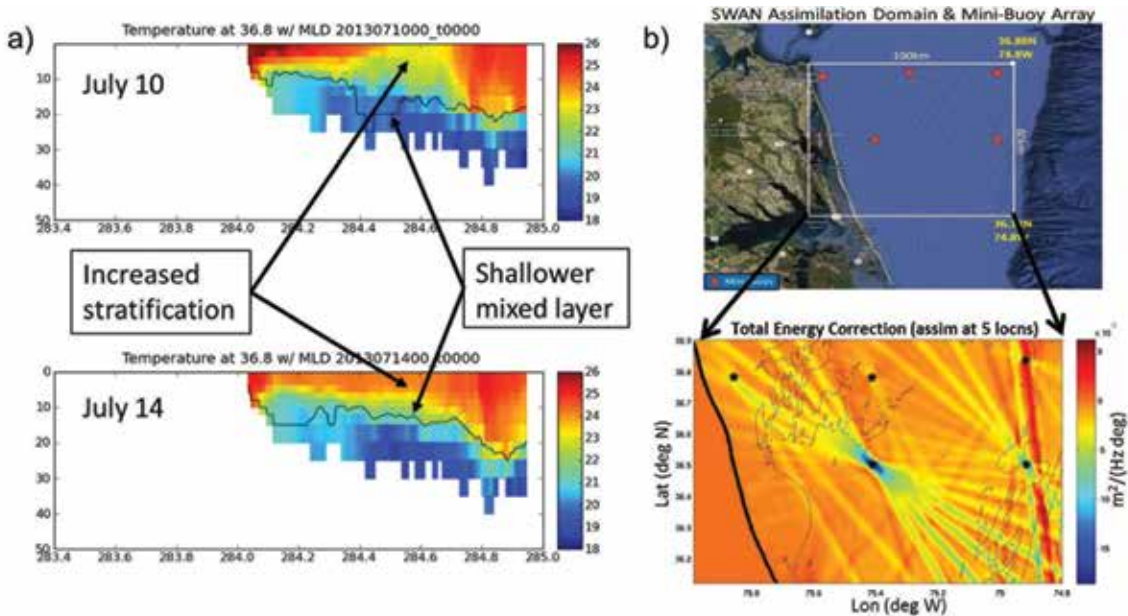


FIGURE 8
 The highest resolution models capture processes important to the warfighter in the nearshore environment, including (a) shallowing of the mixed layer and increased stratification during a wind relaxation event forecast in the 400 m resolution air-sea COAMPS and (b) correction of total wave energy by assimilating wave buoy observations in the 50 m resolution nearshore SWAN.

Acknowledgments: Our work in Trident Warrior 2013 was made possible through the support of the Office of Naval Research (ONR) and its efforts to leverage this exercise to test a wide range of technologies being

developed to support Navy and Air Force operations. We want to thank Jeffrey Kerling, Naval Oceanographic Office, Robert Liang, NRL, and Jaime Pupek, JP Technical Consulting, for collecting and processing the

AXBT data on the flights and Robert Barthelmes and the pilots and crews of VX-20 at Patuxent Naval Air Station for getting us in the air on P-3 774.
[Sponsored by ONR]

References

- ¹ C. Rowley and A. Mask, "Regional and Coastal Prediction with the Navy Coastal Ocean Model," *Oceanography*, submitted.
- ² G.A. Jacobs, J.G. Richman, J.D. Doyle, P.L. Spence, B. Bartels, and F. Bub, "Simulating Conditional Deterministic Predictability within Ocean Frontogenesis," *Ocean Modeling*, submitted.
- ³ J. Veeramony, M.D. Orzech, and K.L. Edwards, "Navy Nearshore Ocean Prediction Systems," *Oceanography*, submitted.

Integrating the Marine Biosphere into Coupled Ocean–Atmosphere Models

J.K. Jolliff and T.A. Smith
Oceanography Division

Introduction: Marine phytoplankton are vital to the functioning of Earth's biosphere. Whereas these ubiquitous microscopic organisms account for only ~1% of the Earth's photosynthetic biomass, they contribute to more than half of the global primary production. This fecund productivity forms the foundation for the marine food web and it is the requisite engine of biogeochemical cycling that enables life on Earth to flourish. Phytoplankton thrive precisely where atmospheric and oceanic planetary boundary layers meet. Exchanges of thermal energy and transfers of momentum impact the physical environment with which planktonic organisms must cope. Biological oceanography has thus been largely concerned with identifying how the physics of the ocean–atmosphere system determine microalgal prolificacy via turbulent mixing and the upwelling of deep ocean nutrients in zones of wind-forced hydrodynamic divergence.

Recently, however, numerical modeling studies^{1,2} have revitalized a long dormant paradigm in oceanography: phytoplankton and associated organic detritus absorb a significant quantity of the Sun's radiant energy and this additional energy may have a net warming effect on the surface ocean, thereby impacting density gradients. Thus, phytoplankton are not merely passive recipients of the ocean's physical dynamics, they are instead active participants in those dynamics.

Integrated Modeling of the Maritime Battlespace Environment: Motivated by these findings, we have integrated a model of biochemical nitrogen cycling and attendant bio-optical dynamics into NRL's state-of-the-art Coupled Ocean–Atmosphere Mesoscale Prediction System (COAMPS®). This numerical forecasting system

includes atmospheric and oceanic components that exchange information regarding transfers of heat and momentum at very high temporal frequency, such that the atmospheric and oceanic density fields develop concomitantly. We use the term "integrate" to emphasize that the surface biota absorb substantial quantities of solar shortwave energy that is accounted for in the modeling system (Fig. 9). Since it is the ocean biology that is driving this additional near-surface retention of thermal energy, we refer to this process as biothermal feedback.

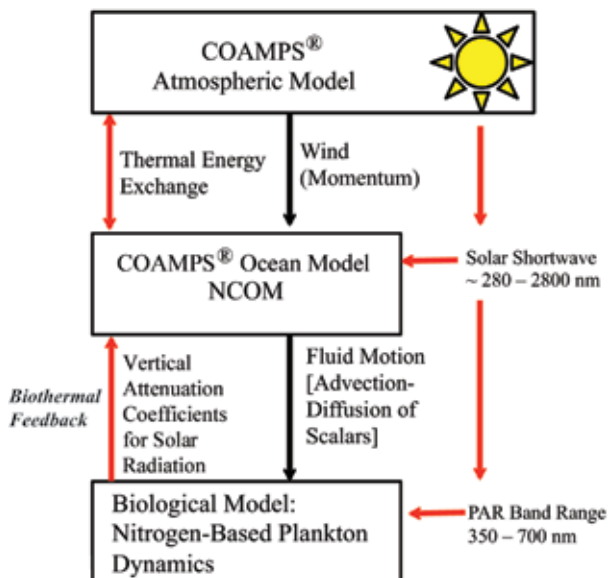


FIGURE 9 Schematic representation of COAMPS is shown with the integrated biological model using the photosynthetically available radiation (PAR) band fraction of the COAMPS solar shortwave and providing the Navy Coastal Ocean Model (NCOM) with the required optical attenuation coefficients.

Indeed, the integrated COAMPS–biology modeling results verify that biothermal feedback may influence the thermal variability of geophysical boundary layer fluids. A simulated phytoplankton bloom develops in northern Monterey Bay (Fig. 10(a)) as a result of coastal upwelling. In contrast to COAMPS simulations wherein no biothermal feedback is represented, the bio-optical properties of phytoplankton provide an additional ~1–2 °C of surface warming to the area (Fig. 10(b)). Elevated sea surface temperatures (SSTs) increase simulated latent heat flux transfers, resulting in a warmer, moister marine atmospheric boundary layer (MABL). The surface warming also increases the upper ocean thermal stratification. Since it is light rather than nitrogen that is most limiting to microalgal growth within this regime, improved vertical stability increases the photosynthetic yield by ~20%. Hence, the simulated thermal and biological fields evolve synergistically in time.

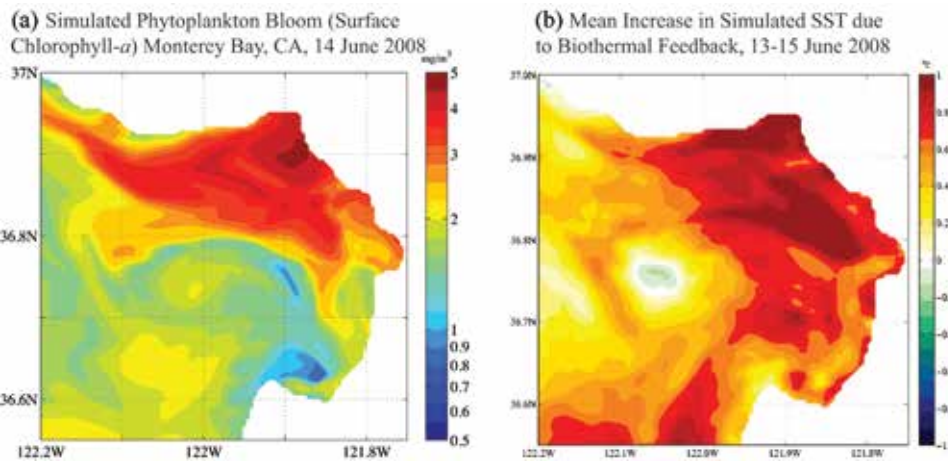


FIGURE 10

(a) The COAMPS simulated phytoplankton bloom in northern Monterey Bay, California, is shown for June 14, 2008; (b) the difference in mean SST between COAMPS with biology and COAMPS without (i.e., no biothermal feedback) is shown.

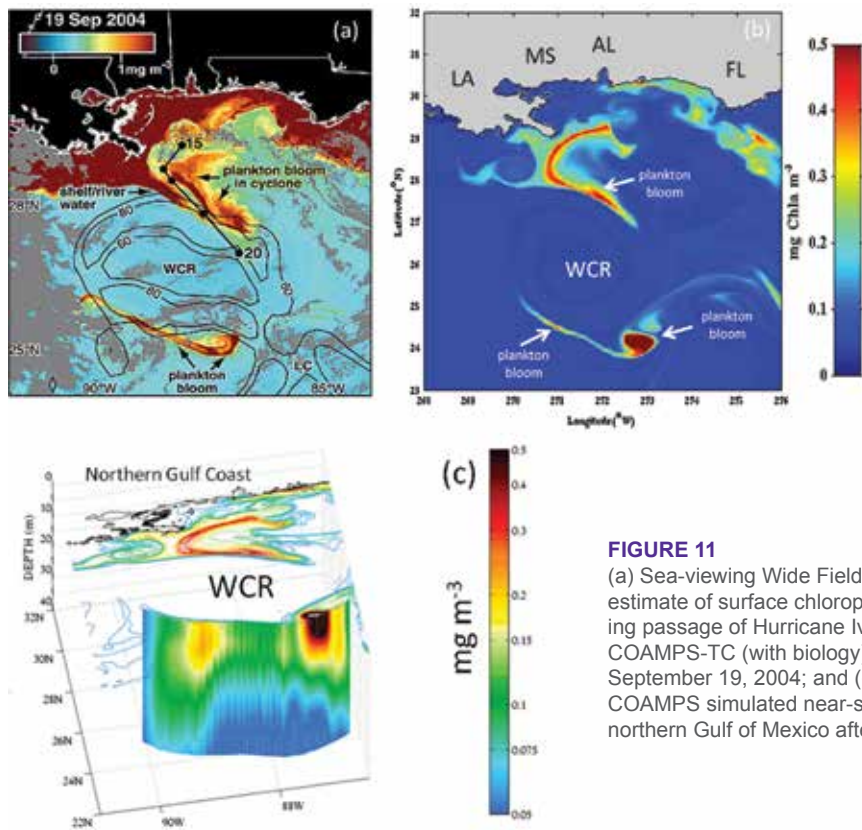


FIGURE 11

(a) Sea-viewing Wide Field-of-View Sensor (SeaWiFS) satellite estimate of surface chlorophyll-a distribution is shown following passage of Hurricane Ivan in the northern Gulf of Mexico; (b) COAMPS-TC (with biology) simulated chlorophyll-a distribution for September 19, 2004; and (c) three-dimensional rendering of the COAMPS simulated near-surface phytoplankton distributions in the northern Gulf of Mexico after the passage of Hurricane Ivan.

These results verify that the integrated modeling approach has a direct impact on aspects of environmental forecasting pertinent to U.S. Naval operations. Surface ocean bio-optical properties will impact the performance of electro-optical detection systems used for mine warfare operations. Changing conditions within the MABL will impact other operationally per-

inent variables such as humidity, surface visibility, and electromagnetic radiation propagation.

New Research Opportunities: Integrating the marine biosphere into COAMPS also provides for novel research opportunities. For example, COAMPS-Tropical Cyclone (COAMPS-TC³) is NRL's integrated

air–ocean–wave modeling system that provides a means to simulate the intense air–sea interactions and the dynamical surface wave–current interactions that are endemic to tropical cyclones. Another consequence of cyclone passage is the disturbance of the upper ocean planktonic ecosystem due to the intense turbulent motions of fluid parcels. Embedding a biological model into COAMPS-TC allows for an examination of these potential bio-optical interactions.

Hurricane Ivan traversed the northern Gulf of Mexico on September 16, 2004, directly perturbing the dynamical mesoscale surface ocean circulation. COAMPS-TC with biology simulates the resulting uplift of deeper water isotherms and the associated introduction of new nutrients into the surface mixed layer. These nutrients stimulated biological productivity that was detected in satellite radiometer data (Fig. 11(a)). The simulated biophysical processes mimic the observations (Fig. 11(b)). Phytoplankton blooms emerge in the centroid of mesoscale cyclones flanking the larger anticyclonic feature (a warm-core ring, WCR). The fidelity of COAMPS-TC to satellite observations provides a unique opportunity to examine the synoptic time evolution of the three-dimensional ocean's integrated biophysical phenomena (Fig. 11(c)).

Summary: Collectively, these results suggest that the continuing development of an Earth systems prediction capability, with applications ranging from operational forecasts for U.S. Naval operations to long-term climate simulations, must consider the synergistic interaction between the Earth's biosphere, atmosphere, and oceans. NRL is uniquely poised to advance numerical modeling of integrated biological-physical systems in ways that improve environmental forecasting tools and expand scientific understanding of complex oceanographic phenomena.

[Sponsored by ONR]

References

- ¹L. Patara, M. Vichi, S. Masina, P.G. Fogli, and E. Manzini, "Global Response to Solar Radiation Absorbed by Phytoplankton in a Coupled Climate Model," *Climate Dynamics* **39**(7–8), 1951–1968, doi: 10.1007/s00382-012-1300-9 (2012).
- ²J.K. Jolliff, T.A. Smith, C.N. Barron, S. Derada, S.C. Anderson, R.W. Gould, and R.A. Arnone, "The Impact of Coastal Phytoplankton Blooms on Ocean-Atmosphere Thermal Energy Exchange: Evidence from a Two-Way Coupled Numerical Modeling System," *Geophys. Res. Lett.* **39**(24), doi: 10.1029/2012GL053634 (2012).
- ³T.A. Smith, S. Chen, T. Campbell, P. Martin, W.E. Rogers, S. Gaberšek, D. Wang, S. Carroll, and R. Allard, "Ocean-wave Coupled Modeling in COAMPS-TC: A Study of Hurricane Ivan (2004)," *Ocean Modeling* **69**, 181–194, doi:10.1016/j.oceomod.2013.06.003 (2013).



space research and satellite technology



226 High-Precision Remote Sensing of Ionospheric Disturbances

229 SWORD: Improving the Simulation Experience

231 Project CHRONOS

High-Precision Remote Sensing of Ionospheric Disturbances

J. Helmboldt
Remote Sensing Division

Analyzing the Ionosphere: The ionosphere, the ionized portion of Earth's upper atmosphere (60 to 1000 km altitude), is a dynamic medium, providing a kind of plasma laboratory in our own "backyard." Disturbances commonly occur within the ionosphere, manifesting as temporal and spatial perturbations in the electron/ion density. These are generated by a variety of mechanisms ranging from gravity waves originating from the lower atmosphere, the impact of geomagnetic storms and substorms, and inherent ionospheric instabilities. Thus, obtaining a better inventory and understanding of such disturbances is key to understanding not only the ionosphere itself, but also the coupled nature of Earth's atmosphere, plasmasphere, magnetosphere, and indeed, the Sun–Earth system.

In addition to the numerous basic research questions that may be addressed through the study of ionospheric disturbances, these phenomena have a measurable impact on assets such as GPS and over-the-horizon (OTH) radar. The ionosphere interacts with any radio-frequency (RF) wave that propagates through it, delaying the signal and resulting in refraction similar to visible light passing through water. Ionospheric disturbances effectively cause variations in the index of refraction, distorting the signal path. This causes, for instance, significant errors in GPS-derived positions, as well as degradation of geolocation accuracy within OTH radar systems. Because of this, assets such as GPS receivers have been turned into ionospheric remote sensors by leveraging techniques that correct for the ionosphere's detrimental effects. These corrections are used to characterize observed disturbances in the total electron content (TEC), the electron density integrated along the line of sight to the satellite.

The ionosphere has a similar impact on RF astronomical observations, especially in the high frequency (HF)/very high frequency (VHF) regime, since the time delay caused by the ionosphere is inversely proportional to the square of the frequency. In fact, for decades, ionospheric distortions/disturbances constituted the chief factor that limited the size of a VHF interferometer used for imaging cosmic radio sources (roughly, <1 km). Thanks in part to pioneering work performed by NRL astronomers, calibration techniques were developed to overcome the effect of the ionosphere, allowing interferometers to operate within the VHF regime with baselines ~35 km or more. This helped open up a new sub-field within radio astronomy as it allowed, for the

first time, images to be made at frequencies below 100 MHz with angular resolution better than one minute of arc.

New Ionospheric Measurement Techniques:

Spurred by this pioneering work, scientists within the NRL Remote Sensing Division have developed new techniques to convert the calibration techniques developed for VHF interferometry for remote sensing of ionosphere disturbances. Using data from the Very Large Array (VLA) in New Mexico, for which NRL helped develop two VHF systems (at 74 and 300 MHz), changes in ionospheric TEC were measured to a precision more than two orders of magnitude better than what is achieved with similar GPS-based methods. These new high-precision techniques have been paired with advanced spectral analysis algorithms to characterize wavelike disturbances, commonly referred to as traveling ionospheric disturbances (TIDs). These have been applied to many VLA data sets, yielding new insights into the nature of TIDs.

Tracking TIDs: An example of an application of these new techniques is a climatological study of TIDs that was conducted using data from an NRL-led, VLA all-sky imaging survey at 74 MHz. Figure 1 shows maps of wave activity, averaged by time of day and season, representing the magnitudes, directions, and sizes of detected TIDs. While some of the observed phenomena are well known (southwestward-propagating TIDs during summer nighttime; southeastward-propagating TIDs during winter daytime), there are many features unique to this survey. These include the activity seen during autumn dusk and nighttime where TIDs were detected moving in virtually all directions, likely due to gravity waves related to the mountainous terrain in the surrounding area.

Another example is a joint detection of a TID generated by one of the last underground nuclear explosions (UNEs) conducted by the U.S. in Nevada in 1992 using both GPS and VLA data. While GPS data were successfully used to detect the wave and estimate its speed and wavelength, the analysis of VLA data revealed its properties in more detail. In particular, the VLA detected small (~2 km in size) distortions along the wavefront, which manifested as small-scale, wavelike disturbances that appeared to propagate perpendicular to the TID's direction of motion near the expected time of arrival at the VLA (see the spectral maps in Fig. 2).

Turning on VLITE: The application of these techniques is being expanded to include radio telescopes in other parts of the world (e.g., India and the Netherlands). They will also be a key component of

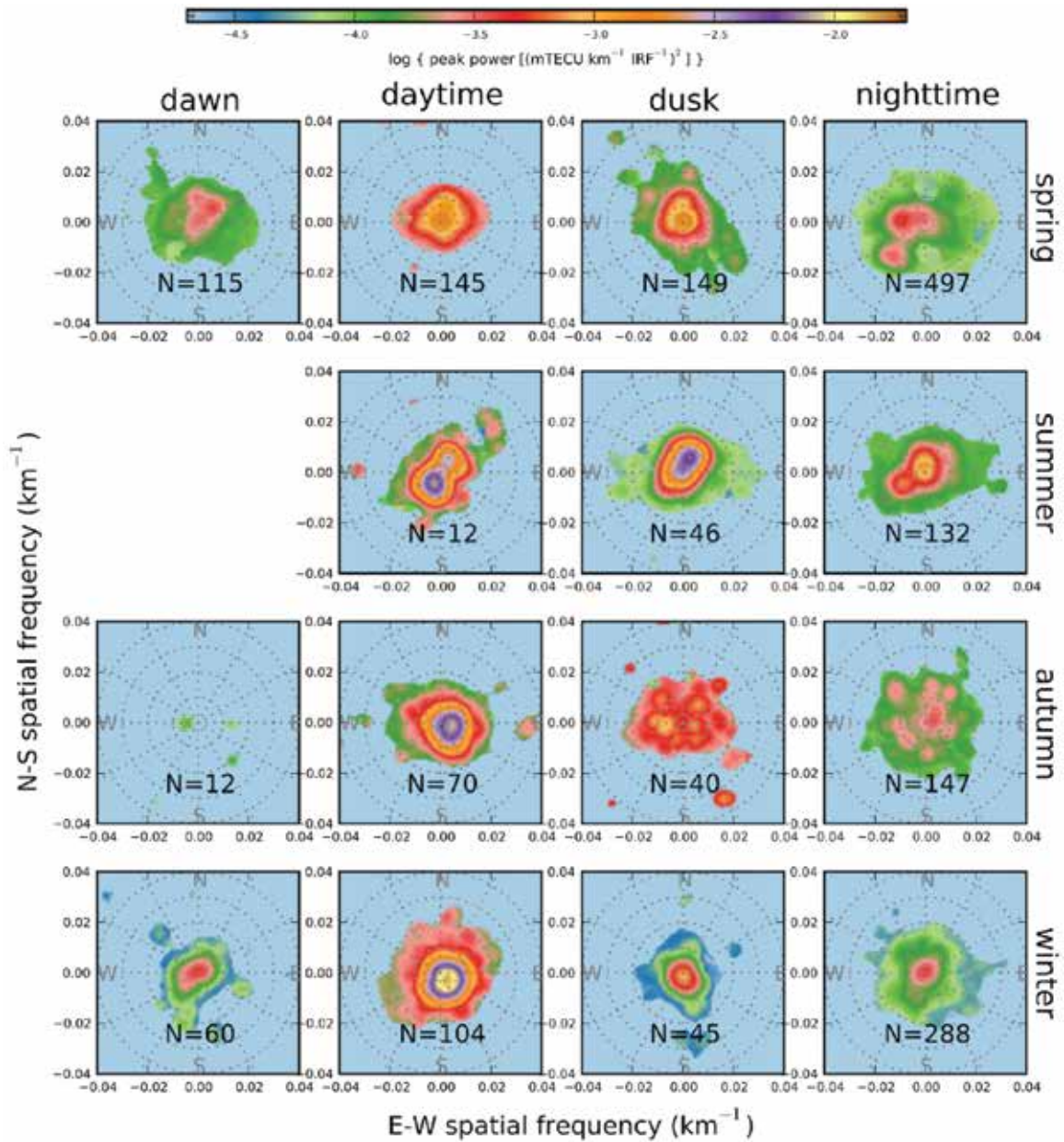


FIGURE 1

A climatological study of TIDs derived from a VLA all-sky survey at 74 MHz. Displayed are maps of TID fluctuation power averaged by time of day and season, where north is up, east is right, and the spatial frequency (the reciprocal of the wavelength) increases radially within each map.

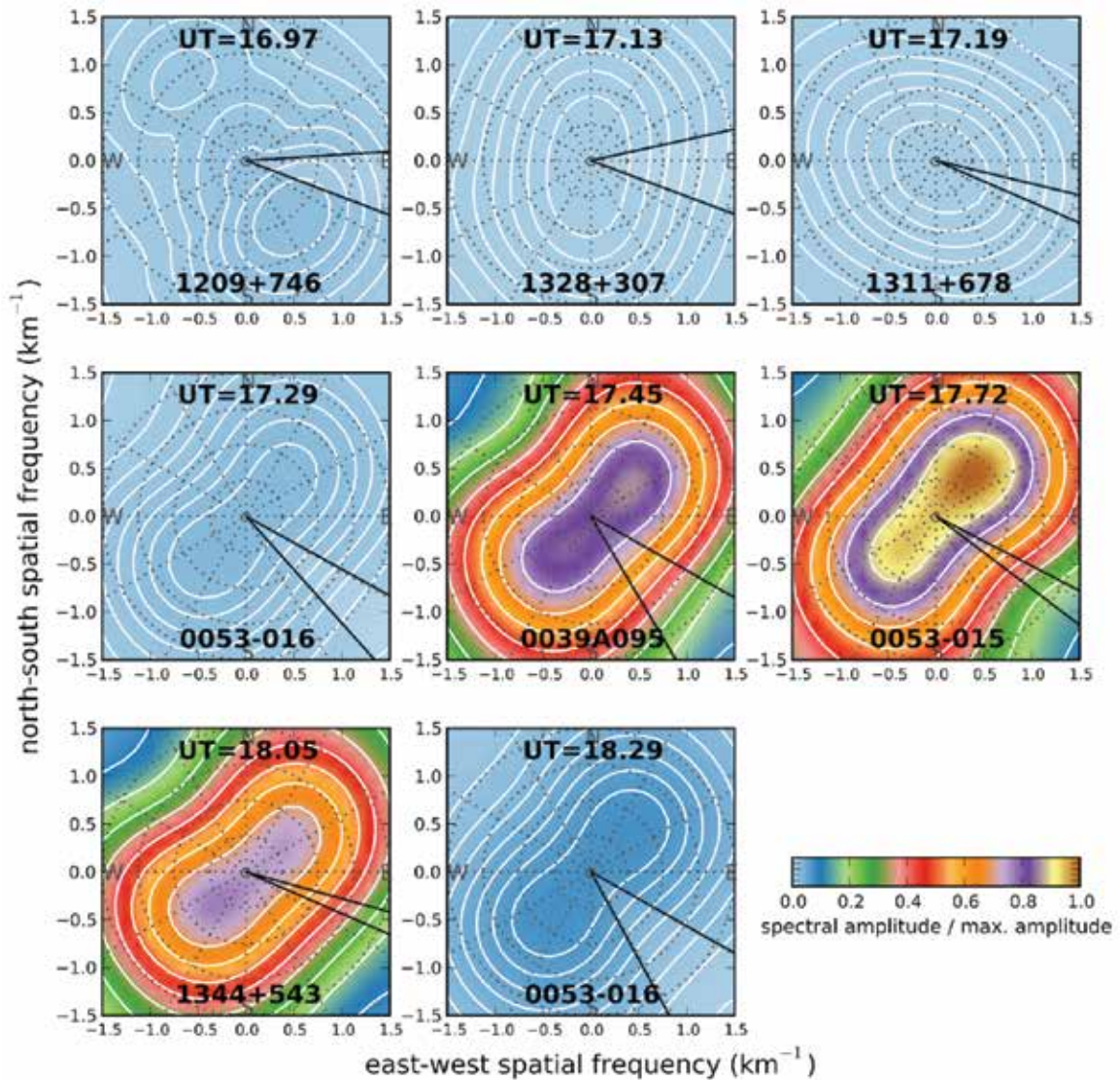


FIGURE 2

Spectral maps (similar to those shown in Fig. 1) derived from VLA observations of bright cosmic sources in the aftermath of a UNE conducted in Nevada in September 1992. The fluctuation power increases dramatically around the expected time of arrival, $\sim 17:30$ UT based on concurrent GPS data. The approximate direction of propagation of the main TID is shown with solid black lines. Small-scale fluctuations/distortions are apparent within the spectral maps, propagating approximately along the wavefront.

an exciting new NRL-supported project, the VLA Low-frequency Transient and Ionospheric Experiment (VLITE). VLITE will continuously monitor the VLA field of view at 350 MHz, and likewise, the ionosphere for three years, yielding an extensive, rich, and unique database of ionospheric disturbances.

[Sponsored by the NRL Base Program (CNR funded)]



SWORD: Improving the Simulation Experience

C. Gwon,¹ M. Strickman,¹ B. Philips,¹ D. Polaski,²
B. Leas,³ and L. Jackson²

¹Space Science Division

²Praxis, Inc.

³SRA International

Introduction: Physics simulation codes have played an integral role in driving the development of modern day computing, dating back to the first electronic general-purpose computer, the ENIAC. Such codes required constant improvements to the performance of computers, and as Moore's Law carried us forward, the capabilities of these codes followed suit. Today, users have the ability to simulate processes that scientists could only dream of a few decades ago, and modern physics codes provide an incredible repository of knowledge that can be used to solve a wide range of problems. The continuing decrease in cost of computing and increase in capabilities provide the means of virtually creating and testing products before devoting significant resources to their construction.

As promising and simple as it seems, the cost of simulation has always been the investment of time and energy into learning how to operate advanced physics codes properly. With high-energy radiation transport codes, this investment has historically been a nontrivial one. For a novice user, preparing the most simplistic scenario with these codes could take weeks, and simulating a realistic scenario could take much longer. Alleviating this steep learning curve has been the primary motivation for creating SWORD, the SoftWare for the Optimization of Radiation Detectors simulation framework.

SWORD Unsheathed...: In 2006, in response to a call for proposals from the Domestic Nuclear Detection Office (DNDO) of the Department of Homeland Security (DHS), NRL Space Science Division proposed the development of a software framework that would drastically reduce the overhead involved with using high-energy radiation transport codes and streamline

the process of running simulations and analyzing the outputs from such codes. This framework, SWORD, consists of a graphical interface and analysis tools for evaluating the performance of instruments used for the detection of nuclear materials, especially those that might be used to create weapons of mass destruction (Fig. 3). The most common radiation transport codes used for this purpose are two Monte Carlo packages: Geant4 from the European Organization for Nuclear Research (CERN), and MCNPX from Los Alamos National Laboratory (LANL). Creating a program with interfaces to both of these codes, with the option for future additions, was a fundamental requirement for SWORD from its inception.

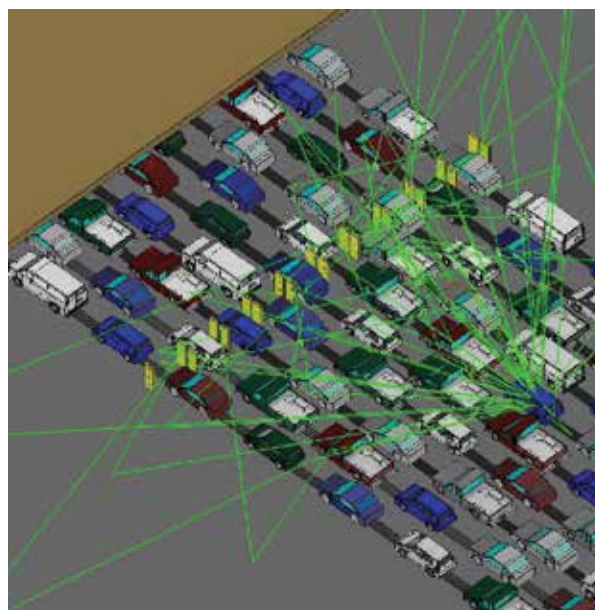


FIGURE 3
NRL SWORD simulation of an operational scenario at the Tijuana border crossing from Mexico to the United States. Green tracks show the gamma emission from the source (in the trunk of the blue car) to the radiation portal detectors (shown in yellow).

Although the physics processes covered by Geant4 and MCNPX have significant overlap, their implementations are vastly different, each having its own strengths and weaknesses. Geant4 is written in C++, and simulation setup is accomplished by writing C++ code. MCNPX is FORTRAN-based, with the simulation setup passed in via an input file of "cards" that emulates a deck of punch cards. Each card has several options that users set in order to define the parameters of their simulation. Differences also exist in the philosophy of the information that the simulation supplies on output. Whereas Geant4 gives the user freedom to decide what information to extract from the simulation on an event-by-event basis, MCNPX supplies histograms or distributions integrated over an entire

run. On the other hand, MCNPX performs extensive statistical checks on the results, informing the user of the trustworthiness of the results. With SWORD, users are insulated from these details and may proceed with a simulation and obtain an accurate complex-geometry result with a high degree of confidence.

...and Sharpened: Today, the SWORD framework has evolved into a fully functional software suite, whose core remains a CAD-like graphical interface for building simulation scenarios, but also includes an extensive and extensible standard library of objects (air/land/sea vehicles, buildings, containers, rail cars, commercial off-the-shelf detectors), and gamma-ray and neutron emission spectra (including terrestrial and sea backgrounds, naturally occurring radioactive backgrounds, common medical isotopes, and special nuclear materials) (see Fig. 4). Support for one additional radiation transport code beyond the initially supported Monte

models for use in simulation and the ability to generate keyhole markup language (KML) files of particle traces and heat maps for overlaying on Google Earth, thereby providing users visual feedback on the simulation results and threat assessment.

Wielding SWORD: Both DHS and DoD agencies make significant use of SWORD. It has been used to predict and interpret results from test campaigns run by both the Defense Threat Reduction Agency (DTRA) and the Office of Naval Research (ONR). Simulations were also performed of the background gamma radiation of the DC area in order to compare with aerial measurements performed by the National Nuclear Security Administration (NNSA) of the Department of Energy (DOE).

Since the physics involved with detecting covert nuclear materials is very similar to that involved in X-ray and gamma-ray astronomy, SWORD is also being

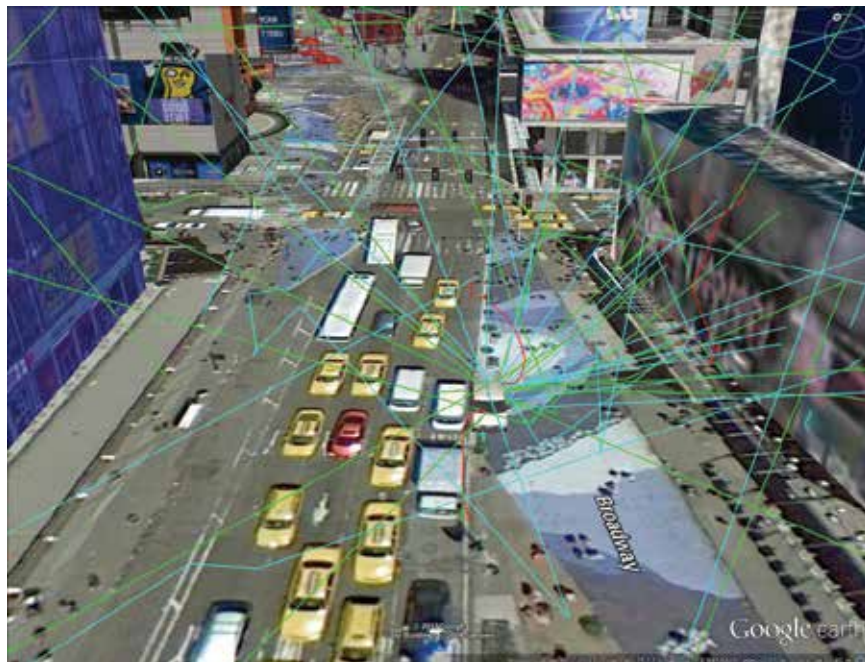


FIGURE 4

NRL SWORD simulation of a neutron source in a building with radiation detectors in the white van. Cyan tracks show path of neutrons that are emitted from the source and enter the detector. Green tracks show secondary from neutron interactions in air that enter the detector.

Carlo codes Geant4 and MCNPX has recently been added: the Denovo discrete ordinates code from Oak Ridge National Laboratory (ORNL), which is operable within SWORD through the ORNL ADVANTG python interface. The addition of a deterministic code such as Denovo allows users to obtain faster results to problems, albeit with potential tradeoffs from the approximations used in the solution. SWORD now also includes the ability to parse geographic information system (GIS) data to automatically generate city-scale

applied to simulation of space instrumentation, including the NRL-led Solar Orbiter Heliospheric Imager (SoloHI) as well as various proposed future instruments. Simulations using SWORD address questions of expected instrument performance and the effects of orbital radiation environment on instrument lifetime. Further, NRL researchers use SWORD to simulate the effects of terrestrial gamma-ray flashes (TGFs), or “dark lightning,” the intense submillisecond bursts of ionizing radiation from thunderstorms, and have simulated both

the source of the TGFs — i.e., the particle accelerator buried within thunderstorms — and dose calculations for individuals in a Boeing 737 aircraft, should a TGF event strike their plane (Fig. 5).

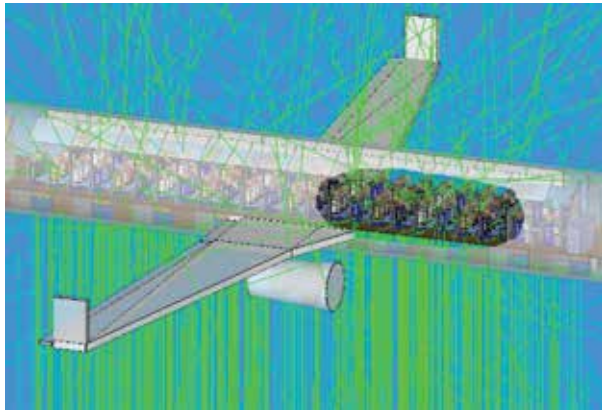


FIGURE 5
NRL SWORD simulation of a terrestrial gamma-ray flash (TGF) as it enters a 737 aircraft. Dose calculations to the passengers on the airliner were performed using the SWORD framework.

SWORD as Shield: The SWORD framework, now the primary tool used by DNDO and DTRA for running simulations involving the detectability of radiological and nuclear threats, has brought the vast capabilities of high-energy radiation transport simulation to a crucial segment of the WMD detection cadre: the technically astute but computationally nonexpert members of this community. Active collaborations with LANL, ORNL, and Sandia National Laboratories strengthen SWORD's integration with the underpinning radiation transport simulation codes as they evolve. With a growing user base, and increasing functionality, SWORD provides an effective means for reliable and efficient access to powerful, accurate simulation.

This work has been supported by the U.S. Department of Homeland Security, Domestic Nuclear Detection Office. This support does not constitute an express or implied endorsement on the part of the Government.

[Sponsored by DNDO–DHS]



Project CHRONOS

K. Senior
Space Systems Development Department

Introduction: The Global Positioning System (GPS) and the receiver technologies that have developed along with it have revolutionized modern warfare,

as well as many civilian industries such as transportation, and has spawned whole new industries because of its unique capability to provide inexpensive precise navigation and positioning to users anywhere globally in the near-Earth vicinity. The GPS system routinely delivers positioning and navigation precisions for most users at the meter level but also at the centimeter level or even millimeter level for some specialized geophysical applications using other GPS data products available from services like the International GNSS Service (IGS).^{1,2} While the largest numbers of applications serving both civil and military users fall under the category of positioning and navigation, a fair number also rely on GPS for precise time or frequency dissemination or synchronization. In fact, the use of GPS for timing, synchronization, or both is so ubiquitous that many engineers and technicians even technically aware within some programs sometimes overlook just how tightly integrated and dependent the level of integration of GPS is within their systems. For example, the U.S. electric grid, cell phone networks (see Fig. 6), and many computer networks are heavily dependent on GPS for maintaining synchronicity (or syntonicity) of their network such that a loss of GPS for extended periods could mean significant service outages within their respective networks. Because the relatively weak signals from the GPS satellites can be easily jammed, either inadvertently or perhaps maliciously, the sole dependence on GPS in such applications represents significant vulnerability to many of our nation's infrastructures.

CHRONOS Approach: In order to address these vulnerabilities, the Naval Research Laboratory has developed and deployed several new technologies as part of Project CHRONOS. The chief aim of this project is to provide to various DoD customers in support of our national defense a robust nanosecond-level global time and frequency capability that is both GPS compatible and GPS independent, delivering credible, highly precise and accurate timing signals and associated data products across various platforms.

CHRONOS uses GPS for its primary time recovery but also employs other techniques to augment GPS, including commercial atomic clocks, Two-Way Satellite Time and Frequency Transfer (TWSTFT) over military satellites, and specialized clock-ensembling algorithms to provide GPS independence and independent monitoring of the GPS timing signals. The overall CHRONOS approach has four main tenets:

1. *Accurate, Credible Time Source*

- All timing signals provided by the CHRONOS Time and Frequency Infrastructure (TFI) are traceable to the DoD time standard, UTC(USNO), as maintained at the U.S. Naval Observatory



FIGURE 6
Visualization of cell phone networks in the United States by "America Revealed."

- Globally distributed time and frequency (T&F) sources
- GPS time recovery is the primary means of time recovery
- Additional atomic clocks provide holdover capability
- Additional robustness assured through system redundancy

2. *Distribution*

- Transport high-quality/verifiable T&F signals and products to users
- Nearly all time and frequency signal formats are supported (e.g., 1PPS, 1/5/10MHz, IRIG, NTP, and PTP).
- Additional reference emitters can provide additional T&F dissemination to reach regionally remote users

3. *GPS Independence*

- Multiple redundant local atomic clocks for increased holdover
- Two-Way Satellite Time and Frequency Transfer
- Ensembling of clocks to provide even more holdover and provide robust characterization of the local clocks and those clocks seen remotely via GPS or TWSTFT

4. *Closed Loop Monitor and Control*

- All system component telemetry and clock measurement information and data are relayed to a central database
- All stations monitored in real time from a centralized operations floor

Existing approaches to providing timing and synchronization are generally stove-piped or “top-down” solutions as characterized in Fig. 7. Isolated GPS receivers are often deployed for this purpose without any external monitoring of the timing they provide. In

limited cases where monitoring does occur, it generally only entails monitoring of the GPS receiver (internal) telemetry, which could be in error or spoofed. Where other GPS independent techniques, such as TWSTFT, have been employed, they are often single linkages to a single time dissemination source and are therefore dependent on single points or single links of failure. In addition to single points of failure, errors in such top-down approaches also tend to cascade down.

CHRONOS differs from these other approaches in that it is a fully distributed timing and synchronization capability, as summarized in the diagram of Fig. 8. Here, multiple linkages of comparison are maintained between the full network of timing nodes including GPS as well as multiple TWSTFT linkages. Single points of failure are avoided since all nodes are intercompared through multiple techniques and through multiple links. Redundancy of system elements and the use of commercial atomic clocks further increase the robustness and holdover capabilities during any GPS outages or during more significant jamming events where both GPS and TWSTFT may not be available.

CHRONOS Clock Ensembling Algorithm

(NITRO): Additionally, NRL has developed specialized clock ensembling algorithms^{3,4,5} that increase the system robustness and holdover even further by harnessing the timing from all of the local clocks as well as remote clocks together. By averaging the signals/measurements from multiple clocks, one may achieve timing that is better than what would be provided by any of the clocks alone. The ensembling methods use measurements of the local clocks as well as GPS and TWSTFT measurements of the remote clocks in order to achieve this. Another benefit of this

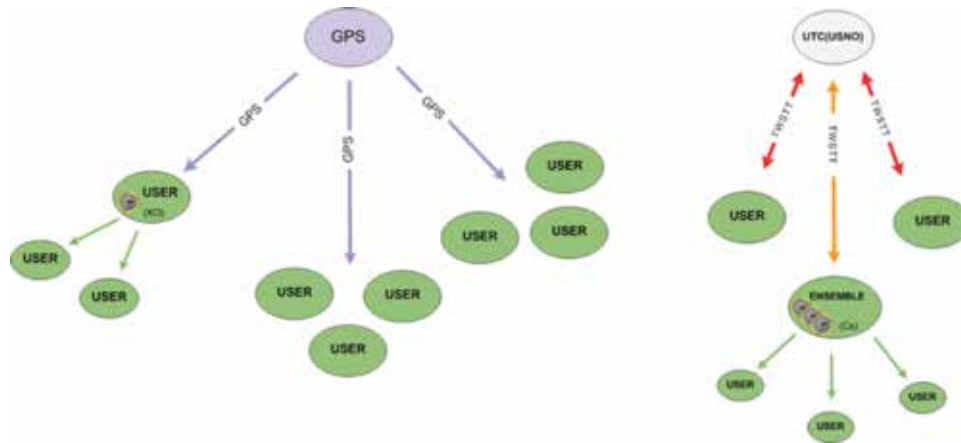


FIGURE 7 Current approaches to timing and synchronization are often GPS-centric and stove-piped or “top-down” approaches, leading to single source vulnerabilities and isolated unmonitored elements.

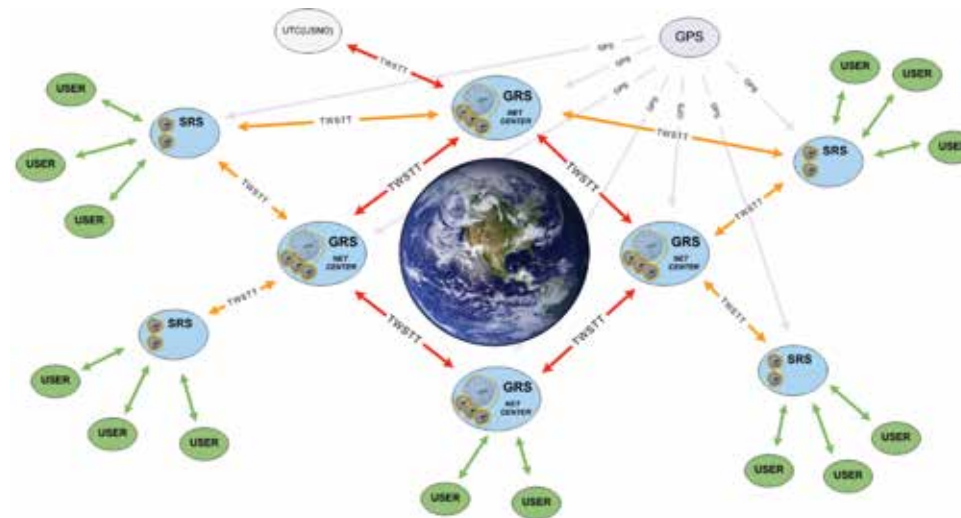


FIGURE 8 CHRONOS represents a fully distributed approach to timing and synchronization. Synchronicity is assured through redundant high-quality links between the clocks, including both GPS and TWSTFT, as well as local and remote clock intercomparison and combination using ensembling. This approach is not single-source dependent and uses all of the clocks maximally together.

technique is that ill-behaving clocks or ill-behaving measurement techniques (e.g., GPS or TWSTFT) are easily identifiable as a result of the combination and intercomparison. A self-contained clock measurement and ensembling system called “NITRO” was developed and deployed by NRL for this purpose.

NITRO performs several functions including the measurement and estimation in near real time of the states of all clocks that are available, including local clock measurements, as well as GPS and TWSTFT measurements of clocks that are seen remotely. NITRO combines the state information from multiple clocks in order to generate a more stable virtual clock than any of the constituent physical clocks would otherwise generate alone. Figure 9 shows a simulation example of the increased timekeeping performance that one

can achieve by using such an ensembling approach. The figure shows a class of three simulated clocks, each having different frequency stability characteristics over different averaging intervals, as measured by the Hadamard deviation statistic. Lower Hadamard deviation means better frequency stability and, hence, better timekeeping performance at that given averaging interval. As the figure demonstrates, NITRO generates timekeeping better than any of the constituent clocks themselves as well as extracting the best performance characteristics from each of the classes.

NRL Calibration Facility and Roving Calibration Units: In order to ensure traceability and verifiability of timing signals across the TFI network, it is crucial to provide nanosecond-level calibrations of all fielded

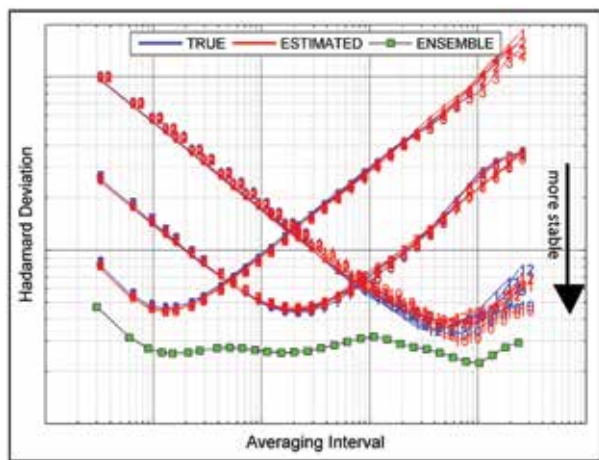


FIGURE 9
A simulation example demonstrating the improved timekeeping performance yielded from ensembling clocks together using the NITRO clock-ensembling algorithm. The plot shows the frequency stability as measured by the Hadamard deviation statistic for three classes of simulated clocks, each performing differently over different averaging intervals. The NITRO algorithm achieves a resulting ensemble that is better at all averaging intervals by using the best performance from each class of clocks. Note that the lower on the curve, the more stable.

equipment. The NRL Precise Clock Evaluation Facility (PCEF) has provided absolute calibration capabilities for GPS receive equipment for several decades and has also developed methods for calibrating TWSTFT equipment. The PCEF includes an anechoic chamber for accurately measuring delays through GPS antennas as well as several GPS simulators for injecting known signals into receivers for the purpose of measuring absolute delays through GPS receivers. Atomic clocks and accurate measurement devices are also available to support such measurements. The NRL PCEF calibration facility includes an anechoic chamber, network analyzers, and GPS simulators.

While the PCEF laboratory equipment is adequate for accurately measuring calibration delays for equipment collocated at the laboratory, it does not provide an adequate means of calibrating equipment that is installed in the field. In order to support field installations, NRL has developed techniques and procedures as well as three roving GPS calibration kits for recovering nanosecond calibrations in the field. Absolute calibrations are made routinely on each kit and the kits subsequently are used in the field.

Calibration of the remote fielded GPS equipment is achieved by running the calibration kit in situ with the fielded GPS system where a common local atomic clock signal is provided to both. Using very precise GPS ephemerides and specialized geodetic reduction software, GPS data collected from each of the two systems may be compared to recover the unknown

GPS equipment delays for the fielded system with nanosecond-level accuracy.

Additional equipment delays for all other equipment are also measured post installation on site, including all relevant 1 pulse per second cable delays and TWSTFT equipment delays. TWSTFT equipment calibrations may be inferred either from the GPS calibrations or independently using specialized roving TWSTFT units as well.

[Sponsored by DoD]

References

- ¹ J. Kouba, "A Guide to Using International GNSS Service (IGS) Products," Geodetic Survey Division, Natural Resources Canada, May 2009.
- ² IGS Product Accuracies and Latencies, <http://igsacc.igs.org/components/prods.html>, 2009; R. Beard, J. White, E. Detoma, and P. DuPuis, "Common Time Reference for Naval Systems," U.S. Naval Research Laboratory Report, NRL/FR/8150--04-10,079, October 12, 2004.
- ³ S.R. Stein, "Time Scales Demystified," Proceedings of the 2003 IEEE Frequency Control Symposium and PDA Exhibition Jointly with the 17th European Frequency and Time Forum, May 2003, pp. 223–227.
- ⁴ K. Senior and D. Percival, "Multiscale Clock Ensembling Using Wavelets," Proceedings of the 42nd Annual Precise Time and Time Interval Systems and Applications Meeting, November 2010, pp. 527–540.
- ⁵ D.B. Percival and K.L. Senior, "A Wavelet-Based Multiscale Ensemble Time-Scale Algorithm," *IEEE Trans. Ultrasonics, Ferroelectrics, and Frequency Control* **59**(3), 510–522 (2012).

special awards and recognition



236 Special Awards and Recognition

249 Alan Berman Research Publication and NRL Edison (Patent) Awards

252 NRC-ASEE Postdoctoral Research Publication Awards



2012 PRESIDENTIAL EARLY CAREER AWARD FOR SCIENTISTS AND ENGINEERS (PECASE)

Dr. Jeremy Robinson
Electronics Science and Technology Division

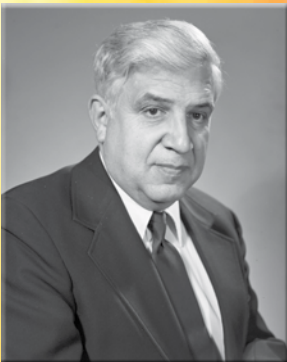
The White House announced the recipients of the 2012 Presidential Early Career Award for Scientists and Engineers (PECASE) on December 23, 2013. This award is the U.S. Government's highest honor for scientists and engineers in the early stages of their careers. President Obama said, "Coupling relentless curiosity with fidelity to facts, our Nation's scientists and engineers have driven American progress for generations. With unwavering commitment to scientific excellence and technological advancement, you are helping carry this tradition forward and keeping America on the cutting-edge of innovation and discovery." Dr. Robinson, a materials research engineer at NRL, was recognized for his "outstanding research accomplishments in the development of graphene-based materials; dedication to community service; and mentoring work with students." Dr. Robinson's research focuses on the synthesis, characterization, and processing of graphene and other nanomaterials for applications such as chemical detection, quantum information processing, nanoelectronic devices, and RF communications.



THE UNDER SECRETARY OF DEFENSE (ACQUISITION, TECHNOLOGY, AND LOGISTICS) AWARD FOR EXCELLENCE

Dr. Bhakta Rath
Materials Science and Component Technology Directorate

Dr. Rath was presented this award in recognition of his support to the Defense Trade and Technology Initiative (DTI). He played an essential role in helping manage the U.S.-India strategic relationship. During a June 2012 trip to India, Secretary of Defense Leon Panetta announced a new initiative to deepen and streamline defense cooperation with India and to make it more "practical and collaborative." The initiative was spearheaded by Deputy Secretary of Defense Dr. Ashton Carter. Dr. Carter noted that the only limit to U.S.-India defense cooperation "should be our independent strategic decisions, not bureaucratic obstacles or inefficient procedures." Dr. Rath's efforts had positive impact in three key elements of the DTI: streamlining export control and acquisition procedures related to India, identifying significant and achievable opportunities for co-production and co-development with India, and working with Indian counterparts to develop cooperative science and technology priorities. The DTI has already significantly advanced defense cooperation with India.



2012 HIS HIGHNESS SHEIKH SALEM AL-ALI AL-SABAH INFORMATICS AWARD

Mr. Roger Easton
Naval Center for Space Technology (deceased)

Launched in 2001, the Informatics Award is one of the most important information technology awards from the State of Kuwait. It was created to develop human capabilities in the field of information development and consolidate the role of institutions in society to cope with rapid developments in informatics. The "Informatics Badge of Honor" is awarded for the personality, public or corporate, with a distinctive contribution in informatics and society. In recognition of Mr. Easton's invention of the Time Navigation (TIMATION) system that forms the basis of the Global Positioning System (GPS), Kuwait's Sheikh Salem Al-Ali Al-Sabah bestowed the highest award in Kuwait upon Mr. Easton. Mr. Easton was represented by his son, Roger Easton, Jr., in the ceremony.

DEPARTMENT OF THE NAVY ACQUISITION EXCELLENCE TECHNOLOGY AWARD

Marine Meteorology Division and Space Science Division

This award was presented by the Honorable Sean J. Stackley, the Assistant Secretary of the Navy for Research, Development and Acquisition. Recognizing individuals and teams for outstanding contributions in promoting competition and innovation in the Navy and Marine Corps acquisition process, the NRL team received the award for a new generation atmospheric global prediction system. The Navy Global Environmental Model (NAVGEM) is a high-resolution global weather prediction system representing a significant milestone in numerical weather prediction (NWP) system development, introducing a semi-Lagrangian/semi-implicit (SL/SI) dynamical core with advanced moisture and ozone physical parameterization schemes. NAVGEM was delivered to the Fleet Numerical Meteorology and Oceanography Center (FNMOC) on September 30, 2012, and entered official operation in March 2013. NAVGEM is part of the global modeling “bridging strategy” in which the Navy and the National Weather Service jointly develop a national global forecasting system named Earth System Prediction Capability (ESPC) to be fielded in the 2020 time frame.



2012 DR. DELORES M. ETTER TOP SCIENTISTS AND ENGINEERS OF THE YEAR AWARD

This award, sponsored by the Assistant Secretary of the Navy for Research, Development and Acquisition, is presented annually to Navy civilian and military personnel who have made significant contributions to their fields and to the Fleet. It is named after former Assistant Secretary of the Navy Dr. Delores Etter, who established the awards in 2006 to recognize these contributions and to promote continued scientific and engineering excellence. More than 35,000 scientists and engineers across the Department of the Navy are eligible. Nominees must have demonstrated exceptional scientific and engineering achievement in their field during the preceding calendar year of the award. Achievements are considered significant when they establish a scientific basis for subsequent technical improvements of military importance, materially improve the Navy’s technical capability, and/or materially contribute to national defense.

Top Scientists and Engineers

Optical Sciences Division

Dr. Jesse Frantz – Optical Materials and Devices Branch

Dr. David Tulchinsky – Photonics Technology Branch

Mr. Allen Davis – Optical Techniques Branch

Plasma Physics Division

Dr. Joseph Huba – Beam Physics Branch

Electronics Science and Technology Division

Microfabrication Techniques Team – Dr. Colin Joye and Dr. Alan Cook

Center for Bio/Molecular Science and Engineering

Dr. Gary Vora – Laboratory for Biosensors and Biomaterials

Space Systems Development Department

Mr. Christopher Huffine – Advanced Systems Technology Branch

Space Science Division

SuperMISTI Team – Dr. Bernard Philips, Dr. Eric Wulf, Dr. Lee Mitchell, and

Dr. Anthony Hutcheson



2012 OFFICE OF NAVAL RESEARCH PRIZE FOR AFFORDABILITY

Mr. Arthur Webb, Mr. Paul Slebodnick, Mr. James Martin, and Mr. Jan Bergh
Chemistry Division

Scientists in NRL's Chemistry Division have been recognized for their development of Rapid Cure Single Coat Tank Coatings. Intended for use in shipboard tanks and voids, this team formulated, synthesized, and commercialized coatings that have revolutionized the Navy's approach to tank maintenance. This technology, which has been implemented Fleet-wide, has provided a \$7 million annual costs savings to date and is making a significant contribution toward reducing the total ownership costs associated with the corrosion control of U.S. Navy ships and submarines. Corrosion control of tanks and voids is the number one corrosion-related maintenance cost in the U.S. Navy, as documented by the Department of Defense. The new coatings have resulted in cost savings of nearly 35% in tank/void painting cost, 40% reduction in tank/void preservation time, with a material cost equal to legacy systems. The NRL-developed technology was fully implemented by the Naval Sea Systems Command (NAVSEA) in September 2008. To date, 1178 tanks have been painted with single coat systems on U.S. Navy surface ships, carriers, and submarines.



2013 JAMES CLERK MAXWELL PRIZE

Dr. Phillip Sprangle
Plasma Physics Division

The James Clerk Maxwell Prize was established to recognize outstanding contributions to the field of plasma physics. This award, presented annually by the American Physical Society (APS), was established in 1975 by Maxwell Technologies, Inc., in honor of the Scottish physicist James Clerk Maxwell and is currently sponsored by General Atomics. Dr. Sprangle was recognized for pioneering contributions to the physics of high intensity laser interactions with plasmas and to the development of plasma accelerators, free electron lasers, gyrotrons, and high current electron accelerators. His research at NRL spans several decades and a multitude of research disciplines that include the atmospheric propagation of high-energy lasers, ultra-short-pulse laser-matter interaction and propagation, nonlinear optics, free electron lasers, and laser-driven accelerators.



2013 E.F. GROSS MEDAL

Dr. Alexander Efros
Materials Science and Technology Division

Established in 2012 by the Russian Optical Society, the E.F. Gross Medal is awarded annually for pioneering discoveries and fundamental contributions to the fields of optics and solid-state spectroscopy. Dr. Efros is a recipient of the medal awarded by the D.S. Rozhdestvensky Optical Society for pioneering work in the discovery and theoretical description of quantum size effects in the optical spectra of semiconductor nanocrystals. He is most notably recognized for his work on the tunable emission spectra of nanocrystals that launched a revolution in the development of affordable, highly efficient devices for use as sensors and displays, and his contributions to the theory of nanocrystal quantum dots to include the establishment of the basic model used for describing their electronic and optical properties.

2013 ARTHUR S. FLEMMING AWARD FOR EXCEPTIONAL FEDERAL SERVICE (BASIC SCIENCE)

Dr. Igor Medintz
Center for Bio/Molecular Science and Engineering

Dr. Medintz was recognized for his vision and dedication as a research biologist which has established him as a world-recognized leader in the growing field of bionanotechnology. Under the National Nanotechnology Initiative, the Department of Defense is tasked with developing new materials by functionally integrating biological molecules with nanoparticles to provide breakthroughs in biosensing, nanomedicine, and energy harvesting for enhancing warfighter capabilities and battle system components. Dr. Medintz is one of the very few who realized at an early point the technological importance of such bio-nano hybrids and the role the interface between these two materials plays in defining the biological function. One of the most important achievements of Dr. Medintz is his elucidation of how quantum dots (a special type of nanoparticle) transfer energy with other nanoparticles and bio/organic molecules. He has demonstrated that such nanoscale assemblies can lead to biosensors capable of monitoring the chemical states within a single human. Sensing and understanding biological function at a single cell level can lead to a better understanding of diseases and hence enable developments of new treatments.

2013 ARTHUR S. FLEMMING AWARD FOR EXCEPTIONAL FEDERAL SERVICE (SCIENCE AND ENGINEERING)

Dr. Kenneth Senior
Space Systems Development Department

Dr. Senior was recognized for his innovative and significant contributions and leadership as a mathematician, engineer, and section head in NRL's Space Systems Development Department. Dr. Senior is internationally known for the development of major advances in techniques and algorithms for time keeping, system synchronization, and determination of precise Global Position System (GPS) time. By creatively combining data from disparate systems' output whose performance varies with clock type, measurement interval, environmental parameters, and even relativistic relationships with other system elements, he was able to recursively estimate clock noise in the presence of system dynamics and operational parameters to a degree not previously possible. This knowledge provides the basis for unprecedented system accuracies, thereby increasing military and civilian positioning and navigation, communications, and data fusion capabilities.

2013 PETER MARK MEMORIAL AWARD

Dr. Daniel Gunlycke
Chemistry Division

The Peter Mark Memorial Award was established in 1979 in memory of Dr. Peter Mark, who served as editor of the *Journal of Vacuum Science and Technology* from 1975 to 1979. The award is presented by the American Vacuum Society (AVS) to a "young scientist or engineer for outstanding theoretical or experimental work." Dr. Gunlycke was recognized "for significant contributions to the understanding of the electronic properties of low-dimensional graphene nanostructures." He is the first NRL scientist to receive this internationally competitive award. He is known for his research on the importance of edge effects on the electronic properties of graphene nanoribbons. Dr. Gunlycke and colleagues showed that the conductance in ribbons narrow enough to generate an acceptable band gap is severely degraded by edge roughness, which causes strong Anderson localization that ultimately turns the nanoribbons into insulators. The findings, since confirmed by many other groups, have changed the direction of the field and led leading experimental groups to search for alternative methods of making nanoribbons with smooth edges, including chemical derivation, bottom-up synthesis, Joule heating, cutting graphene with nanoparticles, and unzipping of carbon nanotubes.





2013 P.S. THEOCARIS AWARD OF THE ACADEMY OF ATHENS

Dr. John Michopoulos
Materials Science and Technology Division

This award represents the highest honor bestowed by the Academy of Athens, and by implication by the nation of the Hellenic Republic, upon innovators in the area of mechanics of materials. The intention of the award is to draw distinction to researchers and scholars for the best scientific publication in the technical area of mechanics of materials, with an emphasis on fracture mechanics, experimental strength of materials, and mechanics of polymers. Dr. Michopoulos received this award for outstanding research work titled, "Direct strain tensor approximation of full-field strain measurement methods," published July 2013 in the *International Journal for Numerical Methods in Engineering*. His multidisciplinary and significant contributions extend to forward and inverse approaches of multiphysics modeling and simulation methods and algorithms and computational tools on high performance computing architectures, as they relate to areas such as electromagnetic launcher systems, data-driven environments for multiphysics applications, artificial muscle smart materials, electromagnetic propulsion, sensor networks for structural and environment monitoring, optical methods for displacement and strain measurement, failure theories, coupled electromagneto and hygrothermoelastic theories of continua, electromagnetic discharge imaging, and catastrophe theory applications.



2013 COPERNICUS AWARD

Mr. Dale Linne von Berg
Optical Sciences Division

Mr. Linne von Berg was recognized for his leadership that has resulted in notable accomplishments in the technical, managerial, and financial aspects of C4ISR capabilities for the warfighter. He has been a principal leader, architecture designer, and facilitator in the development/fielding of advanced C4ISR systems across the Department of Defense and the Intelligence Community (IC). As a Navy working capital fund manager, he routinely provides direction and technical management of more than 40 C4ISR programs annually (\$50 million to \$200 million), which require him to address and directly solve system design, development, integration, testing, and real-time demo/operational issues for a variety of community sponsors. Mr. Linne von Berg also has significantly advanced C4ISR with several innovative sensor technologies that have transitioned to operational use in operations Iraqi Freedom and Enduring Freedom. Specifically, his efforts include leading technical and management roles in the development of the F-14 and F/A-18 reconnaissance systems, Angel Fire/Blue Devil dual-band wide area persistent surveillance sensor system, and multiple MX-20SW long-range oblique gimballed short-wave infrared hyperspectral sensors for multiple community operational groups. When transitioned and fielded, each of these advanced C4ISR systems established a new standard in the state of the art by providing unparalleled coverage, coverage rate, range, resolution, day/night, or material/target detection capabilities.

2013 SIGMA XI PURE SCIENCE AWARD

Dr. Steven Erwin

Materials Science and Technology Division

The Sigma Xi Pure Science Award is presented for distinguished contributions in pure science and to acknowledge exemplary technical success in scientific research at NRL. The award is based on unclassified articles in reviewed scientific publications or on classified reports. Dr. Erwin was recognized for his pioneering contributions toward understanding how electronic and magnetic properties of solids are determined by impurities, surface adsorbates, and structural defects. His work has earned worldwide recognition in the areas of semiconductor surface physics, doped nanocrystals, dilute magnetic semiconductors and C60 fulleride solids.

2013 SIGMA XI APPLIED SCIENCE AWARD

Dr. Stephen Eckermann

Space Science Division

Winners of this award are selected for their distinguished contributions to pure and applied science during their research at NRL. The awards are given to encourage investigation in pure and applied science and to promote the spirit of scientific research at NRL. Dr. Eckermann received the award for contributions to the Navy's high-altitude analysis and forecasting capabilities leading to major improvements in Navy operational numerical weather prediction models. He is internationally recognized for his innovative research in the fields of upper atmosphere meteorology and near space environments. His development of the Mountain Wave Forecast Model, adopted for operational use by the U.S. Air Force, is a significant tool in identifying and forecasting middle and upper atmosphere turbulence and reducing risks to in-flight military and civilian aircraft and occupants.

2013 SIGMA XI YOUNG INVESTIGATOR AWARD

Dr. Daniel Gunlycke

Chemistry Division

The Young Investigator Award recognizes researchers in the early stages of their careers whose outstanding contributions best exemplify the ideals of Sigma Xi. The award is given to young investigators for outstanding research performed within 10 years of earning their highest degree and for their ability to communicate that research to the public. Dr. Gunlycke was recognized for pioneering contributions to the understanding of the electronic properties of graphene nanostructures. He has explored the properties of an extended line defect observed and controllably fabricated in graphene. This line defect holds much promise because it is well defined at the atomic level and could therefore be made reproducibly. His pioneering contributions to the understanding of graphene nanostructures are paving the way to future diverse applications for the Navy in areas ranging from ballistic electronic devices to anti-static coatings.





2013 SIGMA XI YOUNG INVESTIGATOR AWARD

Dr. Sophia Economou
Electronics Science and Technology Division

The Young Investigator Award recognizes researchers in the early stages of their careers whose outstanding contributions best exemplify the ideals of Sigma Xi. The award is given to young investigators for outstanding research performed within 10 years of earning their highest degree and for their ability to communicate that research to the public. Dr. Economou was recognized for developing novel theoretical concepts and tools for the coherent control of semiconductor nanostructure systems such as quantum dots. The ability to control quantum systems coherently is at the heart of new quantum technologies in the vibrant field of quantum information processing around the world. Her theoretical designs form a new paradigm that experiments in this field are using to perform spin manipulations, which are the basic logic gates in this new kind of information processing. This work has enabled the fundamental and often abstract theoretical ideas of quantum information to be implemented in real systems in simple and experimentally intuitive ways.



DEPARTMENT OF DEFENSE (DOD) LABORATORY SCIENTIST OF THE QUARTER

Dr. Jeffrey Long
Chemistry Division

The Laboratory Scientist of the Quarter Award was established to recognize a DoD scientist's extraordinary service to the DoD science and technology community. Dr. Long received the inaugural Laboratory Scientist of the Quarter Award in a ceremony in April 2014 hosted by Mr. Frank Kendall, Under Secretary of Defense (Acquisition, Technology, and Logistics). He was recognized for advancements in the field of electrochemical energy storage (EES), where his recent work has centered on redesigning the electrodes used in electrochemical capacitors (a.k.a. "supercapacitors") and Zn-air batteries to impart unprecedented pulse-power capability, efficiency, and rechargeability. Dr. Long engages in basic and early applied research projects at NRL that focus on the development, characterization, and validation of advanced nanostructured materials that enhance the performance of military-critical technologies ranging from electrochemical power sources to air filtration.



U.S. AIR FORCE SPACE COMMAND DIRECTOR'S CIRCLE AWARD

Mr. Arthur Merat
Space Systems Development Department

The Director's Circle Award annually recognizes the top 1.5 percent of the Air Force sponsor's total workforce who have made significant contributions to the Air Force mission and goals and whose performance exemplifies the Air Force sponsor's values — integrity and accountability, mission excellence, and teamwork. Mr. Merat received the Director's Circle Award for his innovative leadership on two major projects, which resulted in the fielding of products with critical impact on the Air Force at a considerable savings to the organization. Mr. Merat and his team successfully upgraded an existing antenna asset to improve mission support while in parallel expanded the antenna's ability to support additional mission partners. Mr. Merat also led his team in the infrastructure redesign of NRL's radar range facility, expanding the range's capabilities through the addition of the repurposed transmission systems, which resulted in an increased utility and significant cost savings to the Air Force sponsor. He demonstrated superb resource management, accomplishing the mission quickly and at the lowest cost while exceeding mission requirements.

2013 ARMY RESEARCH LABORATORY AWARD FOR PARTNERING

Mr. Joseph Molnar
Information Technology Division

Mr. Molnar was recognized for his exceptional efforts in the research and engineering of new developments in the continuous monitoring and risk scoring to create a common operating picture. This program provides the foundation for a new approach to improving the common operating picture against cyber threats. His achievements required great dedication and perseverance and reflect upon his professionalism. The extraordinary dedication demonstrated in these accomplishments bring great credit to him, the Army Research Laboratory, the High Performance Computing Modernization Program, the Defense-wide Information Assurance Program, the U.S. Army Cyber Command, REDCOM, and the Department of the Navy.



U.S. ENVIRONMENTAL PROTECTION AGENCY (EPA) 2012 SCIENCE AND TECHNOLOGICAL ACHIEVEMENT AWARD LEVEL III

Dr. Richard Gould
Remote Sensing Division

The Level III awards are for those who have accomplished an unusually notable research or technological effort. The awards are for a substantial revision or modification of a scientific/technological principle or procedure, or an important improvement to the value of a device, activity, program, or service to the public. Awarded research relates to a mission or organizational component of the EPA, or significantly affects a relevant area of science/technology. Dr. Gould received this award for being a co-author of one of the winning research publications, "An Analysis of Diffuse Light Attenuation in the Northern Gulf of Mexico Hypoxic Zone Using the SeaWiFS Satellite Data Record." The publication was evaluated by a subcommittee of the EPA's Science Advisory Board and recommended for Level III recognition in the category of Ecological Research.



2013 IEEE BEST PAPER AWARD

Dr. Anthony Hutcheson, Dr. Bernard Philips, Dr. Eric Wulf,
Dr. Lee Mitchell, Dr. Neil Johnson, and Dr. Byron Leas
Space Science Division and SRA International, Inc.

Scientists at NRL are conducting research to improve the detection of weapons of mass destruction in maritime environments. In recognition for their efforts, Drs. Anthony Hutcheson, Bernard Philips, Eric Wulf, Lee Mitchell, Neil Johnson, and Byron Leas received a Best Paper Award at the 2013 IEEE Conference on Technologies for Homeland Security. Their paper, "Maritime Detection of Radiological/Nuclear Threats with Hybrid Imaging System," won the Best Paper Award in the Land and Maritime Border Security track at the IEEE conference. The Best Papers will be published in *Homeland Security Affairs*, the peer-reviewed online journal of the Naval Postgraduate School Center for Homeland Defense and Security. The award-winning paper tells how the NRL team has developed the SuperMISTI standoff detection system for maritime environments as part of the Office of Naval Research's (ONR's) Maritime Weapons of Mass Destruction Detection program. The instrument was deployed at Norfolk Naval Station in July 2012 as part of the ONR's Manta technology demonstration to determine the on-water performance of the system. SuperMISTI is a hybrid detection, identification, and imaging system for sources of gamma-ray radiation at standoff distances.





U.S. AIR FORCE SPACE COMMAND (AFSPC) MOST OUTSTANDING ANALYST

Mr. Jeffrey Hawkins
Marine Meteorology Division

Mr. Hawkins was recognized by the U.S. Air Force Space Command for significant leadership in the effectiveness analysis group for the Space Based Environmental Monitoring Analysis of Alternatives Concepts program. He was selected from 88 participants in the study that lasted from August 2012 to August 2013. The team addressed current and future capability gaps in sensing three key meteorological and oceanic parameters critical in supporting Navy and Department of Defense (DoD) global forces: ocean surface vector winds, tropical cyclone intensity, and theater weather imagery. Mr. Hawkins was specifically recognized for presenting exceptional educational briefings and providing valuable demonstration of how space-based sensing supports global DoD operations by producing daily high quality environmental forecasts.



AMERICAN COUNCIL OF ENGINEERING EXCELLENCE AWARDS COMPETITION (ACEC) – GRAND AWARD AND PINNACLE AWARD

Dr. Rich Colton
Chemistry Division (retired)

The design firm Wiley Wilson, of Lynchburg, Virginia, received the ACEC Grand Award for the design of NRL's Laboratory for Autonomous Systems Research (LASR) building. The LASR building also won the council's Pinnacle Award. According to the project manager, Bob Bibee, "Taken on the whole, [a facility like] this building has never been done before to our knowledge anywhere." LASR, a 47,000 sq ft building, is a unique laboratory that provides specialized facilities to support highly innovative research in intelligent autonomy, sensor systems, power and energy systems, human-system interaction, networking and communications, and platforms. LASR supports a broad range of research related to autonomous systems, from basic to applied, and for integration across different disciplines. Some of its unique features include a prototyping high bay, a littoral high bay, a desert high bay, a tropical high bay, an outdoor test range, and electrical and machine shops.



2013 NATIONAL ASSOCIATION OF ROCKETRY (NAR) HOWARD GALLOWAY SPACEMODELING SERVICE AWARD

Mr. Ivan Galysh
Space Systems Development Department

Mr. Galysh was honored for contributions over the last decade focused on educating and motivating students in the technical disciplines of aerospace engineering. He is recognized by NAR's highest award for the development of novice student rocketeers into confident mission teams designing sophisticated payloads and high-power rockets and presenting their work for review by a panel of NASA engineers. As a mentor and organizer for student teams in the NAR's Team America Rocketry Challenge and NASA's Student Launch Initiative national programs, Mr. Galysh has spent hundreds of hours each year providing direct hands-on instruction, supervision, and motivation to multiple teams of students in grades 7 through 12. Mr. Galysh organizes and runs an annual summer camp, teaching students to design, build, and fly instrument payloads for rockets. He also organizes and runs the CanSat Competition, a competition created to provide a unique opportunity for teams to design and build a satellite that fits inside a soda can. Held annually in Texas, the CanSat rocket launch involves student teams from around the world and is sponsored by aerospace industries, associations, and NRL. He is also the founder of the Battle of the Rockets competition developed for high school and university student teams that involves the design and launch of rover-type payloads on large rockets.

OPTICAL SOCIETY OF AMERICA ALL-IN-ONE (AIO) BEST SPEAKER AWARD

Dr. Gary Miller
Optical Sciences Division

This Best Speaker Award was given to Dr. Miller at the Optical Society of America's Applied Industrial Optics: Spectroscopy, Imaging, and Metrology All-in-One (AIO) Topical Meeting in July 2013. The award was presented by the organizing committee based on the presentation titled, "Fiber Laser Sensors: From Prototype to Practical," which captured the essence of the conference theme.



2012 VICE ADMIRAL SAMUEL L. GRAVELY, JR., SCIENCE, TECHNOLOGY, ENGINEERING, AND MATHEMATICS (STEM) EDUCATION AND DIVERSITY CHAMPION OF THE YEAR AWARD

Mr. Paul Jaffe
Spacecraft Engineering Department

This award is named for Vice Admiral Samuel L. Gravelly, Jr., the first African-American in the U.S. Navy to command a combatant ship, to be promoted to flag rank, and to command a naval fleet (the Third Fleet). The Office of Naval Research presents the Gravelly award to a champion who has excelled at fostering STEM education and diversity growth to expand future generations of students in the naval science and technology workforce. Mr. Jaffe received the award for his encouragement, mentoring, and education of aspiring scientists and engineers over more than a decade. Mr. Jaffe participates in the Science and Engineering Apprenticeship Program (SEAP) by sponsoring and mentoring high school students at NRL. He has participated in this program for over six years, providing challenging assignments to many aspiring scientists and engineers. He also provided supervision to Student Temporary Employment Program students for more than five years. Mr. Jaffe is a coordinator for the NRL Community Outreach Program and manages the tutorial support program at W.B. Patterson Elementary School in Washington, D.C. He has also led numerous other STEM and diversity efforts at local schools.



2013 OUTSTANDING YOUNG ALUMNUS AWARD FROM VIRGINIA TECH COLLEGE OF ENGINEERING

Dr. Sastry Kompella
Information Technology Division

Dr. Kompella is recognized for his work in developing new theoretical foundations for wireless networks and cognitive radios, with a focus on tactical networks for wartime environments, underwater acoustic communication, and dynamic spectrum access. Beginning his basic research in wireless ad hoc networks and breaking ground in the area of wireless link scheduling, high-tech network and sensor design, and radio control for the battlefield, Dr. Kompella's research is currently focused on developing new approaches for pushing performance limits of complex wireless network systems. He continues to work with cognitive radios, which are super-smart radios aware of their own environment, capabilities, and operating rules, adaptable to changing scenarios. Dr. Kompella is also involved in developing new methodologies for optimal relay placement and media access control (MAC) in underwater acoustic networking that are important to the U.S. Navy.





NAVY MERITORIOUS CIVILIAN SERVICE AWARD

Dr. Peter Gaiser
Remote Sensing Division

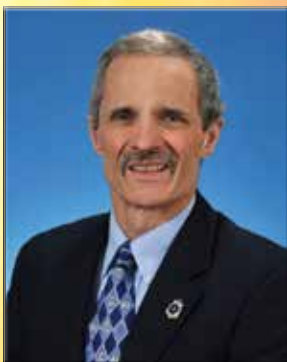
The Meritorious Civilian Service Award is the third highest award bestowed by the Navy on its civilian employees. Dr. Gaiser was honored for his outstanding performance and record of achievements over the past 15 years on the NRL WindSat mission, and the leading role he has played in enabling WindSat to be the great success it has been for the Naval Research Laboratory. WindSat is the first fully polarimetric spaceborne microwave radiometer. In January 2013, it achieved 10 years of on-orbit operations, and it has been a highly visible and successful mission. The WindSat mission's primary objective was to test and fully evaluate the viability of using passive polarimetric radiometry to retrieve the ocean surface wind vector (wind speed and direction). WindSat is a large and complex mission involving a large team and a strong interdivisional collaboration at NRL between the Naval Center for Space Technology and the Remote Sensing Division. Dr. Gaiser is now playing the same critical role in the WindSat Follow-on mission proposal development, and on the Risk Reduction and Analysis of Alternatives activities now underway as part of start-up activities for the next-generation Department of Defense Weather Satellite Systems program.



NAVY MERITORIOUS CIVILIAN SERVICE AWARD

Dr. Robert Morris
Chemistry Division

The Meritorious Civilian Service Award is the third highest award bestowed by the Navy on its civilian employees. Dr. Morris was recognized for his superlative scientific achievements in fuel analytics that have been the singular driving factor in the Navy's development of advanced diagnostics and prognostics for Navy mobility fuels. He has revolutionized fuel analytics with his work in compositional mapping of Navy mobility fuels and through the development of tools for fuel diagnostics using sensing technologies and chemometric modeling capabilities to perform aviation and ship propulsion fuel quality surveillance. He has consistently provided the Navy with leadership and guidance for finding solutions to the many complex problems associated with Navy mobility fuels that power the Navy's ships and aircraft. In addition, Dr. Morris conducts basic and applied research and provides technical support in a wide range of Navy fuel issues to the Fleet.



2013 E.O. HULBURT ANNUAL SCIENCE AWARD

Dr. Jerry Meyer
Optical Sciences Division

The E.O. Hulburt Award is the highest award the NRL Commanding Officer can confer on an NRL civilian employee. Dr. Meyer is cited for "his exceptional contributions to the science of the optoelectronic properties of quantum confined semiconductors, their theory, growth, characterization, structures, and architectures. His technological breakthroughs for both infrared detectors and lasers are of great importance to the Navy and Department of Defense (DoD). Dr. Meyer has combined scientific expertise, service to the research community, and programmatic leadership across DoD to produce new capabilities for the defense of the nation." He is a senior advisor and subject matter expert on photonics technologies and the science underlying them. Performing basic and applied research in broad areas of semiconductor materials and optoelectronic devices, Dr. Meyer is working to develop compact higher power infrared sources that operate at ambient temperatures for chemical sensing, laser spectroscopy, and the protection of military platforms from heat-seeking munitions.

2012 COMMANDING OFFICER'S AWARD FOR EXCELLENCE IN MISSION SUPPORT

Ms. Paula Scholten
Human Resources Office

This award recognizes significant contributions of the NRL support community and is the highest NRL award bestowed for the Laboratory's mission support contributions. Ms. Scholten was cited "for her outstanding contributions to the Naval Research Laboratory in providing exceptional Information Technology support to Laboratory managers and employees." An essential part of the Human Resources Office and setting the model for a positive work ethic, Ms. Scholten's efforts to assist NRL managers through the annual Contribution-based Compensation System (CCS) pay pool process demonstrate dedicated and responsive customer service in support of the NRL mission with commitment to getting the job done in an outstanding manner. She has contributed consistently for years toward the successful implementation of the CCS pay pool process at NRL. Her involvement in every phase of the process has been the key to its success. Additionally, she has been a major contributor toward the development and implementation of the Office of Naval Research's Personnel Demonstration Project and continues to provide support. Ms. Scholten is also the liaison with the Human Resources Service Center Northeast and NRL's local security office and has been instrumental in resolving data reflow issues.

THE 2013 NRL REVIEW ARTICLE AWARDS

Awards for *NRL Review* articles recognize authors who submit outstanding research articles for this publication. The articles are judged on the relevance of the work to the Navy and DoD, readability to the college graduate level, clearness and conciseness of writing, and the effective use of graphics that are interesting and informative. The following awards were presented for articles that appeared in the *2013 NRL Review*.

Featured Research Article

"Graphene as a Tunnel Barrier," by Dr. Olaf van 't Erve, Mr. Enrique Cobas, Dr. Adam Friedman, Dr. Connie Li, Dr. Jeremy Robinson, and Dr. Berry Jonker (Materials Science and Technology Division)

Directorate Awards for Scientific Articles

Systems Directorate

"Frequency Position Modulation," by Mr. Joel Goodman, Dr. Crystal Bertoncini, Mr. Bryan Nousain, and Dr. Gregory Cowart (Tactical Electronic Warfare Division)

Materials Science and Component Technology Directorate

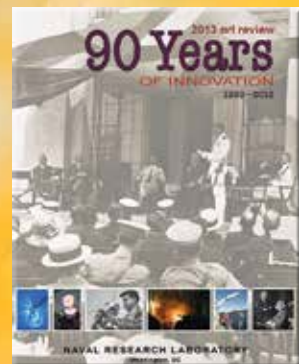
"Measuring Protein Secretions from Individual Live Cells," by Dr. Marc Raphael, Dr. Joseph Christodoulides, and Mr. Jeff Byers (Materials Science and Technology Division), Dr. James Delehanty (Center for Bio/Molecular Science and Engineering), and Mr. James Long and Dr. Pehr Pehrsson (Chemistry Division)

Ocean and Atmospheric Science and Technology Directorate

"Remote Sensing Signatures of Breaking Waves from Multi-Instrument Field Experiment on FLIP," by Dr. Magdalena Anguelova, Mr. David Dowgiallo, Dr. Geoffrey Smith, Dr. Ivan Savelyev, Mr. Glendon Frick, Ms. Charlotte Snow, and Dr. Justin Bobak (Remote Sensing Division), and Dr. Steven Means and Dr. Jeffrey Schindall (Acoustics Division)

Naval Center for Space Technology

"GLADIS Hosted Payload Demonstrates Nanosatellite Technology," by Mr. Jay Middour, Mr. Ivan Galysh, Dr. Kenneth Clark, Mr. Thomas Rodilosso, Mr. Mark Haffner, Mr. Christopher Belmonte, and Mr. Robert Baummer (Space Systems Development Department)





Dr. Berry Jonker, Dr. Jeremy Robinson, Dr. Olaf van 't Erve, Mr. Enrique Cobas, Dr. Adam Friedman, and Dr. Connie Li receive the award for the winning featured research article.



Dr. Gregory Cowart, Mr. Bryan Nousain, Dr. Crystal Bertocini, and Mr. Joel Goodman receive the award for the winning article from the Systems Directorate.



Dr. Joseph Christodoulides and Dr. Marc Raphael receive the award for the winning article from the Materials Science and Component Technology Directorate. Mr. Jeff Byers, Dr. James Delehanty, Mr. Jeffrey Long, and Dr. Pehr Pehrsson were not present.



Mr. Glendon Frick, Dr. Steven Means, Mr. David Dowgiallo, Dr. Magdalena Anguelova, Dr. Ivan Savelyev, and Dr. Geoffrey Smith receive the award for the winning article from the Ocean and Atmospheric Science and Technology Directorate. Ms. Charlotte Snow, Dr. Justin Bobak, and Dr. Jeffrey Schindall were not present.



Mr. Christopher Belmonte, Mr. Robert Baummer, Mr. Ivan Galysh, Mr. Jay Middour, Mr. Mark Haffner, and Mr. Thomas Rodilosso receive the award for the winning article from the Naval Center for Space Technology. Dr. Kenneth Clark was not present.

ALAN BERMAN RESEARCH PUBLICATION AND NRL EDISON (PATENT) AWARDS

The Annual Research Publication Awards Dinner (ARPAD) was established in 1968 to recognize the authors of the best NRL publications each year. These awards not only honor individuals for superior scientific accomplishments in the field of naval research, but also seek to promote continued excellence in research and in its documentation. In 1982, the name of this award was changed to the Alan Berman Research Publication Award in honor of its founder. Of the 207 papers considered for awards in 2013, 33 were selected for recognition. They represent 177 authors.

NRL also recognizes patents as part of its annual publication awards program. The NRL Edison (Patent) Awards were established in 1991 to recognize NRL employees for outstanding patents issued to NRL by the U.S. Patent and Trademark Office during the preceding calendar year. The awards recognize significant NRL contributions to science and engineering, as demonstrated by the patent process, that are perceived to have the greatest potential benefit to the country. Of the 112 patents considered for 2013, 3 were selected, representing 11 inventors and 3 patent attorneys.

PUBLICATION AWARDS

Radar Division

Wideband Multifunction Array Architectures Using Wavelength Scaled Radiating Elements
Dr. Rashmi Mital, Mr. Dharmesh Patel, Mr. Gregory Tavik, and Dr. Jaganmohan Rao

Modeling of Transmission, Scattering, and Reception for Multistatic Polarimetric Radar
Dr. Tegan Webster, Dr. Eric Mokole, and Dr. Margaret Cheney

Information Technology Division

Universal Vocoder Using Variable Data Rate Vocoding
Mr. David Heide, Dr. Aaron Cohen, Ms. Yvette Lee, and Mr. Thomas Moran

Spectrum Database Poisoning for Operational Security in
Policy-Based Spectrum Operations
Dr. Andrew Robertson, Mr. Joseph Molnar, and Dr. Jeffrey Boksiner

Optical Sciences Division


Suppression of Even-Order Photodiode Distortions via Predistortion
Linearization with a Bias-Shifted Mach-Zehnder Modulator
*Dr. Vincent Urick, Dr. Meredith Hutchinson, Mr. Joseph Singley,
Dr. Jason McKinney, and Dr. Keith Williams*

Achromatic GRIN Singlet Lens Design
Dr. Richard Flynn, Dr. Erin Fleet, Dr. Guy Beadie, and Mr. James Shirk

Tactical Electronic Warfare Division

Focusing an Arbitrary RF Pulse at a Distance Using Time Reversal Techniques
*Dr. Sun Hong, Mr. Zachary Drikas, Dr. Tim Andreadis,
Dr. Biniyam Taddese, and Dr. Steven Anlage*





Modeling and Simulation Support for Coordinated Electronic Attack: The NEWCS Suite
Dr. Donald Jarvis, Dr. Jerome Gansman, and Dr. Eric Justh

Laboratories for Computational Physics and Fluid Dynamics

Analysis of the Monotonic Lagrangian Grid as an Air Traffic Simulation Tool
*Dr. Carolyn Kaplan, Dr. Elaine Oran, Dr. Jay Boris, Dr. Johann Dahm,
and Dr. Natalia Alexandrov*

Chemistry Division

Thermodynamic and Kinetic Stabilities of CO₂ Oligomers
*Dr. Brett Dunlap, Dr. Igor Schweigert, Dr. Andrew Purdy,
Dr. Arthur Snow, and Dr. Anguang Hu*

Dual-Function Air Cathode for Metal–Air Batteries with Pulse-Power Capability
*Dr. Jeffrey Long, Dr. Christopher Chervin, Mr. Nathan Kucko,
Dr. Eric Nelson, and Dr. Debra Rolison*

Materials Science and Technology Division

Crowding Induced Entropy-Enthalpy Compensation in Protein Association Equilibria
Dr. Young Kim and Dr. Jeetain Mittal

Quantitative Imaging of Protein Secretions from Single Cells in Real Time
*Dr. Marc Raphael, Dr. Joseph Christodoulides, Dr. Jeff Byers,
Dr. James Delehanty, and Dr. James Long*

Plasma Physics Division

Controlling the Electron Energy Distribution Function of Electron Beam Generated Plasmas with Molecular Gas Concentration: I. Experimental Results
*Dr. David Boris, Dr. George Petrov, Dr. Evgeniya Lock,
Dr. Tzvetelina Petrova, Dr. Richard Fernsler, and Dr. Scott Walton*

Fully Explicit Nonlinear Optics Model in a Particle-in-Cell Framework
Dr. Daniel Gordon, Dr. Michael Helle, and Dr. Joseph Peñano

Electronics Science and Technology Division

Theory and Design of Intrinsically Switched Multiplexers with Optimum Phase Linearity
Dr. Andrew Guyette

Quantum Control of a Spin Qubit Coupled to a Photonic Crystal Cavity
*Dr. Samuel Carter, Dr. Sophia Economou, Dr. Thomas Reinecke, Dr. Allan Bracker,
Dr. Daniel Gammon, Dr. Chul Soo Kim, Dr. Timothy Sweeney, Dr. Dmitry Solenov,
Dr. Lily Yang, and Dr. Mijin Kim*

Center for Bio/Molecular Science and Engineering

Achieving Effective Terminal Exciton Delivery in Quantum Dot Antenna-Sensitized Multistep DNA Photonic Wires
*Dr. Christopher Spillmann, Dr. Ellen Goldman, Dr. Igor Medintz,
Dr. Mario Ancona, Dr. Michael Stewart, Dr. Alan Huston,
Dr. Susan Buckhout-White, Dr. W. Russ Algar, and Dr. Kimihiro Susumu*

Selecting Improved Peptidyl Motifs for Cytosolic Delivery of Disparate Protein and Nanoparticle Materials

Dr. Kelly Boeneman, Dr. James Delehanty, Dr. Jeffrey Deschamps, Dr. Christopher Spillmann, Dr. Igor Medintz, Dr. Michael Stewart, Dr. Alan Huston, Dr. Kimihiro Susumu, Dr. Eunkeu Oh, Dr. Juan Blanco-Canosa, Dr. Sampat Ingale, Dr. Darren Thompson, Dr. Philip Dawson, Dr. Glyn Dawson, Dr. Ryan Walters, Dr. Miriam Domowicz, Dr. W. Russ Algar, Dr. Stassi DiMaggio, Dr. Janet Manono, and Dr. Travis Jennings

Acoustics Division

Empirical and Quadrature Approximation of Acoustic Field and Array Response Probability Density Functions
Dr. Thomas Hayward and Dr. Roger Oba

Convolution Formulations for Non-Negative Intensity
Dr. Earl Williams

Remote Sensing Division

Demonstration of SAR Distortion Correction Using a Ground-Based Multichannel SAR Test Bed
Dr. Mark Sletten

Mapping Surface Currents and Waves with Interferometric Synthetic Aperture Radar in Coastal Waters: Observations of Wave Breaking in Swell-Dominant Conditions
Dr. Paul Hwang, Dr. Jakov Toporkov, Dr. Mark Sletten, and Mr. Steven Menk

Oceanography Division

Covariance Localization with the Diffusion-Based Correlation Models
Dr. Max Yaremchuk and Dr. Dmitry Nechaev

Surface Wave Effects on High-Frequency Currents Over a Shelf Edge Bank
Dr. Hemantha Wijesekera, Dr. David Wang, Dr. William Teague, Dr. Ewa Jarosz, Mr. W. Erick Rogers, Dr. Diane Fribance, and Dr. James Moum

Marine Geosciences Division

Strain-Rate Dependence of Strength of the Gulf of Mexico Soft Sediments
Dr. Andrei Abelev and Dr. Philip Valent


Three-Dimensional Mixture Simulations of Flow Over Dynamic Rippled Beds
Dr. Allison Penko, Dr. Joseph Calantoni, Dr. S. Rodriguez-Abudo, Dr. Diane Foster, and Dr. Donald Slinn

Marine Meteorology Division

Hidden Error Variance Theory Part I: Exposition and Analytic Model
Dr. Craig Bishop and Dr. Elizabeth Satterfield

Observing and Understanding the Southeast Asian Aerosol System by Remote Sensing: An Initial Review and Analysis for the Seven Southeast Asian Studies (7SEAS) Program
Dr. Jeffrey Reid, Dr. Edward Hyer, Dr. James Campbell, Ms. Elizabeth Reid, Dr. Courtney Kearney, Dr. Peng Xian, Dr. Randall Johnson, Dr. Jiangleong Zhang, Mr. Brent Holben, Dr. E. Judd Welton, Dr. Robert Yokelson, Dr. Sundar Christopher, Dr. Larry Di Girolamo, Dr. Guangyu Zhao, Dr. Bethany Norris, Dr. Louis Giglio, Dr. Robert Holz, Dr. Min Oo,





*Dr. Jukka Miettinen, Dr. Rajasekhar Balasubramanian, Dr. Boon Ning Chew,
Dr. Santo Salinas, Dr. Soo Chin Liew, Dr. F. Joseph Turk, Dr. Jun Wang, Dr. Serm Janjai,
Dr. Nofel Lagrosas, Dr. Puji Lestari, Dr. Neng-Huei Lin, Dr. Mastura Mahmud,
Dr. Anh Nguyen, and Dr. Nguyen Oanh*

Space Science Division

On the Remote Detection of Suprathermal Ions in the Solar Corona and their Role as
Seeds for Solar Energetic Particle Production

*Dr. J. Martin Laming, Dr. J. Daniel Moses, Dr. Yuan-Kuen Ko, Dr. Chee Ng,
Dr. Cara Rakowski, and Dr. Allan Tylka*

Sources of GeV Photons and the Fermi Results

Dr. Charles Dermer

Space Systems Development Department

Atmospheric Transmission from an Instrument Measuring Scatter at 1550 nm
*Mr. Michael Vilcheck, Dr. Christopher Moore, Dr. Harris Burris, Dr. Linda Thomas,
Dr. Rita Mahon, Mr. Jim Murphy, Dr. William Rabinovich, and Dr. Anthony Bucholtz*

Spacecraft Engineering Department

Bayesian Inference on Multimodal Distributions from an Interferometer

Dr. Liam Healy and Mr. Christopher Binz

NRL EDISON (PATENT) AWARDS

Real-Time Lines-of-Sight and Viewsheds Determination System

Mr. Robert Doyle, Jr., and Mr. L. George Legg

Detection of Chemicals with Infrared Light

*Dr. Andrew McGill, Dr. Chris Kendziora, Dr. Robert Furstenberg, Dr. Michael Papantonakis,
Dr. Graham Hubler, Dr. James Horwitz, and Ms. Rebecca Forman*

Technique for De-Orbiting Small Debris from the Near-Earth Space Environment

*Dr. Gurudas Ganguli, Dr. Christopher Crabtree, Mr. Scott Chappie,
Dr. Leonid Roudakov, and Ms. Kathleen Chapman*

NRC/AEE POSTDOCTORAL RESEARCH PUBLICATION AWARDS

Chemistry Division

Decoupling Diameter and Pitch in Silicon Nanowire Arrays Made by
Metal-Assisted Chemical Etching

*Junghoon Yeom, Daniel Ratchford, Christopher R. Field,
Todd H. Brintlinger, and Pehr E. Pehrsson*

Plasma Physics Division

Chemical Gradients on Graphene To Drive Droplet Motion

*Sandra C. Hernández, Charlee J. C. Bennett, Chad E. Junkermeier, Stanislav D. Tsoi,
Francisco J. Bezares, Rory Stine, Jeremy T. Robinson, Evgeniya H. Lock,
David R. Boris, Brian D. Pate, Joshua D. Caldwell, Thomas L. Reinecke,
Paul E. Sheehan, and Scott G. Walton*

Electronics Science and Technology Division

First-Principles Determination of Ultrahigh Thermal Conductivity of Boron Arsenide: A Competitor for Diamond?
L. Lindsay, D. A. Broido, and T. L. Reinecke

Center for Bio/Molecular Science and Engineering

Hydrodynamic Shaping, Polymerization, and Subsequent Modification of Thiol Click Fibers
Darryl A. Boyd, Adam R. Shields, Jawad Naciri, and Frances S. Ligler

Macroscopic Self-Assembly and Optical Characterization of Nanoparticle–Ligand Metamaterials
Jake Fontana, Jawad Naciri, Ronald Rendell, and Banahalli R. Ratna

Space Science Division

Broadband Pulsations from PSR B1821–24: Implications for Emission Models and the Pulsar Population of M28
T. J. Johnson, L. Guillemot, M. Kerr, I. Cognard, P. S. Ray, M. T. Wolff, S. Bégin, G. H. Janssen, R. W. Romani, C. Venter, J. E. Grove, P. C. C. Freire, M. Wood, C. C. Cheung, J. M. Casandjian, I. H. Stairs, F. Camilo, C. M. Espinoza, E. C. Ferrara, A. K. Harding, S. Johnston, M. Kramer, A. G. Lyne, P. F. Michelson, S. M. Ransom, R. Shannon, D. A. Smith, B. W. Stappers, G. Theureau, and S. E. Thorsett





programs for professional development

256 Programs for NRL Employees — Graduate Programs, Continuing Education, Professional Development, Equal Employment Opportunity (EEO) Programs, and Other Activities

258 Programs for Non-NRL Employees — Postdoctoral Research Associateships, Faculty Member Programs, Professional Appointments, and Student Programs

260 NRL Employment Opportunities

PROGRAMS FOR NRL EMPLOYEES

The Human Resources Office supports and provides traditional and alternative methods of training for employees. NRL employees are encouraged to develop their skills and enhance their job performance so they can meet the future needs of NRL and achieve their own goals for growth.

One common study procedure is for employees to work full time at the Laboratory while taking job-related courses at universities and schools local to their job site. The training ranges from a single course to undergraduate, graduate, and postgraduate course work. Tuition for training is paid by NRL. The formal programs offered by NRL are described here.

GRADUATE PROGRAMS

The **Advanced Graduate Research Program** (formerly the Sabbatical Study Program, which began in 1964) enables selected professional employees to devote full time to research or pursue work in their own or a related field for up to one year at an institution or research facility of their choice without the loss of regular salary, leave, or fringe benefits. NRL pays all travel and moving expenses for the employee. Criteria for eligibility include professional stature consistent with the applicant's opportunities and experience, a satisfactory program of study, and acceptance by the facility selected by the applicant. The program is open to employees who have completed six years of Federal service, four of which have been at NRL.

The **Edison Memorial Graduate Training Program** enables employees to pursue graduate studies in their fields at local universities. Participants in this program work 24 hours each workweek and pursue their studies during the other 16 hours. The criteria for eligibility include a minimum of one year of service at NRL, a bachelor's or master's degree in an appropriate field, and professional standing in keeping with the candidate's opportunities and experience.

To be eligible for the **Select Graduate Training Program**, employees must have a bachelor's degree in an appropriate field and must have demonstrated ability and aptitude for advanced training. Students accepted into this program receive one-half of their salary and benefits and NRL pays for tuition and travel expenses.

The **Naval Postgraduate School (NPS)**, located in Monterey, California, provides graduate programs to enhance the technical preparation of Naval officers and civilian employees who serve the Navy in the fields of science, engineering, operations analysis, and management. NRL employees desiring to pursue

graduate studies at NPS may apply; thesis work is accomplished at NRL. Participants continue to receive full pay and benefits during the period of study. NRL also pays for tuition and travel expenses.

In addition to NRL and university offerings, application may be made to a number of noteworthy programs and fellowships. Examples of such opportunities are the **Capitol Hill Workshops**, the **Legislative Fellowship (LEGIS) program**, the **Federal Executive Institute (FEI)**, and the **Executive Leadership Program for Mid-Level Employees**. These and other programs are announced from time to time, as schedules are published.

CONTINUING EDUCATION

Undergraduate and graduate courses offered at local colleges and universities may be subsidized by NRL for employees interested in improving their skills and keeping abreast of current developments in their fields.

NRL offers **short courses** to all employees in a number of fields of interest including administrative subjects and supervisory and management techniques. Laboratory employees may also attend these courses at nongovernment facilities. HRO advertises training opportunities on the NRL intranet, HRO website, and in the email newsletter, *HRO Highlights*.

For further information on any of the above Graduate and Continuing Education programs, contact the Employee Development and Management Branch (Code 1840) at (202) 767-8306 or via email at Training@hro.nrl.navy.mil.

The **Scientist-to-Sea Program (STSP)** provides opportunities for Navy R&D laboratory/center personnel to go to sea to gain first-hand insight into operational factors affecting system design, performance, and operations on a variety of ships. NRL is a participant of this Office of Naval Research (ONR) program. Contact (202) 404-2701.

PROFESSIONAL DEVELOPMENT

NRL has several programs, professional society chapters, and informal clubs that enhance the professional growth of employees. Some of these are listed below.

The **Department of the Navy Civilian Employee Assistance Program (DONCEAP)** provides confidential assessment, referral, and short-term counseling for employees (or their eligible family members) regarding personal concerns to help avoid adversely affecting job performance. Types of personal concerns may include

challenging relationships (at work or at home); dealing with stress, anxiety, or depression; grief and loss; or substance abuse. The DONCEAP also provides work/life referral services such as live or on-demand webinars; discussion groups; and advice on parenting, wellness, financial and legal issues, education, and much more. Contact (844)-366-2327 or visit <http://donceap.foh.hhs.gov>.

The NRL chapter of **Women In Science and Engineering (WISE)** was established to address current issues concerning the scientific community of women at the NRL such as networking, funding, work-life satisfaction, and effective use of our resources. We address these issues by empowering members through the establishment of a supportive and constructive network that serves as a sounding board to develop solutions that address said issues, and then serve as a platform in which members work together to implement these solutions. The NRL chapter of WISE has started several new initiatives for the 2013–2014 year, including a seminar series entitled “Working Smarter Not Harder at NRL — Effective Use of Our Resources” and a Science as Art competition, which is open to all NRL sites. Membership is open to all employees. For more information, contact (202) 404-3355.

Sigma Xi, The Scientific Research Society, encourages and acknowledges original investigation in pure and applied science. It is an honor society for research scientists. Individuals who have demonstrated the ability to perform original research are elected to membership in local chapters. The NRL Edison Chapter, comprising approximately 200 members, recognizes original research by presenting annual awards in pure and applied science to two outstanding NRL staff members per year. In addition, an award seeking to reward rising stars at NRL is presented annually through the Young Investigator Award. The chapter also sponsors several lectures per year at NRL on a wide range of topics of general interest to the scientific and DoD community. These lectures are delivered by scientists from all over the world. The highlight of the Sigma Xi Lecture Series is the Edison Memorial Lecture, which traditionally is given by an internationally distinguished scientist. Contact (202) 767-5528.

The **NRL Mentor Program** was established to provide an innovative approach to professional and career training and an environment for personal and professional growth. It is open to permanent NRL employees in all job series and at all sites. Mentees are matched with successful, experienced colleagues having more technical and/or managerial experience who can provide them with the knowledge and skills needed to maximize their contribution to the success of their immediate organization, to NRL, to the Navy, and to their chosen career fields. The ultimate goal of the program is to increase job productivity, creativity, and satisfaction through better communication, understanding, and training. NRL

Instruction 12400.1B provides policy and procedures for the program. For more information, please contact mentor@hro.nrl.navy.mil or (202) 767-6736.

Employees interested in developing effective self-expression, listening, thinking, and leadership potential are invited to join the NRL Forum Toastmasters Club, a chapter of **Toastmasters International**. Members of this club possess diverse career backgrounds and talents and learn to communicate not by rules but by practice in an atmosphere of understanding and helpful fellowship. NRL's Commanding Officer and Director of Research endorse Toastmasters. Contact (202) 404-4670.

EQUAL EMPLOYMENT OPPORTUNITY (EEO) PROGRAMS

Equal employment opportunity (EEO) is a fundamental NRL policy for all employees regardless of race, color, national origin, sex, religion, age, sexual orientation, or disability. The NRL EEO Office is a service organization whose major functions include counseling employees in an effort to resolve employee/management conflicts, processing formal discrimination complaints and requests for reasonable accommodation, providing EEO training, and managing NRL's MD-715 and affirmative employment recruitment programs. The NRL EEO Office is also responsible for sponsoring special-emphasis programs to promote awareness and increase sensitivity and appreciation of the issues or the history relating to females, individuals with disabilities, and minorities. Contact the NRL Deputy EEO Officer at (202) 767-2486 for additional information on programs or services.

OTHER ACTIVITIES

The award-winning **Community Outreach Program** directed by the NRL Public Affairs Office fosters programs that benefit students and other community citizens. Volunteer employees assist with and judge science fairs, give lectures, provide science demonstrations and student tours of NRL, and serve as tutors, mentors, coaches, and classroom resource teachers. The program sponsors student tours of NRL and an annual holiday party for neighborhood children in December. Through the program, NRL has active partnerships with three District of Columbia public schools. Contact (202) 767-2541.

Other programs that enhance the development of NRL employees include sports groups and the **Amateur Radio Club**. The **NRL Fitness Center** at NRL-DC, managed by Naval Support Activity Washington Morale, Welfare and Recreation (NSAW-MWR), houses a fitness room with treadmills, bikes, ellipticals, step mills, and a full strength circuit; a gymnasium for basketball, volleyball, and other activities; and full locker

rooms. The Fitness Center is free to NRL employees and contractors. Various exercise classes are offered for a nominal fee. NRL employees are also eligible to

participate in all NSAW-MWR activities held on Joint Base Anacostia–Bolling and Washington Navy Yard, less than five miles away.

PROGRAMS FOR NON-NRL EMPLOYEES

Several programs have been established for non-NRL professionals. These programs encourage and support the participation of visiting scientists and engineers in research of interest to the Laboratory. Some of the programs may serve as stepping-stones to Federal careers in science and technology. Their objective is to enhance the quality of the Laboratory's research activities through working associations and interchanges with highly capable scientists and engineers and to provide opportunities for outside scientists and engineers to work in the Navy laboratory environment. Along with enhancing the Laboratory's research, these programs acquaint participants with Navy capabilities and concerns and may provide a path to full-time employment.

POSTDOCTORAL RESEARCH ASSOCIATESHIPS

Every year, NRL hosts several postdoctoral research associates through the National Research Council (NRC) and American Society for Engineering Education (ASEE) postdoctoral associateship and fellowship programs. These competitive positions provide postdoctoral scientists and engineers the opportunity to pursue research at NRL in collaboration with NRL scientists and engineers. Research associates are guest investigators, not employees of NRL.

NRL/NRC Cooperative Research Associateship Program: The National Research Council conducts a national competition to recommend and make awards to outstanding scientists and engineers at recent postdoctoral levels for tenure as guest researchers at participating laboratories. The objectives of the NRC program are (1) to provide postdoctoral scientists and engineers of unusual promise and ability opportunities for research on problems, largely of their own choice, that are compatible with the interests of the sponsoring laboratories and (2) to contribute thereby to the overall efforts of the Federal laboratories. The program provides an opportunity for concentrated research in association with selected members of the permanent professional laboratory staff, often as a climax to formal career preparation.

NRL/NRC Postdoctoral Associateships are awarded to persons who have held a doctorate less

than five years at the time of application, and are made initially for one year, renewable for a second and possible third year. Information and applications may be found at <http://www.national-academies.org/rap>. To contact NRL's program coordinator, call (202) 404-7450 or email nrc@hro.nrl.navy.mil.

NRL/ASEE Postdoctoral Fellowship Program:

The ASEE program is designed to significantly increase the involvement of creative and highly trained scientists and engineers from academia and industry in scientific and technical areas of interest and relevance to the Navy. Fellowship awards are based upon the technical quality and relevance of the proposed research, recommendations by the Navy laboratory, academic qualifications, reference reports, and availability of funds.

NRL/ASEE Fellowship awards are made to persons who have held a doctorate for less than seven years at the time of application, and are made for one year, renewable for a second and possible third year. Information and applications may be found at <http://www.asee.org/nrl/>. To contact NRL's program coordinator, call (202) 404-7450 or email asee@hro.nrl.navy.mil.

FACULTY MEMBER PROGRAMS

The **Office of Naval Research Summer Faculty Research and Sabbatical Leave Program** provides for university faculty members to work for ten weeks (or longer, for those eligible for sabbatical leave) with professional peers in participating Navy laboratories on research of mutual interest. Applicants must hold a teaching or research position at a U.S. college or university. Contact NRL's program coordinator at sfrp@hro.nrl.navy.mil.

The **NRL/United States Naval Academy Cooperative Program for Scientific Interchange** allows faculty members of the U.S. Naval Academy to participate in NRL research. This collaboration benefits the Academy by providing the opportunity for USNA faculty members to work on research of a more practical or applied nature. In turn, NRL's research program is strengthened by the available scientific and engineering expertise of the USNA faculty. Contact NRL's program coordinator at usna@hro.nrl.navy.mil.

PROFESSIONAL APPOINTMENTS

Faculty Member Appointments use the special skills and abilities of faculty members for short periods to fill positions of a scientific, engineering, professional, or analytical nature at NRL.

Consultants and experts are employed because they are outstanding in their fields of specialization or because they possess ability of a rare nature and could not normally be employed as regular civil servants.

Intergovernmental Personnel Act Appointments temporarily assign personnel from state or local governments or educational institutions to the Federal Government (or vice versa) to improve public services rendered by all levels of government.

STUDENT PROGRAMS

The student programs are tailored to high school, undergraduate, and graduate students to provide employment opportunities and work experience in naval research.

The **Naval Research Enterprise Intern Program (NREIP)** is a ten-week summer research opportunity for undergraduate sophomores, juniors, and seniors, and graduate students. The Office of Naval Research (ONR) offers summer appointments at Navy laboratories to current college sophomores, juniors, seniors, and graduate students from participating schools. Application is online at www.asee.org/nreip through the American Society for Engineering Education. Electronic applications are sent for evaluation to the point of contact at the Navy laboratory identified by the applicant. Contact NRL's program coordinator at nreip@nrl.navy.mil.

The **National Defense Science and Engineering Graduate Fellowship Program** helps U.S. citizens obtain advanced training in disciplines of science and engineering critical to the U.S. Navy. The three-year program awards fellowships to recent outstanding graduates to support their study and research leading to doctoral degrees in specified disciplines such as electrical engineering, computer sciences, material sciences, applied physics, and ocean engineering. Award recipients are encouraged to continue their study and research in a Navy laboratory during the summer. Contact NRL's program coordinator at (202) 404-7450 or ndseg@hro.nrl.navy.mil.

The **Pathways Intern Program** (formerly STEP and SCEP) provides students enrolled in a wide variety of educational institutions, from high school to graduate level, with opportunities to work at NRL and explore Federal careers while still in school and while getting paid for the work performed. Students can work full-time or part-time on a temporary or non-temporary appointment. Students must be continuously enrolled on at least a half-time basis at a qualifying educational

institution and be at least 16 years of age. The primary focus of our **Non-temporary** intern appointment is to attract students enrolled in undergraduate and graduate programs in engineering, computer science, or the physical sciences. Students on non-temporary appointments are eligible to remain on their appointment until graduation and may be noncompetitively converted to a permanent appointment within 120 days after completion of degree requirements. Conversion is not guaranteed. Conversion is dependent on work performance, completion of at least 640 hours of work under the intern appointment before completion of degree requirements, and meeting the qualifications for the position. The **Temporary** intern appointment is initially a one year appointment. This program enables students to earn a salary while continuing their studies and offers them valuable work experience. NRL's Pathways Intern Program opportunities are announced on USAJOBS four times per year. Visit USAJOBS at <https://www.usajobs.gov/> to create an account, search for jobs, set up an email notification alert of when positions of interest are posted (see "Saved Searches") and apply for our intern opportunities when posted. For additional information on NRL's Intern Program, contact (202) 767-8313.

The **Department of Defense Science and Engineering Apprenticeship Program (SEAP)** provides an opportunity for high school students who have completed at least grade 9, and are at least 15 years of age, to serve as junior research associates. Under the direction of a mentor, for eight weeks in the summer, students gain a better understanding of research, its challenges, and its opportunities through participation in scientific, engineering, and mathematics programs. Criteria for eligibility are based on science and mathematics courses completed and grades achieved; scientific motivation, curiosity, the capacity for sustained hard work; a desire for a technical career; teacher recommendations; and exceptional test scores. The NRL program is the largest in the Department of Defense. For detailed information visit <http://seap.asee.org/>, or call (202) 767-8324, or email seap@hro.nrl.navy.mil.

VOLUNTEER OPPORTUNITIES

The **Student Volunteer Program** helps students gain valuable experience by allowing them to voluntarily perform educationally related work at NRL. It provides exposure to the work environment and also provides an opportunity for students to make realistic decisions regarding their future careers. Applications are accepted year-round. For additional information, contact (202) 767-8313.

NRL EMPLOYMENT OPPORTUNITIES

for Highly Innovative, Motivated, and Creative Professionals

NRL offers a wide variety of challenging S&T positions that involve skills from basic and applied research to equipment development. The nature of the research and development conducted at NRL requires professionals with experience. Typically there is a continuing need for electronics, mechanical, aerospace, and materials engineers, metallurgists, computer scientists, and oceanographers with bachelor's and/or advanced degrees and physical and computer scientists with Ph.D. degrees.



■ **Biologists.** Biologists conduct research in areas that include biosensor development, tissue engineering, molecular biology, genetic engineering, proteomics, and environmental monitoring.

■ **Chemists.** Chemists are recruited to work in the areas of combustion, polymer science, bioengineering and molecular engineering, surface science, materials synthesis, nanostructures, corrosion, fiber optics, electro-optics, microelectronics, electron device technology, and laser physics.

■ **Electronics Engineers and Computer Scientists.** These employees may work in the areas of communications systems, electromagnetic scattering, electronics instrumentation, electronic warfare systems, radio frequency/microwave/millimeter-wave/infrared technology, radar systems, laser physics technology, radio-wave propagation, electron device technology, spacecraft design, artificial intelligence, information processing, signal processing, plasma physics, vacuum science, microelectronics, electro-optics, fiber optics, solid-state physics, software engineering, computer design/architecture, ocean acoustics, stress analysis, and expert systems.

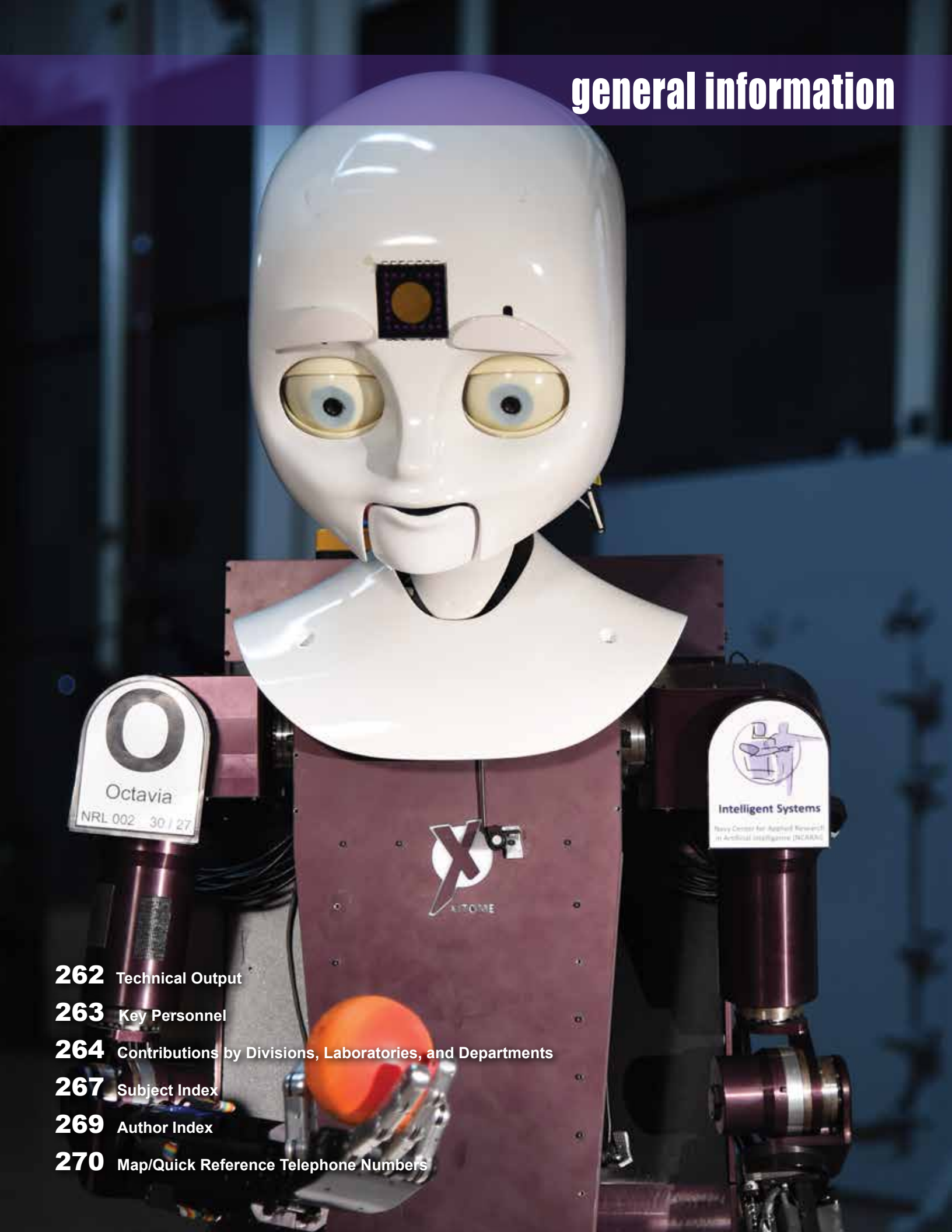
■ **Materials Scientists/Engineers.** These employees are recruited to work on materials, microstructure characterization, electronic ceramics, solid-state physics, fiber optics, electro-optics, microelectronics, fracture mechanics, vacuum science, laser physics and joining technology, and radio frequency/microwave/millimeter-wave/infrared technology.

■ **Mechanical and Aerospace Engineers.** These employees may work in areas of spacecraft design, remote sensing, propulsion, experimental and computational fluid mechanics, experimental structural mechanics, solid mechanics, elastic/plastic fracture mechanics, materials, finite-element methods, nondestructive evaluation, characterization of fracture resistance of structural alloys, combustion, CAD/CAM, and multifunctional material response.

■ **Oceanographers, Meteorologists, and Marine Geophysicists.** These employees work in the areas of ocean and atmospheric dynamics, air-sea interaction, upper-ocean dynamics, oceanographic bio-optical modeling, oceanic and atmospheric numerical modeling and prediction, data assimilation and data fusion, retrieval and application of remote sensing data, benthic processes, aerogeophysics, marine sedimentary processes, advanced mapping techniques, atmospheric physics, and remote sensing. Oceanographers and marine geophysicists are located in Washington, DC, and at the Stennis Space Center, Bay St. Louis, Mississippi. Meteorologists are located in Washington, DC, and Monterey, California.

■ **Physicists.** Physics graduates may concentrate on such fields as materials, solid-state physics, fiber optics, electro-optics, microelectronics, vacuum science, plasma physics, fluid mechanics, signal processing, ocean acoustics, information processing, artificial intelligence, electron device technology, radio-wave propagation, laser physics, ultraviolet/X-ray/gamma-ray technology, electronic warfare, electromagnetic interaction, communications systems, radio frequency/microwave/millimeter-wave/infrared technology, computational physics, radio and high-energy astronomy, solar physics, and space physics.

For more information and current vacancy listings,
visit <http://hroffice.nrl.navy.mil/>

- 
- 262** Technical Output
 - 263** Key Personnel
 - 264** Contributions by Divisions, Laboratories, and Departments
 - 267** Subject Index
 - 269** Author Index
 - 270** Map/Quick Reference Telephone Numbers

TECHNICAL OUTPUT

The Navy continues to be a leader in initiating new developments and applying these advancements to military requirements. The primary method of informing the scientific and engineering community of the advances made at NRL is through the Laboratory's technical output — reports, articles in scientific journals, contributions to books, papers presented to scientific societies and topical conferences, patents, and inventions.

The figures for calendar year 2013 presented below represent the output of NRL facilities in Washington, D.C.; Bay St. Louis, Mississippi; and Monterey, California.

In addition to the output listed, NRL scientists made more than 1239 oral presentations during 2013.

<u>Type of Contribution</u>	<u>Unclassified</u>	<u>Classified</u>	<u>Total</u>
Articles in periodicals, chapters in books, and papers in published proceedings	1472*	0	1472*
NRL Formal Reports	9	7	16
NRL Memorandum Reports	33	5	38
Books	7	0	7
U.S. patents granted	114	2	116
Foreign patents granted	10		10
U.S. Trademark Registrations	1		1

*This is a provisional total based on information available to the Ruth H. Hooker Research Library on June 3, 2015. Additional publications carrying a 2013 calendar year publication date are anticipated. Total includes refereed and nonrefereed publications.

KEY PERSONNEL

Area Code (202) unless otherwise listed
 Personnel Locator - 767-3200
 DSN-297 or 754

Code	Office	Phone Number
EXECUTIVE DIRECTORATE		
1000	Commanding Officer	767-3403
1000.1	Inspector General	767-3621
1001	Director of Research	767-3301
1001.1	Executive Assistant for the Director of Research	767-2445
1002	Chief Staff Officer	767-3621
1004	Head, Technology Transfer Office	767-3083
1006	Head, Office of Program Administration and Policy Development	767-3091
1008	Office of Counsel	767-2244
1030	Public Affairs Officer	767-2541
1100	Director, Institute for Nanoscience	767-3261
1200	Head, Command Support Division	767-3621
1220	Head, Information Assurance and Communications Security	767-0793
1400	Head, Military Support Division	767-2273
1600	Commander, Scientific Development Squadron One	301-342-3751
1700	Director, Laboratory for Autonomous Systems Research	767-2684
1800	Director, Human Resources Office	767-3421
1830	Deputy EEO Officer	767-5264
3005	Deputy for Small Business	767-6263
3540	Head, Safety Branch	767-2232
BUSINESS OPERATIONS DIRECTORATE		
3000	Comptroller/Associate Director of Research	767-2371
3200	Head, Contracting Division	767-5227
3300	Head, Financial Management Division	767-3405
3400	Head, Supply and Information Services Division	767-3446
3500	Director, Research and Development Services Division	404-4054
SYSTEMS DIRECTORATE		
5000	Associate Director of Research	767-3425
5300	Superintendent, Radar Division	404-2700
5500	Superintendent, Information Technology Division/ NRL Command Information Officer*	767-2903
5600	Superintendent, Optical Sciences Division	767-7375
5700	Superintendent, Tactical Electronic Warfare Division	767-6278
MATERIALS SCIENCE AND COMPONENT TECHNOLOGY DIRECTORATE		
6000	Associate Director of Research	767-3566
6040	Director, Laboratories for Computational Physics and Fluid Dynamics	767-2402
6100	Superintendent, Chemistry Division	767-3026
6300	Superintendent, Materials Science and Technology Division	767-2926
6700	Superintendent, Plasma Physics Division	767-2723
6800	Superintendent, Electronics Science and Technology Division	767-3693
6900	Director, Center for Bio/Molecular Science and Engineering	404-6000
OCEAN AND ATMOSPHERIC SCIENCE AND TECHNOLOGY DIRECTORATE		
7000	Associate Director of Research	404-8690
7100	Superintendent, Acoustics Division	767-3482
7200	Superintendent, Remote Sensing Division	767-3391
7300	Superintendent, Oceanography Division	228-688-4670
7400	Superintendent, Marine Geosciences Division	228-688-4650
7500	Superintendent, Marine Meteorology Division	831-656-4721
7600	Superintendent, Space Science Division	767-6343
NAVAL CENTER FOR SPACE TECHNOLOGY		
8000	Director	767-6547
8100	Superintendent, Space Systems Development Department	767-0410
8200	Superintendent, Spacecraft Engineering Department	404-3727

*Additional Duty

CONTRIBUTIONS BY DIVISIONS, LABORATORIES, AND DEPARTMENTS

Radar Division

- 76 2D Oversampled Receive Arrays for Over-the-Horizon Radar
G. San Antonio and Y.I. Abramovich

Information Technology Division

- 166 TRIDENT SPECTRE 2013: FIREFLY: Multimodal Signatures for Increased Confidence in Remote Object Detection and Classification
G.C. Gilbreath, D.J. Bonanno, C.O. Font, B. Bajramaj, T.J. Walls, F. Pipitone, C.T. Hawley, and M. Sartor

- 168 TALON — Robust DoD Laser Communications through the Air
C.I. Moore, L. Thomas, W. Rabinovich, T.N. Smith, D. Baker, H.R. Burris, R. Mahon, D. Rabinovich, W.R. Smith IV, M. Vilcheck, N. Walker, and L. Willstatter

- 208 Broadband Dielectric Spectroscopy of Several Energetic and Nonenergetic Materials
B. Bajramaj, M.A. Nurge, and D.J. Bonanno

Optical Sciences Division

- 116 Multiple Order Staircase Etalon Spectroscopy
M. Yetzbacher, C. Miller, A. Boudreau, and M. Christophersen

- 156 Multilayer Polymer Composites for High Energy Density Capacitors
M.A. Wolak

- 168 TALON — Robust DoD Laser Communications through the Air
C.I. Moore, L. Thomas, W. Rabinovich, T.N. Smith, D. Baker, H.R. Burris, R. Mahon, D. Rabinovich, W.R. Smith IV, M. Vilcheck, N. Walker, and L. Willstatter

- 185 Energy Distribution through Quantum Dot Anchored Nanoscale Photonic Wires
C.M. Spillmann, S. Buckhout-White, E.R. Goldman, I.L. Medintz, M.G. Ancona, M.H. Stewart, K. Susumu, A.L. Huston, and W.R. Algar

- 202 Infrared Gradient Index Optics for Multiband Imagers
D. Gibson, S. Bayya, and J. Sanghera

Tactical Electronic Warfare Division

- 157 Wideband Dynamic Range Extender (DRE)
B. Nousain, J. Goodman, K. Lorenz, M. McKeon, and G. Stantchev

- 203 Broadband Nonlinear Metamaterial
W.S. Wall, S.M. Rudolph, S.K. Hong, K.L. Morgan, and V.M. Mendez

- 210 Camouflage Paint Scheme for the USS Fort Worth (LCS 3)
R. Gignilliat

Laboratories for Computational Physics and Fluid Dynamics

- 216 Considering Blast Response in Helmet Design
D.R. Mott, T.R. Young, Jr., and D.A. Schwer

Chemistry Division

- 83 Structure and Crystallography of the Barnacle *Balanus amphitrite*
A.C. Lewis, R.K. Everett, K.J. Wahl, and D.K. Burden

- 134 Geochemical Data Application to Enhance Seismic Interpretation of Deep Sediment Methane Hydrate Deposits
R. Coffin, W. Wood, and I. Pecher

- 146 Biomolecular Analyses of Ship Hull Biofouling Communities
D.H. Leary, W.J. Hervey IV, L.J. Hamdan, N. Lebedev, Z. Wang, J.R. Deschamps, R.W. Li, A.W. Kusterbeck, and G.J. Vora

- 176 Long-Term Hydrogen-Assisted Cracking Evaluation of Monel K-500
R. Bayles, T. Lemieux, F. Martin, D. Lysogorski, B. Weathers, K. Williams, L. Drake, P. Pao, E. Hogan, A. Geltmacher, T. Newbauer, W. Hyland, W. Kinee, M.R. First, A. Rubinoff, P. Stencel, E. Arnold, E. Knudsen, and D. Horton

- 182 Photochemistry in 3D Using Visible-Light Plasmonic-Sensitization
P.A. DeSario, J.J. Pietron, D.R. Rolison, T.H. Brintlinger, and R.M. Stroud

190 Ballast Water Compliance Testing
*L.A. Drake, T.P. Wier, J.F. Grant, M.R. First,
S.H. Robbins-Wamsley, S.C. Riley,
M.N. Tamburri, and C.S. Moser*

Materials Science and Technology Division

83 Structure and Crystallography of the Barnacle
Balanus amphitrite
*A.C. Lewis, R.K. Everett, K.J. Wahl, and D.K.
Burden*

144 Identification of Trace Explosives on Relevant
Surfaces at Standoff Distances
*C. Kendziora, R. Furstenberg, V. Nguyen,
M. Papantonakis, J. Byers, and R.A. McGill*

172 Novel Spintronic Device for Reconfigurable
Logic
M.B. Johnson

176 Long-Term Hydrogen-Assisted Cracking
Evaluation of Monel K-500
*R. Bayles, T. Lemieux, F. Martin, D. Lysogorski,
B. Weathers, K. Williams, L. Drake, P. Pao,
E. Hogan, A. Geltmacher, T. Newbauer,
W. Hyland, W. Kinee, M.R. First, A. Rubinoff,
P. Stencel, E. Arnold, E. Knudsen, and D. Horton*

182 Photochemistry in 3D Using Visible-Light
Plasmonic-Sensitization
*P.A. DeSario, J.J. Pietron, D.R. Rolison,
T.H. Brintlinger, and R.M. Stroud*

Plasma Physics Division

159 An Attractive Hybrid Indirect and Direct Drive
Approach to Laser Fusion
*M. Karasik, J.L. Weaver, A.J. Schmidt, J.W. Bates,
V. Serlin, S.P. Obenschain, Y. Aglitskiy, and J. Oh*

173 Simulation of Cold-X-Ray Effects Using Intense
Ion Beams
*D.D. Hinshelwood, D. Phipps, G. Williams,
M. Lynch, and G. Paderewski*

217 The X-Ray Flash of a Z Pinch
*J.L. Giuliani, J.W. Thornhill, A. Dasgupta,
A.L. Velikovich, Y.K. Chong, T.A. Mehlhorn,
E. Kroupp, Y. Maron, J.P. Apruzese, and
C. Deeney*

Electronics Science and Technology Division

157 Wideband Dynamic Range Extender (DRE)
*B. Nousain, J. Goodman, K. Lorenz, M. McKeon,
and G. Stantchev*

161 Multi-Kilowatt Millimeter-Wave Sheet Beam
Amplifiers
*J. Pasour, D. Abe, S. Cooke, B. Levush, K. Nguyen,
E. Wright, D. Pershing, and A. Balkcum*

175 Prediction of New High Thermal Conductivity
Materials for Cooling Electronics
L. Lindsay, T.L. Reinecke, and D.A. Broido

183 Strained $\text{In}_x\text{Ga}_{1-x}\text{As}$ HEMTs for Complementary
Logic
*J.G. Champlain, B.R. Bennett, J.B. Boos, D. Park,
H.S. Newman, N.A. Papanicolaou, and R. Bass*

185 Energy Distribution through Quantum Dot
Anchored Nanoscale Photonic Wires
*C.M. Spillmann, S. Buckhout-White, E.R. Gold-
man, I.L. Medintz, M.G. Ancona, M.H. Stewart,
K. Susumu, A.L. Huston, and W.R. Algar*

Center for Bio/Molecular Science and Engineering

146 Biomolecular Analyses of Ship Hull Biofouling
Communities
*D.H. Leary, W.J. Hervey IV, L.J. Hamdan,
N. Lebedev, Z. Wang, J.R. Deschamps, R.W. Li,
A.W. Kusterbeck, and G.J. Vora*

149 Hierarchically Organized Microvessels for
Vascularized Tissue Models
M.A. Daniele, S.H. North, and A.A. Adams

152 X-Ray Crystal Structures of Engineered Ricin
Vaccine Immunogens
P.M. Legler, J.R. Compton, and C.B. Millard

185 Energy Distribution through Quantum Dot
Anchored Nanoscale Photonic Wires
*C.M. Spillmann, S. Buckhout-White, E.R. Gold-
man, I.L. Medintz, M.G. Ancona, M.H. Stewart,
K. Susumu, A.L. Huston, and W.R. Algar*

Acoustics Division

126 Atmospheric Acoustic Propagation and Detec-
tion of Rotorcraft Noise
*J.F. Lingeitch, J. Cook, C. Hutchins, and
D. Martinez*

127 Novel Thermophone Acoustic Projectors
B. Dzikowicz, J. Baldwin, and J. Tressler

128 Elastic Point Contact and Mechanical
Resonators
*D.J. Goldstein, D.M. Photiadis, and
M.K. Zalalutdinov*

Remote Sensing Division

- 212 Hyperspectral Imager for the Coastal Ocean (HICO) Goes Public under NASA Sponsorship
M. Kappus
- 226 High-Precision Remote Sensing of Ionospheric Disturbances
J. Helmboldt

Oceanography Division

- 136 Monitoring Maritime Conditions with Unmanned Systems During Trident Warrior 2013
C.N. Barron, S.D. Ladner, A.J. Quaid, L.F. Smedstad, K.P. Grembowicz, A. Mask, E.M. Coehlo, E.A. Holmberg, and G. Peggion
- 139 Probing the World's Greatest Source of Variability — Madden Julian Oscillation
M. Flatau, S. Chen, T. Jensen, T. Shinoda, J. Cummings, and P. May
- 219 From the Stream to the Shore: Forecasting Complex Ocean Environments in Trident Warrior '13
C.N. Barron, T.J. Campbell, K.L. Edwards, G.A. Jacobs, J.G. Richman, T.A. Smith, T.L. Townsend, J. Veeramony, and P.L. Spence
- 222 Integrating the Marine Biosphere into Coupled Ocean–Atmosphere Models
J.K. Jolliff and T.A. Smith

Marine Geosciences Division

- 89 Measuring Arctic Sea Ice Motion in Real Time
R.A. Hagen, M.F. Peters, R.T. Liang, J.M. Brozena, and D.E. Ball
- 134 Geochemical Data Application to Enhance Seismic Interpretation of Deep Sediment Methane Hydrate Deposits
R. Coffin, W. Wood, and I. Pecher
- 192 Direct Measurements of Tensile Strength of Artificial Marine Flocs under Microscopic Micromanipulation
A. Abelev and P. Amarasinghe
- 194 Laser Profiling System for Laboratory Sediment Beds
A.M. Penko, A. Bordelon, and B. Landry
- 197 Biogeochemical Control of the Particle Flux in River-Dominated Coastal Regions
Y. Furukawa, A.H. Reed, and G. Zhang

Marine Meteorology Division

- 97 Using Unmanned Aircraft to Probe Hurricanes
J.D. Doyle, J. Moskaitis, P. Black, E. Hendricks, P.A. Reinecke, Y. Jin, and S. Braun
- 126 Atmospheric Acoustic Propagation and Detection of Rotorcraft Noise
J.F. Lingeitch, J. Cook, C. Hutchins, and D. Martinez
- 139 Probing the World's Greatest Source of Variability — Madden Julian Oscillation
M. Flatau, S. Chen, T. Jensen, T. Shinoda, J. Cummings, and P. May

Space Science Division

- 109 Predicting Total Solar Irradiance
R.A. Howard, K. Battams, and H.A. Dennison
- 116 Multiple Order Staircase Etalon Spectroscopy
M. Yetzbacher, C. Miller, A. Boudreau, and M. Christophersen
- 229 SWORD: Improving the Simulation Experience
C. Gwon, M. Strickman, B. Philips, D. Polaski, B. Leas, and L. Jackson

Space Systems Development Department

- 168 TALON — Robust DoD Laser Communications through the Air
C.I. Moore, L. Thomas, W. Rabinovich, T.N. Smith, D. Baker, H.R. Burris, R. Mahon, D. Rabinovich, W.R. Smith IV, M. Vilcheck, N. Walker, and L. Willstatter
- 231 Project CHRONOS
K. Senior

SUBJECT INDEX

- 3D printing, 18
3D zinc sponge electrodes, 27
3DOG, 136
Acoustics Division, 52
Acoustics, 127
Administrative Services, 69
Advanced Graduate Research Program, 256
Aggregation, 197
Airborne Expendable BathyThermographs (AXBT), 219
AltiKa, 219
Amateur Radio Club, 257
Aquatic nuisance species, 190
Arctic, 89
Assimilation, 136, 219
ASW, 136
Atmosphere-ocean interaction, 139
Audible detection, 126
Autoregressive modeling, 76
Avalanche diode, 172
Barnacle adhesion, 23
Barnacle, 83
Bed forms, 194
Benthic microbial fuel cell, 21
Biofouling, 146
Biopolymer, 197
Blast, 216
Blossom Point Satellite Tracking and Command Facility, 73
Boron arsenide, 175
Calcite, 83
Camouflage paint scheme, 210
Capacitors, 156
Center for Bio/Molecular Science and Engineering, 50
Chalcogenide glass, 202
Chemistry Division, 42
Chesapeake Bay Detachment (CBD), 71
Clayey marine sediments, 192
Climate change, 134
CMOS, 183
Coastal ocean, 212
Colloid, 197
Community Outreach Program, 257
Complex permittivity, 208
Composite signatures, 166
Composites, 156
Computer simulation, 222
Coupled forecast, 219
De-orbiting space debris, 23
Debye relaxation, 208
Department of Defense Science and Engineering Apprenticeship Program (SEAP), 259
Department of the Navy Civilian Employee Assistance Program (DONCEAP), 256
Dielectric spectroscopy, 208
Dielectrics, 156
Direction-of-arrival (DOA), 76
Edison Memorial Graduate Training Program, 256
Elastic point contact, 128
Electron backscatter diffraction, 83
Electronics Science and Technology Division, 48
Embrittlement, 176
Energetic material, 208
Energy storage, 156
Energy, 134
Estuary, 197
Ex-USS Shadwell Research Platform, 74
FIB/SEM, 156
Finite rank/finite order approximations, 76
Flimmer, 22
Flocculation, 192, 197
Fluid-structure interaction, 216
Fracture mechanics, 176
Free Space Optical (FSO), 168
Fusion energy, 159
Fusion, 166
Geochemistry, 134
Global distribution, 134
GNSS, 231
GOST, 136
GPS, 231
Gradient index (GRIN), 202
Graphene resonant tunneling transistor, 24
Gulf Stream, 219
Helmet, 216
High electron mobility transistors (HEMT), 183
High frequency (HF), 76
High pressure, 159
Homeland Security, 229
Humic, 197
Hurricanes, 97
Hydrogel, 149
Hydrogen fuel cells, 20
Hydrogen-assisted cracking, 176
Hyperspectral Imager for the Coastal Ocean (HICO), 212
Hyperspectral imaging (HSI), 166
Information Technology Division, 34
Infrared imaging, 144
Infrared spectroscopy, 144
Institute for Nanoscience, 30
Integrated Underwater Hull Shield, 18
Intense charged particle beams, 173
Interband cascade lasers, 24
Interferometry, 226
Invasive species, 190
Ionosphere, 226
IR optics, 202
KrF, 159
Laboratories for Computational Physics and Fluid Dynamics, 40
LASCO, 109
Laser fusion, 22
Laser imprint, 159
Laser power beaming, 19
Lasercom, 168
Lasers, 159
Littoral combat ship, 210
Logic, 183
Low SWAP hyperspectral imaging, 116
Marine biofilms, 146
Marine Corrosion Facility, 74
Marine Geosciences Division, 58
Marine Meteorology Division, 60
Materials Science and Technology Division, 44
Mechanical resonator(s), 128
Mesoporous materials, 19
Metagenome, 146
Metaproteome, 146
Methane hydrates, 134
Micromanipulation, 192
Microfiber, 149
Microfluidic fabrication, 149
Midway Research Center, 72
Millimeter-wave amplifiers, 161
MITW, 136
Monel K-500, 176
Monterey (NRL-MRY), 70
Montmorillonite, 197
Multimodal signatures, 166
Multilayer structure, 156
Nanomaterials, 182
Nanoscale energy distribution, 185
Nanoscale exchange electron spin bias mechanism, 25
Nanoscience, 116
National Defense Science and Engineering Graduate Fellowship Program, 259
National nuclear scientific stewardship, 217
Naval Postgraduate School (NPS), 256
Naval Research Enterprise Intern Program (NREIP), 259
Nearfield, 129
Noise propagation, 126
Nonlinear magnetics, 203
Nonlinear media, 203
NRL Fitness Center, 257
NRL Mentor Program, 257
NRL/ASEE Postdoctoral Fellowship Program, 258
NRL/NRC Cooperative Research Associateship Program, 258
NRL/United States Naval Academy Cooperative Program for Scientific Interchange, 258
NTS-2, 8
Numerical weather prediction, 97
Ocean forecast, 219

Ocean gliders, 136
 Oceanography Division, 56
 Oceanography, 222
 Office of Naval Research Summer Faculty
 Research and Sabbatical Leave Program,
 258
 Optical forecast, 136
 Optical Sciences Division, 36
 Optimal beamforming, 76
 Organic matter, 197
 Oscillatory flow tunnel, 194
 Over-the-Horizon Radar (OTHR), 76
 Oversampled arrays, 76
 Pathfinder, 212
 Pathways Intern Program, 259
 Periodic structures, 203
 Phonons, 175
 Photocatalysis, 182
 Photogrammetry, 89
 Photonic wire, 185
 Plankton, 190
 Plasma Physics Division, 46
 Plasma X-ray radiation sources, 217
 Plasmonic enhancement, 182
 Polymer films, 156
 Pomonkey Facility, 73
 Protein engineering, 152
 Pulsed power, 156
 Quantitative proteomics, 146
 Quantum cascade laser, 144
 Quantum dot, 185
 Radar Division, 32
 Radio frequency receiver, 157
 Radiological/nuclear, 229
 Reconfigurable logic, 172
 Reliant autonomous underwater vehicle, 17
 Remote Sensing Division, 54
 Rotating detonation engines, 26
 Rotorcraft, 126
 Ruth H. Hooker Research Library, 69
 Sand ripples, 194
 Scientific Development Squadron ONE
 (VXS-1), 72
 Scientist-to-Sea Program (STSP), 256
 Sea-ice, 89
 Seabed roughness, 194
 Seafloor evolution, 194
 Seismic profiles, 134
 Select Graduate Training Program, 256
 SENTIENT, 21
 SHARC, 136
 Sheet beam, 161
 Sheet electron beam gun, 25
 Shipboard sampling, 190
 Sigma Xi, 257
 Solar corona, 109
 Solar fuels, 182
 Space research, 229
 Space Science Division, 62
 Space Systems Development Department,
 64
 Spacecraft Engineering Department, 66
 Spintronics, 172
 Spurious free dynamic range, 157
 Standoff detection, 144
 Stennis Space Center (NRL-SSC), 70
 Student Volunteer Program, 259
 Superconductivity, 76
 SWAN, 219
 Synthetic aperture radar (SAR), 166
 Tactical Electronic Warfare Division, 38
 Tactical Line-of-sight Optical Network
 Communications (TALON), 168
 Technical Information Services, 68
 Technology Transfer Office, 68
 Thermal conductivity, 175
 Thermoacoustics, 127
 Thermostable, 152
 Tissue engineering, 149
 Toastmasters International, 257
 TODS, 136
 Total Solar Irradiance (TSI), 109
 Transduction, 127
 Transistor, 183
 Traumatic brain injury (TBI), 216
 Trident Warrior, 136, 219
 Tropical dynamics, 139
 Two-Way Satellite Time and Frequency
 Transfer (TWSTFT), 231
 Ultraviolet Photolithographic Process, 26
 Unmanned Aerial Vehicles, 97
 USV, 136
 UUV, 136
 Vaccine, 152
 Waterspace management, 136
 Wave modeling, 219
 WaveWatch III, 219
 Women in Science and Engineering
 (WISE), 257
 X-ray crystallography, 152
 X-ray effects, 173
 XFC, 20
 Z pinches, 217

AUTHOR INDEX

- Abe, D., 161
Abelev, A., 192
Abramovich, Y.I., 76
Adams, A.A., 149
Aglitskiy, Y., 159
Algar, W.R., 185
Amarasinghe, P., 192
Ancona, M.G., 185
Apruzese, J.P., 217
Arnold, E., 176
Bajramaj, B., 166, 208
Baker, D., 168
Baldwin, J., 127
Balkcum, A., 161
Ball, D.E., 89
Barron, C.N., 136, 219
Bass, R., 183
Bates, J.W., 159
Battams, K., 109
Bayles, R., 176
Bayya, S., 202
Bennett, B.R., 183
Black, P., 97
Bonanno, D.J., 166, 208
Boos, J.B., 183
Bordelon, A., 194
Boudreau, A., 116
Braun, S., 97
Brintlinger, T.H., 182
Broido, D.A., 175
Brozena, J.M., 89
Buckhout-White, S., 185
Burden, D.K., 83
Burris, H.R., 168
Byers, J., 144
Campbell, T.J., 219
Champlain, J.G., 183
Chen, S., 139
Chong, Y.K., 217
Christophersen, M., 116
Coehlo, E.M., 136
Coffin, R., 134
Compton, J.R., 152
Cook, J., 126
Cooke, S., 161
Cummings, J., 139
Daniele, M.A., 149
Dasgupta, A., 217
Deeney, C., 217
Dennison, H.A., 109
DeSario, P.A., 182
Deschamps, J.R., 146
Doyle, J.D., 97
Drake, L., 176
Drake, L.A., 190
Dzikowicz, B., 127
Edwards, K.L., 219
Everett, R.K., 83
First, M.R., 176, 190
Flatau, M., 139
Font, C.O., 166
Furstenberg, R., 144
Furukawa, Y., 197
Geltmacher, A., 176
Gibson, D., 202
Gignilliat, R., 210
Gilbreath, G.C., 166
Giuliani, J.L., 217
Goldman, E.R., 185
Goldstein, D.J., 128
Goodman, J., 157
Grant, J.F., 190
Grembowicz, K.P., 136
Gwon, C., 229
Hagen, R.A., 89
Hamdan, L.J., 146
Helmboldt, J., 226
Hendricks, E., 97
Hervey, W.J., IV, 146
Hinshelwood, D.D., 173
Hogan, E., 176
Holmberg, E.A., 136
Hong, S.K., 203
Horton, D., 176
Howard, R.A., 109
Huston, A.L., 185
Hutchins, C., 126
Hyland, W., 176
Jackson, L., 229
Jacobs, G.A., 219
Jensen, T., 139
Jin, Y., 97
Johnson, M.B., 172
Jolliff, J.K., 222
Kappus, M., 212
Karasik, M., 159
Kendziora, C., 144
Kinee, W., 176
Knudsen, E., 176
Kroupp, E., 217
Kusterbeck, A.W., 146
Ladner, S.D., 136
Landry, B., 194
Leary, D.H., 146
Leas, B., 229
Lebedev, N., 146
Legler, P.M., 152
Lemieux, T., 176
Levush, B., 161
Lewis, A.C., 83
Li, R.W., 146
Liang, R.T., 89
Lindsay, L., 175
Lingeitch, J.F., 126
Lorenz, K., 157
Lynch, M., 173
Lysogorski, D., 176
Mahon, R., 168
Maron, Y., 217
Martin, F., 176
Martinez, D., 126
Mask, A., 136
May, P., 139
McGill, R.A., 144
McKeon, M., 157
Medintz, I.L., 185
Mehlhorn, T.A., 217
Mendez, V.M., 203
Millard, C.B., 152
Miller, C., 116
Moore, C.I., 168
Morgan, K.L., 203
Moser, C.S., 190
Moskaitis, J., 97
Mott, D.R., 216
Newbauer, T., 176
Newman, H.S., 183
Nguyen, K., 161
Nguyen, V., 144
North, S.H., 149
Nousain, B., 157
Nurge, M.A., 208
Obenshain, S.P., 159
Oh, J., 159
Paderewski, G., 173
Pao, P., 176
Papanicolaou, N.A., 183
Papantonakis, M., 144
Park, D., 183
Pasour, J., 161
Pecher, L., 134
Jensen, T., 139
Peggion, G., 136
Penko, A.M., 194
Pershing, D., 161
Peters, M.F., 89
Phipps, D., 173
Phlips, B., 229
Photiadis, D.M., 128
Pietron, J.J., 182
Pipitone, F., 166
Polaski, D., 229
Quaid, A.J., 136
Rabinovich, D., 168
Rabinovich, W., 168
Reed, A.H., 197
Reinecke, P.A., 97
Reinecke, T.L., 175
Richman, J.G., 219
Riley, S.C., 190
Robbins-Wamsley, S.H., 190
Rolison, D.R., 182
Rubinoff, A., 176
Rudolph, S.M., 203
San Antonio, G., 76
Sanghera, J., 202
Sartor, M., 166
Schmitt, A.J., 159
Schwer, D.A., 216
Senior, K., 231
Serlin, V., 159
Shinoda, T., 139
Smedstad, L.F., 136
Smith, W.R., IV, 168
Smith, T.A., 219, 222
Smith, T.N., 168
Spence, P.L., 219
Spillmann, C.M., 185
Stantchev, G., 157
Stencel, P., 176
Stewart, M.H., 185
Strickman, M., 229
Stroud, R.M., 182
Susumu, K., 185
Tamburri, M.N., 190
Thomas, L., 168
Thornhill, J.W., 217
Townsend, T.L., 219
Tressler, J., 127
Veeramony, J., 219
Velikovich, A.L., 217
Vilcheck, M., 168
Vora, G.J., 146
Wahl, K.J., 83
Walker, N., 168
Wall, W.S., 203
Walls, T.J., 166
Wang, Z., 146
Weathers, B., 176
Weaver, J.L., 159
Wier, T.P., 190
Williams, G., 173
Williams, K., 176
Willstatter, L., 168
Wolak, M.A., 156
Wood, W., 134
Wright, E., 161
Yetzbacher, M., 116
Young, T.R., Jr., 216
Zalalutdinov, M.K., 128
Zhang, G., 197

NAVAL RESEARCH LABORATORY

4555 Overlook Ave., SW • Washington, DC 20375-5320

LOCATION OF NRL IN THE CAPITAL AREA



Quick Reference Telephone Numbers

	NRL Washington	NRL- SSC	NRL- Monterey	NRL CBD	NRL VXS-1 Patuxent River
Hotline	(202) 767-6543	(202) 767-6543	(202) 767-6543	(202) 767-6543	(202) 767-6543
Personnel Locator	(202) 767-3200	(228) 688-3390	(831) 656-4763	(410) 257-4000	(301) 342-3751
DSN	297- or 754-	828	878	—	342
Direct-in-Dialing	767- or 404-	688	656	257	342
Public Affairs	(202) 767-2541	(228) 688-5328	(202) 767-2541	—	(202) 767-2541

Additional telephone numbers are listed on page 263.

General information on the research described in this NRL Review can be obtained from the Public Affairs Office, Code 1030, (202) 767-2541. Information concerning Technology Transfer is available from the Technology Transfer Office, Code 1004, (202) 767-7230. Sources of information on the various educational programs at NRL are listed in the NRL Review chapter titled "Programs for Professional Development."

For additional information about NRL, the NRL Fact Book lists the organizations and key personnel for each division. It contains information about Laboratory funding, programs, and field sites. The Fact Book can be obtained from the Technical Information Services Branch, Code 3430, (202) 404-4963. The web-based NRL Major Facilities publication, which describes each NRL facility in detail, can be accessed at <http://www.nrl.navy.mil/media/publications>.

2014

NRL REVIEW

www.nrl.navy.mil

